Daniel S. Duick
Robert A. Levine
Mark A. Lupo *Editors*

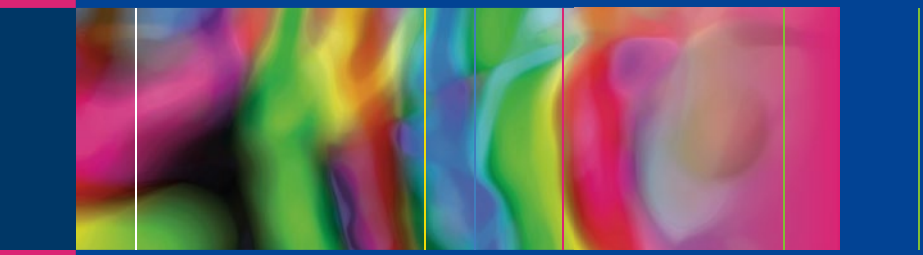

Thyroid and Parathyroid Ultrasound and Ultrasound-Guided FNA

Fourth Edition

Springer

Thyroid and Parathyroid Ultrasound and Ultrasound-Guided FNA

Daniel S. Duick • Robert A. Levine
Mark A. Lupo
Editors

Thyroid and Parathyroid Ultrasound and Ultrasound-Guided FNA

Fourth Edition

Springer

Editors
Daniel S. Duick
University of Arizona, College of Medicine
Phoenix, AZ, USA

Endocrinology Associates, P. A.
Scottsdale, AZ, USA

Mark A. Lupo
Florida State University, College of Medicine
Tallahassee, FL, USA

Thyroid & Endocrine Center of Florida
Sarasota, FL, USA

Robert A. Levine
Geisel School of Medicine at Dartmouth, Thyroid Center of New Hampshire,
St. Joseph Hospital,
Nashua, NH, USA

ISBN 978-3-319-67237-3 ISBN 978-3-319-67238-0 (eBook)
https://doi.org/10.1007/978-3-319-67238-0

Library of Congress Control Number: 2017960819

Printed on acid-free paper

This Springer imprint is published by Springer Nature
The registered company is Springer International Publishing AG
The registered company address is: Gewerbestrasse 11, 6330 Cham, Switzerland

Foreword

Fourth Edition of the "Thyroid and Parathyroid Ultrasound and Ultrasound-Guided FNA"

When I began my career in endocrinology in 1971, and specifically in thyroidology, evaluation of the thyroid nodule simply involved a careful history and physical examination, as well as, in some cases, nuclear scanning. Ultrasound and, for that matter, other imaging techniques were not available. Despite what seems crude by today's standards, we thought we did pretty well. Then, years later, thyroid ultrasound became available, and that revolutionized our approach to patient evaluation and management and especially, with the additional advent of fine needle aspiration, to cytologic evaluation of nodules. Indeed, thyroid ultrasound has become standard practice in the evaluation of patients with thyroid nodules; it is an indispensable extension of our eyes and fingers.

In this fourth edition of the "Thyroid and Parathyroid Ultrasound and Ultrasound-Guided FNA" by Duick, Levine, and Lupo, the authors manage to synthesize the essentials of their prior three editions and provide a comprehensive and expanded review on the latest in the diagnosis and management of thyroid nodules, as well as focusing on parathyroid disease and non-endocrine lesions of the neck. They rely not only on their extensive collective clinical experience but on reviews of prior and current peer-reviewed publications. The authors, all experts in thyroid and parathyroid disease, cover not only thyroid and parathyroid disease but also have a

chapter on imaging of the salivary glands and other non-endocrine lesions of the neck, mindful of the fact that those of us who perform (and evaluate) neck ultrasound also detect non-thyroid and parathyroid lesions. In this edition, the authors expand the chapters on both surgical and nonsurgical management.

Since the publication of the third edition of this book, the use of molecular markers in thyroid evaluation has become both more sensitive and specific, and an excellent chapter addresses this issue.

Finally, as more endocrinologists and surgeons perform ultrasounds in their office practices, it is essential that detailed reports are available to referring physicians and that they also include adequate information for billing purposes. The authors recognize this and include a chapter on authoring ultrasound reports.

In summary, this fourth edition brings together the collective wisdom of specialists who treat patients with thyroid nodules, thyroid cancer, and parathyroid disease and should serve as the "go-to" source for surgeons, endocrinologists, fellows, and residents.

Peter A. Singer, MD
Clinical Endocrinology,
Thyroid Diagnostic Center,
Keck School of Medicine of USC
Los Angeles, CA, USA

Preface

Fourth Edition of the Thyroid Ultrasound and Ultrasound-Guided FNA Textbook

Ultrasound has become ingrained as the classical utilization of applied technology for both diagnostic and interventional therapeutic approaches to the management of thyroid and parathyroid conditions. It is an invaluable tool for the practice of thyroidology and is most beneficial when performed in real time by a physician or a practitioner who is skilled and knowledgeable in the anatomy of the neck.

The recognition of imagery patterns suggestive of a generalized disease state, the presence and evaluation of thyroid nodules, the search for a parathyroid tumor when there is biochemical evidence of hyperparathyroidism, and the assessment for residual tissue and lymphadenopathy of the postoperative thyroid cancer neck are all related issues that ultrasound is capable of optimally imaging.

There continues to be technologic advances in demonstrating ultrasound images on the visual screen which enhance gray scale and employ both color flow Doppler and power Doppler which add additional information to the analysis of the thyroid gland, parathyroid tumors, and lymph nodes as well as other structures in the neck.

Ultrasound remains the number one invaluable tool for assessing the endocrine neck, and the performance of real-time ultrasound is unquestionably the optimum methodology for utilization.

Scottsdale, AZ, USA Daniel S. Duick, MD, MACE

Contents

Contributors

Dev Abraham, MBBS, MRCP(UK) Department of Medicine, University of Utah, Salt Lake City, UT, USA

Ghobad Azizi, MD Endocrinology, Wilmington Endocrinology, Wilmington, NC, USA

H. Jack Baskin Sr., MD, MACE University of Central Florida College of Medicine, Orlando, FL, USA

Hank Baskin, MD, DABR Pediatric Section, Intermountain Healthcare Imaging, Department of Radiology, University of Utah School of Medicine, Medical Imaging, Primary Children's Hospital, Salt Lake City, UT, USA

Vijaya Chockalingam, MD Endocrinology, Banner University Medical Center, Phoenix, AZ, USA

Daniel S. Duick, MD, MACE University of Arizona College of Medicine, Phoenix, AZ, USA

Endocrinology Associates, PA, Scottsdale, AZ, USA

Vinay T. Fernandes, MD, FRCSC Otolaryngology – Head & Neck Surgery, University of Toronto, Toronto, ON, Canada

Andrea Frasoldati, MD, PhD Endocrinology Unit, Medical Specialities Department, Arcispedale S. Maria Nuova – IRCCS, Reggio Emilia, Italy

Susan J. Hsiao, MD, PhD Department of Pathology & Cell Biology, Columbia University Medical Center, New York, NY, USA

Dipti Kamani, MD Department of Otolaryngology, Division of Thyroid and Parathyroid Surgery, Massachusetts Eye and Ear Infirmary, Boston, MA, USA

Stacey Klyn, DO Department of Surgery, Banner University Medical Center, Phoenix, AZ, USA

Jill E. Langer, MD Department of Radiology, Perelman School of Medicine, University of Pennsylvania, Philadelphia, PA, USA

Stephanie L. Lee, MD, PhD, FACE, ECNU Section of Endocrinology, Diabetes and Nutrition, Thyroid Health Center, Boston Medical Center, Boston, MA, USA

Robert A. Levine, MD, FACE, ECNU Geisel School of Medicine at Dartmouth College, Thyroid Center of New Hampshire, St. Joseph Hospital, Nashua, NH, USA

Mark A. Lupo, MD, FACE, ECNU Thyroid & Endocrine Center of Florida, Sarasota, FL, USA

Florida State University, College of Medicine, Sarasota Florida Campus, Sarasota, FL, USA

Carl D. Malchoff, MD, PhD Internal Medicine and Neag Comprehensive Cancer Center, UConn Health, Farmington, CT, USA

Susan J. Mandel, MD, MPH Division of Endocrinology, Diabetes and Metabolism, Department of Medicine, Perelman School of Medicine, University of Pennsylvania, Philadelphia, PA, USA

Mira Milas, MD, FACS Thyroid, Parathyroid & Adrenal Disorders Center, Diabetes and Endocrinology Institute, Phoenix, AZ, USA

Department of Surgery, Endocrine Surgery Center, University of Arizona College of Medicine – Phoenix, Phoenix, AZ, USA

Banner – University Medical Center Phoenix, Phoenix, AZ, USA

Yuri E. Nikiforov, MD, PhD Department of Pathology, Division of Molecular & Genomic Pathology, University of Pittsburgh Medical Center, Pittsburgh, PA, USA

Lisa A. Orloff, MD, FACE, FACS Otolaryngology, Stanford University Medical Center, Stanford, CA, USA

Gregory W. Randolph, MD, FACS, FACE Thyroid Surgery Oncology, Harvard Medical School, Boston, MA, USA

Division of Thyroid and Parathyroid Endocrine Surgery, Department of Otolaryngology – Head and Neck Surgery, Massachusetts Eye and Ear Infirmary, Boston, MA, USA

Department of Surgery, Endocrine Surgery Service, Massachusetts General Hospital, Boston, MA, USA

Barry Sacks, MD Beth Israel Deaconess Medical Center, Natick, MA, USA

Catherine F. Sinclair, BMBS(Hons), FRACS, BSc(Biomed) Department of Otolaryngology, Icahn School of Medicine at Mount Sinai, New York, NY, USA

J. Woody Sistrunk, MD, FACE, ECNU Jackson Thyroid & Endocrine Clinic, PLLC, Jackson, MS, USA

Sarah Smith Sonographer, Medsmart Inc. and Alumnus, West Coast Ultrasound Institute, Phoenix, AZ, USA

Petros Tsamatropoulos, MD Endocrinology Unit, Centro Palmer, Reggio Emilia, Italy

Roberto Valcavi, MD, FACE Endocrinology Unit, Centro Palmer, Reggio Emilia, Italy

Chapter 1
History of Thyroid Ultrasound

Robert A. Levine and J. Woody Sistrunk

Abbreviations

AACE	American Association of Clinical Endocrinologists
AIUM	American Institute of Ultrasound Medicine
ATA	American Thyroid Association
ECNU	Endocrine Certification in Neck Ultrasound
MHz	Megahertz

R.A. Levine, MD, FACE, ECNU (✉)
Geisel School of Medicine at Dartmouth College, Thyroid Center of New Hampshire, St. Joseph Hospital, Nashua, NH, USA
e-mail: thyroidmd2@gmail.com

J.W. Sistrunk, MD, FACE, ECNU
Jackson Thyroid & Endocrine Clinic, PLLC, Jackson, MS, USA

D.S. Duick et al. (eds.), *Thyroid and Parathyroid Ultrasound and Ultrasound-Guided FNA*,
https://doi.org/10.1007/978-3-319-67238-0_1

Introduction

The visual application of sound in medicine has revolutionized the diagnosis and management of thyroid disease. The safety of ultrasound, along with improvements in image quality and equipment availability, underlies the importance of thyroid ultrasound to today's endocrinologist and endocrine surgeon.

The thyroid is amenable to ultrasound study because of its superficial location, vascularity, size, and echogenicity [1]. In addition, the thyroid has a very high incidence of nodular disease, the vast majority benign. Most structural abnormalities of the thyroid need evaluation and monitoring but may not require intervention [2]. Between 1965 and 1970, there were seven articles published specific to thyroid ultrasound. In the last 5 years, there have been over 10,000 articles published. Thyroid ultrasound has undergone a dramatic transformation from the cryptic deflections on an oscilloscope produced in A-mode scanning, to barely recognizable B-mode images, followed by initial low-resolution gray scale, to current high-resolution images. Recent advances in technology, including harmonic imaging, spatial compound imaging, elastography, and three-dimensional reconstruction, have all furthered the field.

The development of high-resolution thyroid ultrasound required decades of study in both the acoustics of sound and data processing. Some animals, for example, dolphins and bats, have the ability use ultrasound in their daily activities in everything from catching prey to finding a mate. As early as the 1700s, the Italian biologist Lazzaro Spallanzani demonstrated that bats use high frequency sound waves to navigate in complete darkness [3]. The aim of this chapter is provide an overview of the basic advancements in the field of ultrasound that have provided the ability to easily and safely see and interpret structures inside the neck.

Beginnings of Ultrasound History

One of the earliest experiments regarding transmission of sound was performed in 1826 in Lake Geneva by Jean-Daniel Colladon. Using an underwater bell he determined the speed of sound transmission in water. In the 1800s, properties of sound including wave transmission, propagation, reflection, and refraction were defined. In 1877 Lord Rayleigh's English treatise, "Theory of Sound," added mathematics and became the basis for the applied study of sound. The principles described lead to the science of using reflected sound in identifying and locating objects. In 1880, Pierre and Jacques Curie discovered the piezoelectric effect, determining that an electric current applied across a crystal would result in a vibration that would generate sound waves and that sound waves striking a crystal would, in turn, produce an electric voltage. Piezoelectric transducers were capable of producing sonic waves in the audible range and ultrasonic waves above the range of human hearing [3].

Sonar

The first patent for a sonar device was issued to Lewis Richardson, an English meteorologist, only 1 month after the Titanic sank following collision with an iceberg. The first functional sonar system was made in the United States, by Canadian Reginald Fessenden, in 1915. The Fessenden "fathometer" could detect an iceberg 2 miles away. As electronics improved, Paul Langevin designed a device called a hydrophone. It became of the one of the first measures available to detect German U-Boats during World War I. The hydrophone was the basis of the pulse-echo sonar that is still employed in ultrasound equipment today [3, 4].

Rudimentary high frequency ultrasound analysis was used on a commercial basis in the 1930s and 1940s to detect defects

in steel such as the hull of a ship. Although crude by today's standards, inhomogeneity suggested abnormalities, whereas a flawless appearance suggested uniform material [4]. With the end of World War II, the development of the computer and the invention of the transistor advanced the development of medical ultrasound [3].

Early Medical Applications of Ultrasound

The initial use of ultrasound in medicine in the 1940s was therapeutic rather than diagnostic. Following the observation that very high-intensity sound waves had the ability to damage tissues, lower intensities were tried for therapeutic uses. Focused sound waves were used to mildly heat tissue for therapy of rheumatoid arthritis, and early attempts were made to destroy the basal ganglia to treat Parkinson's disease [4]. The American Institute of Ultrasound in Medicine (AIUM) was formed in 1952 with therapeutic ultrasound in physical medicine being the primary focus. Although members performing diagnostic ultrasound were not accepted until 1964, diagnostic ultrasound is currently the primary focus of this organization [3].

Early in the twentieth century, Paul Langevin described the ability of high-intensity ultrasound to induce pain in a hand placed in a water tank. The 1940s saw therapeutic ultrasound tried in numerous applications ranging from gastric ulcers to arthritis. Attempts to destroy the basal ganglia in patients with Parkinson's disease now seem archaic. At the time therapeutic ultrasound was headed toward the museum of medical quackery, consideration of ultrasound as a diagnostic tool in medicine had begun. Although Drs. Gohr and Wedekindt at the Medical University of Koln, Germany, suggested that ultrasound could detect tumors, exudates, and abscesses, the results were not convincing. Karl Theodore Dussik is credited as the first physician to use diagnostic ultrasound. In his 1952 report, "Hyperphonography of the Brain," ultrasound was utilized in localizing brain tumors and

the cerebral ventricles by transmitting ultrasonic sound through the skull. While the results of these studies were later discredited as predominantly artifact, this work played a significant role in stimulating research into the diagnostic capabilities of ultrasound [3].

A-Mode Ultrasound

One of the first studies of diagnostic ultrasound was performed by George Ludwig. Using A-mode ultrasound, his main focus was using ultrasound to detect gallstones, shown as reflected sound waves on an oscilloscope screen. Through his study of various tissues, including the use of live subjects, clinical utility of diagnostic ultrasound was described. Despite the limited efficacy of his rudimentary ultrasound system, Ludwig's most important achievement may be his determination of the velocity of sound transmission in animal soft tissues. Ludwig also determined that the optimum frequency of an ultrasound transducer for deep tissue was between 1 and 2.5 MHz. The ultrasound characteristics of mammalian tissue were further defined by physicist Richard Bolt at Massachusetts Institute of Technology and neurosurgeon H. Thomas Ballantine, Jr. at Massachusetts General Hospital [3].

Most of early ultrasound used a transmission technique, but by the mid-1950s that was supplanted by a reflection technique. Providing information limited to a single dimension, A-mode scanning showed deflections on an oscilloscope indicating distance to reflective surfaces [4] (see Fig. 2.7). A-mode ultrasonography was used for detection of brain tumors, shifts in the midline structures of the brain, localization of foreign bodies in the eye, and detection of detached retinas [4]. In the first presage that ultrasound may assist in the detection of cancer, John Julian Wild reported the observation that gastric malignancies were more echogenic than normal gastric tissue. Along with Dr. John Reid, he later studied 117 breast nodules using a 15 MHz sound source and

reported the ability to determine their size with an accuracy of 90% [3].

B-Mode Ultrasound

During the late 1950s, the first two-dimensional B-mode scanners were developed. B-mode scanners display a compilation of sequential A-mode images to create a two-dimensional image (see Fig. 2.8). Douglass Howry developed an immersion tank B-mode ultrasound system which was featured in the Medicine section of Life Magazine in September 1954 [3]. Several additional models of immersion tank scanners followed. All utilized a mechanically driven transducer that would sweep through an arc, with an image reconstructed to demonstrate the full sweep. Continued development led to the "Pan-scanner," a more advanced B-mode device, but it still employed a cumbersome bathtub of water. Later advances included a handheld transducer that still required a mechanical connection to the unit to provide data regarding location and water-bag coupling devices to eliminate the need for immersion [3].

By 1964, the work of Joseph H. Holmes along with William Wright and Ralph (Edward) Meyerdirk lead to the prototype of the "compound contact" scanner, with direct contact of the transducer with the patient's body. As stated in a 1958 Lancet article describing ultrasound evaluation of abdominal masses, "Any new technique becomes more attractive if its clinical usefulness can be demonstrated without harm, indignity or discomfort to the patient" [5].

Applying Ultrasound Technology to the Thyroid

The 1960s brought continued development of microelectronics including semiconductors that revolutionized the ability to process signals and produce visual displays. The phased

array transducer utilized in modern day ultrasound derived from highly classified submarine technology. During the 1970s additional advances in transducer design, including the linear array and mechanical oscillating transducers, lead to the two-dimensional imaging which remains the standard today. With these improvements and the addition of gray-scale displays, ultrasound representation of the thyroid began to resemble that seen in the operative field or gross anatomy lab [4].

In 1967 Fujimoto reported data on 184 patients studied with a B-mode ultrasound "tomogram" utilizing a water bath [6]. The authors reported that no internal echoes were generated by the thyroid in patients with normal thyroid function and non-palpable thyroid glands. They described several basic patterns generated by palpably abnormal thyroid tissue. Thyroid tissue with strong internal echo attenuation characteristics was considered "malignant." Unfortunately, 25% of benign adenomas showed the malignant pattern, and 25% of papillary carcinomas were found to have the benign pattern. Although the first major publication of thyroid ultrasound attempted to establish the ability to determine malignant potential, the results were nonspecific in a large percentage of the cases. However, this was a seminal paper in ultrasound and is considered the first on thyroid ultrasound to attempt to establish the malignant appearance of nodules [4, 6].

In 1971 Manfred Blum published a series of A-mode ultrasounds of thyroid nodules (see Fig. 2.7). He demonstrated the ability of ultrasound to distinguish solid from cystic nodules, as well as accuracy in measurement of the dimensions of thyroid nodules [7]. Additional publications in the early 1970s further confirmed the capacity for both A-mode and B-mode ultrasound to differentiate solid from cystic lesions but consistently demonstrated that ultrasound was unable to distinguish malignant from benign solid lesions with acceptable accuracy [8].

The advent of gray-scale display resulted in images that were far easier to view and interpret [6]. In 1974 Ernest Crocker published *The Gray Scale Echographic Appearance*

of Thyroid Malignancy. Using an 8 MHz transducer with a 0.5 mm resolution, he described "low amplitude, sparse and disordered echoes" characteristic of thyroid cancer when viewed with a gray-scale display [9]. The pattern felt to be characteristic of malignancy was what would now be considered "hypoechoic and heterogeneous".

With each advance in technology, interest was rekindled in ultrasound's ability to distinguish benign from malignant lesions. Initial reports of ultrasonic features typically described findings as being diagnostically specific. Later, reports followed showing overlap between various disease processes. For example, following an initial report that the "halo sign," a rim of hypoechoic signal surrounding a solid thyroid nodule, was seen only in benign lesions [10], Propper reported that two of ten patients with this finding had carcinoma [11]. As discussed in Chap. 7, the halo sign is still considered to be one of the numerous features that can be used in determining the likelihood of malignancy in a nodule.

In 1977 Walfish recommended combining fine-needle aspiration biopsy with ultrasound in order to improve the accuracy of specimen acquisition [12]. Subsequent studies demonstrated that biopsy accuracy is greatly improved when ultrasound is used to guide needle placement. Most patients with prior "nondiagnostic" biopsies will have an adequate specimen obtained when ultrasound-guided biopsy is performed [13]. Ultrasound-guided fine-needle aspiration results in improved sensitivity and specificity, as well as a greater than 50% reduction in nondiagnostic and false-negative biopsies [14].

Over the past several years, the value of ultrasound in screening for suspicious lymph nodes prior to surgery in patients with biopsy proven cancer has been established. Current guidelines for the management of thyroid cancer indicate a pivotal role for ultrasound in monitoring for locoregional recurrence [15].

During the 1980s Doppler ultrasound was introduced, allowing detection of blood flow in tissues. As discussed in detail in Chap. 3, the role of Doppler in assessing the

likelihood of malignancy has undergone a recent reevaluation. Doppler imaging may demonstrate the increased blood flow characteristic of Graves' disease [16] and may be useful in distinguishing between Graves' disease and thyroiditis, especially in pregnant patients or when radioisotope scanning is unavailable (see Chap. 3). Doppler imaging is useful in determining the subtype of amiodarone-induced thyrotoxicosis [17].

Recent Advances in Technology

Recent technological advancements include intravenous sonographic contrast agents, three-dimensional ultrasound imaging, and elastography. Intravenous sonographic contrast agents are available in Europe but remain experimental in the United States. All ultrasound contrast agents consist of microspheres, which function both by reflecting ultrasonic waves and, at higher signal power, by reverberating and generating harmonics of the incident wave. Ultrasound contrast agents have been predominantly used to visualize large blood vessels and have shown promise in imaging peripheral vasculature as well as liver tumors and metastases [18]. While no studies have been published demonstrating any advantage of contrast agents in routine thyroid imaging, the use of contrast agents or B-flow imaging may be helpful in the immediate assessment of successful laser or radiofrequency ablation of thyroid nodules [19].

Three-dimensional display of reconstructed images has been available for CT scan and MRI for many years and has demonstrated practical application. While three-dimensional ultrasound has gained popularity for fetal imaging, its role in diagnostic neck ultrasound remains unclear. Obstetrical ultrasound has the great advantage of the target being surrounded by a natural fluid interface, greatly improving surface rendering, whereas 3D thyroid ultrasound is limited by the lack of a similar interface distinguishing the thyroid from adjacent neck tissues. It has been predicted that breast

biopsies may eventually be guided in a more precise fashion by real time 3D imaging [20], and it is possible that, in time, thyroid biopsy will similarly benefit. At present, however, 3D ultrasound technology does not provide a demonstrable advantage in thyroid imaging.

Elastography is a promising technique in which the compressibility of a nodule is assessed by ultrasound, while external pressure is applied. With studies showing good predictive value for detection of malignancy in breast nodules, recent investigations of its role in thyroid imaging have been promising. Additional prospective trials are ongoing to assess the role of elastography in predicting the likelihood of thyroid malignancy. The role of elastography in the selection of nodules for biopsy or surgery is discussed in Chap. 16.

Application of Neck Ultrasound by Endocrinologists and Endocrine Surgeons

With the growing recognition that real time ultrasound performed by a clinician provides far more useful information than that obtained from a radiology report, point of care ultrasound has gained acceptance. The first educational course specific to thyroid ultrasound was offered in 1998 by the American Association of Clinical Endocrinologists (AACE). Under the direction of Dr. H. Jack Baskin, 53 endocrinologists were taught to perform diagnostic ultrasound and ultrasound-guided fine-needle aspiration biopsy. By the turn of the century, 300 endocrinologists had been trained. Endocrine University, established in 2002 by AACE, began providing instruction in thyroid ultrasound and biopsy to all graduating endocrine fellows. By 2016 over 6000 endocrinologists had completed an AACE ultrasound course. In 2007 a collaborative effort between the American Institute of Ultrasound in Medicine (AIUM) and AACE established a certification program for endocrinologists trained in neck ultrasound. By 2016 the ECNU (Endocrine Certification in Neck Ultrasound) program had certified over 470 endocrinologists as having the

training, experience, and expertise needed to perform thyroid and parathyroid ultrasound and fine-needle aspiration biopsy. In 2011 the American Institute of Ultrasound in Medicine began accrediting qualified endocrine practices as centers of excellence in thyroid and parathyroid imaging. To date, 89 practices have received AIUM site accreditation in thyroid and parathyroid ultrasound.

Conclusion

When the American Association of Clinical Endocrinologists began its efforts to teach thyroid ultrasound to Endocrinologists in 1998, an ultrasound machine seemed a foreign concept in the office. At present, it is becoming the exception to find endocrinologists who do not have thyroid ultrasound and ultrasound-guided FNA biopsy as part of their practice.

In parallel with the growth of thyroid ultrasound in endocrinology, the American Thyroid Association (ATA) guidelines for the management of thyroid nodules and thyroid cancer have placed an increasing emphasis on the sonographic characteristics of thyroid nodules. The 2006 guidelines mention ultrasound characteristics of thyroid nodules five times [21]. The 2009 ATA guidelines make 14 references to ultrasound characteristics [22], and the latest 2015 ATA guidelines mention ultrasound characteristics of thyroid nodules and thyroid cancer 100 times [15].

In the 50 years since ultrasound was first used for thyroid imaging, there has been a profound improvement in the technology and quality of images. The transition from A-mode to B-mode to gray-scale images was accompanied by dramatic improvements in clarity and interpretability of images. Current high-resolution images are able to identify virtually all lesions of clinical significance. Ultrasound characteristics can predict which nodules are likely to be benign and detect features including irregular margins, microcalcifications, and central vascularity that may deem a nodule suspicious [4]. Ultrasound

plays a clear fundamental role in thyroid nodule and lymph node evaluation as well as the selection of which should undergo biopsy [15]. Ultrasound has proven utility in the detection of recurrent thyroid cancer in patients with negative whole body iodine scan or undetectable thyroglobulin [15, 23]. Recent advances including the use of contrast agents, tissue harmonic imaging, elastography, and multiplanar reconstruction of images have further enhanced the diagnostic value of ultrasound images. Ultrasound guidance of fine-needle aspiration biopsy has been demonstrated to improve both diagnostic yield and accuracy and has become the standard of care. Routine point of care use of ultrasound is often considered an extension of the physical examination by endocrinologists and endocrine surgeons. High-quality ultrasound systems are now available at prices that make this technology accessible to virtually all providers of endocrine care [4].

Acknowledgment The authors wish to acknowledge the work of Dr. Joseph Woo and his excellent web-based overview of the history of ultrasound. Relevant parts of his work with application to thyroid ultrasound have been presented here. For his full text, please access http://www.ob-ultrasound.net/ history1.html.

References

1. Solbiati L, Osti V, Cova L, Tonolini M. Ultrasound of the thyroid, parathyroid glands and neck lymph nodes. Eur Radiol. 2001;11(12):2411–24.
2. Tessler FN, Tublin ME. Thyroid sonography: current applications and future directions. AJR. 1999;173:437–43.
3. Woo JSK. A short history of the development of ultrasound in obstetrics and gynecology. http://www.ob-ultrasound.net/history1.html. Accessed 29 June 2016.
4. Levine RA. Something old and something new: a brief history of thyroid ultrasound technology. Endocr Pract. 2004;10(3):227–33.
5. Donald I, Macvicar J, Brown TG. Investigation of abdominal masses by pulsed ultrasound. Lancet. 1958;271:1188–95.
6. Fujimoto F, Oka A, Omoto R, Hirsoe M. Ultrasound scanning of the thyroid gland as a new diagnostic approach. Ultrasonics. 1967;5:177–80.

7. Blum M, Weiss B, Hernberg J. Evaluation of thyroid nodules by A-mode echography. Radiology. 1971;101:651–6.
8. Scheible W, Leopold GR, Woo VL, Gosink BB. High resolution real-time ultrasonography of thyroid nodules. Radiology. 1979;133:413–7.
9. Crocker EF, McLaughlin AF, Kossoff G, Jellins J. The gray scale echographic appearance of thyroid malignancy. J Clin Ultrasound. 1974;2(4):305–6.
10. Hassani SN, Bard RL. Evaluation of solid thyroid neoplasms by gray scale and real time ultrasonography: the "halo" sign. Ultrasound Med. 1977;4:323.
11. Propper RA, Skolnick ML, Weinstein BJ, Dekker A. The nonspecificity of the thyroid halo sign. J Clin Ultrasound. 1980;8:129–32.
12. Walfish PG, Hazani E, Strawbridge HTG, et al. Combined ultrasound and needle aspiration cytology in the assessment and management of hypofunctioning thyroid nodule. Ann Intern Med. 1977;87(3):270–4.
13. Gharib H. Fine-needle aspiration biopsy of thyroid nodules: advantages, limitations, and effect. Mayo Clin Proc. 1994;69:44–9.
14. Danese D, Sciacchitano S, Farsetti A, Andreoli M, Pontecorvi A. Diagnostic accuracy of conventional versus sonography guided fine-needle aspiration biopsy in the management of nonpalpable and palpable thyroid nodules. Thyroid. 1998;8:511–5.
15. Haugen BR, Alexander EK, Bible KC, Doherty G, et al. 2015 American Thyroid Association management guidelines for adult patients with thyroid nodules and differentiated thyroid cancer. Thyroid. 2016;26(1):1–133.
16. Ralls PW, Mayekowa DS, Lee KP, et al. Color-flow Doppler sonography in Graves' disease: "thyroid inferno.". AJR. 1988;150:781–4.
17. Bogazzi F, Bartelena L, Brogioni S, et al. Color flow Doppler sonography rapidly differentiates type I and type II amiodarone induced thyrotoxicosis. Thyroid. 1997;7(4):541–5.
18. Grant EG. Sonographic contrast agents in vascular imaging. Semin Ultrasound CT MR. 2001;22(1):25–41.
19. Andrioli M, Valcavi R. Ultrasound B-flow imaging in the evaluation of thermal ablation of thyroid nodules. Endocrine. 2015;48(3):1013–5.
20. Lees W. Ultrasound imaging in three and four dimensions. Semin Ultrasound CT MR. 2001;22(1):85–105.

21. Cooper DS, Doherty GM, Haugen BR, Kloos RT, et al. Management guidelines for patients with thyroid nodules and differentiated thyroid cancer. Thyroid. 2006;16(2):109–42.
22. Cooper DS, Doherty GM, Haugen BR, Kloos RT, et al. Revised American Thyroid Association management guidelines for patients with thyroid nodules and differentiated thyroid cancer. Thyroid. 2009;19(11):1167–214.
23. Antonelli A, Miccoli P, Ferdeghini M. Role of neck ultrasonography in the follow-up of patients operated on for thyroid cancer. Thyroid. 1995;5(1):25–8.

Chapter 2
Thyroid Ultrasound Physics

Robert A. Levine

Abbreviations

Hz	Hertz
MHz	Megahertz
m/s	Meters per second

Sound and Sound Waves

Some animal species such as dolphins, whales, and bats are capable of creating a "visual" image based on receiving reflected sound waves. Our unassisted vision is limited to electromagnetic waves in the spectrum of visible light. Humans require technology and an understanding of physics to use sound to create a picture. This chapter will explore how we have developed a technique for creating a visual image from sound waves [1].

R.A. Levine, MD, FACE, ECNU
Geisel School of Medicine at Dartmouth College, Thyroid Center of New Hampshire, St. Joseph Hospital, Nashua, NH, USA
e-mail: thyroidmd2@gmail.com

D.S. Duick et al. (eds.), *Thyroid and Parathyroid Ultrasound and Ultrasound-Guided FNA*,
https://doi.org/10.1007/978-3-319-67238-0_2

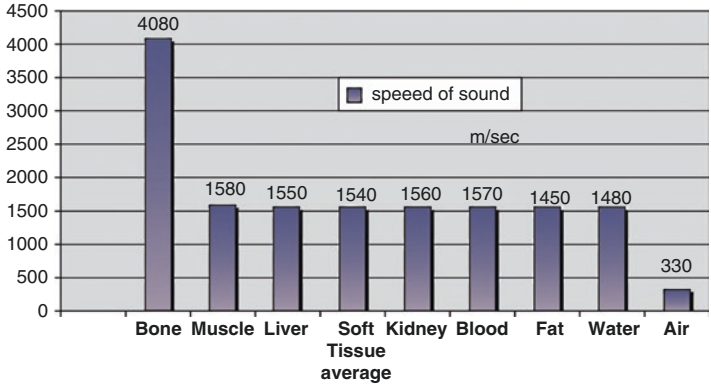

FIGURE. 2.1 Speed of sound. The speed of sound is constant for a specific material and does not vary with frequency. Speed of sound for various biological tissues is illustrated

Sound is transmitted as mechanical energy, in contrast to light, which is transmitted as electromagnetic energy. Unlike electromagnetic waves, sound waves require a propagating medium. Light is capable of traveling through a vacuum, but sound will not transmit through a vacuum. The qualities of the transmitting medium have a direct effect on how sound is propagated. Materials have different speeds of sound transmission and acoustic impedance. Speed of sound is constant for a specific material and does not vary with sound frequency (Fig. 2.1). Acoustic impedance is a measure of the opposition that a system presents to the flow of acoustic energy. When sound travels through a material and encounters a boundary separating two different areas of acoustic impedance, a portion of the sound energy will be reflected, and the remainder will be transmitted. The amount reflected is proportionate to the degree of mismatch of acoustic impedance. Acoustic impedance of a material depends on its density, stiffness, and speed of sound [2].

Sound waves propagate by compression and rarefaction of molecules in space (Fig. 2.2). Molecules of the propagating

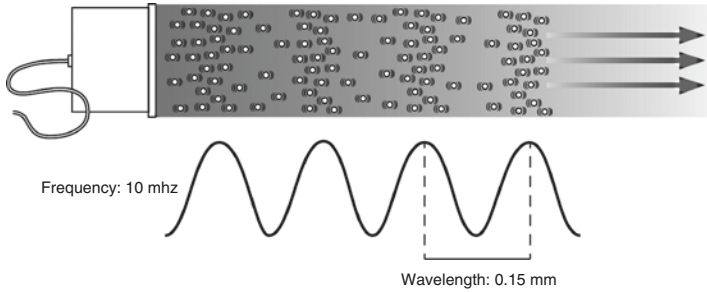

FIGURE. 2.2 Sound waves propagate in a longitudinal direction but are typically represented by a sine wave where the peak corresponds to the maximum compression of molecules in space, and the trough corresponds to the maximum rarefaction

medium vibrate around their resting position and transfer their energy to neighboring molecules. Sound waves carry energy rather than matter through space.

As shown in Fig. 2.2, sound waves propagate in a longitudinal direction but are typically represented graphically by a sine wave where the peak corresponds to the maximum compression of molecules in space, and the trough corresponds to the maximum rarefaction. Frequency is defined as the number of cycles per time of the vibration of the sound waves. A Hertz (Hz) is defined as one cycle per second. The audible spectrum is between 30 and 20,000 Hz. Ultrasound is defined as sound waves at a higher frequency than the audible spectrum. Typical frequencies used in diagnostic ultrasound vary between five million and sixteen million cycles per second (5 and 16 MHz) [1, 3].

Diagnostic ultrasound uses pulsed waves, allowing for an interval of sound transmission, followed by an interval during which reflected sounds are received and analyzed. Typically three cycles of sound are transmitted as a pulse. The spatial pulse length is the length in space filled by three cycles (Fig. 2.3). Spatial pulse length is one of the determinants of resolution. Since higher frequencies have a smaller pulse

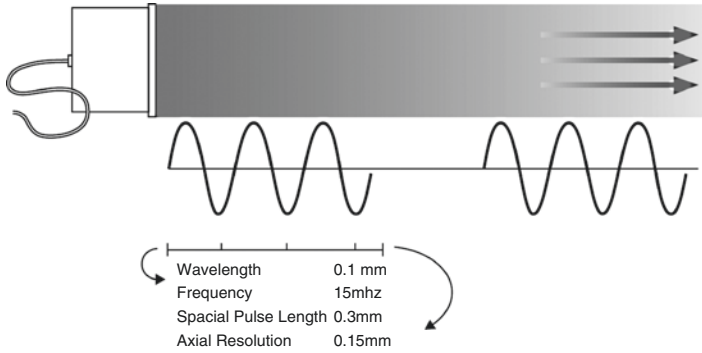

FIGURE. 2.3 Diagnostic ultrasound uses pulsed waves, allowing for an interval of sound transmission, followed by an interval during which reflected sounds are received and analyzed. Typically three cycles of sound are transmitted as a pulse

length, higher frequencies are associated with improved resolution. As illustrated in Fig. 2.3, at a frequency of 15 MHz, the wavelength in biological tissues is approximately 0.1 mm, allowing an axial resolution of 0.15 mm. Although resolution improves with increased frequency, the depth of penetration of the ultrasound waves decreases, limiting the visualization of deeper structures.

As mentioned above, the *speed of sound* is constant for a given material or biological tissue. It is not affected by frequency or wavelength. It increases with stiffness and decreases with density of the material. As seen in Fig. 2.1, common biologic tissues have different propagation velocities. Bone, as a very dense and stiff tissue, has a high propagation velocity of 4080 meters per second (m/s). Fat tissue, with low stiffness and low density, has a relatively low speed of sound of 1450 m/s. Most soft tissues have a speed of sound near 1540 m/s. Muscle, liver, and thyroid have a slightly faster speed of sound. By convention, all ultrasound equipment uses an average speed of 1540 m/s. The distance

to an object displayed on an ultrasound image is calculated by multiplying the speed of sound by half of the time interval for a sound signal to return to the transducer [2, 3]. By using the accepted 1540 m/s as the assumed speed of sound, all ultrasound equipment will provide identical distance or size measurements.

Reflection is the redirection of a portion of a sound wave from the interface of tissues with unequal acoustic impedance. Larger differences in impedance will result in greater amounts of reflection. A material that is homogeneous in acoustic impedance does not generate any internal echoes. A pure cyst is a typical example of an anechoic (echoless) structure. Most biological tissues have varying degrees of inhomogeneity both on a cellular and macroscopic level. Connective tissue, blood vessels, and cellular structure all provide mismatches of acoustic impedance, which lead to the generation of characteristic ultrasonographic patterns (Figs. 2.4, 2.5, and 2.6).

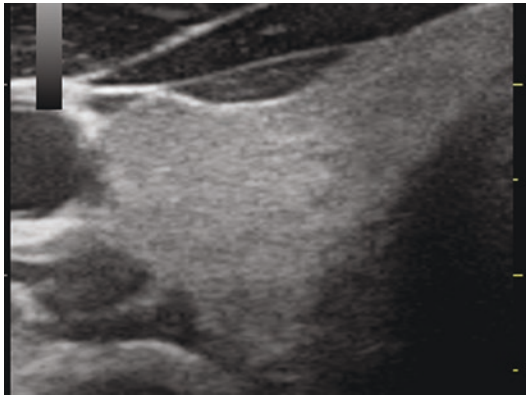

FIGURE. 2.4 The echotexture of normal thyroid tissue. It has a ground glass appearance and is brighter than muscle tissue

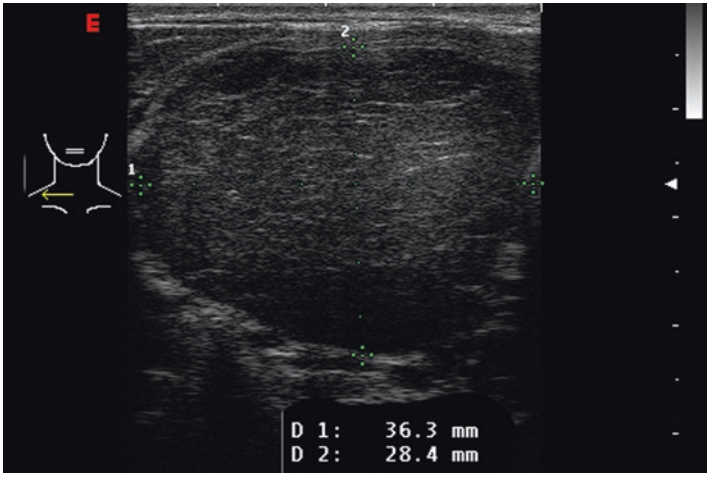

FIGURE. 2.5 The thyroid from a patient with the acutely swollen inflammatory phase of Hashimoto's thyroiditis. Massive infiltration by lymphocytes has decreased the echogenicity of the tissue resulting in a more homogeneous hypoechoic pattern

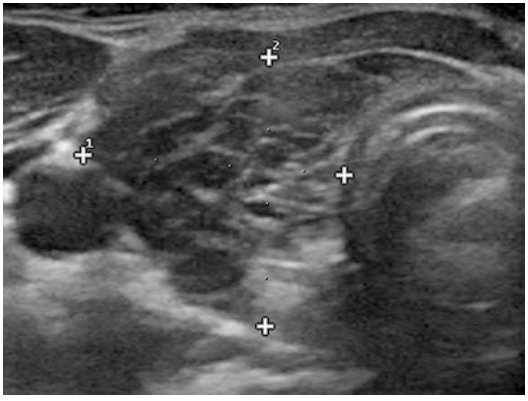

FIGURE. 2.6 A typical heterogeneous and hypoechoic pattern from Hashimoto's thyroiditis with hypoechoic inflammatory regions separated by hyperechoic fibrous tissue

Creation of an Ultrasound Image

The earliest ultrasound imaging consisted of a sound transmitted into the body, with the reflected sound waves displayed on an oscilloscope. Referred to as A-mode ultrasound, these images in the 1960s and 1970s were capable of providing measurements of internal structures such as thyroid lobes, nodules, and cysts. Figure 2.7a shows an A-mode ultrasound image of a solid thyroid nodule. Scattered echoes are present from throughout the nodule. Figure 2.7b shows an image from a cystic nodule. The initial reflection is from the proximal wall of the cyst, with no significant signal reflected by the cyst fluid. The second reflection originates from the posterior wall. Figure 2.7c shows the A-mode image from a complex nodule with solid and cystic components. A-mode ultrasound was capable of providing size measurements in one dimension but did not provide a visual image of the structure [1].

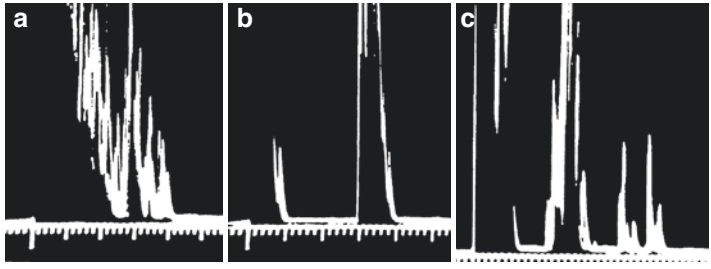

FIGURE. 2.7 A-mode ultrasound images. (**a**) An A-mode ultrasound image of a solid thyroid nodule. Scattered echoes are present from throughout the nodule. (**b**) The image from a cystic nodule. The initial reflection is from the proximal wall of the cyst, with no significant signal reflected by the cyst fluid. The second reflection originates from the posterior wall. (**c**) The A-mode image from a complex nodule with solid and cystic components

In order to provide a visual two-dimensional image, a series of one-dimensional A-mode images are aligned as a transducer is swept across the structure being imaged. Early thyroid ultrasound images were created by slowly moving a transducer across the neck. By scanning over a structure and aligning the A-mode images, a two-dimensional image is formed. The two-dimensional image formed in this manner is referred to as a B-Mode scan (brightness mode) (Fig. 2.8). Most ultrasound transducers used for thyroid imaging use a series of piezo-electric crystals in a linear array to electronically simulate a sweep of the transducer. Firing sequentially, each crystal sends a pulse of sound wave into the tissue and receives subsequent reflections.

The final ultrasound image shows a cross sectional image through the tissue defined by the thin flat beam of sound emitted from the transducer. Resolution is the ability to distinguish between two separate, adjacent objects. For example, with a resolution of 0.2 mm, two adjacent objects measuring <0.2 mm would be shown as a single object. Objects smaller

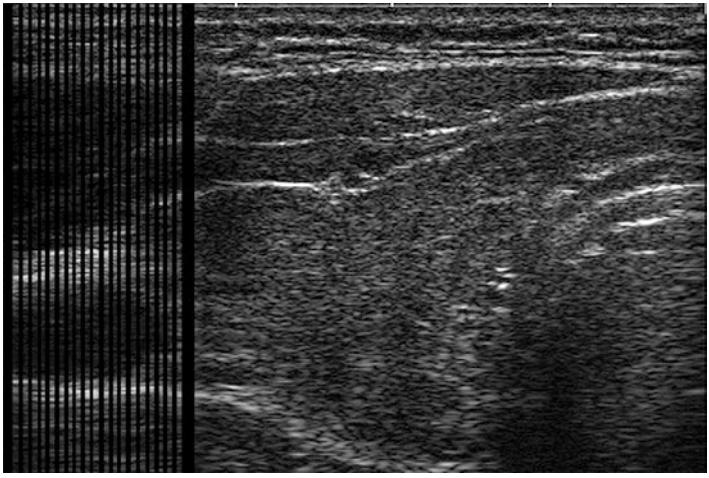

FIGURE. 2.8 A B-mode ultrasound image is composed of a series of A-mode images aligned to provide a two-dimensional image

than the resolution will not be realistically imaged. Lateral resolution refers to the ability to discriminate in a transverse, or side to side, direction. Azimuthal resolution refers to the image perpendicular to the axis of the ultrasound beam; this is inherent to the transducer and cannot be adjusted. Axial resolution is the ability to discriminate objects along the path of the ultrasound beam. Axial resolution is determined by the spatial pulse length and therefore frequency. Lateral and azimuthal resolutions are dependent on the quality and focusing of the ultrasound beam.

The Usefulness of Artifacts in Ultrasound Imaging

A number of artifacts commonly occur in ultrasound images. Unlike most other imaging techniques, such as CT scanning, artifacts are very helpful in interpreting ultrasound images. Artifacts such as shadows behind objects or unexpected areas of brightness can provide additional understanding of the properties of the materials being imaged.

When sound waves impact on an area of extreme mismatch of acoustic impedance, such as a tissue-air interface or a calcification within soft tissue, the vast majority of the sound waves are reflected, providing a very bright signal from the object's surface and an absence of imaging beyond the structure. Figure 2.9 demonstrates *acoustic shadowing* behind a calcified nodule. Figure 2.10 illustrates a coarse calcification within the thyroid parenchyma with acoustic shadowing behind the calcification. Figure 2.11 shows the typical appearance of the trachea on an ultrasound image. Because there is virtually no transmission of sound through the air-tissue interface of the anterior wall of the trachea, no imaging of structures posterior to the trachea occurs. As explained below the reflections seen behind the trachea represent reverberation artifact.

Conversely, a cystic structure transmits sound with very little attenuation, resulting in a greater intensity of sound waves behind it, compared to adjacent structures. This

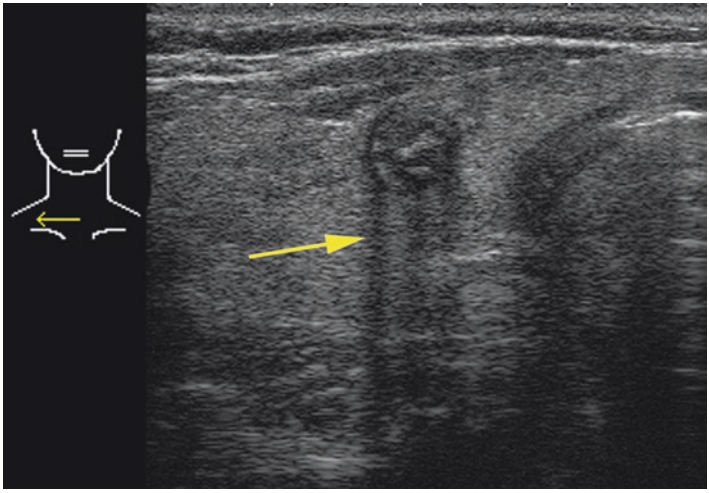

FIGURE. 2.9 Acoustic shadowing. When sound waves impact on an area of extreme mismatch of acoustic impedance, such as a calcification, the vast majority of the sound waves are reflected, resulting in the shadow beyond the structure. This calcified nodule is from a patient with familial papillary carcinoma

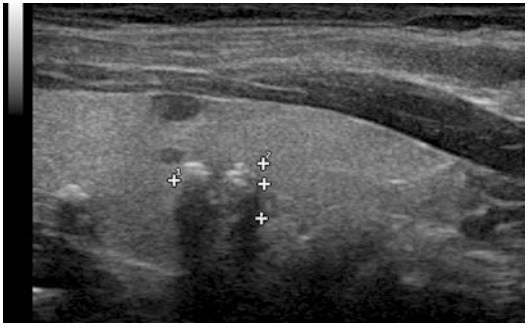

FIGURE. 2.10 Acoustic shadowing. A shadow is observed behind a coarse calcification within the thyroid parenchyma. Unlike calcification within a nodule, amorphic calcification within the parenchyma is not typically associated with malignancy

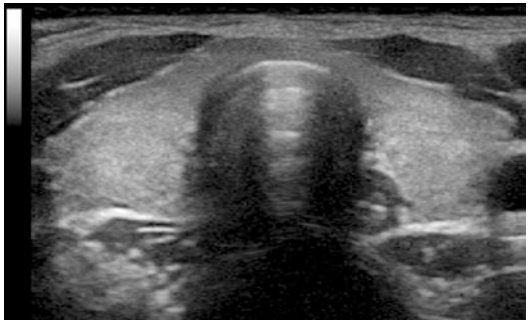

FIGURE. 2.11 Acoustic shadowing. Due to the extreme reflection from the tissue-air interface of the trachea, no image is seen behind the trachea on an anterior ultrasound

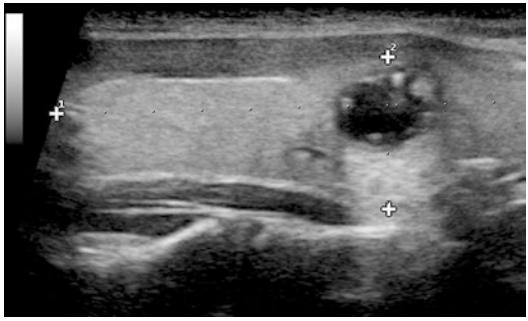

FIGURE. 2.12 Enhancement. A cystic structure transmits sound with very little attenuation, resulting in a greater intensity of sound waves behind it. Enhancement is typical behind a cystic nodule

"through transmission" results in acoustic *enhancement* with a brighter signal behind a cystic or anechoic structure. This enhancement can be used to distinguish between a cystic and solid nodule within the thyroid. Figure 2.12 illustrates enhancement behind a cystic nodule. Enhancement is not limited to cystic nodules, however. Any structure that causes minimal attenuation of the ultrasound signal will have

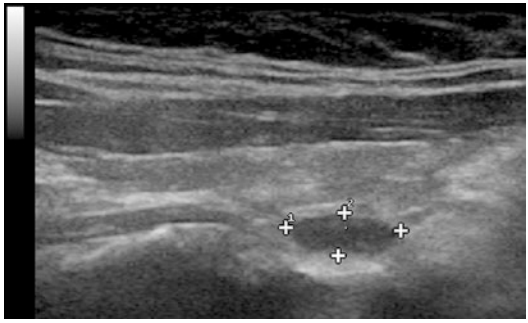

FIGURE. 2.13 Enhancement. Parathyroid adenomas have relatively homogeneous tissue and, like a parathyroid cyst, may demonstrate enhancement behind them

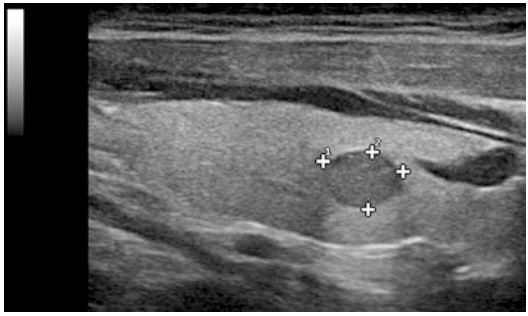

FIGURE. 2.14 Enhancement. This benign colloid nodule has a high content of fluid and colloid with a result in decrease in cellularity. The decreased attenuation of signal within the nodule results in enhancement despite it being a solid nodule

enhancement posterior to it. Figure 2.13 illustrates enhancement behind a solid parathyroid adenoma. Figure 2.14 illustrates enhancement behind a benign colloid nodule. Due to the high content of fluid and colloid within the nodule, and resultant decrease in cellularity, there is less attenuation of signal within the nodule than within the surrounding thyroid

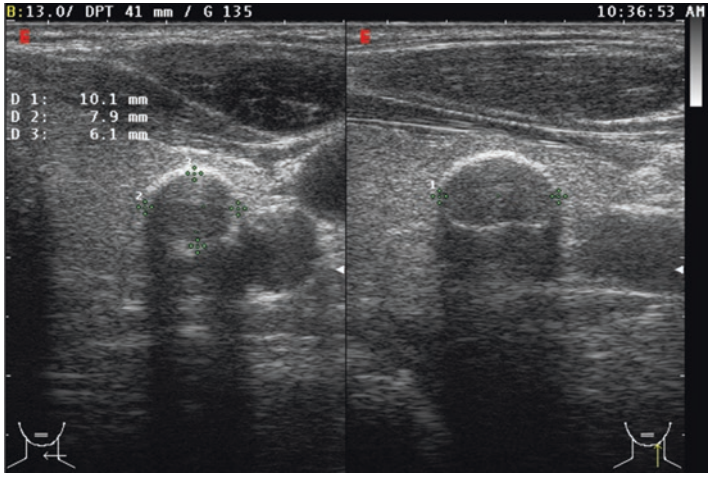

FIGURE. 2.15 Eggshell calcification. A layer of calcium surrounding the nodule results in reflection from the surface, along with marked posterior acoustic shadowing

tissue. To establish that a structure is cystic, use Doppler (as described in Chap. 3) to confirm there is no internal flow as would be seen in a vascular solid nodule with which posterior enhancement can also be seen.

Figure 2.15 shows a nodule exhibiting "eggshell" calcification. A thin layer of calcium surrounding the nodule results in an absence of reflected signal behind the nodule. As can be seen in the figure, reflection is greatest from the surfaces perpendicular to the sound waves: the front and back walls. Because the angle of incidence approaches 180° along the side walls, most of the reflected waves are reflected away from the transducer, resulting in a decreased signal corresponding to the sides of the structure.

Edge artifacts are extremely useful in identifying nodules in the thyroid. Figure 2.16 shows dark lines extending posteriorly from the sides of a nodule, aligned with the ultrasound beam. This is also an example of a reflection artifact. As

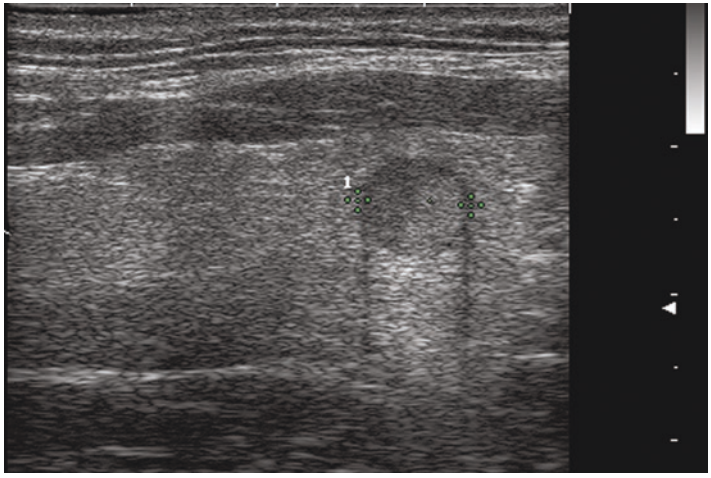

FIGURE. 2.16 Edge artifact. *Dark lines* are seen extending posteriorly from the sides of a nodule. This artifact can be used to help identify a nodule or other structure

described above, the sound waves striking the object tangentially along the sides are reflected away, rather than back toward the transducer. When two parallel dark lines are seen aligned vertically in an image, they can be followed "up" on the display to help identify a nodule or other structure.

Several artifacts arise due to reverberation. When sound waves reflect off of a very reflective surface, some may be re-reflected from the skin surface producing multiple phantom images beyond the actual image. Figure 2.17 illustrates the very common *reverberation artifact* that occurs due to this reverberation of sound waves between the skin surface and deeper tissue interfaces. Since some of the reflected sound waves will bounce back from the skin surface into the tissue multiple times, phantom images are produced. As shown, it is very common to see this artifact in the anterior aspect of cysts, raising doubt as to whether the lesion is a true cyst or partly solid. Changing the angle at which the sound strikes the lesion will usually clarify the situation. Figure 2.18 shows this common artifact behind the anterior wall of the trachea.

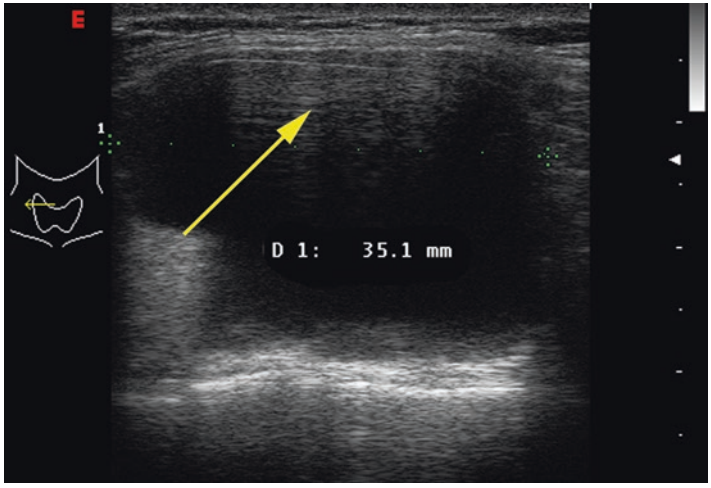

FIGURE. 2.17 Reverberation artifact. It is very common to see this artifact in the anterior aspect of cysts. This arises due to reverberation of signal between the skin surface and the anterior wall of the cyst, resulting in the late signals being received and giving the appearance of solid tissue in the anterior aspect of the cyst

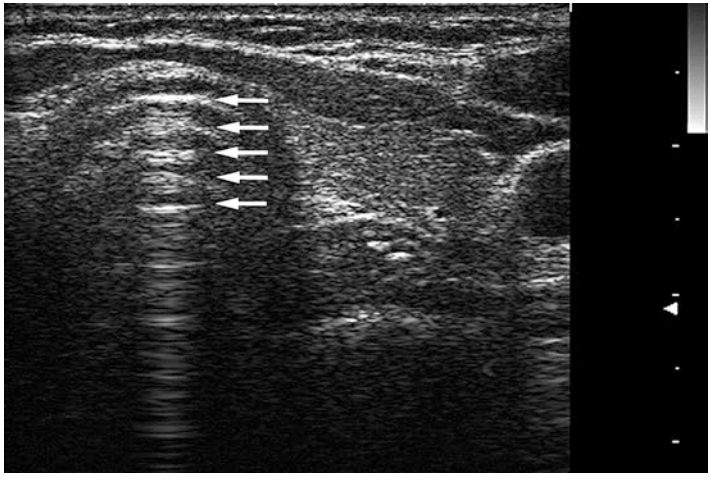

FIGURE. 2.18 Reverberation artifact. Numerous *parallel lines* are seen posterior to the anterior wall of the trachea. These may be misconstrued as tracheal rings but are actually reverberation artifact

The "comet tail" artifact is another extremely common finding arising due to reverberation [4] (Figs. 2.19, 2.20, 2.21, 2.22, and 2.23). Colloid nodules may contain tiny crys-

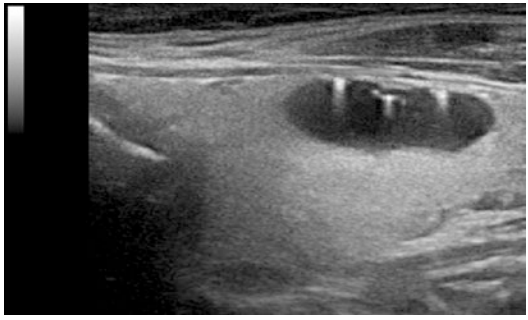

FIGURE. 2.19 "Comet tails." Colloid nodules and cysts may contain tiny crystals resulting from the desiccation of the gelatinous colloid material. Reflection of the sound waves off of the crystal results in a bright spot. However, in contrast to a soft tissue calcification, the crystals begin to vibrate under the influence of the ultrasound energy. The vibration generates sound waves, which return to the transducer after the initial reflected signal, resulting in the "tail"

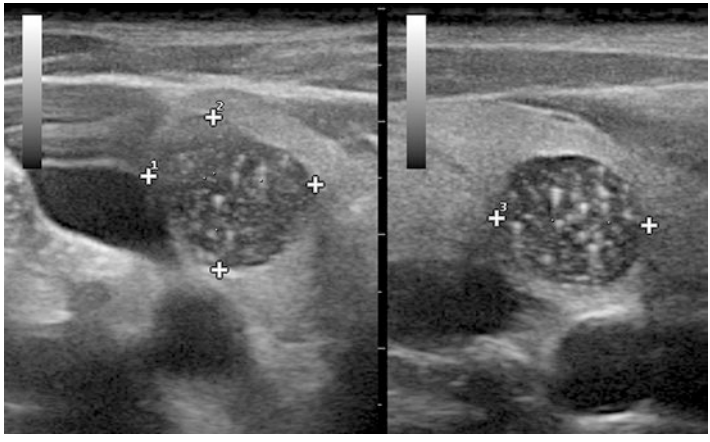

FIGURE. 2.20 "Comet tails." Another example of comet tail artifacts within a benign spongiform nodule

tals resulting from the desiccation of the gelatinous colloid material (colloid bodies). Reflection of the sound waves off of the crystal results in a bright spot. However, in contrast to a soft tissue calcification, the suspended crystals begin to vibrate under the influence of the ultrasound energy. The vibration generates sound waves, which return to the transducer after the initial reflected signal. Also referred to as a *ring-down artifact* or *stepladder artifact*, these "comet tails" help differentiate between the typically benign densities found in a colloid nodule and highly suspicious microcalcifications. When a single comet tail is present in a small colloid cyst, it is referred to as a "cat's eye" (Fig. 2.21). While comet tail artifacts most commonly arise within a benign colloid nodule, they may also be seen in resolving hematomas and have rarely been described within papillary carcinoma [5].

At times differentiating a comet tail density from a microcalcification may be challenging, resulting in different opinions regarding how reassuring it is to observe comet tail densities within a nodule. Tahvildari et al. assessed the characteristics of punctate echogenic reflectors in papillary carcinoma and elucidated "microcalcifications" as arising from a variety of etiologies including psammomatous calcifications, dystrophic calcifications, and eosinophilic colloid. Thus the

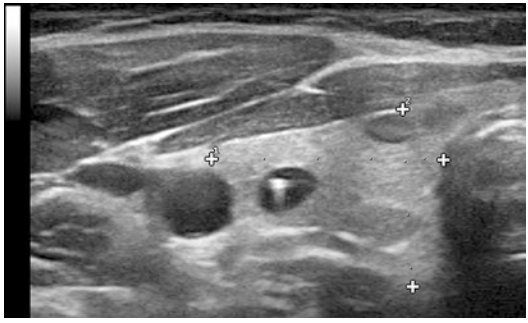

FIGURE. 2.21 "Cat's eye" artifact. The comet tail artifact is also referred to as a ring-down artifact, a stepladder artifact, or, when a single comet tail is seen within a small colloid cyst, a cat's eye

terms “punctate echogenic foci” or microreflectors may be more accurate terms [6]. Beland et al. suggested that non-shadowing brightly echogenic linear foci with or without a comet tail artifact may be a benign finding [5]. On the other hand, Malhi et al. concluded that all categories of echogenic foci, except those with large comet tail artifacts, are associated with cancer risk [7]. It helps in the distinction between comet tails and microcalcifications to note that comet tails typically are located either within or on the edge of a cyst, whereas microcalcifications occur within solid tissue.

Figure 2.22 illustrates a large comet tail artifact, exceeding one mm in size, in a clearly benign colloid cyst. Figure 2.23 demonstrates multiple tiny punctate echogenic reflectors in a benign hyperplastic colloid nodule. Some, but not all, have a small comet tail artifact associated. Those reflectors not showing a clear comet tail may be posterior acoustic enhancement behind the microcystic areas. In contrast, Fig. 2.24 shows typical microcalcifications within a papillary carcinoma. Visualization of these various echogenic foci is best appreciated in real-time imaging and can be enhanced by imaging at lower frequencies.

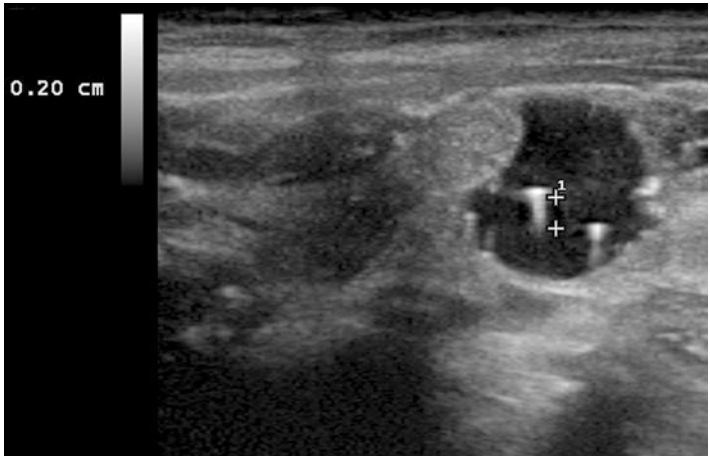

Figure. 2.22 A large comet tail artifact, exceeding 1 mm in size, in a benign colloid cyst

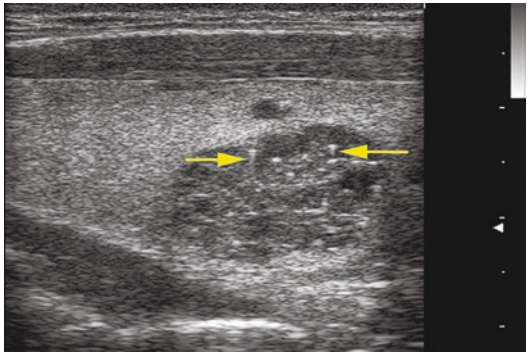

FIGURE. 2.23 Multiple comet tails and punctate echogenic foci or microreflectors within a benign spongiform nodule. Some, without tails could be mistaken for microcalcifications. Note the association with the numerous microcystic areas, behind which posterior acoustic enhancement is seen

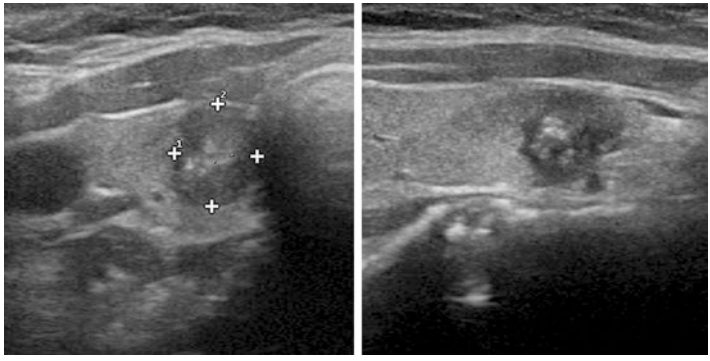

FIGURE. 2.24 Microcalcifications. Compare to the punctate echogenic foci shown in Figs. 2.20 and 2.23. Microcalcifications are typically found in solid nodules, while comet tails are seen associated with cystic or microcystic areas

Refraction is the alteration of direction of the transmitted sound at an acoustic interface when the angle of incidence is not 90°. A portion of a sound wave striking an interface at 90° is transmitted straight through. When waves strike at an angle

other than 90°, the transmitted wave is bent as it propagates through the interface. A greater degree of mismatch of acoustic impedance between tissues results in a greater degree of refraction. While not typically seen in near field ultrasound used in thyroid and other small parts imaging, refraction artifacts can result in a second "ghost" image when a refracting object exists in the path of an ultrasound beam.

As sound waves propagate through any tissue, the intensity of the wave is *attenuated*. Attenuation of acoustic energy results from a combination of reflection, scattering, and absorption, with conversion of sound energy to heat. Attenuation is frequency dependent, with higher frequencies having greater attenuation. As a result, while higher frequencies provide improved resolution, the depth of imaging decreases with increasing frequency. Current ultrasound technology utilizes sound waves as high as 18 MHz for thyroid imaging. However, imaging is limited to less than 5 cm of depth at this frequency. Visualization of deeper structures, as with abdominal or pelvic ultrasound, requires lower frequencies. In obese patients or when imaging very deep structures, frequencies of 5–7.5 MHz may be needed for adequate penetration and visualization of the deep neck structures. Figures 2.25 and 2.26 compare images made at 7.5 and 15 MHz. Loss of detail of proximal structures with improved imaging of deeper structures is evident with the lower frequency.

Shadowing and enhancement, as described above, are examples of attenuation artifacts. Shadowing occurs behind structures with extreme acoustic mismatch due to the attenuation of transmission of sound waves caused by nearly complete reflection. Enhancement occurs behind structures with little to no attenuation, with higher intensity sound waves present behind the structure in comparison to the adjacent tissues.

Advances in Ultrasound Imaging

Ultrasound transducers consist of an array of crystals capable of transmitting and receiving ultrasound energy. Piezoelectric crystals vibrate when exposed to an electrical

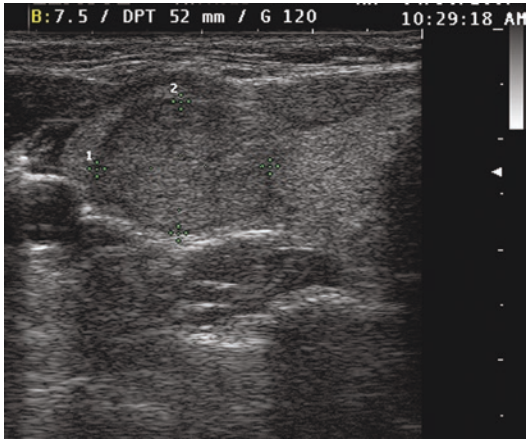

FIGURE. 2.25 Comparison of images produced with frequencies of 7.5 and 13 MHz. In this image utilizing 7.5 MHz, the nodule is less well defined, but the posterior structures are better visualized. Compare to Fig. 2.23

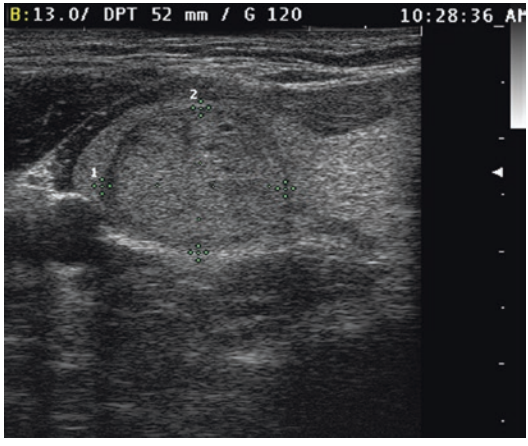

FIGURE. 2.26 Comparison of images produced with frequencies of 7.5 and 13 MHz. In this image, utilizing 13 MHz the nodule show much better definition. Compare to Fig. 2.22

current. Conversely, when energy strikes the crystal, it results in an electrical signal, with a frequency corresponding to the frequency of the incident sound wave. Thyroid ultrasound typically uses a linear array of several hundred crystals within a transducer. The transverse width of the image produced is equal to the length of the array of crystals in the transducer (often referred to as the "footprint"). Curved array (convex) transducers are less often used in thyroid ultrasound (but are commonly used in abdominal, pelvic, and cardiac imaging). By producing a divergent beam of ultrasound they allow visualization of structures larger than the transducer. Microconvex transducers are occasionally used as an aid in fine-needle aspiration biopsy, but the image produced has spatial distortion due to the lack of a linear relationship between the transverse and longitudinal planes (see Chap. 12).

Once received, the ultrasound signal undergoes image reconstruction, followed by image enhancement. Noise reduction and edge sharpening algorithms are used to clarify the image. Most ultrasound equipment allows the user to select the degree of noise reduction, dynamic range, and edge sharpening, to optimize image quality. Ultrasound equipment allows for user adjustment of the gain of the received signal. Overall gain can be adjusted, and separate channels corresponding to individual depths may be adjusted (time gain compensation) to provide the best image quality at the region of interest. Most ultrasound equipment also allows for user adjustment of the focal zone, the depth at which the ultrasound beam is optimally focused in order to improve lateral resolution. Multiple focal zones may also be selected on most ultrasound equipment. While providing an increase in the area of optimal image sharpness, the use of multiple focal zones typically slows the refresh rate of the image, resulting in a more jumpy image when visualized during real-time scanning.

While standard ultrasound receives only the frequency identical to that transmitted for imaging, tissue harmonic imaging capitalizes on the tendency of tissues to reverberate when exposed to higher power ultrasound energy. Different

tissues have a different degree of reverberation and produce unique signatures of tissue harmonics (multiples of the original frequency). Selective detection and processing of the harmonic signal produces an alternative image. Because higher frequencies are being detected, the resolution may be improved, but the original transmitted frequency is typically lower when using tissue harmonic imaging. Since the distance traveled by a harmonically generated signal is one half that of the transmitted and received signal, there is less noise. The increased resolution and decreased noise may result in increased conspicuity of some objects [8], but tissue harmonic imaging has not had widespread application in thyroid imaging.

Recently ultrasound image quality has benefitted by transition to complete digital processing. In conventional ultrasound a linear transducer transmits and receives parallel ultrasonographic waves in a single direction. With compound spatial imaging, the ultrasound beam is electronically or mechanically steered into multiple angles. Compound spatial imaging combines multiple images obtained from different angles and reconstructs them into a single image [9]. This results in much less speckle and noise and a much more realistic appearing image (Figs. 2.27 and 2.28). Artifacts are

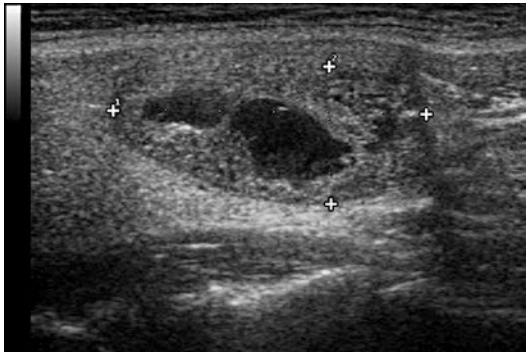

FIGURE. 2.27 A conventional ultrasound image without spatial compound imaging shows speckle artifact and more noise than the processed image shown in Fig. 2.25

reduced, but careful selection of the degree of noise reduction applied allows useful artifacts such a shadowing, enhancement, and edge artifacts to remain, aiding in interpretation of the image [10] (Figs. 2.29 and 2.30).

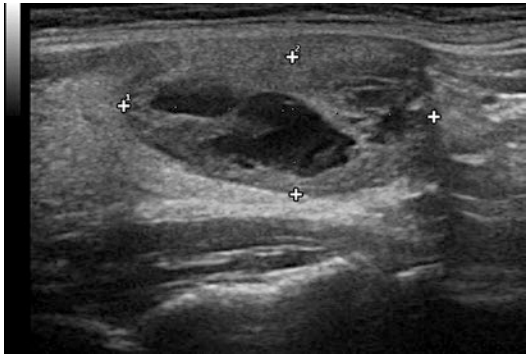

FIGURE. 2.28 After application of spatial compound imaging, there is a reduction of speckle artifact, less noise, and overall improved image quality

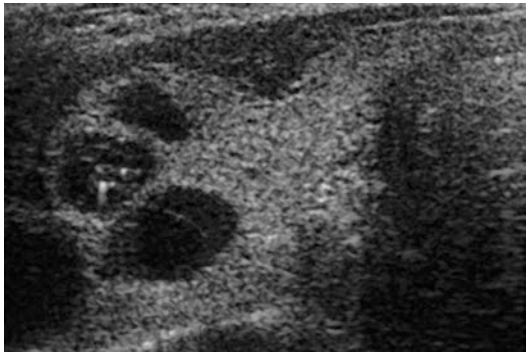

FIGURE. 2.29 A comet tail artifact and posterior acoustic enhancement are present prior to application of spatial compound imaging

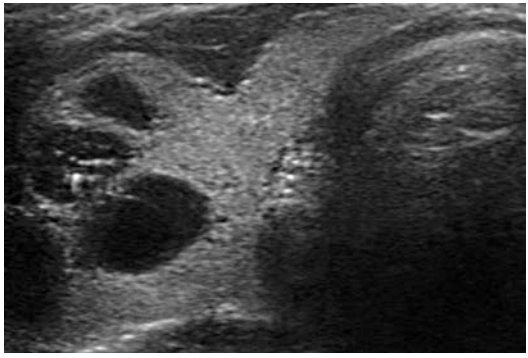

FIGURE. 2.30 The comet tail artifact and posterior enhancement remain visible with compound spatial imaging despite the reduction of speckle and noise artifact

Quantifying Ultrasound Information

Rather than just describing a thyroid nodule as "hypoechoic and heterogeneous," it would be preferable to describe the degree of hypoechogenicity and heterogeneity. In an effort to quantify the ultrasonographic characteristics typically used to predict malignancy, several investigators have applied mathematical analysis of the ultrasound data. Kim et al. [11] performed histogram analysis of grayscale ultrasound images and demonstrated the ability to differentiate lymphocytic thyroiditis from normal thyroid tissue. As discussed in Chap. 6, hypoechogenicity and heterogeneity are typical characteristics of thyroiditis. Histogram analysis allows for quantitation of the degree of hypoechogenicity and heterogeneity, as well as the skew and kurtosis (flatness or pointiness around the peak), providing an objective and reproducible mathematical analysis of the image. It is likely that similar assessment will be performed on thyroid nodules to assess the degree of degree of hypoechogenicity and characteristics of heterogeneity, with possible application to prediction of malignant potential. Several additional studies have begun

preliminary investigation of quantifying ultrasound characteristics of nodules. Song et al. analyzed 16 texture-based gray-level co-occurrence matrix features, providing objective quantified data with the ability to help in the prediction of malignancy of thyroid nodules [12]. Similarly, Ardakani et al. utilized wavelet texture analysis to provide a quantification of the texture of thyroid nodules, also demonstrating utility in differentiating benign from malignant nodules [13]. It is likely that in the future, mathematical quantitative analysis of ultrasound images will lead to more reproducible quantified information regarding nodules with increased power to recognize malignant features and to identify more aggressive lesions.

Summary

In summary, ultrasound waves differ from electromechanical waves in that sound transmission is dependent on the conducting medium. Acoustic energy is reflected at interfaces of mismatch of acoustic impedance, and analysis of the reflected ultrasound waves allows construction of an image. The resolution of an ultrasound image is dependent on the frequency, the focused beam width, and the quality of the electronic processing. Resolution improves with higher frequencies, but the depth of imaging decreases. Image artifacts such as shadowing and enhancement provide useful information, rather than just interfering with creation of a clear image. The current image quality, affordable cost, and ease of performance make real-time ultrasound an integral part of the clinical evaluation of the thyroid patient.

References

1. Meritt CRB. Physics of ultrasound. In: Rumack CM, Wilson SR, Charboneau JW, Levine D, editors. Diagnostic ultrasound. 4th ed. St. Louis: Mosby; 2011. p. 2–33.
2. Levine RA. Something old and something new: a brief history of thyroid ultrasound technology. Endocr Pract. 2004;10(3):227–33.

3. Coltrera MD. Ultrasound physics in a nutshell. Otolaryngol Clin N Am. 2010;43(6):1149–59.
4. Ahuja A, Chick W, King W, Metreweli C. Clinical significance of the comet-tail artifact in thyroid ultrasound. J Clin Ultrasound. 1996;24(3):129–33.
5. Beland MD, Kwon L, Delellis RA, Cronan JJ, Grant EG. Non-shadowing echogenic foci in thyroid nodules: are certain appearances enough to avoid thyroid biopsy? J Ultrasound Med. 2011;30(6):753–60.
6. Tahvildari AM, Pan M, Kong CS, Desser T. Sonographic pathologic correlation for punctate echogenic reflectors in papillary thyroid carcinoma. What are they? J Ultrasound Med. 2016;35(8):1645–52.
7. Malhi H, Beland MD, Cen SY, Allgood E, et al. Echogenic foci in thyroid nodules: significance of posterior acoustic artifacts. Am J Roentgenol. 2014;203(6):1310–6.
8. Szopinski KT, Wysocki M, Pajk AM, et al. Tissue harmonic imaging of thyroid nodules: initial experience. J Ultrasound Med. 2003;22(1):5–12.
9. Lin DC, Nazarian L, O'Kane PL, et al. Advantages of real-time spatial compound sonography of the musculoskeletal system versus conventional sonography. Am J Roentgenol. 2002;179(6):1629–31.
10. Shapiro RS, Simpson WL, Rauch DL, Yeh HC. Compound spatial sonography of the thyroid gland: evaluation of freedom from artifacts and of nodule conspicuity. Am J Roentgenol. 2001;177:1195–8.
11. Kim GR, Kim EK, Kim SJ, Ha EJ, et al. Evaluation of underlying lymphocytic thyroiditis with histogram analysis using grayscale ultrasound images. J Ultrasound Med. 2016;35(3):519–26.
12. Song G, Xue F, Zhang CA. Model using texture features to differentiate the nature of thyroid nodules on sonography. J Ultrasound Med. 2015;34(10):1753–60.
13. Ardakani AA, Gharbali A, Mohammadi A. Classification of benign and malignant thyroid nodules using wavelet texture analysis of sonograms. J Ultrasound Med. 2015;34(11):1983–9.

Chapter 3
Doppler Ultrasound

Robert A. Levine

Abbreviations

AACE	American Association of Clinical Endocrinologists
AME	Associazione Medici Endocrinologi
ATA	American Thyroid Association
GD	Graves' disease
PI	Pulsatility index
PPV	Positive predictive value
PRF	Pulse repetition frequency
PSV	Peak systolic velocity
RAIU	Radioactive iodine uptake
RI	Resistive index
RR	Relative risk
TBFA	Thyroid blood flow area

R.A. Levine, MD, FACE, ECNU
Geisel School of Medicine at Dartmouth College, Thyroid Center of New Hampshire, St. Joseph Hospital, Nashua, NH, USA
e-mail: thyroidmd2@gmail.com

D.S. Duick et al. (eds.), *Thyroid and Parathyroid Ultrasound and Ultrasound-Guided FNA*,
https://doi.org/10.1007/978-3-319-67238-0_3

Doppler Physics

The Doppler shift is a change in frequency that occurs when sound (or light) is emitted from, or bounced off of, a moving object. When a moving target reflects a sound, the frequency of the reflected sound wave is altered. The frequency is shifted up by an approaching target and shifted down by a receding target. This is illustrated in Fig. 3.1. The amount of frequency shift is proportional to the velocity of the moving object. Because the Doppler shift was originally described for energy in the visible light spectrum, an upward Doppler shift is referred to as a blue shift (a shift to a higher visible light frequency) and a downward Doppler shift is referred to as a red shift.

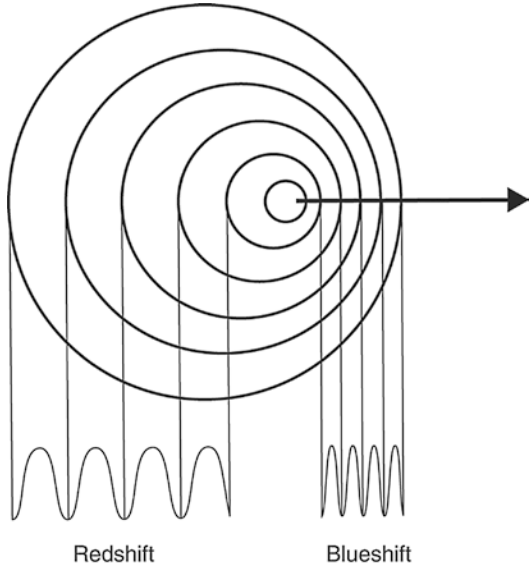

FIGURE. 3.1 Illustration of the Doppler shift. When a moving target reflects a sound, the frequency of the reflected sound wave is altered. The frequency is shifted up by an approaching target and shifted down by a receding target. The amount the frequency is shifted is proportional to the velocity of the moving object

Ultrasound utilization of the Doppler shift falls into three main categories. Analysis of the Doppler frequency spectrum allows for calculation of velocity, pulsatility index, and resistive index and is primarily used in vascular studies. Color-flow Doppler and power Doppler superimpose a color image representing motion onto a B-mode image to illustrate location and degree of motion (blood flow).

In thyroid applications, Doppler imaging is used predominantly to assess the vascularity of tissues. The role of Doppler ultrasound in thyroid imaging has recently experienced a significant change. The prior belief that power Doppler imaging plays an important role in the prediction of the likelihood of malignancy in a thyroid nodule has undergone a reassessment and will be discussed in detail. Other applications of Doppler imaging include helping to determine the etiology of hyperthyroidism, assessing the etiology or subtype of amiodarone-induced thyrotoxicosis or thyroiditis, and clarifying images.

Analysis of the Doppler spectrum allows for determination of flow velocity and calculation of resistance to flow. By analyzing the waveform, the peak systolic and diastolic velocities can be calculated. Resistive index (RI) and pulsatility index (PI) can be calculated using the formulas below but are typically calculated directly by the ultrasound machine. While these values are more often used in studies of peripheral vascular disease, the peak flow velocity and resistive index are also used to provide a reproducible quantification in reporting the degree of vascularity of thyroid tissue.

Resistive Index = (systolic velocity − diastolic velocity)/systolic velocity
Pulsatility Index = (systolic velocity − diastolic velocity)/mean velocity

For most thyroid imaging, color-flow Doppler and power Doppler are utilized. In color-flow Doppler, a unique color (or brightness) is assigned to an individual frequency. Typically a greater frequency shift (corresponding to a higher velocity) is assigned a brighter color. Analysis of the color-flow image

gives a graphic illustration of the direction and speed of blood flow within soft tissue. In contrast, power Doppler considers all frequency shifts to be equivalent, integrating the total amount of motion detected. The assigned color represents the total amount of flow present, independent of the speed and direction of flow. The color image therefore is indicative of the total amount of flow present, without information regarding velocity (Figs. 3.2 and 3.3).

Color-flow Doppler provides information regarding both direction and speed and is more useful in vascular studies. In contrast, power Doppler does not provide information regarding velocity. However, it provides increased sensitivity for the detection of low degrees of flow, has less noise interference, and is less dependent on the angle of incidence between the ultrasound waves and the moving object. Power Doppler is generally the preferred imaging technique for assessing the vascularity of thyroid tissue [1].

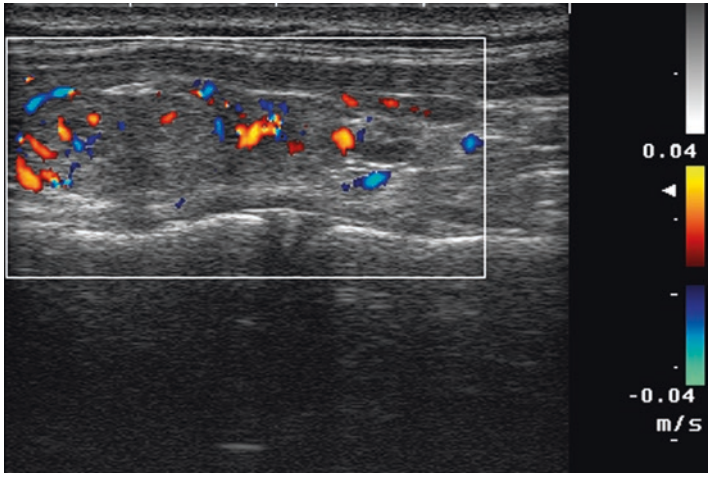

FIGURE. 3.2 Color Doppler. In color-flow Doppler a unique color (or brightness) is assigned to an individual frequency. Typically a greater frequency shift (corresponding to a higher velocity) is assigned a brighter color. Analysis of the color-flow image gives a graphic illustration of the direction and speed of blood flow within soft tissue

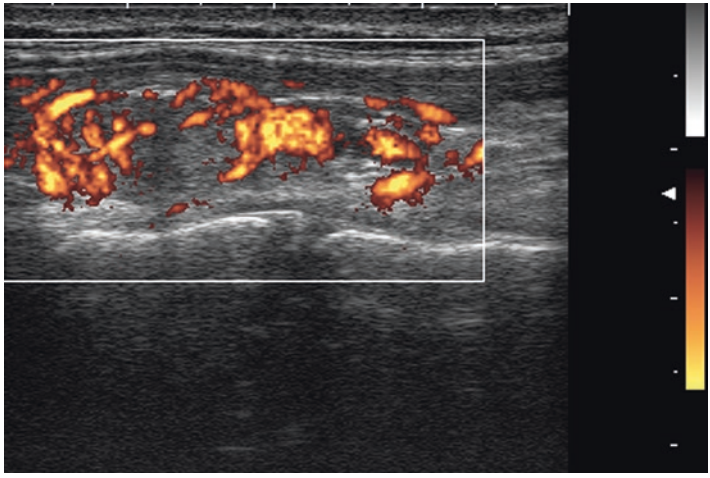

FIGURE. 3.3 Power Doppler. In contrast, power Doppler considers all frequency shifts to be equivalent, integrating the total amount of motion detected. The assigned color represents the total amount of flow present, independent of the velocity. Power Doppler has increased sensitivity for the detection of low degrees of flow, has less noise interference, and is less dependent on the angle of incidence between the ultrasound waves and the moving object

Doppler Analysis of Thyroid Nodules for the Assessment of Probability of Malignancy

Figure 3.4 shows a follicular carcinoma in the inferior pole of the thyroid, with a very high degree of blood flow. The inferior thyroid artery can be seen feeding the nodule. In contrast, Fig. 3.5 shows a nodule with no significant intranodular vascularity, with only scattered blood vessels around the periphery. This nodule was a benign follicular adenoma.

The assessment of whether Doppler plays a role in the determination of malignant potential of a nodule has undergone a major change over the last decade. In 2002 Papini et al. reported on 494 consecutive patients with nonpalpable

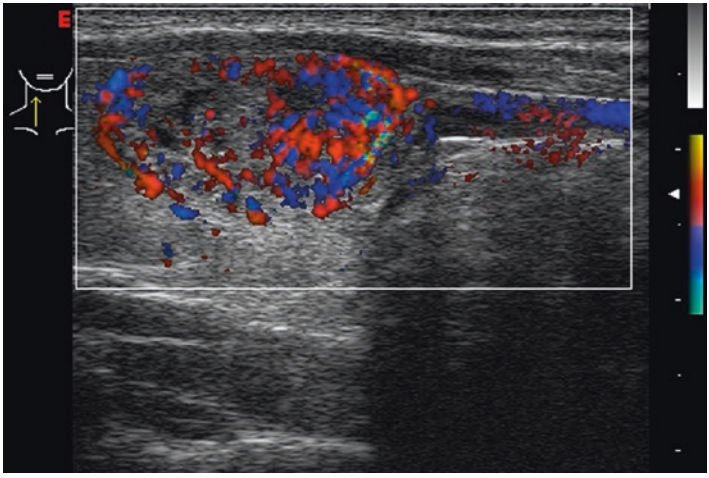

FIGURE. 3.4 Vascular nodule. A follicular carcinoma is present in the inferior pole of the thyroid, with a very high degree of blood flow. The inferior thyroid artery can be seen feeding the nodule

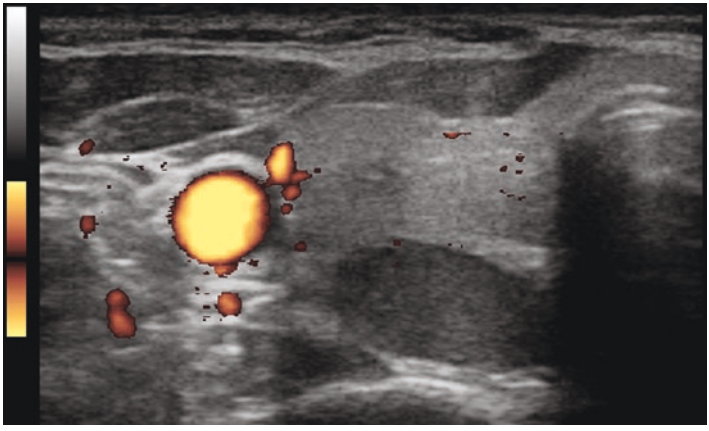

FIGURE. 3.5 Avascular nodule. This benign follicular adenoma has no intranodular blood flow

nodules measuring 8–15 mm. All patients had a Doppler ultrasound study performed prior to fine-needle aspiration biopsy. An intranodular vascular pattern was observed in

74% of all nodules with thyroid cancer. Eighty-seven percent of the cancers were solid and hypoechoic, and 77% of the cancers had irregular or blurred margins. Only 29% of the cancers had microcalcifications. Independent risk factors for malignancy included irregular margins (RR = 16.8), intranodular Doppler blood flow (RR = 14.3), and microcalcifications (RR = 5) [2].

In 2002 Berni et al. analyzed 108 patients with thyroid nodules demonstrated to be hypofunctioning on nuclear medicine study. All of the patients had subsequent surgical excision of the nodule. Half of the patients were found to have malignancy, so this clearly was not a random population. Of the 108 patients, 92 would have been correctly diagnosed based on their color Doppler pattern. There were six false-negative cancers with no blood flow and ten false-positive benign lesions with significant intranodular flow. The calculated sensitivity was 88.8%, and the specificity was 81.5%. The positive predictive value of blood flow was 83%, and the negative predictive value was 88% [3]. The following year Frates et al. demonstrated a 42% rate of malignancy in solid hypervascular nodules, compared to 14% in solid nonhypervascular nodules [4]. In 2006 Appetecchia and Solivetti reported that the addition of Doppler pattern to conventional gray-scale ultrasound modestly improved sensitivity and specificity from 75 and 71.9% to 83.3 and 75.4% [5].

More recently, in 2010 Moon et al. reported a retrospective review of Doppler images of 1083 nodules (with 269 malignancies) in 1024 patients and determined that vascularity was not associated with malignancy [6]. Vascularity was classified as none, peripheral, and intranodular. Vascularity was present in 31% of the benign nodules and only 17% of papillary cancers. Absent vascularity was more common in malignant nodules (60%) than in benign nodules (43%). It is not clear why such disparate results were seen in the Moon study when compared to the earlier studies. It is possible that it relates to a very high number of (small) papillary cancers in the Moon series (>97% classic papillary cancers). Moon suggests that prior studies may have suffered from selection bias, analyzing only hypoechoic, cold nodules, or nodules only >1 cm. In con-

trast, Moon included nodules regardless of size, echogenicity, or results of radioisotope scan [6]. It has been suggested that a pattern of central versus peripheral vascularity may be more predictive of malignancy, but this was not considered in the Moon series [7, 8]. Similarly, in a recent study of over 1500 nodules measuring larger than 1 cm, Rosario et al. found no additional predictive value for adding Doppler ultrasound to gray-scale ultrasound in assessing the benign or malignant nature of thyroid nodules [9].

Several studies have investigated whether quantifying the degree of vascularity using spectral Doppler analysis would help predict the probability of malignancy in thyroid nodules. Bakhshaee et al. concluded that Doppler US parameters of resistive index (RI), pulsatility index (PI), and the vascular pattern of malignant versus benign nodules show significant overlap. He concluded that malignant nodules could not be distinguished reliably from benign nodules on the basis of Doppler US characteristics including RI, PI, or the vascular pattern [10]. Algin et al. measured RI and PI and reported that central, peripheral, and mean resistive and pulsatility index values were significantly higher in malignant nodules according to spectral Doppler measurements. However, the overall predictive values were poor, with substantial overlap of all values [11].

Several studies have attempted to improve the predictive value of Doppler imaging by utilizing ultrasonographic contrast material. Ma et al. reported that contrast-enhanced Doppler images added predictive value to gray-scale parameters but found that color Doppler ultrasound without contrast had no predictive value [12]. Similarly, in a preliminary study, Zhang et al. determined that peripheral ring enhancement was more predictive of benign lesions (PPV 94%), whereas heterogeneous internal enhancement was associated with malignancy (PPV 92.5%) [13]. Both of these studies were relatively small, and further investigations of the value of contrast-enhanced Doppler are warranted. Future studies will need to explore the cost benefit ratio and practicality of contrast administration. In addition, currently ultrasound

contrast agents are not approved for thyroid imaging in the United States.

The prior 2009 ATA and 2010 AACE/AME guidelines for the management of thyroid nodules considered intranodular vascularity to be a risk factor for cancer [14, 15]. However, guidelines published by the Korean Society of Radiology eliminated vascularity as a risk factor, initially in 2011 and again in the revised guidelines published in 2016 [16]. The 2015 American Thyroid Association guidelines no longer integrate nodule vascularity in the assessment of the probability of malignancy in thyroid nodules [17]. The revised AACE/AME guidelines published in 2016 similarly removed vascularity as a risk factor for papillary carcinoma but maintained vascularity as a concerning feature for follicular nodules [18].

Doppler Analysis of Nodules with Follicular Cytology

Doppler ultrasound may play a role in prediction of malignancy in nodules with microfollicular (Bethesda 4) cytology, but this remains controversial [16]. Fukunari et al. studied 310 patients with a solitary thyroid nodule in which a prior fine-needle aspiration biopsy had demonstrated a follicular lesion. All patients underwent a color Doppler flow-mapping study prior to surgery. The amount of flow in the nodule was classified on a four-point scale. Grade 1 nodules had no flow detectable. Grade 2 nodules had only peripheral flow, without intranodular flow. Grade 3 nodules had low-velocity central flow, and grade 4 nodules had high-intensity central flow (Figs. 3.6, 3.7, 3.8, 3.9, and 3.10). For purposes of statistical analysis, the absence of intranodular flow (grade 1–2) was considered a negative result, and the presence of central flow (grade 3–4) was considered a positive result. Of 177 benign adenomatous nodules, 95% were grade 1 or 2, and only 5% were grade 3. No benign adenomatous nodules had grade 4 blood flow. Of 89 benign follicular adenomas, 66% showed

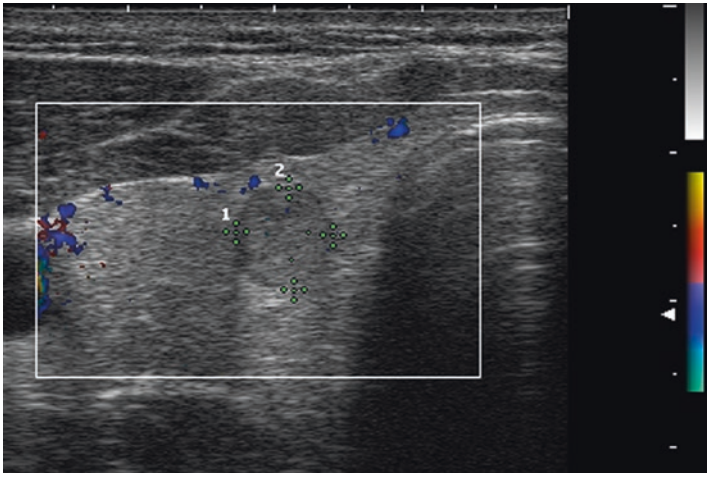

FIGURE. 3.6 Grade 1 Doppler flow. Grade 1 lesions have no intranodular flow and no flow to the periphery

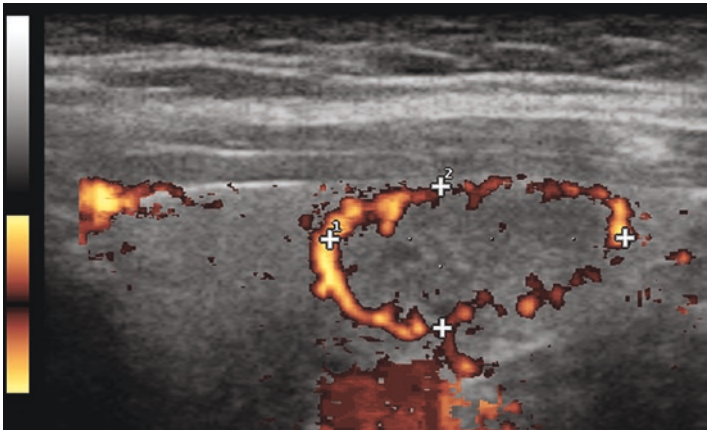

FIGURE. 3.7 Grade 2 Doppler flow. Grade 2 lesions have peripheral flow only, without intranodular flow

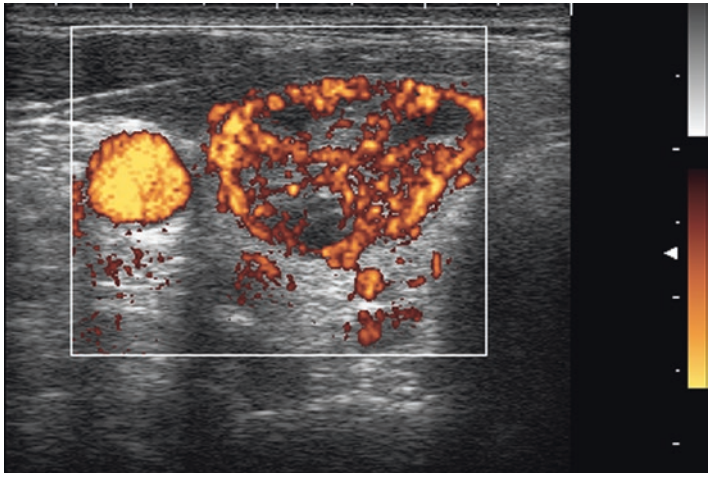

FIGURE. 3.8 Grade 3 Doppler flow. Great 3 lesions have low to moderate velocity central flow. The pattern illustrated here, with peripheral vascularity greater than central, is often felt to be of lower suspicion for malignancy

grade 1 or 2 Doppler flow, and 34% showed grade 3 or 4 flow. Of the 44 follicular carcinomas diagnosed, none showed grade 1 Doppler flow, 13.6% showed grade 2 flow, and 86.4% showed either grade 3 or 4 flow [19].

Using the data of Fukunari, the sensitivity of intranodular blood flow in predicting malignancy in a microfollicular nodule was 86%. The specificity was 85%, and the diagnostic accuracy was 81%. The prevalence of cancer in this group of follicular nodules was 14% [19].

In a similar analysis, De Nicola et al. studied 86 patients in whom nodules had prior follicular biopsies. The flow pattern was characterized on a scale from 0 to 4, with 0 defined as no visible flow, 1 as peripheral flow only, 2 as peripheral flow with a small amount of central flow, 3 as peripheral flow plus extensive intranodular flow, and 4 as central flow only. Patterns 0–2 were grouped as negative results, and nodules

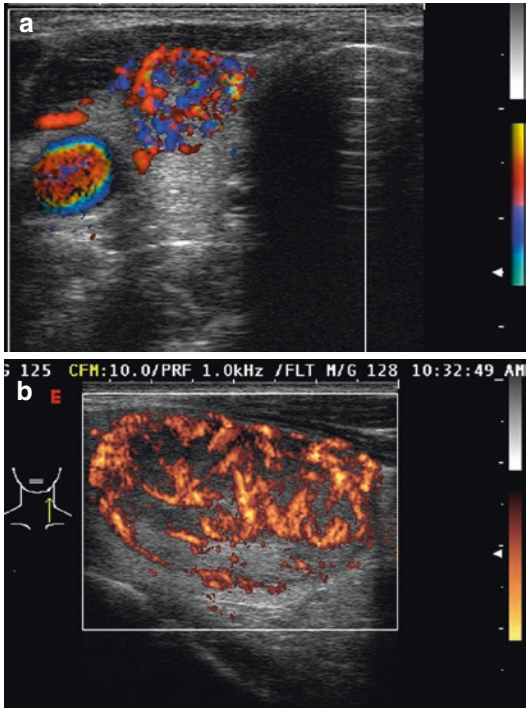

FIGURE. 3.9 Grade 4 Doppler flow. Grade 4 lesions have high-intensity central blood flow. (**a**) Illustrates color Doppler imaging and (**b**) shows power Doppler imaging

with pattern 3–4 were considered positive. Of 59 nonneoplastic nodules, 93% were grade 0–2, and only 7% were grade 3. No nonneoplastic nodules had grade 4 blood flow. Of 14 benign follicular adenomas, 71% showed grade 0–2 Doppler flow, and 29% showed grade 3 or 4 flow. Of the 10 carcinomas, 20% showed grade 0–2 Doppler flow, and 80% showed grade 3 or 4 flow. Based on this analysis, sensitivity was 80% and the specificity was 89% [20].

Applying Bayes' theorem to the data of Fukunari and De Nicola suggests that follicular nodules with no intranodular flow have only a 3% probability of malignancy rather than

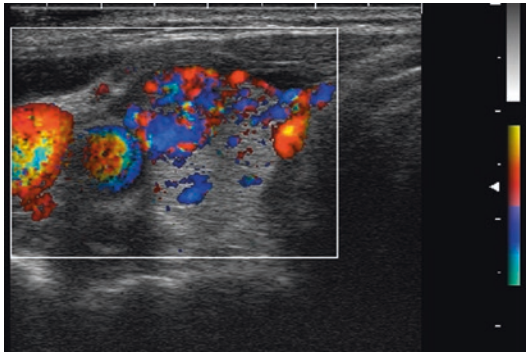

FIGURE. 3.10 Grade 4 Doppler flow in a benign nodule. While intranodular vascularity was previously felt to reflect an increased risk of malignancy, more recent data suggests no relationship between vascularity and the risk of papillary carcinoma. Note the similarity of this image of a benign nodule to the malignant nodule shown in Fig. 3.9a

the generally accepted 15–20% likelihood in unselected follicular nodules. Conversely, vascular nodules with a prior microfollicular biopsy have a probability of malignancy approaching 50% [21, 22].

Miyakawa et al. compared the vascular pattern and spectral parameters between patients with follicular adenoma and follicular carcinoma. Eighty percent of the carcinoma patients showed a moderate increase in intranodular vascularity, whereas 84% of adenoma patients showed only a peripheral rim of vascularity (sensitivity 87.5%, specificity 92%). Use of spectral parameters increased sensitivity slightly to 90% and decreased specificity slightly to 89% [23].

Conversely other studies have failed to show Doppler imaging to be useful in predicting malignancy in nodules with follicular biopsy. While Choi et al. found a statistically significant higher incidence of peripheral color flow present in benign nodules compared to malignant nodules (37.1 vs. 22.2%) and internal central vascularity in malignant nodules (77.8 vs. 62.9%) ($p = 0.03$), the clinical applicability of this

finding is limited [24]. Trimboli et al. studied 93 patients with prior cytology indicating follicular neoplasm and found a low value for color-flow Doppler in predicting malignancy in biopsy proven follicular neoplasms. Of 15 nodules with follicular cancer, eight demonstrated no internal vascularity and seven had internal vascularity. However, of the 78 benign nodules, 37 had internal flow, and 41 showed no internal flow. Thus there was no predictive value to the Doppler analysis [25].

If vascularity is considered a risk factor for malignancy in follicular nodules but not in papillary cancer, how is the clinician to use the Doppler information? Doppler imaging may be irrelevant in a deeply hypoechoic nodule with microcalcifications and infiltrative margins (suspicious for papillary carcinoma) but may remain relevant in an ovoid, isoechoic nodule with a variable thickness peripheral halo (suspicious for a follicular lesion).

In summary, the absence of flow *in a nodule with a prior follicular biopsy* makes malignancy much less likely, and conversely significant intranodular flow increases the risk of malignancy. The power Doppler flow pattern should be interpreted along with other ultrasonographic characteristics including echogenecity, edge definition, and calcifications, as well as clinical features such as nodule size, age, and sex of the patient to help in the decision regarding the need for biopsy, and the need for, and extent of surgery.

Doppler Ultrasound of Amiodarone-Induced Thyrotoxicosis

Amiodarone may cause thyroid dysfunction in 15–20% of treated patients. Doppler ultrasound has been shown to help in the differentiation of the etiology of amiodarone-induced thyrotoxicosis. Type 1 amiodarone thyrotoxicosis resembles Graves' disease. It typically occurs in patients with preexisting thyroid autoimmunity. The gland is

hyperthyroid, overproducing thyroid hormone. It may respond to treatment with thionomides and perchlorate. (Perchlorate is not available currently in the United States.) Typically type 1 amiodarone-induced thyrotoxicosis is associated with normal or increased vascularity on Doppler ultrasound. Type 2 amiodarone-induced thyrotoxicosis more closely resembles painless thyroiditis. In this entity, inflammation and destruction of thyroid tissue results in the release of preformed thyroid hormone. It may respond to glucocorticoid therapy and typically does not respond to thionomides or perchlorate. Typically type 2 amiodarone thyrotoxicosis is associated with absent or a very low degree of vascularity on power Doppler analysis [26, 27]. An elevated serum interleukin-6 level has been described as indicative of type 2 amiodarone thyrotoxicosis, but its predictive value is poor [28].

Eaton et al. demonstrated color-flow Doppler to be useful in the differentiation between the types of amiodarone thyrotoxicosis but did report 20% falling into an "indeterminate" subtype [28]. Unlike in evaluation of the utility of Doppler in thyroid nodules, in which biopsy or surgery provides a confirmation of diagnosis, most patients with amiodarone thyrotoxicosis will not have a histologic confirmation of subtype. The response to therapy has been used as a surrogate marker in several studies. Wong et al. demonstrated a 58% response to steroid therapy when flow was absent on color Doppler imaging, and only a 14% steroid response rate when flow was present [29].

A suggested treatment algorithm, using power Doppler analysis, suggests the use of steroid therapy when no flow is present. If flow is present, and especially if extremely vascular, thionomides with or without perchlorate are recommended. Using such an algorithm, Loy et al. demonstrated 20 of 21 patients to be treatment responsive [30]. Combined therapy or surgery should be considered for gravely ill patients, any patient who does not respond to the initial treatment protocol [31, 32] and those who present with an indeterminate pattern of mild vascularity.

Doppler Ultrasound of Graves' Disease and Thyroiditis

With the recognition that the Doppler image was useful in amiodarone-induced thyrotoxicosis, it seemed likely that Doppler would be useful for distinguishing hyperthyroidism of Graves' disease from thyrotoxicosis due to thyroiditis. Graves' disease has been described as the "thyroid inferno" [33], with intense blood flow and peak systolic velocity is up to 20 cm/s. On the other hand, the vascular pattern observed in thyroiditis is extremely variable, ranging from totally absent to extremely hypervascular. Figure 3.11 illustrates hypervascularity associated with Graves' disease. Figure 3.12 demonstrates increased blood flow in a patient with the early recovery phase of postpartum thyroiditis, most likely due to rise in TSH. Decreased blood flow would be more typical early in the destructive phase. Figure 3.13 shows intense blood flow in a patient with hashitoxicosis, and Fig. 3.14 shows an example of low vascularity in focal subacute thyroiditis.

The 2011 Guidelines for the Management of Hyperthyroidism and Other Causes of Thyrotoxicosis issued by the American Thyroid Association (ATA) and the American Association of

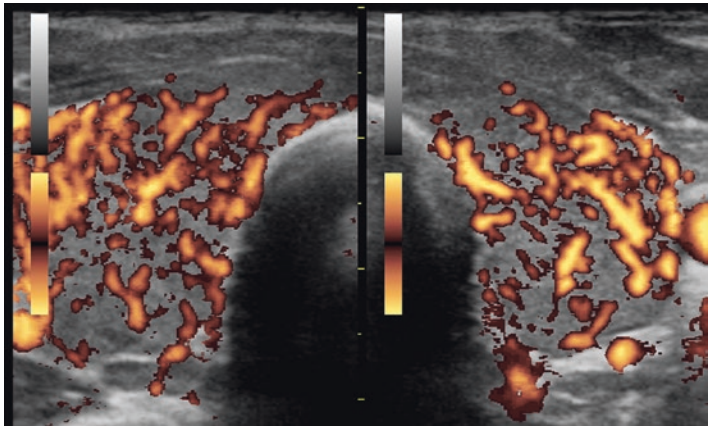

FIGURE. 3.11 Graves' disease. Graves' disease has been described as the "thyroid inferno" typically showing very intense blood flow

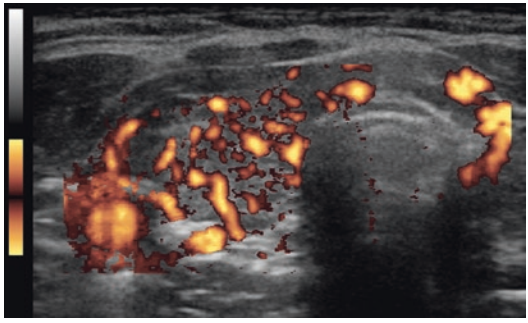

FIGURE. 3.12 Postpartum thyroiditis. Thyroiditis may be associated with any level of vascular flow, ranging from totally absent to intense, as is seen in this patient during the early recovery phase of postpartum thyroiditis

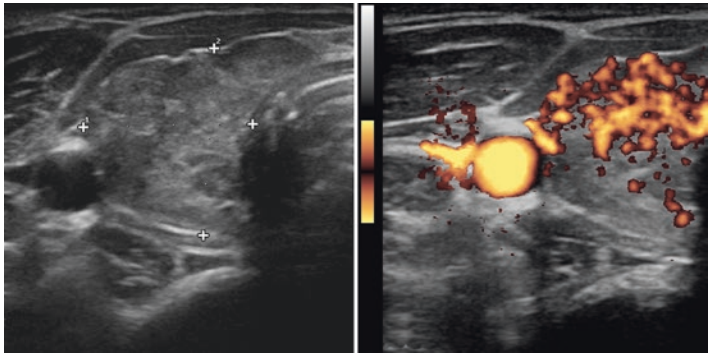

FIGURE. 3.13 Hashitoxicosis. Hashimoto's thyroiditis may also be associated with any degree of vascular flow. This patient with the hyperthyroid phase of early Hashimoto's thyroiditis (hashitoxicosis) has intense blood flow and could be easily confused with Graves' disease. Note that the gray-scale image demonstrates the typical hypoechoic and heterogeneous characteristics more associated with Hashimoto's thyroiditis

Clinical Endocrinologists (AACE) recommended against the routine use of ultrasound in the evaluation of the thyrotoxic patient, stating, "Ultrasonography does not generally contribute to the differential diagnosis of thyrotoxicosis." The authors

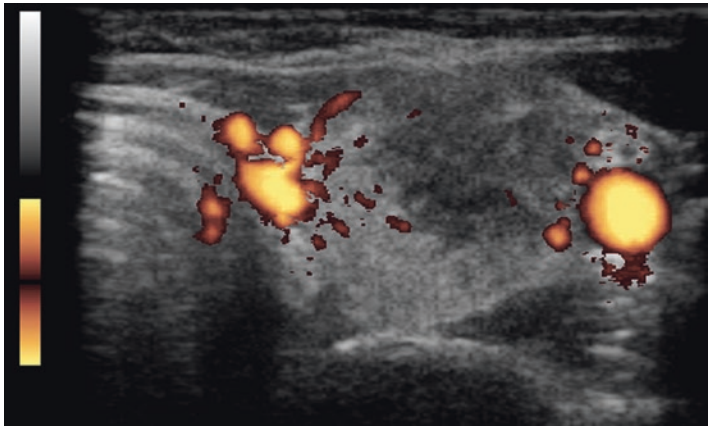

FIGURE. 3.14 Subacute thyroiditis. Subacute thyroiditis may also be associated with any degree of vascular flow. This image shows decreased flow in a hypoechoic inflammatory pseudonodule associated with subacute thyroiditis

did concede that in situations in which radioactive iodine scanning was contraindicated or not useful (e.g., pregnancy, breast feeding, or recent iodine exposure) that "increased color Doppler flow may be useful in confirming a diagnosis of thyroid hyperactivity" [34]. In an editorial discussing these guidelines, Kahaly, Bartelena, and Hegedus argued that, "Thyroid US is a highly sensitive, convenient, inexpensive and noninvasive technique to aid in determining the underlying pathophysiology of thyrotoxicosis." They further stated that, "Addition of color-flow Doppler US improves the diagnostic spectrum and accuracy through its ability to quantify thyroid vascularity. This method accurately distinguishes GD from destructive thyroiditis" [35]. The 2016 ATA guidelines for the management of hyperthyroidism state that, "Where expertise is available, ultrasonography with color Doppler flow can distinguish thyroid hyperactivity (increased flow) from destructive thyroiditis" [36].

However, there is clearly an overlap in color Doppler imaging between Graves' disease and destructive thyroiditis,

and for many cases the distinction is not clear, such as when there is mild to moderate flow observed. Several attempts have been made to apply quantitative techniques to differentiate the two. Kurita et al. calculated the "thyroid blood flow area" (TBFA) by measuring the percentage of thyroid area exhibiting Doppler flow. While demonstrating a statistically significant difference between 22 patients with untreated Graves' disease and 10 patients with destructive thyroiditis, there was considerable overlap. Using a TBFA cutoff of 8, 14% of patients with Graves' disease had low blood flow area and would have been misdiagnosed, and 10% of destructive thyroiditis patients had higher flow and would have been erroneously classified as Graves' disease [37].

Uchida et al. attempted to differentiate Graves' from destructive thyroiditis, using spectral analysis of the superior thyroid artery mean peak systolic velocity. While also demonstrating a statistical difference between 44 patients with untreated Graves' disease and 13 with destructive thyroiditis, there again was a significant overlap, with over 15% of the Graves' disease patients having a peak systolic velocity low enough to be misdiagnosed as destructive thyroiditis [38]. Hari Kumar et al. reported the ability to distinguish GD from destructive thyroiditis using color-flow Doppler imaging and peak systolic velocity (PSV) of the inferior thyroid artery. They reported a small overlap between the groups using both modalities [39]. Recently Gaberšček et al. reported excellent 94.7% sensitivity and 96.8% specificity of peak systolic velocity in discriminating hyperthyroid postpartum thyroiditis from Graves' disease. Due to some overlap of the values, 5–6% of patients would be misclassified by using PSV in isolation [40]. Ota et al. [41] reported results of a novel technique, with dedicated software calculating the TBFA. Comparing 56 patients with GD to 58 patients with destructive thyroiditis, they observed no overlap with a cutoff of 4% TBFA.

Thus, most Doppler techniques, whether qualitative or quantitative, show statistical significance in differentiating Graves' from destructive thyroiditis but suffer a limitation of

overlap of values between the two. Since Graves' disease typically has very intense flow, the absence of flow in a thyrotoxic patient is strongly suggestive of thyroiditis, and the presence of the "thyroid inferno" is highly suggestive of Graves' disease. However, the presence of normal or mildly increased vascularity may reflect either Graves' disease or destructive thyroiditis in a thyrotoxic patient. Significant overlap exists, even in most reports of quantitative techniques, and caution should be used in assignment of diagnosis solely based on color or power Doppler images. Both ultrasound and Doppler ultrasound are extremely operator dependent. As stated by Professor Fausto Bogazzi in a commentary to the Ota study: "Thyroidal RAIU still maintains full validity in helping to distinguish between hyperthyroid, thyrotoxic and euthyroid individuals. Color Doppler can be considered a supplemental technique that might overtake RAIU only if further technical improvement and standardization can be achieved" [42]. When evaluating a thyrotoxic patient, the clinician should consider the clinical history, physical examination, and laboratory studies. Ultrasonography and Doppler analysis will frequently provide evidence supporting the clinical impression. If doubt remains, RAIU may provide additional diagnostic information.

Other Uses of Doppler Imaging

Doppler imaging may be useful to clarify images. For example, the margins of an isoechoic nodule may be difficult to discern, but Doppler imaging may show peripheral vascularity, helping to identify the boundaries of the nodule. Figure 3.15a shows a nodule that appears to have an irregular and ill-defined lateral margin (arrows), but on Doppler imaging (Fig. 3.15b), it can be seen that the irregularity is due to peripheral blood vessels giving the appearance of a jagged margin.

Doppler imaging is useful in determining whether a very hypoechoic nodule is a pure cyst or a solid lesion. Figure 3.16a illustrates a hypoechoic nodule with significant posterior acoustic enhancement. However, the presence of grade 3

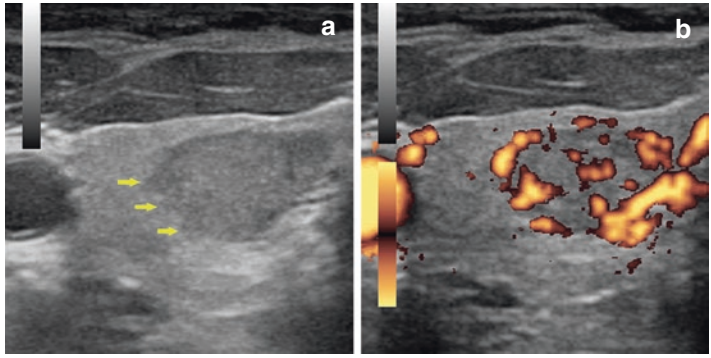

FIGURE. 3.15 (**a**) A nodule that appears to have an irregular and ill-defined lateral margin (*arrows*), but on Doppler imaging (**b**) it can be seen that the irregularity is due to peripheral blood vessels giving the appearance of a jagged margin

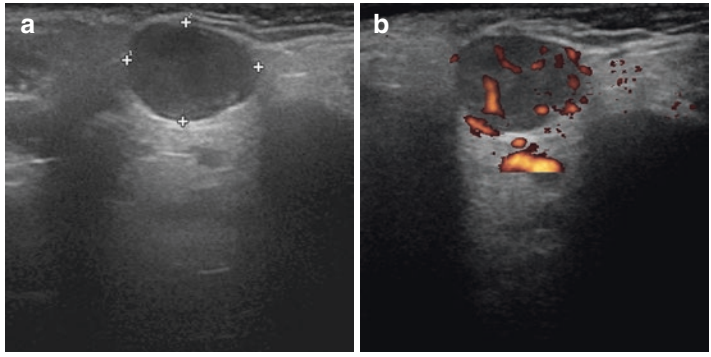

FIGURE. 3.16 (**a**) A hypoechoic nodule with significant posterior acoustic enhancement. However, the presence of grade 3 vascularity, shown in (**b**), clearly identifies this as a solid nodule and not a cyst

vascularity, shown in Fig. 3.16b, clearly identifies this as a solid nodule and not a cyst.

Doppler imaging is also useful prior to biopsy, both to determine if any superficial vessels are located along the planned needle track and to avoid laceration of large feeding vessels (Fig. 3.17).

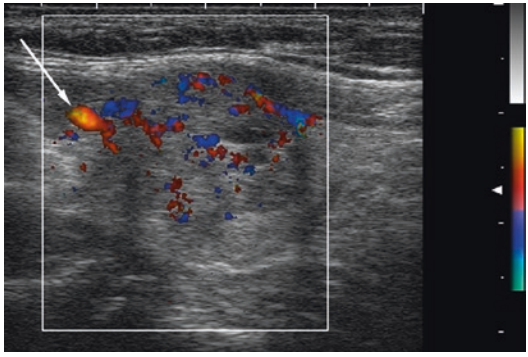

Figure. 3.17 Doppler imaging is useful prior to biopsy. The high-intensity signal associated with a thyroidal artery (*arrow*) is noted in the projected path of the biopsy needle in this image. Repositioning prior to biopsy can help avoid the rare complication of trauma to the artery

Doppler imaging may help distinguish benign from malignant lymph nodes. As discussed in Chap. 8, in a normal lymph node, the vascular supply enters centrally at the hilum and spreads along the long axis, within the central hilar line. In malignant lymph nodes, aberrant vessels enter peripherally through the lymph node capsule. Increased and disordered vascularity may be seen both peripherally and centrally. Figures 3.18 and 3.19 demonstrate the vascular pattern in benign and malignant lymph nodes. Doppler flow study may indicate compression of the jugular vein by a malignant lymph node, as seen in Fig. 3.20.

When examining lymph nodes for possible metastatic disease, it is important to set the ultrasound equipment to be able to detect very small amounts of flow in the hilum and cortex of the lymph node. Maximum sensitivity can be achieved by setting the Doppler pulse repetition frequency (PRF) to less than 800 cycles/s and the wall filter to the lowest setting. This is in contrast to standard thyroid imaging, in which a PRF of 1000 and a medium wall filter will provide acceptable detection of parenchymal or nodular vascularity.

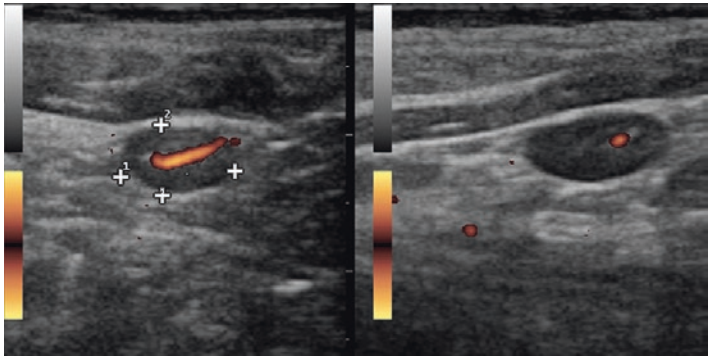

FIGURE. 3.18 Normal lymph node. In a normal lymph node the vascular supply enters centrally at the hilum and spreads along the long axis, within the hilar line

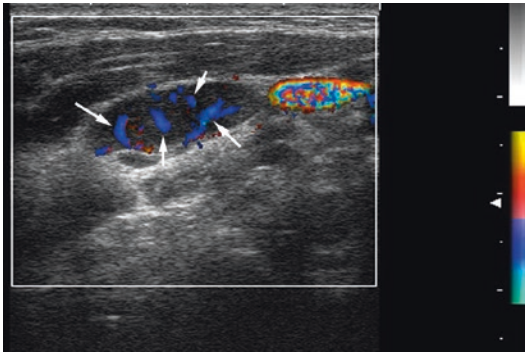

FIGURE. 3.19 Lymph node with metastatic papillary carcinoma. In contrast to the preceding figure, this malignant lymph node has disordered and chaotic blood flow

As discussed in Chap. 9, parathyroid adenomas frequently have a pulsatile polar artery, and Doppler imaging may be useful in establishing that a nodule posterior to the thyroid represents a parathyroid rather than a central compartment lymph node (Fig. 3.21).

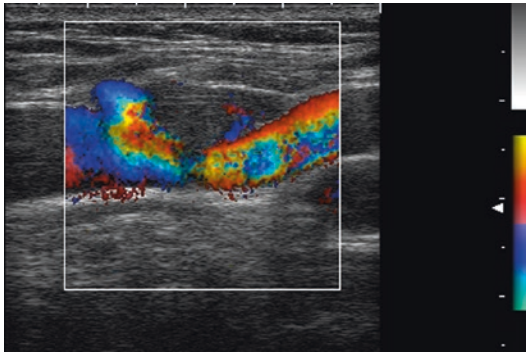

FIGURE. 3.20 A malignant lymph node in a patient with papillary carcinoma is seen compressing the jugular vein in this Doppler image. Benign lymph nodes may cause deviation of the major vessels but typically do not indent the vessel or cause abnormality in the blood flow

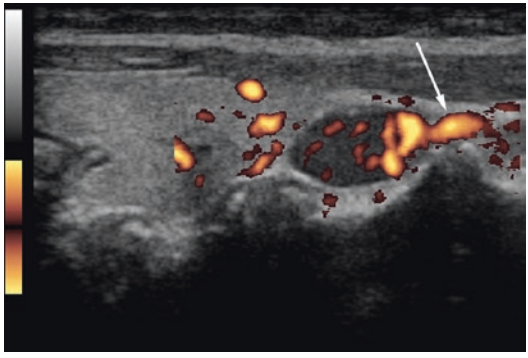

FIGURE. 3.21 Parathyroid adenomas frequently have a pulsatile polar artery, and Doppler imaging may be useful in establishing that a nodule posterior to the thyroid represents a parathyroid rather than a central compartment lymph node

Conclusions

In summary, Doppler ultrasound continues to play an important role in thyroid imaging. While no longer felt to be a feature independently correlated with risk of malignancy in

most thyroid nodules, power Doppler imaging may play a role in the prediction of the likelihood of malignancy in thyroid nodules with follicular cytology. All current guidelines continue to recommend that Doppler assessment of vascularity be documented for all significant thyroid nodules. However, the flow pattern does not have sufficient predictive value to establish the need for biopsy of a nodule. Doppler imaging is useful in the evaluation of goiter, thyroid nodules, lymph nodes, and parathyroid glands.

References

1. Cerbone G, Spiezia S, Colao A, Sarno D, et al. Power Doppler improves the diagnostic accuracy of color Doppler ultrasonography in cold thyroid nodules: follow-up results. Horm Res. 1999;52(1):19–24.
2. Papini E, Guglielmi R, Bianchini A, Crescenzi A, et al. Risk of malignancy in nonpalpable thyroid nodules: predictive value of ultrasound and color Doppler features. J Clin Endocrinol Metab. 2002;87(5):1941–6.
3. Berni A, Tromba L, Falvo L, Marchesi M, et al. Malignant thyroid nodules: comparison between color Doppler diagnosis and histological examination of surgical samples. Chir Ital. 2002;54(5):643–7.
4. Frates MC, Benson CB, Doubilet PM, Cibs ES, Marqusee E. Can color Doppler sonography aid in the prediction of malignancy of thyroid nodules? J Ultrasound Med. 2003;22:127–31.
5. Appetecchia M, Solivetti FM. The association of colour flow Doppler sonography and conventional ultrasonography improves the diagnosis of thyroid carcinoma. Horm Res. 2006;66(5):249–56.
6. Moon HJ, Kwak JY, Kim MJ, et al. Can vascularity at power Doppler US help predict thyroid malignancy? Radiology. 2010;255(1):260–9.
7. Chammas MC, Gerhard R, de Oliveira IR, et al. Thyroid nodules: evaluation with power Doppler and duplex Doppler ultrasound. Otolaryngol Head Neck Surg. 2005;132(6):874–82.
8. Chammas MC. Why do we have so many controversies in thyroid nodule Doppler US? Radiology. 2011;259(1):304.
9. Rosario P, Silva A, Borges M, Calsolari MI. Doppler ultrasound of additional value to gray-scale ultrasound in differentiating

malignant and benign thyroid nodules? Arch Endocrinol Metab. 2015;59(1):79–83.
10. Bakhshaee M, Davoudi Y, Mehrabi M, et al. Vascular pattern and spectral parameters of power Doppler ultrasound as predictors of malignancy risk in thyroid nodules. Laryngoscope. 2008;118(12):2182–6.
11. Algin O, Algin E, Gokalp G, et al. Role of duplex power Doppler ultrasound in differentiation between malignant and benign thyroid nodules. Korean J Radiol. 2010;11(6):594–602.
12. Ma JJ, Ding H, BH X, Xu C, Song LJ, Huang BJ, Wang WP. Diagnostic performances of various gray-scale, color Doppler, and contrast-enhanced ultrasonography findings in predicting malignant thyroid nodules. Thyroid. 2014;24(2):355–63.
13. Zhang B, Jiang Y, Liu J, et al. Utility of contrast-enhanced ultrasound for evaluation of thyroid nodules. Thyroid. 2010;20(1):51–7.
14. Cooper DS, Doherty GM, Haugen BR, et al. The American Thyroid Association Guidelines Task Force. Revised management guidelines for patients with thyroid nodules and differentiated thyroid cancer. Thyroid. 2009;19:1167–214.
15. Gharib H, Papini E, Paschke R, Duick DS, et al. American Association of Clinical Endocrinologists, Associazione Medici Endocrinologi, and European Thyroid Association medical guidelines for clinical practice for the diagnosis and management of thyroid nodules. Endocr Pract. 2010;16(Suppl 1):1–43.
16. Shin JH, Baek JH, Chung J, Ha EJ, et al. Ultrasonography diagnosis and imaging-based management of thyroid nodules: revised Korean Society of Thyroid Radiology consensus statement and recommendations. Korean J Radiol. 2016;17(3):370–95.
17. Haugen BR, Alexander EK, Bible KC, Doherty GM, et al. 2015 American Thyroid Association Management guidelines for adult patients with thyroid nodules and differentiated thyroid cancer: The American Thyroid Association guidelines task force on thyroid nodules and differentiated thyroid cancer. Thyroid. 2016;26(1):1–133.
18. Gharib H, Papini E, Garber JR, Duick DS, et al. American Association of Clinical Endocrinologists, American College of Endocrinology, and Associazione Medici Endocrinologi medical guidelines for clinical practice for the diagnosis and management of thyroid nodules – 2016 update. Endocr Pract. 2016;22(5):622–39.
19. Fukunari N, Nagahama M, Sugino K, et al. Clinical evaluation of color Doppler imaging for the differential diagnosis of thyroid follicular lesions. World J Surg. 2004;28(12):1261–5.

20. De Nicola H, Szejnfeld J, Logullo AF, et al. Flow pattern and vascular resistance index as predictors of malignancy risk in thyroid follicular neoplasms. J Ultrasound Med. 2005;24:897–904.
21. Levine RA. Value of Doppler ultrasonography in management of patients with follicular thyroid biopsies. Endocr Pract. 2006;12(3):270–4.
22. Iared W, Shigueoka DC, Cristófoli JC, et al. Use of color Doppler ultrasonography for the prediction of malignancy in follicular thyroid neoplasms: systematic review and meta-analysis. J Ultrasound Med. 2010;29(3):419–25.
23. Miyakawa M, Onoda N, Etoh M, et al. Diagnosis of thyroid follicular carcinoma by the vascular pattern and velocimetric parameters using high resolution pulsed and power Doppler ultrasonography. Endocr J. 2005;52(2):207–12.
24. Choi YJ, Yun JS, Kim DH. Clinical and ultrasound features of cytology diagnosed follicular neoplasm. Endocr J. 2009;56(3):383–9.
25. Trimboli P, Sorrenti S. Low value of color flow-Doppler in predicting malignancy of thyroid follicular neoplasms. Diagn Cytopathol. 2009;37(5):391–2.
26. Macedo TA, Chammas MC, Jorge PT, et al. Differentiation between the two types of amiodarone-associated thyrotoxicosis using duplex and amplitude Doppler sonography. Acta Radiol. 2007;48(4):412–21.
27. Bogazzi F, Bartelena L, Brogioni S, et al. Color flow Doppler sonography rapidly differentiates type I and type II amiodarone-induced thyrotoxicosis. Thyroid. 1997;7(4):541–5.
28. Eaton SE, Euinton HA, Newman CM, et al. Clinical experience of amiodarone-induced thyrotoxicosis over a 3-year period: role of colour-flow Doppler sonography. Clin Endocrinol. 2002;56(1):33–8.
29. Wong R, Cheung W, Stockigt JR, Topliss DJ. Heterogeneity of amiodarone-induced thyrotoxicosis: evaluation of colour-flow Doppler sonography in predicting therapeutic response. Intern Med J. 2003;33(9-10):420–6.
30. Loy M, Perra E, Melis A, Cianchetti ME, Piga M, Serra A, Pinna G, Mariotti S. Color-flow Doppler sonography in the differential diagnosis and management of amiodarone-induced thyrotoxicosis. Acta Radiol. 2007;48(6):628–34.
31. Bogazzi F, Bartelena L, Martino E. Approach to the patient with amiodarone-induced thyrotoxicosis. J Clin Endocrinol Metab. 2010;95(6):2529–35.

32. Erdogan MF, Güleç S, Tutar E, Başkal N, Erdogan G. A stepwise approach to the treatment of amiodarone-induced thyrotoxicosis. Thyroid. 2003;13(2):205–9.
33. Ralls PW, Mayekowa DS, Lee KP, et al. Color-flow Doppler sonography in Graves disease: thyroid inferno. Am J Roentgenol. 1988;150:781–4.
34. Bahn RS, Burch HB, Cooper DS, et al. Hyperthyroidism and other causes of thyrotoxicosis: management guidelines of the American Thyroid Association and American Association of Clinical Endocrinologists. Thyroid. 2011;21(6):593–646.
35. Kahaly GJ, Bartalena L, Hegedus L. The American Thyroid Association/American Association of Clinical Endocrinologists guidelines for hyperthyroidism and other causes of thyrotoxicosis: a European perspective. Thyroid. 2011;21(6):585–91.
36. Ross DS, Burch HB, Cooper DS, Greenlee MC, et al. 2016 American Thyroid Association guidelines for diagnosis and management of hyperthyroidism and other causes of thyrotoxicosis. Thyroid. 2016;26(10):1343–421.
37. Kurita S, Sakurai M, Kita Y, et al. Measurement of thyroid blood flow area is useful for diagnosing the cause of thyrotoxicosis. Thyroid. 2005;15(11):1249–52.
38. Uchida T, Takeno K, Goto M, Kanno R, et al. Superior thyroid artery mean peak systolic velocity for the diagnosis of thyrotoxicosis in Japanese patients. Endocr J. 2010;57(5):439–43.
39. Hari Kumar KVS, Pasupuleti V, Jayaraman M, et al. Role of thyroid Doppler in differential diagnosis of thyrotoxicosis. Endocr Pract. 2009;15(1):6–9.
40. Gaberšček S, Osolnik J, Zaletel K, Pirnat E, Hojker S. An advantageous role of spectral Doppler sonography in the evaluation of thyroid dysfunction during the postpartum period. J Ultrasound Med. 2016;35(7):1429–36.
41. Ota H, Amino N, Morita S, et al. Quantitative measurement of thyroid blood flow for differentiation of painless thyroiditis from Graves' disease. Clin Endocrinol. 2007;67:41–5.
42. Bogazzi F, Vitti P. Could improved ultrasound and power Doppler replace thyroidal radioiodine uptake to assess thyroid disease? Nat Clin Pract Endocrinol Metab. 2008;4(2):70–1.

Chapter 4
Normal Neck Anatomy and Method of Performing Ultrasound Examination

Vijaya Chockalingam, Sarah Smith, and Mira Milas

V. Chockalingam, MD
Endocrinology, Banner University Medical Center, Phoenix, AZ, USA

S. Smith
Sonographer, Medsmart Inc. and Alumnus, West Coast Ultrasound Institute, Phoenix, AZ, USA

M. Milas, MD, FACS (✉)
Thyroid, Parathyroid and Adrenal Disorders Center, Diabetes and Endocrinology Institute, Phoenix, AZ, USA

Department of Surgery, Endocrine Surgery Center, University of Arizona College of Medicine – Phoenix, Phoenix, AZ, USA

Banner – University Medical Center Phoenix, Phoenix, AZ, USA
e-mail: Mira.milas@bannerhealth.com

D.S. Duick et al. (eds.), *Thyroid and Parathyroid Ultrasound and Ultrasound-Guided FNA*,
https://doi.org/10.1007/978-3-319-67238-0_4

Introduction

Ultrasound is the single most informative and versatile radiologic modality applied to the evaluation of thyroid and parathyroid glands. Ultrasound is also useful for the examination of neck anatomy in general and for the assessment of suspected abnormalities beyond these endocrine glands. Modern ultrasound machines provide unprecedented high-resolution detail of anatomy and disease features. Physicians of multiple specialty types have acquired the expertise to perform neck ultrasound and ultrasound-guided biopsies, bringing access to diagnostic and therapeutic benefits of ultrasound to patients beyond the hospital setting. Endocrinologists, surgeons, primary care specialists, and the original operators—radiologists and sonographers—all participate in the care of a patient with neck ultrasound. While certification and accreditation to perform ultrasound may come from different professional organizations representing each of these specialists, there are several key common requirements for optimal neck ultrasound. These include availability of and familiarity with ultrasound equipment, knowledge of normal neck anatomy, skillfulness of performing sonographic exam and/or ultrasound-guided biopsy accurately, and competence in correct pattern recognition and clinical diagnostic assessment. The clinical applications of neck ultrasound are summarized below to provide an overarching context in which to review each of the key requirements. Literature that emphasizes and further expands on the key concepts of performing neck ultrasound is also provided in the References [1–10].

Clinical Utility of Sonography of Thyroid and Parathyroid Glands

- Confirmation that a palpable or suspected neck mass arises from the thyroid or parathyroid glands
- Characterization of the features of thyroid nodular disease and diffuse thyroid disease
- Characterization of the features of abnormal parathyroid glands (enlargement, location)

- Establish diagnosis of thyroid disorder
  - via pattern recognition
  - via ultrasound-guided fine needle aspiration biopsy
- Provide precise guidance of biopsy into target tissue
- Evaluate cervical lymph nodes for presence of metastatic thyroid cancer
- Detection of other cervical pathologies (involving non-endocrine organs such as salivary glands, glomus tumors, and lymphoma)
- Monitoring of disease (e.g., benign thyroid nodules)
- Assessment of response to treatment (e.g., treatment of thyroid cancer)
- Screening of patients with increased risk of developing hereditary thyroid malignancies
- Correlation of abnormalities detected on other radiology modalities used for endocrine disorders (radioiodine and sestamibi scans, CT, MRI, PET)
- Extension of physical examination

Ultrasound Equipment

Fundamentally, an ultrasound system consists of the processing unit or console, the transducer, and the monitor. Whereas early generation ultrasound machines were built with large and cumbersome frames, current models are compact, portable, and even small enough to fit into a physician's coat like a stethoscope. There are multiple high-quality manufacturers and multiple models of ultrasound so that potential users have many options and should familiarize themselves with machine aspects that meet their clinical application needs (Fig. 4.1). Software is available to enhance imaging, to brighten the needle and predict the path of its direction during biopsy, to organize display of target organs, to store and display prior thyroid nodule images for side-to-side comparison over time, and even to produce detailed ultrasound reports for documentation.

The ultrasound processing unit, essentially a sophisticated computer and keyboard, merges complex operations, yet the

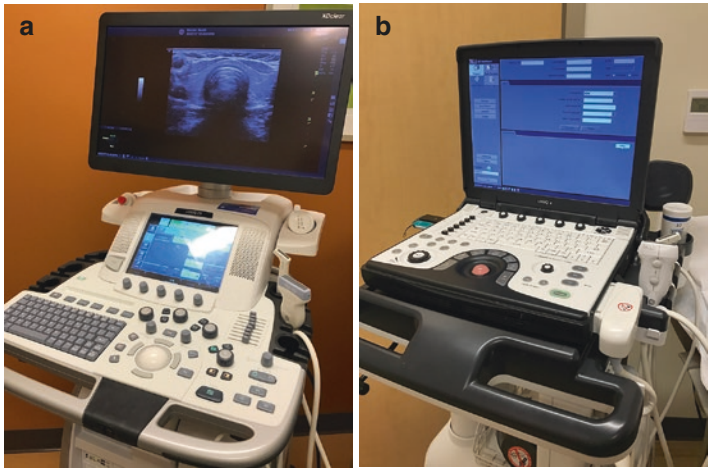

FIGURE 4.1 Ultrasound console units are manufactured in numerous versions. Shown here are the clinic- or radiology-based platform (**a**) and the portable, laptop-sized unit that can be mounted on a stand [as shown in (**b**)] or can be carried in a briefcase and thus be versatile in access to many locations of patient care

sonographer typically uses just a few basic functionalities: input of patient data, control knobs for gain adjustment, depth of view, localization and number of focal zones, frequency selection, zoom mode, freeze frame, Doppler imaging, measurement calipers, icon and labeling markers, and storage of still images or cine-clip segments. The standard transducer is a multi-frequency linear array probe in the 8–15 MHz range that optimizes imaging of superficial structures with fine structural details. Probes of this frequency come in different lengths (2, 4 cm; Fig. 4.2a–d) and also different widths of the footprint (Fig. 4.2b, d) that is positioned on the skin for imaging. Some manufacturers also build small linear or curved transducers that facilitate examination or biopsy in areas such as the sternal notch where clavicular heads limit the scanning path of larger linear probes (Fig. 4.3). Monitors range in display design from basic to sophisticated, with

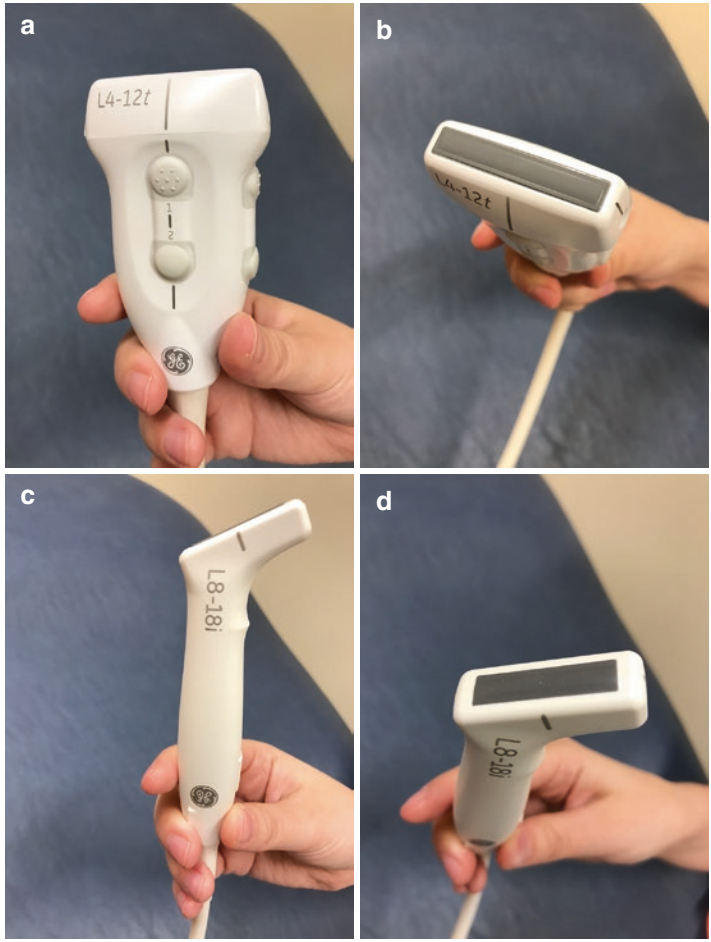

FIGURE 4.2 Examples of ultrasound transducer probes (**a**, **c**) and their linear "footprints" (**b**, **d**). The entire footprint surface should contact the patient's skin for optimal image acquisition

touch-screen features, and flexibility to swivel to be viewed from different angles. Additional monitors can be connected to the ultrasound unit and displayed so that the patient can view the exam in real time.

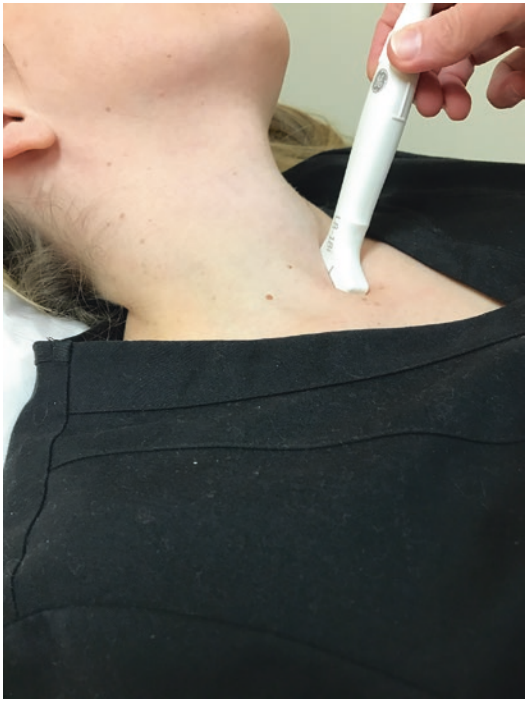

FIGURE 4.3 A small linear footprint transducer is ideal for positioning in anatomical regions where the bone (clavicles and sternal notch as shown in model) or other anatomies prevent a good fit for traditional larger transducers

A practical necessity of any ultrasound usage is to set up a reliable method for image storage, backup, and transmission to electronic health records or radiology picture archiving and communication systems (PACS) if applicable. These methods will be unique to the ultrasound system, the user's preference, the hospital or clinic regulatory requirements, and the need to access archived material. Additional adjuncts to the equipment include printers, ultrasound gel warmers, and storage cases for the console and transducer probes.

Scanning Technique

Patient Positioning

For a right-handed individual who performs ultrasound, the traditional setup entails the ultrasound unit being to the left of the exam table (Fig. 4.4), with the patient supine on the table. This allows the sonographer (henceforth this term will apply

FIGURE 4.4 The traditional arrangement between the ultrasound console unit and the patient exam table. The sonographer stands facing the ultrasound and uses their right hand to move the transducer on the patient's neck, thus simultaneously facing both the ultrasound monitor (*on the left*) and the patient's face (*on the right*)

to any physician or radiology technician performing the ultrasound exam) to face both the patient and the monitor. The goals of positioning are to expose the neck to allow movement of the transducer probe to all relevant anatomic areas and to ensure that the patient remains comfortable during the process, protecting those who may have spine issues or arthritis (Fig. 4.5a, b). Typically, the position entails gentle hyperextension of the neck with a soft pillow for support beneath the shoulders. The sonographer can ask the patient to bend their knees for comfort and protection of the lower back. It is helpful to ask the patient periodically if they remain comfortable and to remind them to indicate if this is not the case.

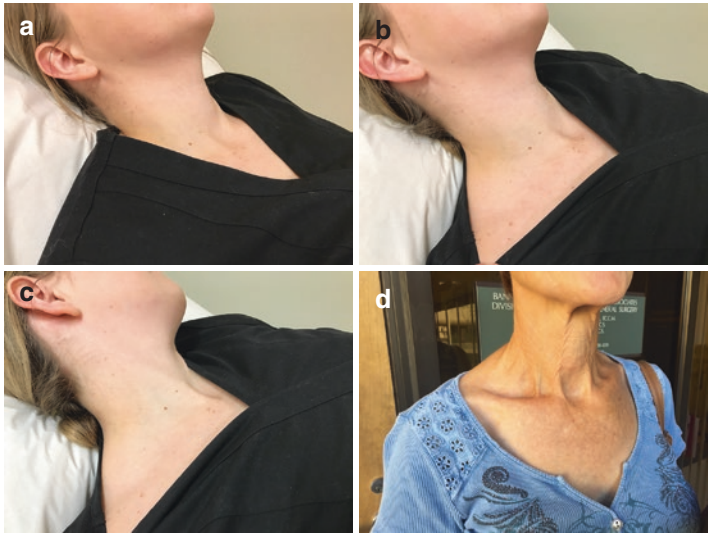

Figure 4.5 Optimal positioning and exposure of the neck for ultrasound of the thyroid and parathyroid glands (**a**, **b**) and lateral neck for lymph node examination and mapping (**c**). While the vast majority of patients are supine on the exam table with a pillow supporting the shoulders to allow gentle neck extension, keep in mind that some patients have beautiful anatomy (**d**) that allows ultrasound exam even in a sitting position. Other patients who have medical constraints (wheelchair-bound) can also have an effective ultrasound exam without needing to be repositioned on an exam table

For patients who need lymph node mapping in the setting of known or suspected thyroid cancer, positioning needs to provide wide exposure of the lateral neck from the hairline and the angle of the mandible to the clavicles, with the chin averted to the contralateral side (Fig. 4.5c).

It is important to realize that a good ultrasound exam can be achieved despite positional challenges. For example, patients in a wheelchair can remain so and be supported when they simply stretch their neck backward. A patient sitting or standing even may have adequate neck exposure to capture the needed ultrasound image, especially if they have a long, thin neck (Fig. 4.5d).

Basic Orientation

The simple acronym "PPP" has remained a guiding cue to the authors since first receiving this instruction in 1994: patient, probe, and preset. These three topics represent, in order, the safest method to start an ultrasound exam. First, the patient information needs to be entered accurately to ensure that the subsequent imaging is linked properly for interpretation, documentation, and storage. Next, the probe is selected based on the type of imaging planned. This is most relevant when ultrasound machines have several different probes connected. To detect if the desired probe is actually selected and engaged for display on the monitor, the sonographer can quickly note the shape of the footprint on the monitor (linear or curved) and as quickly touch one end of the footprint on the transducer to see if motion appears on the monitor. Finally, the preset refers to the exam-specific programming for optimal image resolution with emphasis on small parts or vascular features or even on thyroid-focused features at a specific depth. This may change between exams if different users have access to the ultrasound, thus it is valuable to make sure that the desired display setting is selected prior to the start of each new patient exam.

The proper orientation of the transducer probe is that when placed transversely on the front of the patient's neck, the anatomy touching the left of the probe is displayed on the left

of the monitor. By convention, the probe is rotated 90° clockwise so that in longitudinal (sagittal) placement, the cephalad anatomy touches the left of the probe and remains displayed on the left of the monitor ("head on left, feet on right"). It is tempting to look at the various notchings, dots, or other markings that are etched on the transducer probe to determine if the orientation is correct. Please avoid this tactic. Manufacturers make different markings and none correlate to uniform orientation. Furthermore, the ultrasound console has a keyboard function that allows the image on the monitor to be flipped. The easiest, most reliable way to orient the probe correctly is to place ultrasound gel on the footprint and touch one end of the probe to see where it moves on the display; similarly, it is easiest then simply to turn the probe in the hand to change orientations.

Sequence of Examination

The ultrasound exam is best performed by the strategy of "do it the same way every time all the time." The precise sequence may vary among specialists and sonographers. The main point is to form a consistent habit of the procedure that will maximize performing a complete exam and reduce omission of information needed for assessment and diagnosis. Protocols are available from respected professional associations: American Institute of Ultrasound in Medicine, AIUM [6] and Thyroid Cancer Care Collaborative, TCCC [7]. An example of a checklist protocol provided by the West Coast Ultrasound Institute (Phoenix, AZ) to sonography students during training is itemized in Table 4.1.

Highlighted here is a suggested sequence for a comprehensive endocrine neck ultrasound exam. Place the probe transversely on the anterior of the neck at the level of the isthmus, and scan superiorly until the hyoid bone (to detect the presence of a thyroglossal duct cyst in rare instances) and inferiorly into the upper mediastinum (Fig. 4.6). Note the visible portions of the thyroid lobes, the larynx/vocal cords, and the central neck and upper mediastinal lymph nodes (level 6

TABLE 4.1 Protocol for ultrasound scanning of the thyroid and parathyroid glands (West Coast Ultrasound Institute, Phoenix, AZ)

- Sequence
  - Neck should be hyperextended (as much as comfortably possible)
  - Bilateral TRV RT/LT, color
  - Isthmus, measure, color
  - RT TRV INF
  - RT TRV MID, measure, color
  - RT TRV SUP

    Video sweep RT TRV I-S
  - RT SAG LAT
  - RT SAG MID, measure, color
  - RT SAG MED

    Video sweep RT SAG L-M
  - LT TRV INF
  - LT TRV MID, measure, color
  - LT TRV SUP

    Video sweep LT TRV I-S
  - LT SAG LAT
  - LT SAG MID, measure, color
  - LT SAG MED

    Video sweep LT SAG L-M
  - RT TRV LYMPH CHAIN sweep I-S
  - LT TRV LYMPH CHAIN sweep I-S
- Equipment protocol
  - Linear TX

(continued)

Table 4.1 (continued)

– Range of 10–14 MHz or greater can use lower frequency TX for depth penetration (curvilinear)

– Virtual convex for full scan view

– Power Doppler for full vascularity

- Standards for documenting thyroid

– Sonographic echogenicity of thyroid gland (overall)

Normal: homogeneous mid-gray

– Size (normal adult ranges)

Isthmus: <0.4 cm

Length: 40–60 mm

AP: 20–30 mm

Width: 15–20 mm

– Size (normal child ranges)

Length: 20–30 mm

AP: 12–15 mm

Width: 10–15 mm

– Documentation of any nodules

Size (in 3 dimensions)

Architecture

Location

Color (vascularity)

– Overall vascularity

– Thyroid margins contour

– Parathyroid region

- Standards for documenting lymph node chain

– Size

Table 4.1 (continued)

– Architecture
– Location
– Suspicious features such as calcification, cystic areas, absence of a central hilum, round shape, and abnormal blood flow
– Blood flow patterns detectable through Doppler

The acronyms are *TRV* (transverse), *RT* (right), *LT* (left), *INF and I* (inferior), *MID* (midpoint), *SUP and S* (superior), *SAG* (sagittal), *LAT and L* (lateral), *MED and M* (medial), *color* (Doppler color flow assessment), *TX* (transducer), *AP* (anteroposterior)

Figure 4.6 Orientation of the ultrasound in transverse position in the usual starting point of a thyroid ultrasound, centered on the thyroid isthmus

and 7; see schematic in Fig. 4.7). Move the probe to the center on the right thyroid lobe, and scan transversely to demonstrate the entire span of the right lobe from the upper pole to the lower pole, noting any abnormal findings. Rotate the probe 90° clockwise to acquire longitudinal images from the medial aspect adjacent to the trachea to the lateral edge adjacent to the carotid artery (Fig. 4.8). Repeat these same image acquisitions for the left thyroid lobe. Return to measure the thickness of the isthmus and three dimensions of the right and left lobes (anterior-posterior depth (D) × transverse width (W) × longitudinal length (L)). Volume if needed can be calculated for each lobe by the formula $D \times W \times L \times (\pi/6)$ which can be easily remembered as $D \times W \times L \times ½$. Note and describe the abnormal thyroid pathology, and measure dominant nodules in the same three-dimensional convention. Categorize thyroid nodules in terms of the American Thyroid Association (ATA) risk of malignancy features [2]. Begin to form a diagnostic impression based on ATA pattern recognition strategies (thyroiditis, multinodular goiter, diffuse goiter, solitary nodule, thyroid cancer). Note the location of any abnormal parathyroid glands, and measure their size (normal

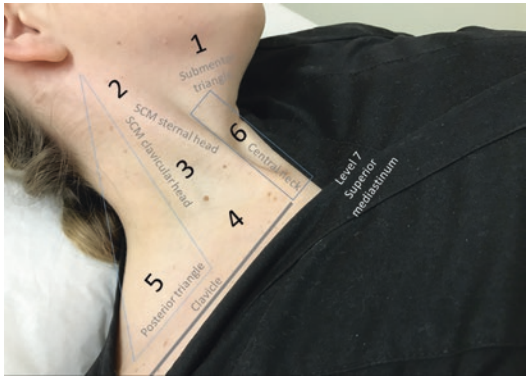

Figure 4.7 Levels of the neck used to classify anatomic location of cervical lymph nodes

FIGURE 4.8 Orientation of the ultrasound in longitudinal (sagittal) position achieved by 90° rotation clockwise from the transverse position

parathyroid glands are not visible by ultrasound, but their expected distribution is depicted in Fig. 4.9). Note the presence of abnormal central neck lymph nodes, their features (reactive from thyroiditis versus abnormal from cancer metastases), and size. Apply the color Doppler analysis to assess overall thyroid gland vascularity and the vascular patterns specific to any discrete nodules. Scan the lateral neck briefly through levels 2–5 to detect any grossly evident lymphadenopathy. In real time, return to examine any area of the thyroid or the central and lateral neck that needs a more thoughtful or detailed evaluation.

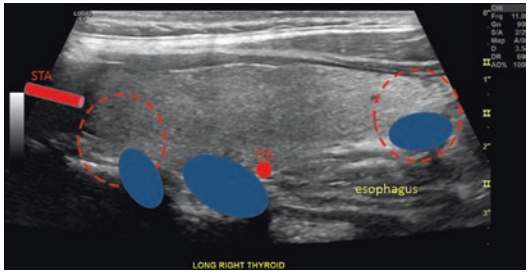

FIGURE 4.9 Typical anatomic distribution of normal superior and inferior parathyroid glands (*within dotted circles*) with superimposed examples for the location of enlarged parathyroid glands (*blue ovals*). The right thyroid gland is shown in longitudinal (sagittal) orientation. The superior thyroid artery (STA) is at the left of the image; inferior thyroid artery (ITA) is at the posterior midportion of the thyroid. Published with kind permission of © Mira Milas, MD 2017. All Rights Reserved

Normal Neck Anatomy in Ultrasound

The Thyroid and Parathyroid Glands

The thyroid gland is a symmetrical, butterfly-shaped gland draped over the trachea with the isthmus positioned over tracheal rings 1–3 (Fig. 4.10). The dimensions of a typical thyroid lobe are 1–2 cm deep, 1–2 cm wide, and 4–6 cm long (Fig. 4.11a, b). The isthmus is usually <0.5 cm thick (Fig. 4.11c). The echogenicity of the normal thyroid is a silver gray that is brighter than the surrounding strap muscles and similar to the echogenicity of the submandibular glands. The pyramidal lobe is an embryologic remnant of descent from the foramen caecum visible usually on the left aspect of thyroid cartilage (Fig. 4.12a, b), while the tubercle of Zuckerkandl is located along the posterior midportion of the thyroid lobe and represents lateral ingress of embryologic thyroid tissue (Fig. 4.13). Tubercles take many different shapes and sizes; some appear to have a "cleft-like" partition that leads to erroneous

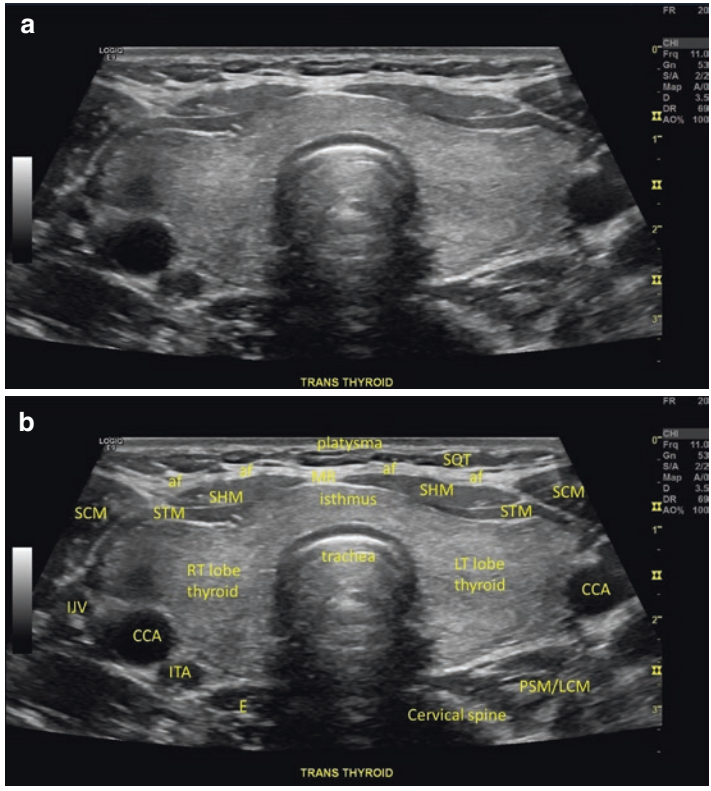

FIGURE 4.10 (**a**) Transverse view of the thyroid gland and surrounding structures. Use this image to identify the sonographic appearance of anatomic structures, and check your knowledge using **b**. (**b**) Normal anatomy seen on transverse view of thyroid ultrasound with labeled structures: platysma, *SQT* (subcutaneous tissue), *af* (anterior layer of deep cervical fascia), isthmus, *RT* (right) and *LT* (left) lobes of thyroid, trachea, *MR* (midline raphe between the strap muscles—*SHM*, sternohyoid muscle; *STM*, sternothyroid muscle), *SCM* (sternocleidomastoid muscle), *CCA* (common carotid artery), *ITA* (inferior thyroid artery), *IJV* (internal jugular vein), *E* (esophagus), *PSM*/*LCM* (paraspinous muscles/longus colli muscle), cervical spine. Published with kind permission of © Mira Milas, MD 2017. All Rights Reserved

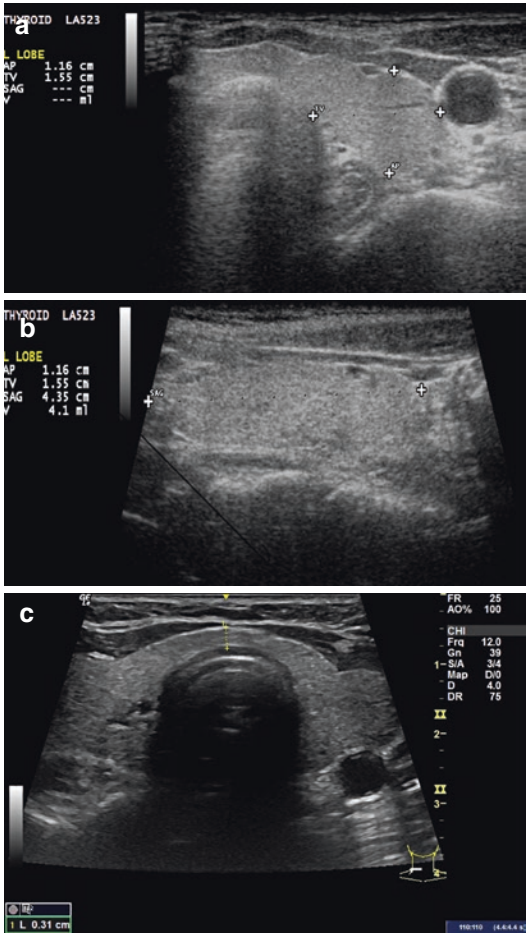

FIGURE 4.11 Transverse and longitudinal measurements of the left lobe. Note the use of virtual convex imaging to capture the entire length of the lobe. Additionally, the machine automatically calculates the volume of the lobe based on the three measured dimensions. The AP dimension can be obtained in either the transverse or longitudinal view. (**a**) Transverse view of left lobe, taking the AP and transverse measurements. (**b**) Sagittal (longitudinal) view of the left lobe, taking the length measurement. Note that the AP dimension can be obtained on either the transverse or sagittal image. (**c**) Measuring the AP dimension of the isthmus

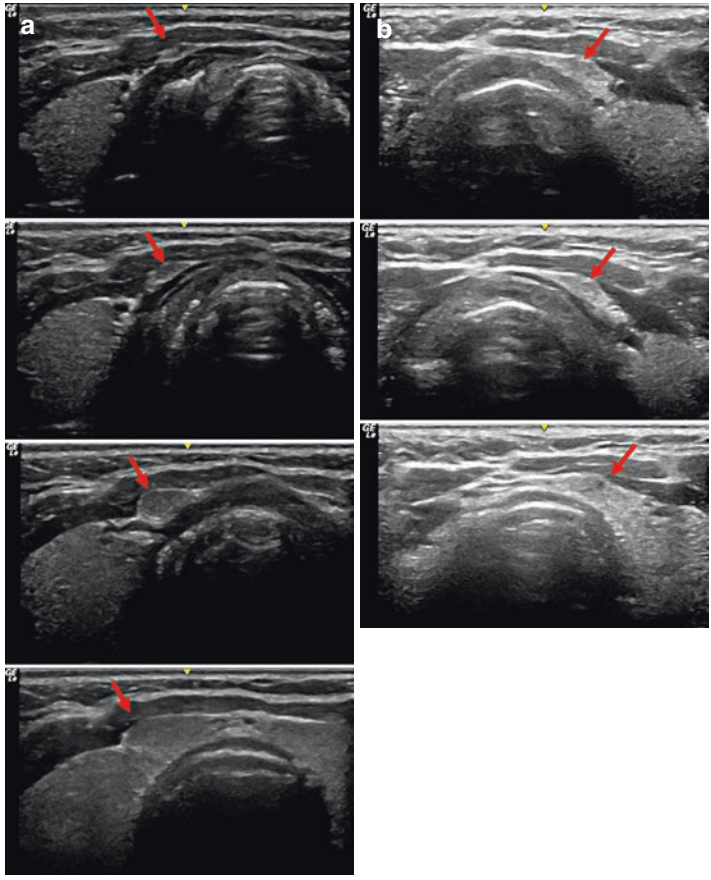

FIGURE 4.12 The pyramidal lobe can be seen progressing from the isthmus superiorly along the edge of the cricoid and thyroid cartilages. (**a**) A right-sided pyramidal lobe. (**b**) A left-sided pyramidal lobe

interpretation and even measurement (Fig. 4.13a, b) as a thyroid nodule. Normal parathyroid glands are too small and too similar in tissue composition to their surrounding structures to be differentiated by ultrasound waves; they are not visible as discrete structures.

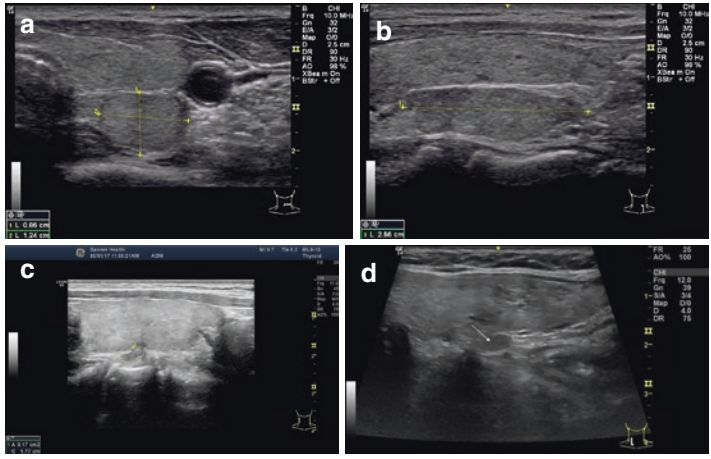

FIGURE 4.13 (**a**–**d**) Tubercle of Zuckerkandl examples. This tubercle is an embryologic remnant and exists in various shapes protruding off of the posterior aspect of the thyroid lobe. It is often misinterpreted as a thyroid nodule

The Cervical Lymph Nodes

Hundreds of normal lymph nodes populate the cervical spaces, yet on ultrasound only a small fraction (up to 10–20) may be detectable in the lateral neck. They are less often visible in the central neck except in patients with thyroiditis. The normal lymph node appears as a hypoechoic oval structure with a central hyperechoic line representing the vascular hilum from which a color Doppler signal can be detected (Fig. 4.14a). There is tremendous variability in the sonographic appearance of normal lymph nodes, including variable size, variable presence and shape of the hilar stripe, and variable position. The absence of a hilar stripe in and of itself does not necessarily signify an abnormal lymph node. At the lateral edge of each submandibular gland is a common location for a large lymph node that maintains normal architecture (size even up to 2–3 cm long); the symmetry of this large node, when it is detectable adjacent to both the left and right submandibular glands, serves also as a reassurance of benign pattern (Fig. 4.14b, c).

The Architecture of the Neck: Vascular, Nervous, Musculoskeletal and Soft Tissues

Surrounding the thyroid are essential anatomical structures that are important to recognize as they form a constant background against which pathology stands out and needs to be distinguished. Arteries and veins are most prominently visible in both transverse and longitudinal views. The common carotid artery frames the lateral boundary of the central neck (level 6) and is visible at the edges of the thyroid gland in transverse views (Fig. 4.15a). The red color scheme of Doppler flow indicates that flow is detected moving toward the ultrasound transducer, while blue color means flow is moving away; hence the internal jugular vein appears red in Fig. 4.15a. The inferior thyroid artery travels deep (posterior) to the plane of the carotid artery, then can be seen as cross-sectional small circles approaching the esophagus and then via the tracheoesophageal groove enters the posterior mid-portion of a thyroid lobe (Fig. 4.15b, c); this artery can also be traced using ultrasound to its origin off of the subclavian artery. This path is in contrast to the superior thyroid artery that, as its name implies, enters directly into the triangular apex of the thyroid lobe, giving off anterior and posterior branches. The middle thyroid vein can be visible in some patients and travels above (anterior) to the common carotid artery then joins into the internal jugular vein. Other vascular structures surrounding the inferior poles of the thyroid and visible in the midline of the central neck do not have eponyms. Scanning toward the upper mediastinum, it is possible in some patients to image the juncture of the common carotid and subclavian arteries and even see a significant portion of the innominate artery (Fig. 4.15d, e). In the venous system, all main branches of the jugular system—internal, external, and anterior—are imageable by ultrasound. Often, large fluttering valves (thin hyperechoic lines) can be seen within the internal jugular vein, which enlarges with a Valsalva maneuver demonstrating elongation of the valves' turbulent vascular flow (hyperechoic swirls) between the valves and thin vein walls (Fig. 4.15f–h).

The large muscles of the neck and the more delicate muscles surrounding the larynx are labeled in Figs. 4.10b, 4.15c, and 4.16. The platysma, as a thin flat muscle, covers most of the anterior neck; in most individuals it is very attenuated

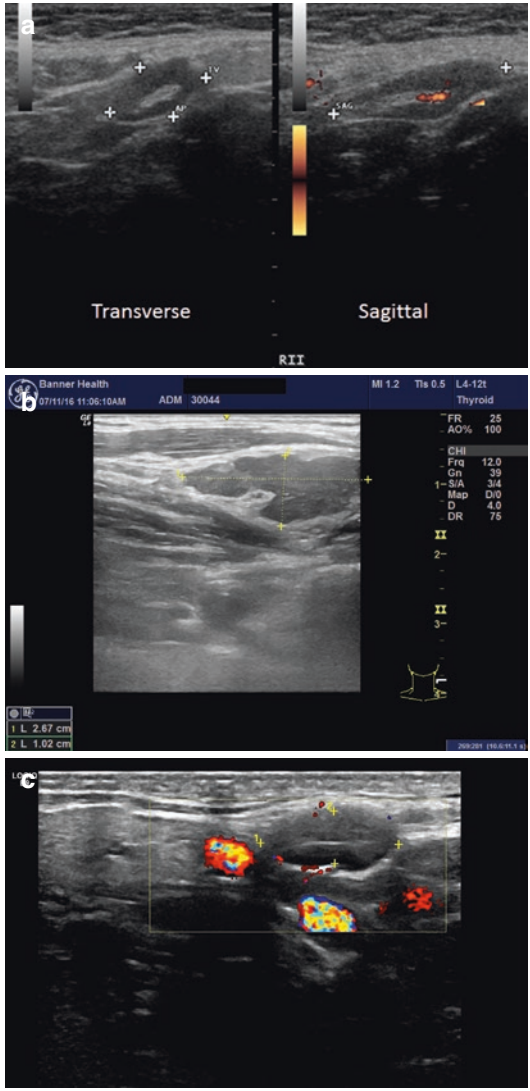

and thus may be visible best in men where this muscle layer is thicker. The term "strap muscles" most practically refers to the centrally located sternohyoid and sternothyroid muscles. The sternohyoid muscle will always be "higher" or more anterior on the transverse view; it is attached to the hyoid bone and the sternum. The sternothyroid muscle will always be immediately adjacent on the anterior surface of the thyroid gland; however, its name derives from the fact that it attaches to the thyroid cartilage and sternum. These two muscles form the "roof" of the central neck compartment (Fig. 4.16b). The sternocleidomastoid muscle is the largest muscle always evident on neck ultrasound. The omohyoid muscle, like its name implies, is attached to the hyoid bone and the shoulder bones/ligaments. Hence its path is oblique in the lateral neck; occasionally in individuals with beautiful anatomic definition, the omohyoid can be tracked by ultrasound, but routinely it is difficult to detect (Fig. 4.16c). Likewise, body mass index (BMI) and tissue composition determine the visibility or clarity of the trapezius muscles (Fig. 4.16d) and scalene muscles (Fig. 4.17). In patients with high BMI, these muscles may blend into the general gray-scale echogenicity of fibrofatty tissue that fills the lateral neck and envelopes these muscles (Fig. 4.17a for scalene muscles). In contrast, the paraspinous muscles (longus colli) adjacent to the cervical spine column maintain a routinely visible path on transverse ultrasound views of the central neck.

FIGURE 4.14 (**a**) Normal lymph node at the lateral edge of the right submandibular gland. Note the flat shape and the echogenic hilum with Doppler flow. (**b**) Benign, reactive lymph node in transverse view. It is not uncommon to see large, benign lymph nodes adjacent to the submandibular glands. The shape and presence of echogenic hilum (in this case, slightly eccentric) are reassuring features. (**c**) Transverse view of a normal lymph node just lateral to the submandibular gland and above the bifurcation of the common carotid artery. Note the echogenic hilum and lack of peripheral/chaotic Doppler signal

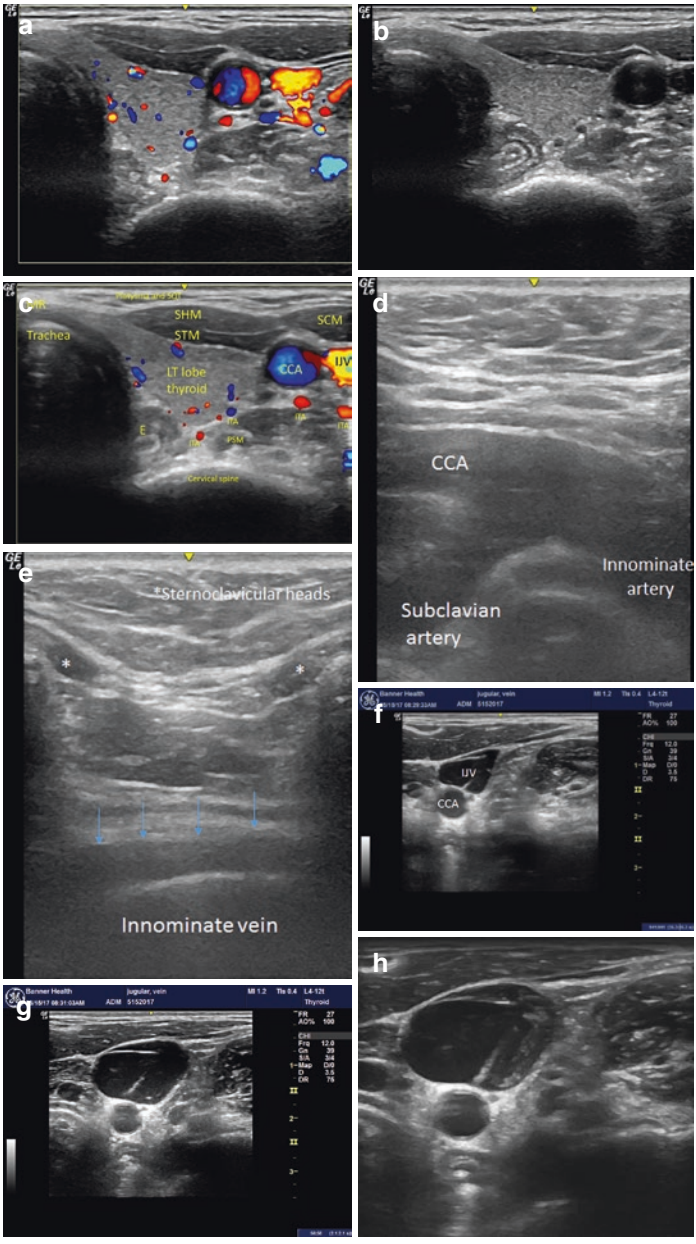
a
b
c
Trachea
SHM
STM
SCM
LT lobe thyroid
CCA
IJV
PSM
Cervical spine
d
CCA
Innominate artery
Subclavian artery
e
*Sternoclavicular heads
Innominate vein
f
IJV
CCA
g
h

The more delicate muscles of the larynx are rarely visible with sufficient distinctiveness because of the air shadowing interference from the tracheolaryngeal complex that, literally and visually, blacks out ultrasound waves. The midline anchors of the tracheolaryngeal complex are the hyoid bone (most cephalad and located in cervical level 1), the thyroid cartilage, and the cricoid cartilage; these are all hypoechoic thick structures. The thyroid cartilage in some individuals may be so dense that ultrasound waves are reflected back to the transducer, and thus the only detectable shape is an inverted V of thick echogenic lines. With such constraints and with variable body anatomy, consistent imaging of the laryngeal muscles can be challenging. The reader is guided to more detailed resources [5, 11] for ultrasound imaging of the larynx and vocal cord ultrasonography.

The vagus nerve is visible as a small 2–3 mm hypoechoic circle usually between the carotid artery and jugular veins (Fig. 4.15a). The vagus can be tracked cephalad as high as the

FIGURE 4.15 (**a**, **b**) Transverse view of the left lobe with (**a**) and without (**b**) Doppler. Try to identify the anatomic structures and blood vessels then use (**c**) to confirm your answers. (**c**) Normal vascular anatomy seen on transverse view of thyroid ultrasound with labeled structures: platysma, *SQT* (subcutaneous tissue), *af* (anterior layer of deep cervical fascia), isthmus, *RT* (right) and *LT* (left) lobes of thyroid, trachea, *MR* (midline raphe between the strap muscles—*SHM*, sternohyoid muscle; *STM*, sternothyroid muscle), *SCM* (sternocleidomastoid muscle), *CCA* (common carotid artery), *ITA* (inferior thyroid artery), *IJV* (internal jugual vein), *E* (esophagus), *PSM*/*LCM* (paraspinous muscles/longus colli muscle), cervical spine. Ultrasound can even detect large vessels in the upper mediastinum such as the innominate artery (**d**) and innominate vein [(**e**) traced by the *blue arrows*]. (**f**, **g**, **h**) Transverse views of the internal jugular vein (IJV) and common carotid artery (CCA). In (**g**) the IJV is dilated as the patient performs a Valsalva maneuver. (**h**) "Zooms in" on the IJV where the echogenic lines represent fluttering valves of the IJV. Published with kind permission of © Mira Milas, MD 2017. All Rights Reserved

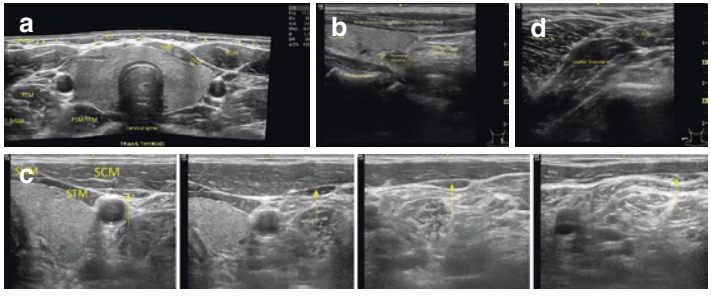

Figure 4.16 (**a**) Normal muscular anatomy seen on transverse view of thyroid ultrasound with labeled structures: platysma (thin *yellow arrows* all along anterior neck), *SQT* (subcutaneous tissue), *af* (anterior layer of deep cervical fascia), *MR* (midline raphe between the strap muscles—SHM, sternohyoid muscle; STM, sternothyroid muscle), *SCM* (sternocleidomastoid muscle), *PSM*/*LCM* (paraspinous muscles/longus colli muscle), cervical spine, *ASM* (anterior scalene muscle), *MSM* (middle scalene muscle). While these structures are all symmetrical and present on both the left and right sides of the neck, for clarity the labels are placed on one side only. (**b**) Strap muscles seen in longitudinal view. The area between the inferior pole of the thyroid and the sternal notch is part of the central neck that is filled with fibrofatty tissue, as shown here. When this area has visible thyroid lobe and the spinal vertebral bodies, it is therefore more lateral to the trachea and called paratracheal central neck. When the trachea itself is visible (not shown here), the tissues anterior to the trachea are called paratracheal central neck. (**c**) Omohyoid muscle (*yellow arrow*) tracking from medial to lateral (*left to right across the frames*) in the left neck. *SHM*, sternohyoid muscle; *STM*, sternothyroid muscle; *SCM*, sternocleidomastoid muscle. (**d**) Trapezius muscle (*yellow arrow*) and the adjacent levator scapulae muscle are located in the far lateral and posterior neck, at the edge of the *SCM*, sternocleidomastoid muscle

Figure 4.17 The brachial plexus is between the anterior and medial scalene muscles as labeled in (**b**). Seen as a cluster of circles, the brachial plexus (*arrows*) can resemble blood vessels in cross section. Doppler interrogation as seen in (**a**) and (**c**) confirms these circles are not vessels

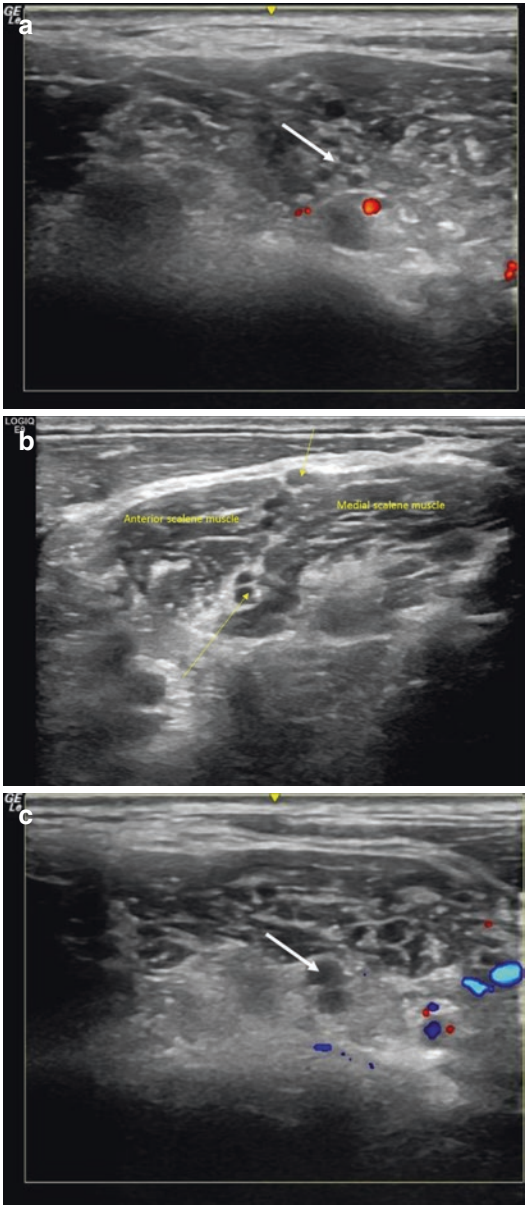
a
b
Anterior scalene muscle
Medial scalene muscle
c

carotid bifurcation and becomes less visible there due to the density of other hypoechoic anatomies in the region. The brachial plexus is also detectable in between the anterior and middle scalene muscles (Fig. 4.17b). It has a distinctive appearance as a cluster of circles that may initially seem like cross sections of vascular structures, until absence of color Doppler flow confirms them as nerve roots (Fig. 4.17a–c). The recurrent laryngeal nerves (RLN) and the superior laryngeal nerves are too small in caliber to be detectable by modern ultrasound technology. The normal anatomic path of the RLN is along the tracheoesophageal groove, and it enters into the cricothyroid muscle.

The trachea, esophagus, and spine feature prominently in nearly all sectional images of the thyroid due to their immediate proximity. The trachea is at the center of all transverse views of the thyroid, though perhaps its most peculiar and distinct image is in longitudinal view where the tracheal cartilage rings alternating with the soft membranous portions appear like black-white zebra stripes (Fig. 4.18a, trachea underlies a long isthmus). Ultrasound views of the thyroid cartilage, which encases the true vocal cords (most hyperechoic thin bright white lines at the center (Fig. 4.18b), and arytenoid cartilages (here show as hyperechoic round densities lateral to the true vocal cords closed in midline, Fig. 4.18b, c) are being acquired more often in modern ultrasound exams because of the ability to perform laryngeal ultrasound to evaluate the voice. The esophagus has the unique echogenic pattern of a “bull’s eye” target: a central hypoechoic circle representing the lumen that is filled with air and sometimes saliva (hyperechoic spots), then a concentric circular layer of mucosa that is hyperechoic, and then finally the outer muscular hypoechoic circle. Typically the esophagus is positioned in the left central neck slightly lateral to the trachea (Fig. 4.15b), but in some patients, the position favors the right side or with sufficient transducer pressure can be moved to the right (Fig. 4.19a). These layers and their echogenicity remain visible in longitudinal views as well (Fig. 4.19b). The cervical spine vertebral bodies are

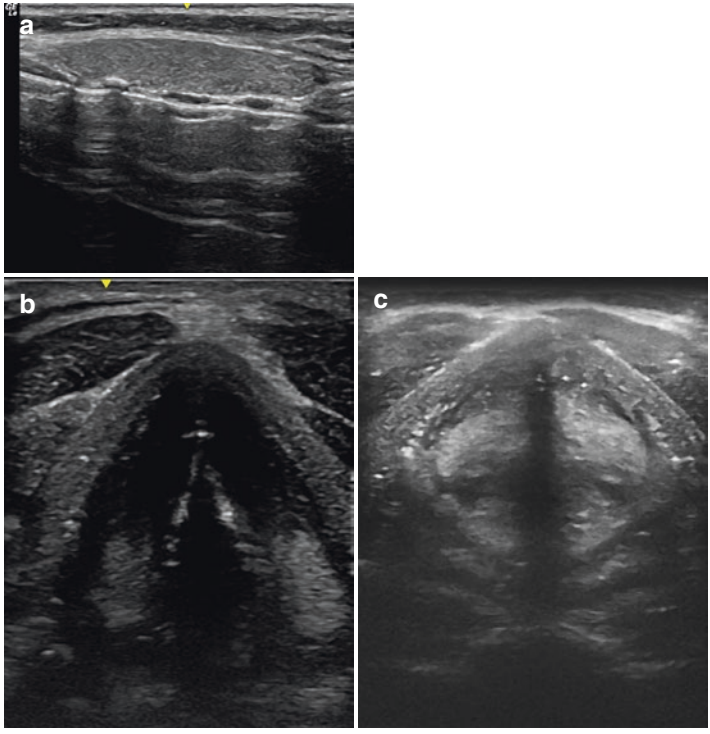

FIGURE 4.18 A long isthmus overlies the bright hyperechoic lines of the trachea, seen in this longitudinal view (**a**). The cartilage of the tracheal rings appears as hypoechoic oval segments in line one after another. Nothing is visible deep to the trachea as air interferes with ultrasound wave progression. The strap muscles are again seen as the hypoechoic layer along the entire top frame of the image, with the *yellow triangle* situated along the midportion of their path. In this particular view, the isthmus occupies so much of the anterior tracheal surface that no "pretracheal central neck" remains visible at the right half of the image. (**b**, **c**) Illustrate the ultrasound view of the larynx in transverse orientation. The hyperechoic thin bright white lines are the true vocal cords (TVC), seen as an "upside-down V" in the middle of the image (**b**), surrounded by laryngeal cartilage and muscles. The TVC lines are not visible in image (**c**) because of the thicker encasing thyroid cartilage and anatomy present in another patient

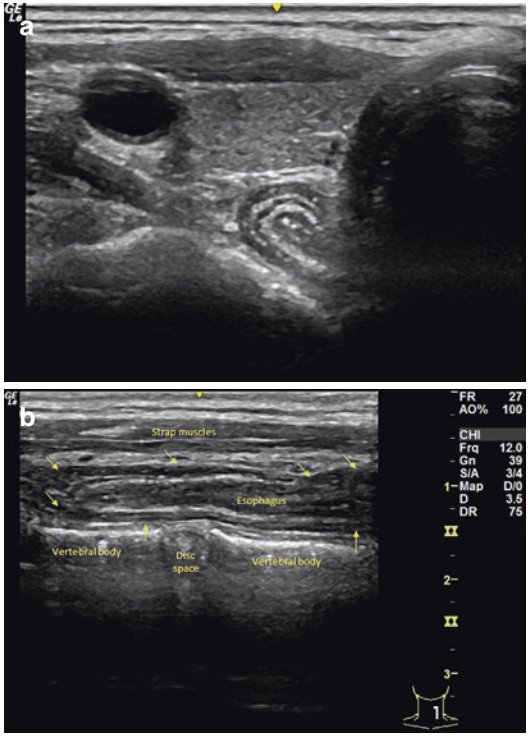

FIGURE 4.19 The esophagus can sometimes be situated in the right neck as seen in (**a**), where all of the "bull's eye" layers of the esophagus clearly appear in the ultrasound image. Those same layers can also be appreciated in the longitudinal view (**b**) of the esophagus with the outer muscular layer outlined by arrows

hyperechoic and block-like in longitudinal view (Fig. 4.20a). It can be more challenging to appreciate that the transverse cervical spine processes is also hyperechoic though somewhat more ambiguous in outline. Thus, its distal tip has been known to be misinterpreted as a calcified lateral neck mass (shown in the middle of the image, associated with posterior acoustic shadowing, in Fig. 4.20b).

The submandibular glands (Fig. 4.14c, in the left upper corner and outside of the Doppler square) are visible on

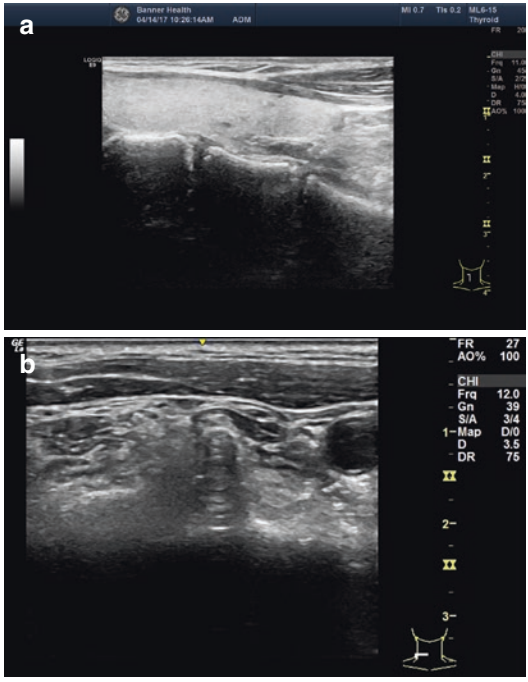

FIGURE 4.20 In the middle of image (**a**), the cervical vertebral spine is seen as a series of the most hyperechoic line segments (individual vertebral bodies) separated by vertebral disks. The thick bone of the spine prevents ultrasound waves from traveling deeper; hence the bottom half of the image is anechoic—*black*. In the lateral neck, the cervical spinous process ends in the middle of the image and is surrounded by soft tissues (**b**). The tip of this spinous process is hyperechoic and creates posterior acoustic shadowing (series of small thin *white arrows*); this has sometimes been misinterpreted as a calcified lateral neck mass

ultrasound in nearly all patients and have a silver echotexture similar to a normal thyroid gland. Rarely, and typically only in young patients or children, thymus is apparent in the low central neck deep to the strap muscles (Fig. 4.21 which shows an image obtained by a small curved transducer that could fit into the sternal notch of a child).

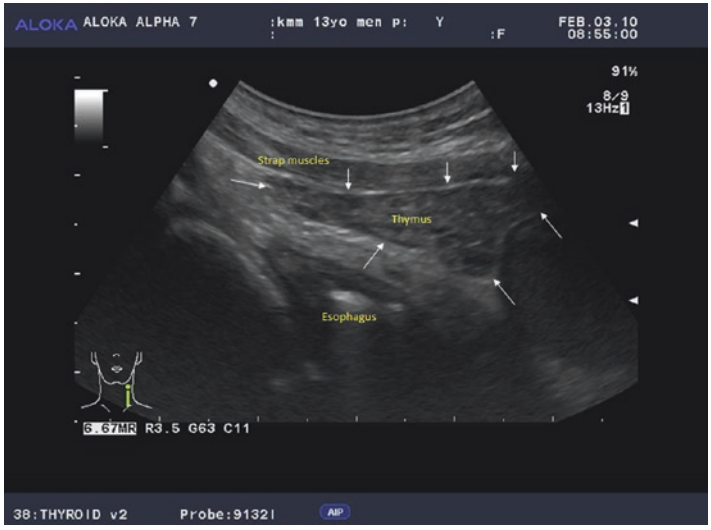

FIGURE 4.21 In young individuals and especially children, the thymus is seen as a triangular structure (*white arrows*) immediately deep to the strap muscles. This is a longitudinal view with a small curvilinear transducer probe that captures the left-sided thymus in view; typically there will be a symmetrical structure for the other limb of the cervical thymus on the contralateral side. Published with kind permission of © Mira Milas, MD 2017. All Rights Reserved

Pearls of Practice

Included here are the top ten practical concepts born of the authors' ultrasound experience and treatment of patients with thyroid and parathyroid disorders:

1. **Increase transducer pressure** to improve the clarity of tissue and organ planes. This adjustment of pressure also sometimes brings to exposure pathology that is situated in deeper neck regions (e.g., large parathyroid adenoma or central neck lymph node metastasis in the tracheoesophageal groove). Novice users of ultrasound tend to be too delicate in the application of transducer probe, sometimes just having it glide on the ultrasound gel and barely touch the skin. Without proper transducer pressure

anatomy will not properly display. Alert your patient that you may increase the pressure, and ask them to tell you when it is too firm so you can make adjustments as needed.

2. **Vary magnification and field display to scrutinize anatomy for more detail. Zoom out** to view the region of interest in low magnification. This is key for patients with large goiters, for men, and for the elderly whose thyroid glands tend to be situated at the level of the clavicle or below. This allows visualization of a wider expanse of territory of the anatomy that is relevant to detect pathology. This maneuver allows observation of both nuances (e.g., tracheal deviation and/or substernal extension of goiters) and essential elements (e.g., enlarged parathyroid glands—these are unlikely to be detected if the ultrasound protocol setting focuses just on the main outline of the thyroid because the parathyroid glands are deeper along the posterior capsule of the thyroid). **Zoom in** to provide greater magnification when relevant; for example, this may be helpful to discern whether a hyperechoic focus is an artifact (colloid ring down) or a true microcalcification. Select the **virtual convex** setting on your ultrasound console. Using a linear transducer probe, this allows a trapezoidal display of the anatomy, with inclusion of an expanded view of structures on the lateral sides of the thyroid (Fig. 4.10a).
3. **Vary overall gain** as needed for image clarity.
4. **Beware of imitators of pathology**. The paraspinous muscle/longus colli muscle can appear as hypoechoic teardrop-shaped structure, for example, and be labeled as parathyroid adenoma in some patients.
5. **Remember that normal anatomic structures "keep going"**—they do not appear and disappear from view. This is one method that can help distinguish architectural structures from pathology (such as the longus colli from a parathyroid adenoma or scalene muscles from cervical lymph node or mass).
6. **Size of the thyroid varies** with the size of a person, thus carefully consider what constitutes an enlarged thyroid lobe. For example, a thyroid lobe that is 6 cm long may be normal for a muscular person who is 6′5″ tall and weighs 250 lbs. Be careful when applying conclusions that repre-

sent judgments about pathology; provide enough objective descriptions that will help support your assessment.

7. **Echogenicity of the normal thyroid gland** is comparable to that of the submandibular gland. When the initial transverse appearance of the thyroid looks darker than expected and resembles the hypoechogenicity of the surrounding strap muscles (alerting perhaps to thyroiditis), it is helpful to view the submandibular gland for comparison.
8. **Make your documentation as succinct yet inclusive of key aspects as possible**. For example, do not assume that lack of mention of cervical lymph nodes means they are normal. The best way to state this assessment is to actually explicitly state it: "No abnormal cervical lymph nodes were evident in the central or lateral neck." This is relevant whether you are reading an outside ultrasound report or whether you are composing your own ultrasound documentation.
9. **"Phone a friend."** Consultation with a trusted colleague with ultrasound expertise is invaluable at any stage of clinical practice or career. If available, you can invite such a colleague to perform or review the ultrasound with you in real time. If unavailable, review of saved images and cine clips is always possible with experts within and beyond your clinic setting, medical institution, and even geography.
10. **Ultrasound is a "real-time" exercise where "practice makes perfect."** Many phrases have come to epitomize the mind-set of expert sonographers ("the ultrasound is an extension of the physical exam"; the "ultrasound is just like a stethoscope") or the phrase coined by the original editors of this textbook: **"Ultrasound**. **Just do it."** [12]. If you need to reexamine an area of the thyroid or the neck on initial ultrasound while the patient is still in your presence, you can pick up the transducer and repeat the exam. Surgeons have the privilege of the additional encounter with a patient in the operating room to repeat the ultrasound. Repetition creates mastery. Mastery in turn benefits your patients, your community of physicians, the education of future sonographers, and innovation and evolution of future ultrasound applications.

Conclusion

The field of thyroid and parathyroid endocrinology, radiology, and surgery continues to evolve and become more reliant on imaging to guide individually tailored patient management. Ultrasound has proven to be superior to CT, MRI, radioiodine, and sestamibi scans for imaging normal endocrine neck anatomy and for the diagnosis and guided interventions in diseased thyroid and parathyroid glands. Ultrasound provides real-time information to the clinician and functions as an extension of the physical exam. It avoids radiation and contrast agent exposures and is cost-effective. Ultrasound is an elegant and precise modality to examine the elegant anatomy of neck structures gently and effectively. The phenomenal and detailed image resolution allows sensitivity in detection of both obvious abnormalities and subtle nuances that guide clinical management options for thyroid and parathyroid disorders. Dedicated effort by physicians and sonographers to gain ultrasound expertise is a lasting and invaluable investment for exceptional patient care and exciting ultrasound innovations.

References

1. Milas M, Stephen A, Berber E, Wagner K, Miskulin J, Siperstein A. Ultrasonography for the endocrine surgeon: a valuable clinical tool that enhances diagnostic and therapeutic outcomes. Surgery. 2005;138(6):1193–201.
2. Haugen B, Alexander E, Bible K, Doherty G, Mandel S, Nikiforov Y, et al. 2015 American Thyroid Association management guidelines for adult patients with thyroid nodules and differentiated thyroid cancer: the American Thyroid Association guidelines task force on thyroid nodules and differentiated thyroid cancer. Thyroid. 2016;26(1):1–133.
3. Park S, Park S, Choi Y, Kim D, Son E, Lee H, et al. Interobserver variability and diagnostic performance in US assessment of thyroid nodule according to size. Ultraschall Med. 2012;33(07):E186–90.
4. Park C, Kim S, Jung S, Kang B, Kim J, Choi J, et al. Observer variability in the sonographic evaluation of thyroid nodules. J Clin Ultrasound. 2010;38:287–93.

5. Carneiro-Pla D, Solorzano C, Wilhelm S. Impact of vocal cord ultrasonography on endocrine surgery practices. Surgery. 2016;159(1):58–64.
6. American Institute of Ultrasound in Medicine; American College of Radiology; Society for Pediatric Radiology; Society of Radiologists in Ultrasound. AIUM practice guideline for the performance of a thyroid and parathyroid ultrasound examination. J Ultrasound Med. 2013;32:1319–29. http://www.Aium.Org/Resources/Guidelines/Thyroid.pdf
7. HK S, Dos Reis LL, Lupo MA, Milas M, et al. Striving toward standardization of reporting of ultrasound features of thyroid nodules and lymph nodes: a multidisciplinary consensus statement. Thyroid. 2014;24(9):1341–9.
8. Yuen HY, Tong CSL, Ahuja AT. Sonography of the normal thyroid. RA Sofferman, AT Ahuja, editors. Ultrasound of the thyroid and parathyroid glands. 41–59. Springer, Berlin 2012.
9. Choi SH, Kim EK, Kim SJ, Kwak JY. Thyroid ultrasonography: pitfalls and techniques. Korean J Radiol. 2014;15(2):267–76.
10. Nagarkatti SS, Mekel M, Sofferman RA, Parangi S. Overcoming obstacles to setting up office-based ultrasound for evaluation of thyroid and parathyroid diseases. Laryngoscope. 2011;121(3):548–54.
11. Arruti A, Poumayrac DM. Larynx ultrasonography: an alternative technique in the evaluation of the aero-digestive crossroad. Rev Imagenol. 2010;14(1):30–6.
12. Baskin HJ. Thyroid ultrasound-just do it. Thyroid. 2004;14(2):91–2.

Chapter 5
Pediatric Ultrasound of the Neck

Hank Baskin

Introduction

The spectrum of imaging abnormalities encountered during pediatric neck ultrasound extends well beyond the thyroid gland—both anatomically and conceptually—to include normal anatomic variants and embryologically derived pathologies that are less commonly seen in older patients. This chapter will briefly discuss an approach to scanning children's necks and then focus on the spectrum of abnormalities that may be encountered during pediatric neck ultrasound, first addressing embryologically derived pathology, normal variants, and non-thyroidal cervical abnormalities, before focusing on the appearance of specific diseases that involve the thyroid itself.

H. Baskin, MD, DABR
Pediatric Section, Intermountain Healthcare Imaging, Department of Radiology, University of Utah School of Medicine, Medical Imaging, Primary Children's Hospital, Salt Lake City, UT, USA
e-mail: hank.baskin@gmail.com

D.S. Duick et al. (eds.), *Thyroid and Parathyroid Ultrasound and Ultrasound-Guided FNA*,
https://doi.org/10.1007/978-3-319-67238-0_5

Patient Preparation

The key to successful pediatric neck lies in appropriate patient preparation. For a very young child, the procedure can be frightening. Understanding the child's perspective helps one prepare better for this examination and thus allows better diagnostic imaging.

Ideally, as with all pediatric medical care, an ultrasound should be performed in an environment that is welcoming and nonthreatening to children. Age-appropriate toys and, if available, child life specialists should be at hand to comfort the child. Newborns are especially soothed by ceiling projectors and warming pads on the scanning bed. Transducer gel warmers should be used to make the gel a comfortable temperature, and, if appropriate, the child should be offered a chance to feel the gel and transducer prior to the examination. If not actually performing the study, the interpreting physician should be closely involved in image acquisition so as to decrease the time that the child needs to stay still.

Ultrasound performed by the physician is also helpful because many pediatric neck abnormalities extend into the lateral neck, where children's small size and the complex regional anatomy can become quite confusing, and real-time scanning helps to better conceptualize any complex transspatial lesions. In addition to being skilled and experienced with imaging pediatric neck lesions, the interpreting physician should be knowledgeable as to when computed tomography (CT), magnetic resonance imaging (MRI), or scintigraphy would better elucidate a given abnormality. Moreover, they should be facile in correlating ultrasound abnormalities with findings made visible by other modalities; for example, a physician interpreting ultrasound should be able to anticipate how suspected blood products or fatty components of a lesion seen by ultrasound will manifest on CT and/or MRI so that they are able to confirm or exclude various diagnostic considerations. For these reasons, all pediatric neck ultrasound at our institution is performed or directly supervised by subspecialty-trained pediatric radiologists.

Finally, it is crucial to use a high-resolution, high-frequency (at least 15 MHz), linear-array transducer to best visualize the pediatric thyroid gland and cervical soft tissues. Unfortunately, traditional high-resolution transducers offered with most ultrasound packages are often too large to comfortably use on the very short necks of neonates and young infants. Likewise, infants and toddlers often have quite chubby chins and necks, and—because the thyroid lies relatively higher in the neck at this age—the transducer may not be able to obtain close contact with the skin. In these young children, the thyroid gland may be best imaged by a specialized small footprint probe, such as those used in neonatal echoencephalography; of course, the sonographer should be familiar with and experienced at using such probes.

Embryologically Derived Pathology

Embryology of the Thyroid Gland

The thyroid gland originates at the base of the tongue in an embryological structure known as the foramen cecum and then descends into the lower neck by way of the thyroglossal duct. As the developing gland descends into the lower neck, it divides into separate lobes connected to each other by an isthmus. After the thyroid gland reaches its final location—inferior to the hyoid bone and anterior to the trachea—the thyroglossal duct involutes. Aberrations of this normal development result in various forms of thyroid dysgenesis or thyroglossal duct remnants that one may encounter during pediatric neck ultrasound.

Congenital Hypothyroidism

Congenital hypothyroidism (CH) is relatively common, occurring in approximately 1 per 3000 births. It is classified as either transient or permanent; the transient form accounts for

20% of newborns with CH and occurs as a result of maternal iodine deficiency or secondary to in utero exposure to antithyroid drugs, maternal TSH-receptor antibodies, or very high levels of iodine. Permanent CH results from dyshormonogenesis, from autoimmune disease in the newborn, or from thyroid dysgenesis (aplasia, hypoplasia, or ectopy).

CH is the most easily treated form of developmental delay, and ultrasound is clinically useful to help differentiate its many causes. In patients with transient CH or with CH due to dyshormonogenesis or autoimmune thyroiditis, ultrasound will demonstrate an orthotopic thyroid gland; the gland may be normal sized in transient CH or enlarged in cases of dyshormonogenesis (Fig. 5.1) or autoimmune disease. If CH is secondary to thyroid dysgenesis, then ultrasound will demonstrate an absent or small thyroid gland.

Thyroid Aplasia

Thyroid aplasia presents with CH and an absence of any thyroidal tissue. The defect is usually sporadic, but there are some familial forms, and both autosomal dominant and autosomal recessive inheritance patterns have been reported. Neck ultrasound fails to reveal any thyroid tissue in the thyroid bed, and no uptake is seen with I-123 scintigraphy.

Thyroid Hypoplasia

Ultrasound in children with CH may sometimes demonstrate a small but otherwise normal-appearing thyroid gland (Fig. 5.2). This is particularly common in those children who have CH and trisomy 21 (children with trisomy 21 are also more likely to have small benign thyroid cysts) (Fig. 5.3). There are published charts of normal thyroid volumes for different populations, and these should be used to evaluate the size of the thyroid in children with hypothyroidism, congenital, or otherwise.

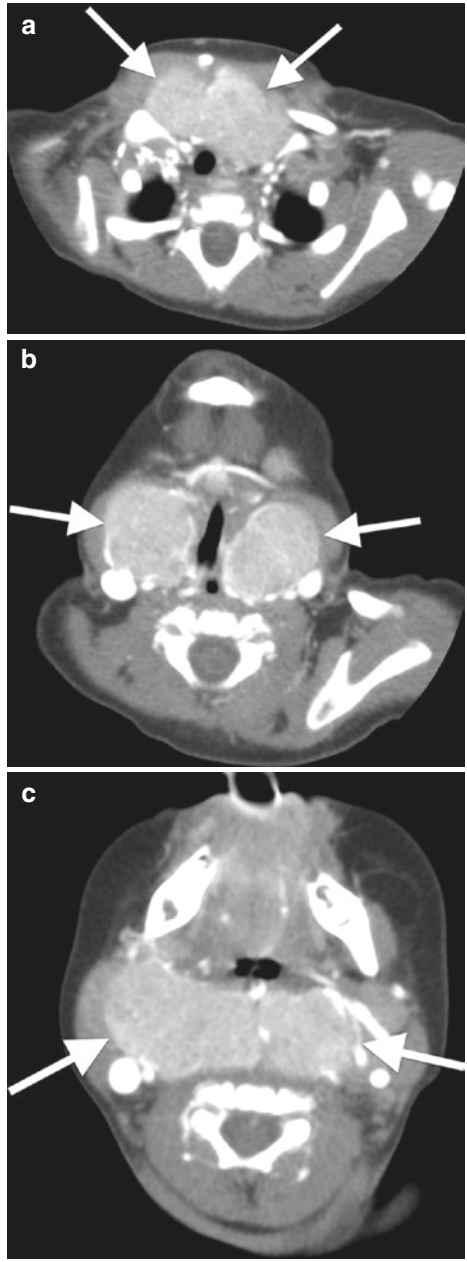

FIGURE 5.1 Goitrous thyroid in congenital hypothyroidism. Axial CT images (**a**–**c**) show a massively enlarged thyroid (*arrows*) in a 5-month-old with a TSH over 300. Full ultrasonic visualization of the thyroid gland is difficult in young children because of the overall short length of their necks compared to the size of most high-frequency transducers and because of the relatively high positioning of the thyroid gland in the neck compared to adults. This is best appreciated on sagittal CT images from the same patient, which well demonstrates the patient's short neck and how the path of least resistance for the thyroid to enlarge is posterior (*arrows*, **d**). On a 3D CT reconstruction (**e**), note how the thyroid gland (*arrow*) wraps around the airway (*asterisk*)

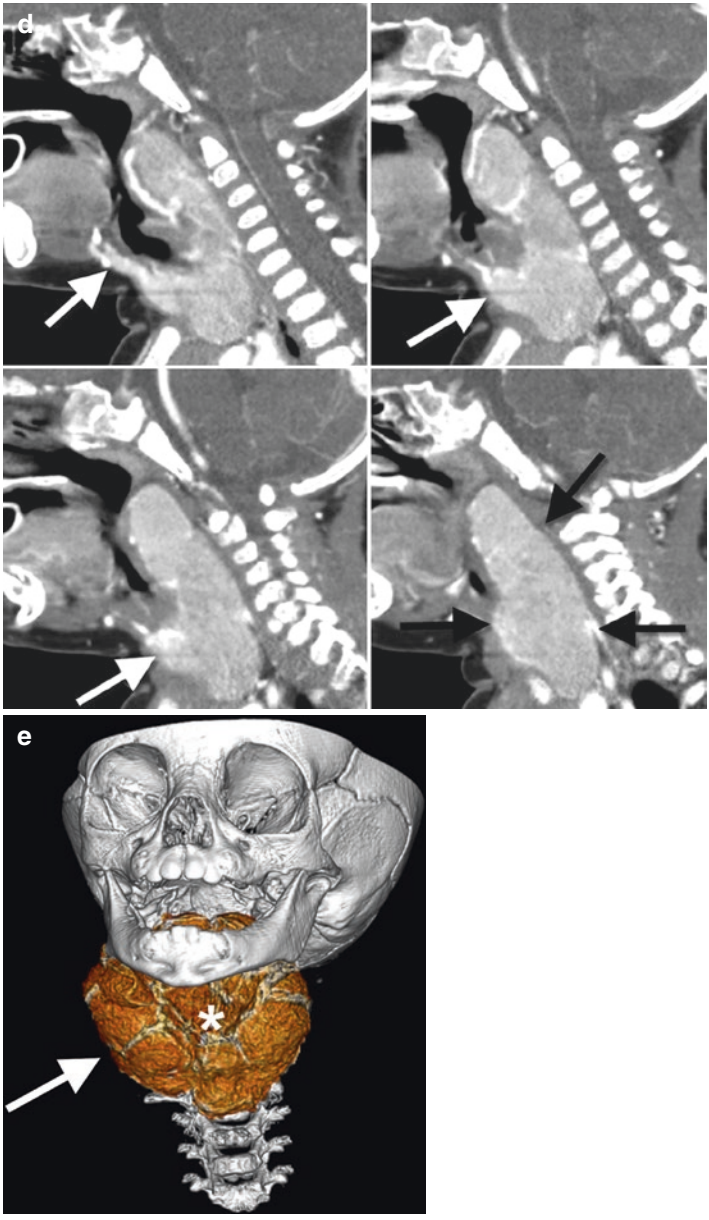

Figure 5.1 (continued)

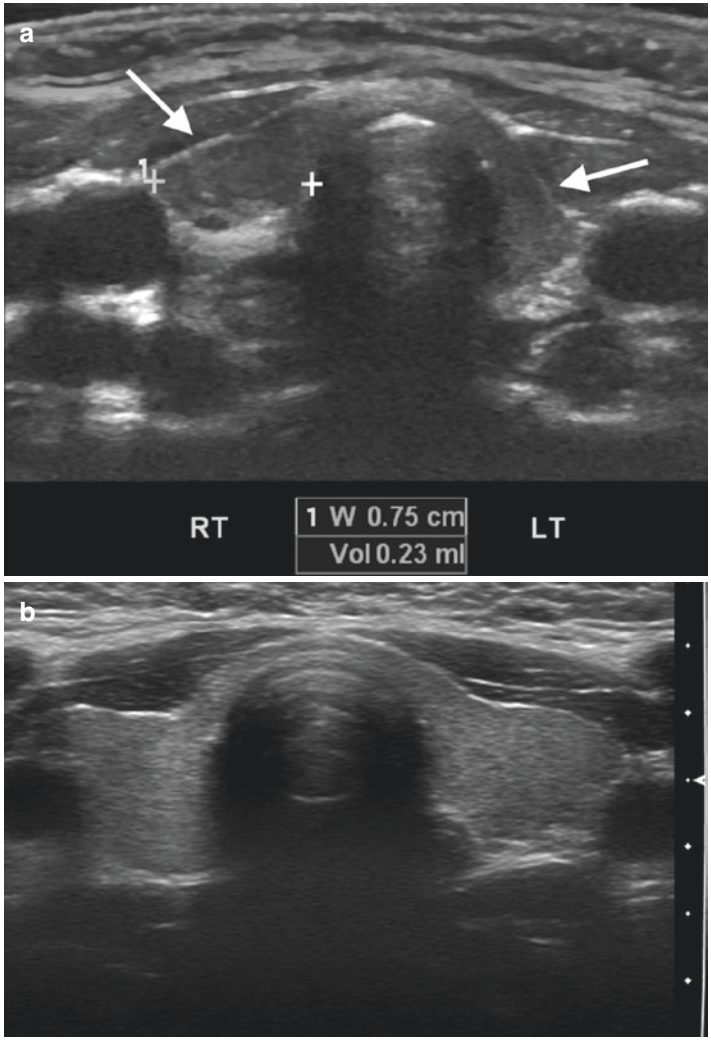

FIGURE 5.2 Thyroid hypoplasia. In thyroid hypoplasia (**a**), the gland is small and difficult to visualize; the right and left lobes may both be small (*arrows*; *left lobe measured*), and the isthmus may be relatively normal thickness, as shown in a patient with congenital hypothyroidism and trisomy 21. Compare this to the thyroid of a normal child (**b**), which is well-defined, normal volume, and well-proportioned

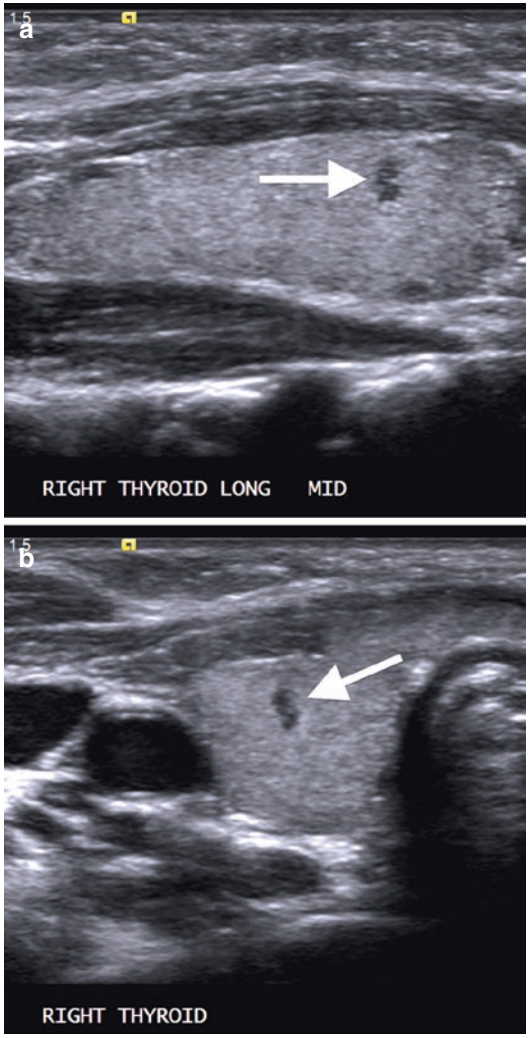

FIGURE 5.3 Benign thyroid cyst in trisomy 21. Longitudinal (**a**) and transverse (**b**) ultrasound images in a 26-month-old boy with trisomy 21 show the typical appearance of a very small hypoechoic cyst (*arrows*) seen in patients with Down syndrome. Note lack of significant posterior acoustic enhancement because these cysts are so small

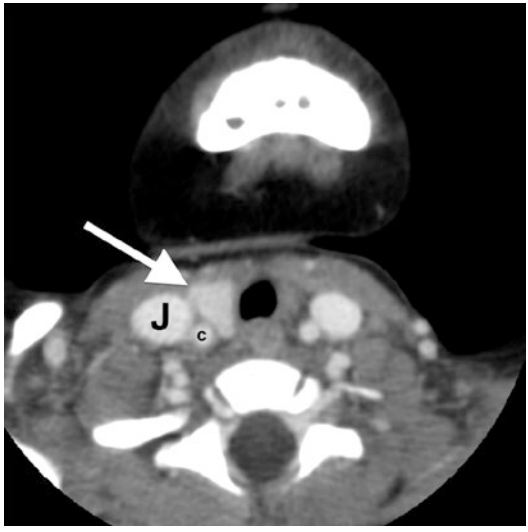

FIGURE 5.4 Left thyroid hemiagenesis. Axial CT image in a 26-month-old with a retropharyngeal abscess shows absence of the left lobe of the thyroid gland. The right lobe is shown with an arrow, and the right jugular vein (*J*) and carotid artery (*c*) are also annotated. Although not present in this child, patients with an absent left thyroid lobe usually have a small but blunted isthmus

Thyroid Hemiagenesis

Thyroid hemiagenesis is a rare congenital anomaly in which one lobe of the thyroid fails to form. It is the most innocuous form of thyroid dysgenesis and is much more common in girls. In hemiagenesis it is almost always the left lobe that is absent; the right lobe has a normal size and appearance, and, although blunted, the isthmus is usually present (Fig. 5.4). For unknown reasons, the isthmus will be absent in rare cases of right hemiagenesis (Fig. 5.5). Although hemiagenesis is considered an incidental finding, numerous studies have shown that these patients have a slightly increased rate of all forms of thyroid pathology, from hyperthyroidism to carcinoma. The diagnosis of thyroid hemiagenesis should be clearly communicated to the surgeon in patients who are to undergo any type of neck surgery.

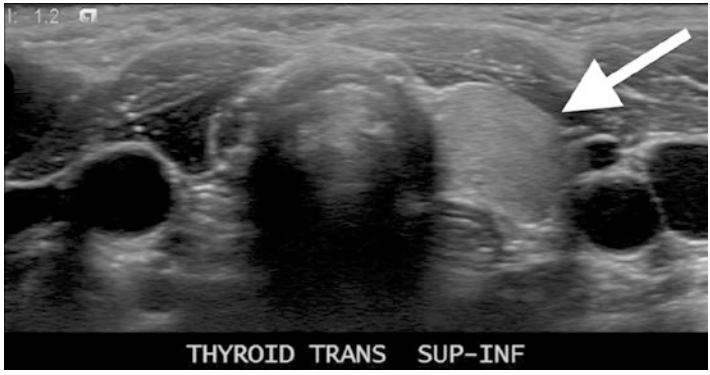

FIGURE 5.5 Right thyroid hemiagenesis. A transverse image of the thyroid reveals a normal left lobe (*arrow*) but no right lobe or isthmus. Right thyroid hemiagenesis is quite rare

Ectopic Thyroid

Ectopic, or aberrant, thyroid tissue can be found anywhere along the normal path of thyroid descent but is most commonly found at the base of the tongue, in which case it may be referred to as a lingual thyroid (Fig. 5.6). Ultrasound of the thyroid bed may reveal a hypoplastic thyroid or no thyroid tissue at all. Further imaging workup varies according to local preferences and practice; although I-123 scintigraphy is very sensitive for the presence of ectopic thyroid tissue, it fails to localize exactly where along the path from the base of the tongue to the inferior neck any potential aberrant thyroid tissue exists. Contrast-enhanced CT is especially helpful for the evaluation of thyroid ectopia because of its excellent spatial resolution and ability to provide multiplanar images, which best identify smaller rests of ectopic thyroid tissue (Fig. 5.7), or any potential thyroglossal duct remnants.

Thyroglossal Duct Cysts

The thyroglossal duct is a normally transient structure that involutes during fetal life; if it fails to do so, any remnants may slowly collect fluid and eventually manifest as a cystic neck

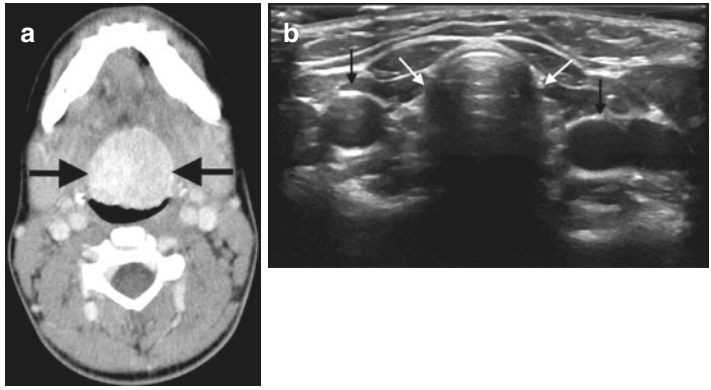

FIGURE 5.6 Lingual thyroid. An axial enhanced CT scan through the neck in a young child with hypothyroidism (**a**), a long-standing sensation of neck fullness, and tongue mass on radiographs show a clump of high attenuation thyroid tissue in the base of the tongue, known as a lingual thyroid. Ultrasound of the thyroid bed revealed no thyroid tissue in the expected location between the shadow of the tracheal air column (*white arrows*, **a**) and the carotid arteries (*black arrows*, **b**)

mass. Ninety percent of thyroglossal duct cysts (TGCs) present before age 10, and the typical history is a young child with a painless and compressible midline or paramidline mass. There is often a history of waxing and waning size, which occurs when there is irritation from recurrent upper respiratory tract infection or minor trauma. Sometimes TGCs become secondarily infected and present as an acutely painful, inflamed mass. If a TGC has not been complicated by prior infection or bleeding, then it appears as an anechoic cystic mass with increased through transmission and sharp, well-defined margins. They are usually spherical but may have tubular configuration (Fig. 5.8). About half are found at the level of the hyoid bone, a quarter above it, and another quarter below it; they should never be found below the level of the thyroid. If complicated by prior hemorrhage or infection, TGCs may have more echogenic contents, small septations, and a thickened, irregular margin; they occasionally appear solid (although should still cause increased through transmission) (Fig. 5.9). Complete surgical resection is needed, or TGCs will recur.

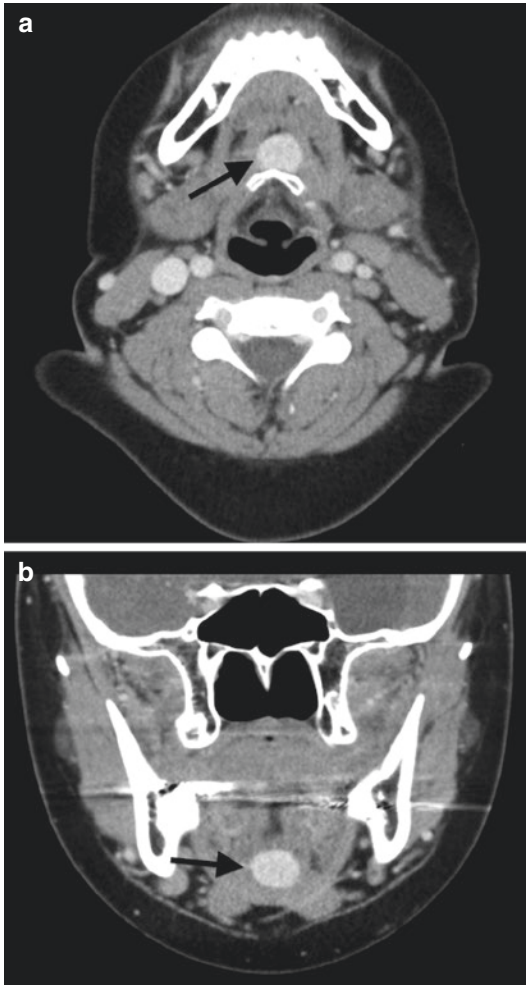

FIGURE 5.7 (**a**, **b**) Ectopic thyroid. Aberrant thyroid tissue may be found anywhere along the course of the thyroglossal duct, from the base of the tongue to the thyroid bed. Although scintigraphy is often espoused as the study of choice to identify ectopic thyroid tissue, it provides little spatial resolution. CT has the advantage of significantly better spatial resolution and the ability to provide multiplanar reconstructions, which can often better demonstrate rest of aberrant tissue, as shown in this patient with hypothyroidism, no thyroid tissue in the thyroid bed, and a small rest of aberrant thyroid (*arrows*) anterior to the hyoid bone

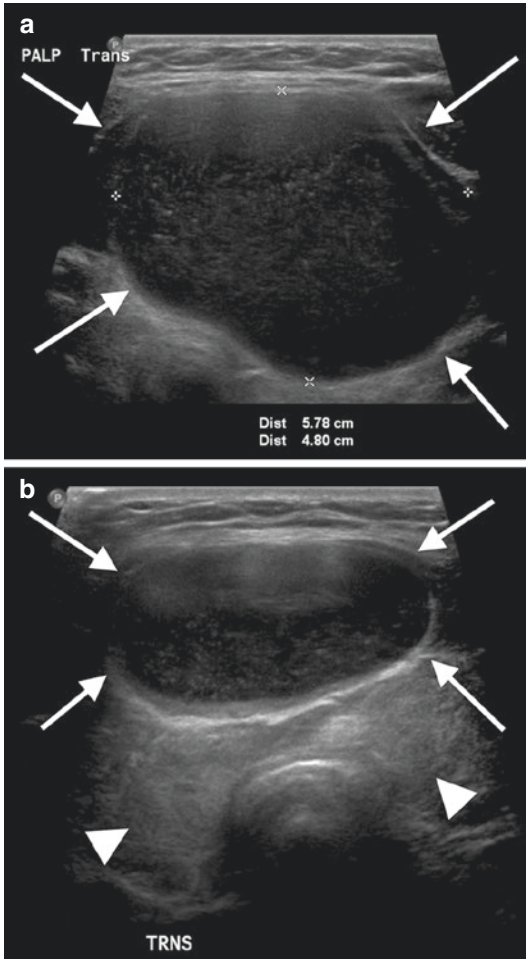

FIGURE 5.8 Thyroglossal duct cyst. An US was obtained on this teenager to evaluate a long-standing palpable thyroid mass. The mass turned out to be a thyroglossal duct cyst. Transverse US images show a predominantly anechoic cyst with scattered low-level echoes (*arrows*, **a** and **b**). This minimally complex thyroglossal duct cyst sits just above the level of the thyroid gland (*arrowheads*, **b**)

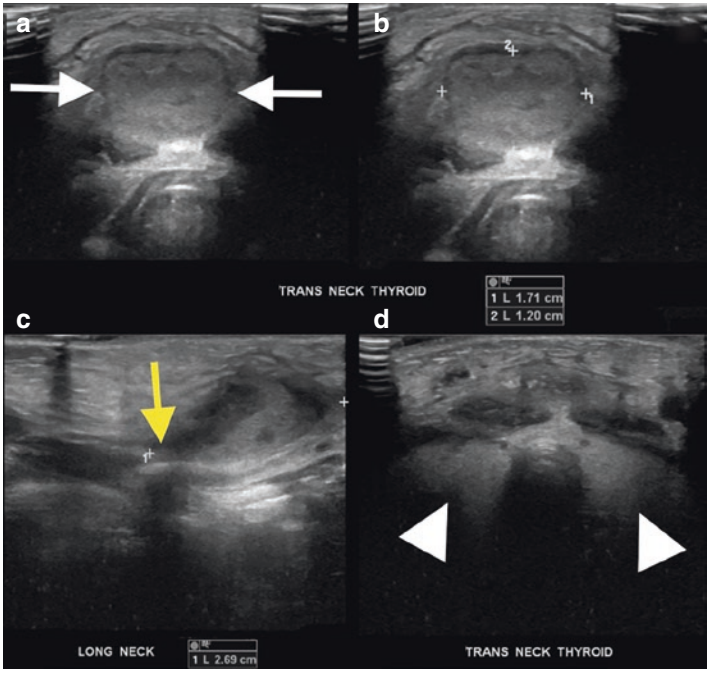

FIGURE 5.9 (**a**–**d**) Complex thyroglossal duct cyst. US was performed to evaluate a new painful thyroid mass in a 2-year-old boy. The images demonstrate that the mass is actually a heterogeneous, isoechoic cystic collection (*calipers and white arrows*) separate from the thyroid gland (*arrowheads*). This was an infected thyroglossal duct cyst; note its "tail" (*yellow arrow*) extending cephalad toward the tongue, reflecting this TGC's embryologic origins

Branchial Apparatus Anomalies

Another embryologic anlage that may cause pediatric thyroid abnormalities is the branchial apparatus. Branchial apparatus anomalies (BAAs) include a spectrum of epithelial-lined remnants that only involve the left lobe of the thyroid. Third and fourth BAAs may become infected and cause suppurative thyroiditis, abscess, cystic mass, or sinus tract to the

pyriform sinus; imaging depends on the specific patient's complication. Suppurative thyroiditis—which can be caused by a BAA or occur primarily—begins as a focal area of abnormally decreased echogenicity within the thyroid (Fig. 5.10). With worsening infection and abscess formation, a complex focal fluid collection may develop, usually with heterogeneous but hypoechoic internal contents; if caused by a BAA, a sinus tract may extend up into the deep neck toward the pyriform sinus. Such complications are best visualized by contrast-enhanced CT imaging (Fig. 5.11).

Inclusion Cysts

Small epidermal inclusion cysts are another common cause of palpable neck or "thyroid" masses in children. These cysts are characterized pathologically as either dermoids or epidermoids, both of which are benign congenital cysts derived from inclusion of ectodermic elements. On ultrasound, they appear as well-defined, avascular masses with internal echogenicity similar to the thyroid gland. The ultrasound findings of inclusion cysts are nonspecific (Fig. 5.12), but, because they contain dermal appendages, dermoids may have imaging characteristics identical to fat and therefore have a pathognomonic appearance on MRI and CT.

Vascular Malformations

Vascular malformations are a common cause of pediatric neck masses. Broadly speaking, these lesions are a group of nonneoplastic congenital malformations caused by disordered development of vascular channels. They are categorized by the predominant channel involved and are therefore termed either lymphatic, venous, venolymphatic, or arteriovenous malformations. They may range from predominately solid to mostly cystic masses. Although they often infiltrate the thyroid gland, vascular malformations usually extend into the lateral neck.

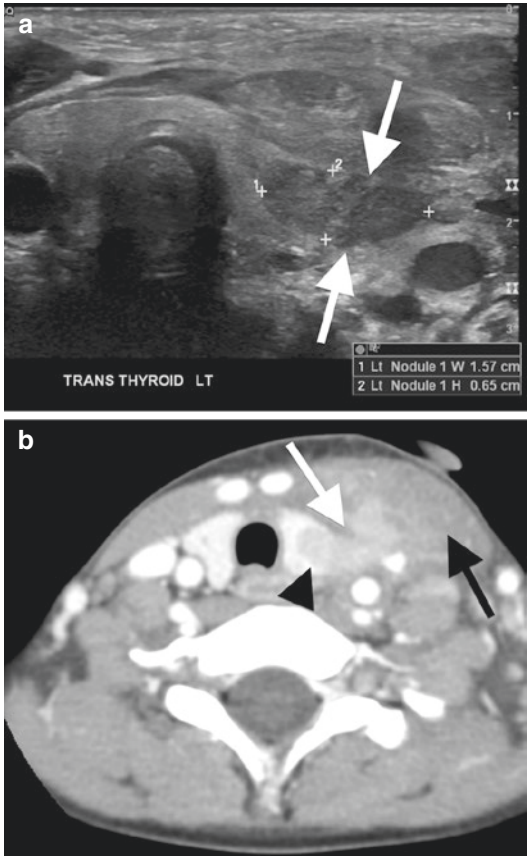

FIGURE 5.10 Fourth branchial apparatus anomalies. Suppurative thyroiditis in a 6-year-old boy with fever and neck pain. Embryologic remnants from the fourth branchial apparatus are almost always left-sided and may lead to any one of several abnormalities, from suppurative thyroiditis to a sinus track to infected cysts or abscesses. In this child, transverse US shows a well-defined, focal, heterogeneously hypoechoic nodule (*calipers*, **a**) extending through the thyroid capsule (*arrows*, **a**). Axial CT in the same patient also shows the focal area of suppuration in the upper pole of the left lobe (*arrowhead*, **b**) as well as more detail of the extracapsular extension (*white arrow*, **b**) and inflammation of the overlying strap musculature (*black arrow*, **b**)

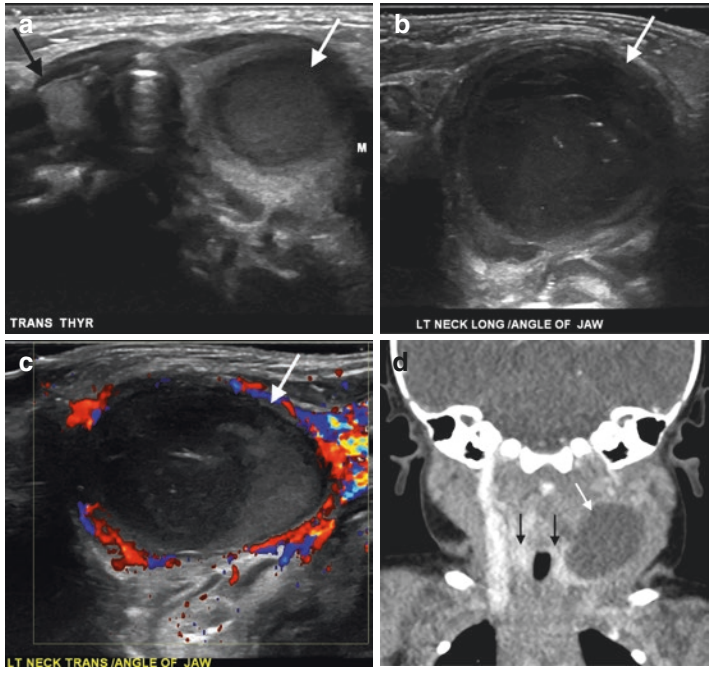

FIGURE 5.11 Branchial apparatus anomaly in a 10-day-old with 1 week of neck swelling and 1 day of fever. Transverse ultrasound shows a large, spherical lesion (*white arrow*, **a**) in the left lobe of the thyroid that is hypoechoic relative to normal thyroid tissue (*black arrow*, **a**). High-resolution, zoomed-in grayscale ultrasound shows the complex nature of the lesion (*arrow*, **b**), and color Doppler ultrasound reveals that it lacks internal blood flow (*arrow*, **c**), suggesting that this is a complex fluid collection rather than a solid mass. A coronal CT better characterizes the relationship of this large lesion (*white arrow*, **d**) with respect to the remainder of the neck and thyroid gland (*black arrow*, **d**). At microlaryngoscopy, this lesion was shown to have a small fistulous tract to the pyriform sinus, typical for an infected third BAA cyst

Lymphatic malformations are usually trans-spatial, multicystic masses with numerous fluid–fluid levels (as a result of prior hemorrhage or infection) (Fig. 5.13). If predominately microcystic, lymphatic malformations may appear solid on ultrasound.

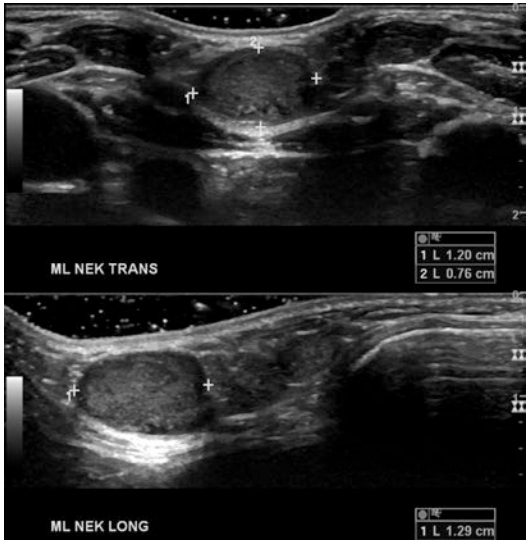

Figure 5.12 Epidermal inclusion cyst. Transverse and longitudinal US images show a well-defined isoechoic nodule (*calipers*) in the subcutaneous soft tissues of the infrahyoid midline neck, just above the thyroid gland. Images are characteristic, but not diagnostic, of an epidermal inclusion cyst; tissue diagnosis is needed and in this case confirmed the diagnosis of dermoid

Venous malformations generally appear as a lobulated, hyperechoic soft tissue mass that may contain phleboliths (which cause posterior acoustic shadowing) (Fig. 5.14). CT and MRI are very useful to demonstrate enhancement of the solid components of these lesions and are much better than ultrasound for delineating the entire extent of disease; these modalities usually help provide a confident diagnosis without biopsy.

Infantile Hemangioma

Unfortunately, the adult medical literature is littered with reports of masses related to the thyroid (and elsewhere in the body) that are inaccurately classified as a "hemangioma." These

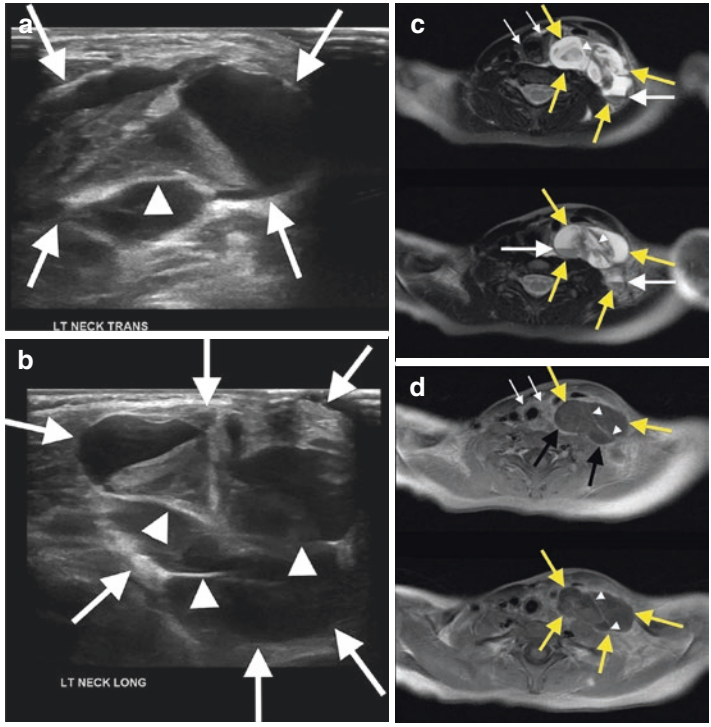

FIGURE 5.13 Lymphatic malformation. Transverse (**a**) and longitudinal (**b**) neck ultrasound in a 3-year-old boy with new swelling near the thyroid gland reveals a very complex, trans-spatial, multiloculated fluid collection (*white arrows*, **a** and **b**) extending from the region of the thyroid (not shown) into the left lateral neck. Note the presence of thin septations (*arrowheads*, **a** and **b**), typical of macrocystic lymphatic malformations. Two axial fluid-sensitive sequence MR images (**c**) better show the internal characteristics of this complex cystic lesion (*yellow arrows*) as well as its relationship regional structures, including the thyroid gland (*small white arrows*, upper image). Again, note numerous thin septations (*arrowheads*) and fluid–fluid levels (*large white arrows*) from prior internal hemorrhage. Two contrast-enhanced MR images (**d**) show that the lesion (*yellow arrows*) does not enhance, supporting the diagnosis of lymphatic malformation. The thin septations (*arrowheads*) are again well seen, as are regional soft tissues, including the thyroid gland (*small white arrows*, upper image)

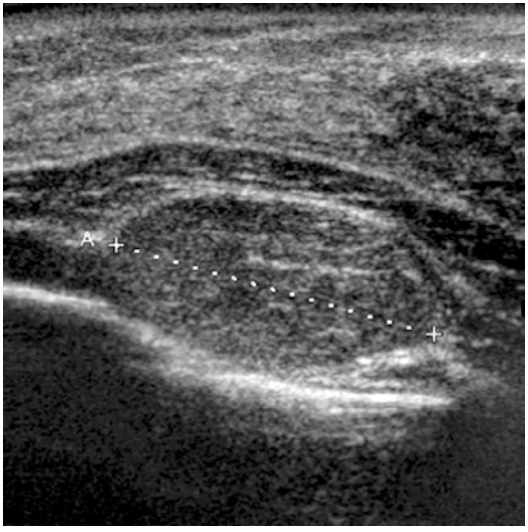

FIGURE 5.14 Venous malformation. A longitudinal US image shows a well-defined, hypoechoic neck mass (*calipers*) in a 14-year-old girl. This appearance is nonspecific, and excisional biopsy is mandatory to exclude a soft tissue sarcoma; biopsy in this case revealed a venous malformation

masses are in fact venous malformations and should be referred to as such. True infantile hemangiomas are benign neoplasms seen exclusively in young children. They also follow a very predictable natural history: they develop in early infancy, proliferate during the first year of life, and involute shortly thereafter. They may be seen near the thyroid gland, but, unlike the aforementioned malformations, infantile hemangiomas are never seen in older children and adults. Infantile hemangiomas should not be confused with other lesions and are treated conservatively.

Thymic Tissue

The thymus is also derived from the branchial apparatus and, like the thyroid, descends into the neck early during fetal life. The two lobes of the thymus course behind the thyroid and

sternocleidomastoid muscles and fuse at the level of the aortic arch, but occasionally a portion of the thymus will extend into the upper neck and may be visible on thyroid ultrasound. Knowledge of its normal appearance helps avoid any diagnostic dilemma. In younger children, the thymus is hypoechoic with an echotexture similar to that of the liver (Fig. 5.15). As children grow, the thymus becomes infiltrated with fat, which accentuates its internal septations, and gives it a pattern sometimes referred to as a "starry sky" appearance. The thymus gland should never cause mass effect or displacement of vessels or other structures. On real-time imaging, the thymus gently pulsates with cardiac motion.

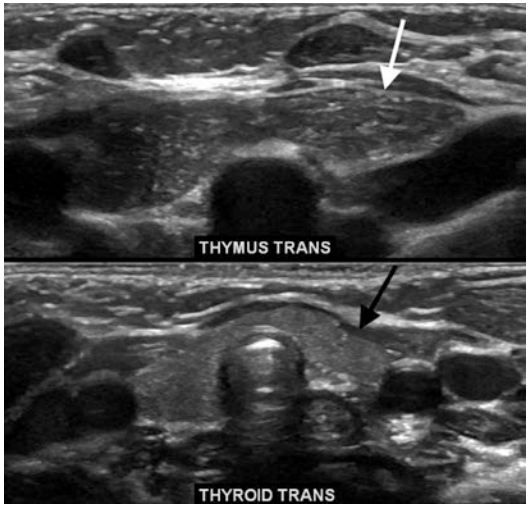

Figure 5.15 Normal thymus tissue. The thymus may extend well into the neck in younger children and may be confounding when unexpectedly seen on ultrasound. One should be suspicious that midline or paramidline tissue is actually extension of normal thymus if such tissue has an aberrant echotexture or unusual shape. In these images from the same 5-month-old who presented with a palpable suprasternal mass, note how the normal thymus (*white arrow*) is more hypoechoic and less well-defined in shape compared to the normal thyroid gland (*black arrow*)

Diffuse Thyroid Diseases

Hashimoto thyroiditis is by far the most common diffuse thyroid abnormality seen in children. Early changes almost always involve the posterior portion of the gland, first manifesting as subtle coarsening of the normally smooth, homogeneous echotexture in the deeper part of the gland. As thyroiditis progresses, the posterior portion of the gland will develop very small (1–2 mm) round or oval areas of hypoechogenicity. Eventually these subtle sonographic abnormalities progress to involve the entire gland, and over several years (or with particularly pernicious disease, even sooner), the entire thyroid becomes increasingly heterogeneous (Fig. 5.16). Although these abnormalities are almost always present in children with Hashimoto thyroiditis, these sonographic features may at first

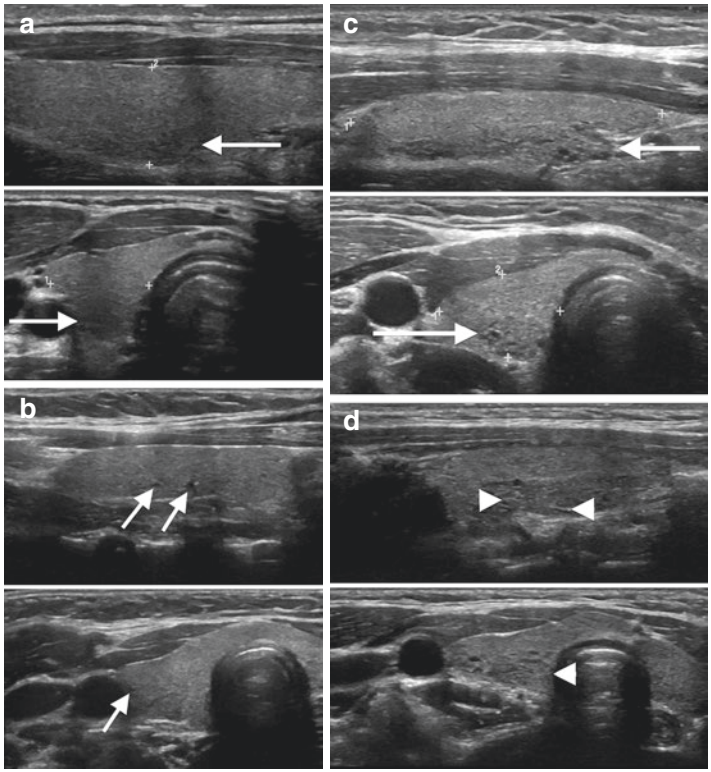

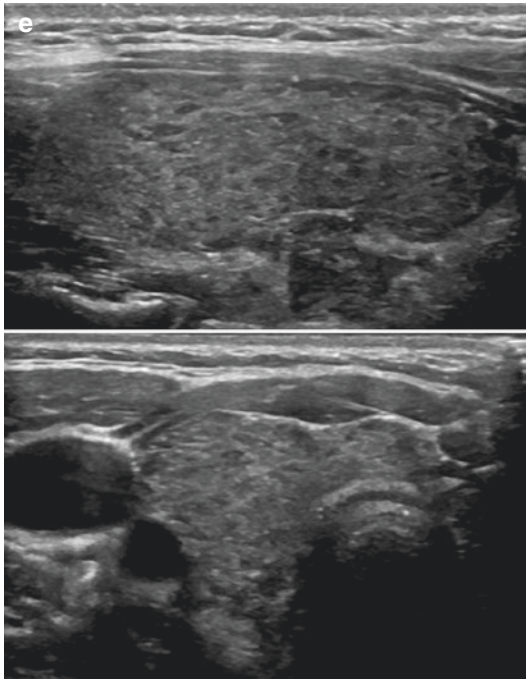

FIGURE 5.16 (continued)

FIGURE 5.16 Ultrasound findings in five children with thyroiditis of increasing severity. (**a**) 17-year-old boy: There is subtle coarsening of the thyroid echotexture in the posterior portion of the gland (*arrows*). (**b**) 13-year-old boy: In addition to mild coarsening, there are a few oval hypoechoic foci (*arrows*) in the posterior portion of the gland. (**c**) 12-year-old boy: The posterior gland has become progressively more heterogeneous (*arrows*), losing the smooth echotexture that characterizes the normal thyroid. (**d**) 7-year-old girl: Numerous thin, echogenic septations (*arrowheads*) have become visible within the area of coarse echogenicity. (**e**) 13-year-old girl: The whole gland now has a coarse, heterogeneous echotexture with thin septations and innumerable small hypoechoic foci visible throughout

be quite subtle, and therefore it is important to use a high-resolution transducer to achieve adequate image resolution.

With chronic Hashimoto disease, the thyroid develops coarse, thickened septa that appear on ultrasound as branching, echogenic reticulations that form conspicuous rounded or oval foci of relatively hypoechoic thyroid tissue, small lesions known as pseudonodules (Fig. 5.17). It is this pattern of coarse reticular echoes and pseudonodules that becomes the dominant ultrasound feature in children with severe or chronic thyroiditis (Fig. 5.18).

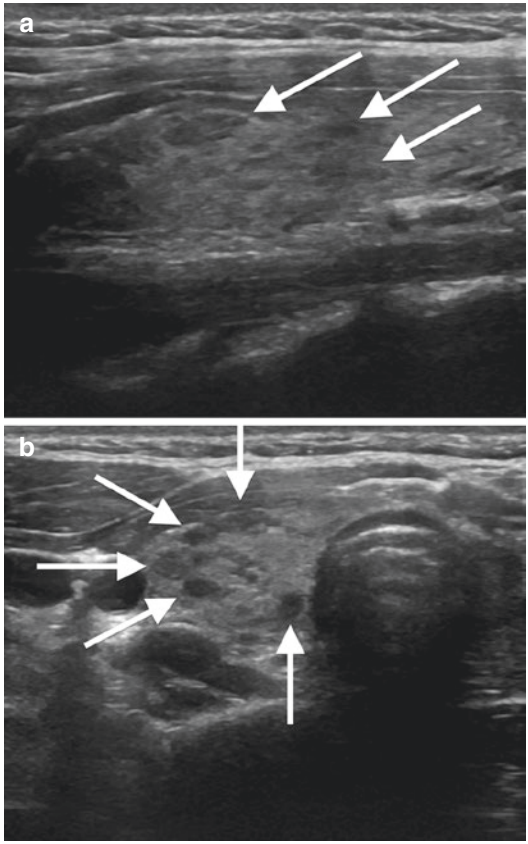

FIGURE 5.17 Pseudonodules. Longitudinal (**a**) and transverse (**b**) US in a 14-year-old girl with chronic Hashimoto disease show innumerable rounded and oval hypoechoic foci known as pseudonodules (*arrows*)

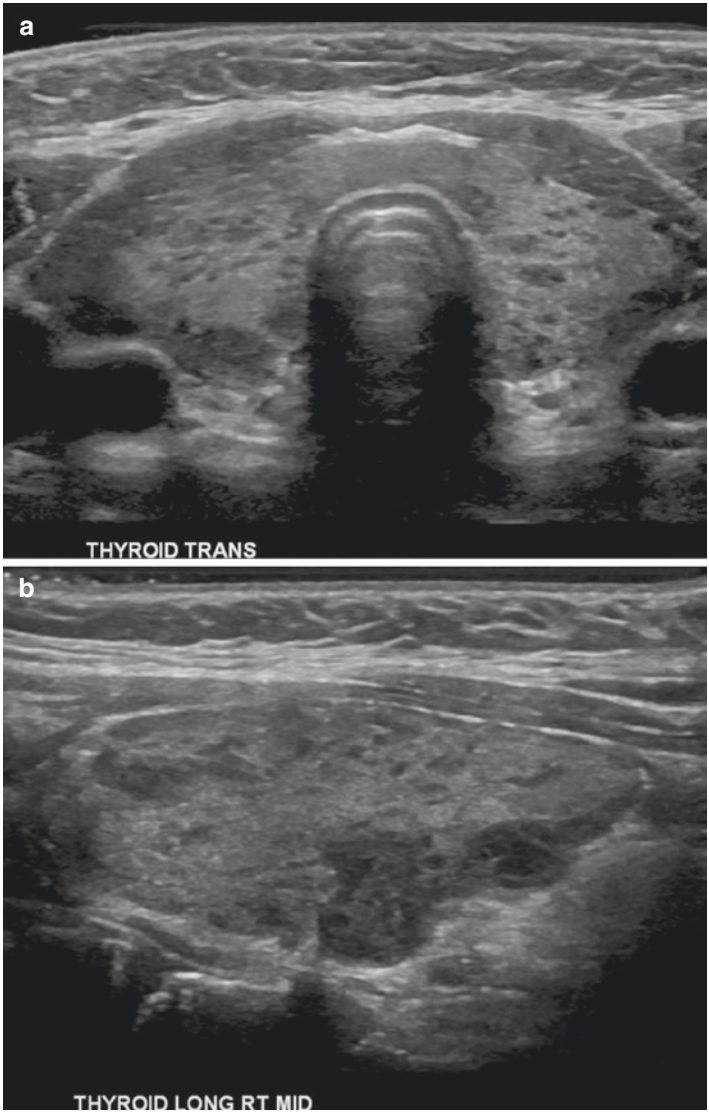

FIGURE 5.18 Chronic Hashimoto disease. Transverse (**a**) and longitudinal (**b**) US in a 12-year-old boy show the typical appearance of chronic Hashimoto disease: a diffuse pattern of coarse reticular echoes and pseudonodules throughout the gland

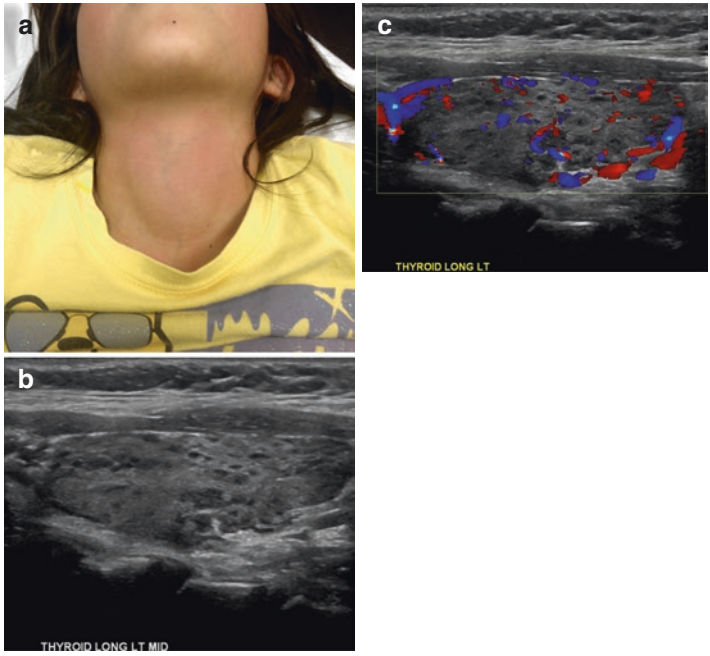

FIGURE 5.19 Thyromegaly. Photograph (**a**) of a 9-year-old girl with severe thyroiditis shows marked enlargement of the thyroid gland. Grayscale (**b**) and color Doppler (**c**) images show the typical pattern of severe thyroiditis with innumerable pseudonodules. The gland is hyperemic and enlarged, with a volume over twice the upper limits of normal for her age

Severe thyroiditis—especially early on—may cause diffuse enlargement of the gland, sometimes accompanied by marked hyperemia visible with power Doppler (Fig. 5.19). These changes are generally not, but may be, encountered in chronic disease. Also, unlike the early grayscale findings described earlier, increased Doppler flow seen in Hashimoto thyroiditis is often inhomogeneous and has no predictable pattern, sometimes sparing large swaths of the gland (Fig. 5.20).

One should not expect thyroid ultrasound to offer specificity with regard to other diffuse thyroid diseases; there are no

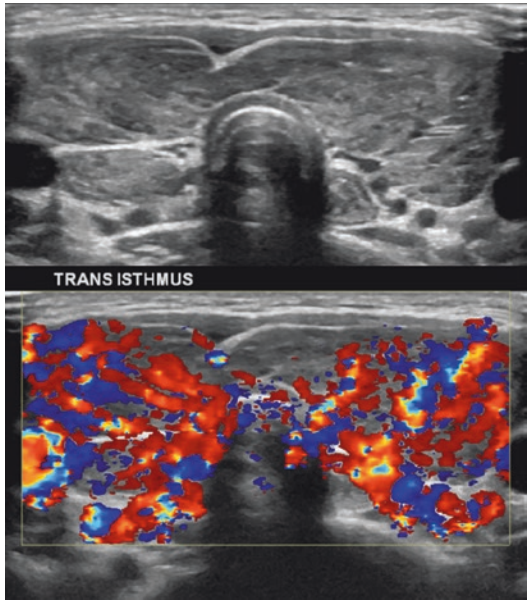

FIGURE 5.20 Thyromegaly and hyperemia. Grayscale and color Doppler US images demonstrate diffuse thyroid enlargement and typical findings of severe thyroiditis. Note the diffuse, but inhomogeneous, pattern of hyperemia

imaging features that accurately suggest alternative diagnoses such as Graves' disease or nodular hyperplasia (both of which are far less common than Hashimoto thyroiditis in children) (Fig. 5.21). The clinical usefulness of ultrasound in the evaluation of children with Hashimoto thyroiditis lies in the identification of the very early grayscale abnormalities described earlier. In children, these subtle findings can suggest the diagnosis well before thyroid antibodies become positive.

Other important ultrasonic findings to be cognizant of in children with thyroiditis are the potential of associated lymphoma (which may cause regional lymphadenopathy) or the presence of a dominant nodule (which may represent a superimposed adenoma or thyroid malignancy).

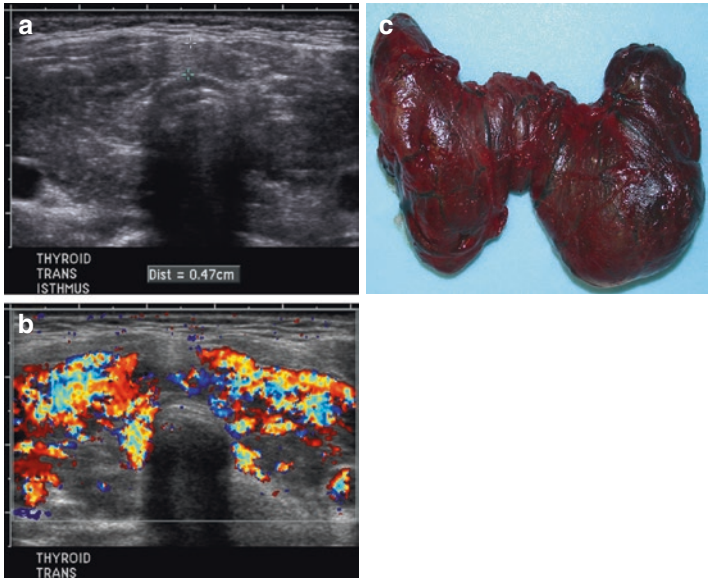

FIGURE 5.21 Graves' disease. US cannot reliably differentiate between Hashimoto thyroiditis and Graves' disease in children. Grayscale (**a**) and color Doppler (**b**) US images in a 16-year-old girl with Graves' disease show sonographic features similar to those seen in Hashimoto thyroiditis, including diffuse enlargement and coarsening of the echotexture and echogenic septations. (**c**) A gross pathologic photograph of the thyroid from the same patient

Focal Thyroid Lesions

Focal thyroid nodules and masses are rare in children, accounting for less than 2% of pediatric thyroid diseases. Thyroid cancer in this age group is rarer still, occurring in less than 2 per 100,000 children. There are no specific imaging features unique to pediatric thyroid nodules, and any dominant lesion should be biopsied as discussed in other chapters of this book.

The vast majority of pediatric thyroid nodules are benign, the most common diagnosis being benign follicular adenoma. Adenomas may have variable echogenicity, ranging from

mostly solid (Fig. 5.22) to mostly cystic (Fig. 5.23) masses. Other common benign thyroid lesions seen in children include colloid cysts and cystic degenerating or hemorrhagic nodules (Fig. 5.24).

Like in adults, papillary carcinoma is the most common thyroid neoplasm in the pediatric age group. Unfortunately, it tends to behave more aggressively than in adults, with higher rates of multifocality, neck lymph node disease, and extracapsular extension (Fig. 5.25). Other malignancies that may be seen include follicular carcinoma, medullary carcinoma, papillary oncocytic neoplasm, and metastatic disease, none of which have any specific imaging features.

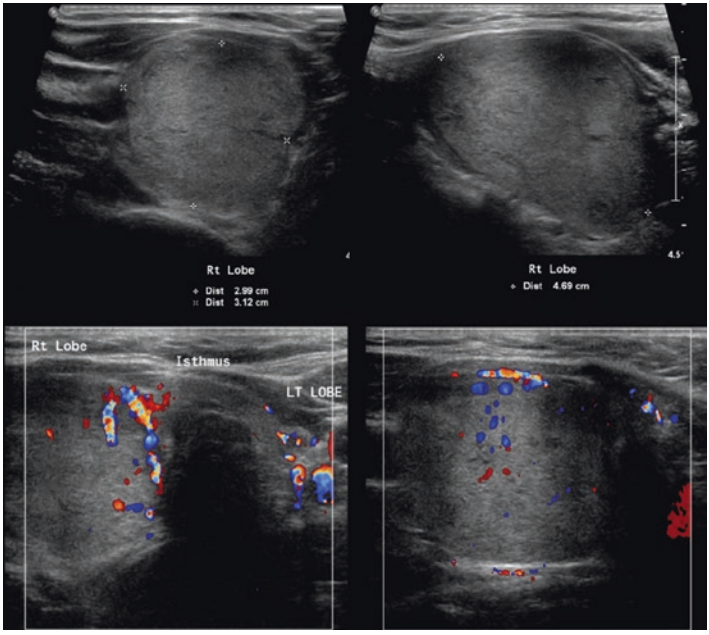

Figure 5.22 Follicular adenoma. Imaging features of thyroid neoplasms are not specific. The most common thyroid neoplasm in children is benign follicular adenoma, which may range from completely solid to mostly cystic. Here, grayscale and color Doppler US images show a large, well-defined mass (*calipers*) in the right lobe of the thyroid of a 12-year-old boy with follicular adenoma

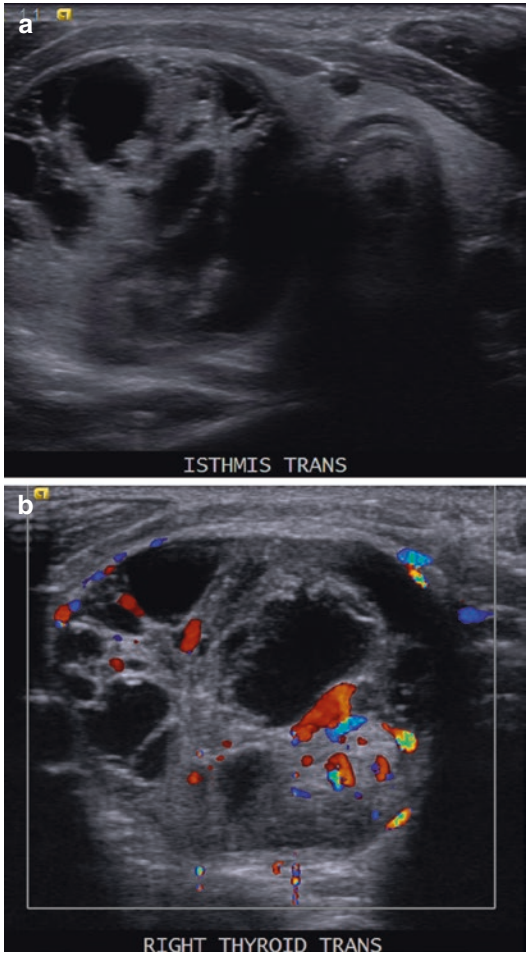

FIGURE 5.23 Follicular adenoma. Transverse grayscale (**a**) and color Doppler (**b**) US images in a 17-year-old boy show an example of a mostly cystic follicular adenoma

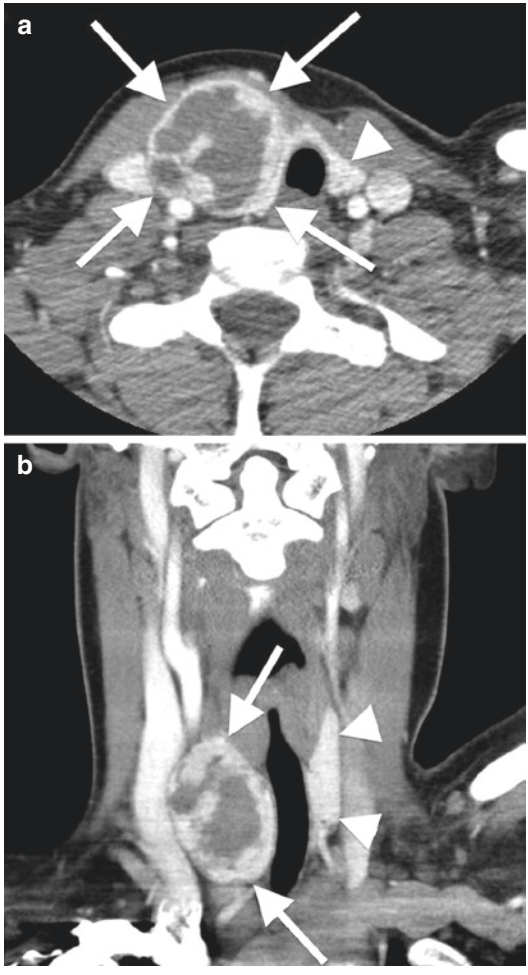

FIGURE 5.24 Degenerating nodule. Axial (**a**) and coronal (**b**) enhanced CT in a 11-year-old boy with a long-standing thyroid mass show a nonspecific, partially enhancing cystic mass (*arrows*) found to be a degenerating nodule on pathology. Note the normal left thyroid lobe (*arrowheads*)

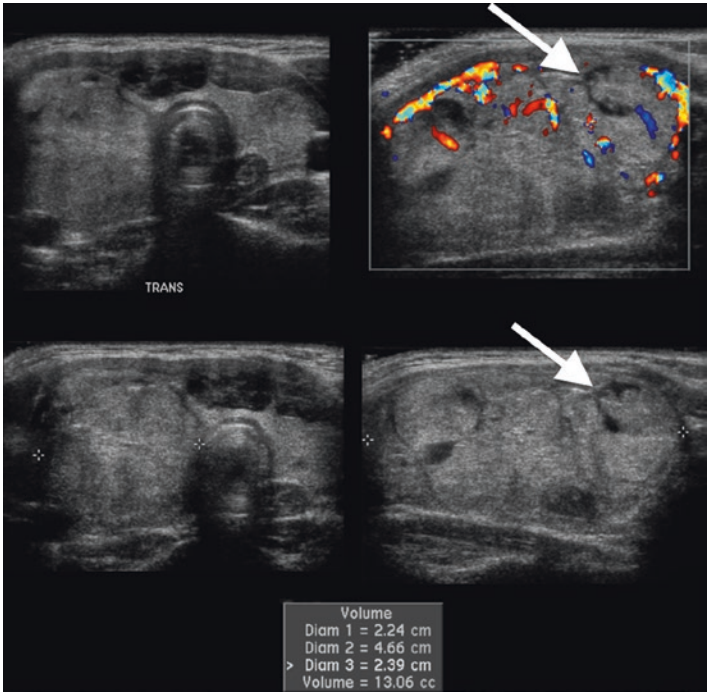

FIGURE 5.25 Papillary carcinoma. Transverse (*top left & bottom left*) and longitudinal color Doppler (*top right*) and grayscale (*bottom right*) US images show a large, heterogeneous, multilobulated mass (*calipers*) almost replacing the entire right lobe of the thyroid in a 12-year-old boy. There is focal extracapsular extension (*arrows*) of this papillary carcinoma

Summary

The most important concepts to remember about pediatric thyroid ultrasound can be distilled into two points. The first is that one must keep an open mind about what ultrasound of a "thyroid mass" may actually reveal in a child. The complex embryologic development of neck can result in disparate, but

predictable abnormalities that are, in fact, separate from the thyroid gland itself and the interpreting physician must be familiar with how to best diagnose these abnormalities, especially when further workup involves the use of other imaging techniques.

The second important concept to remember when performing pediatric thyroid ultrasound is that early thyroiditis may be quite subtle and often precedes the clinical detection of antithyroid antibodies in children. When imaging children with thyroiditis, one should be highly sensitive to subtle abnormalities seen in early disease. In children with chronic thyroiditis, the focus should be on the identification of any dominant nodule or regional lymphadenopathy. The sonographic approach and features of focal thyroid nodules in children are not unique, and the other chapters of this text cover these topics in excellent detail.

Chapter 6
Diffuse Thyroid Disease (DTD) and Thyroiditis

Stephanie L. Lee

Introduction

Ultrasound (US) of the thyroid is well established as the most sensitive imaging test available for the examination of the thyroid gland to (1) establish the size of the thyroid, (2) detect and characterize lesions, (3) identify the diffuse characteristics suggesting disease such as thyroiditis, (4) determine vascular flow using color flow Doppler imaging (CDI), and (5) characterize anatomic variations such as a pyramidal lobe, thyroglossal duct masses, and tubercle of Zuckerkandl (Table 6.1). Thyroid US is able to confirm the presence of a thyroid nodule and differentiate between non-nodular thyroid enlargement (goiter and cervical masses of other origins. This chapter will focus on non-nodular diffuse thyroid disease (DTD) including simple goiter, adenomatous goiter, and thyroiditis

S.L. Lee, MD, PhD, FACE, ECNU
Section of Endocrinology, Diabetes and Nutrition,
Thyroid Health Center, Boston Medical Center,
Boston, MA, USA
e-mail: stlee@bmc.org

D.S. Duick et al. (eds.), *Thyroid and Parathyroid Ultrasound and Ultrasound-Guided FNA*,
https://doi.org/10.1007/978-3-319-67238-0_6

Table 6.1 US examination for diffuse thyroid disease

Thyroid gland	Characteristic
Size	Measure sagittal × AP × transverse dimensions
Unusual shape	Note and measure extension of lobe(s) below clavicles, pyramidal lobe, and thyroglossal duct masses
Echotexture	Homogeneous or heterogeneous
Echogenicity	Compare to strap muscles: hypoechoic, isoechoic, hyperechoic (normal echogenicity is simlar to the submandibular gland)
Vascular pattern	Increased, decreased, or normal by Doppler analysis, note if vascular flow outlines isoechoic nodule
Calcification	Note clusters of microcalcification, macrocalcification, or disrupted eggshell calcification

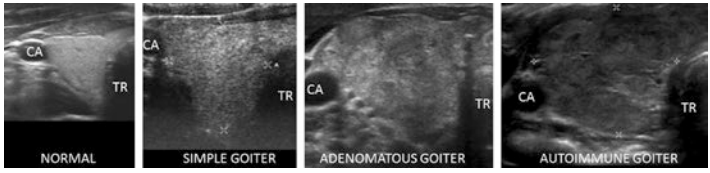

Figure 6.1 Normal thyroid and diffuse thyroid disease (DTD) goiters. Right transverse view. (**a**) Normal size and echotexture. (**b**) Simple goiter with mildly heterogeneous echotexture. (**c**) Adenomatous goiter with heterogeneous echotexture. (**d**) Autoimmune goiter with thyroiditis. *CA* carotid artery, *TR* trachea

(Fig. 6.1). The evaluation of nodular thyroid disease can be found in Chap. 7.

Diffuse and Adenomatous Goiter

Any nonmalignant increase in the size of the thyroid above normal is referred to as a goiter [1]. Thyroid size, shape, and volume vary with age, gender, and iodine sufficiency. The normal thyroid

volume for a male (14 mL) is larger than a female (12 mL). The normal dimensions of an adult thyroid are 40–60 mm longitudinal and 13–18 mm in AP diameter. A practical measurement of the thyroid >2 cm in the AP or transverse dimensions or >5 in the longitudinal measurement is considered be enlarged. The characteristic of the thyroid enlargement may be diffuse or nodular. Non-thyroiditis DTD includes simple goiter, adenomatous goiter, and infiltrative disease (amyloid and iron deposition). The causes of simple goiter are multifactorial and involve interactions between genetics, gender (female > male), environmental (iodine intake), pregnancy, and other factors [2, 3]. The most common cause of thyroid enlargement worldwide is iodine deficiency [4, 5]. Insufficient iodine intake reduces thyroid hormone output that stimulates follicular epithelium compensatory hypertrophy and polyclonal follicles hypertrophy and results a simple goiter. There is continued goiter growth in an attempt to maintain a euthyroid state. The alternating follicular growth, hemorrhagic degeneration, and scarring over the course of growth result in the development of nodular thyroid disease [3].

Conventional B Mode Gray-Scale Ultrasound

The normal thyroid examined by ultrasound shows the parenchyma to be finely granulated (ground-glass appearance), and the echogenicity is similar to the salivary glands but of higher echogenicity compared to the adjacent strap muscles or sternocleidomastoid muscle [6] (Figs. 6.1a, b and 6.2). The individual nodules that can be seen on histopathology of a sonographic simple goiter (Figs. 6.1 and 6.2) or adenomatous goiter (Fig. 6.3) are difficult to distinguish on B mode US because the echotexture of the nodules are similar to the normal thyroid parenchyma and the nodules have incomplete capsules. This results in an ultrasound image that shows thyroid enlargement with minimal parenchymal heterogeneity without distinct nodules and is described as a simple goiter on US (Fig. 6.2). An enlarged thyroid with more parenchymal heterogeneity with variable amounts of cystic degeneration, vascular flow, and dystrophic or eggshell

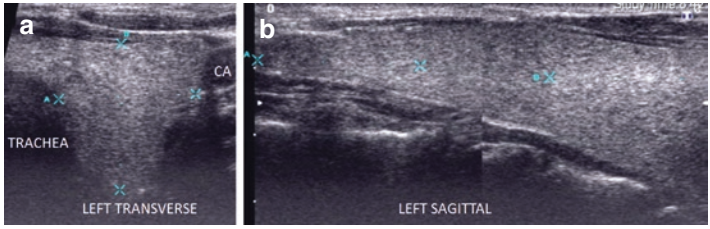

Figure 6.2 Simple goiter. The echotexture is minimally heterogeneous without discrete nodules. The thyroid is enlarged and measures 6.5 × 2 × 2.5 cm (sagittal × AP × transverse) in a small 50 kg female. *CA* carotid artery. (**a**) Left transverse view. (**b**) Left sagittal view

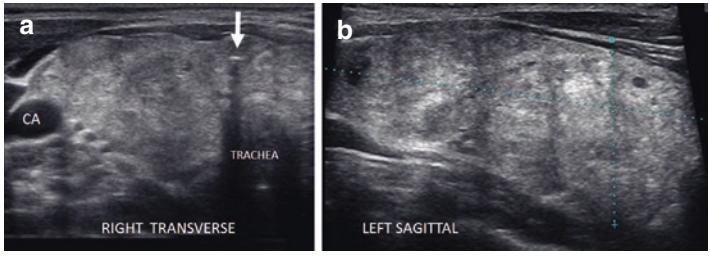

Figure 6.3 Adenomatous goiter. The echotexture is heterogeneous with confluent isoechoic nodules. Examining the individual nodular areas in transverse and sagittal dimensions, a discrete nodule could not be seen due to either the confluence of nodules or the lack of a complete capsule in adenomatous nodules. The thyroid is enlarged and measures 7.1 × 2.6 × 3.2 cm (sagittal × AP × transverse) in an 80 kg female. *CA* carotid artery. (**a**) Right transverse view. (**b**) Right sagittal view. Dystrophic macrocalcification in the isthmus (*arrow*)

calcification but without a distinct nodule is called an adenomatous goiter on US imaging (Fig. 6.3). By definition, simple or diffuse adenomatous goiters do not have sonographically distinct nodules that can be assessed for the risk of malignancy by the AACE [7] and ATA [8] nodule guidelines. The overall size of the enlarged thyroid (sagittal × AP × transverse measurements) and the absence of high-risk nodules should be noted in the US report.

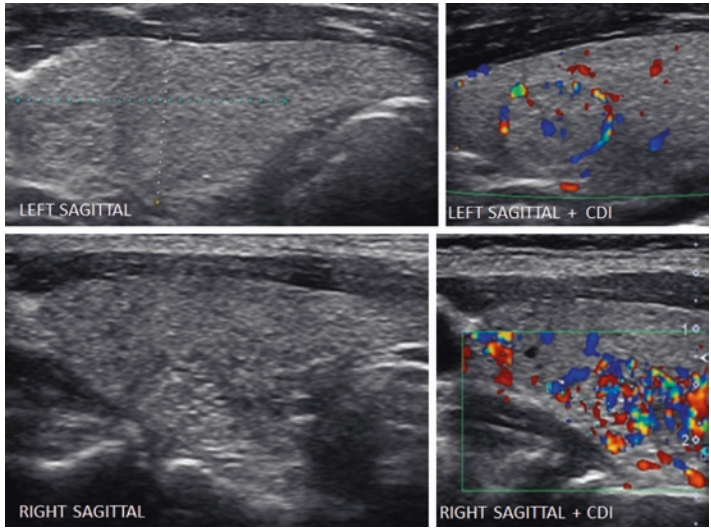

FIGURE 6.4 Adenomatous goiter and isoechoic nodules detected by CDI. The echotexture is heterogeneous with confluent isoechoic nodules. Examining the individual nodular areas in transverse and sagittal views did not show distinct nodules. A discrete isoechoic nodule with peripheral vascular flow (grade 2) was detected in the left lobe by the use of CDI (**a**, **b**). Vascular flow that was increased in a low to moderate intranodular pattern (grade 3/grade 4) confirmed isoechoic nodules in the left and right lobes by CDI (**c**, **d**)

Color Doppler Imaging (CDI)

CDI should be used to examine a diffusely enlarged goiter because the vascular flow may identify otherwise non-visualized isoechoic nodules which if >1.5–2 cm could be considered for FNA biopsy (Fig. 6.4) or reveal early thyroiditis with a diffuse increase in vascularity (see Fig. 6.8).

Elastography

There have been no studies using elastography in the US evaluation of simple or adenomatous goiters that do not have distinct nodules. Elastography is not recommended for the routine evaluation of diffuse or adenomatous goiters.

Table 6.2 Types of thyroiditis

Hashimoto's thyroiditis (chronic lymphocytic thyroiditis)
Subacute thyroiditis (postpartum; silent painless or lymphocytic; painful or subacute pseudogranulomatous)
Riedel's thyroiditis
Suppurative thyroiditis
Drug-induced thyroiditis (amiodarone, lithium, interferon alfa, interleukin-2, tyrosine kinase inhibitors, high iodine intake)

Thyroiditis

There are different etiologies of thyroid inflammation including autoimmune, infection, medication, and ionizing radiation. The most common forms of thyroiditis will be covered in this chapter: Hashimoto's thyroiditis, Graves' thyroiditis, subacute thyroiditis, and Riedel's thyroiditis. Types of thyroiditis that can be identified by US are located in Table 6.2. The appearance of pseudonodules and thyroid malignancies will be discussed in the context of the difficulty in detection by B mode gray-scale US in the hypoechoic heterogeneous background of thyroiditis.

Hashimoto's Thyroiditis

Hashimoto's thyroiditis (HT) or chronic lymphocytic thyroiditis is the most prevalent autoimmune disease and the most common cause of hypothyroidism in the United States [9]. The disease most often occurs in young or middle-aged women and leads to progressive thyroid destruction and hormone production failure. The etiology of the thyroiditis is an organ-specific autoimmune response in which cytotoxic T cells, with the assistance of T-helper cells, are responsible for the direct destruction of thyroid cells, leading to hypothyroidism [10]. When examined histopathologically (Fig. 6.5a), the gland has either focal or diffuse lymphocytic infiltration with occasional germinal centers, small thyroid follicles with sparse colloid, and

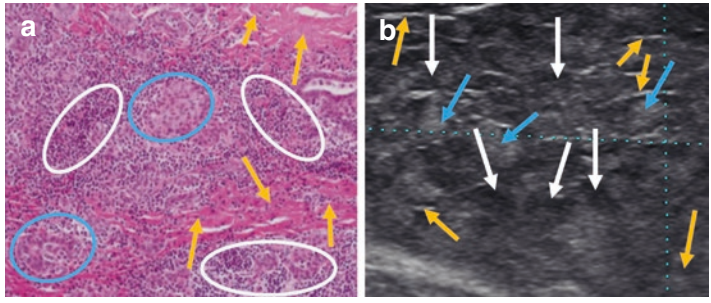

FIGURE 6.5 Hashimoto's thyroiditis pathology (**a**) and ultrasound correlation (**b**). *White circle* and *white arrows*: hypoechoic lymphocytic infiltration. *Blue circle and blue arrows*: isoechoic thyroid follicular cells. *Yellow arrows*: hyperechoic fibrotic lines

variable amounts of fibrosis [10–12]. HT develops in genetically predisposed individuals who are exposed to an environmental trigger [9–11]. Although all the triggers are not understood, pregnancy appears to be one of the important events leading to clinical thyroid dysfunction. The diagnosis is strongly suggested by an elevation of the thyroperoxidase (TPO) antibodies, which is highly sensitive and specific for this disease [13]. High serum TPO antibody concentrations are present in more than 90–95% of patients with Hashimoto's thyroiditis [9, 10].

Conventional B Mode Gray-Scale Ultrasound

The normal thyroid examined by ultrasound shows the parenchyma to be finely granulated (ground-glass appearance), and the echogenicity is similar to the salivary glands but of higher echogenicity compared to the adjacent strap muscles or sternocleidomastoid muscle [6] (Fig. 6.6). HT can be identified with ultrasound by hypoechoic changes in the thyroid (Figs. 6.5b and 6.6b) prior to thyroid dysfunction or elevation of the TPO antibody [14, 15]. Autoimmune thyroid disease may change the thyroid volume (normal values: women 12 mL, men 14 mL) and echogenicity of the thyroid gland. Raber quantified thyroid echogenicity into five grades

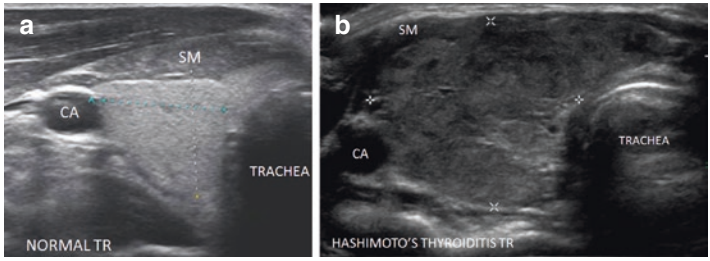

Figure 6.6 Normal thyroid compared to HT. (**a**) Normal size and echotexture. (**b**) Enlarged and hypoechoic echotexture of Hashimoto's thyroiditis. The normal thyroid is brighter (hyperechoic) compared to the strap muscle. The HT gland is enlarged and hypoechoic and isoechoic compared to the SM. *CA* carotid artery, *SM* strap muscle

Table 6.3 Risk of autoimmune thyroiditis and echogenicity

Grade	Pattern	PPV/NPV (any TSH)
Grade 1	Echogenicity similar to submandibular gland, hyperechoic to strap muscles	NPV 91%
Grade 2	Hypoechoic compared to submandibular gland, hyperechoic to strap muscles	PPV 87%
Grade 3	Iso- or hypoechoic compared to strap muscles	PPV 96%

PPV positive predictive value, *NPV* negative predictive value. Data derived from Raber (2002)

(Table 6.3) and correlated the degree of change with thyroid function and TPO antibody levels [15]. The extent of echogenicity decrease accurately predicted autoimmune thyroiditis and thyroid dysfunction with a 96% probability. The positive predictive values (PPV) of grade 3 pattern (thyroid parenchyma is iso- or hypoechoic compared to strap muscles) for detection of autoimmune thyroiditis were 94% (with overt hypothyroidism) and 96% (with any degree of hypothyroidism). The negative predictive value (NPV) of grade 1 pattern (thyroid echogenicity similar to submandibular gland,

hyperechoic to strap muscles) for detection of euthyroid and TPO antibody negative subjects was 91%. In this study, goiter (larger than normal) or atrophy of the gland did not correlate with TPO antibody status.

The sonographic appearance of HT is extremely variable and depends on the degree of autoimmune involvement and the resulting patient-specific amount of follicular destruction, lymphocytic infiltration, and fibrosis. Figure 6.5 illustrates the ultrasound changes associated with the histopathology (follicular destruction, lymphocyte infiltration, and fibrosis) of HT. Early in the course of thyroiditis, the gland may be normal in size with a diffuse fine micronodular change, with increased diffuse vascularity by Doppler, with short echogenic fibrous bands within the parenchyma, and with an overall normal echogenicity (Figs. 6.7 and 6.8). Frequently,

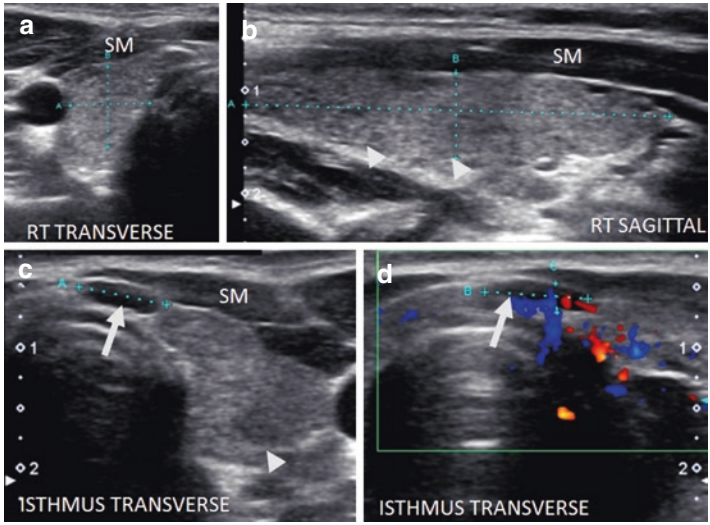

Figure 6.7 Early HT. A normal size thyroid with diffuse fine micronodular change a few short fibrous hyperechoic (*arrowheads*) bands and peri-isthmus benign nodes (*arrows*). The overall echogenicity of the surrounding thyroid parenchyma of the surrounding thyroid parenchyma is normal and hyperechoic compared to the strap muscle (SM). (**a**) Right transverse view. (**b**) Medial sagittal view. (**c**) Transverse isthmus and left lobe view. (**d**) Transverse isthmus view

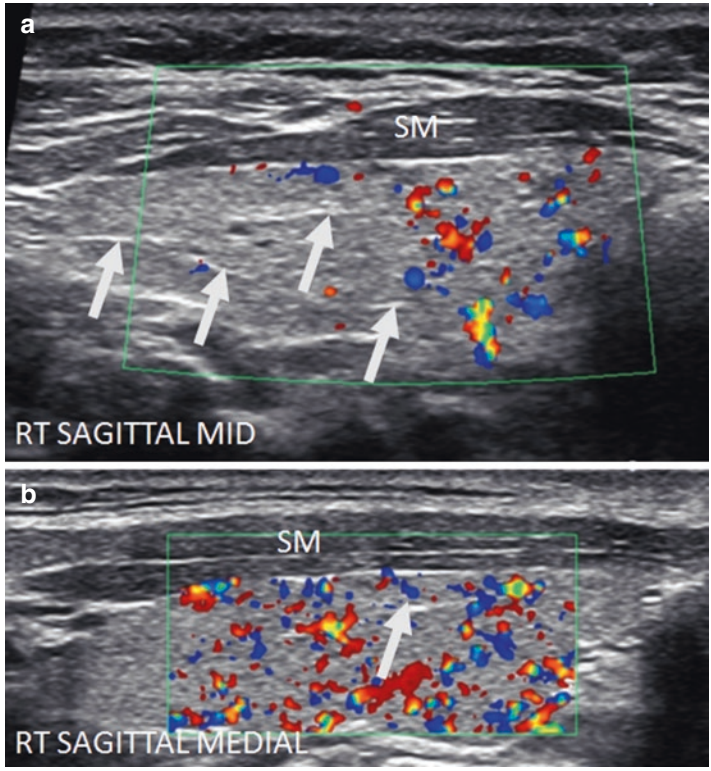

FIGURE 6.8 Early HT. A normal size thyroid with diffuse micronodular change, prominent hyperechoic fibrous bands (arrow), and mild increased vascularity by CDI. The overall echogenicity is normal and hyperechoic compared to the strap muscle (SM). (**a**) Right sagittal mid-lobe view. (**b**) Right sagittal medial lobe view

even with early HT and normal thyroid function, there may be benign reactive nodes located around the isthmus and inferior to each thyroid lobe (Figs. 6.7 and 6.9). The micronodular change in a normal size thyroid gland (Figs. 6.7, 6.8, and 6.9) or an enlarged thyroid (Fig. 6.10) with a diffuse increase in vascular flow by CDI can be seen before the overall thyroid echogenicity is significantly reduced and is an important signal that the patient has autoimmune thyroiditis.

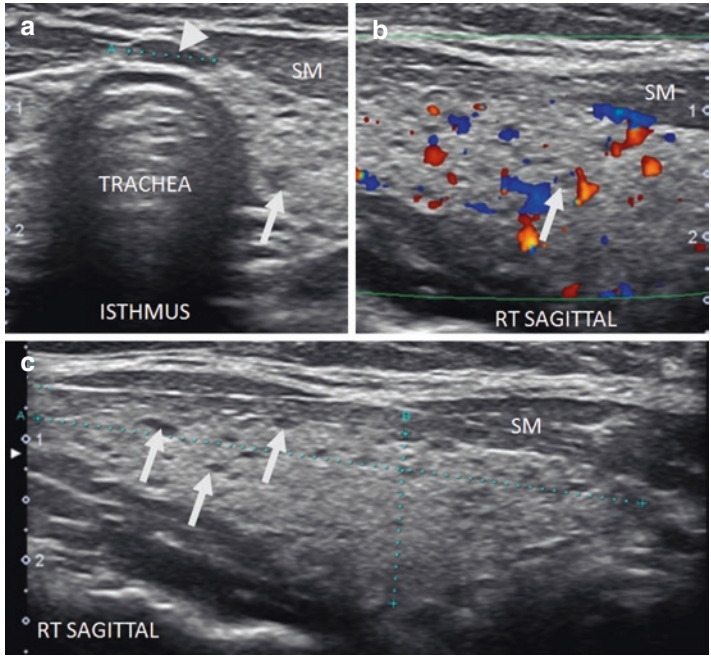

FIGURE 6.9 Early HT. (**a**) Right transverse image. (**b**, **c**) Right sagittal image. A normal size thyroid with more pronounced micronodular change (*arrows*). The overall echogenicity is normal and hyperechoic compared to the strap muscle (SM). A benign reactive node (*arrowhead*) is seen next to the isthmus. The vascular flow is minimally elevated by CDI. Note the increased vascular flow occurs in the normal parenchyma surrounding the micronodules

As thyroiditis progresses, the gland enlarges and becomes more hypoechoic (Figs. 6.10 and 6.11). The entire gland increases in size with HT including the isthmus and pyramidal lobe. The enlarged pyramidal lobe may appear to be a nodule on transverse imaging (Figs. 6.12c and 6.13), but if the isthmus is scanned in transverse view from superior to inferior,the apparent mass (Fig. 6.12b) will be contiguous with the isthmus to create the HT pseudonodule type 1 (Table 6.4) without a distinct nodule margin.

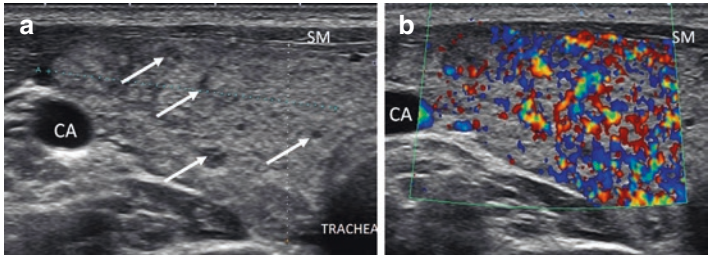

Figure 6.10 Early HT. (**a**) Right transverse view. (**b**) Right sagittal view. An enlarged thyroid with heterogeneous micronodular change (*arrows*). The overall echogenicity is normal and hyperechoic compared to the strap muscle (SM). The vascular flow is significantly elevated by CDI. *CA* carotid artery

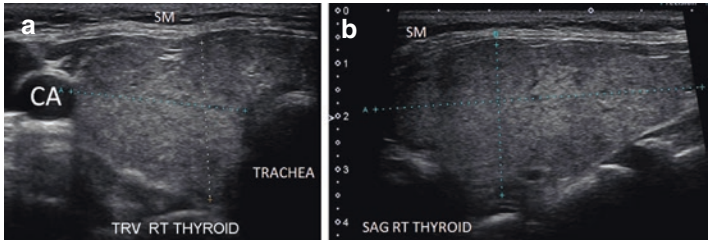

Figure 6.11 HT. An enlarged, mildly hypoechoic thyroid with heterogeneous with micronodular change. The overall echogenicity is reduced but still more echogenic than the strap muscle (SM). (**a**) Right transverse view. (**b**) Right sagittal view. *CA* carotid artery

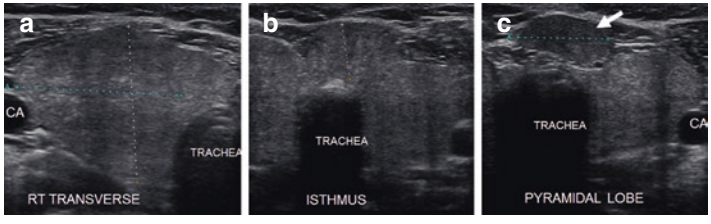

Figure 6.12 HT with a pyramidal lobe that mimics a nodule. A hypoechoic enlarged thyroid, isthmus, and pyramidal lobe with HT. The pyramidal lobe in the transverse view rostral to the isthmus gives the appearance of a pseudonodule (*arrow*; HT pseudonodule type 1). (**a**) Right transverse view. (**b**) Transverse isthmus. (**c**) Transverse pyramidal lobe. *CA* carotid artery

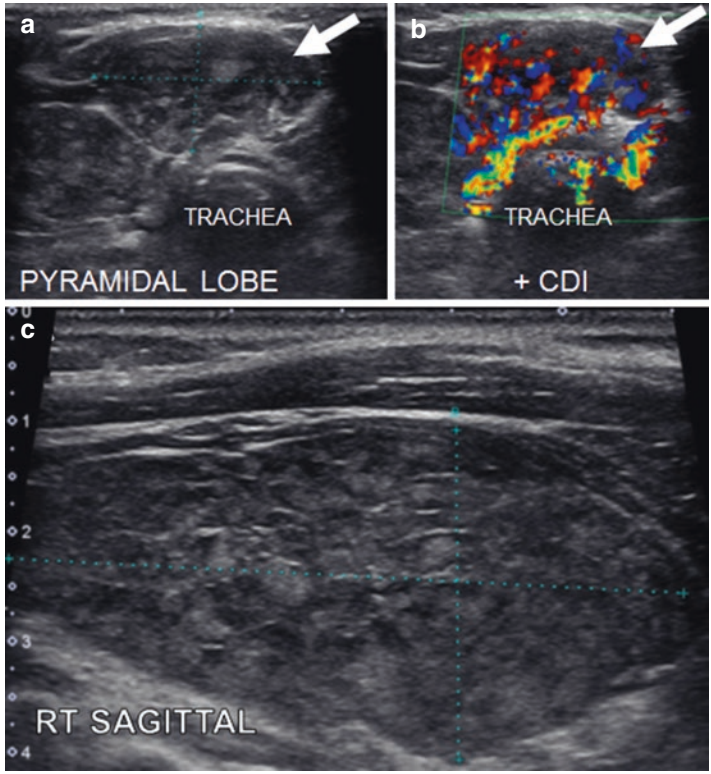

Figure 6.13 HT with a pyramidal lobe—HT pseudonodule type 1. (**a**) Pyramidal lobe, transverse view. (**b**) Pyramidal lobe, transverse + CDI. (**c**) Right sagittal view of thyroid with HT. This thyroid gland is enlarged with a heterogeneous echotexture with hyperechoic fibrous strands. The pyramidal lobe in the transverse view rostral to the isthmus gives the appearance of a pseudonodule (*arrow*; HT pseudonodule type 1)

As HT progresses, the thyroid ultrasound develops more obvious fibrous bands, and increased parenchymal vascularity is seen with Doppler color imaging (Fig. 6.14). The thyroid parenchyma with HT becomes progressively coarser with patchy hypoechoic micronodular change (Fig. 6.14). The micronodular changes are poorly defined hypoechoic patches measuring 1–7 mm in size that can become confluent resulting

Table 6.4 Types of HT pseudonodules

Type 1	Enlarged pyramidal lobe with HT	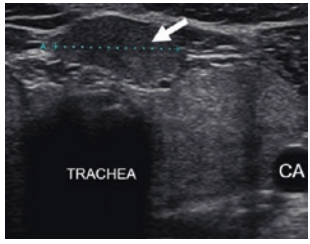
Type 2	Hypoechoic micronodular change surrounding more normal parenchyma	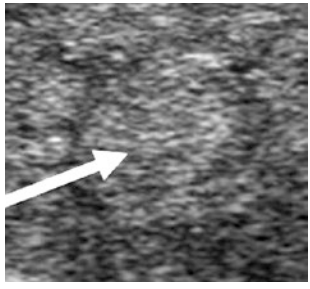
Type 3	Hypoechoic micronodules 1–7 mm	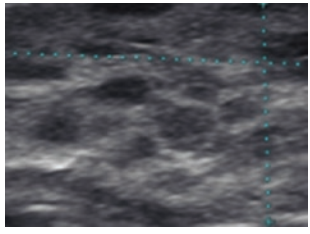
Type 4	Tubercle of Zuckerkandl (posterior lateral thyroid tissue)	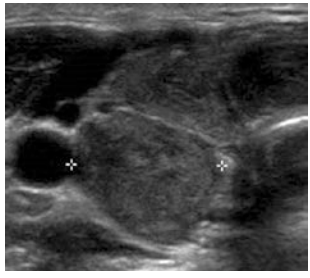

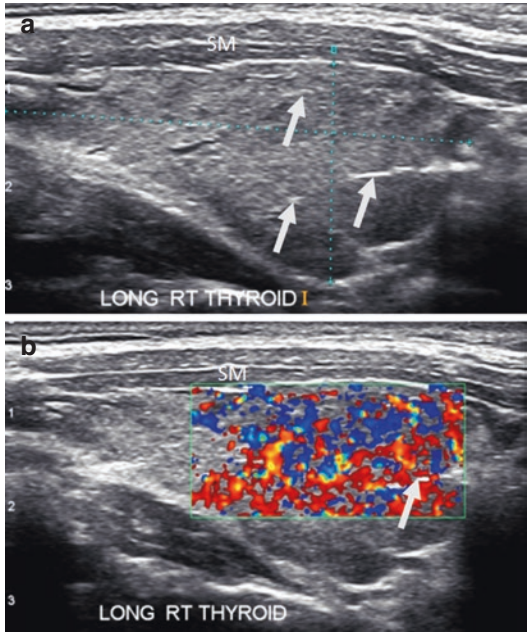

Figure 6.14 HT and fibrosis. A slightly enlarged thyroid with micronodular change, prominent hyperechoic fibrous bands (*arrows*), and overall significant increased vascularity by CDI. The overall echogenicity is less than normal and similar to the strap muscle (SM). (**a**) Right sagittal view. (**b**) Right sagittal view + CDI

in the appearance of pseudonodules (HT pseudonodule type 2) of the relatively normal isoechoic tissue surrounded by the hypoechoic micronodules (Fig. 6.15 and Table 6.4) [14, 16–18]. The hypoechoic patches can be relatively large (up to 7 mm) in a regular pattern that resembles the spots on a giraffe. The "giraffe" pattern has been reported as "innumerable" small hypoechoic nodules, but this is the type 3 pseudonodule (Figs. 6.9, 6.10, 6.16, and 6.17 and Table 6.4). The micronodular change is highly specific for HT with a PPV 95% [16]. The amount of fibrosis is variable with HT. Some HT glands have extensive fibrosis in the thyroid parenchyma. The fibrosis is seen on ultrasound as hyperechoic strands that often have

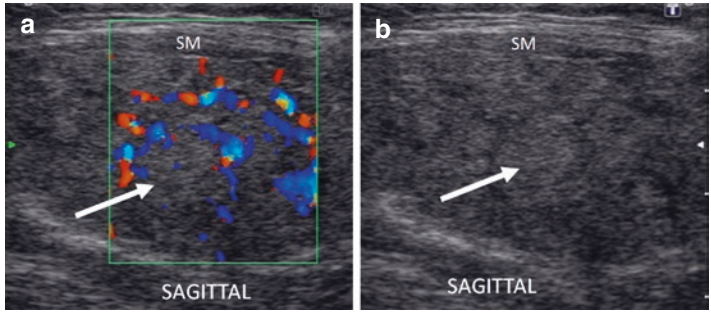

Figure 6.15 HT and pseudonodule type 2. The patchy hypoechoic regions coalesce to create pseudonodules that cannot be identified in the orthogonal image. The overall echogenicity is less than normal and similar to the strap muscle (SM). A pseudonodule (*arrow*; HT pseudonodule type 2) composed of relatively normal isoechoic tissue surrounded by hypoechoic micronodules. (**a**) Pseudonodule + CDI. (**b**) Pseudonodule

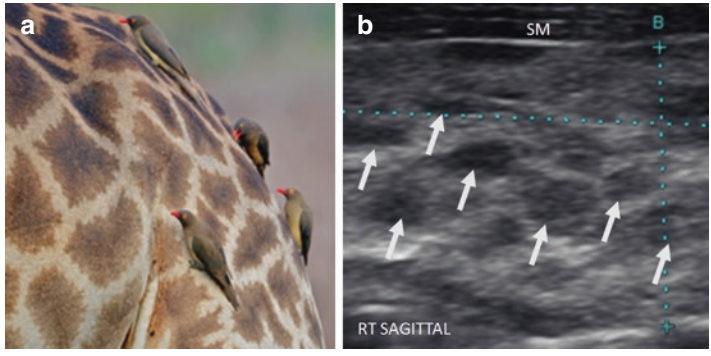

Figure 6.16 Giraffe pattern of HT and HT pseudonodule type 3. Distinct micronodular change (*arrows*) in a pattern that resembles a giraffe's spots (**a**). The echogenicity of the thyroid (**b**) between the hypoechoic patches is normal and hyperechoic compared to the strap muscle (SM). These hypoechoic patches do not have a sharp margin and are an example of HT pseudonodule type 3. Photograph provided by Dr. Robert Levine.

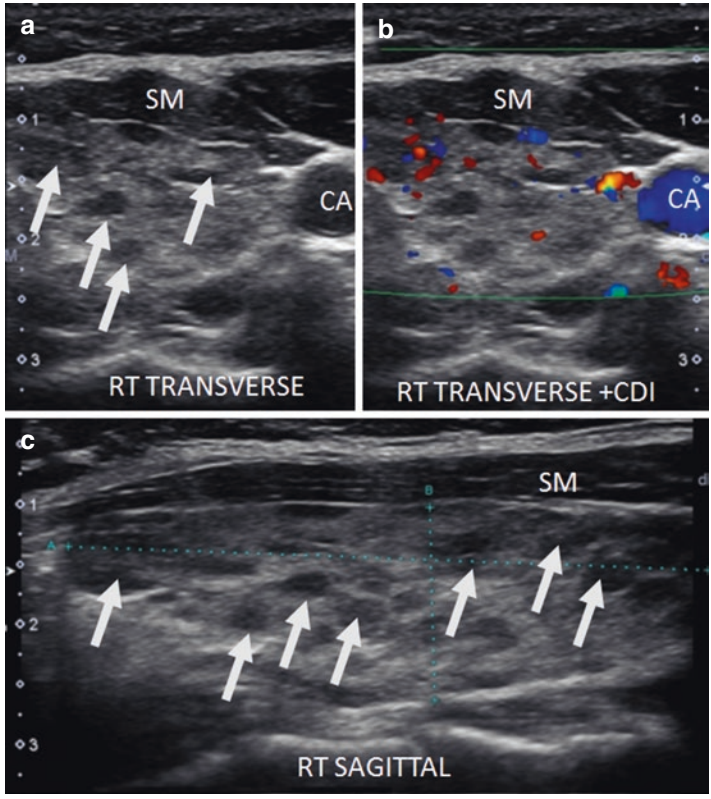

FIGURE 6.17 Giraffe pattern of HT and HT pseudonodule type 3. (**a**) Right transverse image with color Doppler. (**b**) Right transverse image with color Doppler. (**c**) Right sagittal image. A slightly enlarged thyroid with distinct pronounced micronodular change (*arrows*). The overall echogenicity is normal and hyperechoic compared to the strap muscle (SM). The vascular flow by CDI is within the normal parenchyma and not the hypoechoic patches. These hypoechoic patches are thought to be focal deposits of lymphocytes. This is an example of HT pseudonodule type 3. *CA* carotid artery

vascular flow along them by CDI (Figs. 6.18 and 6.19). Fibrous bands may separate the thyroid parenchyma giving a false appearance of a nodule. Generally, when the area of concern is examined in orthogonal directions, a discrete nodule is not seen. The hypoechoic parenchyma of HT allows visualization of the hyperechoic thyroid capsule separating a normal anatomic variant, the tubercle of Zuckerkandl. The tubercle of Zuckerkandl is normal thyroid tissue derived from the fourth branchial cleft and the ultimobranchial body extending posteriorly from the posterior thyroid (Fig. 6.20). The tubercle of Zuckerkandl can be mistaken for a thyroid

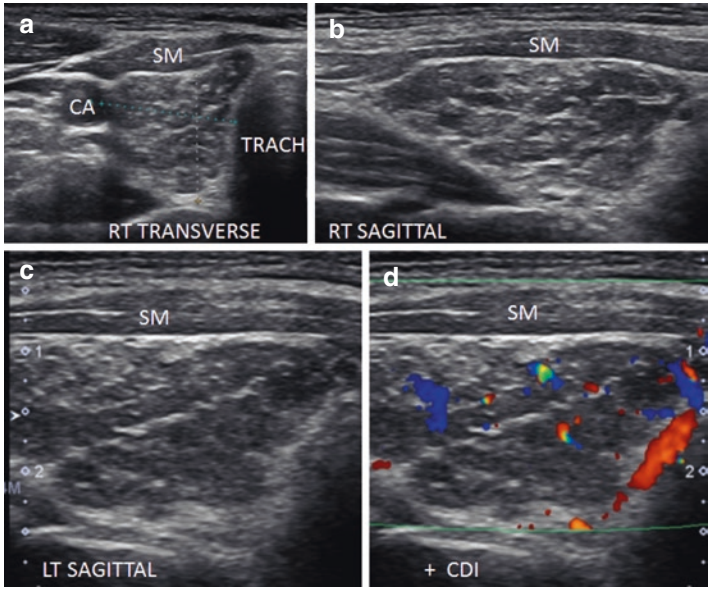

Figure 6.18 Micronodular and fibrous change of HT in an enlarged thyroid. Distinct micronodular change with extensive hyperechoic strands of fibrosis. The echogenicity of the thyroid between the fibrous bands is hypoechoic and isoechoic compared to the strap muscle (SM). The vascular flow is minimally elevated especially along the fibrous bands by CDI. (**a**) Right transverse. (**b**) Right sagittal. (**c**) Left sagittal. (**d**) Left sagittal with CDI

nodule on US imaging, but it is an important caveat that thyroid nodules are not surrounded by hyperechoic fibrous bands (Figs. 6.21 and 6.22). Care should be taken to examine the tubercle of Zuckerkandl for a true nodule that can be distinguished by a difference in echogenicity from the thyroid lobe, well-formed nodular margins, and peri-nodular vascular flow (Fig. 6.23).

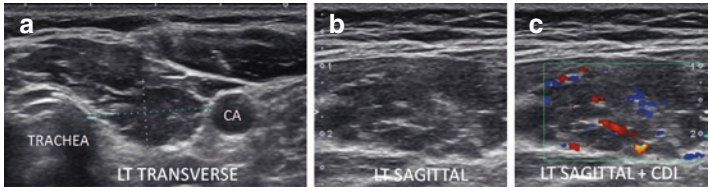

FIGURE 6.19 Micronodular and fibrous change of HT in a normal size thyroid. Hypoechoic thyroid with hyperechoic strands of fibrosis. The echogenicity of the thyroid between the fibrous bands is hypoechoic (isoechoic compared to the strap muscle (SM)). The vascular flow is seen along the fibrous bands by Doppler analysis. (**a**) Left transverse image. (**b**) Left sagittal image. (**c**) Left sagittal + CDI

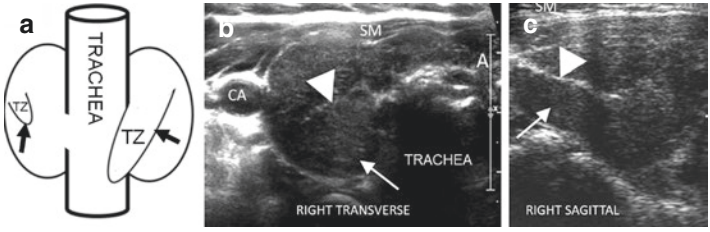

FIGURE 6.20 HT and the tubercle of Zuckerkandl. (**a**) Diagram of posterior view of the thyroid with an enlarged right posterior lateral tissue, the tubercle of Zuckerkandl. The hypoechoic parenchyma allows visualization of the double layer of hyperechoic capsule (*arrowhead*) separating the body of the thyroid from the tubercle of Zuckerkandl (TZ; *arrow*). (**b**) Right transverse view. (**c**) Right sagittal view. *CA* carotid artery

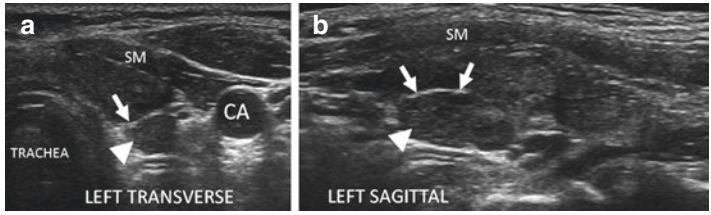

Figure 6.21 HT, Tubercle of Zuckerkandl and HT pseudonodule type 4. The echogenicity of the thyroid is hypoechoic and isoechoic with the strap muscle (SM). The hyperechoic thyroid capsule (*arrow*) separates the body of the thyroid from the tubercle of Zuckerkandl (*arrowhead*) creating a HT pseudonodule type 4. (**a**) Left transverse view. (**b**) Left sagittal view. *CA* carotid artery

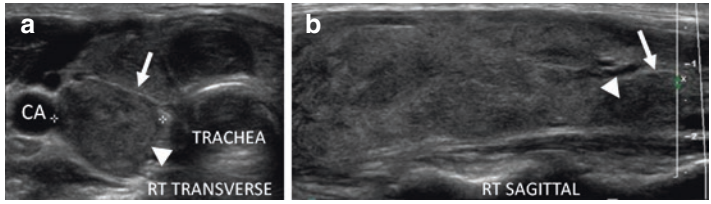

Figure 6.22 HT, tubercle of Zuckerkandl, and pseudonodule type 4. The thyroid is enlarged and heterogeneous with patchy hypoechogenicity. The hyperechoic thyroid capsule (*arrow*) separates the tubercle of Zuckerkandl (*arrowhead*) from the body of the thyroid creating the HT pseudonodule type 4. (**a**) Right transverse view. (**b**) Right sagittal view. *CA* Carotid artery

The micronodular change and overall hypoechogenicity observed on ultrasound is thought to reflect lymphocytic infiltration [1, 19]. Diffuse decrease in thyroid echogenicity (Figs. 6.6b, 6.12, 6.13, 6.21, and 6.23) has a PPV for AITD of 88.3% [95% CI, 85–91%]. Hashimoto's thyroiditis can be detected by ultrasound before clinical disease or the presence of serum TPO antibodies [14]. A prospective study demonstrated that diffuse hypoechogenicity was a better sensitivity (100% vs 63.3%) at predicting current or future thyroid dysfunction than TPO antibody level [20]. However,

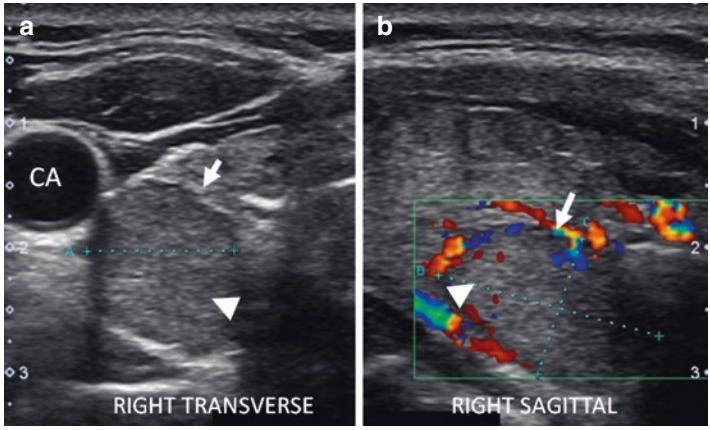

FIGURE 6.23 HT and nodule in tubercle of Zuckerkandl. The hypoechoic parenchyma allows visualization of the hyperechoic thyroid capsule (*arrow*) separating a hypoechoic nodule (*arrowhead*) located in the tubercle of Zuckerkandl from the body of the thyroid. The nodule has a distinct margin and peripheral vascular flow (grade 3) by CDI. (**a**) Right transverse view. (**b**) Right sagittal view. *CA* carotid artery

the ability of observers to reliably detect degrees of thyroid hypoechogenicity is poor (generalized $\kappa = -0.002–0.781$) and depends on the US equipment, equipment settings, and experience of the observer [21, 22]. One attempt to normalize detection is to use histogram analysis that does not depend on equipment or US settings. The degree of hypoechogenicity assessed by this standardized method called the histogram analysis of gray scale is associated with higher TSH levels [21, 23].

Clinically, hypothyroidism can be categorized as goitrous or atrophic thyroiditis (Ord's thyroiditis; Fig. 6.24) [9, 24]. Although it is assumed that the US changes of thyroiditis starts with an enlarged gland with hypoechoic micronodules, progresses to the diffusely hypoechoic gland with fibrous bands, and ends with a small hypoechoic atrophic gland, this progression has never been specifically documented. Recent

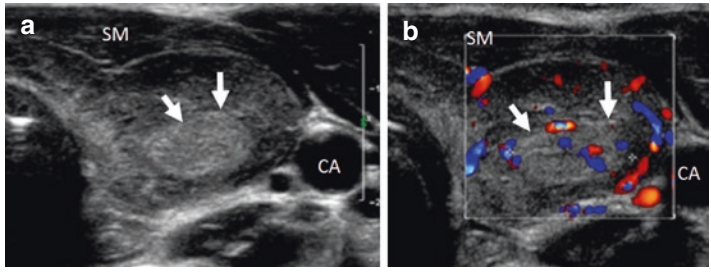

FIGURE 6.24 "White knight nodule" and HT. A nodule can be called a benign white knight nodule (*white arrows*) only if the nodule has a smooth well-defined margin without calcification and is homogeneously hyperechoic on a hypoechoic background of HT. (**a**) Right transverse image. (**b**) Right transverse image + Doppler. *CA* carotid artery, *SM* strap muscle

investigations suggest that HT is a multifaceted disease including various subtypes which exhibit distinct clinicopathological characteristics [25]. Several subclassification schemes of HT have been introduced [11]. The fibrous variant of HT is regarded as end stage of HT, but IgG4 thyroiditis may overlap the so-called fibrous variant of HT to a large extent because of the close histologic similarities [25, 26] (Fig. 6.25). Recently, the enlarged, very hypoechogenic gland (Figs. 6.6b, 6.11, and 6.12) has been associated with a new syndrome of IgG4-related sclerosing systemic disease. IgG4-related sclerosing disease is a systemic disease that is characterized by elevated gamma globulins with a predominant increase in IgG4 levels with lymphoplasmacytic infiltration, fibrosis, obliterative phlebitis, and increased numbers of IgG4-positive plasma cells in affected organs [27]. It has suggested there are four types of IgG-related thyroid disease including IgG4-related HT, fibrosing variant of HT, Graves' disease with elevated IgG4, and Riedel thyroiditis [28]. IgG4 Hashimoto's thyroiditis showed higher grade of stromal fibrosis, lymphoplasmacytic infiltration, and follicular cell degeneration than non-IgG4 thyroiditis [25]. IgG4 thyroiditis is associated with younger age, male gender, subclinical hypothyroidism with a large and diffusely

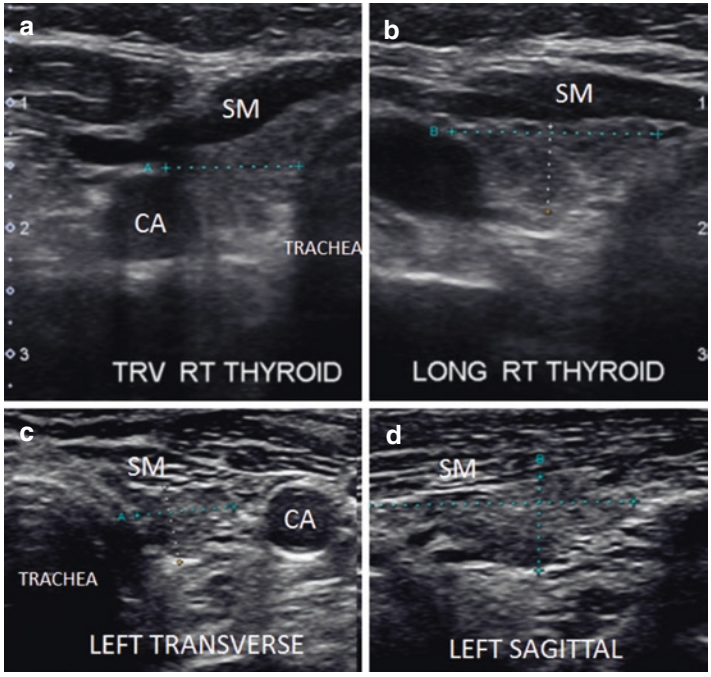

FIGURE 6.25 End-stage atrophic HT. Two examples of end-stage HT in hypothyroid patients. Patient 1: The thyroid is small (1.6 × 0.8 × 0.6 cm; sagittal × AP × transverse) with a heterogeneous echotexture. The echogenicity of the thyroid is hypoechoic but slightly more echogenic than the strap muscle (SM). (**a**) Right transverse image. (**b**) Right sagittal image. Patient 2: A small thyroid (1.7 × 0.5 × 0.6 cm; sagittal × AP × transverse) with heterogeneous and hypoechoic echotexture. (**c**) Left transverse image. (**d**) Left sagittal image. *CA* carotid artery

hypoechoic thyroid gland on ultrasound, and higher level of circulating thyroid antibodies [28, 29]. Prospective studies will need to be performed to determine if the variable sonographic appearances of HT is a continuum or whether they represent different variants of Hashimoto's thyroiditis.

It has been suggested that a brightly echogenic "white knight" nodule in a patient with HT is nearly always benign

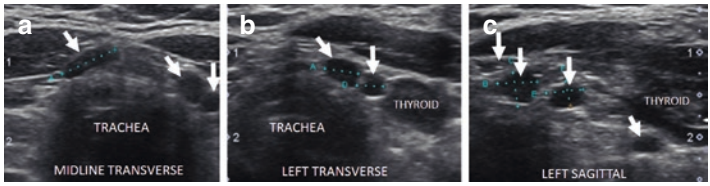

FIGURE 6.26 Perithyroidal benign nodes and HT. A: Benign peri-isthmus nodes. B: Benign nodes superior to the upper left thyroid lobe with HT. C: Benign nodes inferior to the left thyroid lobe with HT. Arrows: benign nodes. (**a**) Midline transverse view. (**b**) Left transverse view at the superior tip of the left thyroid lobe. (**c**) Left sagittal view showing the inferior pole of the thyroid

(Fig. 6.24) [30, 31]. But it is important to understand that the background must be hypoechoic from HT; the nodule must be smoothly rounded with well-defined margins, uniformly hyperechoic; and the CDI should show flow in the surrounding parenchyma and not within the nodule. Only if all these criteria are seen can you be sure the nodule is benign. FNB should be considered if the nodule is large or has significant growth per the AACE [7] and ATA [8] nodule guidelines.

Perithyroidal lymph nodes are frequently found in patients with HT. One study found paratracheal lymph nodes in 184 of 199 (92.5%) patients with HT and 28 of 100 (28%) controls ($P < 0.001$). Paratracheal nodes were fewer (2.8 vs. 4.7) and smaller (10.7 mm vs. 8.2 mm) in control patients compared to patients with HT [32]. Perithyroidal nodes are usually located next to the isthmus or inferior to the thyroid lobes. These reactive nodes have a typical benign appearance with an oval shape (Figs. 6.7, 6.9, and 6.26).

Color Doppler Imaging (CDI)

CDI of the thyroiditis gland may show hypervascularity when inflammation is actively present, but, over time, with the development of fibrosis, vascularity may be become sparse. Peak systolic flows of the perithyroidal arteries is normal in

all stages of Hashmimoto's which may distinguish from the enlarged hypoechoic, hypervascular Graves' disease in which the PSV are elevated [33, 34]. CFI estimate of TBF may be useful to distinguish between patients with Graves' disease and HT, as both may have a similar hypoechoic heterogeneous echotexture pattern on US.

Elastography

HT with lymphocytic infiltration and fibrosis results in an increase in stiffness of the thyroid parenchyma [22]. Shear wave elastography (SWE) with a cutoff value of >2.53 m/s can differentiate normal thyroid from thyroiditis (Graves' disease $P < 0.001$; Hashmimoto's thyroiditis $P = 0.004$) with a positive predictive value (PPV) of >90% [35]. Using a different method of elastography using the carotid artery pulsations as the internal compression source, the elasticity index decreased (increased stiffness) according to the thyroid antibody tier and the extent of thyroid dysfunction [36]. Elastography measurements of thyroid nodules may be inaccurate in the presence of Hashimoto's thyroiditis due to the increased stiffness of the surrounding parenchyma (see Chap. 16).

Graves' Disease (GD)

GD is an autoimmune disorder that causes increased production of thyroid hormones and hyperthyroidism. B cells produce an activating immunoglobulin that binds to the thyrotropin receptor (TSH receptor) and activates the thyrotroph cell cascade to produce thyroid hormone in the absence of serum TSH. The activating antibody, the thyroid-stimulating immunoglobulin (TSI), binds to the TSH receptor and activates every thyrotroph cell to grow and produce thyroid hormone, resulting in diffuse enlargement of the thyroid gland and hyperthyroidism.

Conventional B Mode Gray-Scale Ultrasound

On sonography, the GD gland is typically diffusely enlarged, with convex bowing of the anterior gland margin and mild textural coarsening (Figs. 6.27, 6.28, and 6.29). The echogenicity is decreased compared to the normal thyroid parenchyma. The cause of the hypoechoic echotexture is hypothesized to be due to increased vascular flow, increased cellularity, and decreased colloid content compared to the more echogenic normal thyroid gland. Compared to HT, the gland is less heterogeneous and micronodular with a lobulated contour of the thyroid gland capsule (Figs. 6.27, 6.28, and 6.29) [20, 37]. Occasionally after radioactive iodine therapy of GD, there will be clinical detection of transient thyroid enlargement or development of nodules. In these cases, it is important to know the expected changes after radioactive iodine ablation. The typical sonographic features of the thyroid after radioactive iodine ablation include a significant reduced mean total volume (87%; $P < 0.05$), hypovascularity, coarse echotexture, and hyperechogenicity compared to the pretreatment ultrasound [37]. It is not typical to develop discrete nodules after radioactive iodine ablation. Any nodule detected in GD must be evaluated with an ultrasound-guided fine-needle biopsy (USGFNB) based on the AACE [7] or ATA [8] nodule guidelines.

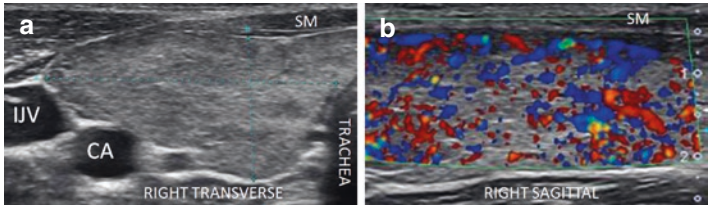

Figure 6.27 Graves' hyperthyroidism. The thyroid is heterogeneous and hypoechoic compared with the strap muscle (SM). Graves' thyroiditis is often less hypoechoic and heterogeneous with less micronodular change or fibrosis than in HT. The vascular flow is high in a diffuse pattern by CDI. (**a**) Right transverse view. (**b**) Right sagittal view. *CA* carotid artery, *IJV* internal jugular vein

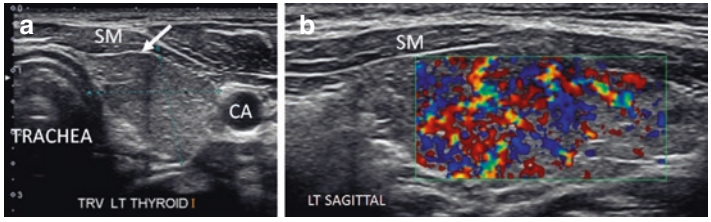

FIGURE 6.28 Graves' hyperthyroidism. The thyroid is hypoechoic and isoechoic with the strap muscle (SM). The vascular flow is extremely high by CDI giving the appearance of a "thyroid inferno." Note the lobular convex bowing of the anterior capsule (*arrow*) typical of Graves' disease. *CA* carotid artery. (**a**) Left transverse view. (**b**) Left sagittal view

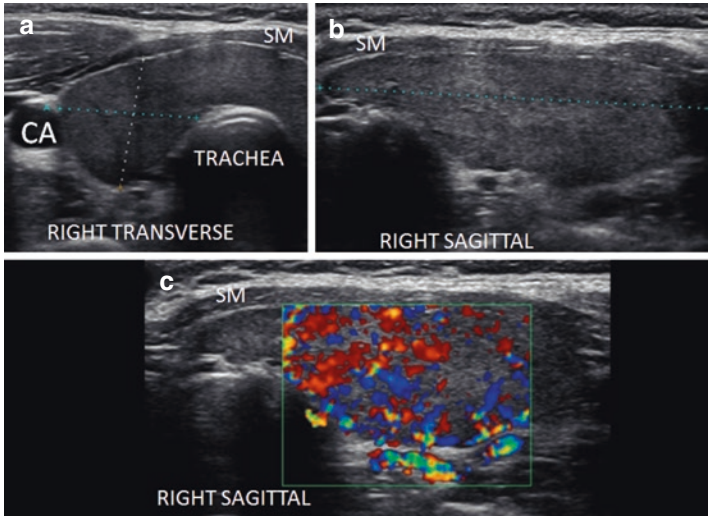

FIGURE 6.29 Very hypoechoic Graves' hyperthyroidism. The thyroid is very hypoechoic and similar to the strap muscle (SM) with very smooth lobular contour of the gland. This appearance is consistent with Igg4-related thyroid disease. The vascular flow is increased compared to normal by CDI. (**a**) Right transverse view. (**b**) Right sagittal view. (**c**) Right sagittal view + CDI. *CA* carotid artery

Color Doppler Imaging (CDI)

CDI of normal thyroid will show occasional spots or vascular channels with peak systolic velocities (PSV) between 15 and 30 cm/s in the inferior thyroid artery and 3 and 5 cm/s in the intrathyroid arteries [38]. The mean PSV of blood flow is elevated in GD in the inferior thyroid artery (25.5 cm/s) and perithyroidal arteries (48.2 cm/s) [38]. PSV are significantly higher in GD than HT ($P < 0.001$) and normal thyroid glands ($P < 0.001$). CDI and measurement of PSV can differentiate GD from HT despite a similar enlarged hypoechoic gray-scale image [34]. Increased vascularity and arteriovenous shunts are the etiology of intense vascular flow observed with CDI referred to as the "thyroid inferno" (Fig. 6.28). Advanced dynamic flow (ADF) is a high-resolution power Doppler mode used to quantitate calculated Doppler patterns of the glands. ADFs were scored, and peak systolic velocity (PSV) measurements were obtained from intrathyroidal, perithyroidal, and peri-nodular vasculature. Vascular patterns were significantly more prominent, and the mean PSV values were significantly higher in the GD patients compared to the HT patients ($P < 0.001$) and controls ($P < 0.001$). ADF could differentiate the untreated GD from HT, with similar gray-scale hypoechoic findings. ADF can be also used to quantitatively measure thyroid blood flow (TBF). TBF was significantly higher (>4%; $P < 0.001$) in patients with GD compared to patients with silent subacute thyroiditis, subacute granulomatous thyroiditis, or normal controls, although there was overlap of values [39].

Elastography

Thyroid stiffness by SWE is higher in Graves' disease (2.82 ± 0.47 m/sec; P <0.001) and Hashimoto's thyroiditis (2.49 ± 0.48 m/s,; $P = 0.004$) compared to normal controls (2.07±0.44 m/s) [35]. However, there was no difference in stiffness between Graves' disease and HT ($P = 0.053$).

Subacute Thyroiditis

Subacute thyroiditis can be separated into three forms that have a similar clinical course: 4–8 weeks of thyrotoxicosis and 2–4 months of hypothyroidism and then return to normal thyroid function in >90% of patients. The three forms of subacute thyroiditis are the painless "silent" subacute thyroiditis, the painful pseudo granulomatous subacute thyroiditis, and the postpartum subacute thyroiditis. The pseudo granulomatous subacute thyroiditis presents as a painful swelling of the lower neck, odynophagia, fever, and myalgias, with an elevated ESR. Postpartum and painless subacute thyroiditis is associated with a painless thyroid enlargement, the typical changes in thyroid hormone level but without the thyroid pain, fever, and myalgias. Postpartum subacute thyroiditis may occur within the first year after childbirth or abortion, most commonly within the first 6 months. Subacute thyroiditis is a self-limited inflammatory disease of the thyroid. Although the etiologies are not entirely understood, the subacute granulomatous condition occurs after a wide variety of viral infections, while postpartum subacute thyroiditis is typically associated with subclinical autoimmune disease before pregnancy.

Conventional B Mode Gray-Scale Ultrasound

The typical ultrasound finding of thyrotoxic phase of subacute thyroiditis is an ill-defined moderate or markedly heterogeneous and hypoechoic areas in one or more locations within the enlarged thyroid gland (Figs. 6.30 and 6.31). The hypoechoic areas can extend over the long axis of the gland and involve one or both lobes of the thyroid. The hypoechoic areas are patchy without distinct margins [40–46]. Pain of granulomatous subacute thyroiditis is found in the largest areas of hypoechoic change ($P < 0.001$) [47]. Permanent hypothyroidism after resolution of the subacute thyroiditis was most often found in patients who initially presented with bilateral hypoechoic areas and small thyroid size after the resolution of the thyroid inflammation [48].

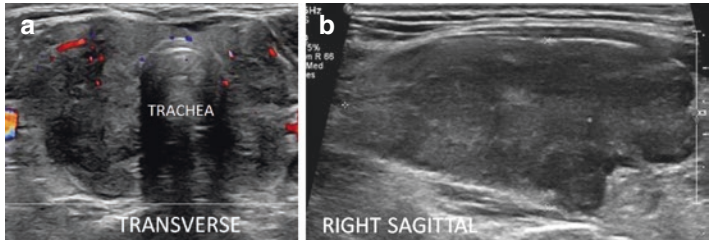

Figure 6.30 Granulomatous subacute thyroiditis. The patient presented with 1 week of anterior neck pain, fever, myalgia, and tachycardia. Her thyroid functions were high with an ESR 60. The thyroid is very enlarged, hypoechoic, and very heterogeneous. The vascular flow in the hypoechoic regions is very low by CDI. (**a**) Transverse view. (**b**) Right sagittal view

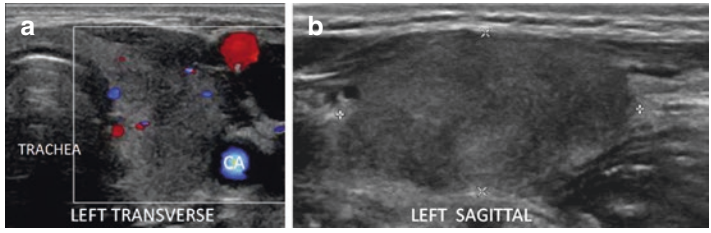

Figure 6.31 Lymphocytic or silent subacute thyroiditis. The patient presented with 3 weeks of rapid heartbeat and thyrotoxicosis, and normal ESR. I-123 thyroid scan showed <1% uptake at 24 h. The thyroid is mildly enlarged, heterogeneous, and hypoechoic. The vascular flow in the hypoechoic regions is low by CDI. (**a**) Left transverse view. (**b**) Left sagittal view. *CA* carotid artery

Color Doppler Imaging (CDI)

A hallmark of subacute thyroiditis that separates it from GD on sonography is absent or reduced vascularity within the hypoechoic areas (Figs. 6.30 and 6.31), while the remaining surrounding thyroid has normal vascularity (Fig. 6.31a) [33, 40, 41, 47, 49]. Peak systolic velocity of CDI of the different thyroid arteries are normal [49] and lower than patients with GD [50]. Especially with postpartum thyroiditis, the

surrounding thyroid parenchyma may have increased vascularity because of the concomitant HT [1]. While intense flow in a thyrotoxic patient strongly supports the presence of GD, and absent flow strongly supports subacute (destructive) thyroiditis, there is overlap, and the diagnosis may not be clear in the presence of mild to moderate flow.

Elastography

The hypoechoic areas of subacute thyroiditis are hard and stiffer than HT. The stiffness is similar to thyroid cancer [51, 52]. Statistically significant difference ($P < 0.05$) in stiffness measured as strain ratio between the thyroid and the SCM can differentiate between GD (2.3 ± 1.08) versus HT (7.04 ± 7.74) and subacute thyroiditis (24.09 ± 13.56) [53].

Acute Suppurative Thyroiditis

The thyroid is an uncommon location for infection or acute suppurative thyroiditis. It may develop locally or by hematogenous spread in septicemia. The most common pathogens causing acute suppurative thyroiditis are Gram-positive bacteria, including staphylococcal and streptococcal species, but a fungal etiology is possible in immunosuppressed patients. Patients present with a painful mass or swelling over the thyroid gland along with fever. When the left lobe of the thyroid is involved, the possibility of a left third pharyngeal pouch remnant and a fistula between the thyroid lobe and the ipsilateral pyriform sinus should be considered [54].

Conventional B Mode Gray-Scale Ultrasound

The areas of thyroid infection will appear enlarged and heterogeneous on US (Fig. 6.32) but rarely may present as a fluid-filled cystic mass in the thyroid with gas collection within the soft tissue of the anterior neck [33, 55]. Acute

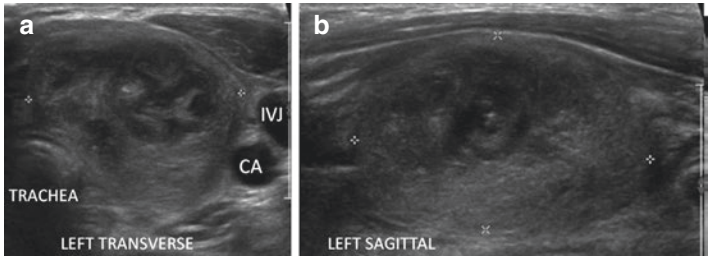

FIGURE 6.32 Suppurative acute thyroiditis. The patient presented with 2 weeks of fever, severe dysphagia, thyroid mass, and normal thyroid function. The entire left lobe was enlarged and very painful to palpation. The left lobe is enlarged and heterogeneous. There is no vascular flow in the hypoechoic mass by CDI (not shown). (**a**) Left transverse view. (**b**) Left sagittal view. *CA* carotid artery, *IJV* internal jugular vein

suppurative thyroiditis can be associated with swelling of the adjacent perithyroidal soft tissue resulting from associated cellulitis with unilateral vocal cord paralysis [56].

Color Doppler Imaging (CDI)

There may be increased vascular flow in the area of the thyroid infection and inflammation by CDI.

Elastography

No studies has been found using elastography in the US evaluation of acute suppurative thyroiditis.

Riedel's Thyroiditis (RT)

Riedel's thyroiditis or fibrosing thyroiditis is a local manifestation of a systemic disease of fibrosclerosis that involves fibrosis of the mediastinum and retroperitoneum. The etiology

is unclear, but a small series of surgical specimens were stained positively for IgG4-bearing plasma cells suggesting that RT in some patients is part of the IgG4-related systemic disease spectrum [57]. It is a rare inflammatory disease that is characterized by replacement of normal thyroid tissue by dense fibrotic connective tissue, with obliteration of normal thyroid architecture and vascular structures, and involvement of adjacent tissues following extension through the thyroid capsule. Diffuse or partial involvement of the thyroid may occur. RT differs from HT in which the fibrosis is limited to within the thyroid capsule [58]. Patients present with a painless thyroid mass that can be rapidly growing. On examination, there is usually an enlarged thyroid which is fixed and hard, sometimes described as stony or woody [59].

Conventional B Mode Gray-Scale Ultrasound

The ultrasound of RT will show an enlarged thyroid gland with either a hypoechoic coarsened echotexture and fibrous septations resulting in a pseudonodular appearance or an extremely hypoechoic mass with irregular margins [60–63] that extends outside the thyroid (Fig. 6.33) [60, 61, 63]. Linear echogenic

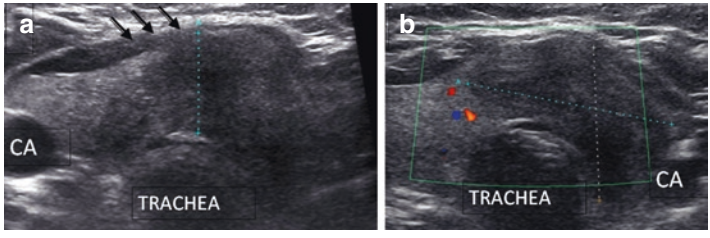

FIGURE 6.33 Riedel's thyroiditis. The patient presented a hard isthmus mass, normal thyroid function, and negative TPO antibody titer. The mass is very hypoechoic with an infiltrative margin that interrupts the thyroid capsule and extends beyond the thyroid in multiple sites (*arrows*). There is no vascular flow in the hypoechoic mass by CDI. (**a**) Transverse isthmus view. (**b**) Transverse isthmus + CDI. *CA* carotid artery

linear streaks may represent fibrosis early in the disease. As the disease progresses, the gland becomes replaced by fibrous tissue resulting in the hypoechogenic mass without internal echoes that may extend to surround the carotid artery [63].

Color Doppler Imaging (CDI)

RT will have decreased vascular flow by CDI especially after complete fibrosclerotic replacement of the thyroid parenchyma with obliteration of vascular structures [63, 64].

Elastography

The hypoechoic areas of the thyroid with RT are extremely hard and stiff measuring 142–281 kPa by shear wave elastography [63] compared to the adjacent normal thyroid with normal stiffness [53].

Thyroiditis and Papillary Thyroid Cancer (PTC) and Lymphoma

HT and GD can occur concomitantly with thyroid malignancy. It is controversial whether there is an increased risk of PTC in HT and GD. Some studies have shown an increased risk, perhaps only in patients who are euthyroid and not in patients with end-stage HT, compared to the background risk of cancer in thyroid nodules [65–67]. Prospective studies also indicate an increase in prevalence of PTC in patients with GD, and metastatic spread was associated with GD and an age >45 years [68]. As in the general population, papillary thyroid cancer is the most common type of thyroid malignancy in patients with HT and GD. Primary thyroid lymphoma is strongly associated with HT, although it is exceedingly rare in absolute prevalence compared to HT. Primary thyroid lymphoma occurs almost exclusively in patients with preexisting HT. Thyroid lymphoma is more common in women and the mean age at onset is 60 years old.

The main symptom is rapidly growing goiter with compressive symptoms. The majority of histopathologic types are extranodal marginal zone B-cell lymphomas of mucosa-associated lymphoid tissue, diffuse large B-cell lymphomas, and mixed types of the above two. Most thyroid lymphomas are of B-cell origin, with six different histologic subtypes. The more indolent lymphomas are the subgroup of mucosa-associated lymphoid tissue (MALT) lymphomas comprising approximately 6–27% of thyroid lymphomas.

Conventional B Mode Gray-Scale Ultrasound

It can be difficult distinguish between an area of focal thyroiditis and adenomatous hyperplasia from thyroid cancer in HT and GD because they have similar suspicious hypoechoic sonographic findings making infiltrative margins difficult to identify in the hypoechoic background of thyroiditis. The US characteristics of PTC (hypoechogenicity, microcalcification, macrocalcification, halo, and infiltrative margins) are similar in patients with or without HT [67, 69, 70]. Thus, malignant nodules in a background of thyroiditis tend to be solid and hypoechoic, but there is no single sonographic characteristic that will identify all malignancies [69–71]. Infiltrative margins are particularly difficult to detect since the hypoechoic cancer will blend into the heterogeneous, hypoechoic background of HT and GD (Fig. 6.34). Hypoechoic nodules in the heterogeneous, hypoechoic echotexture of HT and GD may be detected by a difference in vascular pattern of the nodule compared to the surrounding parenchyma detected by color Doppler (Fig. 6.35). All types of calcification are more prevalent in malignant nodules including microcalcification, nonspecific tiny bright reflectors, macrocalcification, and eggshell calcification [69]. An area of calcification, especially microcalcification, in the background of HT, should be considered for biopsy to exclude malignancy, even if a distinct nodule is not seen (Fig. 6.36) [69, 72, 73]. Diffuse sclerosing papillary thyroid carcinoma (DSPTC) is a relatively rare variant of papillary thyroid carcinoma characterized by scattered

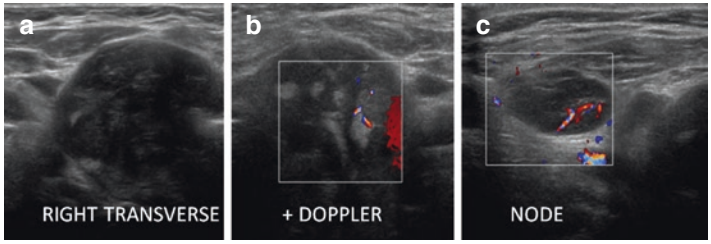

Figure 6.34 Hypoechoic HT and lymphoma. The 74-year-old female patient presented with 6 months of an enlarging neck after a 25-year history of HT. The ultrasound shows the right lobe was enlarged and very hypoechoic. There is no vascular flow in the hypoechoic mass by CDI. An abnormal 1.8 cm node was found in the right lateral neck with blood flow in the hilum but also abnormal peripheral flow by CDI. (**a**) Right transverse view. (**b**) Right transverse view + CDI. (**c**) Right level 3 node + CDI

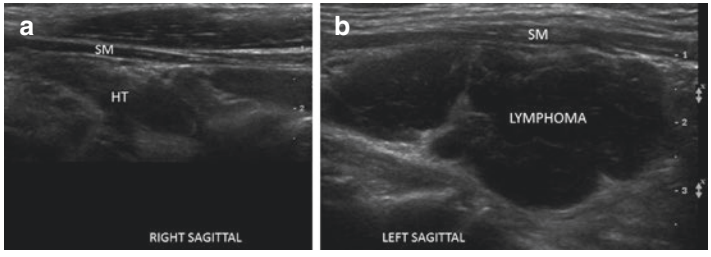

Figure 6.35 Hypoechoic HT with lymphoma and asymmetric enlargement. A 68-year-old male with HT complained of having to buy shirts with larger neck size twice in the last 8 months. (**a**) Right sagittal view shows a small atrophic lobe consistent with end-stage HT. (**b**) Left sagittal view shows a very enlarged, severely hypoechoic lobe with lobulated margins with open biopsy consistent with lymphoma

microscopic tumor foci, diffuse fibrosis, calcification, and abundant lymphocytic aggregation. This tumor may present without a discrete mass with thyroid ultrasound showing a

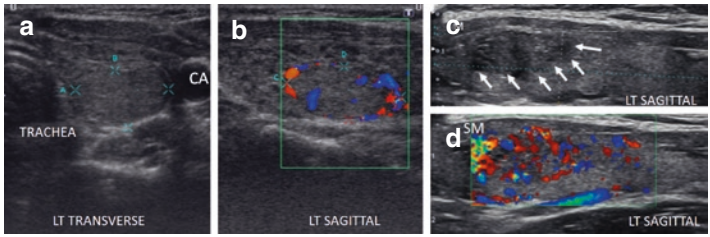

Figure 6.36 Hypoechoic HT and hypoechoic nodule detected by CDI. The echotexture of the thyroid is hypoechoic with micronodules consistent with HT. Patient 1 (**a**, **b**): A discrete hypoechoic nodule with peripheral vascular flow (grade 2) was detected in the left lobe by CDI. This nodule was benign (Bethesda II) on fine-needle biopsy. Patient 2 (**c**, **d**): Vascular flow that was increased in a low flow intranodular pattern (grade 3/grade 4) confirmed a mildly hypoechoic nodule in the right lobe by CDI (*arrows*). This nodule was a papillary thyroid carcinoma (Bethesda VI) on fine-needle biopsy. *CA* carotid artery

diffuse thyroid enlargement, extensive fibrosis, abundant lymphocytic infiltration mimicking thyroiditis, and innumerable microcalcification (Fig. 6.37). Fine-needle biopsy should be performed in a focal area of microcalcification of diffuse microcalcification of the entire lobe even if a discrete nodule cannot be detected by ultrasound [74, 75].

Ultrasonographic characteristics predictive of primary thyroid lymphoma can be diffuse involvement of the entire thyroid or a single lobe or a nodular form with marked hypoechogenicity in the lesion and asymmetrical enlargement of the thyroid gland (Figs. 6.38, 6.39, and 6.5) [76, 77]. When localized MALT lymphoma was found during a sonographic survey of HT, only three of nine patients clinically had an enlarging goiter, but when the detection of a hypoechoic nodular lesion is observed in the background of HT, a primary lymphoma should be considered [78].

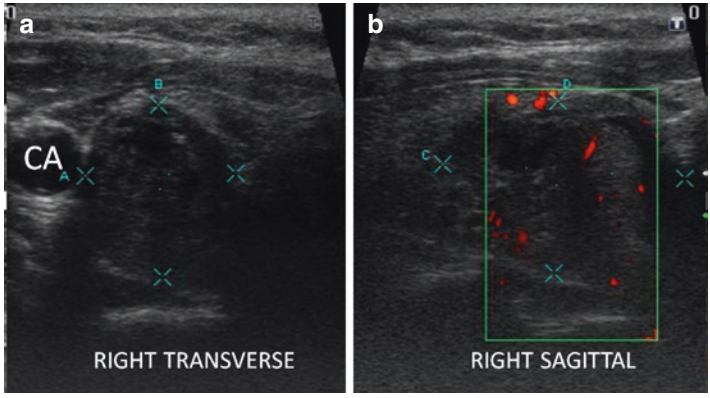

Figure 6.37 Hypoechoic HT and hypoechoic taller than wide nodule. The echotexture is hypoechoic consistent with HT. A discrete hypoechoic nodule with taller than wide shape is difficult to visualize in the hypoechoic thyroid gland. The nodule does not have increased vascular flow by power Doppler analysis. This nodule was a papillary thyroid carcinoma (Bethesda VI) on fine-needle biopsy. (**a**) Right transverse view. (**b**) Right transverse view + CDI. *CA* carotid artery

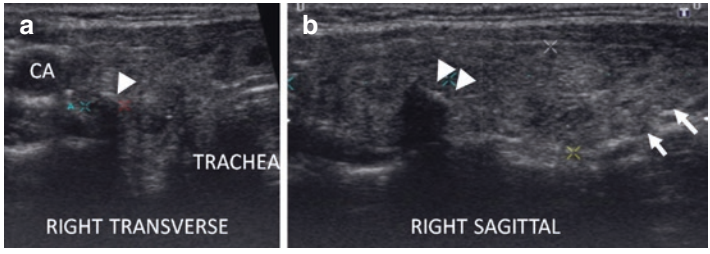

Figure 6.38 Hypoechoic HT and macrocalcification. The echotexture is hypoechoic with giraffe pattern of micronodular change (*arrows*) consistent with HT. A discrete linear macrocalcification was found in the right thyroid lobe. A discrete nodule was not seen. Fine-needle biopsy was suspicious for malignancy (Bethesda V). Right lobectomy confirmed a micro-PTC with surface calcification. (**a**) Right transverse view. (**b**) Right sagittal view. *CA* carotid artery

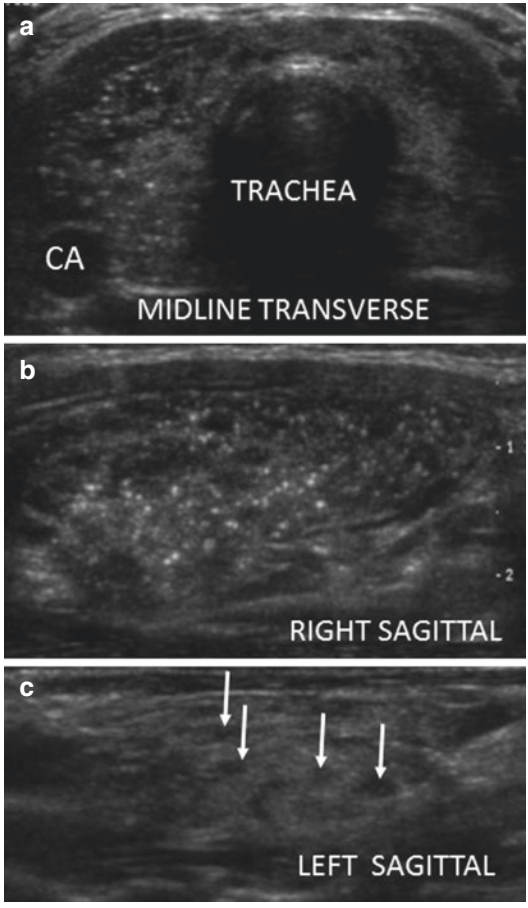

FIGURE 6.39 Hypoechoic HT and unilateral microcalcification. The echotexture is hypoechoic with giraffe pattern of micronodular change (*arrows*) consistent with HT (**c**). Innumerable non-shadowing hyperechoic foci (microcalcification) are seen only in the right lobe (**a**, **b**). A discrete nodule was not seen. Fine-needle biopsy targeting microcalcification and avoiding the microcysts in the right lobe was suspicious for malignancy (Bethesda V). Total thyroidectomy showed innumerable foci of sclerosing variant of papillary thyroid carcinoma. (**a**) Midline view. (**b**) Right sagittal view. (**c**) Left sagittal view. *CA* carotid artery

Color Doppler Imaging (CDI)

Differentiated thyroid cancer may be associated with intranodular vascularity, but often the surrounding parenchyma with HD or GD will be hypervascular allowing for the detection of the outline of a hypoechoic thyroid nodule. Thyroid lymphoma typically does not have vascular flow by CDI.

Elastography

There have been no studies using elastography in the US evaluation of thyroid lymphoma.

Conclusions

A wide spectrum of diffuse thyroid diseases commonly affects the thyroid gland. These thyroid diseases can be detected and evaluated by conventional B mode US and CDI. In some cases, like Hashimoto's thyroiditis, US can diagnose disease before clinically evident and exclude focal thyroid disease including malignancies. US elastography is a new technology that may be helpful in distinguishing between different types of diffuse thyroid disease, but larger studies are needed to evaluate the clinical utility in the diagnosis and management of diffuse thyroid diseases.

References

1. Dighe M, Barr R, Bojunga J, Cantisani V, Chammas MC, Cosgrove D, et al. Thyroid ultrasound: state of the art part 1 – thyroid ultrasound reporting and diffuse thyroid diseases. Med Ultrason. 2017;19(1):79–93.
2. Hegedus L, Bonnema SJ, Bennedbaek FN. Management of simple nodular goiter: current status and future perspectives. Endocr Rev. 2003;24(1):102–32.
3. Hegedus L, Brix TH, Paschke R. Etiology of simple goiter. Thyroid. 2009;19(3):209–11.

4. Zimmermann M, Saad A, Hess S, Torresani T, Chaouki N. Thyroid ultrasound compared with World Health Organization 1960 and 1994 palpation criteria for determination of goiter prevalence in regions of mild and severe iodine deficiency. Eur J Endocrinol. 2000;143(6):727–31.
5. Zimmermann MB. The adverse effects of mild-to-moderate iodine deficiency during pregnancy and childhood: a review. Thyroid. 2007;17(9):829–35.
6. Ghervan C. Thyroid and parathyroid ultrasound. Med Ultrason. 2011;13(1):80–4.
7. Gharib H, Papini E, Garber JR, Duick DS, Harrell RM, Hegedus L, et al. American Association of Clinical Endocrinologists, American College of Endocrinology, and Associazione Medici Endocrinologi medical guidelines for clinical practice for the diagnosis and management of thyroid nodules—2016 update. Endocr Pract. 2016;22(5):622–39.
8. Haugen BR, Alexander EK, Bible KC, Doherty GM, Mandel SJ, Nikiforov YE, et al. 2015 American Thyroid Association management guidelines for adult patients with thyroid nodules and differentiated thyroid cancer: the American Thyroid Association guidelines task force on thyroid nodules and differentiated thyroid cancer. Thyroid. 2016;26(1):1–133.
9. Pearce EN, Farwell AP, Braverman LE. Thyroiditis. N Engl J Med. 2003;348(26):2646–55.
10. Dayan CM, Daniels GH. Chronic autoimmune thyroiditis. N Engl J Med. 1996;335(2):99–107.
11. LiVolsi VA. The pathology of autoimmune thyroid disease: a review. Thyroid. 1994;4(3):333–9.
12. Caturegli P, De Remigis A, Rose NR. Hashimoto thyroiditis: clinical and diagnostic criteria. Autoimmun Rev. 2014;13(4–5):391–7.
13. Hollowell JG, Staehling NW, Flanders WD, Hannon WH, Gunter EW, Spencer CA, et al. Serum TSH, T(4), and thyroid antibodies in the United States population (1988 to 1994): National Health and Nutrition Examination Survey (NHANES III). J Clin Endocrinol Metab. 2002;87(2):489–99.
14. Pedersen OM, Aardal NP, Larssen TB, Varhaug JE, Myking O, Vik-Mo H. The value of ultrasonography in predicting autoimmune thyroid disease. Thyroid. 2000;10(3):251–9.
15. Raber W, Gessl A, Nowotny P, Vierhapper H. Thyroid ultrasound versus antithyroid peroxidase antibody determination: a cohort study of four hundred fifty-one subjects. Thyroid. 2002;12(8):725–31.
16. Yeh HC, Futterweit W, Gilbert P. Micronodulation: ultrasonographic sign of Hashimoto thyroiditis. J Ultrasound Med. 1996;15(12):813–9.

17. Simeone JF, Daniels GH, Mueller PR, Maloof F, vanSonnenberg E, Hall DA, et al. High-resolution real-time sonography of the thyroid. Radiology. 1982;145(2):431–5.
18. Carle A, Pedersen IB, Knudsen N, Perrild H, Ovesen L, Jorgensen T, et al. Thyroid volume in hypothyroidism due to autoimmune disease follows a unimodal distribution: evidence against primary thyroid atrophy and autoimmune thyroiditis being distinct diseases. J Clin Endocrinol Metab. 2009;94(3):833–9.
19. Willms A, Bieler D, Wieler H, Willms D, Kaiser KP, Schwab R. Correlation between sonography and antibody activity in patients with Hashimoto thyroiditis. J Ultrasound Med. 2013;32(11):1979–86.
20. Rago T, Chiovato L, Grasso L, Pinchera A, Vitti P. Thyroid ultrasonography as a tool for detecting thyroid autoimmune diseases and predicting thyroid dysfunction in apparently healthy subjects. J Endocrinol Investig. 2001;24(10):763–9.
21. Kim GR, Kim EK, Kim SJ, Ha EJ, Yoo J, Lee HS, et al. Evaluation of underlying lymphocytic thyroiditis with histogram analysis using grayscale ultrasound images. J Ultrasound Med. 2016;35(3):519–26.
22. Kim I, Kim EK, Yoon JH, Han KH, Son EJ, Moon HJ, et al. Diagnostic role of conventional ultrasonography and shearwave elastography in asymptomatic patients with diffuse thyroid disease: initial experience with 57 patients. Yonsei Med J. 2014;55(1):247–53.
23. Schiemann U, Avenhaus W, Konturek JW, Gellner R, Hengst K, Gross M. Relationship of clinical features and laboratory parameters to thyroid echogenicity measured by standardized grey scale ultrasonography in patients with Hashimoto's thyroiditis. Med Sci Monit. 2003;9(4):MT13–7.
24. Doniach D, Bottazzo GF, Russell RC. Goitrous autoimmune thyroiditis (Hashimoto's disease). Clin Endocrinol Metab. 1979;8(1):63–80.
25. Li Y, Nishihara E, Hirokawa M, Taniguchi E, Miyauchi A, Kakudo K. Distinct clinical, serological, and sonographic characteristics of Hashimoto's thyroiditis based with and without IgG4-positive plasma cells. J Clin Endocrinol Metab. 2010;95(3):1309–17.
26. Zhang J, Zhao L, Gao Y, Liu M, Li T, Huang Y, et al. A classification of Hashimoto's thyroiditis based on immunohistochemistry for IgG4 and IgG. Thyroid. 2014;24(2):364–70.
27. Sato Y, Notohara K, Kojima M, Takata K, Masaki Y, Yoshino T. IgG4-related disease: historical overview and pathology of hematological disorders. Pathol Int. 2010;60(4):247–58.

28. Kottahachchi D, Topliss DJ. Immunoglobulin G4-related thyroid diseases. Eur Thyroid J. 2016;5(4):231–9.
29. Jokisch F, Kleinlein I, Haller B, Seehaus T, Fuerst H, Kremer M. A small subgroup of Hashimoto's thyroiditis is associated with IgG4-related disease. Virchows Arch. 2016;468(3):321–7.
30. Bonavita JA, Mayo J, Babb J, Bennett G, Oweity T, Macari M, et al. Pattern recognition of benign nodules at ultrasound of the thyroid: which nodules can be left alone? AJR Am J Roentgenol. 2009;193(1):207–13.
31. Virmani V, Hammond I. Sonographic patterns of benign thyroid nodules: verification at our institution. AJR Am J Roentgenol. 2011;196(4):891–5.
32. Serres-Creixams X, Castells-Fuste I, Pruna-Comella X, Yetano-Laguna V, Garriga-Farriol V, Gallardo-Agromayor E. Paratracheal lymph nodes: a new sonographic finding in autoimmune thyroiditis. J Clin Ultrasound. 2008;36(7):418–21.
33. Blank W, Braun B. Sonography of the thyroid—part 2: thyroid inflammation, impairment of thyroid function and interventions. Ultraschall Med. 2008;29(2):128–49; quiz 50-5
34. Vitti P, Rago T, Mazzeo S, Brogioni S, Lampis M, De Liperi A, et al. Thyroid blood flow evaluation by color-flow Doppler sonography distinguishes Graves' disease from Hashimoto's thyroiditis. J Endocrinol Investig. 1995;18(11):857–61.
35. Sporea I, Vlad M, Bota S, Sirli RL, Popescu A, Danila M, et al. Thyroid stiffness assessment by acoustic radiation force impulse elastography (ARFI). Ultraschall Med. 2011;32(3):281–5.
36. Magri F, Chytiris S, Capelli V, Alessi S, Nalon E, Rotondi M, et al. Shear wave elastography in the diagnosis of thyroid nodules: feasibility in the case of coexistent chronic autoimmune Hashimoto's thyroiditis. Clin Endocrinol. 2012;76(1):137–41.
37. English C, Casey R, Bell M, Bergin D, Murphy J. The sonographic features of the thyroid gland after treatment with radioiodine therapy in patients with Graves' disease. Ultrasound Med Biol. 2016;42(1):60–7.
38. Erdogan MF, Anil C, Cesur M, Baskal N, Erdogan G. Color flow Doppler sonography for the etiologic diagnosis of hyperthyroidism. Thyroid. 2007;17(3):223–8.
39. Ota H, Amino N, Morita S, Kobayashi K, Kubota S, Fukata S, et al. Quantitative measurement of thyroid blood flow for differentiation of painless thyroiditis from Graves' disease. Clin Endocrinol. 2007;67(1):41–5.

40. Cappelli C, Pirola I, Gandossi E, Formenti AM, Agosti B, Castellano M. Ultrasound findings of subacute thyroiditis: a single institution retrospective review. Acta Radiol. 2014;55(4):429–33.
41. Park SY, Kim EK, Kim MJ, Kim BM, KK O, Hong SW, et al. Ultrasonographic characteristics of subacute granulomatous thyroiditis. Korean J Radiol. 2006;7(4):229–34.
42. Ohmori N, Miyakawa M, Ohmori K, Takano K. Ultrasonographic findings of papillary thyroid carcinoma with Hashimoto's thyroiditis. Intern Med. 2007;46(9):547–50.
43. Nishihara E, Ohye H, Amino N, Takata K, Arishima T, Kudo T, et al. Clinical characteristics of 852 patients with subacute thyroiditis before treatment. Intern Med. 2008;47(8):725–9.
44. Shahbazian HB, Sarvghadi F, Azizi F. Ultrasonographic characteristics and follow-up in post-partum thyroiditis. J Endocrinol Investig. 2005;28(5):410–2.
45. Miyakawa M, Tsushima T, Onoda N, Etoh M, Isozaki O, Arai M, et al. Thyroid ultrasonography related to clinical and laboratory findings in patients with silent thyroiditis. J Endocrinol Investig. 1992;15(4):289–95.
46. Brander A. Ultrasound appearances in de Quervain's subacute thyroiditis with long-term follow-up. J Intern Med. 1992;232(4):321–5.
47. Omori N, Omori K, Takano K. Association of the ultrasonographic findings of subacute thyroiditis with thyroid pain and laboratory findings. Endocr J. 2008;55(3):583–8.
48. Nishihara E, Amino N, Ohye H, Ota H, Ito M, Kubota S, et al. Extent of hypoechogenic area in the thyroid is related with thyroid dysfunction after subacute thyroiditis. J Endocrinol Investig. 2009;32(1):33–6.
49. Kunz A, Blank W, Braun B. De Quervain's subacute thyroiditis – colour Doppler sonography findings. Ultraschall Med. 2005;26(2):102–6.
50. Zuhur SS, Ozel A, Kuzu I, Erol RS, Ozcan ND, Basat O, et al. The diagnostic utility of color Doppler ultrasonography, Tc-99m Pertechnetate uptake, and TSH-receptor antibody for differential diagnosis of Graves' disease and silent thyroiditis: a comparative study. Endocr Pract. 2014;20(4):310–9.
51. Xie P, Xiao Y, Liu F. Real-time ultrasound elastography in the diagnosis and differential diagnosis of subacute thyroiditis. J Clin Ultrasound. 2011;39(8):435–40.

52. Ruchala M, Szczepanek E, Sowinski J. Sonoelastography in de Quervain thyroiditis. J Clin Endocrinol Metab. 2011;96(2):289–90.
53. Yang Z, Zhang H, Wang K, Cui G, Fu F. Assessment of diffuse thyroid disease by strain ratio in ultrasound elastography. Ultrasound Med Biol. 2015;41(11):2884–9.
54. Ahuja AT, Griffiths JF, Roebuck DJ, Loftus WK, Lau KY, Yeung CK, et al. The role of ultrasound and oesophagography in the management of acute suppurative thyroiditis in children associated with congenital pyriform fossa sinus. Clin Radiol. 1998;53(3):209–11.
55. Bukvic B, Diklic A, Zivaljevic V. Acute suppurative klebsiella thyroiditis: a case report. Acta Chir Belg. 2009;109(2):253–5.
56. Boyd CM, Esclamado RM, Telian SA. Impaired vocal cord mobility in the setting of acute suppurative thyroiditis. Head Neck. 1997;19(3):235–7.
57. Dahlgren M, Khosroshahi A, Nielsen GP, Deshpande V, Stone JH. Riedel's thyroiditis and multifocal fibrosclerosis are part of the IgG4-related systemic disease spectrum. Arthritis Care Res (Hoboken). 2010;62(9):1312–8.
58. Papi G, LiVolsi VA. Current concepts on Riedel thyroiditis. Am J Clin Pathol. 2004;121(Suppl):S50–63.
59. Hennessey JV. Clinical review: Riedel's thyroiditis: a clinical review. J Clin Endocrinol Metab. 2011;96(10):3031–41.
60. Ozbayrak M, Kantarci F, Olgun DC, Akman C, Mihmanli I, Kadioglu P. Riedel thyroiditis associated with massive neck fibrosis. J Ultrasound Med. 2009;28(2):267–71.
61. Perez Fontan FJ, Cordido Carballido F, Pombo Felipe F, Mosquera Oses J, Villalba Martin C. Riedel thyroiditis: US, CT, and MR evaluation. J Comput Assist Tomogr. 1993;17(2):324–5.
62. Papi G, Corrado S, Cesinaro AM, Novelli L, Smerieri A, Carapezzi C. Riedel's thyroiditis: clinical, pathological and imaging features. Int J Clin Pract. 2002;56(1):65–7.
63. Slman R, Monpeyssen H, Desarnaud S, Haroche J, Fediaevsky Ldu P, Fabrice M, et al. Ultrasound, elastography, and fluorodeoxyglucose positron emission tomography/computed tomography imaging in Riedel's thyroiditis: report of two cases. Thyroid. 2011;21(7):799–804.
64. Perez Fontan FJ, Cordido Carballido F, Pombo Felipe F, Mosquera Oses J, Villalba Martin C. J Comput Assist Tomogr. 1993;17(2):324–5.

65. Chen YK, Lin CL, Cheng FT, Sung FC, Kao CH. Cancer risk in patients with Hashimoto's thyroiditis: a nationwide cohort study. Br J Cancer. 2013;109(9):2496–501.
66. Paparodis R, Imam S, Todorova-Koteva K, Staii A, Jaume JC. Hashimoto's thyroiditis pathology and risk for thyroid cancer. Thyroid. 2014;24(7):1107–14.
67. Gul K, Dirikoc A, Kiyak G, Ersoy PE, Ugras NS, Ersoy R, et al. The association between thyroid carcinoma and Hashimoto's thyroiditis: the ultrasonographic and histopathologic characteristics of malignant nodules. Thyroid. 2010;20(8):873–8.
68. Kim WB, Han SM, Kim TY, Nam-Goong IS, Gong G, Lee HK, et al. Ultrasonographic screening for detection of thyroid cancer in patients with Graves' disease. Clin Endocrinol. 2004;60(6):719–25.
69. Anderson L, Middleton WD, Teefey SA, Reading CC, Langer JE, Desser T, et al. Hashimoto thyroiditis: part 2, sonographic analysis of benign and malignant nodules in patients with diffuse Hashimoto thyroiditis. AJR Am J Roentgenol. 2010;195(1):216–22.
70. Durfee SM, Benson CB, Arthaud DM, Alexander EK, Frates MC. Sonographic appearance of thyroid cancer in patients with Hashimoto thyroiditis. J Ultrasound Med. 2015;34(4):697–704.
71. Liu FH, Hsueh C, Chang HY, Liou MJ, Huang BY, Lin JD. Sonography and fine-needle aspiration biopsy in the diagnosis of benign versus malignant nodules in patients with autoimmune thyroiditis. J Clin Ultrasound. 2009;37(9):487–92.
72. Topaloglu O, Baser H, Cuhaci FN, Sungu N, Yalcin A, Ersoy R, et al. Malignancy is associated with microcalcification and higher AP/T ratio in ultrasonography, but not with Hashimoto's thyroiditis in histopathology in patients with thyroid nodules evaluated as Bethesda Category III (AUS/FLUS) in cytology. Endocrine. 2016;54(1):156–68.
73. Ye ZQ, DN G, HY H, Zhou YL, XQ H, Zhang XH. Hashimoto's thyroiditis, microcalcification and raised thyrotropin levels within normal range are associated with thyroid cancer. World J Surg Oncol. 2013;11:56.
74. Kwak JY, Kim EK, Hong SW, KK O, Kim MJ, Park CS, et al. Diffuse sclerosing variant of papillary carcinoma of the thyroid: ultrasound features with histopathological correlation. Clin Radiol. 2007;62(4):382–6.

75. Jeong SH, Hong HS, Lee EH, Kwak JJ. The diffuse sclerosing variant of papillary thyroid cancer presenting as innumerable diffuse microcalcifications in underlying adolescent Hashimoto's thyroiditis: a case report. Medicine. 2016;95(12):e3141.
76. Jeon EJ, Shon HS, Jung ED. Primary mucosa-associated lymphoid tissue lymphoma of thyroid with the serial ultrasound findings. Case Rep Endocrinol. 2016;2016:5608518.
77. Ma B, Jia Y, Wang Q, Li X. Ultrasound of primary thyroid non-Hodgkin's lymphoma. Clin Imaging. 2014;38(5):621–6.
78. Mizokami T, Hamada K, Maruta T, Higashi K, Yamashita H, Noguchi Y, et al. Development of primary thyroid lymphoma during an ultrasonographic follow-up of Hashimoto's thyroiditis: a report of 9 cases. Intern Med. 2016;55(8):943–8.

Chapter 7
Ultrasound of Thyroid Nodules

Susan J. Mandel and Jill E. Langer

Introduction

Thyroid ultrasound is an exquisitely sensitive technique for the detection of thyroid nodules and is able to image nodules as small as 2–3 mm. The prevalence of sonographically detected nodules that cannot be palpated is up to 50–60% in individuals older than 60 [1]. The significant increase in thyroid cancer incidence both in the United States and in other countries with higher health-care utilization is directly linked to the increase in diagnostic imaging with incidental detection

S.J. Mandel, MD, MPH (✉)
Division of Endocrinology, Diabetes and Metabolism, Department of Medicine, Perelman School of Medicine, University of Pennsylvania, Philadelphia, PA, USA
e-mail: Susan.Mandel@uphs.upenn.edu

J.E. Langer, MD
Department of Radiology, Perelman School of Medicine, University of Pennsylvania, Philadelphia, PA, USA

D.S. Duick et al. (eds.), *Thyroid and Parathyroid Ultrasound and Ultrasound-Guided FNA*,
https://doi.org/10.1007/978-3-319-67238-0_7

of thyroid nodules [2, 3]. Coupled with the rising incidence rates is the knowledge that a significant number of thyroid cancers are now recognized to be low risk, such that even if never diagnosed, these would not harm the patient [3]. Therefore, the challenge confronting the clinician is the identification of those nodules that have a higher probability of being a clinically relevant malignancy so that these can be targeted for fine-needle aspiration biopsy (FNA) and the recognition of those that may undergo sonographic surveillance because of a lower malignant potential. Although other factors influence a patient's thyroid cancer risk, such as history of neck irradiation as a child or presence of certain genetic syndromes, the sonographic imaging properties of a thyroid nodule have a definite impact on FNA decision-making [4].

Over the last two decades, multiple publications have investigated the correlation of nodule sonography and cancer risk. Initially, the focus was to define risk based upon the presence or absence of individual imaging features. More recently, however, the focus has been on defining classification systems of sonographic patterns, each representing a composite of specific imaging features. This chapter will first review the specific ultrasound features and then describe how these comprise sonographic patterns and their association with thyroid cancer risk.

Ultrasound Characteristics of Thyroid Nodules

Ultrasound not only detects the presence, location, and size of nodules within the thyroid gland but also provides details about the composition and other characteristics of nodules that are related to their histopathology. Over the last decade, multiple reports have evaluated sonographic features of thyroid nodules as predictors of malignancy. However, these studies neither utilize consistent methodologies nor uniformly address all characteristics. Some inconsistencies may

be related to technical improvements in thyroid sonography, with earlier reports typically using a 7 MHz probe, while more recent studies use higher-frequency probes, typically 10 MHz and higher, which provide better resolution. But, differences in pathological and imaging classification criteria account for the largest proportion of variability among the studies [5]. For example, benign nodules may be identified by cytology or by histology; consequently, the proportion of thyroid cancers in these series varies from 4 to 32% [6–15]. Furthermore, the analysis and reporting of sonographic features differ among the series. Some only consider echogenicity for solid nodules; others include cystic nodules, and echogenicity is determined by the solid portion. Most studies dichotomize a halo as absent or present, but some separate those with a partial halo from those with a complete halo [15]. Some series group all macrocalcifications together [6, 12], whereas others divide them into subtypes [14, 15]. Finally, identification of these qualitative ultrasound features is highly operator dependent, especially for characterization of nodule margins [16].

A description of the individual sonographic characteristics of thyroid nodules follows, with a focus on the features that are associated with thyroid cancer. Table 7.1 lists these sonographic characteristics and summarizes their published median sensitivities and specificities for detection of malignancy summarized from 14 published reports [6–15, 17–20]. In order to minimize the effects of the varying methodologies, we have chosen to include studies that have met the following criteria: (1) report at least 100 nodules; (2) analyze at least three sonographic characteristics; and (3) report both sensitivity and specificity for thyroid cancer.

Echogenicity

The echogenicity of a thyroid nodule refers to its brightness relative to the normal thyroid parenchyma. Normal parenchyma appears homogeneously hyperechoic or relatively

Table 7.1 Grayscale sonographic features reported to be associated with thyroid cancer

	Median sensitivity (range)	**Median specificity (range)**
Hypoechoic c/w surrounding thyroid [6–12, 14, 15, 17–20]	81% (48–90%)	53% (36–92%)
Marked hypoechogenicity c/w strap muscle [13, 18, 20]	41% (27–59%)	94% [92–94%)
Microcalcifications [6–9, 13–15, 17, 18, 20]	44% (26–73%)	89% (69–98%)
Macrocalcifications [9, 14, 15, 18, 20]	10% (2–17%)	94% (84–98%)
Absence of halo [9, 14, 15, 18, 20]	66% (33–100%)	43% (30–77%)
Irregular, microlobulated margins [6, 7, 9, 12, 14, 15, 17–20]	55% (17–84%)	80% (62–85%)
Solid consistency [9, 12, 14, 15, 20]	86% (78–91%)	48% (30–58%)
Taller-than-wide shape on transverse view [6, 13, 18, 20]	48% (33–84%)	92% (82–93%)

bright on sonography as a consequence of the high number of acoustic interfaces within the normal follicles of the thyroid gland. The echogenicity of a nodule is described relative to this bright background of the normal thyroid as either (1) hypoechoic, meaning darker than the normal thyroid (Fig. 7.1a); (2) hyperechoic, meaning brighter than normal thyroid (Fig. 7.1b); or (3) isoechoic, meaning equal in echogenicity compared to the normal thyroid (Fig. 7.1c). Many nodules have regions of varying echogenicity and may be described by the dominant echogenicity (e.g.,, predominantly hypoechoic) or when there is no dominant pattern, as

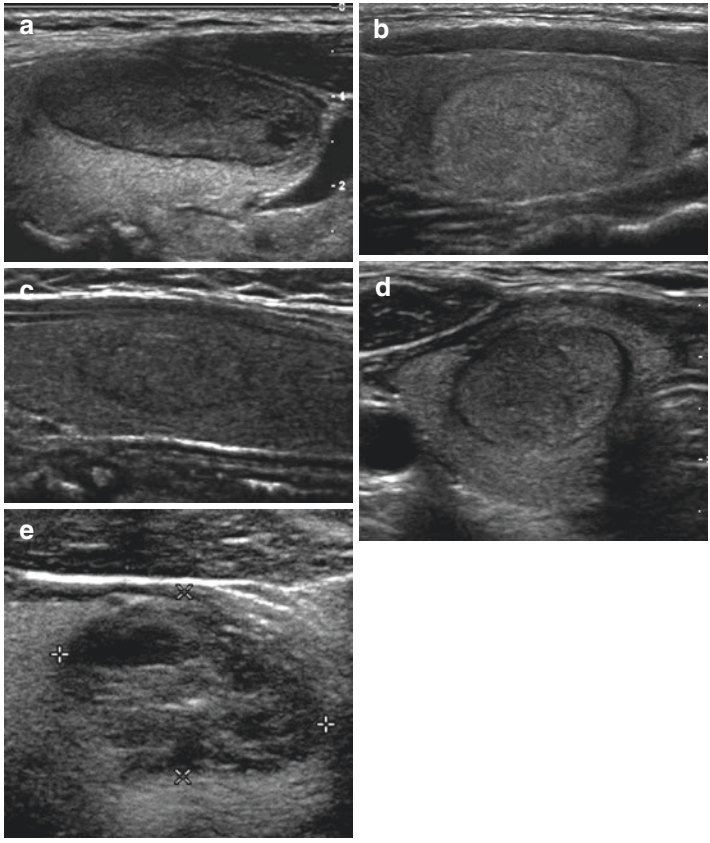

FIGURE 7.1 Nodule echogenicity. Images from ultrasound exams performed on different patients show (**a**) a hypoechoic nodule, (**b**) a hyperechoic nodule, (**c**) an isoechoic nodule, (**d**) a heterogeneous solid nodule with both hyperechoic and hypoechoic solid portions, and (**e**) a mixed cystic and solid nodule in which the solid component is isoechoic to the parenchyma. The nodules depicted in (**b**) and (**d**) proved to be follicular variant of papillary thyroid carcinoma, and the reminder had benign cytology

heterogeneous in echogenicity (Fig. 7.1d). For nodules that are partially cystic, the echogenicity of the solid part should be used to describe the nodule's echogenicity, and cystic

components are considered anechoic, meaning devoid of echoes, with hypoechoic used only in reference to solid components of a nodule [21] (Fig. 7.1e).

Most thyroid cancers appear dark, or hypoechoic, as compared with thyroid parenchyma. Histologically, the increased cellularity and cellular compaction present in classic papillary thyroid cancer and medullary thyroid cancer produce less acoustic interfaces than micro-follicles and therefore typically cause these lesions to appear hypoechoic compared with surrounding normal thyroid tissue [6–12, 14, 15, 17]. However, not all neoplasms of the thyroid are hypoechoic in appearance. Follicular neoplasms, including benign follicular adenomas, follicular carcinomas, and follicular variant of papillary cancers, are composed of small micro-follicles with variable amounts of colloid. Therefore, the echogenicity of these follicular-predominant neoplasms, both carcinomas and adenomas, is less commonly hypoechoic and instead is much more commonly isoechoic or hyperechoic compared with the parenchyma (Fig. 7.1b, d) [22, 23].

Additionally, many benign nodules will also appear hypoechoic. Since benign nodules are much more common than malignant nodules, a nodule that is hypoechoic but otherwise lacks any additional features associated with malignancy will statistically most likely be benign. Hypoechogenicity, as a unique characteristic of a nodule, is therefore only a moderately sensitive finding for malignancy, with a reported median sensitivity of about 80%. The reported specificity of hypoechogenicity for malignancy varies greatly depending on the histological subtypes of cancers in the population studied as well as the association of hypoechogenicity with other coexisting nodule features such as all solid consistency, calcifications, and central vascular flow. Some authors have identified a sonographic feature called “marked hypoechogenicity” that describes a nodule with echogenicity that is darker than the neck strap muscles [13, 18, 20]. Compared to nodules that are hypoechoic with respect to parenchyma but not as hypoechoic as strap muscles, marked hypoechogenicity is less sensitive for identification of thyroid cancer but much more specific, typically over 90% [13, 18] (Fig. 7.2).

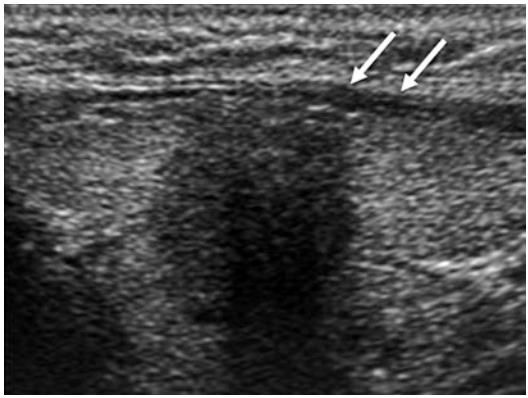

FIGURE 7.2 Marked hypoechogenicity. This nodule which proved to be a papillary thyroid carcinoma demonstrates echogenicity that is more hypoechoic than the strap muscles (*arrows*) overlying the thyroid

The assessment of echogenicity is subjective and tends to have only fair to moderate interobserver reproducibility even among expert observers (Kappa values 0.3–0.5) [16, 18, 24]. Echogenicity can be altered by differing sonographic techniques including changes in the overall gain and transducer frequency. Additionally, in patients with autoimmune thyroid disease such as Hashimoto's thyroiditis, the echogenicity of the parenchyma is much more heterogeneous in appearance making classification of the nodule's echogenicity more subjective.

Composition

Nodule composition describes the amount or proportion of solid soft tissue and fluid in a nodule. Nodules can be described as (a) solid, meaning composed entirely or nearly entirely of soft tissue with only a few small scattered cystic spaces (Fig. 7.3a); (b) predominantly solid, meaning that soft tissue components comprise at least 50% or greater of the volume of the nodule (Fig. 7.3b); (c) predominantly cystic,

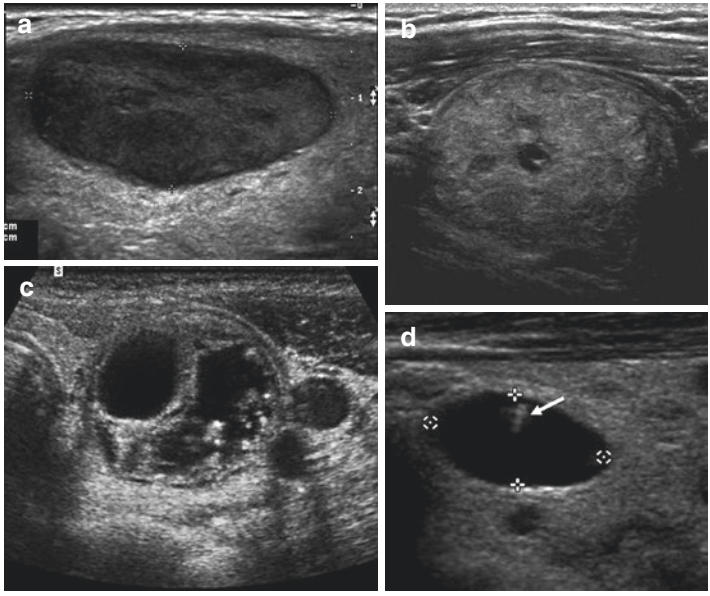

FIGURE 7.3 Nodule composition. Images from ultrasound exams performed on different patients show (**a**) an entirely solid nodule, (**b**) a predominantly solid nodule with scattered cystic spaces, (**c**) a predominantly cystic nodule, and (**d**) an entirely cystic nodule. Note the comet-tail artifact in this nodule (*arrow*)

meaning that soft tissue components comprise less than 50% of the volume of the nodule (Fig. 7.3c); or (d) entirely cystic, meaning fluid filled without appreciable solid component (Fig. 7.3d). Some authors have used numerical percentages of cystic or solid elements to describe nodule composition, most commonly by quartiles [21, 25, 26].

Thyroid cancers are most commonly solid or nearly entirely solid and are more likely to be solid than benign nodules [9, 12, 14, 15, 20]. However, because benign nodules outnumber malignant ones, this feature carries a relatively low specificity for malignancy as an isolated feature. It is estimated that a solid nodule has a 15–27% likelihood of being malignant [25]. Although there is some subjectivity in report-

ing the degree of cystic change present in a nodule, the interobserver agreement for reporting solid nodule consistency is reported to be quite high [16, 18, 24].

Cystic change within a nodule is very common. Hyperplastic nodules contain abundant colloid which appears cystic on sonography, and neoplasms may undergo cystic degeneration or necrosis, producing cystic areas [27]. It is uncommon for cancers to have a predominantly cystic appearance, with only 6.1% of predominately cystic nodules being malignant [28]. The evaluation of a partially cystic nodule for malignancy risk should focus on an analysis of the solid component. Features concerning for a malignancy include an intralesional solid component that is hypoechoic and lobulated, has an irregular border, and/or contains calcifications (Fig. 7.4). From a recent Mayo clinic review of ultrasound findings in 360 consecutive patients undergoing thyroidectomy for thyroid cancer, only nine (2.5%) were more than 50% cystic, and of these, all except one had another suspicious ultrasound feature that included either microcalcifications, intranodular vascularity, a mural nodule, or a thick irregular wall surrounding the cystic area [28]. In addition, if the solid component is eccentrically (peripherally) located within a partially cystic nodule and the margin of the solid component has an acute angle with the wall of the nodule, the risk for malignancy is also increased. Conversely, if the solid component is isoechoic, is centrally located within the nodule, or is distributed concentrically, lacking an acute angle with the nodule wall, or has a smooth margin, the nodule is likely benign (Figs. 7.4 and 7.5) [29].

Pure cysts over 1.5–2 cm are rare, comprising <2% of all thyroid nodules, but if present, these are reported to always be benign [15] (Fig. 7.3d). In addition, a "spongiform appearance" has a very low (<3%) risk of malignancy [30]. Moon et al. [18] defined a spongiform appearance as one in which the nodule has multiple microcystic areas that occupy more than 50% of the nodule volume and found that only 1 of the 360 thyroid cancers appeared spongiform in their series (Fig. 7.6). Bonavita et al. [19] defined spongiform to mean tiny spaces involving the entire nodule and found all 210 nonvascular nodules with

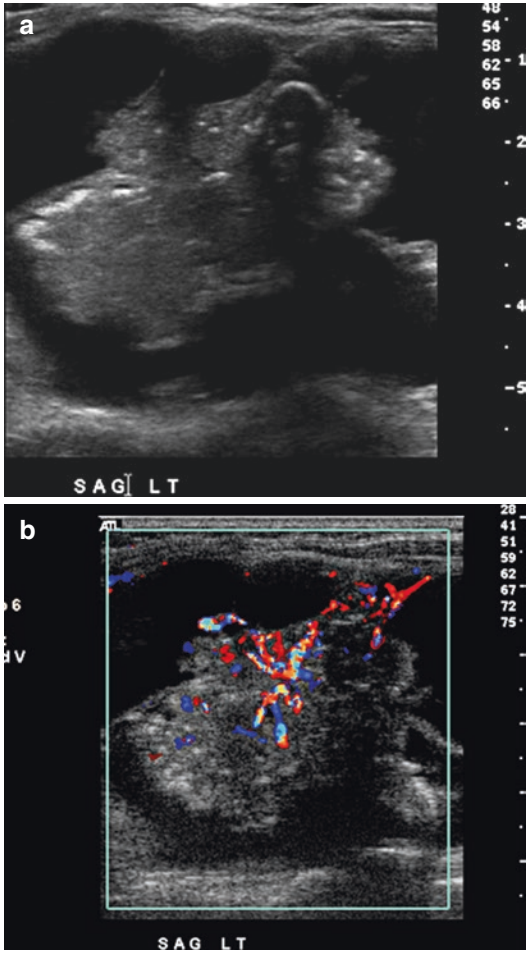

FIGURE 7.4 Cystic papillary cancer. (**a**) Grayscale and (**b**) color Doppler images of this cystic papillary thyroid carcinoma show the solid competent to be frond-like, lobulated, calcified, and have marked vascular flow

this sonographic appearance to be benign. These spongiform nodules often have echogenic foci, generally linear, that are associated with the back wall of the small internal cystic spaces. These bright foci should not be confused with

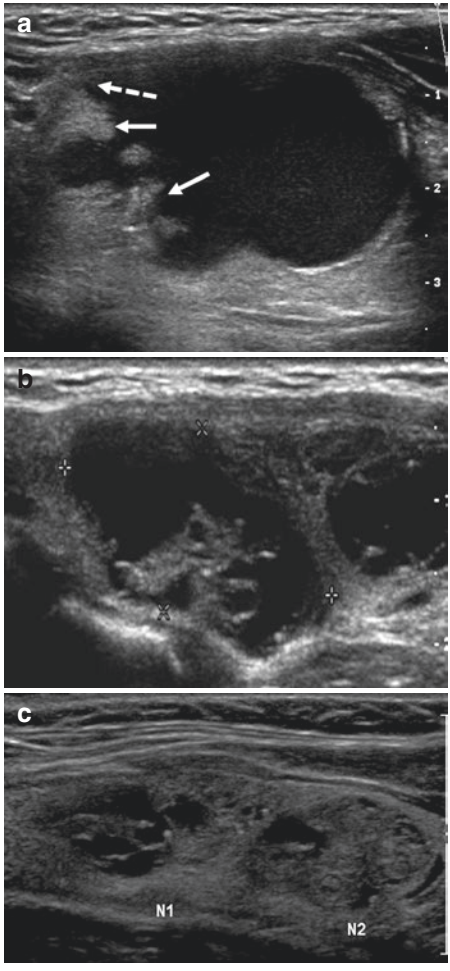

FIGURE 7.5 Partially cystic nodules. (**a**) The soft tissue component (*solid arrows*) of this predominately cystic nodule is eccentric and nodular and forms an acute angle with the wall of the nodule (*dashed arrow*) and proved to be a cystic papillary thyroid carcinoma. (**b**) The solid component of this cystic nodule is isoechoic to the parenchyma, with straight margins and spongiform in appearance, typical of a benign cystic nodule. (**c**) Two adjacent nodules (labeled N1 and N2) have a solid component that is central, concentric and smooth margin, typical of benign hyperplastic nodules

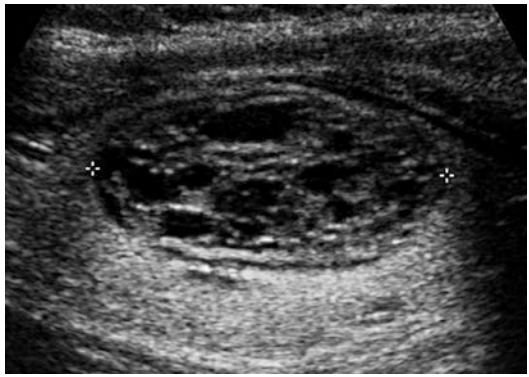

FIGURE 7.6 Spongiform nodule. This nodule has interspersed cystic spaces throughout, an appearance termed spongiform and is associated with a very low risk of malignancy

microcalcifications which are much smaller and punctate in appearance (Fig. 7.7). Often, comet-tail artifacts, which appear as an inverted triangle of parallel linear echoes, representing reverberation of sound waves caused by inspissated colloid [31], are present in both entirely cystic-appearing and spongiform nodules (Figs. 7.3d and 7.7b, c). It is worth noting that colloid may be present in both benign and malignant nodules. As noted above, very few thyroid cancers will be predominantly cystic, but these cystic carcinomas will typically have another suspicious US feature such as frond-like solid tissue and/or calcifications [28] (Fig. 7.4).

Calcifications

Calcifications may be present in up to 30% of nodules and can be divided into different categories. Microcalcifications appear as small, punctate echogenic foci, less than 1 mm, and are more specific (in some studies, up to 96%) than sensitive for thyroid cancer [32]. Microcalcifications, which are thought to represent aggregates of psammoma bodies, are found in about 40% of papillary thyroid cancers and much less

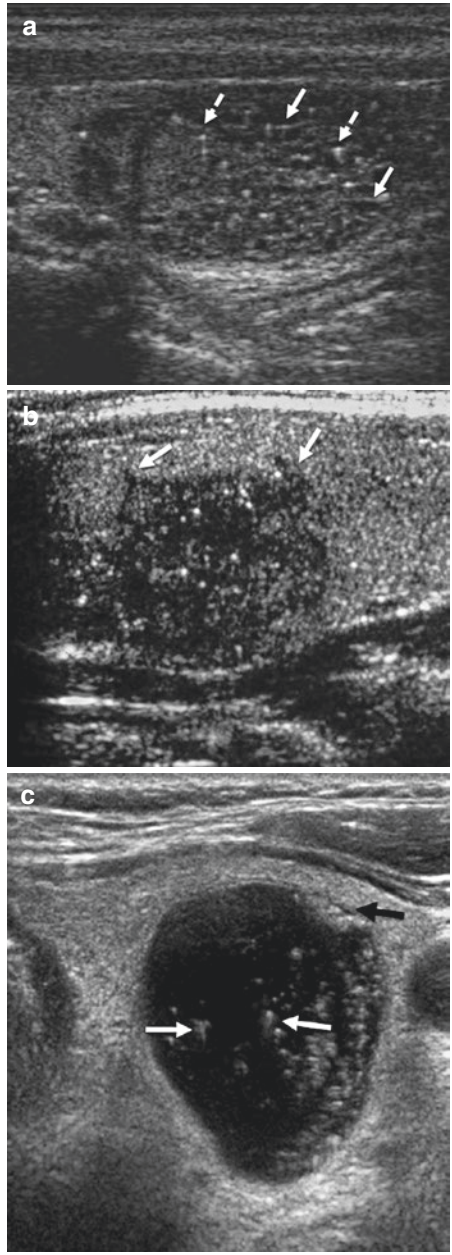

FIGURE 7.7 Echogenic foci. (**a**) Two types of echogenic foci are seen in this nodule. Some are short and linear and have comet-tail artifact (*dashed arrows*), whereas other are longer and linear (*solid arrows*) related to sound reflection from the back wall of the small internal cystic spaces in this spongiform nodule. FNA cytology is benign. (**b**) This nodule has microcalcifications which appear as punctate echogenic foci within the solid stroma of this hypoechoic solid nodule with irregular, jagged margins (*arrows*). FNA cytology is papillary thyroid cancer. (**c**) This nearly entirely cystic nodule shows multiple comet-tail artifacts (*white arrows*), which appear as inverted triangles of parallel linear echoes due to sound reverberation from colloid. An isoechoic solid component with smooth borders is seen anteriorly (*black arrow*)

commonly in benign nodules and Hashimoto's thyroiditis [32]. Due to the very small size of microcalcifications, they do not reflect the ultrasound beam sufficiently to cause distal acoustic shadowing, a feature dissimilar to larger or macrocalcifications. They most commonly are noted in nodules that have other malignant features such as all solid consistency, hypoechogenicity (often marked), and infiltrative margins, which help to distinguish them from other nonneoplastic and non-shadowing echoic foci in thyroid nodules (Fig. 7.7b). The interobserver agreement for the identification of microcalcifications is quite good [16]. Coarse or dense calcifications are larger than 2 mm and cause posterior acoustic shadowing (Fig. 7.8). Occurring within both benign and malignant nodules, these dystrophic calcifications are present in areas of fibrosis and tissue degeneration and necrosis. However, coarse calcifications, either associated with microcalcifications or appearing in the center of a hypoechoic nodule, may be worrisome for malignancy [15, 33]. Calcifications may also occur along the periphery of a nodule and can be thin and regular, often called "eggshell" calcification, which is most commonly noted in a benign nodule and less commonly in a malignancy [32] (Fig. 7.8c). Irregular or interrupted calcification is more concerning for a malignancy, and a particular worrisome finding is the interruption of this rim calcification by a soft tissue component of the nodule indicating probable invasion by the cancer (Fig. 7.8d, e).

Margins

Sonography performed with high-frequency, high-resolution transducers allows detailed assessment of the interface of thyroid nodules with the surrounding parenchyma. The margins of a nodule can be defined because of either a difference in echogenicity between the nodule and the thyroid parenchyma or a border that demarcates a nodule when it is similar in echogenicity to the background thyroid. If the thyroid parenchyma has a normal homogeneous hyperechoic appearance, a hypoechoic nodule is easily identified, but

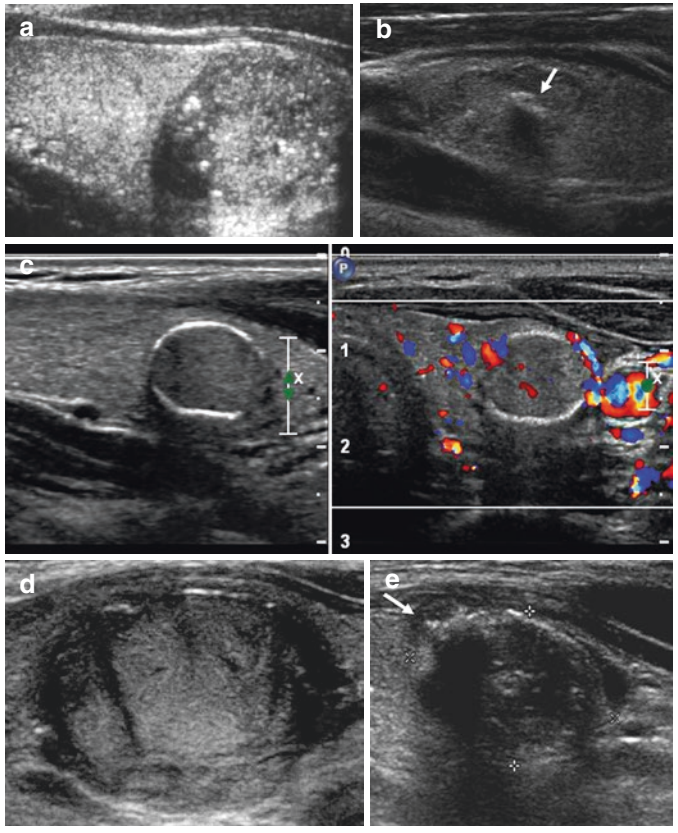

FIGURE 7.8 Macrocalcifications. (**a**) Hypoechoic solid nodule with both micro- and macrocalcifications. The macrocalcifications demonstrate posterior acoustic shadowing which appears as a dark area distal to the calcification due to complete reflection of sound by the large calcification. FNA cytology is papillary thyroid cancer. (**b**) A central linear calcification (*arrow*) is noted in this nodule. FNA cytology is benign. (**c**) A smooth peripheral rim of "eggshell" calcification is noted as well as central flow. FNA cytology is follicular variant of papillary carcinoma. (**d**) Note the interruption of the anterior calcified border that corresponded with localized invasion into the surrounding thyroid. FNA cytology is follicular variant of papillary carcinoma. (**e**) Note the extension of hypoechoic soft tissue with microcalcification beyond the peripheral rim of calcification. FNA cytology is papillary carcinoma

detection of a hypoechoic nodule can be more challenging if the parenchyma is heterogeneous such as with Hashimoto's thyroiditis. Certain margin features have been associated with thyroid malignancy. Infiltrative, spiculated, and/or jagged margins as well as lobular borders (Figs. 7.7b and 7.9) are concerning for an unencapsulated, invasive thyroid carcinoma. However, the distinction of infiltrative borders from

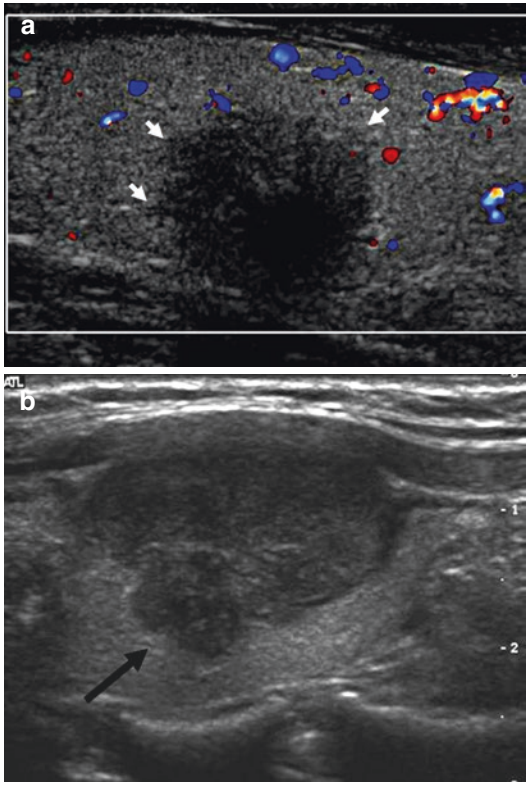

FIGURE 7.9 Nodule margins. (**a**) Hypoechoic solid nodule with jagged and spiculated margins (*arrows*) extending into the adjacent parenchyma. FNA cytology is papillary thyroid cancer. (**b**) Hypoechoic solid nodule with a lobulated margin (*arrow*). FNA cytology is papillary thyroid cancer

indistinct borders is important because many small hyperplastic nodules will have poorly defined or indistinct margins at the interface between the nodule and the adjacent normal tissue, but these are not infiltrative and not considered to be a sign of a malignant growth pattern [18]. Interobserver variability for assessment of nodule margins carries the poorest agreement [16], likely reflecting the subtlety of this analysis. Additionally, studies did not distinguish between poor-defined and more aggressive margin features which may account for its reported lack of association with malignancy in several studies.

Nodules may also demonstrate the presence of a halo, defined as a sonolucent ring that surrounds a nodule. This generally forms the margin for iso- and hyperechoic nodules. Since benign hyperplastic nodules grow slowly and displace and compress the surrounding blood vessels as they expand, this may produce a thin halo, which demonstrates the nodule's peripheral vascularity on color flow Doppler, and is found in about half of benign nodules (Fig. 7.10a, b). However, a halo can also be thick, irregular, and avascular [11] and may signify the presence of a fibrous capsule surrounding a neoplastic growth, either follicular or Hürthle cell, and is therefore more concerning (Fig. 7.10c).

When evaluating a known or potential thyroid malignancy, it is important to assess for invasion beyond the thyroid to the adjacent soft tissues. Ultrasound may detect extrathyroidal extension when the tumor growth extends through either the anterior or posterior thyroid capsule, which normally appears as a bright white outline surrounding the thyroid. In such instances, the margin of the tumor has an ill-defined edge that interrupts this capsule [34] (Fig. 7.11). Only rarely is intratracheal growth demonstrated by sonography.

Taller-than-Wide Shape

Several series have reported that thyroid cancer is associated with a nodule's anteroposterior to transverse diameter ratio

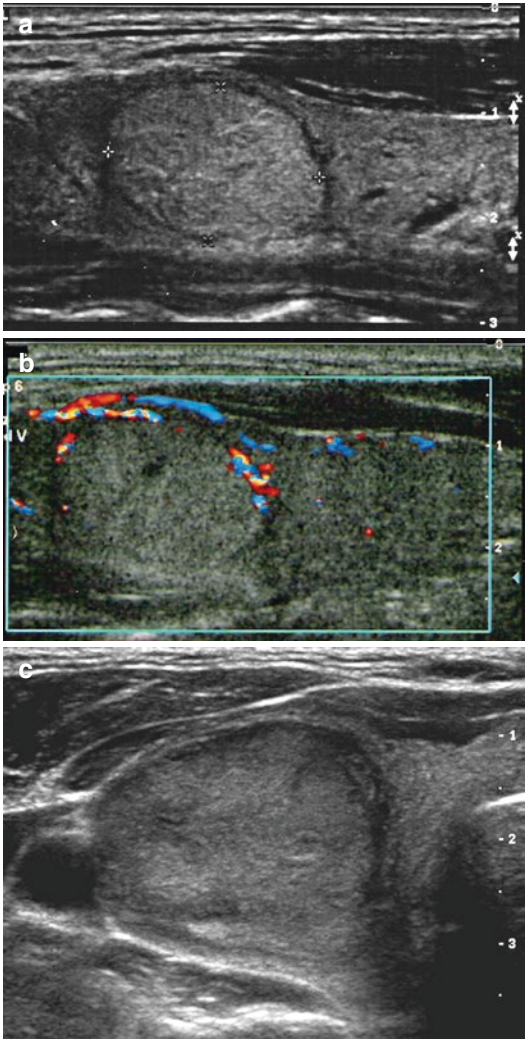

FIGURE 7.10 Halo. (**a**) Grayscale image of isoechoic nodule with thin regular halo. Cytology is benign. (**b**) Color flow Doppler image of the same nodule indicating the halo corresponds with peripheral vascularity. (**c**) Thick, irregular, and incomplete halo surrounding solid iso- to hyperechoic nodule. Histology is Hürthle cell cancer

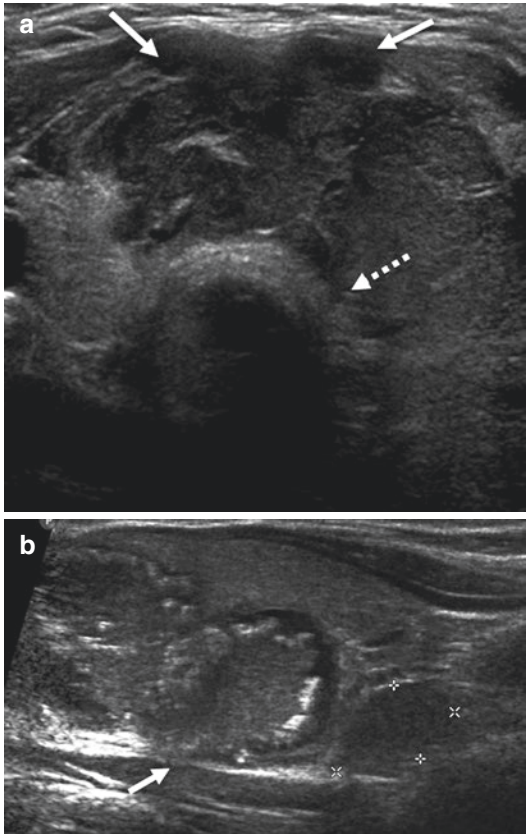

Figure 7.11 Extrathyroidal extension. (**a**) This anaplastic carcinoma shows clear extrathyroidal extension anteriorly (*solid arrows*) with tumor extending through the anterior capsule. Posteriorly there is lack of a clear margin with the adjacent trachea (*dashed arrow*) which proved to be tracheal invasion during surgery. (**b**) Sagittal image of the thyroid shows a calcified papillary thyroid carcinoma occupying much of the lobe. Posteriorly, there is discontinuity of the posterior capsule (*arrow*) which proved to be extrathyroidal extension of the tumor at surgery. Additionally, a metastatic central compartment lymph node is present (marked by electronic calipers)

(A/T) being greater than one as measured on the transverse view [6, 13, 18, 20]. This finding replicates the results in the sonographic literature evaluating breast carcinomas [13]. Disproportionate growth in the anteroposterior dimension is considered an aggressive growth pattern across, rather than within, the normal tissue planes. This finding may not be very sensitive for thyroid cancer, but it has a specificity ranging from 82 to 93% and is most commonly noted in smaller cancers under 1 cm [20, 35]. In studies that specify how measurements are made, there are no significant differences comparing transverse or longitudinal imaging planes for determining the ratio [35].

Vascularity

The vascularity of a thyroid nodule is evident with color flow Doppler (CFD) imaging. Based upon the Doppler frequency shift detected in the reflected ultrasound beam caused by moving blood, CFD imaging can show which regions have vascular flow, as well as measure the velocity of the blood flow. High-quality CFD imaging of the thyroid requires ultrasound units and imaging settings that are sensitive to detect the small size of vessels and the low velocity of flow within the thyroid. Power Doppler (PD) imaging, which is more sensitive than CFD, has also been applied to nodule assessment. Power Doppler is more sensitive to flow in small vessels, has relative independence from the incident angle of the ultrasound beam, and suffers less from background noise [11].

Generally speaking, the analysis of the pattern of flow has been the most investigated Doppler feature of thyroid nodules. Several systems exist for grading Doppler vascularity (see Chap. 3, Doppler Ultrasound). Using Doppler, nodule vascularity can be categorized as absent (type I), peripheral (type II), or peripheral and intranodular (type III) (Fig. 7.12). Although increased intranodular vascularity has been reported by earlier studies to be a worrisome feature, a recent report analyzing over 1000 nodules did not confirm an independent association with papillary thyroid

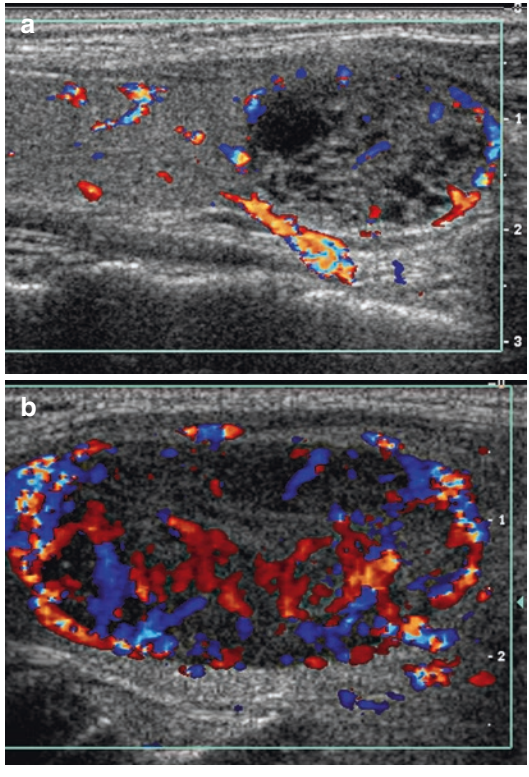

FIGURE 7.12 Nodular flow. (**a**) Peripheral vascularity in spongiform nodule. Cytology is benign. (**b**) Increased intranodular vascularity in hypoechoic nodule. Cytology is benign

cancer, after accounting for grayscale features of hypoechogenicity, taller-than-wide shape and noncircumscribed margins. Intranodular vascularity was observed in 31% of benign nodules and only 17% of papillary cancers [36]. One possible explanation for the discrepancy in reports on vascularity may be related to the specific type of thyroid cancer. Small papillary cancers, such as analyzed by Moon et al., may lack vascularity [36], whereas intranodular vascularity may more commonly be associated with follicular cancers [37].

Cervical Lymph Nodes

Cervical lymph node metastases from thyroid carcinoma may have a variety of abnormal findings including cystic regions, punctuate calcifications, hyperechoic foci, increased peripheral vascularity, and a rounded shape [30] (see Chap. 8 "Ultrasound and Mapping of the Neck Lymph Nodes"). Both the ATA [4, 38] and AACE [39, 40] guidelines for evaluating patients with thyroid nodules state that sonographic evaluation of the cervical lymph nodes should be part of standard diagnostic thyroid US of thyroid nodules. The AIUM practice guidelines indicate that an assessment of the lateral cervical lymph nodes should be part of all neck ultrasound exams, and any abnormal-appearing nodes should be imaged, and the location, size, and abnormal features of the node should be reported [41]. Because of the presence of the thyroid, it is more difficult to evaluate the central neck or paratracheal lymph nodes.

Ultrasound Patterns of Thyroid Nodules

The exclusive reliance on identification of individual sonographic features for FNA decision-making is tempered by two main observations. First, two recent meta-analyses of the extensive literature of observational reports correlating ultrasound features and thyroid cancer detected significant heterogeneity among studies [42, 43]. In part, this may be attributed to significant interobserver variability for accurate sonographic feature classification [18, 24]. In fact, the correct identification of microcalcifications, one of the individual features associated with the highest likelihood of cancer, is correlated to the proficiency of the sonographer, with overcall by less-experienced operators [42], potentially leading to inappropriate recommendations for FNA. Second, focus on the individual features is predicated upon the erroneous assumption that these features are present independently of each other; rather the appearance of some are highly

correlated with others. For example, microcalcifications almost exclusively appear in solid hypoechoic nodules. Similarly, irregular borders, which demarcate the interface between the nodule's echogenicity and the surrounding thyroid, by definition, are generally only apparent in a hypoechoic nodule when the background thyroid echotexture is normal. This natural relationship among features leads to the concept of identifying sonographic patterns, specifically defining characteristic nodule appearances that are each composed of a constellation of individual sonographic features simultaneously manifest together.

Currently, there are several systems of sonographic patterns for thyroid nodule risk stratification, developed for the most part by single institutions. They share the fact that pattern recognition is more reproducible among different operators [44–46] and is less influenced by physician experience [44]. Validation for these systems varies, retrospective or prospective, and generally reflects findings from only a single group. In addition, over the last 2 years, secondary publications have begun to appear that apply these classification schemes to different populations, for the most part reporting similar results. However, no one system has achieved universal acceptance, leading to some confusion for the practitioners of sonography. The next paragraphs describe the sonographic pattern classification systems most widely referenced in current practice.

The first Thyroid Imaging Reporting and Data System (TIRADS) was developed in 2009 [46] and was based upon the concepts of the original Breast Imaging Reporting and Data System (BIRADS) that defined mammographic categories according to cancer risk. Using pattern recognition, the objective of this TIRADS classification was not only to identify thyroid nodules for FNA but also to define those associated with a negligible malignancy risk such that FNA could be avoided. This original TIRADS system described in 2009 by Horvath et al. defined six categories, with TIRADS 1, a normal thyroid; TIRADS 2, benign nodules; TIRADS 3, probably benign nodules; TIRADS 4, suspicious nodules; TIRADS 5,

probably malignant nodules; and TIRADS 6, a diagnosed malignancy [46]. Therefore, in essence only four main categories apply to nodules, and these (TIRADS 2–5) are characterized by both grayscale and Doppler ultrasound criteria to define ten patterns. In the defining study of 1097 nodules, all 62 TIRADS 2 nodules were cytologically benign, and the probability of a malignant FNA cytology increased 3.4%, 14%, and 87%, respectively, in TIRADS 3, 4, and 5. In addition the authors subdivided TIRADS 4 into 4a and 4b with respective malignant cytology risks of 7 and 27%. Since its inception, the applicability and clinical use of this original TIRADS have been limited in part due to the perceived intricacy of the ten pattern descriptions subgrouped under TIRADS 2–5.

The goal of the second iteration of TIRADS, a system developed in Korea by Kwak et al. in 2011, was to develop a "practical" and less complex TIRADS stratifying malignancy risk and focused on FNA decision-making [47]. These authors stressed that in parallel to BIRADS, differentiating category 3 from 4 was crucial because surveillance is recommended for the former and biopsy for the latter. In addition, they also introduced a 4c subcategory. The study included 1658 nodules larger than 1 cm that underwent FNA. In a multivariate analysis, five ultrasound features were associated with malignancy: solid composition, hypoechogenicity or marked hypoechogenicity, irregular or microlobulated margins, microcalcifications, and taller-than-wide shape. Using a derived regression equation, cancer risk exponentially increased with the number of suspicious ultrasound features present. With these findings, the authors proposed a new TIRADS classification system: TIRADS 3, no suspicious features; TIRADS 4a, one suspicious feature; TIRADS 4b, two suspicious features; TIRADS 4c, three or four suspicious features; and TIRADS 5, five suspicious features. A main limitation of this classification system was each feature was assigned the same weight even though the authors noted that odds ratios for malignancy of certain features, such as irregular or microlobulated margins and microcalcifications, were higher than those of solid composition and hypoechogenicity. Furthermore, inherent in this type

of checklist classification scheme is the assumption that each feature can occur independent of the other four and is therefore just as likely to be the only suspicious finding. For example, TIRADS 4a is defined by only one suspicious feature. This could certainly be solid composition, but it would be highly unlikely that microlobulated or irregular margins would be the one element defining TIRADS 4a nodule because these types of margins virtually always occur in solid hypo- or marked hypoechoic nodules; hence a total of three characteristics are present, all of which are highly correlated, and these then define a TIRADS 4c nodule.

Subsequently, the Korean Society of Thyroid Radiology sought to modify the initial Kwak TIRADS system by assigning a different risk score to each suspicious ultrasound feature according to their odds ratios for cancer prediction derived from a multicenter retrospective study (Table 7.2) [48]. The total score associated with each nodule could then be used to predict malignancy risk. For example, the scores for hypo- versus marked hypoechogenicity were 2 and 6 points, respectively. No risk score was assigned to composition. However, what resulted from this new scheme was no longer a pattern recognition classification; rather this scoring system has reverted to identification of individual sonographic features and has not yet been widely adopted.

Also recognizing the differing probabilities of malignancy associated with the five ultrasound features, Russ and his colleagues proposed a third TIRADS classification scheme in 2013 [45], now referred to as the French system [49] (Table 7.2). Solid composition was removed from the list of high suspicion sonographic features. In addition, only marked but not mild hypoechogenicity was included in the list. High suspicion features were specifically defined as irregular shape, irregular borders, marked hypoechogenicity, microcalcifications, and, if available, high stiffness on elastography, but elastography was not considered prerequisite for this TIRADS classification. Mild hypoechogenicity in the absence of high suspicion features was categorized as TIRADS 4a. The presence of only one or two high suspicion features led to a TIRADS 4b category, but once three or more features

Table 7.2 Sonographic pattern systems and estimated malignancy risks (%)

ATA 2015 [4]	**AACE/AME 2016** [40]	**TIRADS Horvath 2009** [46]		**K-TIRADS** [48]	**TIRADS Russ** [45, 49]	
Benign 0%	Low risk <1%	2	0%	2 benign	2	0%
Very low suspicion <3%				Cyst <1%		
				Spongiform <3%		
Low suspicion 5–10%	Intermediate risk 5–15%	4a	5–10%	3 low suspicion 3–15%	3	0.25%
Intermediate suspicion 10–20%				4 intermediate suspicion 15–50%	4a	6%
High suspicion >70–90%	High risk 50–90%	4b	10–80%	5 high suspicion >60%	4b	69%
		5	>80%		5	~100%

were present, the nodule was classified as TIRADS 5. This system was validated in a prospective 2-year study of 4550 nodules (4.5% prevalence of thyroid cancer) that underwent US FNA. In addition, the authors estimated a 34% reduction in the number of FNAs if biopsy was not recommended for stable TIRADS 2 and 3 nodules [45].

The current 2015 American Thyroid Association (ATA) Management Guidelines for Adult Patients with Thyroid Nodules and Differentiated Thyroid Cancer sought to make pattern recognition more straightforward and reproducible for physicians who perform sonography on patients in their practices [4]. The ATA task force recognized the existence of three competing TIRADS systems, none of which has achieved universal adoption, as well as their perceived complexity by non-radiologists. The ATA guidelines provide an "atlas" that offers examples of 15 sonographic nodule images and 1 image of a sonographically suspicious lateral cervical lymph node (Fig. 7.13). These 16 images are divided

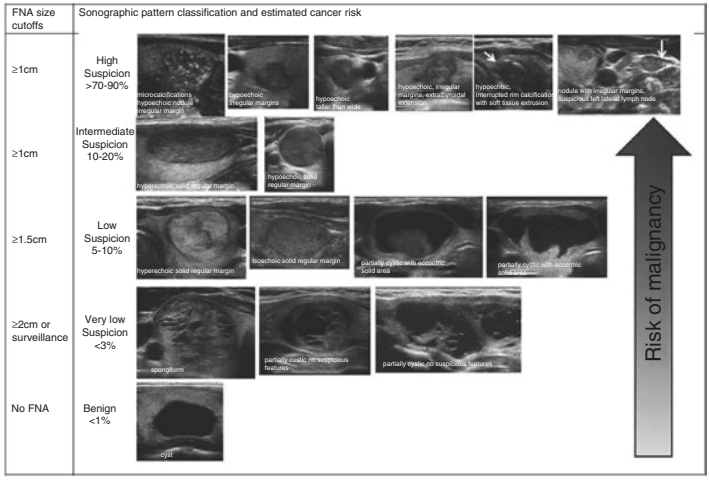

FIGURE 7.13 American Thyroid Association nodule sonographic patterns and risk of malignancy from Haugen BR, et al. [4] Copyright © 2016, Mary Ann Liebert, Inc.

into five defined categories of sonographic patterns with associated cancer risks to triage nodules for FNA with recommendations for either surveillance or FNA with nodule size cutoffs. The patterns in each category were derived from a graded evidence-based literature review. The benign category includes the pure cyst, and FNA is not recommended, unless performed for therapeutic drainage. The very low suspicion patterns (cancer risk estimate <3%) are spongiform nodules and mixed cystic solid nodules without high suspicion features defined as irregular (infiltrative, microlobulated) margins, microcalcifications, taller-than-wide shape, interrupted rim calcifications with small extrusive soft tissue component, evidence of extrathyroidal extension, or sonographically suspicious cervical lymph nodes. Low suspicion nodules (cancer risk estimate 5–10%) include iso- or hyperechoic solid nodules or partially cystic nodules with eccentric solid areas without high suspicion features. Cancer risk increases to 10–20% for intermediate-suspicion nodules that are smoothly marginated hypoechoic and solid. The frequency of cancer is highest (>70–90%) for the high suspicion category that includes solid hypoechoic nodules or solid hypoechoic component of a partially cystic nodule with any of the high suspicion features. Sonographic assessment of cervical lymph nodes is also prerequisite for all imaging as the presence of suspicious lymph nodules mandates FNA of the lymph node regardless of nodule pattern. Recommended FNA size cutoffs are smaller, 1 cm, for the patterns more likely to be associated with cancer and then increase as the likelihood of malignancy decreases, such that for the very low suspicion pattern observation may suffice (see Chap. 12, Table 12.1).

The American Association of Clinical Endocrinologists (AACE) in collaboration with the Italian Associazione Medici Endocrinologi (AME) has recently introduced a three-tiered pattern classification, with recommendation for either surveillance or FNA at size cutoffs determined by cancer risk (Fig. 7.14) [40]. Low-risk nodules (cancer risk estimate 1%) include spongiform nodules and nodules that are

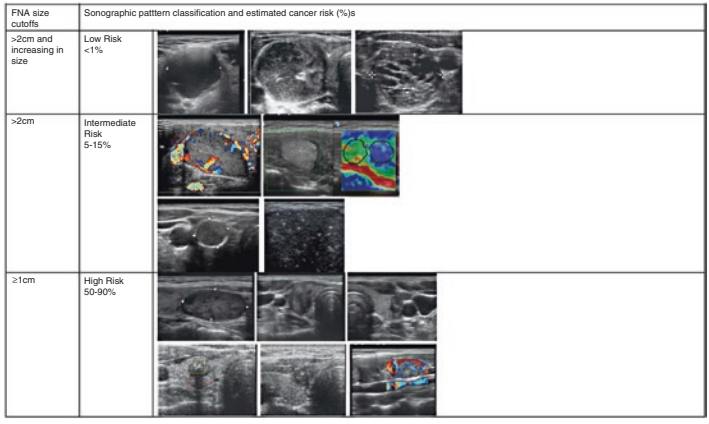

Figure 7.14 AACE/AME thyroid ultrasound features and risk of malignancy. Reprinted from Endocrine Practice, Vol. 22, Gharib H et al., American Association of Clinical Endocrinologists, American College of Endocrinology, and Associazione Medici Endocrinologi Medical Guidelines for Clinical Practice for the Diagnosis and Management of Thyroid Nodules - 2016 update, pp. 622–639 [40]. Copyright 2016, with permission from the American Association of Clinical Endocrinologists

more than 50% cystic nodules without suspicious features. These suspicious features are the same as those identified in the ATA guidelines, with two differences: only marked, not mild, hypoechogenicity is included, and interrupted rim calcifications with a soft tissue excrescence are not. Intermediate risk (cancer risk estimate 5–15%) includes both mildly hypoechoic and isoechoic solid nodules, with both smooth or ill-defined margins and stiffness on elastography if available. High-risk lesions (estimated cancer risk 50–90%) have one of the suspicious features. The AACE/AME 3 level system telescopes some of the five levels of the ATA classification as indicated in Table 7.2.

One of the shortcomings of the pattern approach of nodule classification is the inability to classify all nodules [50]. For this reason, the American College of Radiology (ACR)

began the development of the ACR TIRADS using a point system for the evaluation of nodular features, with the ultimate aim of applying it to risk stratification and triage of nodules for FNA or observation. The ACR has presented a lexicon of defined sonographic features demonstrated to be consistently associated with either benignity or malignancy, which can be used to describe every thyroid lesion. The lexicon contains six ultrasound categories: composition, echogenicity, shape as taller than wide, size based upon maximal diameter, margins, and echogenic foci. Each category contains terms describing the varied appearances within that category, and the spectrum of nodule features within each category has been clearly defined and illustrated to standardize interpretation [25]. This classification system requires the evaluator to assess and report these six categories for each nodule, and each feature in the category is assigned individual points that scale with the risk of malignancy. For example, within the echogenicity category, a hyperechoic or isoechoic nodule is assigned 1 point, a hypoechoic nodules 2 points, and a very hypoechoic nodule 3 points. The points for all six categories are summed to determine the overall TIRADS level, levels 1 through 5. For each level, a specific size cutoff for FNA is recommended. The goal of the ACR TIRADS is to facilitate a standard approach to assessing and reporting nodular features that will be reproducible among interpreters with varying levels of sonographic expertise and allow for future refinement of the individual point assignments. However, once published, this system will still require prospective validation.

Conclusion

Operationalizing thyroid nodule ultrasound for FNA decision-making has evolved over the last two decades with improved understanding of imaging features associated with both malignancy and benignity as well as of limitations due to interobserver variation. The current trend has

been to identify constellations of individual sonographic features, and classify nodules by patterns, which includes the use of TIRADS. The benefits of using sonographic pattern recognition include increased interobserver reliability that promotes standardization of interpretation. However, currently there are several classification systems, and none has undergone multi-institutional prospective validation. Although there is no universal consensus about which should be adopted by the clinician, the classification systems consistently identify the same patterns as either high or low risk. The variabilities are manifest in the categorizations of nodules with patterns in between these extremes. Prospective studies will refine our understanding and optimize sonography as a risk stratification tool for thyroid nodule assessment.

References

1. Mazzaferri EL. Management of a solitary thyroid nodule. N Engl J Med. 1993;328(8):553–9.
2. Davies L, Welch HG. Current thyroid cancer trends in the United States. JAMA Otolaryngol Head Neck Surg. 2014;140(4):317–22.
3. Brito JP, Davies L. Is there really an increased incidence of thyroid cancer? Curr Opin Endocrinol Diabetes Obes. 2014;21(5):405–8.
4. Haugen BR, Alexander EK, Bible KC, Doherty GM, Mandel SJ, Nikiforov YE, et al. 2015 American Thyroid Association management guidelines for adult patients with thyroid nodules and differentiated thyroid cancer: the American Thyroid Association guidelines task force on thyroid nodules and differentiated thyroid cancer. Thyroid. 2016;26(1):1–133.
5. Langer JE, Mandel SJ. Thyroid nodule sonography: assessment for risk of malignancy. Imaging Med. 2011;3:513–24.
6. Cappelli C, Pirola I, Cumetti D, Micheletti L, Tironi A, Gandossi E, et al. Is the anteroposterior and transverse diameter ratio of nonpalpable thyroid nodules a sonographic criteria for recommending fine-needle aspiration cytology? Clin Endocrinol. 2005;63(6):689–93.

7. Papini E, Guglielmi R, Bianchini A, Crescenzi A, Taccogna S, Nardi F, et al. Risk of malignancy in nonpalpable thyroid nodules: predictive value of ultrasound and color-Doppler features. J Clin Endocrinol Metab. 2002;87(5):1941–6.
8. Rago T, Vitti P, Chiovato L, Mazzeo S, De Liperi A, Miccoli P, et al. Role of conventional ultrasonography and color flow-Doppler sonography in predicting malignancy in 'cold' thyroid nodules. Eur J Endocrinol. 1998;138(1):41–6.
9. Takashima S, Fukuda H, Nomura N, Kishimoto H, Kim T, Kobayashi T. Thyroid nodules: re-evaluation with ultrasound. J Clin Ultrasound. 1995;23(3):179–84.
10. Brkljacic B, Cuk V, Tomic-Brzac H, Bence-Zigman Z, Delic-Brkljacic D, Drinkovic I. Ultrasonic evaluation of benign and malignant nodules in echographically multinodular thyroids. J Clin Ultrasound. 1994;22(2):71–6.
11. Cerbone G, Spiezia S, Colao A, Di Sarno A, Assanti AP, Lucci R, et al. Power Doppler improves the diagnostic accuracy of color Doppler ultrasonography in cold thyroid nodules: follow-up results. Horm Res. 1999;52(1):19–24.
12. Leenhardt L, Hejblum G, Franc B, Fediaevsky LD, Delbot T, Le Guillouzic D, et al. Indications and limits of ultrasound-guided cytology in the management of nonpalpable thyroid nodules. J Clin Endocrinol Metab. 1999;84(1):24–8.
13. Kim EK, Park CS, Chung WY, Oh KK, Kim DI, Lee JT, et al. New sonographic criteria for recommending fine-needle aspiration biopsy of nonpalpable solid nodules of the thyroid. AJR Am J Roentgenol. 2002;178(3):687–91.
14. Nam-Goong IS, Kim HY, Gong G, Lee HK, Hong SJ, Kim WB, et al. Ultrasonography-guided fine-needle aspiration of thyroid incidentaloma: correlation with pathological findings. Clin Endocrinol. 2004;60(1):21–8.
15. Frates MC, Benson CB, Doubilet PM, Kunreuther E, Contreras M, Cibas ES, et al. Prevalence and distribution of carcinoma in patients with solitary and multiple thyroid nodules on sonography. J Clin Endocrinol Metab. 2006;91(9):3411–7.
16. Wienke JR, Chong WK, Fielding JR, Zou KH, Mittelstaedt CA. Sonographic features of benign thyroid nodules: interobserver reliability and overlap with malignancy. J Ultrasound Med. 2003;22(10):1027–31.
17. Kovacevic O, Skurla MS. Sonographic diagnosis of thyroid nodules: correlation with the results of sonographically guided fine-needle aspiration biopsy. J Clin Ultrasound. 2007;35(2):63–7.

18. Moon WJ, Jung SL, Lee JH, Na DG, Baek JH, Lee YH, et al. Benign and malignant thyroid nodules: US differentiation--multicenter retrospective study. Radiology. 2008;247(3):762–70.
19. Bonavita JA, Mayo J, Babb J, Bennett G, Oweity T, Macari M, et al. Pattern recognition of benign nodules at ultrasound of the thyroid: which nodules can be left alone? AJR Am J Roentgenol. 2009;193(1):207–13.
20. Ahn SS, Kim EK, Kang DR, Lim SK, Kwak JY, Kim MJ. Biopsy of thyroid nodules: comparison of three sets of guidelines. AJR Am J Roentgenol. 2010;194(1):31–7.
21. Frates MC, Benson CB, Charboneau JW, Cibas ES, Clark OH, Coleman BG, et al. Management of thyroid nodules detected at US: Society of Radiologists in ultrasound consensus conference statement. Radiology. 2005;237(3):794–800.
22. Jeh SK, Jung SL, Kim BS, Lee YS. Evaluating the degree of conformity of papillary carcinoma and follicular carcinoma to the reported ultrasonographic findings of malignant thyroid tumor. Korean J Radiol. 2007;8(3):192–7.
23. Kim DS, Kim JH, Na DG, Park SH, Kim E, Chang KH, et al. Sonographic features of follicular variant papillary thyroid carcinomas in comparison with conventional papillary thyroid carcinomas. J Ultrasound Med. 2009;28(12):1685–92.
24. Choi SH, Kim EK, Kwak JY, Kim MJ, Son EJ. Interobserver and intraobserver variations in ultrasound assessment of thyroid nodules. Thyroid. 2010;20(2):167–72.
25. Grant EG, Tessler FN, Hoang JK, Langer JE, Beland MD, Berland LL, et al. Thyroid ultrasound reporting lexicon: white paper of the ACR Thyroid Imaging, Reporting and Data System (TIRADS) Committee. J Am Coll Radiol. 2015;12(12 Pt A):1272–9.
26. Alexander EK, Hurwitz S, Heering JP, Benson CB, Frates MC, Doubilet PM, et al. Natural history of benign solid and cystic thyroid nodules. Ann Intern Med. 2003;138(4):315–8.
27. Malhi H, Beland MD, Cen SY, Allgood E, Daley K, Martin SE, et al. Echogenic foci in thyroid nodules: significance of posterior acoustic artifacts. AJR Am J Roentgenol. 2014;203(6):1310–6.
28. Henrichsen TL, Reading CC, Charboneau JW, Donovan DJ, Sebo TJ, Hay ID. Cystic change in thyroid carcinoma: prevalence and estimated volume in 360 carcinomas. J Clin Ultrasound. 2010;38(7):361–6.
29. Kim DW, Lee EJ, In HS, Kim SJ. Sonographic differentiation of partially cystic thyroid nodules: a prospective study. AJNR Am J Neuroradiol. 2010;31(10):1961–6.

30. Langer JE, Mandel SJ. Sonographic imaging of cervical lymph nodes in patients with thyroid cancer. Neuroimaging Clin N Am. 2008;18(3):479–89. vii-viii.
31. Ahuja A, Chick W, King W, Metreweli C. Clinical significance of the comet-tail artifact in thyroid ultrasound. J Clin Ultrasound. 1996;24(3):129–33.
32. Taki S, Terahata S, Yamashita R, Kinuya K, Nobata K, Kakuda K, et al. Thyroid calcifications: sonographic patterns and incidence of cancer. Clin Imaging. 2004;28(5):368–71.
33. Reading CC, Charboneau JW, Hay ID, Sebo TJ. Sonography of thyroid nodules: a "classic pattern" diagnostic approach. Ultrasound Q. 2005;21(3):157–65.
34. Ito Y, Kobayashi K, Tomoda C, Uruno T, Takamura Y, Miya A, et al. Ill-defined edge on ultrasonographic examination can be a marker of aggressive characteristic of papillary thyroid microcarcinoma. World J Surg. 2005;29(8):1007–11; discussion 11–2.
35. Moon HJ, Kwak JY, Kim EK, Kim MJ. A taller-than-wide shape in thyroid nodules in transverse and longitudinal ultrasonographic planes and the prediction of malignancy. Thyroid. 2011;21(11):1249–53.
36. Moon HJ, Kwak JY, Kim MJ, Son EJ, Kim EK. Can vascularity at power Doppler US help predict thyroid malignancy? Radiology. 2010;255(1):260–9.
37. Messuti I, Corvisieri S, Bardesono F, Rapa I, Giorcelli J, Pellerito R, et al. Impact of pregnancy on prognosis of differentiated thyroid cancer: clinical and molecular features. Eur J Endocrinol. 2014;170(5):659–66.
38. Cooper DS, Doherty GM, Haugen BR, Kloos RT, Lee SL, Mandel SJ, et al. Revised American Thyroid Association management guidelines for patients with thyroid nodules and differentiated thyroid cancer. Thyroid. 2009;19(11):1167–214.
39. Gharib H, Papini E, Paschke R, Duick DS, Valcavi R, Hegedus L, et al. American Association of Clinical Endocrinologists, Associazione Medici Endocrinologi, and European Thyroid Association medical guidelines for clinical practice for the diagnosis and management of thyroid nodules: executive summary of recommendations. Endocr Pract. 2010;16(3):468–75.
40. Gharib H, Papini E, Garber JR, Duick DS, Harrell RM, Hegedus L, et al. American Association of Clinical Endocrinologists, American College of Endocrinology, and Associazione Medici Endocrinologi medical guidelines for clinical practice for the

diagnosis and management of thyroid nodules - 2016 update. Endocr Pract. 2016;22(5):622–39.
41. AIUM practice guideline for the performance of ultrasound examinations of the head and neck. J Ultrasound Med. 2014;33(2):366–82.
42. Brito JP, Gionfriddo MR, Al Nofal A, Boehmer KR, Leppin AL, Reading C, et al. The accuracy of thyroid nodule ultrasound to predict thyroid cancer: systematic review and meta-analysis. J Clin Endocrinol Metab. 2014;99(4):1253–63.
43. Remonti LR, Kramer CK, Leitao CB, Pinto LC, Gross JL. Thyroid ultrasound features and risk of carcinoma: a systematic review and meta-analysis of observational studies. Thyroid. 2015;25(5):538–50.
44. Ko SY, Kim EK, Moon HJ, Yoon JH, Kim HY, Kwak JY. Application of thyroid imaging reporting and data system in the ultrasound assessment of thyroid nodules according to physician experience. Ultrasound Q. 2016;32(2):126–31.
45. Russ G, Royer B, Bigorgne C, Rouxel A, Bienvenu-Perrard M, Leenhardt L. Prospective evaluation of thyroid imaging reporting and data system on 4550 nodules with and without elastography. Eur J Endocrinol. 2013;168(5):649–55.
46. Horvath E, Majlis S, Rossi R, Franco C, Niedmann JP, Castro A, et al. An ultrasonogram reporting system for thyroid nodules stratifying cancer risk for clinical management. J Clin Endocrinol Metab. 2009;94(5):1748–51.
47. Kwak JY, Han KH, Yoon JH, Moon HJ, Son EJ, Park SH, et al. Thyroid imaging reporting and data system for US features of nodules: a step in establishing better stratification of cancer risk. Radiology. 2011;260(3):892–9.
48. Kwak JY, Jung I, Baek JH, Baek SM, Choi N, Choi YJ, et al. Image reporting and characterization system for ultrasound features of thyroid nodules: multicentric Korean retrospective study. Korean J Radiol. 2013;14(1):110–7.
49. Russ G. Risk stratification of thyroid nodules on ultrasonography with the French TI-RADS: description and reflections. Ultrasonography. 2016;35(1):25–38.
50. Yoon JH, Lee HS, Kim EK, Moon HJ, Kwak JY. Malignancy risk stratification of thyroid nodules: comparison between the thyroid imaging reporting and data system and the 2014 American Thyroid Association management guidelines. Radiology. 2016;278(3):917–24.

Chapter 8
Ultrasound and Mapping of Neck Lymph Nodes

Catherine F. Sinclair, Dipti Kamani, Gregory W. Randolph, Barry Sacks, and H. Jack Baskin Sr.

C.F. Sinclair, BMBS (Hons), FRACS, BSc (Biomed)
Department of Otolaryngology, Icahn School of Medicine at Mount Sinai, New York, NY, USA

D. Kamani, MD
Department of Otolaryngology, Division of Thyroid and Parathyroid Surgery, Massachusetts Eye and Ear Infirmary, Boston, MA, USA

G.W. Randolph, MD, FACS, FACE (✉)
Thyroid Surgery Oncology, Harvard Medical School, Boston, MA, USA

Division of Thyroid and Parathyroid Endocrine Surgery, Department of Otolaryngology – Head and Neck Surgery, Massachusetts Eye and Ear Infirmary, Boston, MA, USA

Department of Surgery, Endocrine Surgery Service, Massachusetts General Hospital, Boston, MA, USA
e-mail: gregory_randolph@meei.harvard.edu

B. Sacks, MD
Beth Israel Deaconess Medical Center, Natick, MA, USA

H. Jack Baskin Sr., MD, MACE
University of Central Florida College of Medicine, Orlando, FL, USA

D.S. Duick et al. (eds.), *Thyroid and Parathyroid Ultrasound and Ultrasound-Guided FNA*,
https://doi.org/10.1007/978-3-319-67238-0_8

Introduction

The strategic value of ultrasound imaging in both treating and following patients with thyroid cancer has become increasingly appreciated over the past decades. Ultrasound plays a prominent role in the recommendations from the 2015 American Thyroid Association's *Guidelines for Adult Patients with Thyroid Nodules and Differentiated Thyroid Cancer* [1]. Neck sonography has become pivotal in planning the preoperative surgical approach in patients undergoing initial thyroid cancer surgery as well as in the postoperative surveillance of patients with thyroid cancer. The key to determining the extent of the appropriate initial surgery as well as the recognition of recurrent cancer is the ultrasound's ability to detect early malignancy in the regional neck lymph nodes.

The format of this chapter will be as follows:

1. Surgical levels and compartments of the neck
2. Ultrasound characteristics that differentiate benign from malignant lymph nodes and cervical node ultrasound-guided FNA (USGFNA)
3. Preoperative use of ultrasound to evaluate the neck in thyroid carcinoma
4. Postoperative utilization of ultrasound, in conjunction with thyroglobulin and/or other imaging modalities, in a cost-effective manner for the long-term surveillance and early detection of residual, recurrent, or metastatic thyroid cancer

Surgical Levels and Compartments of the Neck

Lymphatic metastases from thyroid cancer tend to segregate into specific regions of the neck. To facilitate description and three-dimensional communication of these regions between treating physicians, the neck is divided into six basic compartments or subregions (Fig. 8.1) which have great utility in the preoperative surgical planning of patients with nodal disease.

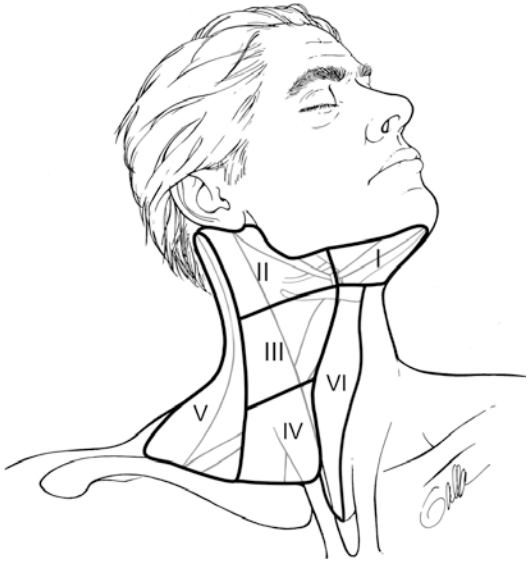

FIGURE 8.1 Surgical levels of the neck

Level I constitutes lymph nodes above the anterior and posterior bellies of the digastric muscle cephalad to the hyoid bone and inferior to the inferior border of the mandible and includes the submental group of nodes. For Levels II–IV, the posterior border is the posterior edge of the sternomastoid muscle, and the anterior border is the laryngeal complex. Level II (upper jugular region) extends from the skull base and spinal accessory nerve superiorly to the hyoid bone inferiorly and is subdivided into IIA below the spinal accessory nerve and IIB above the spinal accessory nerve. Level III (mid-jugular region) extends from the hyoid superiorly to the cricoid cartilage inferiorly. Level IV (lower jugular region) extends from the cricoid cartilage down to the clavicle. Level V is a triangular region bounded anteriorly by the posterior edge of the sternocleidomastoid muscle (SCM) and posteriorly by the anterior edge of the trapezius muscle. It is subdivided into the region 5A above the level of the cricoid cartilage and 5B (supraclavicular region) below the level of

the cricoid cartilage. Level VI (central compartment) is composed of four subcompartments: (1) prelaryngeal (Delphian nodal group), (2) pretracheal, (3) left paratracheal, and (4) right paratracheal. It extends from the hyoid bone superiorly to the clavicle. A Level VII or superior mediastinal group has also been described which appears to be encompassed in the lower part of the central neck dissection group described by ATA [2]. Typically standard neck dissection for papillary carcinoma of the thyroid excludes Levels I, IIB, and V due to the low prevalence of disease in these subareas. An exception to this is a patient with bulky lateral neck nodal disease where these areas may require dissection. In addition to the lymph node levels described above, many classification systems pertaining to the cervical lymph nodes have been published, including Union for International Cancer Control (UICC) classification, American Head and Neck Society (AHNS) classification, Japanese classification and the compartment classification (German classification) [3–6]. Cunnane et al. recently published a thyroid-specific, multidisciplinary, clinically validated nodal classification system that divides the neck into multiple stand-alone surgically distinct, side-specific compartments [7]. Distribution of nodal disease likely varies between primary presentation and recurrent disease. A recent study that mapped nodal distribution in PTC reported that at the first presentation, nodal disease is concentrated in the central neck, while in recurrent disease, this pattern is reversed with the nodes being more focused in the lateral neck [8] (Fig. 8.2). The same study reported that with recurrent nodal disease, ectopic nodal location outside of the typical central and lateral neck regions (retropharyngeal, sublingual region, subcutaneous location, axilla, and chest wall) occurred in almost 10% of patients, suggesting that axial imaging should be performed in patients with recurrent nodal disease [8].

Nodal subgroups can be further classified into the lateral (Levels II–V) or central (Levels VI ± VII) neck which correlates with the current prevailing philosophy of a "compartment-oriented dissection" in surgical management of nodal disease. Lateral neck dissection for thyroid carcinoma generally

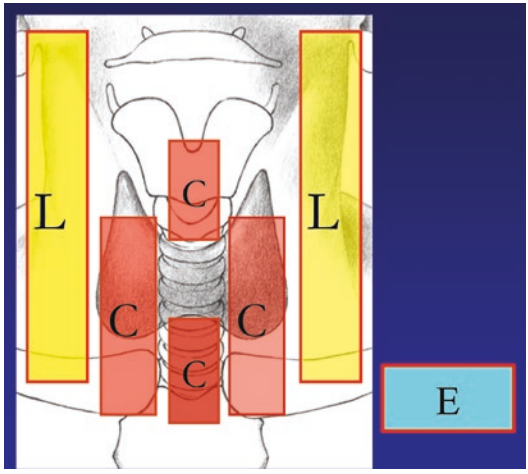

FIGURE 8.2 Thyroid cancer radiographic map. *Outer boxes* (*A*, *B*) indicate the lateral neck nodal compartments, whereas the *inner boxes* (*C*, *D*, *L*, *T*) indicate the central neck nodal compartments. Box labeled (*E*) represents ectopic nodal groups

encompasses Levels II, III, and IV, and central neck dissection encompasses prelaryngeal, pretracheal, and at least one paratracheal region (Fig. 8.3). Note that, occasionally, especially in patients with aggressive subtypes of thyroid cancer, patients may present with nodal metastases which are outside of these known neck regions. However, the vast majority of patients with well-differentiated nodal metastasis can be described with this terminology.

Ultrasound Features of Benign vs. Malignant Lymph Nodes

The normal neck contains approximately 300 lymph nodes. Benign nodes are typically flattened or slightly oval in shape, and most are less than 0.5 cm in size in their *short axis*. They may enlarge for various reasons including infection, inflammation, allergy, and malignancy. Those in Levels I and II commonly

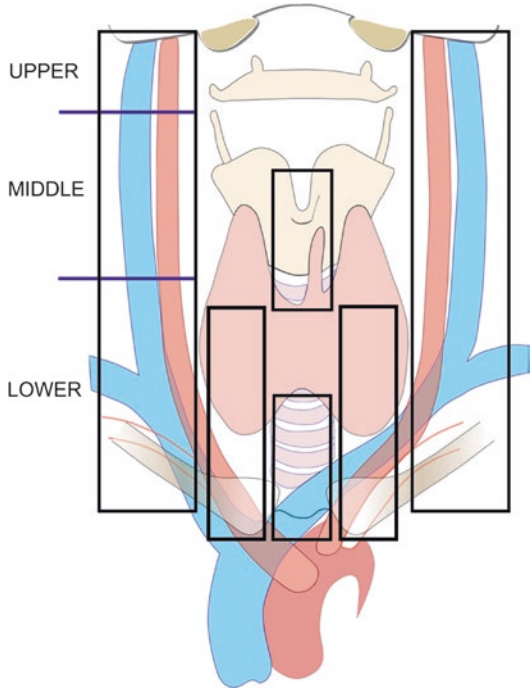

FIGURE 8.3 "Compartment-oriented dissection." Lateral neck dissection is divided into *upper* (Level II lymph nodes), *middle* (Level III lymph nodes), and *lower* (Level IV lymph nodes). Central neck dissection encompasses the pretracheal region, the prelaryngeal region, and at least one paratracheal region

enlarge during upper respiratory infections or inflammation. Therefore, the overall size of a lymph node is of little benefit in determining if a lymph node is malignant or benign, and ultrasound criteria other than size must be used to differentiate benign hyperplastic lymph nodes from those that are malignant. While larger lymph nodes should, and do, attract our attention, additional characteristics such as shape, hilar line, calcifications, cystic degeneration, and vascularity need to be assessed to determine the probability of malignancy.

Unlike thyroid nodules which are measured in true transverse, sagittal, and AP axes, the lymph nodes are measured in long and short axes. The long axis will usually align close to the sagittal plane, but lymph nodes typically orient in an oblique axis. Measurements are made in two planes, initially holding the transducer in the transverse and sagittal planes. The largest diameter of the node is measured and defined as the "long-axis diameter." Then the largest diameter perpendicular to the first plane is measured and defined as the "short-axis diameter." The ratio of the long to short axis is then calculated as the long/short ratio [9]. Benign lymph nodes are usually flattened with a long/short ratio > 2. Inflamed or hyperplastic lymph nodes typically appear enlarged but usually maintain the flat shape and a long/short ratio > 2. Malignant lymph nodes usually have a more rounded morphology with a long/short ratio < 2. In an early publication, Steinkamp et al. reported a 95% accuracy in differentiating benign from malignant cervical nodes using a long/short ratio cutoff of 2 [9]. However Leboulleux subsequently found that the long/short ratio (using the same cutoff of 2) had only a 46% sensitivity and 64% specificity [10].

A normal lymph node has a hypoechoic cortex but often shows a central hyperechoic hilum containing fat and intranodal blood vessels referred to as a hilar line. The hilar line is more prominent in older patients. Malignant lymph nodes in the neck, whether they are metastatic from the thyroid or elsewhere (i.e. squamous cell carcinoma), or lymphoma will seldom show a hilar line, thought to be due to interruption of lymphatic flow by tumor invasion. However, specificity of hilar absence for malignancy is reportedly only 29% as the hilum may be difficult to visualize in a benign node [10, 11]. Thus, the presence of a hilar line is reassuring, but its absence is not a highly suspicious finding. When ultrasound is performed on a patient with nodular goiter, or a patient with a history of thyroid cancer, finding a prominent lymph node with a rounded shape

(*long/short axis ratio* < 2) and absent hilar line warrants further evaluation of the node (Figs. 8.4, 8.5, 8.6, 8.7, and 8.8).

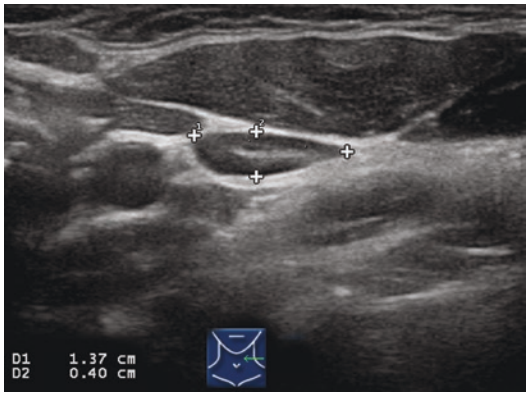

FIGURE 8.4 Benign lymph node. The normal neck contains scores of lymph nodes some of which are easily seen with ultrasound. This lymph node (calipers) appears benign because it is elongated with a long-/short-axis ratio > 2

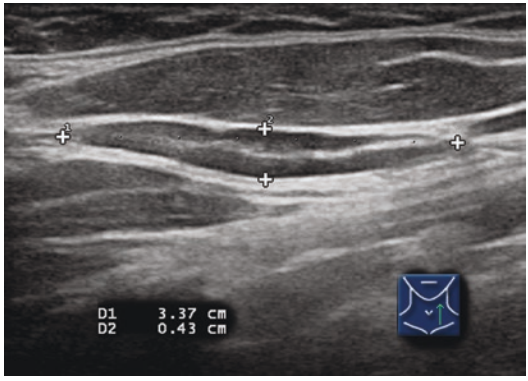

FIGURE 8.5 The same lymph node in Figure 8.4 in sagittal view. Despite a maximum dimension of 3 cm, it is clearly benign with long-/short-axis ratio >>2 and a clear central hilum

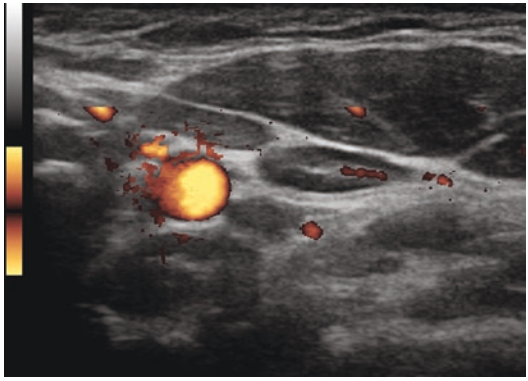

FIGURE 8.6 Power Doppler of the previous lymph node shows vascularization of the hilum which contains small arterioles. Note there is no vascularization seen in the periphery of the node

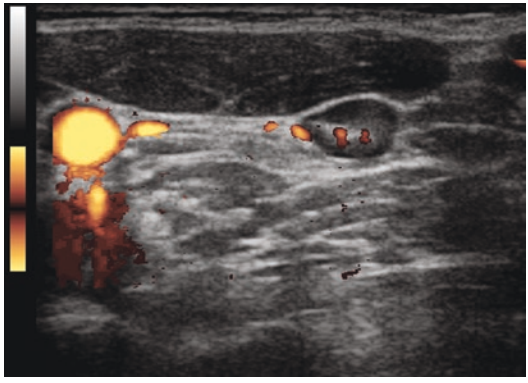

FIGURE 8.7 Benign lymph node. This lymph node is slightly more rounded with a long-/short-axis ratio < 2 in the transverse view. However it has a central hilum, and vascularity is limited to the hilum. The long to short axis can be seen to be >2 in Fig. 8.8 in the sagittal view

Several ultrasound findings, when present, are highly suspicious for malignancy in lymph nodes [12] (Table 8.1). Any lymph node calcification, particularly microcalcifications but also amorphous calcifications with posterior acoustic

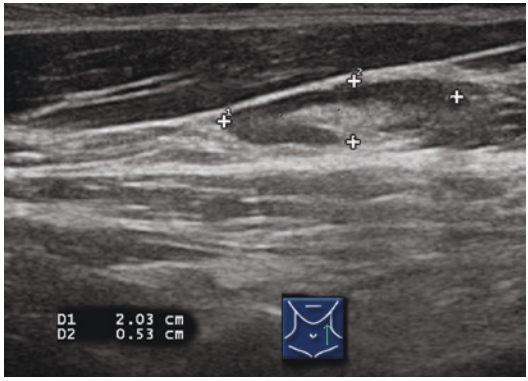

FIGURE 8.8 Same lymph node in sagittal (longitudinal) view. Long/short axis is >2 and a broad central hilum is present

TABLE 8.1 Sensitivity and specificity of suspicious lymph node features

Feature	Sensitivity (%)	Specificity (%)
Short axis > 0.5 cm	61	96
Long axis > 1 cm	68	75
Long/short axis < 2	46	64
Hyperechogenic hilum absent	100	29
Hypoechogenicity	39	18
Hyperechogenic punctuations (calcifications)	46	100
Cystic appearance	11	100
Chaotic or peripheral vascularity	86	82

Data from Leboulleux et al. [10]

shadowing, raises a strong suspicion of malignancy (sensitivity 46%, specificity 100%) [9]. Cystic necrosis, often recognized because of uneven posterior acoustic enhancement, is another highly specific sign of malignancy (although this also may be seen in tuberculosis of lymph nodes) (Figs. 8.9, 8.10, 8.11, 8.12, 8.13, 8.14, 8.15, 8.16, 8.17, 8.18, 8.19, 8.20, and 8.21).

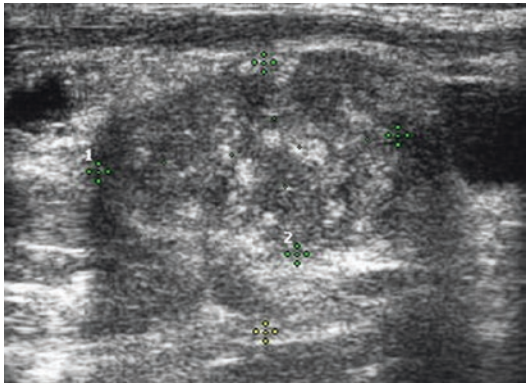

FIGURE 8.9 This markedly heterogeneous lymph node (calipers) contains scattered calcifications indicating metastatic papillary thyroid cancer

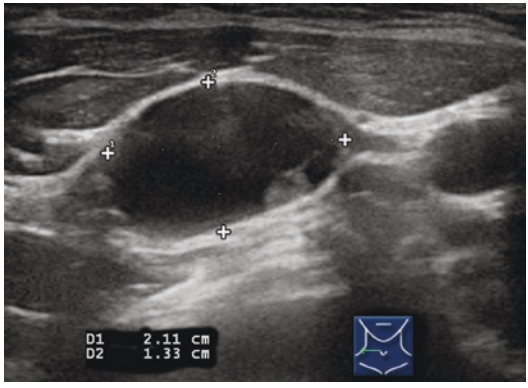

FIGURE 8.10 This 2.1 cm rounded lymph node in the right neck is >90% cystic; note the distal enhancement. Although occasionally seen in tuberculosis, cyst formation within a lymph node usually indicates metastatic papillary thyroid or oropharyngeal carcinoma

Assessment of the pattern of lymph node vascularity using color or power Doppler is instrumental in assessing risk of malignancy in lymph nodes. Power Doppler is preferred over color Doppler for lymph node evaluation, because of its

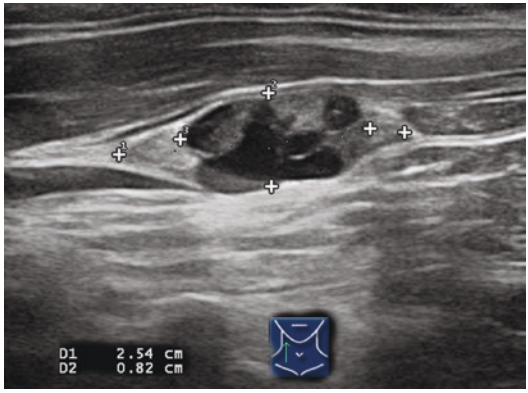

FIGURE 8.11 This atypical appearing lymph node is heterogeneous and demonstrates multiple areas of cystic necrosis. Cystic degeneration within a lymph node is often first suspected because of uneven distal acoustic enhancement (*arrow*)

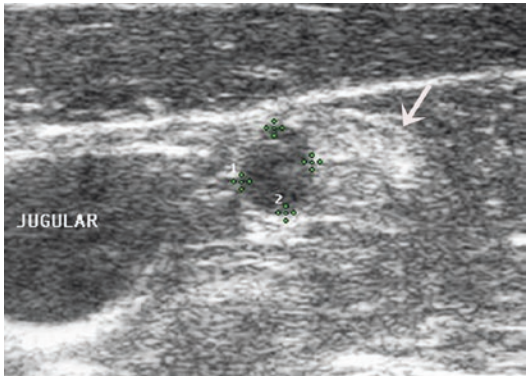

FIGURE 8.12 This metastatic lymph node, less than 1 cm in size, contains cystic necrosis on the medial side which is hypoechoic (calipers) and shows enhancement. The other side (*arrow*) is solid and hyperechoic. US-guided FNA of the hypoechoic area yielded negative cytology but high levels of Tg in needle washout—a finding not unusual when cystic necrosis is present

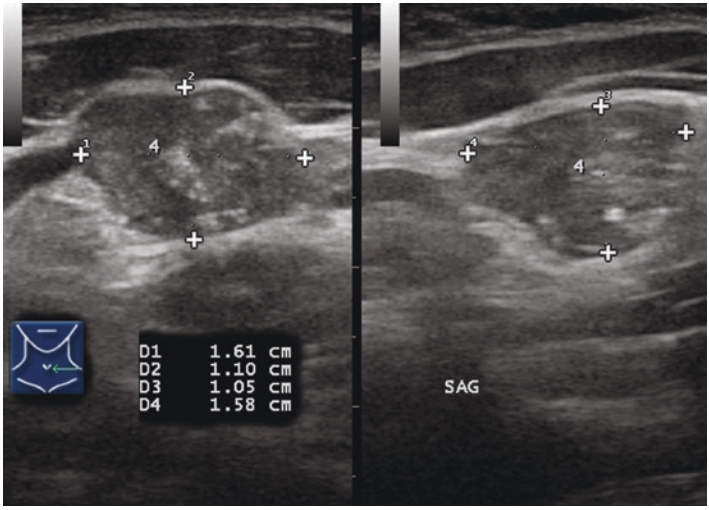

FIGURE 8.13 This compartment IV lymph node, deep to the SCM, shows multiple features highly suggestive of malignancy including rounded morphology and microcalcifications

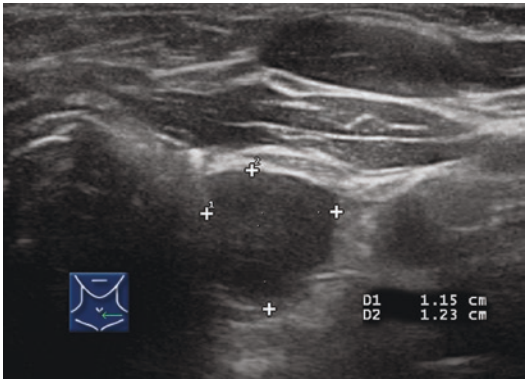

FIGURE 8.14 A central compartment VI paratracheal lymph node with rounded morphology and loss of central hilar line

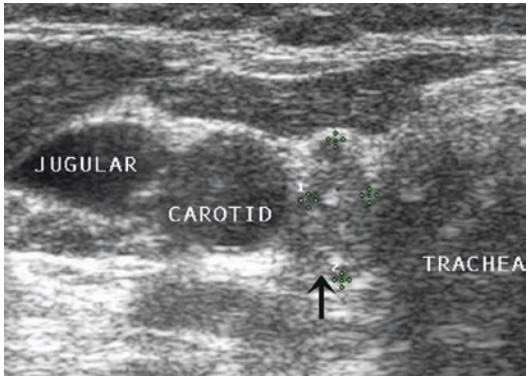

Figure 8.15 Ultrasound of 54-year-old female 36 years after her thyroidectomy reveals a paratracheal lymph node (*arrow*) in the right central compartment. Note the long/short axis is <2, and several calcifications are seen indicating malignancy

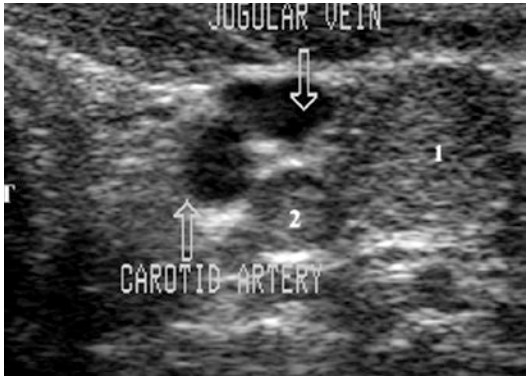

Figure 8.16 A 1 cm lymph node (*1*) and a 0.5 cm lymph node (*2*) in the lateral neck are both rounded without a hilar line. Both nodes had papillary thyroid cancer at surgery

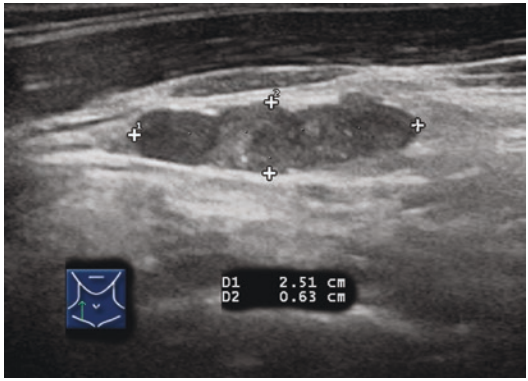

FIGURE 8.17 Despite a long/short ratio > 2, this 2.5 cm lymph node is clearly abnormal with irregular contour, microcalcifications, and absence of hilar line. Figure 8.23 shows a Doppler image of the same node demonstrating disordered peripheral vascularity

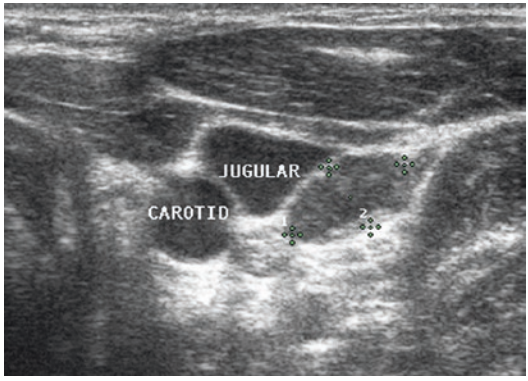

FIGURE 8.18 This lymph node (calipers) was suspicious because of its borderline long/short axis of 2 and absent hilum. Surgery confirmed metastatic papillary thyroid cancer

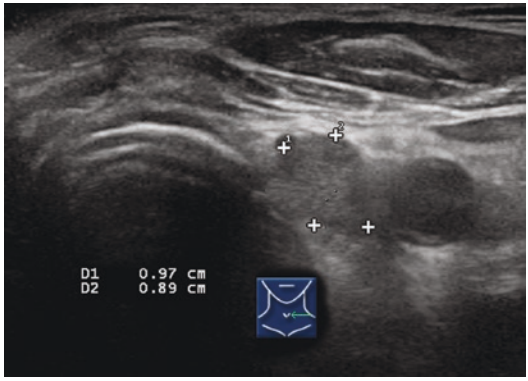

Figure 8.19 Metastatic lymph node (calipers) in left central compartment with long/short axis < 1 and no hilar line

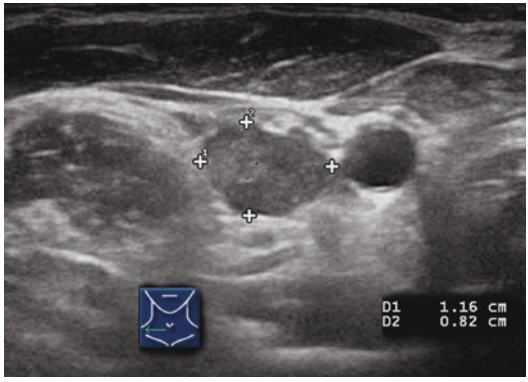

Figure 8.20 Right compartment IV lymph node with rounded morphology (long/short > 2), loss of central hilum, and possible microcalcifications. FNA cytology showed papillary thyroid carcinoma

sensitivity to arteriolar blood flow. In order to achieve adequate sensitivity to small amounts of flow, pulse repetition frequency (PRF) should be set to <1000 and a low wall filter should be utilized. Benign nodes generally show vascularization limited to the central hilum, but malignancy disrupts this flow and causes chaotic vascularization throughout the

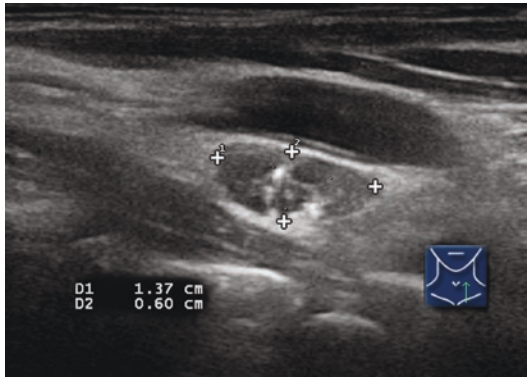

FIGURE 8.21 Despite a normal long/short axis > 2, this lymph node posterior to the carotid artery is suspicious with central microcalcifications. However, biopsy demonstrated sarcoidosis

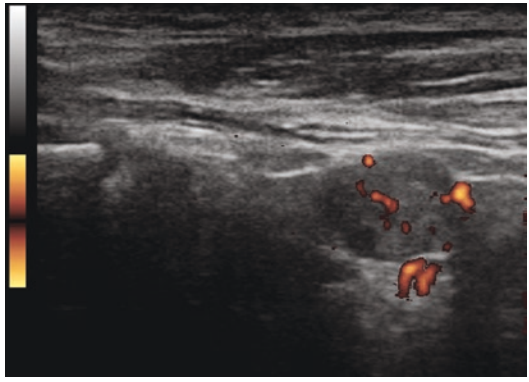

FIGURE 8.22 Power Doppler of lymph node shows vascularization of the periphery of the node rather than the normal hilar vascular pattern

peripheral cortex due to recruitment of vessels into the periphery of the node [13, 14]. The specificity of disordered peripheral vascularity is only 82%, as reactive nodes may also show this feature. However, this feature has been described as having the "best sensitivity specificity compromise" [10], and finding disordered vascularity warrants further evaluation (Figs. 8.22, 8.23, 8.24, 8.25, and 8.26).

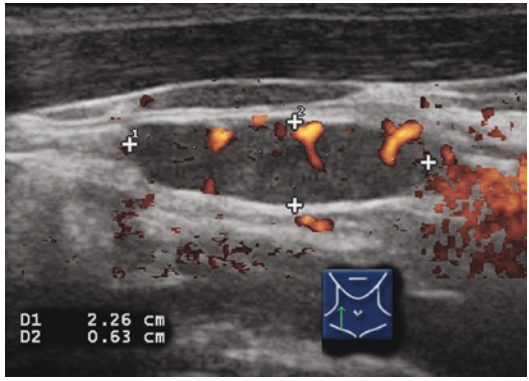

Figure 8.23 Power Doppler of lymph node (same lymph node as in Fig. 8.17) demonstrating chaotic peripheral vascularity

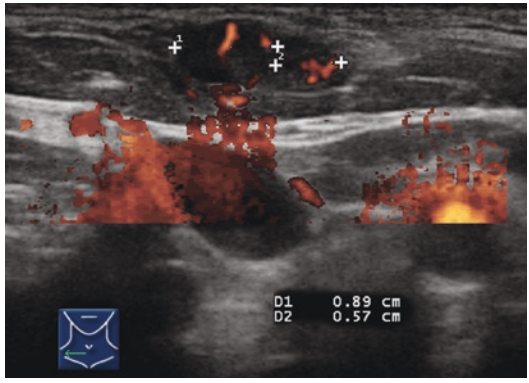

Figure 8.24 This soft tissue metastasis is located superficial to the SCM muscle. Malignancy was suspected due to the abnormal vascular pattern and confirmed by cytology and TG analysis

The internal jugular vein lies adjacent to the carotid artery in the neck. Since metastatic nodes commonly occur in proximity to the jugular vein or in the carotid sheath, any deviation of the jugular vein away from the carotid artery strongly suggests the presence of a malignant lymph node. The entire length of the vessels should be surveyed closely

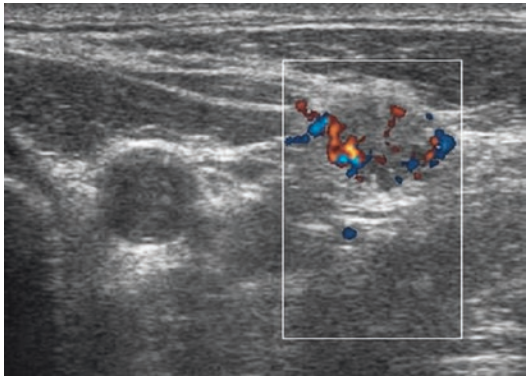

FIGURE 8.25 Power Doppler of lymph node shows a malignant vascular pattern. Tg in needle washout was high confirming malignancy

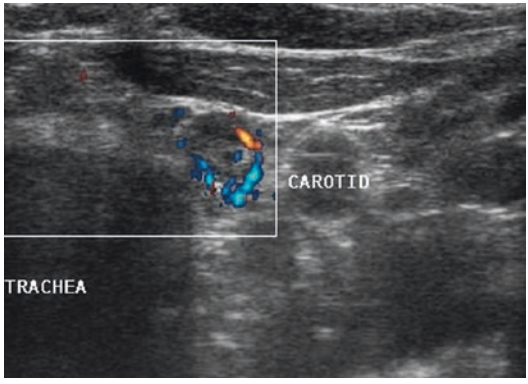

FIGURE 8.26 Power Doppler of lymph node shows peripheral vascular pattern of malignancy. FNA cytology was positive, and Tg in the needle washout was >10,000

with particular attention given to any area where the artery and vein diverge. Moving the ultrasound transducer in several planes may help to reveal an obscure node.

In addition to causing deviation of the internal jugular vein, malignant lymph nodes tend to compress the vein and cause partial obstruction to blood flow. Color or power

Doppler may demonstrate the impeded blood flow in the jugular vein. Benign lymph nodes, unless severely enlarged, rarely deviate or obstruct the jugular vein (Figs. 8.27, 8.28, 8.29, 8.30, 8.31, 8.32, and 8.33).

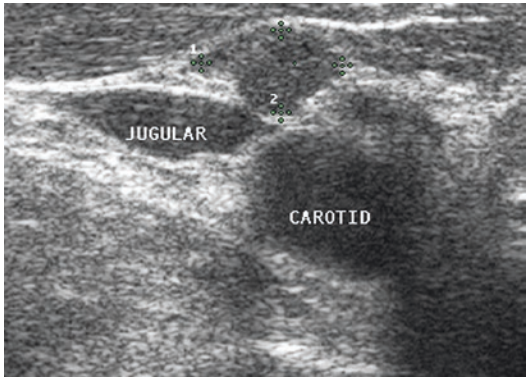

FIGURE 8.27 On transverse view, this small rounded lymph node (calipers) without a hilar line is in close proximity to the great vessels

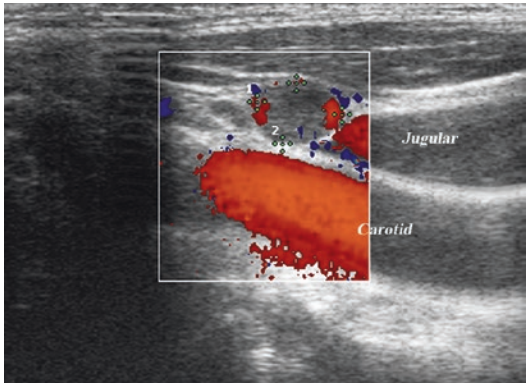

FIGURE 8.28 Same lymph node (calipers) in longitudinal view shows compression of the jugular vein against the carotid. US-guided FNA confirmed malignancy

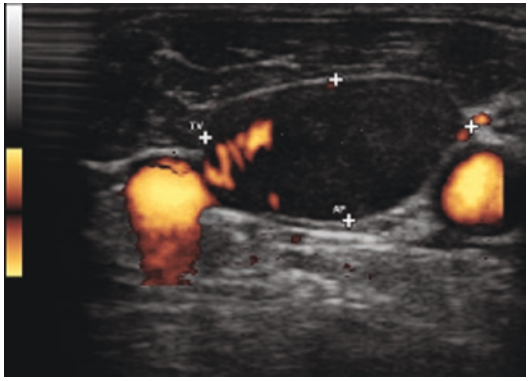

FIGURE 8.29 This 1.7 cm lymph node (calipers) separates the carotid and jugular. Its location and shape (long-/short-axis ratio < 2) strongly suggested malignancy which was confirmed by US-guided FNA

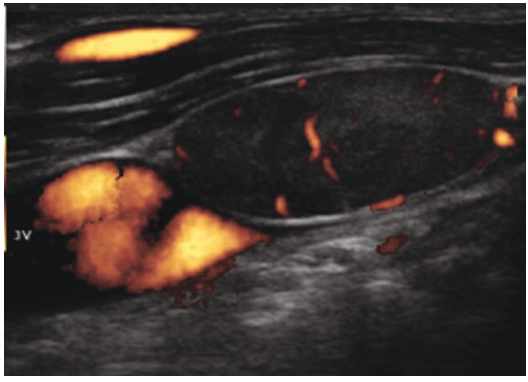

FIGURE 8.30 This 2.6 cm lymph node is compressing the jugular vein and obstructing its blood flow. It is essential to apply very light pressure with the transducer when assessing whether vascular compression is present

Ultrasound characteristics helpful in distinguishing benign from malignant thyroid nodules do not always apply to lymph nodes. Metastatic lymph nodes can have well-defined borders

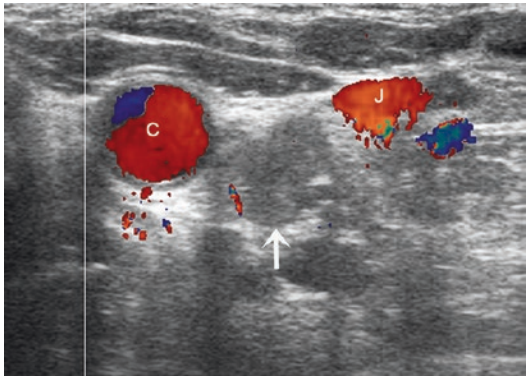

FIGURE 8.31 This irregular rounded lymph node (*arrow*) was discovered because of the separation of the jugular from the carotid. The calcification at 3 o'clock strongly suggests malignancy, but US-guided FNA is required before surgery

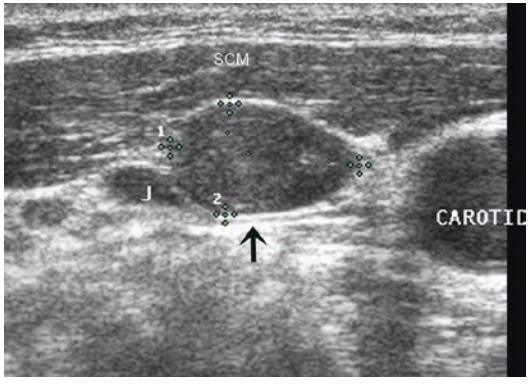

FIGURE 8.32 Transverse view of a metastatic lymph node (calipers) in the right neck beneath the SCM and lateral to the carotid artery. The node is impinging upon the jugular vein (*J*) at the arrow. The long/short axis ratio is ≤1and no hilar line is seen. US-guided FNA had positive cytology, and Tg was found in the needle washout

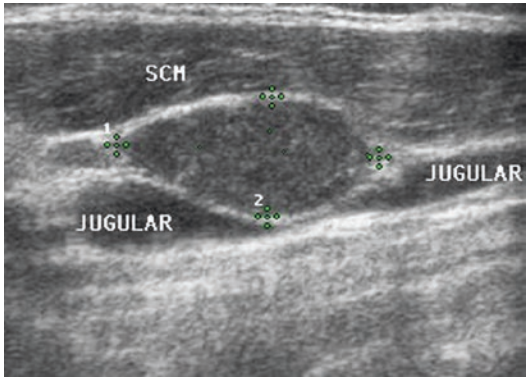

FIGURE 8.33 Longitudinal view of the same lymph node (calipers) showing partial obstruction of the jugular vein

until they become quite large, although the presence of an irregular nodal margin is highly suggestive of malignancy. Both normal and malignant lymph nodes can have varying degrees of echogenicity, although normal nodes are generally hypoechoic compared to thyroid. A recent study found that diffusely increased echogenicity was strongly predictive of metastatic thyroid carcinoma, particularly in small nodes [11]. Matting of lymph nodes occurs with malignancy but is not a helpful sign since it is also seen with inflammation (such as in Hashimoto's thyroiditis) or in patients who have had radiation.

In summary, several features such as size and shape draw our attention to lymph nodes but lack specificity. Others, such as calcifications or cystic degeneration, are highly specific and warrant intervention, depending on the clinical situation. In isolation, lymph node enlargement, rounded shape, or the absence of an echogenic hilum is not specific enough to warrant fine needle aspiration biopsy [10]. However, combinations of atypical features greatly increase the probability of malignancy. The final decision whether to observe over time or perform a biopsy requires analysis of both ultrasonographic and clinical features.

Ultrasound-Guided FNA of Lymph Nodes

Because definitive ultrasonographic features of malignant lymph nodes are not always present and there is overlap in the ultrasound appearance of benign and malignant lymph nodes, US-guided FNA of suspicious nodes is typically required for a definitive diagnosis before recommending surgery. The 2015 ATA guidelines state that US-guided FNA of sonographically suspicious lymph nodes measuring >8–10 mm in the smallest diameter should be performed to confirm malignancy if this would change management [1].

US-guided FNA of lymph nodes is carried out in the same manner as a US-guided FNA of a thyroid nodule with aspirate slides prepared and sent for cytology interpretation. If the entire lymph node is sonographically abnormal, the FNA specimen can be obtained by moving the needle tip throughout the lymph node. However, if the lymph node maintains some normal architecture and only a portion is sonographically suspicious, the needle tip should be directed to the suspicious component of the lymph node [10].

Lymph node cytology is occasionally difficult to interpret [15]. However, differentiated thyroid cancer metastases contain thyroglobulin (Tg) which can be measured and used as a tissue marker. Therefore, after making the slide, the biopsy needle(s) can be flushed with 1 cc normal saline and the washout analyzed for Tg [16, 17]. The material in the needle is diluted approximately 100–1000-fold; therefore, a Tg measurement of >10 in the needle washout is considered positive for malignancy. Because intracellular Tg is not exposed to circulating anti-TgAB, a positive serum anti-TgAB does not interfere with measurement of Tg obtained from lymph nodes [18]. Either a positive cytology report or finding Tg in the needle washout confirms the lymph node is malignant and, by using these criteria, Lee et al. reported 100% sensitivity and specificity in detecting metastatic thyroid cancer [19]. For cystic nodes where cytology may only reveal macrophages without epithelial cells, FNA-Tg

washout is more sensitive than cytology in detecting nodal malignancy [20] (see Fig. 8.10). If medullary thyroid cancer is suspected, calcitonin can be used as the tissue marker. The 2015 ATA guidelines state that the addition of fine needle aspiration – thyroglobulin washout in the evaluation of suspicious cervical lymph nodes – is appropriate in select patients, but its interpretation, particularly for central compartment nodes, may be difficult in patients with an intact thyroid gland.

Preoperative Ultrasound and Surgical Management

PTC is a disease characterized by frequent lymph node metastases. Lymph node metastases have been reported to occur in 12–80% of PTC patients, the majority of this nodal disease being microscopic disease. Clinically apparent nodal disease is present in approximately 35% of patients presenting with PTC and is defined as nodes evident by (1) preoperative physical exam, (2) preoperative radiographic evaluation, or (3) intraoperative detection by the surgeon [21–23]. The main prognostic significance of the presence of nodal disease in a patient with PTC lies in the risk of recurrence rather than in survival. In patients with small volume nodal disease, locoregional recurrence rates in treated patients range from 2 to 6% regardless of whether lymph node dissection is performed or RAI is given [24–36]. The ATA taskforce on thyroid cancer nodal surgery has reported that for patients with pathologically proven cervical LN metastases (pN1), there is markedly variable median risk of locoregional recurrence based on clinical staging; initially clinically N0 (cN0) patients had 2% risk (0–9% range) versus initially clinically N-positive (cN1) patients with a 22% risk (range 10–42%) [37]. Thus, microscopic nodal disease is of little if any clinical significance, and only macroscopic nodal disease warrants opera-

tive treatment to reduce risk of additional nodal recurrence. Additionally, the ATA taskforce demonstrated that the median risk of locoregional recurrence in pN1 patients varies markedly by the number of positive nodes, <5 nodes (4%, range 3–8%) vs. >5 nodes (19%, range 7–21%) [37]. Sensitivity of physical examination for detection of pathologic lymphadenopathy is as low as 15–30% [5, 38–46]. Thus, ultrasound is the most useful modality for screening and mapping of nodal disease in patients with thyroid carcinoma [47]. The 2015 ATA management guidelines recommend that thyroid sonography with survey of the cervical lymph nodes be performed in all patients with known or suspected thyroid nodules (Recommendation 6) and that preoperative neck US for cervical (central and especially lateral neck compartments) lymph nodes is recommended for all patients undergoing thyroidectomy for malignant or suspicious for malignancy cytologic or molecular findings [1]. Neck lymph nodes detected on preoperative neck US in patients with known PTC (i.e., clinically apparent macroscopic nodal disease) convey a higher risk of disease recurrence (>20%), even when treated with therapeutic neck dissection and/or RAI ablation, than either clinical N0 necks or pathologically proven N1a disease [48, 49]. A recent study comparing patients with and without preoperative lateral neck ultrasounds found that patients with preoperative neck US were more likely to have lateral neck dissection compared with patients without preoperative neck US ($P < 0.001$) and that preoperative neck US resulted in a better response to therapy ($P = 0.005$), a greater likelihood of no evidence of disease, and a smaller likelihood of having a biochemical or structural incomplete response or a return for delayed neck dissection. The preoperative US group also had fewer disease recurrences [47]. Thus, all PTC patients should have robust radiographic nodal mapping preoperatively to identify and elucidate the distribution of macroscopic nodal disease (Figs. 8.34 and 8.35).

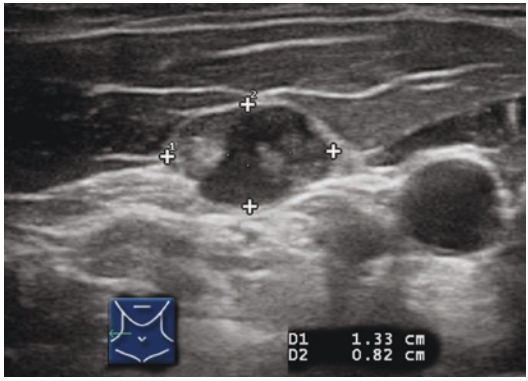

FIGURE 8.34 Preoperative ultrasound of a patient seen for a thyroid nodule in the right lobe (*N*) revealed an abnormal appearing lymph node in right lateral neck compartment III. Note the long/short axis < 2, absent hilum, and calcifications

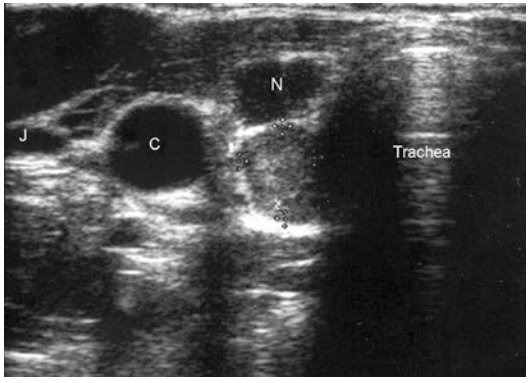

FIGURE 8.35 Preoperative ultrasound of patient with a thyroid nodule (*N*) whose FNA was positive for papillary thyroid cancer shows a suspicious lymph node (calipers) adjacent to the lower pole of the thyroid. A central node dissection at the time of surgery revealed that this was metastatic papillary thyroid carcinoma

Preoperative Ultrasound and the Central Neck

Preoperative ultrasound of the central compartment is much less sensitive for detection of nodal disease than it is in the lateral neck. Most studies report central neck ultrasound sensitivity between 10 and 26%, in part because even macroscopic lymph nodes may be obscured by the thyroid gland [11, 50, 51]. Preoperative FNA of central compartment lymph nodes is fraught with the risk of contamination if the needle passes through the thyroid gland which might cause a false-positive cytology and/or Tg in the washout. It is still recommended that the central compartment be examined at the time of lateral neck ultrasound and all suspicious lymph nodes should be mapped preoperatively. When the thyroid gland is not yet removed, 70–90% of positive lymph nodes in the central neck are not detected by ultrasound; hence, prior to the thyroidectomy, a "negative" ultrasound examination does not rule out central neck metastatic lymph node disease.

Axial CT scan with contrast may provide improvement in detection of central neck nodal disease. In one recent study, sensitivity of ultrasound detection of central neck nodal disease in primary PTC patients was 26%, whereas combined radiographic mapping through ultrasound and axial CT scan with contrast improved sensitivity to 54% with a negative predictive value of 75% in the central compartment. In this study, CT scan was overall found to improve macroscopic nodal dissection; also, it identified compartments that required dissection for macroscopic nodal disease that had been missed on ultrasound in 25% of primary PTC patients allowing appropriate expansion of the nodal surgical plan [50]. The use of iodine contrast for CT scan causes minimal delay in postoperative iodine treatment (if required) and should not be seen as a contraindication for performing a CT scan. Accurate preoperative mapping of macroscopic nodal disease and appropriately planned surgery, based on the extent of nodal disease, affect oncological outcome more significantly than a minor delay in radioiodine administration [52]. The 2015 ATA guidelines recommend preoperative use

of cross-sectional imaging studies (CT, MRI) with intravenous (IV) contrast as an adjunct to US for patients with clinical suspicion for advanced disease, including invasive primary tumor or clinically apparent multiple or bulky lymph node involvement (Recommendation 33) [1].

Postoperative Ultrasound and Surgical Management

In addition to screening and mapping for nodal disease preoperatively, ultrasound also has a primary role in the postoperative surveillance of thyroid cancer patients. Thyroid cancer has a propensity to occur at any age, even in the very young, and to recur many years later; hence, it must be monitored for the lifetime of a patient. Achieving this in a cost-effective manner has been a challenge. Until the 1990s the only diagnostic tool available was ^{131}I whole-body scan (WBS) performed after withdrawal of the thyroid hormone replacement. The sensitivity of WBS in the early detection of residual, recurrent, or metastatic thyroid cancer is poor. This is apparent from the many patients with increased thyroglobulin (Tg) but negative diagnostic scans, who are treated with ^{131}I and have positive posttreatment scans [53–55]. Park et al. has also shown that the dose of ^{131}I used for WBS can stun the uptake of iodine in metastatic lesions and interfere with the subsequent treatment dose of ^{131}I [56]. The expense, poor sensitivity, and risk of stunning make WBS an unsatisfactory test for follow-up of thyroid cancer.

In the last decades two techniques that aid in the early detection of recurrent thyroid cancer have been widely available. The first is a sensitive, reliable, reproducible Tg assay that biochemically detects early signs of cancer recurrence. The second is high-resolution ultrasound of the postoperative neck to identify early lymph node recurrence. These new tools, especially neck ultrasound combined with US-guided FNA of suspicious lymph nodes, have greatly improved the sensitivity of cancer surveillance in these patients.

Postoperative physical examination of the neck of a thyroid cancer patient is seldom helpful in the *early* detection of a recurrence. The scar tissue following surgery combined with the propensity of metastatic lymph nodes to lie deep in the neck beneath the sternocleidomastoid muscle makes palpation of enlarged lymph nodes in the neck difficult. Even lymph nodes several centimeters in diameter are often not palpable. High-resolution ultrasound has proven to be a very sensitive method to find and locate early recurrent cancer and lymph node metastasis. Frasoldati et al. studied 494 patients with a history of low-risk well-differentiated thyroid cancer by withdrawal WBS, stimulated Tg, and ultrasound and found that 51 patients had a recurrence by at least one test [57]. The WBS was positive in 23 patients (45%), the stimulated Tg was positive in 34 patients (67%), and the ultrasound with FNA was positive in 48 patients (94%). Since most thyroid cancer initially metastasize to the neck, it is rare for thyroid cancer to spread elsewhere without neck lymph node involvement. Therefore, neck ultrasound has proven to be the most sensitive test available in locating early recurrent disease even before serum Tg is elevated. In the pediatric population, a study on the use of ultrasound for detection of locoregional recurrence in children with differentiated thyroid cancer reported that the sensitivity of ultrasound was 85.7%, specificity was 89.4%, negative predictive value was 94.4%, and positive predictive value was 75% and that results of stimulated Tg and US were discordant in 17.3% of patients [58]. With regard to frequency of neck ultrasound postoperatively, a recent study showed that in ATA intermediate-risk patients with nonstimulated Tg < 1.0 ng/mL and the posttreatment neck US without suspicious findings, frequent US screening during follow-up was more likely to identify false-positive abnormalities than clinically significant structural recurrence [59]. ATA guidelines recommend that the neck US for evaluation of the thyroid bed and central and lateral cervical nodal compartments should be performed at 6–12 months postoperatively and then periodically, depending on the patient's risk for recurrent disease and Tg status (Recommendation 65).

Identifying and evaluating lymph nodes should be done with high-resolution ultrasound using a 10–15 MHz transducer with power Doppler capability to assess vascularity. When

performing ultrasound of the neck in a patient who has undergone a thyroidectomy, the carotid artery and jugular vein are noted to have migrated medially close to the trachea (Fig. 8.36). To get familiarized with the ultrasound appearance of the postoperative neck, one should first explore the postthyroidectomy neck in patients with benign thyroid disease. This facilitates the accustomization to the neck structures and the altered anatomy of the postoperative neck without the concerns of recurrent thyroid cancer. Postthyroidectomy, the thyroid bed is filled with a varying amount of hyperechoic connective tissue that appears white (dense) on ultrasound. This serves well in demarcating thyroid bed recurrence or a metastatic lymph node, which typically appear dark or hypoechoic. The criteria discussed earlier are used to determine the need to perform a US-guided FNA with both cytology and Tg washout.

The decision to perform revision surgery requires demonstration of a clinically significant structural recurrence. A structural recurrence once identified by ultrasound should be mapped thoroughly by CT scan or MRI with contrast for a comprehensive planning of the revision surgery. Additionally, revision surgery is a multidisciplinary decision based on a

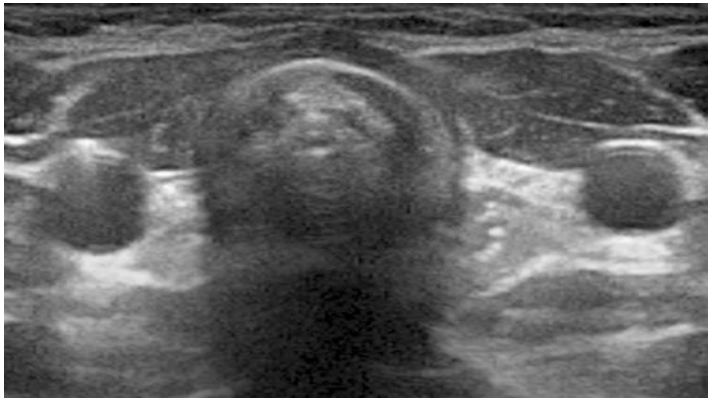

Figure 8.36 Thyroid ultrasound 1 year after total thyroidectomy. Note the medialized carotid artery on the right, separated from the trachea by echoic scar tissue. The left thyroid bed contains the esophagus protruding from posterior to the trachea with echoic scar tissue anterior to it

detailed discussion between endocrinology, surgery, and importantly the patient. Revision surgery is associated with higher rate of complications, specially unilateral or bilateral vocal cord paralysis (VCP) and permanent hypothyroidism, due to the technical challenges arising from altered anatomy, scarring, and altered natural history of the cancer. Figures 8.37 and 8.38 illustrate a comprehensive central and lateral cervical

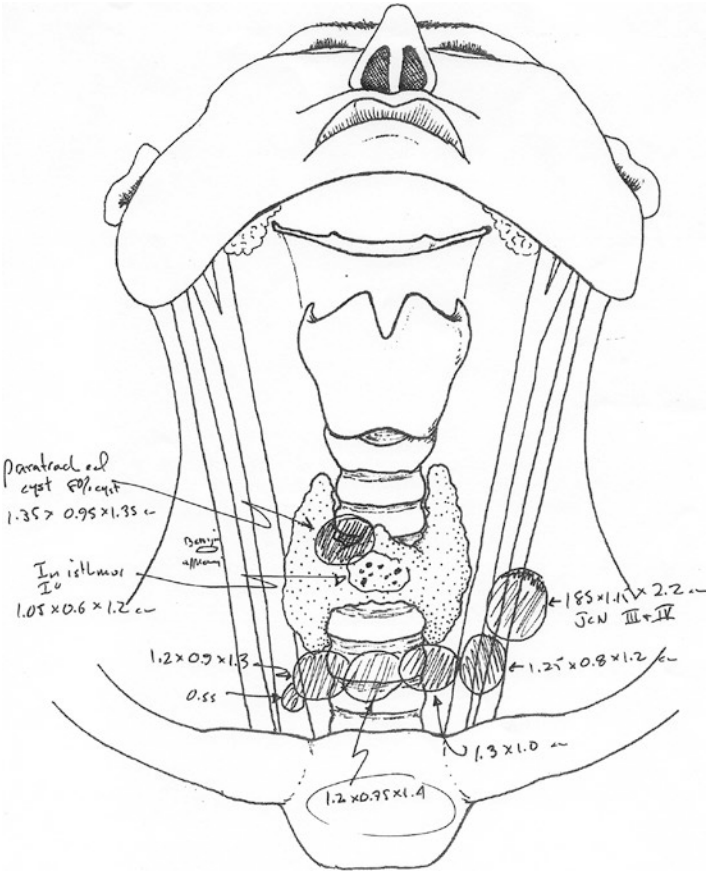

FIGURE 8.37 A map drawn based on the preoperative ultrasound and contrast-enhanced CT, used during surgery. The surgical specimens are shown in Fig. 8.38

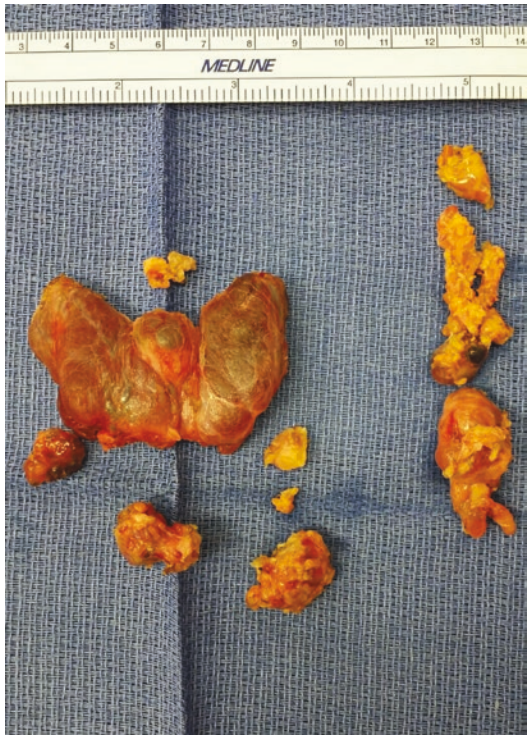

FIGURE 8.38 A photograph of the surgical specimens, including the thyroid, central, and lateral compartments in the patient whose preoperative imaging is summarized in the map shown in Fig. 8.37

ultrasound study with a drawing providing mapping of abnormal nodes prepared prior to surgery and a photograph demonstrating the gross anatomical specimens resected at surgery.

Revision surgery must have clear-cut and definable goals as small nodal recurrences may remain stable in the setting of TSH suppression without other treatments [60]. To this end, ATA 2015 guidelines recommend that suspicious lymph nodes <8–10 mm in smallest diameter should be followed without biopsy with consideration for FNA or intervention if there is growth or if the node threatens vital structures (Recommendation 65C).

Surgery for recurrent thyroid cancer should be meticulous and requires certain expertise to achieve good oncological and surgical outcomes [60, 61]. Intraoperative nerve monitoring can help reduce rate of VCP associated with reoperative surgeries [62, 63]. A recent study of 181 revision surgeries performed in a tertiary center reported occurrence of no permanent or temporary VCP, 9% temporary and 4.2% permanent hypocalcemia, and 5% cervical node recurrence, and biochemical complete remission was 58% in all patients after 3 1/2 years of median follow-up [64].

References

1. Haugen BR, et al. 2015 American Thyroid Association management guidelines for adult patients with thyroid nodules and differentiated thyroid cancer: the American Thyroid Association guidelines task force on thyroid nodules and differentiated thyroid cancer. Thyroid. 2016;26(1):1–133.
2. Carty SE, et al. Consensus statement on the terminology and classification of central neck dissection for thyroid cancer. Thyroid. 2009;19(11):1153–8.
3. Wittekind C, et al. TNM supplement: a commentary on uniform use. New York: Wiley-Liss; 2002.
4. Robbins KT, et al. Consensus statement on the classification and terminology of neck dissection. Arch Otolaryngol Head Neck Surg. 2008;134(5):536–8.
5. Qubain SW, et al. Distribution of lymph node micrometastasis in pN0 well-differentiated thyroid carcinoma. Surgery. 2002;131(3):249–56.
6. Dralle H, et al. Compartment-oriented microdissection of regional lymph nodes in medullary thyroid carcinoma. Surg Today. 1994;24(2):112–21.
7. Cunnane M, et al. A novel thyroid cancer nodal map classification system to facilitate nodal localization and surgical management. Laryngoscope. 2016. [Epub ahead of print].
8. Goyal N, et al. Mapping the distribution of nodal metastases in papillary thyroid carcinoma: where exactly are the nodes? Laryngoscope. 2017;127(8):1959–1964. (accepted Jan 2017).
9. Steinkamp HJ, Cornehl M, Hosten N, et al. Cervical lymphadenopathy: ratio of long- to short-axis diameter as a predictor of malignancy. Br J Radiol. 1995;68(3):266–70.

10. Leboulleux S, et al. Ultrasound criteria of malignancy for cervical lymph nodes in patients followed up for differentiated thyroid cancer. J Clin Endocrinol Metab. 2007;92(9):3590–4.
11. Lee YJ, et al. Pre-operative ultrasound diagnosis of nodal metastasis in papillary thyroid carcinoma patients according to nodal compartment. Ultrasound Med Biol. 2015;41(5):1294–300.
12. Ahuja A, et al. Lymph node hilus: gray scale and power Doppler sonography of cervical nodes. J Ultrasound Med. 2001;20(9):987–92; quiz 994.
13. Ahuja AT, et al. Power Doppler sonography of metastatic nodes from papillary carcinoma of the thyroid. Clin Radiol. 2001;56(4):284–8.
14. Ahuja A, Ying M. An overview of neck node sonography. Investig Radiol. 2002;37(6):333–42.
15. Bellantone R, et al. Management of cystic or predominantly cystic thyroid nodules: the role of ultrasound-guided fine-needle aspiration biopsy. Thyroid. 2004;14(1):43–7.
16. Frasoldati A, et al. Role of thyroglobulin measurement in fine-needle aspiration biopsies of cervical lymph nodes in patients with differentiated thyroid cancer. Thyroid. 1999;9(2):105–11.
17. Pacini F, et al. Detection of thyroglobulin in fine needle aspirates of nonthyroidal neck masses: a clue to the diagnosis of metastatic differentiated thyroid cancer. J Clin Endocrinol Metab. 1992;74(6):1401–4.
18. Baskin HJ. Detection of recurrent papillary thyroid carcinoma by thyroglobulin assessment in the needle washout after fine-needle aspiration of suspicious lymph nodes. Thyroid. 2004;14(11):959–63.
19. Lee MJ, et al. Fine-needle biopsy of cervical lymph nodes in patients with thyroid cancer: a prospective comparison of cytopathologic and tissue marker analysis. Radiology. 1993;187(3):851–4.
20. Cignarelli M, et al. Diagnostic utility of thyroglobulin detection in fine-needle aspiration of cervical cystic metastatic lymph nodes from papillary thyroid cancer with negative cytology. Thyroid. 2003;13(12):1163–7.
21. Gemsenjager E, et al. Lymph node surgery in papillary thyroid carcinoma. J Am Coll Surg. 2003;197(2):182–90.
22. Bardet S, et al. Macroscopic lymph-node involvement and neck dissection predict lymph-node recurrence in papillary thyroid carcinoma. Eur J Endocrinol. 2008;158(4):551–60.
23. Cranshaw IM, Carnaille B. Micrometastases in thyroid cancer. An important finding? Surg Oncol. 2008;17(3):253–8.

24. Yamashita H, et al. Extracapsular invasion of lymph node metastasis. A good indicator of disease recurrence and poor prognosis in patients with thyroid microcarcinoma. Cancer. 1999;86(5):842–9.
25. Baudin E, et al. Microcarcinoma of the thyroid gland: the Gustave-Roussy institute experience. Cancer. 1998;83(3):553–9.
26. Chow SM, et al. Papillary microcarcinoma of the thyroid-prognostic significance of lymph node metastasis and multifocality. Cancer. 2003;98(1):31–40.
27. Ito Y, et al. An observation trial without surgical treatment in patients with papillary microcarcinoma of the thyroid. Thyroid. 2003;13(4):381–7.
28. Wada N, et al. Lymph node metastasis from 259 papillary thyroid microcarcinomas: frequency, pattern of occurrence and recurrence, and optimal strategy for neck dissection. Ann Surg. 2003;237(3):399–407.
29. Roti E, et al. Clinical and histological characteristics of papillary thyroid microcarcinoma: results of a retrospective study in 243 patients. J Clin Endocrinol Metab. 2006;91(6):2171–8.
30. Hay ID. Management of patients with low-risk papillary thyroid carcinoma. Endocr Pract. 2007;13(5):521–33.
31. Mazzaferri EL. Management of low-risk differentiated thyroid cancer. Endocr Pract. 2007;13(5):498–512.
32. Hay ID, et al. Papillary thyroid microcarcinoma: a study of 900 cases observed in a 60-year period. Surgery. 2008;144(6):980–7; discussion 987-8.
33. Noguchi S, et al. Papillary microcarcinoma. World J Surg. 2008;32(5):747–53.
34. Giordano D, et al. Treatment and prognostic factors of papillary thyroid microcarcinoma. Clin Otolaryngol. 2010;35(2):118–24.
35. So YK, et al. Subclinical lymph node metastasis in papillary thyroid microcarcinoma: a study of 551 resections. Surgery. 2010;148(3):526–31.
36. Zetoune T, et al. Prophylactic central neck dissection and local recurrence in papillary thyroid cancer: a meta-analysis. Ann Surg Oncol. 2010;17(12):3287–93.
37. Randolph GW, et al. The prognostic significance of nodal metastases from papillary thyroid carcinoma can be stratified based on the size and number of metastatic lymph nodes, as well as the presence of extranodal extension. Thyroid. 2012;22(11):1144–52.
38. Noguchi M, et al. Indications for bilateral neck dissection in well-differentiated carcinoma of the thyroid. Jpn J Surg. 1987;17(6):439–44.

39. Noguchi S, Murakami N. The value of lymph-node dissection in patients with differentiated thyroid cancer. Surg Clin North Am. 1987;67(2):251–61.
40. Mirallie E, et al. Localization of cervical node metastasis of papillary thyroid carcinoma. World J Surg. 1999;23(9):970–3. discussion 973-4.
41. Wang TS, et al. Incidence of metastatic well-differentiated thyroid cancer in cervical lymph nodes. Arch Otolaryngol Head Neck Surg. 2004;130(1):110–3.
42. Triponez F, et al. Hook needle-guided excision of recurrent differentiated thyroid cancer in previously operated neck compartments: a safe technique for small, nonpalpable recurrent disease. J Clin Endocrinol Metab. 2006;91(12):4943–7.
43. Ito Y, et al. Risk factors for recurrence to the lymph node in papillary thyroid carcinoma patients without preoperatively detectable lateral node metastasis: validity of prophylactic modified radical neck dissection. World J Surg. 2007;31(11):2085–91.
44. Lee SK, et al. Sentinel lymph node biopsy in papillary thyroid cancer: comparison study of blue dye method and combined radioisotope and blue dye method in papillary thyroid cancer. Eur J Surg Oncol. 2009;35(9):974–9.
45. Lim YC, et al. Central lymph node metastases in unilateral papillary thyroid microcarcinoma. Br J Surg. 2009;96(3):253–7.
46. Ross DS, et al. Recurrence after treatment of micropapillary thyroid cancer. Thyroid. 2009;19(10):1043–8.
47. Wang LY, et al. Preoperative neck ultrasound in clinical node-negative differentiated thyroid cancer. J Clin Endocrinol Metab. 2014;99(10):3686–93.
48. Moreno MA, et al. Preoperative lateral neck ultrasonography as a long-term outcome predictor in papillary thyroid cancer. Arch Otolaryngol Head Neck Surg. 2011;137(2):157–62.
49. Ito Y, et al. Clinical significance of metastasis to the central compartment from papillary microcarcinoma of the thyroid. World J Surg. 2006;30(1):91–9.
50. Lesnik D, et al. Papillary thyroid carcinoma nodal surgery directed by a preoperative radiographic map utilizing CT scan and ultrasound in all primary and reoperative patients. Head Neck. 2014;36(2):191–202.
51. Ito Y, et al. Preoperative ultrasonographic examination for lymph node metastasis: usefulness when designing lymph node dissection for papillary microcarcinoma of the thyroid. World J Surg. 2004;28(5):498–501.

52. Caparevic Z, et al. Psychological evaluation of patients with a nodular goiter before and after surgical treatment. Med Pregl. 2002;55(9–10):401–5.
53. Pineda JD, et al. Iodine-131 therapy for thyroid cancer patients with elevated thyroglobulin and negative diagnostic scan. J Clin Endocrinol Metab. 1995;80(5):1488–92.
54. Schumm-Draeger PM, Encke A, Usadel KH. Optimal recurrence prevention of iodine deficiency related goiter after thyroid gland operation. A prospective clinical study. Internist. 2003;44(4):420–6. 429-32.
55. Menendez Torre E, et al. Prognostic value of thyroglobulin serum levels and 131I whole-body scan after initial treatment of low-risk differentiated thyroid cancer. Thyroid. 2004;14(4):301–6.
56. Park HM, et al. Influence of diagnostic radioiodines on the uptake of ablative dose of iodine-131. Thyroid. 1994;4(1):49–54.
57. Frasoldati A, et al. Diagnosis of neck recurrences in patients with differentiated thyroid carcinoma. Cancer. 2003;97(1):90–6.
58. Vali R, et al. The role of ultrasound in the follow-up of children with differentiated thyroid cancer. Pediatr Radiol. 2015;45(7):1039–45.
59. Peiling Yang S, et al. Frequent screening with serial neck ultrasound is more likely to identify false-positive abnormalities than clinically significant disease in the surveillance of intermediate risk papillary thyroid cancer patients without suspicious findings on follow-up ultrasound evaluation. J Clin Endocrinol Metab. 2015;100(4):1561–7.
60. Phelan E, et al. Neural monitored revision thyroid cancer surgery: surgical safety and thyroglobulin response. Otolaryngol Head Neck Surg. 2013;149(1):47–52.
61. Salari B, et al. Revision neural monitored surgery for recurrent thyroid cancer: safety and thyroglobulin response. Laryngoscope. 2016;126(4):1020–5.
62. Chuang YC, Huang SM. Protective effect of intraoperative nerve monitoring against recurrent laryngeal nerve injury during re-exploration of the thyroid. World J Surg Oncol. 2013;11:94.
63. Chan WF, Lang BH, Lo CY. The role of intraoperative neuromonitoring of recurrent laryngeal nerve during thyroidectomy: a comparative study on 1000 nerves at risk. Surgery. 2006;140(6):866–72; discussion 872-3.
64. Amin MR. Thyrohyoid approach for vocal fold augmentation. Ann Otol Rhinol Laryngol. 2006;115(9):699–702.

Chapter 9
Ultrasonography of the Parathyroid Glands

Dev Abraham

Introduction

Primary hyperparathyroidism (PHPT) is a common endocrine condition affecting approximately 100,000 new patients each year in the USA [1]. The apparent increase in incidence was traced to the wide availability and the use of multichannel analyzers for routine testing, resulting in the early detection of subclinical disease since 1970 [2]. This fortuitous biochemical screening has also changed the disease presentation of PHPT in the USA, with the majority of subjects presenting well before the onset of symptoms or end-organ damage. In more than 85% of these cases, a solitary adenoma is the cause of the problem. Point of contact neck ultrasonography (US) has become an integral part of most endocrine and surgery practices. It is also used in the localization of

D. Abraham, MBBS, MRCP (UK)
Department of Medicine, University of Utah,
Salt Lake City, UT, USA
e-mail: dev.abraham@hsc.utah.edu

D.S. Duick et al. (eds.), *Thyroid and Parathyroid Ultrasound and Ultrasound-Guided FNA*,
https://doi.org/10.1007/978-3-319-67238-0_9

parathyroid adenomas enabling the application of minimally invasive surgery as an outpatient procedure resulting in shortened hospitalization and recuperative times [1].

Historical Perspectives

The parathyroid glands are the last known organs identified in humans. The first description of the glands is credited to Sir Richard Owens during dissection of an Indian rhinoceros [3]. Ivar Sandstrom, as a medical student, described the parathyroid glands in other animals and humans [4]. The first parathyroid adenoma surgery was performed by Dr. Felix Mandl on Mr. Albert Gahn, a tram conductor in Vienna. The first parathyroidectomy in the USA was performed by E. J. Lewis at Cook County Hospital in Chicago [5]. The inherent risk of surgical failure due to ectopic location of adenomas was observed in the case of Captain Charles Martell, who required seven surgeries to achieve cure [6]. In the 1990s the chance observation of parathyroid tumors accumulating the isotope Tc99MIBI, due to mitochondrial richness, spurred the concept of presurgical localization and the emergence of minimally invasive surgery [7].

Surgical Anatomy and Embryological Development of Parathyroid Glands

Normal parathyroid glands are variable in size, weight, and location. They measure approximately 5/4 mm in size and weigh 20–40 mg [8]. This variation in size was described astutely by Ivar Sandstrom in his landmark publication in 1877 [4]. Without the knowledge of parathyroid disorders, he may well have described parathyroid adenoma or asymmetric hyperplasia. The parathyroid glands have an anatomically distinct vascular supply from that of the thyroid gland and are enveloped in a pad of fibro-fatty capsule [9]. The glands have a vascular supply that is distinct from that of neighboring thyroid gland (Fig. 9.1). This blood supply is visualized as a

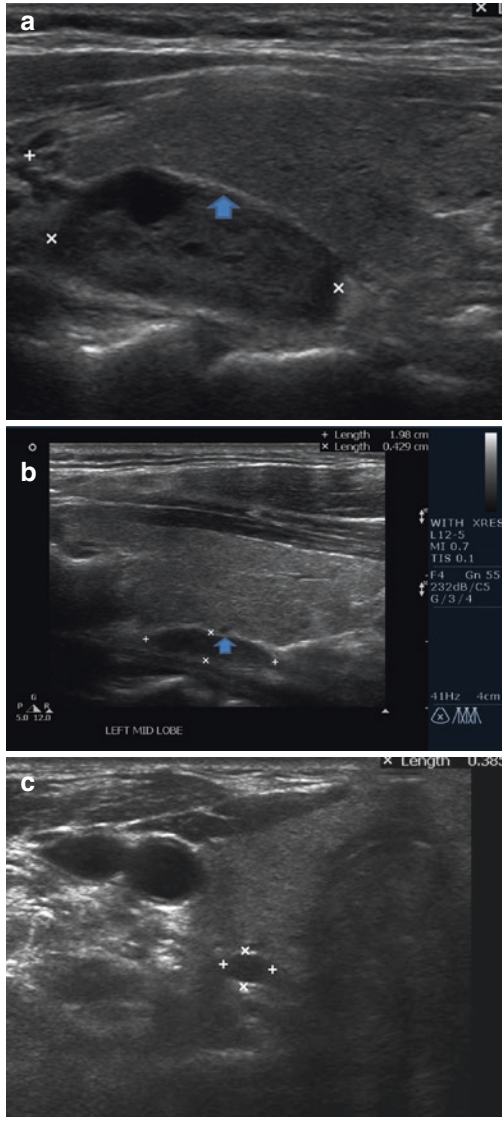

FIGURE 9.1 Superior parathyroid adenoma seen in longitudinal view. Indentation sign. (**a**) Upper PA, craniocaudal view, note indentation. (**b**) Upper PA, note indentation sign, and long pencil shape. (**c**) Small superior adenoma

polar vessel or pedicle during Doppler interrogation of parathyroid adenomas (Fig. 9.2). The unique variations in the anatomic location of parathyroid glands pose challenges to localization and subsequent surgery. The superior parathyroid glands are located along the posterior aspect of the thyroid lobes (Figs. 9.2 and 9.3) as opposed to the inferior pair located more caudally in relation to the inferior pole of the thyroid gland. Due to their small size, it is generally not possible to visualize normal glands with the use of present-day US equipment. In addition, the presence of physiologic central compartment lymph nodes makes it harder if not impossible

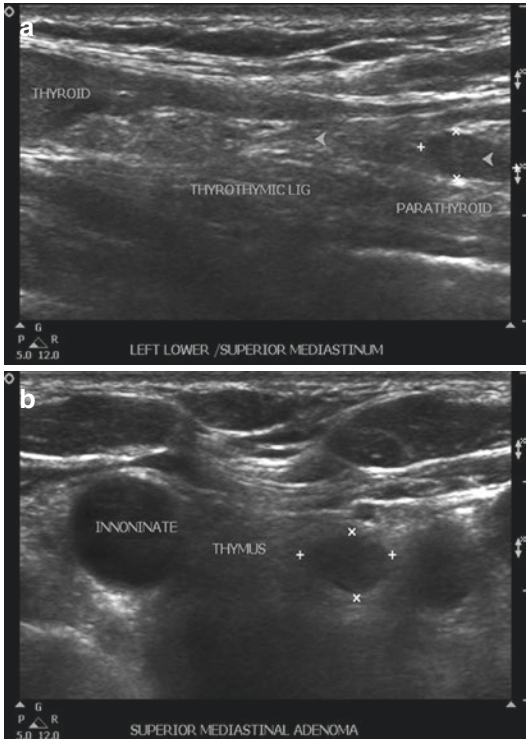

FIGURE 9.2 (**a**, **b**) PA located in the proximal portion of thyrothymic ligament and within the thymus

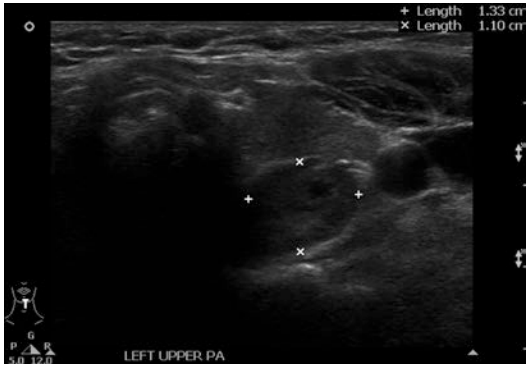

FIGURE 9.3 Superior parathyroid adenoma seen in transverse view

to distinguish extrathyroidal structures as parathyroid glands. Fine needle aspirations may be required in select cases to identify parathyroid glands prior to surgical intervention or ethanol ablations. A thorough understanding of the typical location and the anatomical variations of parathyroid glands is the cornerstone to the successful identification and removal of glands that develop adenomas or hyperplasia.

US Findings of Parathyroid Adenomas

Extrathyroidal and posterior location

Homogenous hypoechoic texture

Echogenic line of separation—this sign is absent in intrathyroidal adenomas

Distinct vascular pedicle or polar vessel on Doppler interrogation

Variable shapes conforming to available space within anatomical planes

Indentation sign—superior or inferior glands that are abutting the posterior capsule

One postmortem series revealed the presence of four glands in 91% of the subjects, three glands in 5%, and five glands in 4% [6]. Supernumerary glands are rare and found in

less than 5% of individuals [10]. The locations of parathyroid glands vary widely due to their embryonic origination from the third and fourth pharyngeal pouches with eventual migration to the lower neck. The superior parathyroid glands develop in the fourth pharyngeal pouch and migrate caudally along with the ultimobranchial bodies, which give rise to parafollicular cells—C cells of the thyroid gland. The superior pair is commonly located posterior to the thyroid lobes along the mid to upper two thirds of the thyroid lobes. The superior parathyroid glands are relatively constant in their location. Anomalous locations of the superior glands include the posterior pharyngeal region and the tracheaesophageal groove; however, they are also more likely to be located within the upper and posterior aspect of the thyroid lobes due to their unique developmental relationship to the C cells. The third branchial pouches give rise to the inferior pair of parathyroid glands and the thymus; together they migrate to the lower neck. Forty-four percent of inferior pair are located within 1 cm of the inferior pole of the thyroid gland, 17% are in close proximity to the inferior margin of the thyroid gland, 26% are found close to the superior portion of the thymus along the thyrothymic ligament (Fig. 9.2), and 2% are found within the thymus [8–10]. The unusual locations of the inferior parathyroid glands include the carotid bifurcation, the carotid sheath, intrathyroidal, and retropharyngeal sites. The reported frequency of ectopic parathyroid glands is quite variable ranging from 5 to 39.3%. This variability is due to the lack of criteria and agreement between investigators as to which locations should be considered as ectopic. A Greek autopsy series involving 942 autopsies revealed 5% of cadavers had supernumerary glands, 2% were intrathyroidal, and 6% of the glands were mediastinal in location. Most glands were located within the immediate vicinity of the thyroid gland [11]. In contrast, in a surgical series involving four gland surgeries for secondary hyperparathyroidism due to chronic renal failure, 39.3% of the glands were reported by the authors as “ectopic” in location [12]. Nevertheless, the variable location of the parathyroid glands underscores the importance of localization to ensure the success of minimally invasive parathyroid surgery.

Epidemiology of Primary Hyperparathyrodism

The predominant clinical phenotype of PHPT in the developed nations is the fortuitous discovery of asymptomatic individuals with normal or mild hypercalcemia undergoing yearly physical examinations. The apparent increase in the incidence of PHPT in the 1970s was traced to the development and wide availability of multichannel analyzers [2]. In a study from the USA, involving 3.5 million people, the incidence of PHPT varied from 34 to 124/100,000 person years. There is an age-related increase in incidence with the highest prevalence in Blacks followed by Whites. Latino and Asian minorities had the lowest incidence. PHPT is also threefold more common in women than in men [13]. The volume of surgeries performed for PHPT has increased 177% in California during 1999–2008 [14].

The typical end-organ damage encountered in PHPT patients is due to bone loss at the cortical bone sites and renal stones. Trabecular bone (spine) is relatively preserved at the expense of cortical bone sites such as the femoral neck and ultra-distal radius [15].

Due to the online heightened awareness among patients and doctors and because of "proactive" PTH testing in normocalcemic subjects, there is an emerging trend in the diagnosis of "eucalcemic" hyperparathyroidism. Selective administration of surgery following careful evaluation of end-organ damage in such patients is reasonable until randomized studies are conducted.

Localization Studies

Ultrasound evaluation of the parathyroid glands should not be performed to diagnose PHPT. Its use should be reserved strictly for localization purposes. Appropriate biochemical testing should be conducted and surgical indication(s) established in each patient prior to proceeding to any type of localization studies.

The two most widely used studies to locate the abnormal parathyroid gland(s) are Tc99MIBI (functional study) and ultrasonography (anatomical study). The respective localization techniques have their strengths and weaknesses and are equally efficacious [16]. Most isotope-based studies "lateralize" the lesion, whereas US studies provide precise localization information. To a practicing endocrinologist, the use of ultrasonography to study a patient with suspected parathyroid adenoma poses several advantages. The most important of these are the proven safety, ease of availability of ultrasound equipment, the lack of ionizing irradiation, short duration of the study, and the potential cost savings. The limitations of parathyroid localization using ultrasonography include operator variability and experience.

The Technique of Performing Ultrasonography for PHPT

Proper positioning of the patient is crucial to the successful visualization of enlarged parathyroid gland(s). The patient should lie flat on a firm table with one or two pillows placed underneath the posterior upper torso and the shoulders to enable full extension of the neck. The head should be supported with a folded towel to enhance patient comfort. Patients with cervical spine diseases such as ankylosing spondylosis may have very limited neck extension making it impossible to conduct an adequate study.

The linear transducer (3–5 cm) is applied to the anterior neck along with appropriate amount of coupling gel, and the thyroid gland is located. The structures of the neck should be carefully studied in multiple axes and at different levels of the neck. Most clinicians use multifrequency transducers (5–15 MHz) to study the thyroid gland. Parathyroid ultrasonography does not require different equipment. The lower frequency settings are more effective at visualizing the deeper portions of the neck. The most common sites of location, such as the posterior margin of the thyroid capsule and

the regions caudal to the thyroid lobes, are inspected first looking for lesions with features of enlarged parathyroid gland. Due to the inherent mobility of parathyroid adenomas, the tumor may not be visualized readily, particularly the superior adenomas located within the tracheaesophageal groove or intrathoracic inferior gland adenomas. Asking patients to cough, strain, turn the head from side to side, or take deep breaths in and out can enable visualization of a mobile adenoma (Fig. 9.4).

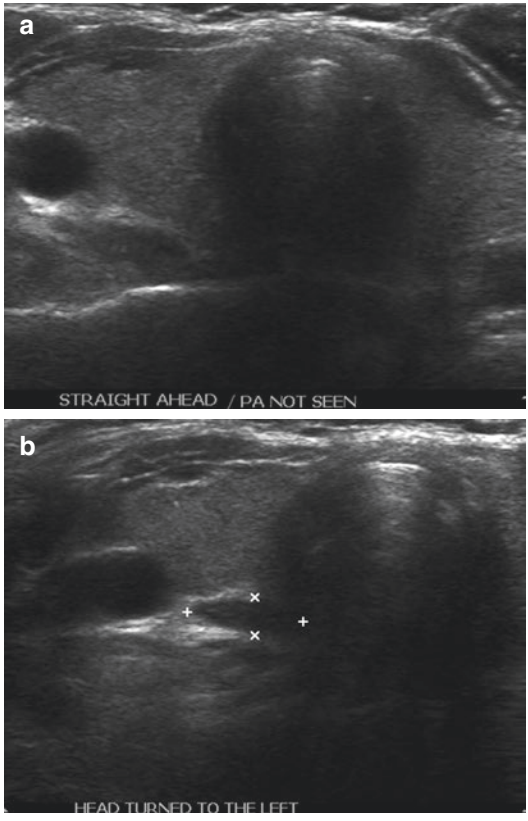

FIGURE 9.4 (**a**, **b**) Mobile right upper TE groove adenoma

Ultrasound Evaluation in MEN Syndromes and Chronic Renal Failure Patients

Multiple Endocrine Neoplasia

Primary hyperparathyroidism occurs in MEN 1 and MEN 2a syndromes. In these syndromes, multigland disease is very common. All gland inspection is required during surgery even if localization studies reveal unilateral abnormality; therefore, US or Tc99MIBI localization is of little value. However, there is a role for performing US evaluation in MEN subjects who have had unsuccessful surgeries.

Renal Failure

In subjects with chronic renal failure, all glands are affected to a variable degree. Surgical intervention should involve inspection of all parathyroid glands; therefore, localization is of limited value. US evaluation is a valuable tool to perform ETOH ablation in ESRD patients who are unable to undergo surgery due to comorbidities. Renal patients also present an excellent opportunity to practice parathyroid ultrasonography.

Ultrasound Features of the Parathyroid Adenomas

Normal or non-enlarged parathyroid glands cannot be visualized with present-day US equipment. In eucalcemic or mildly hypercalcemic subjects, it is possible to have a diminutive adenoma in the typical sites of location which elude US detection. Ultrasound evaluation cannot be used to diagnose PHPT; it is strictly a localization tool. The following are the distinct ultrasonographic features of parathyroid adenomas.

Extrathyroidal Location and Indentation Sign

The vast majority of parathyroid adenomas are located outside the posterior capsule of the thyroid gland [10–12]. These lesions are located in close relation to the posterior capsule of the thyroid gland [17]. The visualization of a lesion along the posterior aspect of thyroid gland in the clinical context of hypercalcemia makes the possibility of a parathyroid gland very likely. It is quite common to see an indentation made by the parathyroid adenoma on the posterior capsule of the thyroid gland: "the indentation sign." There is also a noticeable echogenic line observed, separating the two glands, which represents the fibro-fatty capsule. A parathyroid adenoma is embedded within the thyroid gland in about 2–5% of cases [18, 19] when it is indistinguishable in appearance from a thyroid nodule. The incidence of intraglandular location was higher in patients with multigland disease in one series: 3% in patients with uniglandular disease versus 15% in those with hyperplasia [13] (Figs. 9.3, 9.5, and 9.6).

Homogenous Hypoechoic Texture

This is a distinguishing imaging characteristic of parathyroid adenomas. The enlarged parathyroid glands are homogeneously hypoechoic echotexture in relation to the thyroid gland [20].

Vascular Pedicle and Blood Flow

The presence of an independent artery (polar artery) feeding an adenoma was found in 83% of parathyroid adenomas [21]. Other patterns of blood flow such as the "vascular arc" and diffuse flow within the adenoma have also been described [22] (Fig. 9.7).

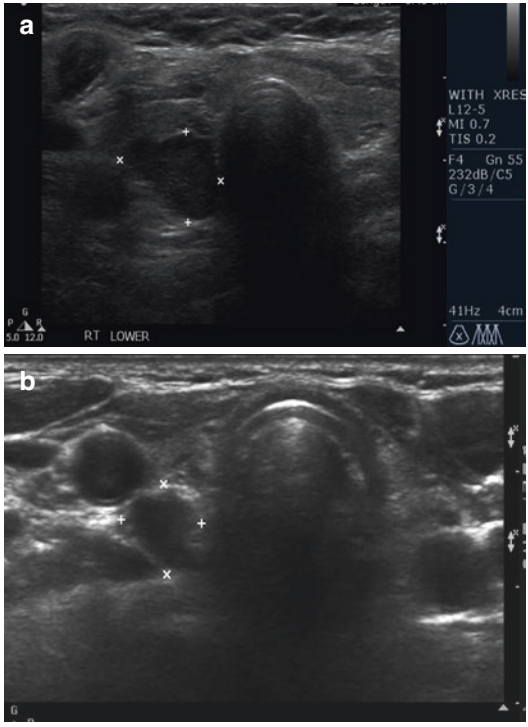

FIGURE 9.5 (**a**, **b**) Inferior parathyroid adenoma in transverse view

Variable Shapes

Parathyroid adenomas develop along the fascial planes and conform to the anatomical pressures of surrounding structures. Therefore, considerable variations in shapes can be observed. Oval, sausage shaped, pencil shaped, triangular, or oblong shapes can all be observed.

Lack of US Visualization of Parathyroid Lesion(s) in Hypercalcemic Subjects

In the hands of experienced operators, parathyroid ultrasonography has high level of sensitivity and specificity. Despite the best of efforts, in about 10–20% of the subjects, adeno-

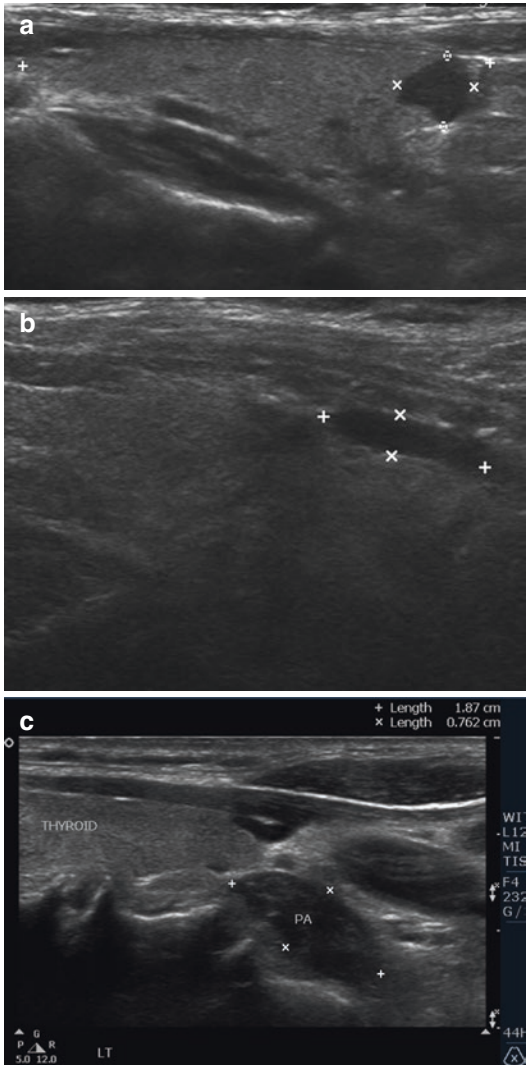

FIGURE 9.6 Inferior parathyroid adenoma seen in longitudinal view. (**a**) Inferior, intrathyroidal, craniocaudal. (**b**) Inferior PA, craniocaudal, pencil-shaped lesion. (**c**) Inferior paravertebral posteriorly located adenoma

mas are not visualized. The likely cause includes posteriorly located lesions, retropharyngeal superior adenomas, intrathoracic location, and parathyroid hyperplasia. In one study,

posteriorly located parathyroid adenomas were observed in 58% of subjects with negative US and Tc99MIBI scans [23].

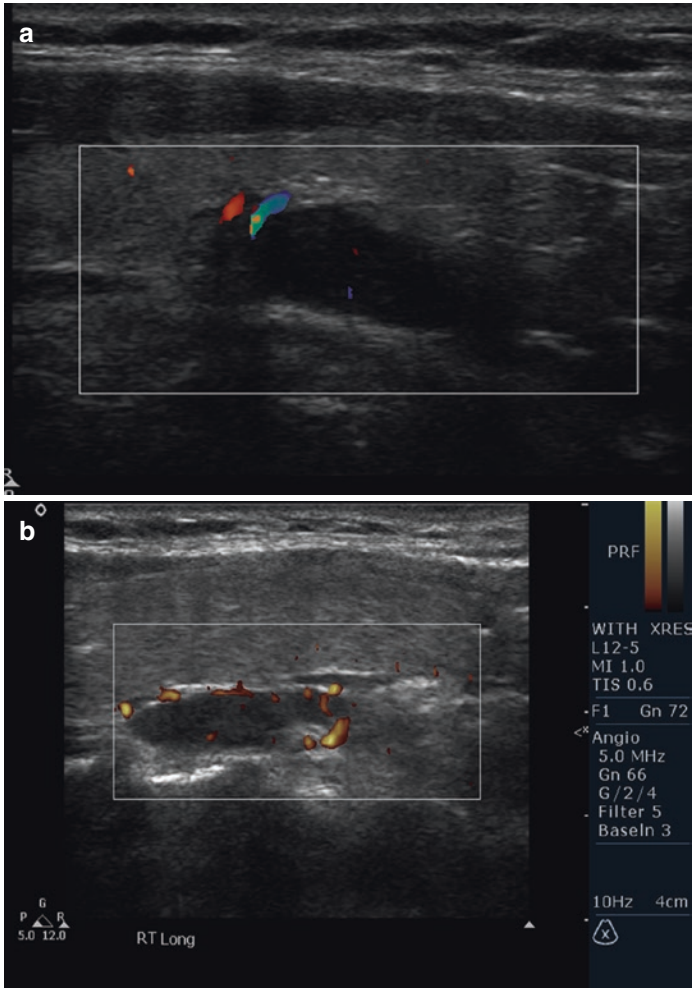

FIGURE 9.7 (**a**) Polar vascular pedicle color Doppler. (**b**) Polar vessels depicted by power Doppler. (**c**) Arc pattern of blood flow. (**d**) Diffuse blood flow seen within adenoma

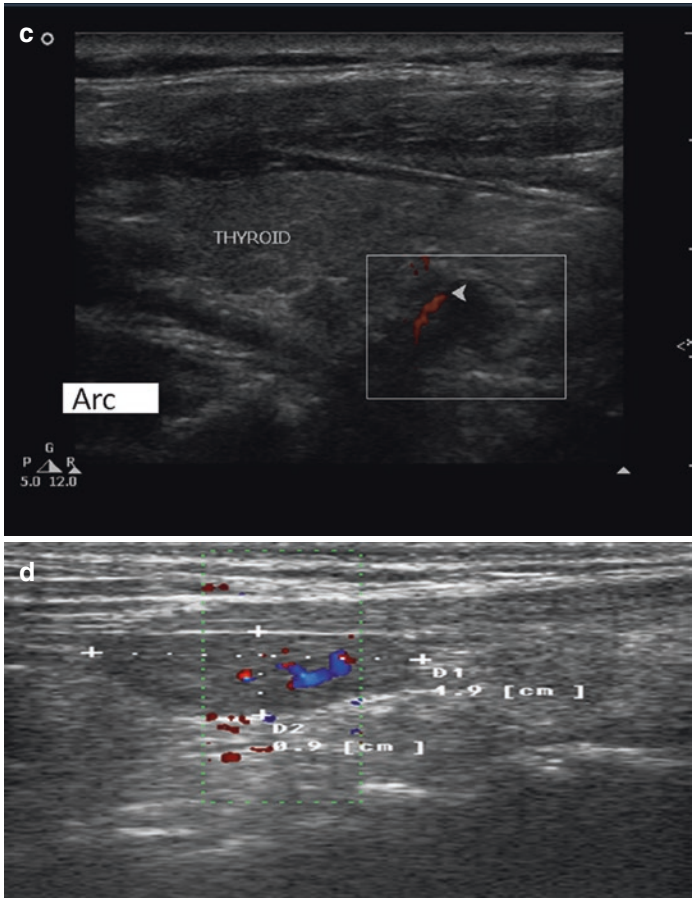

FIGURE 9.7 (continued)

Parathyroid Incidentaloma

Subclinical parathyroid tumors can be discovered incidentally during neck ultrasonography (Figs. 9.8 and 9.9). The frequency of observing these incidental tumors is rare [24, 25]. Fine needle aspiration with PTH estimation in syringe washings is a reliable way to identify these lesions as parathyroid tumors.

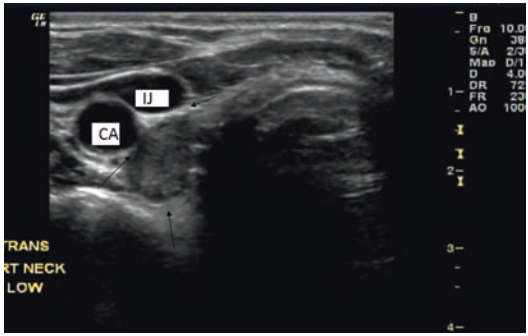

FIGURE 9.8 Adenoma within the carotid sheath

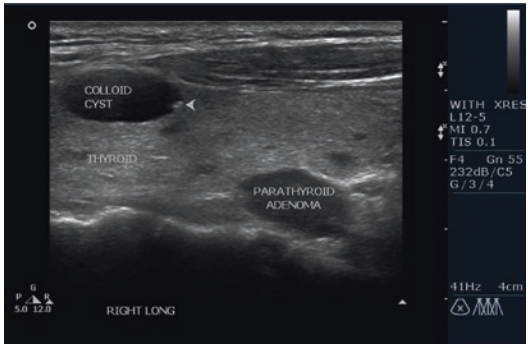

FIGURE 9.9 Parathyroid adenoma visualized alongside incidental thyroid disease

Cystic Parathyroid Adenomas

Cystic parathyroid adenomas are very rare. Simple cysts of the parathyroid glands without hypercalcemia are occasionally encountered during assessment of suspected thyroid cysts. Partial cystic change of adenoma is depicted in Fig. 9.10. Syringe washout PTH estimation is useful to prove the origin of these cysts (Fig. 9.11).

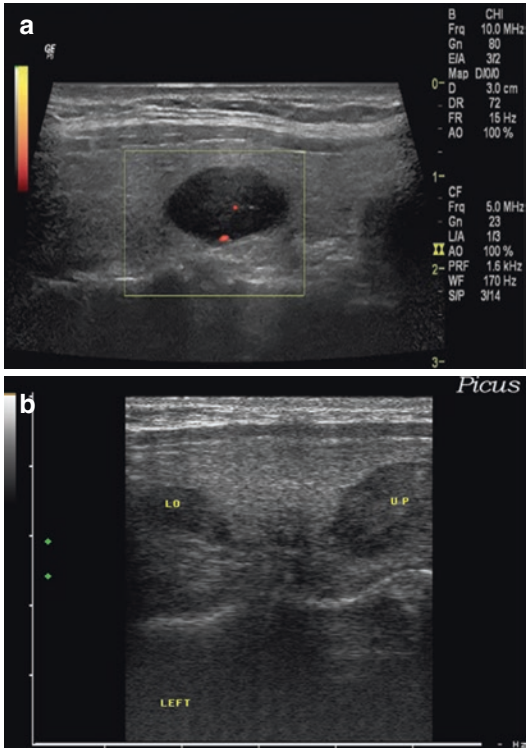

FIGURE 9.10 Intrathyroidal parathyroid adenomas. Double adenoma visualized in longitudinal view. Note also PA located within the thyroid gland capsule. (**a**) (Intrathyroidal) note absent echogenic line. (**b**) Hyperplasia—intrathyroidal

Biopsy of Parathyroid Lesions

Biopsy of suspected parathyroid lesions can be safely performed in the office setting and syringe washings analyzed for parathormone (PTH) [26, 27]. Elevation of PTH in syringe washings provides confirmation with high degree of specificity and differentiates from coexistent posteriorly located thyroid

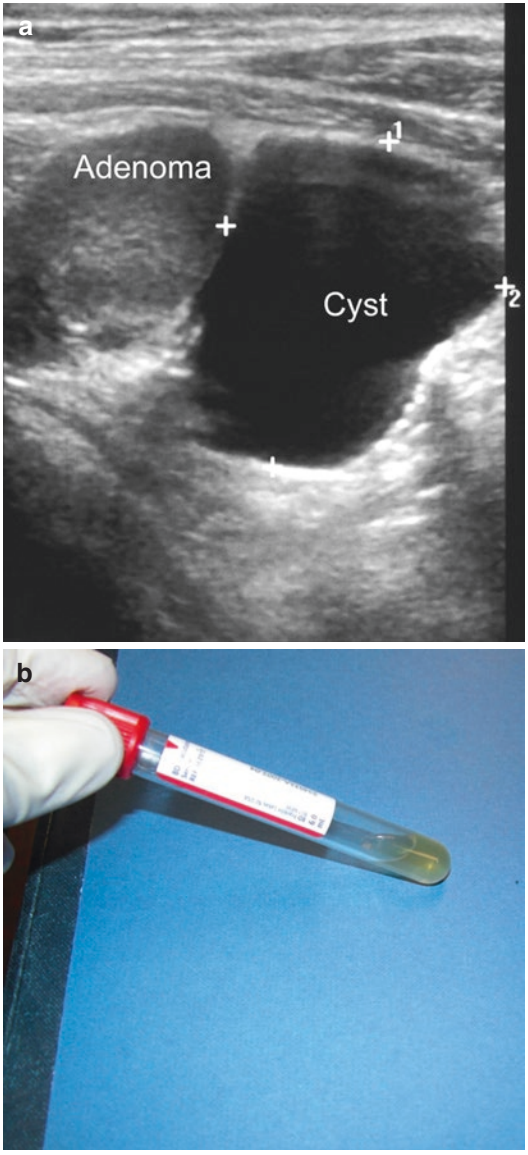

FIGURE 9.11 (**a**) Parathyroid cyst and (**b**) aspirate

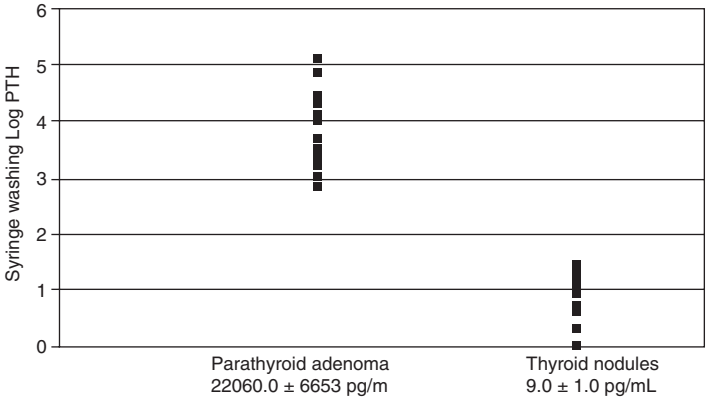

FIGURE 9.12 Parathyroid hormone (*PTH*) levels in syringe washing specimens obtained after fine needle aspiration of parathyroid adenomas of study subjects and proven thyroid nodules as controls, represented in log scale. Findings in the two groups were significantly different ($P < 0.001$). Reprinted with permission from [27]. Copyright 2007 American Association of Clinical Endocrinologists

nodules Fig. 9.12 [27]. Lesions larger than >1.5 cm with obvious ultrasound features of a solitary parathyroid adenoma do not require biopsy confirmation. Subjects with bilateral or multiple lesions, patients who received unsuccessful surgery, negative Tc99MIBI study, atypical location, coexistent multinodular goiter, and prior to percutaneous interventions are some of the indications to perform biopsy confirmation (Figs. 9.10, 9.13, and 9.14). Table 9.1 lists indications and contraindications for fine needle aspiration biopsy of parathyroid lesions. Parathyroid incidentaloma observed during cervical ultrasonography can also be sampled for diagnosis. Central compartment lymph nodes are often seen in subjects with Hashimoto's disease (Fig. 9.15). These reactive appearing lymph nodes should not be confused with parathyroid incidentalomas. The texture of the thyroid gland can provide clues to the diagnosis of Hashimoto's disease in undiagnosed subjects. The reactive lymphadenopathy is often multiple and observed in several areas in the perithyroidal region and may have a hilum.

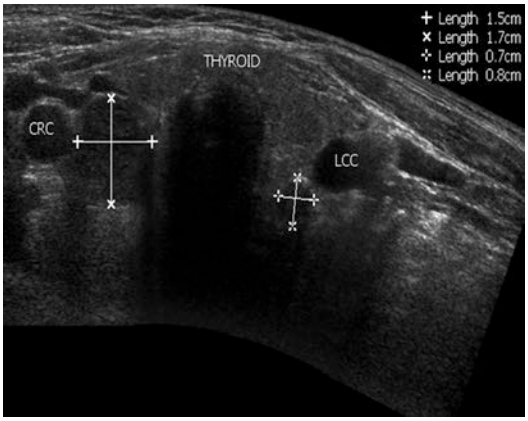

FIGURE 9.13 Double parathyroid adenomas in transverse panoramic view. The findings were confirmed during surgery

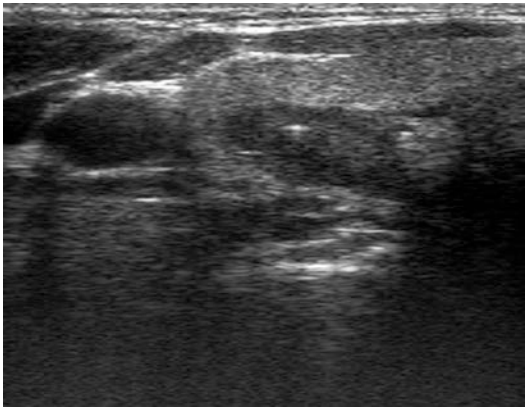

FIGURE 9.14 Biopsy of suspected PA

The technique of biopsy is similar to that of FNA of a thyroid lesion with a few precautions. We advocate the use of 27 or 25 G needles and to attempt fewer passes. Vigorous "jabbing" technique is best avoided. The use of larger needles with multiple passes can lead to fibrosis of the gland or

Table 9.1 Suggested indications and contraindications for parathyroid FNA

Indications	Contraindications
Failed surgery	Anticoagulation (relative)
Multiple lesions	Morbid obesity (relative)
Intrathyroidal location	Deeply located lesion (relative)
Atypical location or appearance	Partial or complete obscuration by vital structures
Ethanol ablation	Suspected parathyroid carcinoma (absolute)

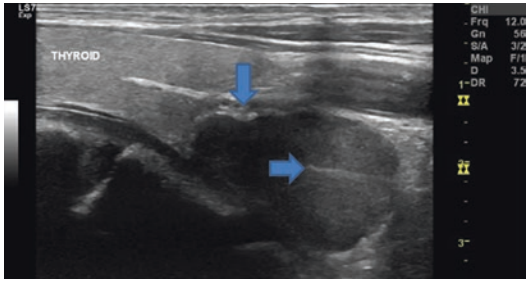

Figure 9.15 Multiple reactive lymphadenopathy at the location of an inferior parathyroid gland. Hashimoto's thyroiditis with lymph nodes, at the location of inferior parathyroid gland

capsule, complicating subsequent surgical excision [28]. These histological changes have not been universally observed by others when appropriate smaller bore needles are used for sampling [29]. Due to the deep location of parathyroid lesions, longer needles may be required to enable biopsy to be performed. Parathyroid tumors can be mobile and may need a sharp and abrupt jab to penetrate the capsule. Parathyroid lesions produce bloody aspirates. The absence of bloody aspirate is typically encountered with non-parathyroid lesions most often, a central compartment lymph node.

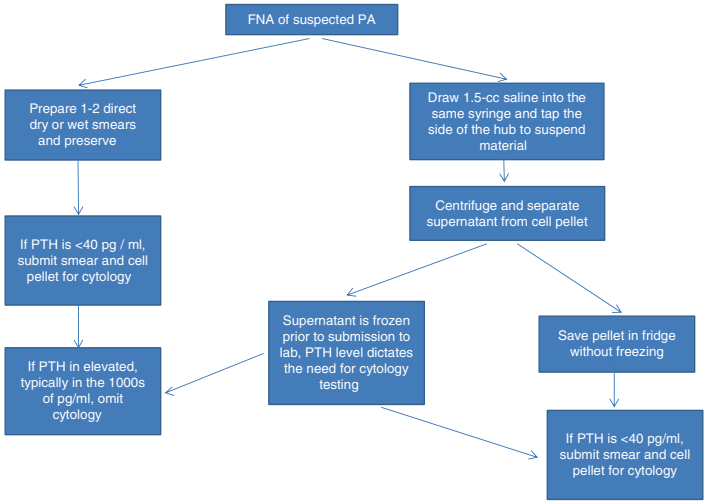

FIGURE 9.16 Specimen processing flow chart following parathyroid FNA

The syringe aspirate can be processed in the following manner (Fig. 9.16):

1. Prepare one or two slides with the specimen obtained during parathyroid FNA, and rinse the reminder of the specimen in 2 mL of normal saline.
2. The fluid is centrifuged immediately, separate the supernatant from the cellular debris, and freeze before transporting to the laboratory.
3. It is not necessary to submit the slides for cytological evaluation until the syringe washing PTH results become available. If the PTH level is low in the syringe aspirate, the prepared slides are submitted for cytological analysis. The latter technique ensures a certain level of safety against the chance sampling of posteriorly located coincidental metastatic lymph nodes. Metastatic lymph nodes in the central compartments are often multiple, unlike parathyroid adenoma.

4. The cell pellet is saved and refrigerated, which serves as a duplicate specimen. This specimen can also be used for cytology if the need arises. This protocol negates the need for second FNA in the event of mishandled specimen.

Most laboratories in the USA are willing to perform intact PTH estimations in tissue specimens if prior arrangements are made with the lab supervisor. It is good practice to save the left over cell pellet. This can be reconstituted in saline and used as a second specimen in the event of loss of the primary specimen. The PTH concentration in aspirates can be very high. Despite such high levels, the "hook effect" has not been observed during PTH estimation [27]. The lowest level observed in this study was 40 pg/mL [27]. Parathyroid cytology is not useful during evaluation for parathyroid adenomas. Irrespective of the presence or absence of parathyroid cells, the PTH levels in FNA fluid were elevated in all specimens obtained from parathyroid tissue. Also, thyroid cells can be observed in 30% of FNA specimens when posteriorly located lesions are biopsied through the thyroid lobe [30].

Coexistent Thyroid Disease

Parathyroid ultrasonography provides the additional advantage of identifying coexistent thyroid nodules and cancers [27, 30, 31]. This alerts surgeons to the coincidental presence of thyroid pathology that can be addressed during the same surgery. Not all thyroid lesions can be visualized during surgery and none by Tc99MIBI imaging.

Special Considerations in Atypical Adenomas and Parathyroid Carcinomas

Parathyroid carcinomas and atypical adenomas present in a rapidly progressive fashion. The long lag of gradual development of hypercalcemia is typically absent. CDC73 gene

codes for a tumor suppressor protein called parafibromin. A common syndrome related to CDC73 mutation is the hyperparathyroidism-Jaw tumor (HPT-JT) syndrome. These subjects are often in their late adolescence or young adulthood. Other accompaniments of this syndrome are ossifying fibromas of the maxilla or mandible, renal, and uterine tumors. The vast majority of individuals with HPT-JT present with benign tumor of the parathyroid (85%), which require careful biochemical monitoring for recurrence in other glands. In suspected parathyroid carcinoma patients, the surgery should be aimed at removal of the tumor en bloc along with intraoperative clear margins, with or without ipsilateral thyroid lobectomy. Genetic testing is recommended in subjects diagnosed with atypical adenoma or parathyroid carcinomas. Germline CDC73-related disorders are inherited in an autosomal dominant fashion. About 20% of individuals with sporadic parathyroid carcinomas harbor CDC73 mutation. About 15% of subjects with CDC73 germline mutations present with parathyroid carcinomas [32]. Parathyroid carcinomas often manifest calcifications, fibrous bands, cystic changes, or irregular margins (Fig. 9.17).

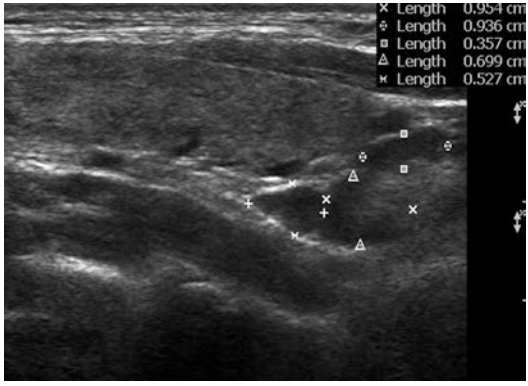

Figure 9.17 Parathyroid carcinoma. Note fibrotic band and calcification

Indications and Procedure of ETOH Ablation

Surgery is the mainstay for the definitive treatment of PHPT. In an occasional patient, who is deemed high surgical risk, percutaneous ethanol ablation can be attempted. The procedure is performed as below.

The skin and subcutaneous tissue is anesthetized using 2 ml of lidocaine under guidance. Lidocaine infiltration is performed under vision, using US transducer along the facial planes anterior to the parathyroid lesion. Once lidocaine infiltration is complete, the lesion is entered with a 27 or 25 G needle that is loaded with 0.5–1 cm^3 of alcohol. The alcohol is injected into the target lesion in question. Great care should be taken to avoid injection outside the lesion. This can result in tissue necrosis. Similarly, puncturing of the posterior or medial aspect of the capsule should be avoided altogether. The risk for injury to recurrent laryngeal nerve is greater in such situations. Patients sometimes complain of a twinge or dull ache for 5–10 min. The disappearance or the "pruning" of blood flow by Doppler predicts success of injection (Fig. 9.18). If blood flow into the gland is unaffected by the injection 5–10 min following the first injection, a second injection may be administered. Ethanol ablation can be effective in MEN 1 subjects who have recurrent primary hyperparathyroidism [33].

Parathyroid Incidentalomas

Parathyroid-like lesions encountered incidentally during neck or thyroid imaging are not uncommon in clinical practice. These tumors have the imaging phenotype and likeness of a parathyroid adenoma. Serum chemistry testing can reveal calcium or PTH elevation in previously unidentified subjects. The confirmatory test is FNA PTH estimation following a biopsy [24].

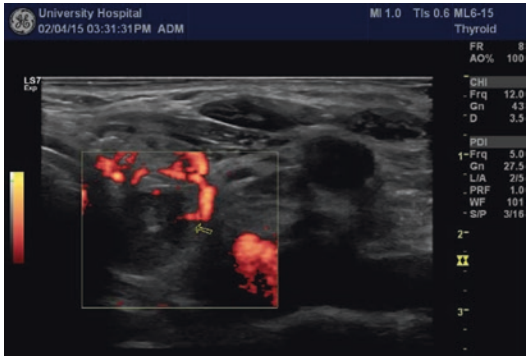

FIGURE 9.18 Postinjection "pruning" of the vascular pedicle

Summary

Parathyroid ultrasonography is a valuable tool for the assessment of diseased parathyroid glands in patients with primary hyperparathyroidism. It is a valuable tool to evaluate the thyroid gland for coincidental nodules and cancers, prior to parathyroid surgery and to perform percutaneous intervention such as alcohol injection.

References

1. Kebebew E, Clark OH. Parathyroid adenoma, hyperplasia and carcinoma: localization, technical details of primary neck exploration and treatment of hypercalcemic crisis. Surg Oncol Clin N Am. 1998;7:721–48.
2. Heath H, Hodgson SF, Kennedy M. Primary hyperparathyroidism: incidence, morbidity and potential economic impact in a community. N Engl J Med. 1980;302:189–93.
3. Owen R. On the anatomy of the Indian Rhinoceros (Rh. Unicornis L.). Trans Zool Soc London. 1862;4:31–58.
4. Johansson H. The Uppsala anatomist Ivar Sandström and the parathyroid gland. Ups J Med Sci. 2015;112:72–7.

5. Rogers-Stevane J, Kauffman GLA. Historical perspective on surgery of the thyroid and parathyroid glands. Otolaryngol Clin N Am. 2008;41(6):1059–67.
6. Spence HM. The life and death of Captain Charles Martell and kidney stone disease. J Urol. 1984;132(6):1204–7.
7. Udelsman R, Donovan PI. Open minimally invasive parathyroid surgery. World J Surg. 2004;28(12):1224–6.
8. Yao K, Singer FR, Roth SI, Sassoon A, Ye C, Giuliano AE. Weight of normal parathyroid glands in patients with parathyroid adenomas. J Clin Endocrinol Metab. 2004;89:320–3213.
9. Gilmore JR. The gross anatomy of parathyroid glands. J Pathol. 1938;46:133–49.
10. Alveryd A. Parathyroid glands in thyroid surgery. Acta Chir Scand. 1968;389:1.
11. Lappas D, Noussios G, Anagnostis P, Adamidou F, Chatzigeorgiou A, Skandalakis P. Location, number and morphology of parathyroid glands: results from a large anatomical series. Anat Sci Int. 2012;87:160–4.
12. Schneider R, Waldmann J, Ramaswamy A, Fernández ED, Bartsch DK, Schlosser K. Frequency of ectopic and supernumerary intra-thymic parathyroid glands in patients with renal hyperparathyroidism: analysis of 461 patients undergoing initial parathyroidectomy with bilateral cervical thymectomy. World J Surg. 2011;35(6):1260–5.
13. Yeh MW, Ituarte PHG, Zhou HC, et al. Incidence and prevalence of primary hyperparathyroidism in a racially mixed population. J Clin Endocrinol Metab. 2013;98(3):1122–9.
14. Abdulla AG, Ituarte P, Harari A, JX W, Yeh MW. Trends in the frequency and quality of parathyroid surgery: analysis of 17,082 cases over 10 years. Ann Surg. 2015;261(4):746–50.
15. Eastell R, Brandi ML, Costa AG, D'Amour P, Shoback DM, Thakker RV. Diagnosis of Asymptomatic primary hyperparathyroidism: proceedings of the fourth international workshop. J Clin Endocrinol Metab. 2014;99:3570–9.
16. Cheung K, Wang TS, Farrokhyar F, Roman SA, Sosa JA. A meta-analysis of preoperative localization techniques for patients with primary hyperparathyroidism. Ann Surg Oncol. 2012;19(2):577–83.
17. Yeh MW, Barraclough BM, Sidhu SB, Sywak MS, Barraclough BH, Delbridge LW. Two hundred consecutive parathyroid ultrasound studies by a single clinician: the impact of experience. Endocr Pract. 2006;12(3):257–63.

18. Andre V, Andre M, Le Dreff P, Granier H, Forlodou P, Garcia JF. Intrathyroid parathyroid adenoma. J Radiol. 1999;80(6):591–2.
19. McIntyre R Jr, Eisenach J, Pearlman N, Ridgeway C, Liechty RD. Intrathyroidal parathyroid glands can be a cause of failed cervical exploration for hyperparathyroidism. Am J Surg. 1997;174(6):750–3; discussion 753-4
20. Kamaya A, Quon A, Jeffrey RB. Sonography of the abnormal parathyroid gland. Ultrasound Q. 2006;22(4):253–62.
21. Lane MJ, Desser TS, Weigel RJ, Jeffrey RB Jr. Use of color and power Doppler sonography to identify feeding arteries associated with parathyroid adenomas. Am J Roentgenol. 1998;171(3):819–23.
22. Wolf RJ, Cronan JJ, Monchik JM. Color Doppler sonography: an adjunctive technique in assessment of parathyroid adenomas. J Ultrasound Med. 1994;13(4):303–8.
23. Harari A, Mitmaker E, Grogan RH, Lee J, Shen W, Gosnell J, Clark O, Duh QY. Primary hyperparathyroidism patients with positive preoperative sestamibi scan and negative ultrasound are more likely to have posteriorly located upper gland adenomas (PLUGs). Ann Surg Oncol. 2011;18(6):1717–22.
24. Pesenti M, Frasoldati A, Azzarito C, Valcavi R. Parathyroid incidentaloma discovered during thyroid ultrasound imaging. J Endocrinol Investig. 1999;22(10):796–9.
25. Frasoldati A, Pesenti M, Toschi E, Azzarito C, Zini M, Valcavi R. Detection and diagnosis of parathyroid incidentalomas during thyroid sonography. J Clin Ultrasound. 1999;27(9):492–8.
26. Doppman JL, Krudy AG, Marx SJ, Saxe A, Schneider P, Norton JA, Spiegel AM, Downs RW, Schaaf M, Brennan ME, Schneider AB, Aurbach GD. Aspiration of enlarged parathyroid glands for parathyroid hormone assay. Radiology. 1983;148(1):31–5.
27. Abraham D, Sharma PK, Bentz J, Gault PM, Neumayer L, McClain DA. The utility of ultrasound guided FNA of parathyroid adenomas for pre-operative localization prior to minimally invasive parathyroidectomy. Endocr Pract. 2007;13(4):333–7.
28. Norman J, Politz D, Browarski E. Diagnostic aspiration of parathyroid adenomas causes severe fibrosis complicating surgery and final histologic diagnosis. Thyroid. 2007;17(12):1251–5.
29. Abraham D, Duick DS, Baskin HJ. Appropriate administration of fine-needle aspiration (FNA) biopsy on selective parathyroid adenomas is safe. Thyroid. 2008;18(5):581–2. author reply 583–4
30. Agarwal AM, Bentz JS, Hungerford R, Abraham D. Parathyroid fine-needle aspiration cytology in the evaluation of parathyroid

adenoma: cytologic findings from 53 patients. Diagn Cytopathol. 2009;37:407–10.
31. Krause UC, Friedrich JH, Olbricht T, Metz K. Association of primary hyperparathyroidism and non-medullary thyroid cancer. Eur J Surg. 1996;162(9):685–9.
32. Sharretts JM, Kebebew E, Simonds WF. Parathyroid Cancer. Semin Oncol. 2010;37(6):580–90.
33. Singh Ospina N, Thompson GB, Lee RA, Reading CC, Young WF Jr. Safety and efficacy of percutaneous parathyroid ethanol ablation in patients with recurrent primary hyperparathyroidism and multiple endocrine neoplasia type 1. J Clin Endocrinol Metab. 2015;100(1):E87–90.

Chapter 10
Surgical Trends in Ultrasound Applications for the Treatment of Thyroid Nodules, Thyroid Cancer, and Parathyroid Disease

Stacey Klyn and Mira Milas

S. Klyn, DO
Department of Surgery, Banner University Medical Center, Phoenix, AZ, USA

M. Milas, MD, FACS (✉)
Thyroid, Parathyroid and Adrenal Disorders Center, Diabetes and Endocrinology Institute, Phoenix, AZ, USA

Endocrine Surgery Center, Department of Surgery, University of Arizona College of Medicine – Phoenix, Phoenix, AZ, USA

Banner – University Medical Center Phoenix, Phoenix, AZ, USA
e-mail: Mira.milas@bannerhealth.com

D.S. Duick et al. (eds.), *Thyroid and Parathyroid Ultrasound and Ultrasound-Guided FNA*,
https://doi.org/10.1007/978-3-319-67238-0_10

Introduction

Using imaging for perioperative planning has continued to increase in popularity as imaging modalities increase in their sensitivity and specificity. Just as the physical exam is essential in a patient encounter in the hospital or clinic, the US exam is equally essential in the surgical evaluation of a patient with endocrine neck disorders.

Clinical Applications of Thyroid and Parathyroid Ultrasound Relevant to Surgeons and Surgery

- Characterization of anatomic/organ abnormality
- Diagnosis:
  - Via pattern recognition
  - Via ultrasound-guided fine needle aspiration biopsy
- Determination of indications for surgery
- Identification of appropriate extent of surgery:
  - Lymph node mapping of central and lateral neck for thyroid cancer
  - Lymph node scanning of central and lateral neck for benign thyroid disease
  - Appreciation of single, multiple, or ectopic parathyroid gland abnormalities
  - Defining size of suspected/known thyroid cancer
  - Defining the presence or absence of disease in contralateral thyroid lobe
  - Signs of local cancer invasion to aerodigestive structures
- Identification of coexisting thyroid and parathyroid disease
- Parathyroid localization
- Detection of other cervical pathology (non-endocrine)
- Identifying any special characteristics for practical relevance during surgery:
  - Hashimoto's thyroiditis
  - Long upper thyroid poles
  - Gland vascularity

  - Thyroid location in the neck or to skin lines
  - Tracheal deviation
  - Tubercle of Zuckerkandl
  - Substernal extension
- Laryngeal ultrasound
- Optimal cosmetic cervical incision placement
- Eligibility for robotic or remote access surgery
- Intraoperative use
- Review of real-time cine images rather than static images for better assessment
- Detection of disease recurrence
- Continuity or care and assessment of surgical outcomes

In this sense it can be considered an extension of the physical exam. Its usefulness for determining pathology and exposing relative anatomy makes the addition of imaging to a surgical procedure easier for the surgeon and safer for the patient. With this in mind, there are many radiological avenues used to evaluate the thyroid and parathyroid glands. However, the one most useful in the hands of a surgeon is the US. The use of surgeon-performed US has been in practice formally for over 25 years by way of the focused assessment with sonography for trauma (FAST) exam [1, 2]. This has led to the change in management of patients in the trauma bay, decreasing invasive diagnostic procedures and facilitating quicker operative intervention [3]. In a similar fashion, perioperative thyroid and parathyroid US has pioneered the way for improved patient care and better surgical outcomes. Clinician-performed US for thyroid and parathyroid evaluation for surgery began in the late 1990s and has increased exponentially. In part, this has been facilitated by innovations in US technology and decreases in machine size and cost [4]. An accompanying trend has been development of continuing medical education courses being offered at annual surgical and medical professional meetings to increase the knowledge and skills of the surgeon and broaden the scope of their practice. With this form of certification and the proper amount of exposure to thyroid and parathyroid pathology, the surgeon and endocrinologist alike can adequately assess their patients with confidence.

Surgeons and the Initial Evaluation with US in the Clinic Setting

The use of US by the surgeon begins in the office setting. The patient will usually have previously an US of their thyroid, identifying a reason for surgical evaluation. While this previous US is helpful in that it identifies the initial abnormality, it can have significant potential limitations to the surgeon or, for that matter, to any treating clinician. The patient often presents with only a report that describes the abnormality of the thyroid or parathyroids in very general terms. The initial exam may be performed by sonographers whose skill or familiarity with endocrine disease may vary widely. Access for sonographers to clinical information may be difficult. Access for clinicians to review images or cine loops may be difficult. A communication gap arises and the variability of US reporting is widely appreciated (see Chap. 17, Authoring Quality Ultrasound Reports).

A dedicated evaluation of the lateral neck to include assessment of cervical lymph nodes may or may not be included. For a surgeon, lack of mention of abnormal cervical lymph nodes in the report cannot be assumed to imply the exam was done or that the lymph nodes are normal. Without a clinical history or communication to guide them, initial sonographers, particularly in a radiology department, could easily overlook the need for lymph node screening. The current 2015 ATA guidelines advise that lymph node evaluation in the lateral neck occurs at the time the original ultrasound detects a thyroid nodule [5].

As discussed in previous chapters, many variants of thyroid and parathyroid pathology and characteristics can be seen on US. Reports generated by clinicians who are not thyroid specialists, based on images acquired by a sonography technician, may frequently misinterpret significant pathology, especially for smaller nodules [6, 7]. Given this variability, the report may not include all of the necessary descriptors or even all of the surgically relevant pathology. Even in the situation of high-quality reporting, the surgeon still must piece

together a mental image based upon the descriptors used in writing. The wisdom of "a picture is worth a thousand words" motivates surgeon-performed and office-based US exams. Awareness of the drawbacks of an "outside" US can help guide the surgeon as to what needs to be further evaluated prior to surgery.

The office US exam allows the surgeon to fill in the gaps between the outside US report and the decision to perform surgery. For example, the patient may present with a report of multiple nodules. An exam in the office reveals that the patient does not have multiple nodules but in fact has Hashimoto's thyroiditis with pseudonodules. With the former diagnosis, the patient may have required an operation; however, with the latter diagnosis, surgery may not be indicated. Without the clinician-performed US, the patient could have undergone unnecessary surgery and assumed unnecessary risks and expenses inherent to surgery. From the opposite aspect, US evaluation of the neck by the surgeon in the case of hyperparathyroidism can aid in identification of concomitant thyroid pathology, thus changing the surgical management of the patient. Patients presenting for hyperparathyroidism have concurrent thyroid disease in 40–60% of cases [2, 4, 8]. This significant proportion of the patient population implies that the planned surgical procedure may likewise significantly change depending on the results of an office US.

The surgeon-performed US can also be used to reassure the patient of any discrepancies between previous exams. Given that US is extremely operator dependent, different views of the same nodule or pathology may yield different characteristics or measurement results. This often causes distress to the patient if the results are inconsistent or unexpected, such as a nodule that can no longer be found or has grown significantly, when in fact it has not. These variable results can lead to a referral for surgical consultation. During this meeting the surgeon can show the patient their ultrasound images and put their mind at ease, whether this means continued monitoring or surgical intervention.

Not only is using the US exam in the office essential in securing the decision for surgery, but an increasing number of surgeons are using it to perform ultrasound-guided fine needle aspirations (FNA). Only 31% of endocrinologists perform fine needle aspiration in their office [9]. Often a patient is referred to a surgeon based upon the findings of the outside US report alone. The primary care provider may feel more comfortable having the patient seen by a specialist prior to making the decision to have the patient undergo an invasive procedure such as FNA. By performing the fine needle aspiration, the surgeon ensures that the suspicious nodule is indeed the one being sampled in the case of multinodular disease. Also when evaluating the thyroid to confirm the findings of an outside US, additional pathology may be found in the contralateral lobe or in the lateral neck. Aside from the possibility of performing the initial diagnostic FNA of a thyroid nodule, surgeons may find themselves performing a second FNA on either contralateral nodules or cervical lymph nodes. The most common scenario reported for surgeon-performed fine needle aspiration is in a patient being evaluated for primary hyperparathyroidism, where a previously unknown thyroid nodule was detected during the course of localizing abnormal parathyroid glands.

A Surgeon's Perspective on Parathyroid US

Currently several modalities can be used to identify enlarged parathyroid glands, whether single adenomas or in multigland hyperplasia. These include dual-phase sestamibi scintigraphy, US, magnetic resonance imaging, and 4DCT (computed tomography). Dual-phase/subtraction scintigraphy has been reported to have an 88–90% sensitivity and over 90% specificity for localizing single adenomas [10]. 4DCT has sensitivity of 86% and MRI of 80% [10]. Surgeon-performed US detected a single, abnormal parathyroid in 72–86% of cases compared to 50% of the time with sestamibi scan [2].

For identification of any parathyroid abnormality, US is accurate in visualizing disease 76–89% of the time [8]. This accuracy decreases to 55–75%, though, if the subject has had a previous operation [4, 9, 11]. Studies have also shown that the sensitivity of a surgeon-performed US is equivalent to that of a sestamibi scan; therefore it can be used as the sole localization study if combined with intraoperative parathyroid hormone monitoring [4, 12, 13]. This level of accuracy is invaluable in preoperative planning for the surgeon, providing a road map in an ordinarily difficult dissection and localization endeavor. Surgeons also try to identify the embryologic origin of the enlarged parathyroid in order to optimally position the neck incision (Fig. 10.1).

Despite the high yield and usefulness of US in parathyroid disease, there are inherent drawbacks to successful evaluation. These include decreased detection secondary to thyroid nodular disease and thyroiditis, increased body mass index, the presence of multiglandular or ectopic parathyroid disease, and the presence of a small parathyroid adenoma [4, 14]. In

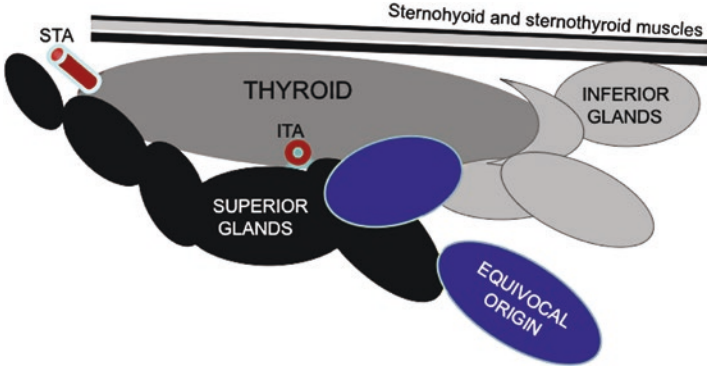

Figure 10.1 Embryologic origin of parathyroid glands can be suspected from the positioning of the enlarged parathyroid relative to the inferior thyroid (ITA) and superior thyroid (STA) arteries. This type of ultrasound detail also provides helpful orientation to surgeons

addition to these factors, thyroid nodules situated in the posterior portion of the thyroid, or benign central compartment lymph nodes, may inadvertently be mistaken for a parathyroid gland and vice versa [4]. Although the minimal amount of tissue between the US probe and the thyroid and parathyroid glands makes US ideal for scanning the neck, it is difficult to visualize a parathyroid gland located behind the trachea, esophagus, in the superior mediastinum, or in patients with thyroiditis who may have significant reactive adenopathy [4]. With the use of US to direct the exposure of the parathyroid glands at surgery, the time to locate the glands is decreased, thereby decreasing the operative time and extent of dissection. Generally speaking, shorter operative times are expected to have quicker recoveries, shorter hospital stays, and increased patient satisfaction.

Thyroid Cancer and Ultrasound Applications Relevant to Surgeons

When presented with a patient with cytology diagnostic of or suspicious for thyroid cancer, the surgeon's primary concern becomes not so much whether to perform surgery but rather what operation is best indicated. The American Thyroid Association's 2015 guidelines provide a framework for this decision; however, in order to follow these recommendations, the patient must first be fully assessed for the information that is the basis of those guidelines. As previously mentioned, the report from an US performed by an outside facility may be lacking in relevant content, even if the prior images are obtained and reviewed by the surgeon personally. A thorough, clinician-performed neck US is ideal in every patient diagnosed with thyroid cancer to evaluate for lymph node involvement and contralateral disease. Preoperative evaluation of the neck changes a surgeon's management in up to 66% of the cases [2]. The most frequent indication for a change in surgical plan was metastatic cervical lymphadenopathy [2]. A partial or near total thyroidectomy may have been the initial plan for a

patient as the results of the outside US are discussed in clinic; however, upon the clinician-performed exam, new findings such as additional suspicious nodules in the contralateral lobe or lateral lymphadenopathy may lead to an indication of a total thyroidectomy or a lateral or central neck dissection. Just as surgical management can increase in invasiveness based upon results of the surgeon-directed US, a shift toward avoiding unnecessary surgeries can also occur. Surgeon-performed US is a valuable resource for evaluating for central lymphadenopathy and thoracic extension of the thyroid and diseased lymph nodes. For central neck lymph node metastases, preoperative US performed prior to the initial surgery provides 95% sensitivity, 90% specificity, 97% negative predictive value and 83% positive predictive value [15]. Surveillance after thyroid surgery in the case of thyroid cancer is pivotal in early diagnosis of recurrence. Radioactive iodine scans and cross-sectional imaging studies are costly, time-consuming, and accompanied by radiation. Standard laboratory studies such as thyroglobulin can also be negative in the presence of antibodies or poorly differentiated recurrent disease [2]. Clinician-performed US can detect recurrent disease in patients with otherwise negative or inconclusive standard surveillance methods [2] (see Chap. 8, Ultrasound and Mapping of the Neck Lymph Nodes).

Perioperative Assessment of Vocal Cords

Damage to the recurrent laryngeal nerve is a known complication of thyroid and parathyroid surgery and can carry significant morbidity to the patient. Therefore, both preoperative and postoperative assessment of the vocal cords can inform the surgeon about their functionality. This is especially relevant in the case of a reoperation for recurrent disease, history of other prior neck surgery such as tracheostomy, history of prior neck radiation, or physical exam findings that would suggest possible nerve dysfunction preoperatively [16]. The traditional approach to evaluating the vocal cords is direct laryngoscopy which allows visual examination

of vocal cord appearance and movement. However, using US to assess the vocal cords can be almost as effective with an 85–100% visualization rate [17, 18]. Vocal cord US brings with it the benefit of being noninvasive, therefore avoiding the risks and expense of direct laryngoscopy. In the event of a suboptimal US exam, the patient may still proceed with the standard direct laryngoscopy without having sacrificed significant time and resources. Despite the high rate of visualization as well as the benefits of laryngeal US, direct laryngoscopy is still advisable for those patients at higher risk of having a prior injury or showing signs of dysfunction preoperatively (Fig. 10.2).

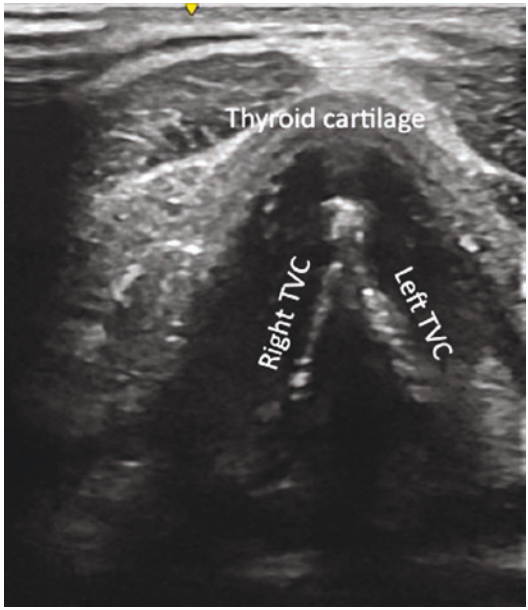

Fig. 10.2 Appearance of true vocal cords (TVC) on laryngeal ultrasound as the brightest white hyperechoic lines in V shape. Laryngeal ultrasound is an application that surgeons are increasingly using for initial assessment of TVC both pre- and postoperatively. Select patients are able to proceed to direct laryngoscopy if appropriate, but many are spared the additional cost and invasiveness of this procedure

Intraoperative US

Not only is surgeon-performed US exam essential in the preoperative clinic setting, but it is also extremely valuable in the operating room for several applications. The use of US imaging once the patient is anesthetized is becoming more popular among endocrine surgeons. There are a number of advantages to this practice, and, aside from the small amount of time to perform the exam, there are no disadvantages to its use. One advantage is aiding optimal placement of the surgical incision (Fig. 10.3). It is the authors' practice to assess the patient in the preoperative area and look for a natural skin crease for best cosmetic results in the sitting and supine positions. Based on the location of the pathology and the skin creases, more than one crease may be marked, and the most appropriate one is selected based on intraoperative US evaluation. Once the

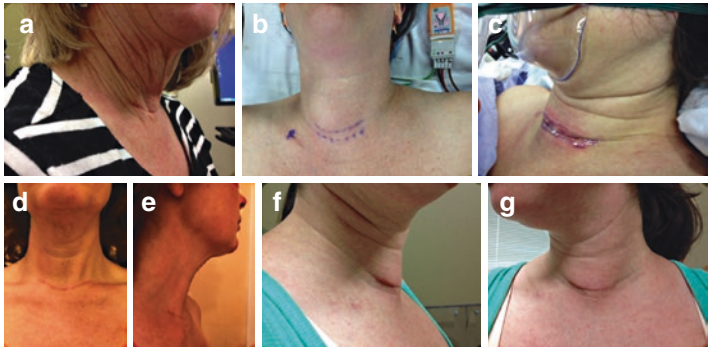

Fig. 10.3 A well-healed cervical incision is barely visible several years after surgery (**a**). Marking of potential skin incision along existing natural creases is ideally started while the patient is awake and in the preoperative area (**b**). Surgeon preference varies for using higher- vs lower-situated incisions (**c**). Two weeks after surgery, this patient was pleased with her scar (**d**, **e**). Three months after surgery, this patient (**f**, **g**) took her own photos appreciating the cosmetic position of her scar. Ultrasound done after anesthesia and prior to surgery can help select incision placement relative to underlying pathology as well

patient is under anesthesia, the head and neck are positioned in the ideal location for the operation. At this point, prior to the sterile skin prep, the neck is examined with the US probe. This study may reveal additional pathology prompting a change in the surgical procedure or extent of the surgical procedure. This view also allows the surgeon to plan their surgical incision more appropriately. In the event there is thoracic extension or newly found lymphadenopathy, the incision may need to be placed further inferior or extended slightly laterally. In patients with parathyroid disease, greater compression of the neck with the transducer probe often elicits deeply situated enlarged glands that were not apparent with office-based US (Fig. 10.4). Once the operation has begun, occasionally despite extensive dissection, a parathyroid gland may not be found and parathyroid hormone levels may still be elevated. At this time, a sterile US probe can be used to evaluate the surrounding tissue for possible ectopic locations of the missing gland. If the gland cannot be located and there appears to be a suspicious nodule within the thyroid tissue

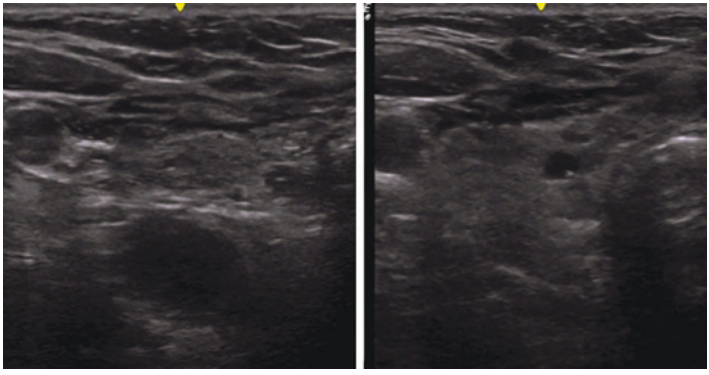

Fig. 10.4 Application of greater transducer pressure (*left panel*) brings out a parathyroid adenoma (large hypoechoic oval) that with light pressure may stay unrecognized deeper in the tracheoesophageal groove (*right panel*). A small thyroid cyst is evident in the right thyroid lobe. Surgeons may be more motivated to apply such maneuvers in order to localize the abnormality and thus make surgery more efficient

on intraoperative US, an aspirate can be sent for parathyroid hormone levels. This saves both the time of dissecting the thyroid and avoids the possibilities of unnecessary thyroid lobectomy or further unrevealing parathyroid exploration.

Robotic and Remote Access Surgery

Although thyroid surgery has become less invasive with smaller incisions, these are nonetheless in a location on the anterior neck that is not easily concealed. This drawback to conventional surgery has led to developments in remote access thyroid surgery allowing for more aesthetically pleasing results. Surgical treatment of thyroid disease via nontraditional approaches is now possible with the use of endoscopic assistance through an axillary, chest, or postauricular incision; the two most frequently used are the robotic axillary thyroidectomy (RAT) and the robotic facelift thyroidectomy (RFT) [4, 19, 20]. Eligibility criteria for such surgeries include benign nodules ≤5 cm or malignant lesions ≤2 cm for the axillary approach and benign nodules <4 cm for the facelift approach [4, 19–21]. While these guidelines exist, there have been studies showing successful RAT and RFT total thyroidectomy as well as total thyroidectomy with bilateral modified neck dissection [4, 22, 23]. These studies, however, are small in size and lack the long-term follow-up needed to fully assess outcomes. The use of US is instrumental in determining eligibility for RAT and RFT because it evaluates the overall size and appearance of the thyroid gland preoperatively and allows the surgeon to establish characteristics of the individual's disease that influence the type of surgery offered [4, 17]. For both the RAT and RFT approaches, US findings of Hashimoto's thyroiditis or extrathyroidal, substernal, or retropharyngeal extension are exclusion criteria [4, 24, 25]. The specific location of the nodule within the thyroid gland is also taken into account, with the ideal position in the midportion of the thyroid lobe [4, 26]. This location enables the surgeon to grasp the superior pole for manipulation without damaging the capsule of the cancer and permitting an easier, thus, quicker operation [4]. Despite the appealing nature of

nontraditional approaches for cosmetic reasons, they have not been widely adopted and are only performed at a small number of facilities in the United States.

Certification in Clinician-Performed Ultrasound at Point of Care

Ultrasound can be a valuable tool for any practitioner; however, it is only as good as its operator. Proper training is crucial, not only in performing the ultrasound but also in interpreting the images. Should physicians with insufficient ultrasound training rely on their evaluation of the neck for treatment, important features may be misinterpreted or missed for many reasons, including lack of technique in acquiring necessary images and lack of correct pattern recognition. This circumstance may lead to misdiagnosis, unnecessary surgery, or even a lack of proper medical or surgical treatment. Given the importance of a proficient ultrasound skill set, several avenues are available to ensure that physicians are equipped with the appropriate knowledge and capabilities to perform their duties safely at the point of care. In this context, point of care refers to physicians who use ultrasound for diagnosis and interventions (FNA) outside the scope of a radiology department, for example, in their outpatient clinics, in the emergency room, or in the operating room settings.

The American College of Endocrinology recognizes this importance and offers the Endocrine Certification in Neck Ultrasound (ECNU) Program. This program is designed for endocrinologists, endocrine and head and neck surgeons, radiologists, and cytopathologists to ensure that practicing clinicians using physician-performed ultrasound are proficient in the skill. In doing so, the goals of promoting patient safety and patient best interests are maintained at the forefront. A series of steps are required for program certification including a written exam, ultrasound course attendance, and submission of a designated number of diagnostic and interventional (fine needle aspiration) ultrasound studies and

reports. Similarly, both introductory and advanced ultrasound courses are made available at national surgical meetings such as the Clinical Congress of the American College of Surgeons and the Annual Meeting of the American Association of Endocrine Surgeons. These courses allow general surgeons the ability to become familiar with physician-performed ultrasound and the varying degrees of thyroid and parathyroid pathology as well as evaluating the lymph node status of the patient. Please see below for existing resources in thyroid and parathyroid ultrasound education.

Educational Resources for Thyroid and Parathyroid Ultrasound

Multidisciplinary-based

ECNU Endocrine Certification in Neck Ultrasound https://www.aace.com/ecnu

WCUME World Congress on Ultrasound in Medical Education http://www.wcume.org/

TCCC Thyroid Cancer Care Collaborative https://www.thyroidccc.org/

Endocrinology-based

AACE American Association of Clinical Endocrinologists https://www.aace.com/

ENDO The Endocrine Society https://www.endocrine.org

Surgery-based

ACS American College of Surgeons https://www.facs.org

AAES American Association of Endocrine Surgeons https://www.endocrinesurgery.org

AHNS American Head and Neck Society http://www.ahns.info/

Radiology-based

AIUM American Institute of Ultrasound in Medicine http://www.aium.org/

Other Educational Resources

Ultrasound manufacturer websites

SonoSim Ultrasound Simulation Systems http://sonosim.com/

Blue Phantom Ultrasound Training Models https://www.bluephantom.com/

Collected Med/ECHO Ultrasound Interactive Interpretation https://collectedmed.com/

Ultrasound Institute Ultrasound Education http://ultrasoundinstitute.med.sc.edu/

Accessed via www on February 13, 2017

Although certification through an accredited course or program gives the clinician an initial foundation of knowledge, it is prudent that the physician frequently exercises their use of ultrasound in order to retain that knowledge and in some instances maintain certification. This level of involvement and ability to accomplish a comprehensive and relevant ultrasound are not always realistic for physicians of all specialties. The wealth of information provided by a detailed and targeted ultrasound is essential and cannot be omitted due to challenges in information access, communication lines, familiarity with guidelines, or ultrasound experience. In these instances, good relationships among a working group of colleagues are essential and take many forms, based on the medical care setting and even region of the country. For example, an experienced sonographer-endocrinologist can partner with a surgeon, while at other times an experienced sonographer-surgeon partners with referring physicians who do not perform ultrasound, or a thyroid-focused radiologist partners with all types of physicians (primary care, endocrinology, surgery) to provide clinically important feedback. Since for patients going to surgery the ultimate "final checkpoint" clinician is the surgeon, surgeons have the unique opportunity to ensure the relevant ultrasound information has been obtained prior to surgery. Useful questions for *all* physicians to consider:

Checklist Questions for Physicians of All *Specialties to Ask Regarding Thyroid and Parathyroid Ultrasound*

- Did my patient receive an appropriate ultrasound evaluation of all relevant areas in the head and neck?
- If my patient has a parathyroid diagnosis, how does their thyroid look on ultrasound?
- If my patient has nodular thyroid disease, was a screening cervical lymph node (central and lateral) ultrasound performed?

- If my patient has a new thyroid cancer diagnosis and has not had their initial surgery yet:
  - Did my patient get a central and lateral neck cervical lymph node ultrasound mapping?
  - Does the ultrasound report clearly comment that cervical lymph nodes were examined?
  - If the ultrasound report does *not* comment specifically about the appearance (normal or abnormal) of cervical lymph nodes (central and lateral), how can I ensure this is done prior to surgery?
- Would it be beneficial for me to see the ultrasound images? To review them in person with the physician who performed the ultrasound?
- What do I need to communicate about ultrasound with my referring physicians or collaborating physicians?

Conclusion

The field of thyroid and parathyroid surgery continues to evolve and becomes more reliant on imaging to guide individually tailored patient management. Although a number of modalities are key in diagnosing disease of the neck, US has proven to be equivalent or superior to CT, MRI, or sestamibi scan in imaging diseased thyroid and parathyroid glands. The versatility of information gained from US is essential to surgeons in planning for appropriate procedures. US has proven itself to be cost-effective, and readily used, able to guide treatment decisions, and achieve optimal outcomes for patients.

References

1. Rozycki G, Ochsner M, Jaffin J, Champion H. Prospective evaluation of surgeons' use of ultrasound in the evaluation of trauma patients. J Trauma. 1993;34(4):516–27.
2. Milas M, Stephen A, Berber E, Wagner K, Miskulin J, Siperstein A. Ultrasonography for the endocrine surgeon: a valuable clinical tool that enhances diagnostic and therapeutic outcomes. Surgery. 2005;138(6):1193–201.

3. Ollerton J, Sugrue M, Balogh Z, D'Amours S, Giles A, Wyllie P. Prospective study to evaluate the influence of fast on trauma patient management. J Trauma. 2006;60(4):785–91.
4. Yehuda M, Westfall E, Milas M, Gianoukakis A. Thyroid and parathyroid ultrasound: comprehensive and problem-focused point-of-care utilization in clinical practice. In: Advanced thyroid and parathyroid ultrasound. Langer: Springer; 2016.
5. Haugen B, Alexander E, Bible K, Doherty G, Mandel S, Nikiforov Y, et al. 2015 American Thyroid Association Management guidelines for adult patients with thyroid nodules and differentiated thyroid cancer: the American Thyroid Association guidelines task force on thyroid nodules and differentiated thyroid cancer. Thyroid. 2016;26(1):1–133.
6. Park S, Park S, Choi Y, Kim D, Son E, Lee H, et al. Interobserver variability and diagnostic performance in US assessment of thyroid nodule according to size. Ultraschall in der medizin. Eur J Ultrasound. 2012;33(7):E186–90.
7. Park C, Kim S, Jung S, Kang B, Kim J, Choi J, et al. Observer variability in the sonographic evaluation of thyroid nodules. J Clin Ultrasound. 2010;38(6):287–93.
8. Arciero C, Shiue Z, Gates J, Peoples G, Dackiw A, Tufano R, et al. Preoperative thyroid ultrasound is indicated in patients undergoing parathyroidectomy for primary hyperparathyroidism. J Cancer. 2012;3:1–6.
9. Mitchell J, Milas M, Barbosa G, Sutton J, Berber E, Siperstein A. Avoidable reoperations for thyroid and parathyroid surgery: effect of hospital volume. Surgery. 2008;144(6):899–907.
10. Minisola S, Cipriani C, Diacinti D, Tartaglia F, Scillitani A, Pepe J, et al. Imaging of the parathyroid glands in primary hyperparathyroidism. Eur J Endocrinol. 2015;174(1):D1–8.
11. Thompson G. Reoperative parathyroid surgery in the era of sestamibi scanning and intraoperative parathyroid hormone monitoring. Arch Surg. 1999;134(7):699.
12. Untch B, Adam M, Scheri R, Bennett K, Dixit D, Webb C, et al. Surgeon-performed ultrasound is superior to 99tc-sestamibi scanning to localize parathyroid adenomas in patients with primary hyperparathyroidism: results in 516 patients over 10 years. J Am Coll Surg. 2011;212(4):522–9.
13. Levy J, Kandil E, Yau L, Cuda J, Sheth S, Tufano R. Can ultrasound be used as the primary screening modality for the localization of parathyroid disease prior to surgery for primary hyperparathyroidism a review of 440 cases. ORL J Otorhinolaryngol Relat Spec. 2011;73(2):116–20.

14. Berber E, Parikh R, Ballem N, Garner C, Milas M, Siperstein A. Factors contributing to negative parathyroid localization: an analysis of 1000 patients. Surgery. 2008;144(1):74–9.
15. Mizrachi A, Feinmesser R, Bachar G, Hilly O, Cohen M. Value of ultrasound in detecting central compartment lymph node metastases in differentiated thyroid carcinoma. Eur Arch Otorhinolaryngol. 2013;271(5):1215–8.
16. Lin Y, Jen Y, Lin J. Radiation-related cranial nerve palsy in patients with nasopharyngeal carcinoma. Cancer. 2002;95(2):404–9.
17. Carneiro-Pla D, Solorzano C, Wilhelm S. Impact of vocal cord ultrasonography on endocrine surgery practices. Surgery. 2016;159(1):58–64.
18. Woo J, Suh H, Song R, Lee J, Yu H, Kim S, et al. A novel lateral-approach laryngeal ultrasonography for vocal cord evaluation. Surgery. 2016;159(1):52–7.
19. Brunaud L, Germain A, Zarnegar R, Klein M, Ayav A, Bresler L. Robotic thyroid surgery using a gasless transaxillary approach: cosmetic improvement or improved quality of surgical dissection? J Visc Surg. 2010;147(6):e399–402.
20. Terris D, Singer M, Seybt M. Robotic facelift thyroidectomy: II. Clinical feasibility and safety. Laryngoscope. 2011;121(8):1636–41.
21. Kang S, Jeong J, Yun J, Sung T, Lee S, Lee Y, et al. Robot-assisted endoscopic surgery for thyroid cancer: experience with the first 100 patients. Surg Endosc. 2009;23(11):2399–406.
22. Byeon H, Holsinger F, Tufano R, Chung H, Kim W, Koh Y, et al. Robotic total thyroidectomy with modified radical neck dissection via unilateral retroauricular approach. Ann Surg Oncol. 2014;21(12):3872–5.
23. Agarwal S, Sabaretnam M, Ritesh A, Chand G. Feasibility and safety of a new robotic thyroidectomy through a gasless, transaxillary single-incision approach. J Am Coll Surg. 2011;212(6):1097.
24. Terris D, Singer M, Seybt M. Robotic facelift thyroidectomy. Surg Laparosc Endosc Percutan Tech. 2011;21(4):237–42.
25. Kang S, Lee S, Lee S, Lee K, Jeong J, Lee Y, et al. Robotic thyroid surgery using a gasless, transaxillary approach and the da Vinci S system: the operative outcomes of 338 consecutive patients. Surgery. 2009;146(6):1048–55.
26. Kang S, Jeong J, Nam K, Chang H, Chung W, Park C. Robot-assisted endoscopic thyroidectomy for thyroid malignancies using a gasless transaxillary approach. J Am Coll Surg. 2009;209(2):e1–7.

Chapter 11
Ultrasound of Salivary Glands and the Non-endocrine Neck

Vinay T. Fernandes and Lisa A. Orloff

Introduction

The thyroid gland is situated in the lower midline neck, but conditions affecting the thyroid itself may also involve adjacent and distant cervical structures and regions. In order to understand the regional anatomy and related pathology, it is instructive to subdivide the neck into sections. In the demonstration and reporting of metastatic lymphadenopathy, the neck is classically separated into six levels (Fig. 11.1). Level I

The authors wish to acknowledge Robert A. Sofferman, who wrote the previous version of this chapter for the third edition and whose images are included here.

V.T. Fernandes, MD, FRCSC
Otolaryngology – Head and Neck Surgery, University of Toronto, Toronto, ON, Canada

L.A. Orloff, MD, FACE, FACS (✉)
Otolaryngology, Stanford University Medical Center, Stanford, CA, USA
e-mail: lorloff@stanford.edu

D.S. Duick et al. (eds.), *Thyroid and Parathyroid Ultrasound and Ultrasound-Guided FNA*,
https://doi.org/10.1007/978-3-319-67238-0_11

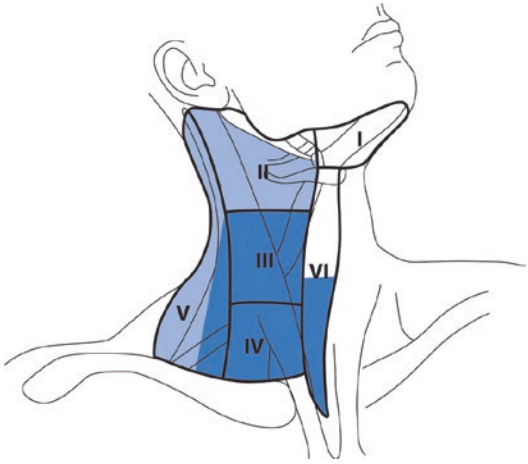

FIGURE 11.1 The six neck levels are demonstrated. The *darker areas* are the likely sites for metastatic papillary and medullary carcinoma

is triangular in shape bounded by the anterior and posterior bellies of the digastric muscle and superiorly by the inferior border of the mandible. Levels II–IV are situated along the internal jugular vein (IJV) with each third designated as a separate level. Level II begins at the skull base and ends inferiorly at the level of the hyoid bone. Level III encompasses the middle third of the IJV between the hyoid bone and cricoid cartilage medially and omohyoid muscle laterally. Level IV is the lower third of the IJV between the cricoid cartilage and clavicle. Level V is triangular in shape, bordered by the posterior aspect of the sternocleidomastoid muscle, anterior aspect of the trapezius muscle, and the clavicle and is often referred to as the posterior cervical triangle. Level VI is a midline rectangular region from the hyoid superiorly to innominate artery inferiorly and lateral extent from right to left carotid artery. There are approximately 200–300 lymph nodes in the neck and facial region [1], and these are distributed among each level. When the relationship between lymph nodes and the structures they drain is understood, the

primary malignancy or source of inflammatory lymphadenopathy can be suspected even before imaging. Lymphadenopathy in level I relates to primary lesions in the oral cavity, sublingual and submandibular salivary glands, and facial skin. Level II lymph nodes serve the oropharynx (i.e., soft palate, tonsils, tongue base), nasopharynx, hypopharynx, and parotid. Level III is the regional distribution from the larynx and adjacent mucosal structures, the hypopharynx, and the thyroid gland. Level IV drains lymphatics from the hypopharynx and esophagus as well as the thyroid gland. Levels IV and V may be indicators from malignancy of the lower esophagus, upper GI tract, pancreas, and lung (Pancoast tumors), especially on the left. The thyroid gland mostly involves lymph nodes in levels II–VI. Lastly, inflammatory and malignant lesions of the skin such as melanoma may produce lymph node enlargement in any level adjacent to the respective primary skin site.

Level I

This level has a close relationship to the oral cavity. As such, lymphatic and vascular conditions of the floor of mouth and submandibular gland demonstrate mass lesions in this area. Although it is rare for thyroid carcinoma to metastasize to level I, in the survey of the neck with ultrasound, this region should still be examined. Lymph nodes are commonly enlarged in level I and into the neighboring level II, especially the jugulodigastric node which is just cranial and superficial to the carotid bulb (Fig. 11.2). It may be considered in the posterior aspect of zone I or in the cranial portion of level II. Its name derives from the fact that it is located at the place where the posterior belly of the digastric muscle passes over the IJV. While present in most individuals, this commonly hypertrophied lymph node is particularly notable in adolescents and young adults who have experienced recent episodes of tonsillopharyngitis.

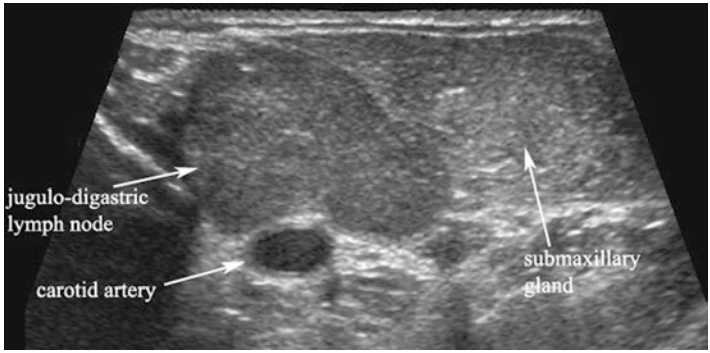

FIGURE 11.2 This gray scale transverse ultrasound in levels I–IIa demonstrates a hypertrophied jugulodigastric lymph node superficial to the carotid artery

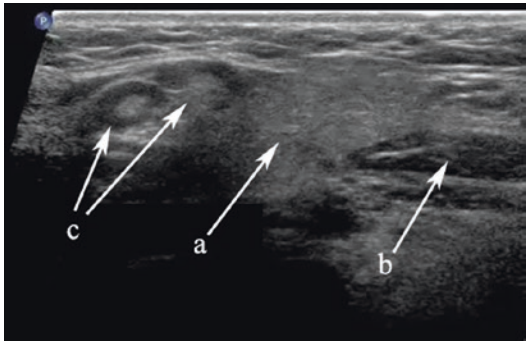

FIGURE 11.3 The submandibular gland (**a**), anterior belly of digastric (**b**), and level I lymph nodes (**c**) are demonstrated in this transverse gray scale ultrasound

Submandibular Gland

The submandibular gland has a homogeneous ground-glass appearance on ultrasound. It is a discrete structure with a deep lobe that extends deep to the mylohyoid muscle (further away from the skin). It is the most recognizable structure in level I and often demonstrates adjacent benign hypertrophic lymph nodes (Fig. 11.3). The duct structure is not generally identified unless there is an obstructing calculus (stone).

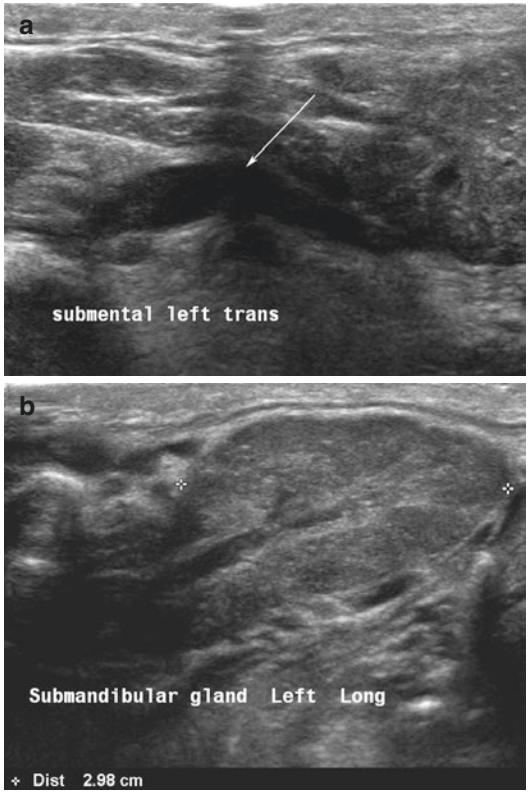

FIGURE 11.4 (**a**, **b**) A distal calculus of the submandibular duct into the floor of mouth produces dilation of the entire ductal architecture as designated by the *arrow* (**a**). This ductal dilation or ectasia can be identified even within the gland parenchyma (**b**)

An obstructing calculus of the main (Wharton's) duct produces dilation and an appearance which could suggest a vascular structure (Fig. 11.4). Doppler is a useful tool to determine that the tubular structure is not vascular. One or more stones can be identified as hyperechoic lines or points with posterior acoustic shadowing as well as the presence of posterior shadowing artifact along the duct structure.

Common salivary gland diseases can be classified into tumors, inflammatory conditions, and sialosis. A mass within

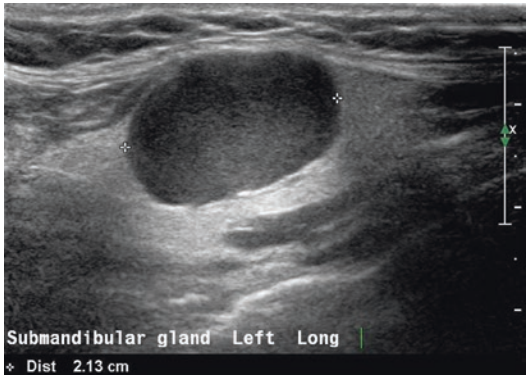

Figure 11.5 A benign mixed tumor (also known as pleomorphic adenoma) of the submandibular gland is demonstrated with gray scale ultrasound. Note posterior acoustic enhancement

the submandibular gland may be benign or malignant. The sonographic features which favor a benign lesion are a discrete homogeneous mass and a surrounding capsule which clearly separates the lesion from surrounding submandibular parenchyma. The most common benign lesion is a pleomorphic adenoma [2] which demonstrates posterior enhancement; it is one of the few tumors which demonstrate this characteristic so often seen in cysts (Fig. 11.5).

The appearance of inflammation of the gland depends on the etiology. Bacterial inflammation can produce decreased parenchymal echogenicity and increased edema, often with dilated ducts. As the inflammation becomes chronic, the gland echogenicity becomes more heterogeneous. Viral infections which are more interstitial are more characterized by heterogeneous and increased echogenicity as well as edematous enlargement. Küttner's tumor, which has been reclassified as IgG4-RSD, is an excellent example of a chronic sclerosing inflammation of the submandibular gland that often presents bilaterally. Sonographic findings include decreased echogenicity of the parenchyma with heterogeneous, cirrhosis-like hyperechoic bands of fibrosis.

Sialosis is noninflammatory, nonneoplastic often bilateral enlargement of the salivary glands with compressed parenchyma. Later stages of sialosis can mimic chronic inflammation [3]. This condition is frequently seen in patients with bulimia. Fatty "jowls," or masseter muscle hypertrophy can both resemble parotid gland enlargement, but both of these conditions can easily be distinguished from parotid gland pathology by US. Shrinkage or atrophy and fibrosis of the salivary glands are commonly seen following radiation therapy for head and neck neoplasms. The sonographic appearance is one of small, heterogeneous, hypovascular, and somewhat indistinct glands. Radioactive ^{131}iodine ablation for thyroid cancer is also associated with salivary gland inflammation and injury. In the acute phase, there is often gland enlargement associated with pain; in the chronic phase, there may be ductal obstruction and the appearance of chronic sialadenitis or gland shrinkage and atrophy.

Ranula

A ranula is a cystic enlargement of a portion of the sublingual gland [4]. It may remain situated in the floor of the mouth or can extend posteriorly and deep to the mylohyoid muscle into the neck, and as such is then designated a "plunging ranula (Fig. 11.6)." It is due to an outflow obstruction of one of the sublingual gland ducts. On aspiration, the fluid is relatively clear and has the consistency of saliva. It usually produces a cystic swelling of the floor of mouth and may elevate the mobile tongue.

Lymphangioma

In contrast to the ranula, a lymphangioma [5] can also produce a cystic mass lesion in level I or floor of mouth, but there are septations and no actual communication with the salivary ducts so it does not contain saliva. Power Doppler is essential to differentiate the lymphangioma from its mate, a hemangi-

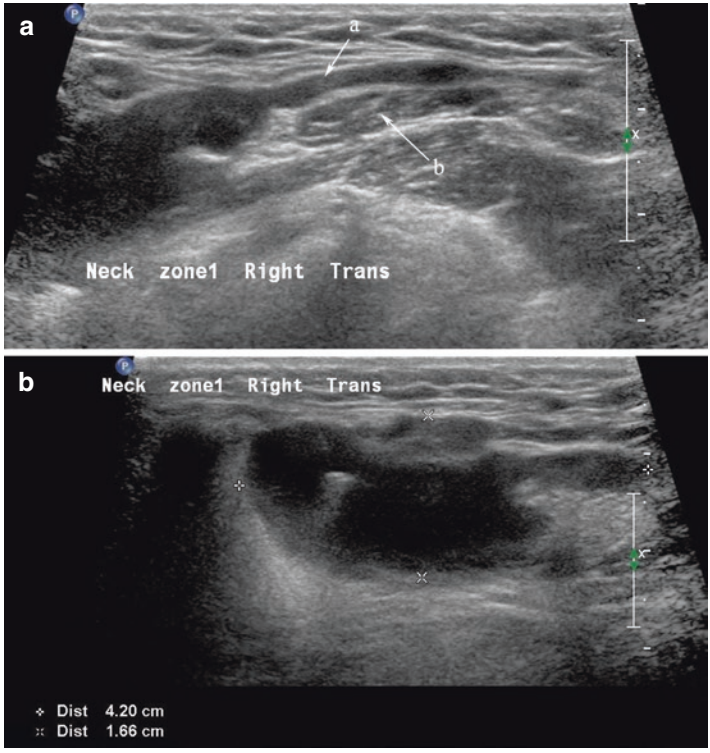

FIGURE 11.6 (**a**, **b**) The hypoechoic homogeneous lesion extending from the sublingual region posteriorly (*a*) deep to the mylohyoid muscle (*b*) ends adjacent to the submandibular gland as a dilated cystic structure. The cystic extension adjacent to the submandibular gland in the neck is demonstrated in image (**b**) where it is designated a "plunging ranula"

oma (Fig. 11.7), and these congenital lesions are collectively known as lymphovascular malformations. A lymphangioma demonstrates its vasculature within the septae rather than within the lesion's parenchyma. Hemangiomas [6] are also found in the parotid gland, and it is the most common parotid mass lesion in children (Fig. 11.8).

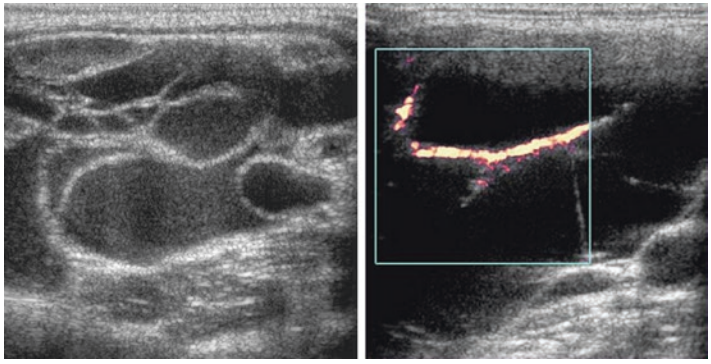

FIGURE 11.7 Septations within this lesion are indicative of a lymphovascular malformation. Power Doppler demonstrates that the contributory vessels are only within the septae, indicating that the lesion is relatively avascular and consistent with a lymphangioma

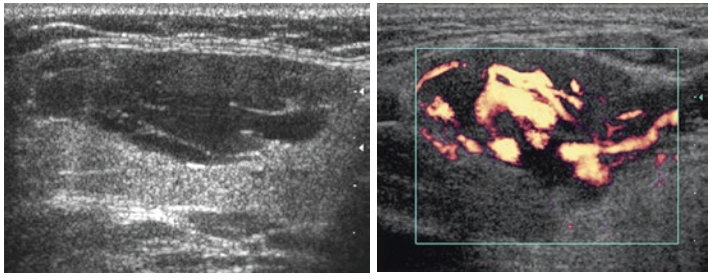

FIGURE 11.8 Septations within this lesion suggest a vascular lesion, but the differential between a lymphangioma and hemangioma cannot be made without Doppler. Power Doppler on the *right* proves that this lesion is highly vascular and therefore more consistent with a hemangioma

Level II

Level II is the most common location for a number of lesions which often cannot be differentiated from one another on physical examination alone. As mentioned previously, the

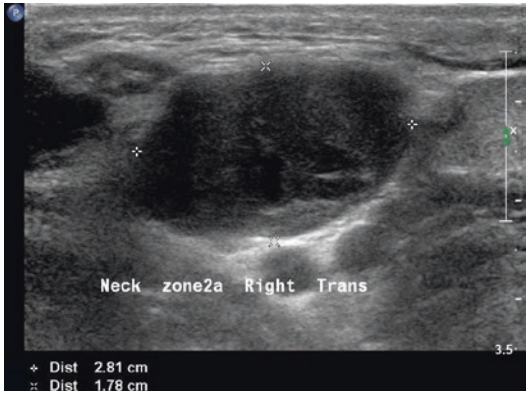

FIGURE 11.9 The differential diagnosis of a purely cystic lesion within level II includes a second branchial cleft cyst. This hypoechoic mass proved to be cystic on FNA, but cytology demonstrated metastatic squamous cell carcinoma

jugulodigastric lymph node is commonly palpated and demonstrated with ultrasound. Usually, sonography demonstrates an appropriate hilum with corresponding hilar vascularity on Doppler both of which suggest likely nodal hypertrophy. A cystic lesion in level II, especially in children and young adults, suggests a possible second branchial cleft cyst [7, 8] in the differential. Fine-needle aspiration cytology is useful to make differential determinations. However, any cystic node in the head and neck must be suspect for metastatic lymphadenopathy (Fig. 11.9). The most common primary origin of a cystic carcinomatous node in level II might be tonsil or tongue base squamous cell carcinoma. Alternatively, thyroid papillary carcinoma can also present as a cystic mass in the neck and even as a solitary mass in level II (Figs. 11.10 and 11.11). The key is to both examine the entire thyroid gland with ultrasound and add thyroglobulin washout to the needle assay of the cystic fluid.

A solid mass in level II may displace the carotid artery into an anterior location. In this circumstance, a lesion of neurogenic origin should be suspected [9, 10]. The cervical plexus or sympathetic chain may be the source of this type of lesion

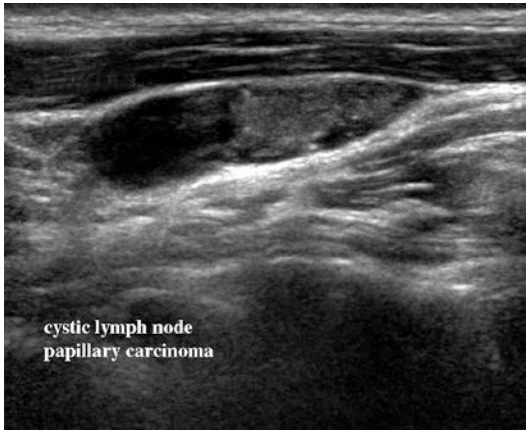

FIGURE 11.10 Sagittal view of a lymph node in level II demonstrates cystic changes in its superior region and microcalcifications. This node was proven to be replaced by metastatic papillary carcinoma

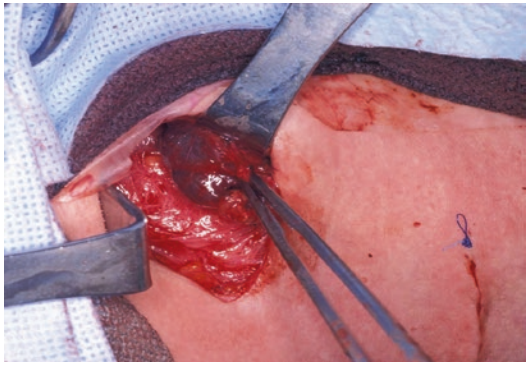

FIGURE 11.11 The surgical field during total thyroidectomy and lateral neck dissection in the same patient as Fig. 11.10. The cystic lymph node with metastatic papillary carcinoma is seen here being delivered from level II

(Fig. 11.12). If a Horner's syndrome is identified, the lesion is most likely to have originated from the sympathetic autonomic system (Figs. 11.13 and 11.14). If the patient has hoarseness and a vocal cord paralysis, the lesion may have originated

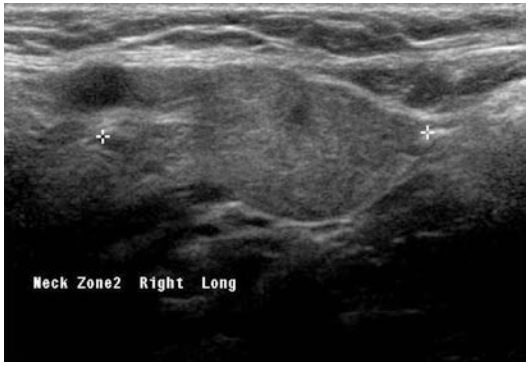

Figure 11.12 A level II cervical rootlet schwannoma is demonstrated. Note the taper of the mass inferiorly which is typical of a neurogenic lesion

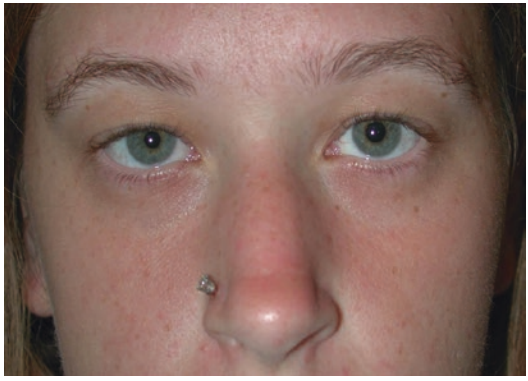

Figure 11.13 A patient with a sympathetic chain neurofibroma presents with a Horner's syndrome

from the vagus nerve. In circumstances where a mass resides at the carotid bulb and separates the internal and external carotid arteries, a carotid body tumor or paraganglioma would be realistic considerations [11] (Fig. 11.15). In this circumstance, Doppler demonstrates both the intense vascularity of the mass which is not noted in a schwannoma [12] (Fig. 11.16). The vascular supply to the mass is actually from

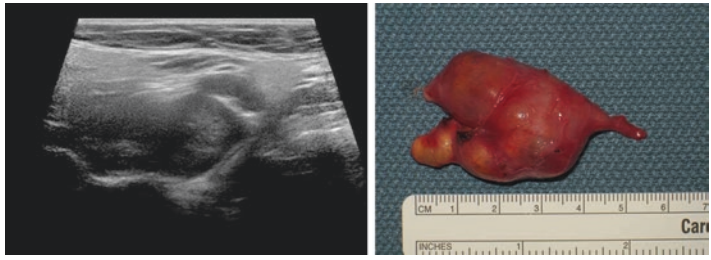

FIGURE 11.14 This composite image of a cervical plexus schwannoma demonstrates that the actual gross image of the surgical specimen is identically reflected in the preoperative sagittal ultrasound

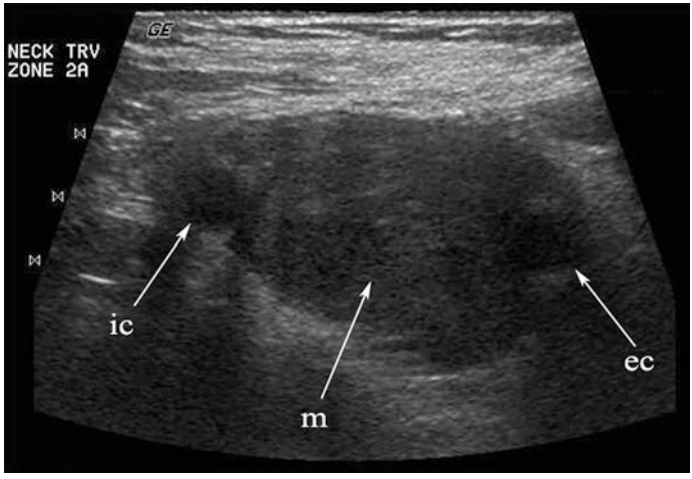

FIGURE 11.15 Any hypoechoic mass in level II may be construed as a lymph node or schwannoma. When the mass (*m*) separates the internal (*ic*) and external (*ec*) carotid arteries, a chemodectoma or carotid body tumor (paraganglioma) must be suspected

the ascending pharyngeal artery branch off the external carotid, which can be seen in the lateral Doppler image in this sagittal image (Fig. 11.17). Although none of these lesions are malignant, it is important to understand how to separate them from the more life-threatening clinical conditions.

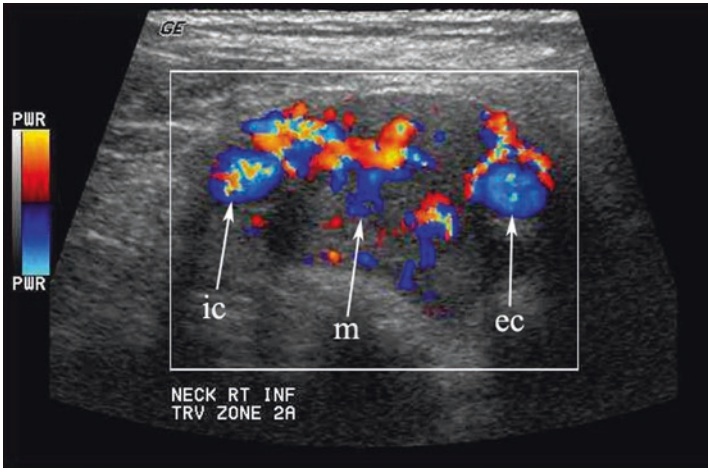

Figure 11.16 This carotid body tumor located in level II at the carotid bifurcation is clearly defined with color Doppler. The internal (*ic*) and external (*ec*) carotid arteries are splayed apart by the vascular mass (*m*)

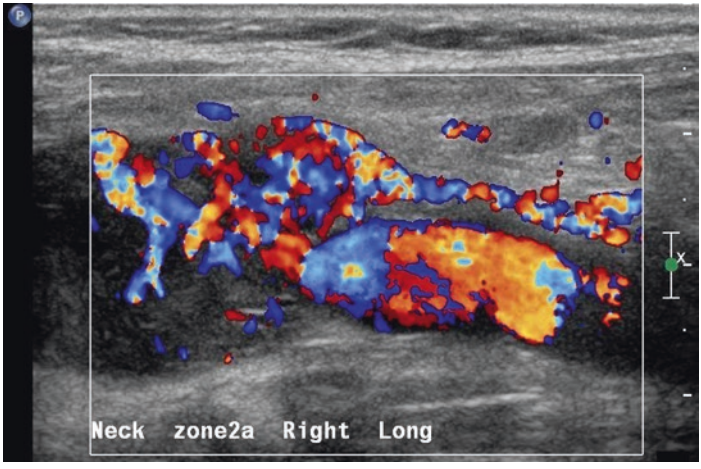

Figure 11.17 Sagittal color Doppler image of a carotid body tumor demonstrates its vascular supply from a vessel separate from the common carotid artery. This ascending pharyngeal artery is a branch of the external carotid system

Level III

This region along with level IV is most often associated with conditions relative to the thyroid gland. Although exceedingly rare, lateral aberrant thyroid tissue [13] may be misinterpreted as the more common metastatic lymphadenopathy (Fig. 11.18). These lesions are separate from the main thyroid gland and are homogeneous and more rounded in structure than a lymph node. However, in the context of a mass lesion adjacent to the thyroid gland which is suspect for metastasis, a thyroglobulin washout would be recommended in addition to cytology. If the cytology is benign, no mass lesion of the thyroid gland is identified, and the thyroglobulin is positive; one still must suspect this as a metastatic node from an occult papillary thyroid carcinoma. A formal excision of the mass will be required and in this rare circumstance would confirm this lesion as benign thyroid tissue.

Patients with recurrent suppurative thyroiditis, especially left sided, may actually have a congenital fourth branchial cleft cyst or fistula which extends from the apex of the

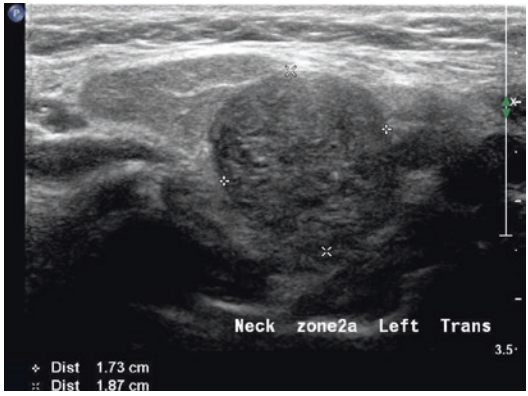

Figure 11.18 A rounded mass in level IIa is demonstrated in transverse gray scale ultrasound. This proved to be one of two lateral thyroid rests which are rare embryonic thyroid remnants completely separate from the thyroid gland. This mass is adjacent to the normal submandibular gland

piriform sinus ending in the thyroid parenchyma [14, 15] (Fig. 11.19). Episodes may actually begin in children as young as 3 months and present as recurrent retropharyngeal abscess. Neck ultrasound may reveal an inflammatory process overlying the thyroid cartilage in addition to the changes in the adjacent thyroid gland (Fig. 11.20). In some cases, an actual fistulous tract can be identified.

The esophagus is an easily recognizable structure deep to the left lobe of the thyroid gland and adjacent to the trachea. Both the muscular and mucosal layers can be identified in the normal state. A Zenker's diverticulum is a mucosal hernia between the cricopharyngeus and inferior constrictor muscles allowing a pouch to form which traps food and fluid [16–18]. It may be mistaken for a mass lesion. The sonographic features are loss of the usual concentric layers, some enlargement of the apparent esophageal structure, and internal, refractile debris (Figs. 11.21 and 11.22). Either on cine loop or sequential post-swallow static images, the debris often evacuates to some degree. Of course, the ultrasound is simply a means to suspect this lesion, and esophagram is the definitive required imaging study.

Finally, patients with primary hyperparathyroidism can have the source localized with ultrasound. Usually enlarged

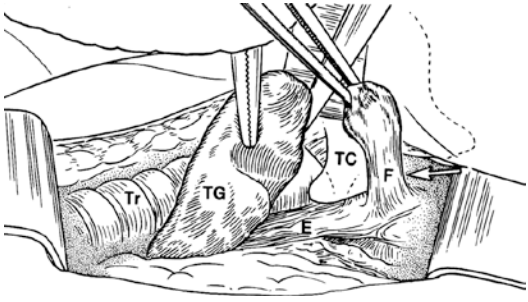

Figure 11.19 This artistic rendering demonstrates a fistula (*F*) arising from the esophagus (*E*) and positioned just lateral to the thyroid cartilage (TC). The fistula is invariably left sided and extends to the thyroid gland, frequently into its parenchyma

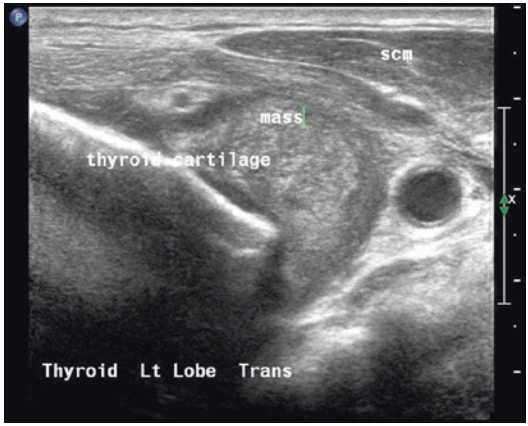

FIGURE 11.20 An inflammatory mass lateral to the thyroid cartilage extending into the thyroid gland is due to a fistula extending from the piriform sinus or esophagus (fourth branchial pouch sinus). Note the small circular structure superficial and to the left of the inflammatory mass; this is the actual fistula

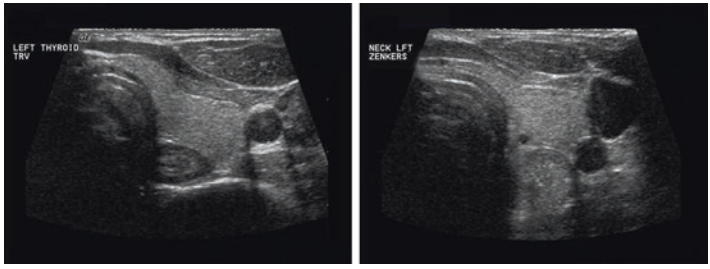

FIGURE 11.21 The *left* demonstrates the normal esophagus and the *right* an expanded esophagus consistent with a Zenker's diverticulum

single hypoechoic lesions suggestive of an adenoma or multiple lesions indicating diffuse hyperplasia in the central neck (level VI) are self-explanatory. When this is noted in the context of hypercalcemia, there is very little confusion about what the images represent. However, a level III nodule in a patient with primary hyperparathyroidism may represent an

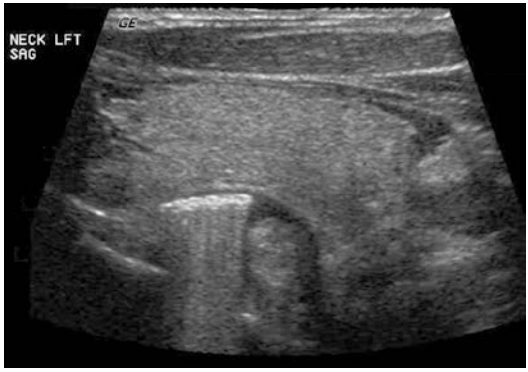

FIGURE 11.22 The sagittal view of this Zenker's diverticulum reveals food debris which demonstrate refractile sound waves. Note the posterior position of the diverticulum relative to the left lobe of the thyroid gland

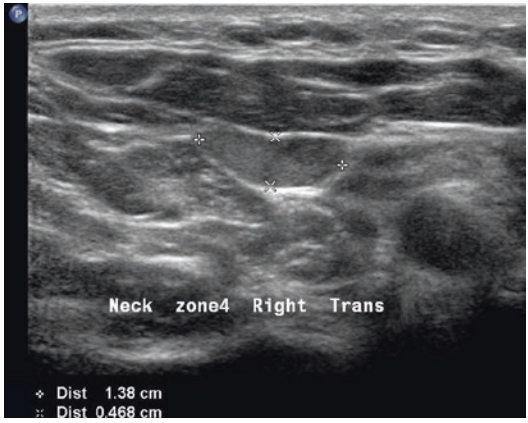

FIGURE 11.23 A parathyroid adenoma may occasionally be ectopic within the lateral neck, in this instance level III

ectopic parathyroid adenoma (Figs. 11.23 and 11.24). The differential diagnosis always includes lymphadenopathy. The vascularity of a parathyroid adenoma [19] differs from that of a lymph node (Figs. 11.25 and 11.26), and the absence of

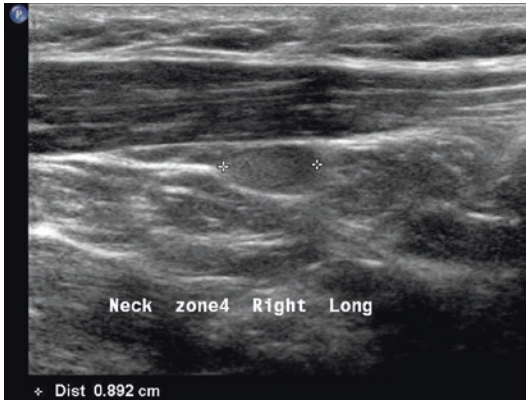

FIGURE 11.24 This sagittal view of the ectopic parathyroid adenoma noted in Fig. 11.23 demonstrates its ovoid shape

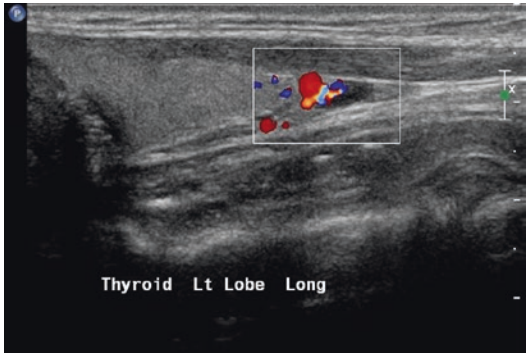

FIGURE 11.25 The blood supply to a parathyroid adenoma ends bluntly in the parenchyma without arborization. This small adenoma has the characteristic vascular supply

lymphocytes on aspiration cytology suggests that the lesion is unusual. Parathyroid cytology is notoriously difficult, but an aspirate for PTH will identify the lesion as ectopic parathyroid. Certainly a serum calcium and intact PTH would give an accurate biochemical diagnosis.

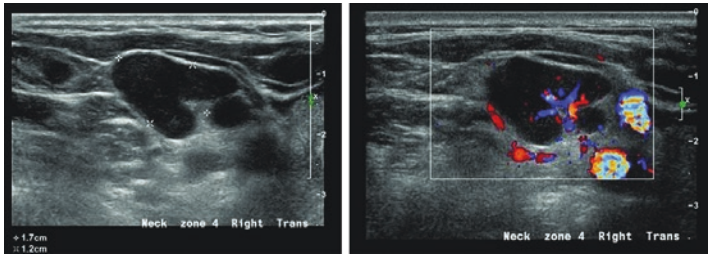

FIGURE 11.26 The arborized pattern of vascularity of a hyperplastic level IV lymph node is demonstrated with color Doppler. Note the axial vasculature entering at the nodal hilum which is nicely shown in gray scale on the *left*

Level IV

Any mass or cystic structure in level IV is suspect for metastatic thyroid carcinoma. The thoracic duct usually enters the venous system on the left side at the posterior junction of the internal jugular and innominate veins. Due to this special anatomical relationship, metastatic malignancy can be identified in this location, especially arising from adenocarcinomas whose origin is from structures below the clavicle. More specifically, the gastrointestinal tract from esophagus to colon may send malignant cells through the thoracic duct to the neck. In addition, other abdominal and pelvic primary tumors such as pancreatic and testicular cancer can produce the same metastatic result. Metastatic squamous cell carcinoma in addition to thyroid cancer should be suspected, especially in adults, when a partially or completely cystic mass is identified in the upper, mid-, or lower jugular chain [20] (Figs. 11.9 and 11.27).

A pure cyst in level IV without any solid component and abutment with the inferior aspect of the thyroid gland may be of parathyroid origin [21]. Pure parathyroid cysts are not associated with hyperparathyroidism (Figs. 11.28 and 11.29). The aspirate is crystal clear as water, and PTH analysis reveals very high levels in the thousands. In fact, the clear

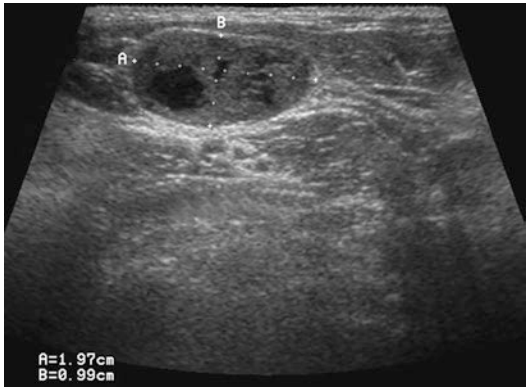

FIGURE 11.27 Anechoic areas within this cervical lymph node are suggestive of necrosis. The FNA cytology confirmed the presence of metastatic squamous cell carcinoma

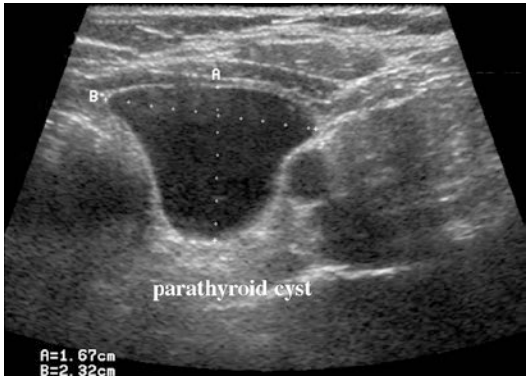

FIGURE 11.28 Transverse view of a parathyroid cyst. Note the anechoic internal signal, posterior enhancement, and thin discrete envelope

appearance of the fluid and the PTH level is what separates this cyst from a thymic cyst. The histopathology of both cysts may appear to be identical since Hassall's corpuscles can be seen in both.

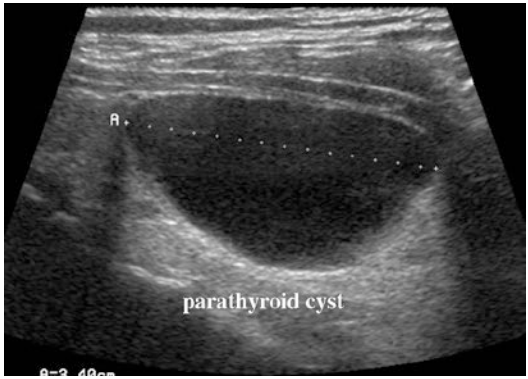

FIGURE 11.29 Sagittal view of the same parathyroid cyst

Level V

Lymphadenopathy

Lymphomas often present as single or multiple enlarged lymph nodes in level V. Although lymphoma may occur in any of the cervical node basins, they are most often noted in level V as enlarged single or multiple rounded, hypoechoic masses [22, 23] (Figs. 11.30 and 11.31). The echoarchitecture is suggestive with an even, homogeneous appearance and loss of the usual hilum. There are no areas of necrosis and the power Doppler pattern may be helpful with peripheral or transnodal vascularity (Fig. 11.32). Multiple and matted adenopathy is a pattern which also frequently defines lymphoma (Fig. 11.33). Although suggestive, these sonographic features are not absolutely diagnostic and demand additional evaluation. When lymphoma is suspected, specimens for cytology should include samples submitted in RPMI solution for flow cytometry.

Inferiorly located nodes in level V with metastatic squamous cell carcinoma are likely to have arisen from a primary of the lung. In addition to an exhaustive search of the head and neck to identify a primary source, a chest CT scan is especially valuable when nodes are noted in this area.

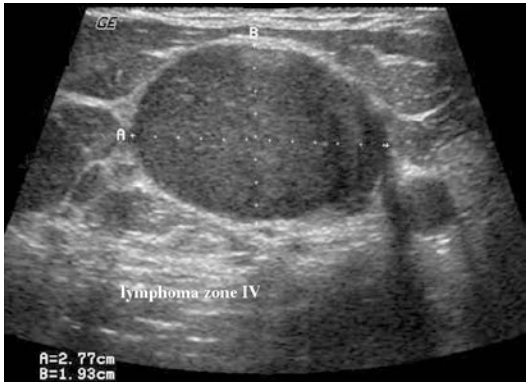

FIGURE 11.30 This large lymph node in level IV fails to demonstrate normal hilar architecture. It is a diffuse non-Hodgkin's lymphoma

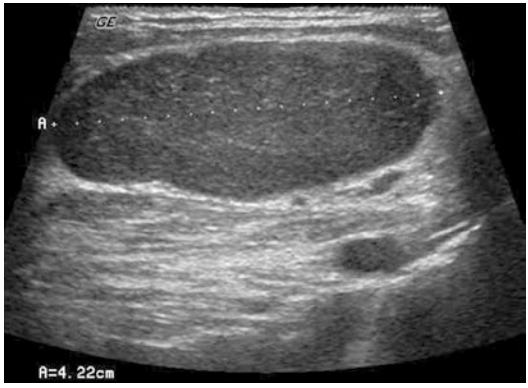

FIGURE 11.31 The sagittal view of this same lymphomatous node demonstrates its large size and suspicious homogeneous echoarchitecture

Neurofibroma

Neurofibromas may be single or multiple lesions. In patients with von Recklinghausen's disease, the diagnosis is relatively straightforward. With ultrasound the mass is noted to be ovoid, homogeneous, and may have a tapered end as noted

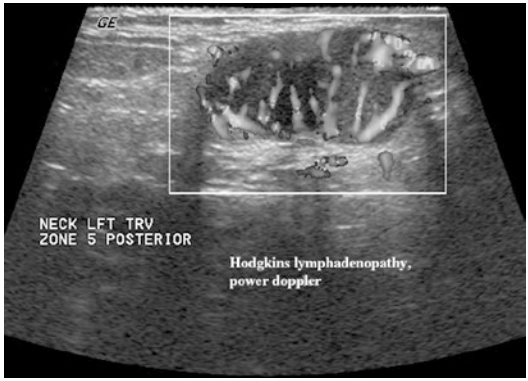

FIGURE 11.32 This gray scale Doppler image of a level V lymph node replaced with Hodgkin's disease demonstrates pathologic transnodal vascularity. This vascular pattern is highly suggestive of malignancy

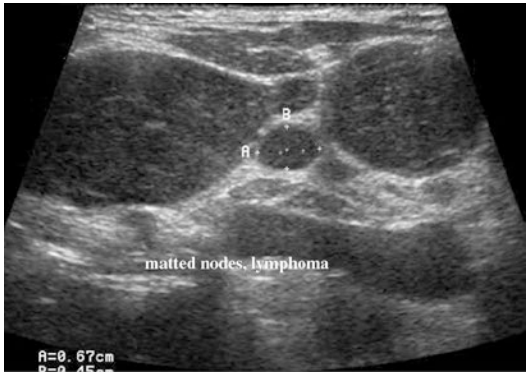

FIGURE 11.33 Multiple matted lymph nodes from Hodgkin's disease are demonstrated in this transverse view

with a schwannoma. There is no internal vascularity or hilar architecture. Cytology may be nondiagnostic. One may suspect that this lesion is of neurogenic origin when a painful dysesthesia occurs at the time of needle sampling. Often the clinician assumes that this is an accidental penetration of an adjacent nerve, but if the same painful scenario occurs with a

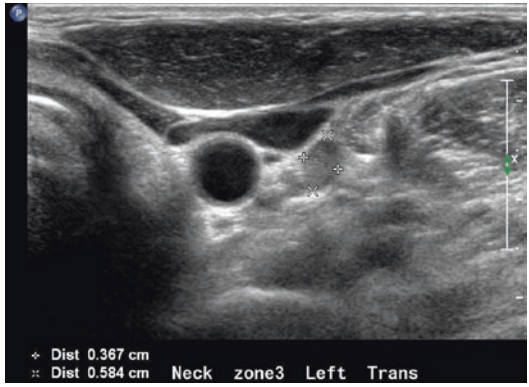

FIGURE 11.34 This patient with prior neck dissection for papillary carcinoma demonstrates a nodule in level III on transverse ultrasound. This lesion was initially suspicious for recurrence

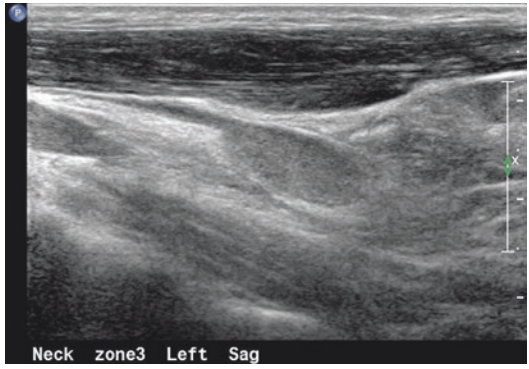

FIGURE 11.35 The sagittal view of the same nodule noted in Fig. 11.34 demonstrates a fusiform configuration suggesting its association with a nerve. This is the typical appearance of a postoperative neuroma and not recurrent carcinoma

subsequent pass, attempts at FNAC should be abandoned in favor of other imaging methods. A traumatic neuroma may resemble a mass lesion (Fig. 11.34). When a linear neural structure enters the mass and FNA is painful, there is little doubt of the diagnosis (Fig. 11.35).

Level VI

Thyroglossal Duct Cyst

These cysts can occur anywhere from the central suprahyoid region to the thyroid isthmus. Although they share the same sonographic characteristics as cysts elsewhere, there are some special anatomical peculiarities [24, 25]. To begin, the cyst may be multidimensional with an extension posterior to the hyoid bone best seen on the sagittal view (Figs. 11.36 and 11.37). Debris are often visible within the cyst which manifest as floating echogenic lesions throughout the fluid (Fig. 11.38). In the circumstance where a solid component is noted in the cyst, the possibility of a papillary carcinoma must be entertained and appropriate mural samples obtained [26].

Delphian Lymph Node

A midline lymph node in the same distribution as a thyroglossal duct cyst or inferior, even to the cricothyroid membrane, is commonly seen with thyroid carcinoma as well as with Hashimoto's thyroiditis. Nodularity within a pyramidal lobe of the thyroid may appear similar to a Delphian lymph node.

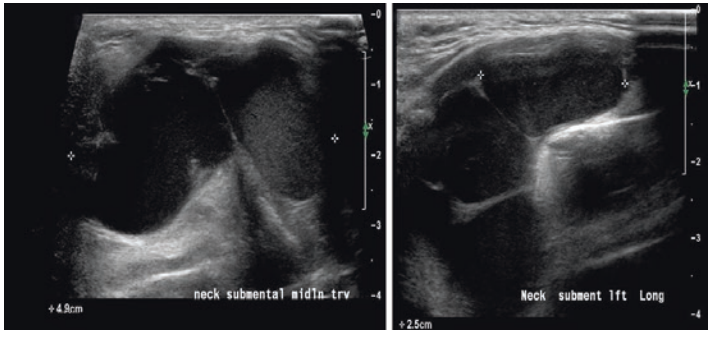

Figure 11.36 This is a composite transverse and sagittal image of a large thyroglossal duct cyst. Note in the *right* that the superior aspect of the cyst extends deep to the hyoid bone

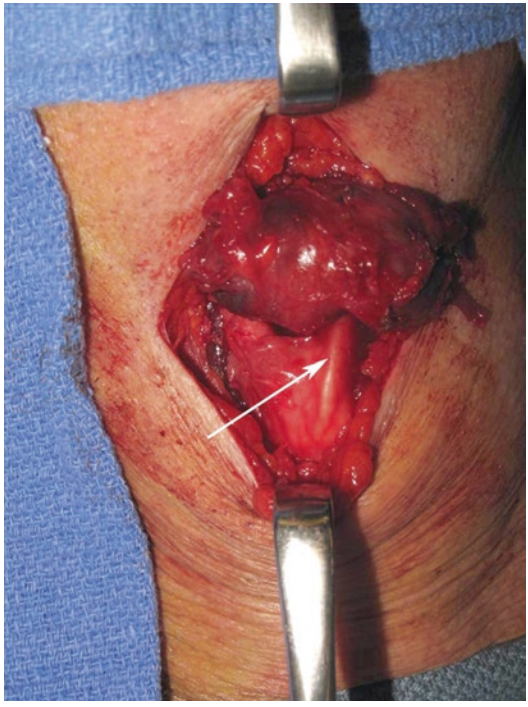

FIGURE 11.37 This is an intraoperative view of the large thyroglossal duct cyst demonstrated in Fig. 11.36. The *arrow* designates the anterior keel of the thyroid cartilage framework

Lingual Thyroid

The key to suspicion of lingual thyroid requires a comprehensive examination of the neck. Lingual thyroid represents an undescended thyroid gland from its origin at the foramen cecum of the midline tongue base. It is an amber submucosal mass and is usually identified through mirror examination of the hypopharynx on routine inspection. However, it may be identified in reverse, i.e., at the time of ultrasound inspection of the neck. If the thyroid gland appears atrophic or absent from its usual orthotopic location (Fig. 11.39), then a routine endoscopic exam and/or nuclear thyroid scan will provide the

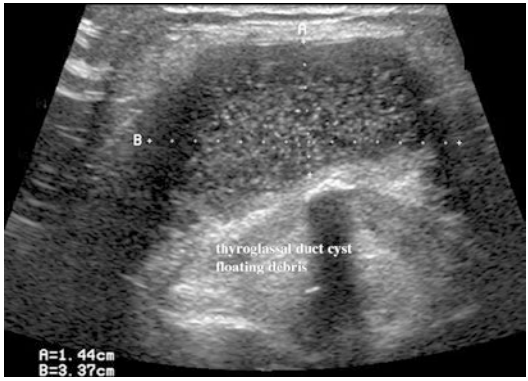

Figure 11.38 This transverse view of a thyroglossal duct cyst demonstrates the central hyoid bone, a discrete hyperechoic structure with posterior shadowing artifact. Note the multiple hyperechoic reflectors within the cyst which represents debris

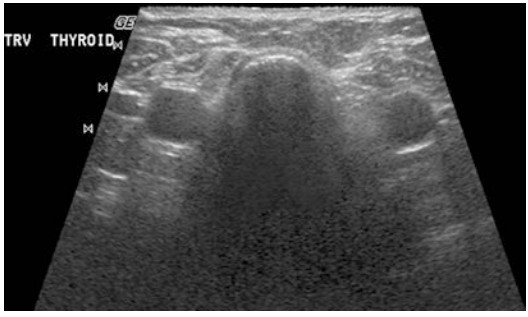

Figure 11.39 This patient with a tongue base mass demonstrates the absence of the normal cervical thyroid gland. Undescended lingual thyroid was diagnosed on initial clinic visit as a result of this ultrasound and demonstration of a typical submucosal tongue base lesion

information necessary to establish the diagnosis (Fig. 11.40). Lingual thyroid is not a condition which generally requires any clinical management and is usually simply an embryologic curiosity.

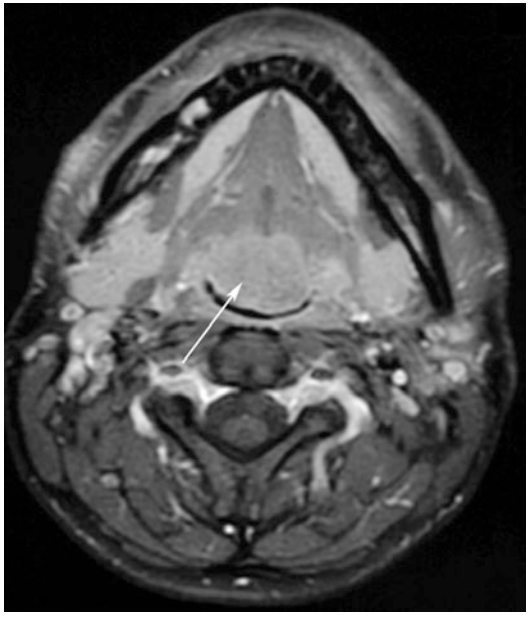

FIGURE 11.40 Transverse MRI shows a tongue base mass denoted by the *arrow*. This is lingual thyroid which has not descended into its normal orthotopic location in the lower neck

Thymus

The thymus gland is usually recognizable in children but generally recedes into adulthood. Its sonographic characteristics are bilateral hypoechoic areas inferior to the lower poles of the thyroid gland with multiple punctate hyperlucencies [27, 28] (Fig. 11.41). These may be misinterpreted as microcalcifications but are actually Hassall's corpuscles usually found in thymus tissue. The area inferior to the thyroid gland is usually void of this type of lesion, and when it is seen by the unwary clinician performing the ultrasound, the aforementioned characteristics may vaguely simulate papillary carcinoma. The features which suggest benign thymus are its bilateral presence and the lack of a confined nodular appearance.

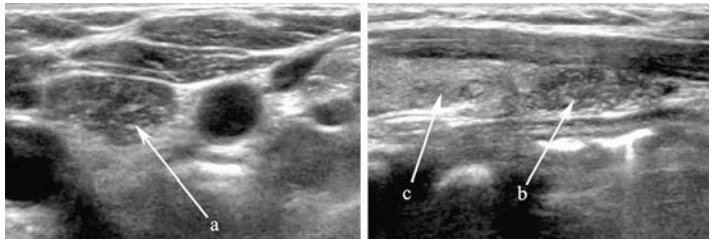

FIGURE 11.41 Composite ultrasound image of thymus tissue (*a*, *b*). The *left* is a transverse image of the left upper mediastinum and the *right* a longitudinal view of the left lobe of thyroid (*c*)

Metastatic Thyroid Carcinoma

Although cervical metastasis from thyroid carcinoma (most often papillary or medullary) is covered elsewhere in this text, it is important to discuss these nodal issues relative to level VI. This is a particularly difficult area to evaluate with ultrasound, especially when the thyroid is present, but it is important to understand how to optimize this inspection both at the time of initial assessment and during surveillance. The obstacles to proper ultrasound are principally based on anatomy. The clavicle and manubrium are obstacles to ideal positioning of the transducer, and these difficulties can be magnified by body habitus. In very slender patients, the depression between the distal sternocleidomastoid muscle and trachea may prevent the transducer from resting evenly on the skin and subcutaneous tissues. Conversely, an obese patient or one with a low-lying larynx may pose a different set of anatomical obstacles. The size of the footprint of the transducer may be a factor, as some narrow probes are easier to manipulate with these anatomical variables in mind. A system which allows manual manipulation to a lower probe frequency may allow better imaging of this deep region. Finally, using a greater depth setting may be assistive in imaging the lower aspect of level VI. Any cystic lesion in the mid or lower neck should be considered to be metastatic papillary thyroid carcinoma until proven otherwise [29] (Fig. 11.42).

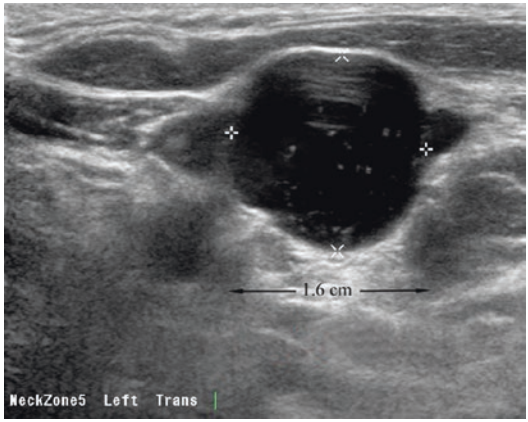

FIGURE 11.42 This round, nearly anechoic lymph node in level V demonstrates posterior enhancement and scattered microcalcifications. It represents metastatic papillary carcinoma. Such metastatic lesions are often seen in levels VI and IV

Parotid Gland

A portion of the parotid gland may reside in level II and upper level V, but this gland is generally thought of as autonomous along with its subcapsular lymph nodes. Ultrasound examination of the parotid is facilitated by orienting the probe in the sagittal plane.

Infection—Acute and chronic parotitis demonstrate many of the same characteristics on ultrasound [30]. Ill-defined areas of hypo- or anechoic signal are noted, and there may be broad areas of loss of the usual parenchymal architecture (Fig. 11.43). Doppler may show hypervascularity. Hyperplastic lymphadenopathy is usually identified in the upper neck and subcapsular parotid. Confluent anechoic areas would suggest abscess formation.

Cysts—A single parotid cyst may either be due to obstruction of a terminal duct or more commonly a first branchial pouch anomaly. These bear the same sonographic characteristics of cysts elsewhere in the neck and body. Multiple cysts

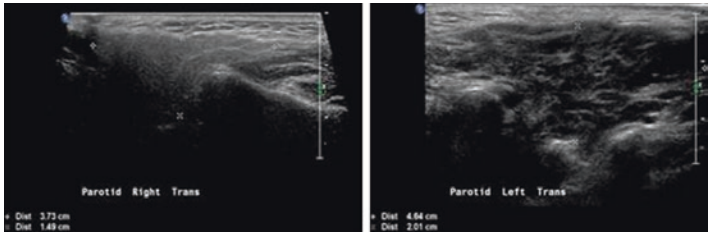

FIGURE 11.43 This comparison ultrasound demonstrates the normal parotid parenchyma in the *left* and a heterogeneous pattern in the *right* in a patient with acute parotitis

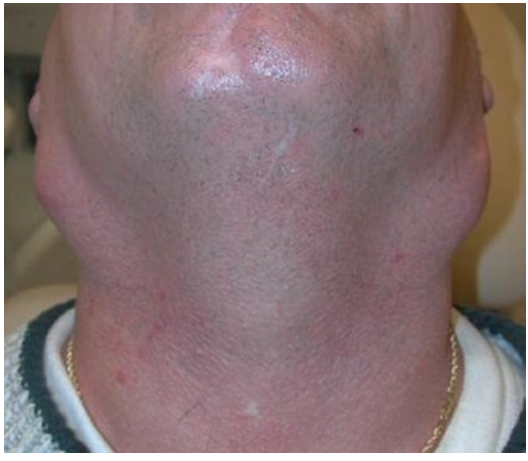

FIGURE 11.44 Submental view of bilateral parotid enlargement from a patient with AIDS

are more important to identify and characterize as they are frequently associated with HIV infection [31]. In fact they are often bilateral and contain debris (Figs. 11.44 and 11.45).

Tumor—The most common tumor of the parotid gland is a pleomorphic adenoma [32, 33] (Fig. 11.46). Also known as a benign mixed tumor, it has the peculiar characteristic which is similar to that of a cyst in that there is usually posterior acoustic enhancement, even though the lesion is solid. This

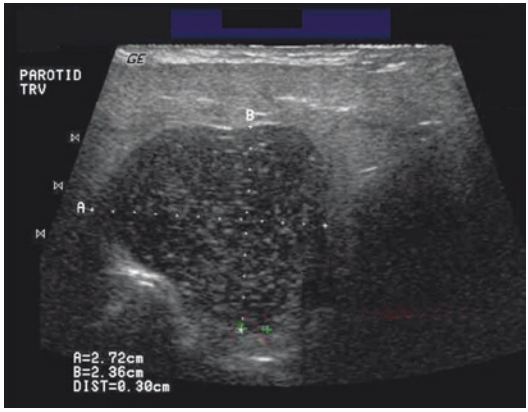

FIGURE 11.45 This parotid cyst contains debris which is actually set in motion by the ultrasound waves when visualized in real time. This benign lymphoepithelial cyst is secondary to the patient's HIV status

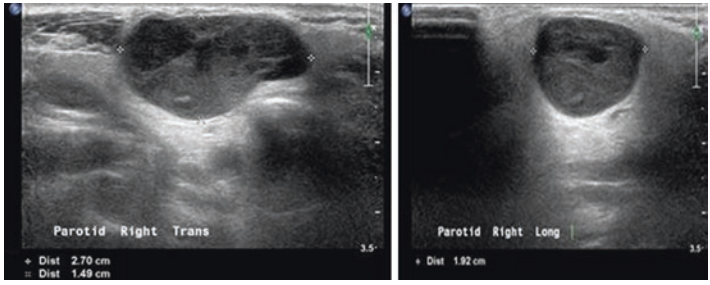

FIGURE 11.46 This gray scale ultrasound is typical of a pleomorphic adenoma. The margins are discrete and irregular, and there is posterior enhancement

finding is likely due to the homogeneous nature of the tumor interior. The tumor capsule is discrete and the lesion does not extend into the surrounding parotid tissues. There are irregular lobulations from the general perimeter of the mass, but these are contained within the same envelope. Other tumors which are malignant often demonstrate more jagged, irregular margins (Fig. 11.47) and occasionally penetration of their

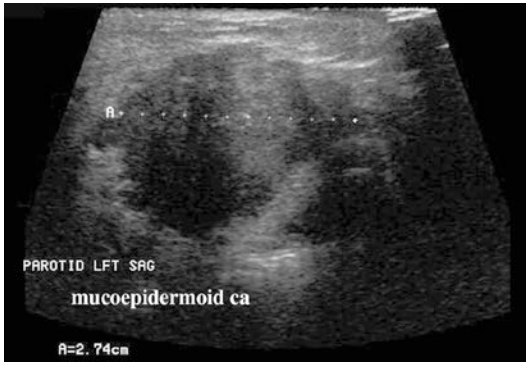

FIGURE 11.47 This mass within the parotid gland demonstrates irregularity of its borders which suggests invasion of the surrounding parenchyma. The lesion proved to be a mucoepidermoid carcinoma

capsule [34]. Often there is no actual separation between the tumor and surrounding parotid tissue. Lesions such as adenoid cystic and mucoepidermoid carcinomas are the most commonly encountered malignancies. In addition to the previously identified malignant features, these tumors often demonstrate adjacent lymphadenopathy.

Calculus [35]—The main parotid duct (Stensen's duct) is normally collapsed and is not visualized with gray scale ultrasound. However, when the duct is ectatic or enlarged from distal obstruction, it is possible to identify it with ultrasound. The duct has the appearance of a tubular structure and without Doppler could be misconstrued as a vessel (Fig. 11.48). The characteristics which identify the actual pathology are as follows: (1) discrete hyperechoic linear object in the position of the obstructing lesion (2) tubular anechoic structure proximal to the calculus, and (3) the absence of vascularity of the duct structure by Doppler (Fig. 11.49). Occasionally, multiple stones can be noted within the duct (Fig. 11.50).

Autoimmune disorder—Sjogren's syndrome is usually noted in patients with recurrent parotid swelling and rheumatoid arthritis (Figs. 11.51 and 11.52). This is condition which affects minor and major salivary glands and produces symptoms of atrophy of the lacrimal glands as well. Thus,

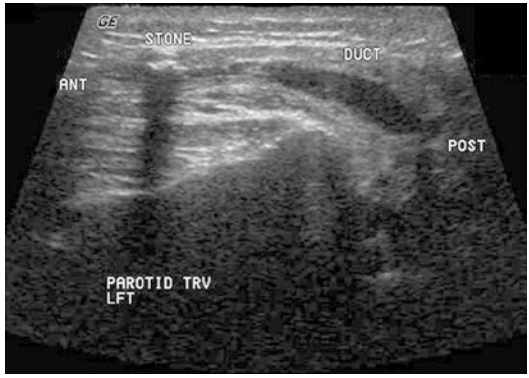

FIGURE 11.48 This is a classic image of an obstructing parotid duct calculus. It demonstrates posterior shadowing artifact behind the stone, and there is enlargement of the obstructed duct proximal to the stone

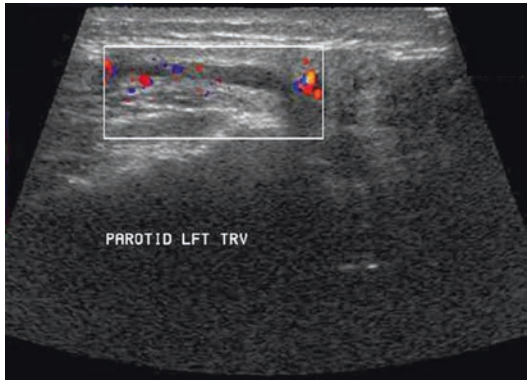

FIGURE 11.49 The dilated elongated structure within the parotid gland is proven to be an ectatic duct with the absence of flow on color Doppler

these patients experience xerostomia and xerophthalmia (dry mouth and eyes) in addition to the parotid symptoms [36]. The histopathology demonstrates a lymphoproliferative process which is remarkably similar to Hashimoto's thyroiditis. With ultrasound, the homogeneous parenchyma of the parotid gland is replaced with an even small nodular change

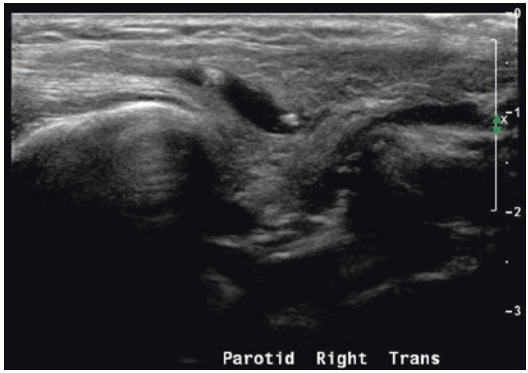

Figure 11.50 An enlarged obstructed parotid duct demonstrates two internal calculi

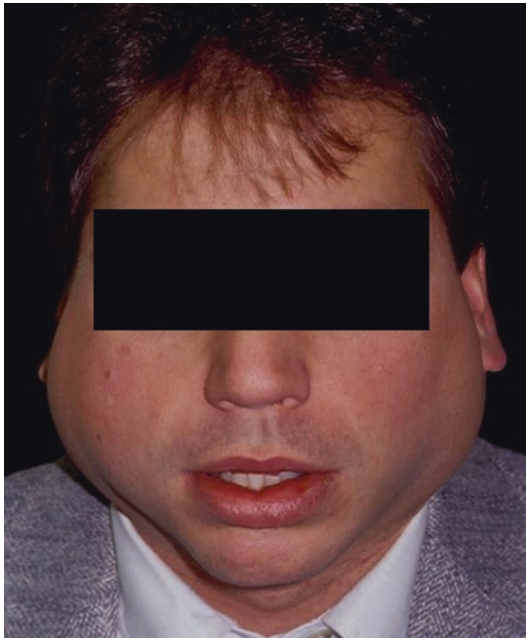

Figure 11.51 Bilateral parotid swelling is noted in a patient with Sjogren's syndrome

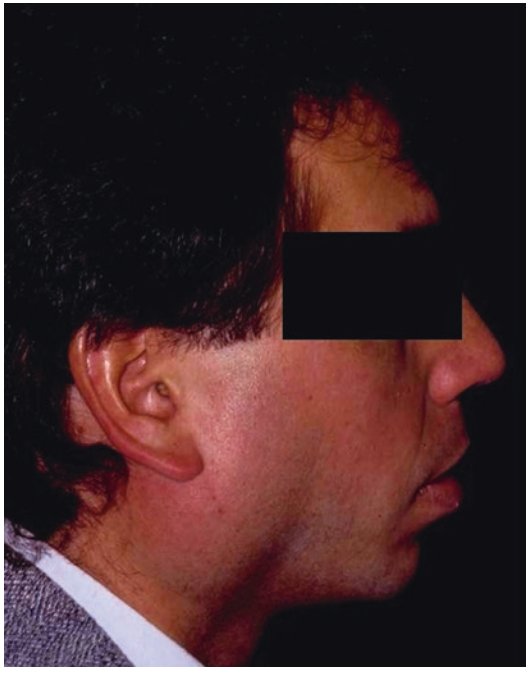

FIGURE 11.52 Lateral view of the patient with Sjogren's syndrome. The diffuse swelling demonstrates the full extent of the parotid gland anterior, inferior, and posterior to the auricle

which has a "Swiss cheese" pattern (Fig. 11.53). This condition is bilateral and usually can be noted by similar ultrasonographic changes in the submandibular glands as well [37].

Miscellaneous Conditions

Lipoma

This is a mass lesion which on physical examination is often difficult to differentiate from lymphadenopathy or other cervical conditions. These are benign, focal lesions which are located in the subcutaneous domain but can also be seen in

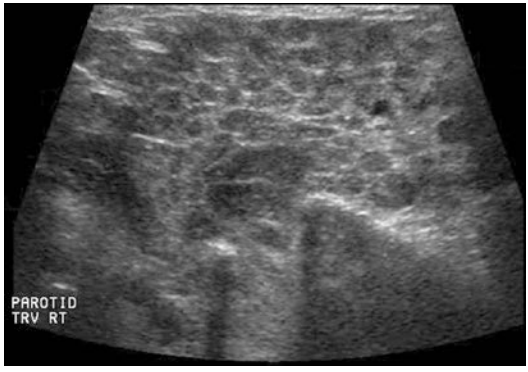

FIGURE 11.53 The normal ground-glass appearance of the parotid gland is replaced by a "Swiss cheese" pattern in the patient with Sjogren's syndrome

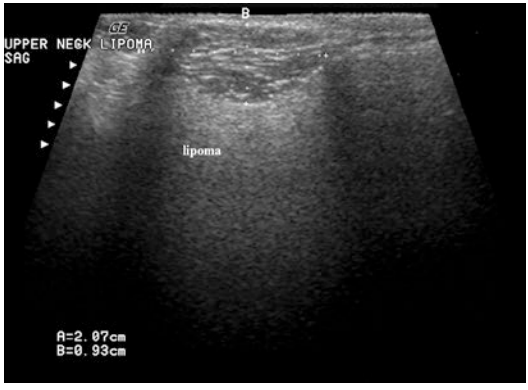

FIGURE 11.54 This discrete, ovoid hypoechoic lesion in the subcutaneous location demonstrates horizontal parallel hyperechoic striations. These findings are typical of a lipoma

other structures which contain lipocytes, such as the parotid gland. The mass is ovoid in shape and is traversed with striations along its long axis [38] (Fig. 11.54). It is discrete, avascular with Doppler, and seems separate from its surrounding adipose tissues.

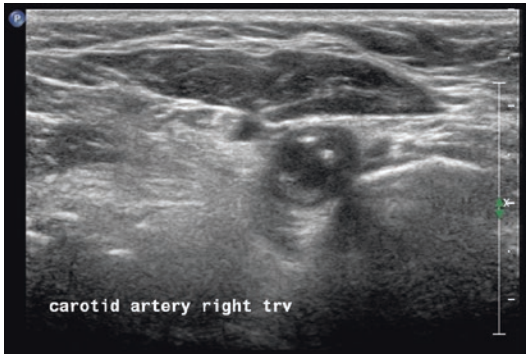

FIGURE 11.55 Atherosclerosis of the carotid system is commonly localized to the bulb region (carotid bifurcation). This transverse gray scale ultrasound image demonstrates typical hyperechoic calcifications

Vascular Lesions

Lymphangioma and hemangioma have already been discussed as important lesions to identify and differentiate in level I. Other conditions can involve the vascular system in random areas of the neck. For example, it is common for patients who undergo carotid ultrasound to demonstrate unsuspected thyroid lesions, and these become a source of referral to endocrinologists and surgeons. Similarly, when performing ultrasound of the thyroid and parathyroid glands, it is imperative to survey the neck to identify pathologic lymphadenopathy and any other process which may not be evident with physical examination alone. Atherosclerosis of the carotid artery is often identified as rim or nodular calcification at the carotid bulb (Figs. 11.55 and 11.56). It is not critical to demonstrate impaired flow distal to the calcification at the bifurcation, as referral for carotid Duplex sonography in an appropriate vascular laboratory will eventually be warranted. Patients who receive or have been administered chemotherapy via a central line may develop IJV thrombosis. This may not have any clinical implications, but some patients

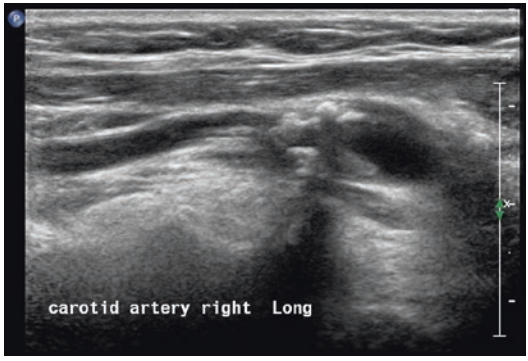

Figure 11.56 This sagittal ultrasound demonstrates calcifications at the carotid bulb, characteristic of atherosclerosis

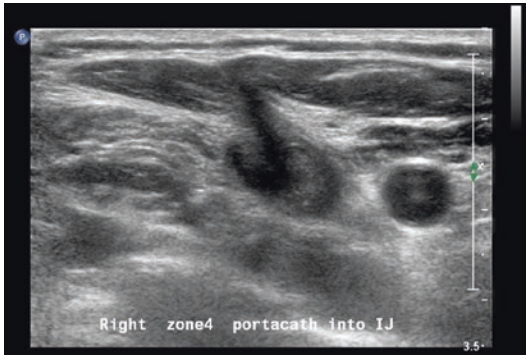

Figure 11.57 This sagittal gray scale ultrasound demonstrates thrombosis of the internal jugular vein (IJV) in a patient with prior central line placement for administration of chemotherapy

may have a progressive thrombophlebitis, neck pain, and serious consequences. The hallmark of identification is the use of Doppler and failure to demonstrate venous flow (Figs. 11.57 and 11.58). Occasionally, patients with invasive thyroid carcinoma may demonstrate thrombosis of the middle thyroid and

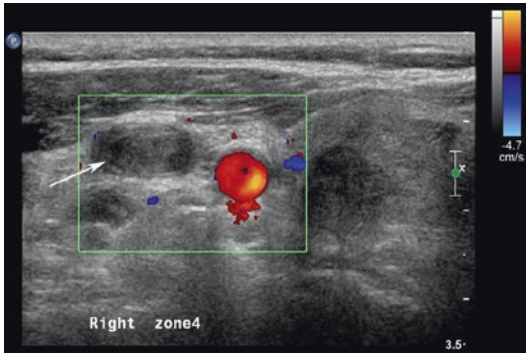

FIGURE 11.58 Color Doppler of the thrombosed IJV (designated by the *arrow*) of the patient in Fig. 11.56

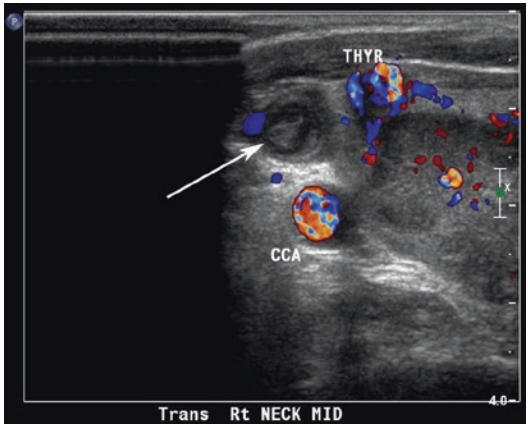

FIGURE 11.59 This is a color Doppler image of a thrombosed IJV as designated by the *arrow*. This preoperative ultrasound was performed in a patient with ipsilateral poorly differentiated thyroid carcinoma

adjacent jugular veins with Doppler, and this important recognition has important implications regarding the extent of surgical planning (Figs. 11.59, 11.60, and 11.61).

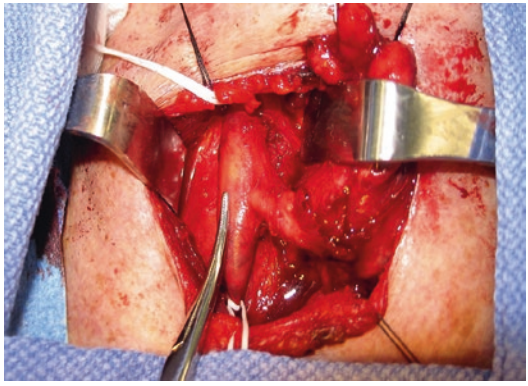

FIGURE 11.60 Intraoperative view of the enlarged middle thyroid vein entering the IJV demonstrated with a hemostat in the patient from Fig. 11.58

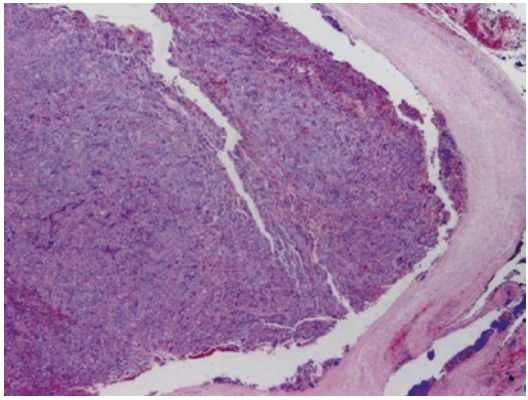

FIGURE 11.61 A tumor thrombus within the IJV correlates with the previous ultrasound and intraoperative view

Summary

In summary, the clinician who understands thyroid and parathyroid conditions may perform ultrasound with all of its recognized advantages for the patient and efficiency of management. Along with this focal interest, it is imperative

for these same clinicians to understand how to assess lymph nodes and to appreciate the ultrasonographic characteristics of metastatic malignancy. This survey process covers the entire neck. Other potential conditions may be identified, and this chapter is an effort to cover some of the more common entities which might be encountered. The reader who performs his or her own ultrasound examination is encouraged to become familiar with normal head and neck anatomy with each examination. Before long, abnormalities will reveal themselves, and even if the exact pathology cannot be cataloged, these changes may be identified as unusual. The decision to invite additional consultation may then be considered.

References

1. Ahuja A, Ying M. Sonography of neck lymph nodes: part II. Abnormal lymph nodes. Clin Radiol. 2003;58:359–66.
2. Dumitriu D, Dudea SM, Botor-Jid C, Baciut G. Ultrasonographic and sonoelastographic features of pleomorphic adenomas of the salivary glands. Med Ultrason. 2010;12(3):175–83.
3. Ching ASC, Ahuja AT. High-resolution sonography of the submandibular space: anatomy and abnormalities. AJR Am J Roentgenol. 2002;179:703–8.
4. Jain P, Jain R, Morton RP, Ahmad Z. Plunging ranulas: high resolution ultrasound for diagnosis and surgical management. Eur Radiol. 2010;20(6):1442–9.
5. Friedman ER, et al. Imaging of pediatric neck masses. Radiol Clin. 2011;49(4):617–32.
6. Lowe L, et al. Swelling at the angle of the mandible: imaging of the pediatric parotid gland and periparotid region. Radiographics. 2001;21:1211–27.
7. Benson MT, Dalen K, Mancuso AA, Kerr HH, Caccicarelli AA, Mafee MF. Congenital anomalies of the branchial apparatus: embryology and pathologic anatomy. Radiographics. 1992;12:942–60.
8. Telander R, Filston H. Review of head and neck lesions in infancy and childhood. Surg Clin North Am. 1992;72:1429–47.
9. Panneton JM, et al. Cervical sympathetic chain schwannomas masquerading as carotid body tumors. Ann Vasc Surg. 2000;14(5):519–24.

10. Fornage BD. Sonography of the peripheral nerves of the extremities. Radiol Med. 1993;5:162–7.
11. Netterville JL, Reely KM, Robertson D, Reiber ME, Armstrong WB, Childs P. Carotid body tumors: a review of 30 patients with 46 tumors. Laryngoscope. 1995;105:115.
12. Arslan H, Unal O, Kutluhan A, Sakarya ME. Power Doppler scanning in the diagnosis of carotid body tumors. J Ultrasound Med. 2000;19(6):367–70.
13. Huang TS, Chen HY. Dual thyroid ectopia with a normally located pre-tracheal thyroid gland: case report and literature review. Head Neck. 2007;29:885–8.
14. Park NH, Park HJ, Park CS, Kim MS, Park SL. The emerging echogenic tract sign of pyriform sinus fistula: an early indicator in the recovery stage of acute suppurative thyroiditis. AJNR Am J Neuroradiol. 2011;32(3):44–6.
15. Mali VP, Prabhakaran K. Recurrent acute thyroid swellings because of pyriform sinus fistula. J Pediatr Surg. 2008;43(4):27–30.
16. Killian G. La boudre de l'oesophage. Ann Mal Orelle Larynx. 1907;34:1.
17. Westrin KM, Ergun S, Carlsoo B. Zenker's diverticulum—a historical review and trends in therapy. Acta Otolaryngol. 1996;116:351–60.
18. Chang C, Payyapilli R, Scher RL. Endoscopic staple diverticulectomy for Zenker's diverticulum: review of literature and experience in 159 consecutive patients. Laryngoscope. 2003;113:957–65.
19. Mazzeo S, et al. Usefulness of echo color Doppler in differentiating parathyroid lesions from other cervical masses. Eur Radiol. 1997;7(1):90–5.
20. King AD, Tse GM, Ahuja AT, Yuen EH, Vlantis AC, To EW, et al. Necrosis in metastatic neck nodes: diagnostic accuracy of CT, MR imaging, and US. Radiology. 2004;230:720–6.
21. Ihm P, Dray T, Sofferman RA, Nathan M, Hardin NJ. Parathyroid cyst diagnosis and management. Laryngoscope. 2001;111:1576–8.
22. Ahuja A, Ying M, Yang WT, Evans R, King W, Metreweli C. The use of sonography in differentiating cervical lymphomatous lymph nodes from cervical metastatic lymph nodes. Clin Radiol. 1996;51:186–90.
23. Tsang RW, Gospodarowicz MK. Non-Hodgkin's lymphoma. In: Gunderson LL, Tepper JE, editors. Clinical radiation oncology. Philadelphia: Churchill Livingstone; 2000. p. 1158–88.

24. Ahuja AT, King AD, Metreweli C. Thyroglossal duct cysts: sonographic appearance in adults. AJNR Am J Neuroradiol. 1999;20:579–82.
25. Oyewumi M, et al. Ultrasound to differentiate thyroglossal duct cysts and dermoid cysts in children. Laryngoscope. 2015;125(4):998–1003.
26. Patel SG, Escrig M, Shaha AR, Singh B, Shah JP. Management of well-differentiated thyroid carcinoma presenting within a thyroglossal duct cyst. J Surg Oncol. 2002;79:134–9.
27. Fausto CSCV, et al. Thymus: ultrasound characterization. Radiol Bras. 2004;7(3):207–10.
28. Han BK, Suh YL, Yoon HK. Thymic ultrasound II. Pediatr Radiol. 2001;31(7):480–7.
29. Landry CS, Grubbs EG, Busaidy NL, Staerkel GA, Perrier ND, Edeiken-Monroe BS. Cystic lymph nodes in the lateral neck are an indicator of metastatic papillary thyroid cancer. Endocr Pract. 2010;16:1–16.
30. Gritzmann N, et al. Sonography of soft tissue masses in the neck. J Clin Ultrasound. 2002;30:356–73.
31. Dave SP, Pernas FG, Roy S. The benign lymphoepithelial cyst and a classification system for lymphocytic parotid gland enlargement in the pediatric HIV population. Laryngoscope. 2007;17(1):106–13.
32. Webb AJ, Eveson JW. Pleomorphic adenomas of the major salivary glands: a study of the capsular form in relation to surgical management. Clin Otolaryngol Allied Sci. 2001;26:134–42.
33. Stennert E, et al. Histopathology of pleomorphic adenoma in the parotid gland: a prospective unselected series of 100 cases. Laryngoscope. 2001;111:2195–200.
34. Lamont JP, McCarty TM, Fisher TL, et al. Prospective evaluation of office-based parotid ultrasound. Ann Surg Oncol. 2001;8:720.
35. Carlson E. Diagnosis and management of salivary gland infections. Oral Maxillofac Surg Clin North Am. 2009;21(3):293–312.
36. Patel R, Shahane A. The epidemiology of Sjögren's syndrome. Clin Epidemiol. 2014;6:247–55.
37. Jousse-Joulin S, et al. Is salivary gland ultrasonography a useful tool in Sjögren's syndrome? A systematic review. Rheumatology (Oxford). 2016;55(5):789–800.
38. Ahuja AT, et al. Head and neck lipomas: sonographic appearance. AJNR Am J Neuroradiol. 1998;19(3):505–8.

Chapter 12
Ultrasound-Guided Fine-Needle Biopsy of Thyroid Nodules

Mark A. Lupo and Daniel S. Duick

Abbreviations

AACE	American Association of Clinical Endocrinologists
ATA	American Thyroid Association
FNA	Fine-needle aspiration
INR	International normalized ratio
LBC	Liquid-based cytology
ROSE	Rapid on-site evaluation
UGFNA	Ultrasound-guided fine-needle aspiration

Introduction

There are multiple benefits in performing a diagnostic ultrasound neck examination prior to a thyroid nodule fine-needle aspiration (FNA). Comprehensive ultrasound will confirm

M.A. Lupo, MD, FACE, ECNU (✉)
Thyroid and Endocrine Center of Florida, Sarasota, FL, USA

Florida State University, College of Medicine, Sarasota Florida Campus, Sarasota, FL, USA
e-mail: marklupo@thyroidflorida.com

D.S. Duick, MD, MACE
University of Arizona College of Medicine, Phoenix, AZ, USA

Endocrinology Associates, PA, Scottsdale, AZ, USA

D.S. Duick et al. (eds.), *Thyroid and Parathyroid Ultrasound and Ultrasound-Guided FNA*,
https://doi.org/10.1007/978-3-319-67238-0_12

that a biopsy is necessary and aid in determining the size and position of a nodule, which allows better selection of needle length and needle size. In patients with a multinodular goiter, ultrasound assures biopsy of the dominant nodule or the nodules most likely to be malignant—those having microcalcifications, increased vascularity, marked hypoechogenicity, blurred irregular borders, or other characteristics associated with malignancy. Finally, ultrasound may redirect the FNA to other areas of suspicion, such as an enlarged, suspicious lymph node or identify an incidental parathyroid adenoma.

UGFNA is a low-risk, cost-effective outpatient method for thyroid nodule evaluation but is highly dependent on operator skill and quality cytopathology. Once a physician acquires the skill to perform neck ultrasonography, it is a simple progression to combine the two procedures into an ultrasound-guided FNA (UGFNA). Indeed, this technique is essential to biopsy non-palpable nodules and most nodules less than 1.5 cm in size. UGFNA is also necessary in many obese, muscular, or large-frame patients or when a nodule is palpated in the upright position but cannot be accurately relocated when the patient is supine. UGFNA is indicated for the biopsy of complex or cystic nodules in order to obtain material from the mural or solid component of the nodule and assure adequate cytology. In solid nodules, the best cytology material is usually obtained from various aspects of the entire nodule. However, many nodules undergo changes centrally as they grow, and UGFNA should be directed to the solid, more peripheral areas of the nodule. This chapter will describe a number of UGFNA techniques utilized to diagnose problematic nodules. In heterogeneous nodules, the biopsy should be taken from the hypoechoic area of the nodule and any area with any additional suspicious findings (e.g., regions of intranodular Doppler blood flow, microcalcifications, etc.). UGFNA allows for more precise placement of the needle tip within the nodule. Contemporary thyroid nodule FNA is virtually always performed under ultrasound guidance.

The introduction of FNA biopsy of thyroid nodules in the 1970s decreased the number of diagnostic surgery by 50%

and doubled the number of cancers discovered at surgery [1]. Multiple investigators have revealed that combining ultrasound and FNA into a single procedure, UGFNA, leads to a three- to five-fold increase in satisfactory cellular yields for cytology interpretation compared to conventional FNA [2, 3]. Others have demonstrated an increase in both FNA specificity and sensitivity when UGFNA was performed [4, 5]. UGFNA assures the needle tip is in the nodule (avoiding false negatives) and allows the operator to avoid the trachea, esophagus, and great vessels in the neck. The technique will usually allow the operator to avoid passing the needle through the sternocleidomastoid muscle and thus significantly decreases the discomfort of the procedure. Because UGFNA maximizes the quality and quantity of the cytology, it has become the single best tool with which to evaluate and manage thyroid nodules.

Guidelines for Thyroid Nodule FNA

Guidelines on which nodules require biopsy have recently been updated in 2015 by the American Thyroid Association (ATA) [6] and in 2016 by a joint collaboration of the American Association of Clinical Endocrinologists (AACE), the American College of Endocrinology (ACE), and the Italian organization, Associazione Medici Endocrinologi (AME) [7]. These guidelines both highlight risk stratification of thyroid nodules by sonographic pattern as outlined in Chap. 7 of this text. The recommendation for UGFNA is based on the risk assessment and nodule size as shown in Tables 12.1 and 12.2. Importantly, the ATA guidelines recommend repeat FNA of sonographically high-risk nodules with initial benign cytology. Patient preference and other clinical features should factor into the decision to perform FNA, which should only be done if it will change management of the patient.

The question of whether to biopsy nodules less than 1 cm (micronodules) remains controversial. These micronodules

Table 12.1 ATA 2015 guidelines for UGFNA of thyroid nodules

Ultrasound pattern	Estimated risk of malignancy (%)	FNA size threshold
High suspicion	>70–90	≥1 cm (repeat FNA within 12 months if initial cytology is benign)
Intermediate suspicion	10–20	≥1 cm
Low suspicion	5–10	≥1.5 cm
Very low suspicion	<3	≥2 cm or consider observation
Benign	<1	No biopsy

Table 12.2 AACE/ACE/AME 2016 guidelines for UGFNA of thyroid nodules

Ultrasound pattern	Estimated risk of malignancy (%)	FNA size threshold
High risk	50–90	≥1 cm
Intermediate risk	5–15	≥2 cm
Low risk	<1	≥2 cm or growing

have the same risk of malignancy as larger nodules with similar sonographic pattern [8, 9] but seldom present a threat. Small nodules are common in the population, and routine biopsy of all potentially suspicious micronodules is not likely cost-effective or clinically beneficial. Clearly some judgment is required in deciding which nodules require FNA. Careful ultrasound evaluation can identify suspicious lymph nodes and high-risk micronodules located at the thyroid capsule with potential invasion into the recurrent laryngeal nerve, trachea, or strap muscles, findings which may prompt FNA over surveillance. These features, when combined with patient age and comorbidities, can aid in clinical decision making [10, 11].

Preparation for UGFNA

Prior to consideration of a thyroid nodule aspiration, a history of relative contraindications and rarely absolute contraindication should be obtained. These include patients who may not be able to lie recumbent due to physical problems, who have difficulty in controlling the rate and depth of respiration, and who are uncooperative because of anxiety. Instead of the recumbent position, UGFNA may be performed at 45–60° elevation of the upper body or in a semi-sitting position. Patients with breathing issues or anxiety may often do well with discussion, reassurance, and directions given during the procedure. Nodule FNA tends to be less painful than lymph nodes (due to overlying sternocleidomastoid muscle), and pain generally correlates with anxiety, young age, and the number of nodules biopsied [12, 13]. Younger children may require anesthesia or sedation, while adults can be premedicated with an anxiolytic medication in order to obtain a satisfactory biopsy provided someone is able to drive them to and from the procedure.

A written and signed informed consent should be obtained after a verbal discussion during which all questions have been answered. Latex or anesthetic allergies should be documented. The consent form should contain in lay language all details and additional information regarding the reason for the procedure who will be performing the UGFNA, a description of the procedure and risks, the possibilities of false-negative results and not obtaining an adequate sample, and patient and witness signatures.

Thorough discussion prior to the procedure usually minimizes patient anxiety. This explanation should include that patients will feel a strange pressure briefly (as the needle passes through strap muscles), and sometimes pain radiates to the ear, jaw, or upper chest. Patients should not hold their breath during the procedure and should be told not to talk or move. Advising patients not to swallow may increase the chance of swallowing during the FNA. Patients should be told of potential complications [14]. Vasovagal reactions are

self-limited and managed by keeping patient supine with legs elevated and a cold compress to forehead. After instructions should include possibility of bruising, recommendations for ice/acetaminophen if pain/swelling (nonsteroidal anti-inflammatory agent after 48 h if needed), and clear communication on how results will be conveyed to the patient.

Fine Needle vs. Core Biopsy

An UGFNA biopsy is defined as utilizing a 25 or 27 gauge needle. Larger needles, cutting needles, coring needles, and spring-loaded, needle projecting devices all have an inherently greater risk for significant bleeding. Also, there is greater risk for puncture site infection and for structural damage to the thyroid, trachea, esophagus, carotid artery, jugular vein, and recurrent laryngeal nerve [15]. Larger needles do not aid in further defining cytologically benign from malignant (indeterminate) follicular nodules but may have a role when FNA shows atypical cytology [16]. Core needle biopsy can help in obtaining an adequate sample for cytologic interpretation after two or three repeated FNA "nondiagnostic" aspirates [17]. Thus, the use of an ultrasound-guided, 25 or 27 gauge FNA biopsy of thyroid nodules has become the standard and the preferred technique for reasons of safety, cost, and efficacy.

Patients on Anticoagulation Therapy

The presence of a severe, uncorrected bleeding, platelet, or coagulation disorder rendering the patient incapable of hemostasis is an absolute contraindication for any type of a thyroid needle biopsy. In most patients receiving aspirin, warfarin (with possible exception of very high INR), heparin, or clopidogrel, it is safe to perform UGFNA of thyroid nodules and cervical lymph nodes using 25 or 27G needles without an increased risk of hematoma [18]. Similarly, it is not necessary to withhold novel oral anticoagulants (dabigatran, rivaroxaban, or apixaban) prior to performing

UGFNA [19]. Additionally, anticoagulation therapy is not likely to result in a higher rate of inadequate cytology [20]. However if a prior FNA was inadequate on anticoagulation, it may be useful to withhold anticoagulation prior to repeat FNA [21].

For patients on anticoagulants, it is recommended to hold pressure for 5–10 min following the procedure and then check with ultrasound to see if a hematoma is forming. If so, this situation is managed by manual tamponage, followed by a pressure-taped dressing and/or an ice pack. The patient should be observed by ultrasound to assure stabilization prior to departure. The individual physician operator's judgment and experience in performing UGFNA in these situations of a potentially increased risk of minor side effects is most important. Full disclosure of risks to the patient is mandatory prior to proceeding with UGFNA. Occasionally for UGFNA, withholding or reducing anticoagulation or other therapies may be appropriate. If there is a decision to defer the procedure or hold anticoagulation therapy, the referring or treating physician should be contacted.

Materials

The ultrasound laboratory should consist of an ultrasound machine with a probe and linear transducer that has a 3.5–5.0 cm footprint and multiple frequency settings ranging between 7.5 and 14 MHz. The machine should also have Doppler imaging capabilities not only for diagnostic evaluation but also to identify blood vessels in the planned needle path (Fig. 12.1).

Larger footprint transducers are cumbersome and may impede biopsy capabilities. An additional utility probe with a similar or lower frequency range is a 2 cm curvilinear or curved linear array transducer (a linear transducer with a convex-curved footprint that produces an image with an increased field of view in a sector format). The smaller curvilinear transducer footprint is useful for imaging and performing an FNA in difficult locations, especially in the

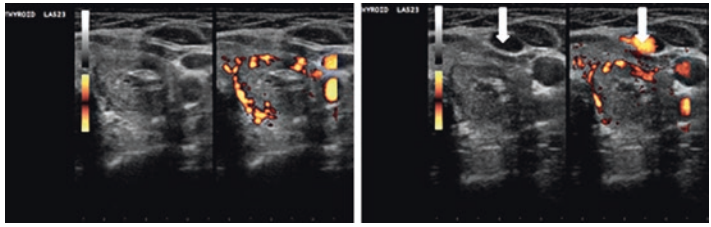

FIGURE 12.1 Left panel shows a transverse view (B-mode and power Doppler) with pressure applied on the transducer, masking the anterior jugular vein which is easily seen on the right panel (*arrow*) when less pressure is used. It is important to identify such blood vessels in order to avoid hematomas and bruising

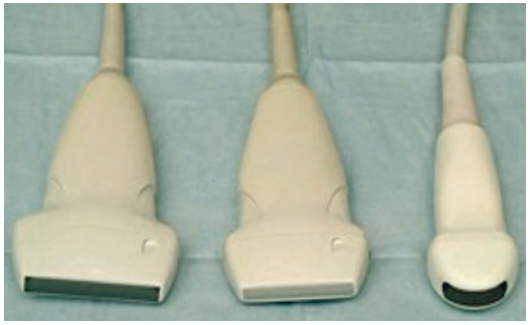

FIGURE 12.2 From left to right demonstrates different footprint sizes, linear array transducers with the transducer on the right demonstrating a smaller, curvilinear array transducer)

lower neck region at the level of the manubrium, clavicles, and insertions of the sternocleidomastoid muscle (Fig. 12.2).

Additional items may include a mobile ultrasound machine, setup tray/cart, and patient imaging table or gurney, each of which can be easily moved for optimum positioning, visualization, and utilization during an UGFNA (Fig. 12.3). A second monitor placed across the imaging table allows the operator to visualize the UGFNA procedure without turning his/her head (Fig. 12.4). The setup tray should include all materials required for topical cleansing,

FIGURE 12.3 (**a**) UGFNA with assistant holding probe and monitor positioned for optimal viewing. (**b**) US-guided drainage of a large cyst with sonographer holding and adjusting the transducer, another assistant draining with large syringe via three-way stopcock, allowing physician to manipulate the large-bore needle to optimize complete drainage

as well as transducer covers, sterile coupling gel, and an assortment of needles readily assembled and accessible to perform UGFNA (Figs. 12.5 and 12.6). Small needles (25–27G), medium needles (21–23G), and specialty needles (25, 23, or 21G stylet-type needles or spinal needles) of variable lengths and types should be part of the routine setup (Fig. 12.2). Shorter (1/2–1 in.) needles can be used for small isthmus nodules to avoid the trachea. The stylet-type needles are used for deep nodules or for aspirating structures

FIGURE 12.4 Room setup: Position the monitor so that it is in clear view during the UGFNA

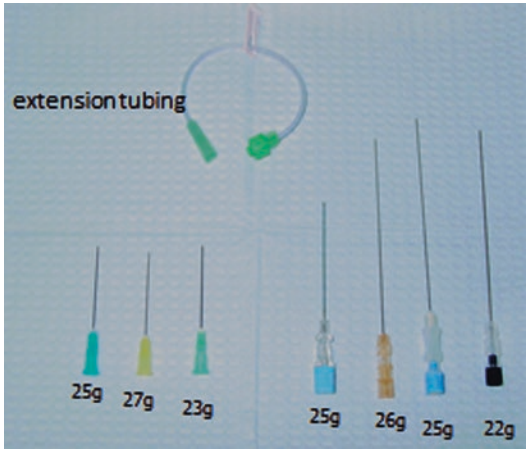

FIGURE 12.5 Various needle gauges and lengths as well as extension tubing should be available

posterior to the thyroid, which may or may not lie within the thyroid (e.g., exophytic thyroid nodule vs. parathyroid tumor or lymph node). The stylet can be left in while advancing the needle preventing the uploading of thyroid

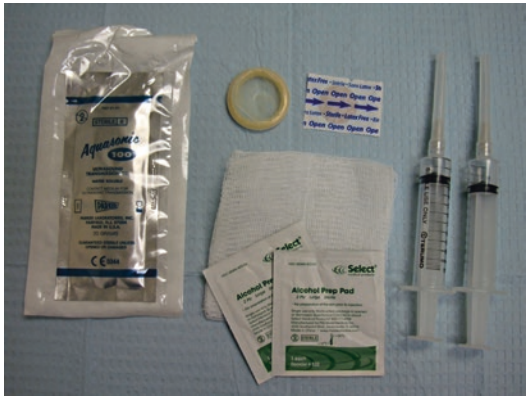

FIGURE 12.6 Basic setup tray: 27 g 1¼" needles on 10 cc syringes (plunger pulled back 1–2 cc), alcohol prep pads, gauze, probe cover, sterile gel (optional as alcohol can serve as coupling agent), and bandage

cells into the needle prior to reaching the target. The stylet also stiffens the needle, making it easier to maneuver prior to withdrawing the stylet when in the nodule and performing an aspirate. A detachable needle guide adapted for the transducer or transmitted on the monitor screen in a biopsy mode setting on some ultrasound machines may be utilized if desired but usually is not necessary for routine UGFNA. These devices can be helpful in the FNA of deep or posteriorly located nodules and in performing specialized and prolonged procedures such as drainage of a large cyst followed by percutaneous ethanol injection. Almost any needle will be visible on modern high-resolution ultrasound equipment, and this makes use of echogenic needles unnecessary.

For aspiration technique, a 3–10 cc syringe is connected to the needle. Pistol grip holders are not recommended since they are cumbersome and often apply excessive negative aspiration pressure, inducing bleeding and poor aspirates. However, these pistol grip holders can be used by an assistant in the drainage of a large cyst (Fig. 12.7).

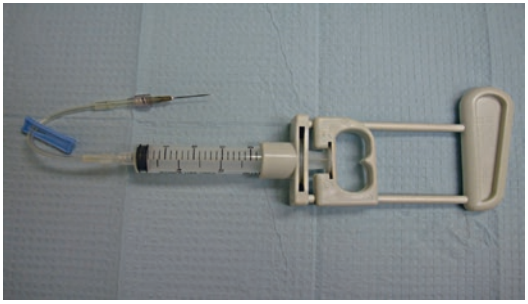

FIGURE 12.7 Pistol grip syringe holder connected to large syringe and needle with extension tubing. The operator controls the needle under ultrasound guidance, and the assistant applies negative pressure using the pistol grip

The use of injectable or topical anesthesia is optional for a 27 or 25G needle procedure. The operator may choose to use one or more of the following for local anesthesia: injectable 1 or 2% lidocaine or, less commonly, ethyl chloride topical spray or a topical lidocaine gel or patch (applied 1 or 2 h prior to the procedure), or ice. Injectable lidocaine should be readily available pending the patient's or physician's preference; or the perceived need of a procedure that is technically difficult (e.g., involving multiple nodules or repetitive aspirations) or if a larger gauge needle is required for cyst drainage.

Technique

The patient should be positioned supine with the neck extended and soft pillow or pad inserted beneath the shoulders to optimize extension of the neck. An additional, small, soft pillow may be placed behind the head for patients who have known neck problems or discomfort with extension of the head and/or rotation of the extended neck. Based on prior knowledge of the planned procedure, the operator should position oneself on either side of the table or at the

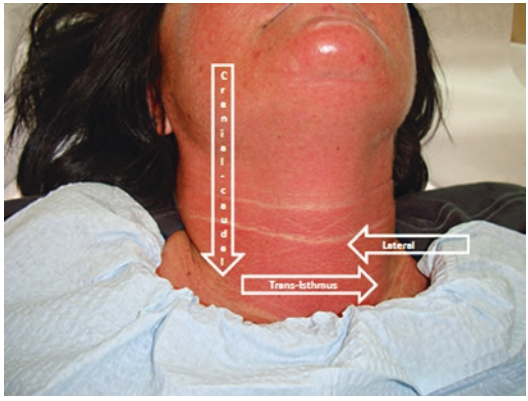

FIGURE 12.8 Three different approaches for parallel technique: Cranial-caudal, trans-isthmus, and lateral

head of the table for optimal target lesion access during the performance of the aspiration procedure (Fig. 12.8). The neck can be rotated slightly toward the side of the nodule to avoid the sternocleidomastoid muscle by moving it laterally. The monitor should be clearly visible to the operator/physician during the entire procedure. Prior to prepping the neck, an extended field of view should be performed before every needle biopsy. Both lobes of the thyroid, the isthmus, low central region, and the lateral neck should all be observed for any abnormalities or lymphadenopathy not previously detected. Coupling gel is applied to the transducer face, and the transducer is then enclosed in a cover or Parafilm to avoid direct contact with any blood products. UGFNA is a clean but not sterile procedure—similar to phlebotomy. The covered transducer is cleaned with alcohol, and the neck area is prepped with alcohol swabs. Sterile coupling gel can be applied to the covered transducer face or directly to the prepped neck area. Alternatively the alcohol swab may serve as a coupling agent then reapplied between passes. This eliminates the possibility of contaminating the sample with gel.

The key to utilizing ultrasound guidance for performance of the FNA is understanding the orientation of the

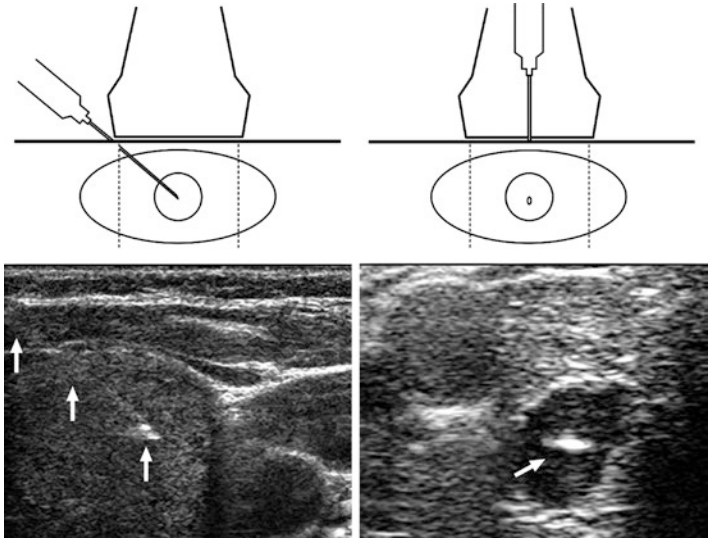

FIGURE 12.9 Left panel shows parallel approach in which the entire needle is visible. Right panel is the perpendicular approach where only the bevel-up tip is seen

azimuthal plane, which is the very thin plane in the middle of the transducer face along which the transducer sends and receives high-frequency ultrasound waves. Utilization of the azimuthal plane during UGFNA imaging allows the operator to visualize the needle pathway or approach, adjust the needle insertion angle, and track the entire needle and bevel-up tip by a parallel approach. Alternatively, the needle can be introduced perpendicular to the azimuthal plane, but in this orientation, only the bevel-up tip of the needle will be visible as it crosses the azimuthal plane (Fig. 12.9). Thus, there are basically two approaches for performing the UGFNA based on orientation to the azimuthal plane. The procedure may be done with an assistant holding the probe or with the operator holding the transducer in one hand and needle in the other (Figs. 12.3 and 12.10). A suggested step-by-step protocol is provided below.

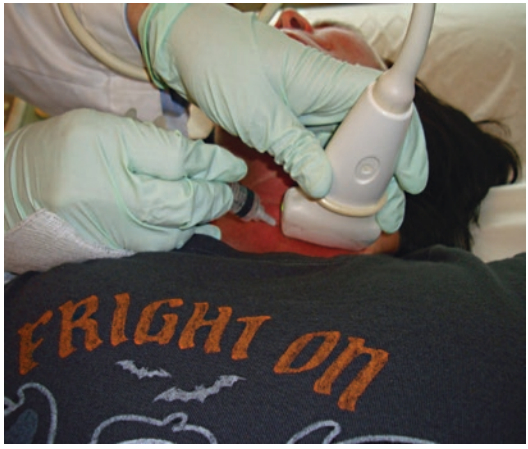

FIGURE 12.10 Parallel approach, trans-isthmus, without assistant

Suggested "Step-by-Step" Protocol for UGFNA

- Perform diagnostic ultrasound to confirm biopsy target and assess for abnormal lymph nodes.
- Discuss procedure with patient and obtain informed consent.
- Procedural "time-out" confirms patient identity, date of birth, procedure planned, and lateralization.
- Decide on best approach to nodule as well as depth of nodule to select needle length.
- Mark skin with pen (optional).
- Place gel on transducer, then apply probe cover.
- Prep the skin with alcohol and administer local or topical anesthesia as indicated.
- Rotate the neck ipsilateral to nodule to displace sternocleidomastoid away from planned needle path if possible.
- Adjust room lights to optimize image on monitor.
- Transducer in non-dominant hand and needle in dominant hand (if no assistant holding transducer).
- Use sterile gel or alcohol for a coupling agent. If prolonged procedure such as cyst drainage, sterile gel should be used. Wipe gel from needle path before insertion.

- Insert needle bevel-up under ultrasound guidance into the nodule.
- Move the needle back and forth with slight twisting motion at a 3 cycle/s cadence until a flash in occurs in the hub of the needle (assistant is watching for the flash).
- Withdraw needle and apply pressure with gauze pad.
- Freeze the image on the ultrasound machine.
- Eject specimen onto slide and make smear or rinse needle in liquid-based cytology.
- If making smears, rinse needle for immunohistochemistry/molecular markers/flow cytometry.
- Annotate and save ultrasound image of FNA for documentation.
- Make additional UGFNA passes with new needle/syringe as necessary (usually 2–4 passes total).
- If patient is on anticoagulation, recheck with ultrasound for hematoma formation.
- Apply bandage to skin.
- Explain to patient how results will be relayed.
- Fill out cytology form: nodule location, size, US characteristics, known malignancy, presence of autoimmune thyroid disease, and prior radiation exposure.

Parallel Approach

The ultrasound-guided parallel approach (also referred to as "in-plane" or "long-axis") tracks the needle from the point of insertion down and along the azimuthal plane to the nodule. The needle is oriented and introduced at the midportion of either end of the transducer, which is in parallel to the azimuthal plane. The transducer may be oriented in the transverse or longitudinal fashion and is held perpendicular to the skin. On the monitor screen, the nodule is positioned off-center and closer to the screen's lateral border on the side of planned needle insertion. The needle is best inserted with the bevel-up tip toward the transducer since this has angular edges with a flat surface producing greater reflectance and a brighter ultrasound image of the tip of the needle. The initial

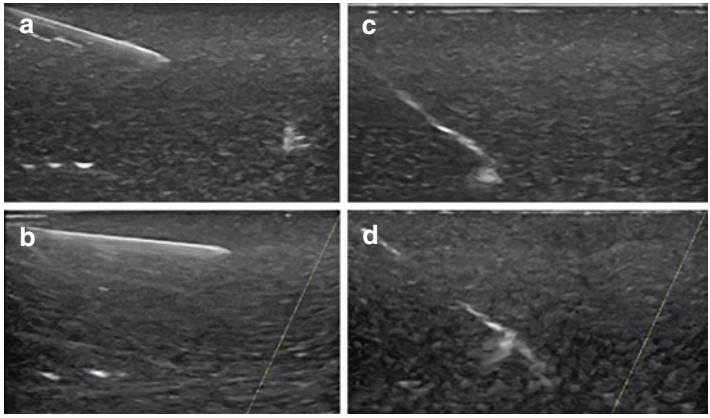

FIGURE 12.11 Needle visualization in parallel approach: Note the shallow approach in (**a**) is better reflected than the deeper approach in (**c**). (**b** and **d**) Use beam steer toward the needle which may improve reflection

angle is typically 45° and can be adjusted from 30–70°, the more shallow the needle, the better the reflection (Fig. 12.11). Utilizing the beam-steer function of the ultrasound machine to "steer" the beam toward the needle may increase reflection/visibility. The transducer and needle need to be maintained in the same plane, as if placing a needle into a pipe. It is recommended to "commit" to this line by inserting the needle and beginning to advance it prior to looking up at the monitor (Fig. 12.12). Upon needle penetration of the subcutaneous tissue, the needle tip appears at the upper right or upper left corner (depending on orientation of the transducer) of the monitor screen. As the needle is advanced forward and into the nodule, it is carefully guided along and within the azimuthal plane in parallel fashion. This approach allows the operator to observe needle penetration, location, and pathway of the entire needle within the neck, thyroid, and nodule, which remain visible on the monitor. If the needle course veers laterally or away from or out of the azimuthal plane even a few degrees, it will be lost from the monitor screen. If the needle is not seen, tilt or slightly move the transducer to

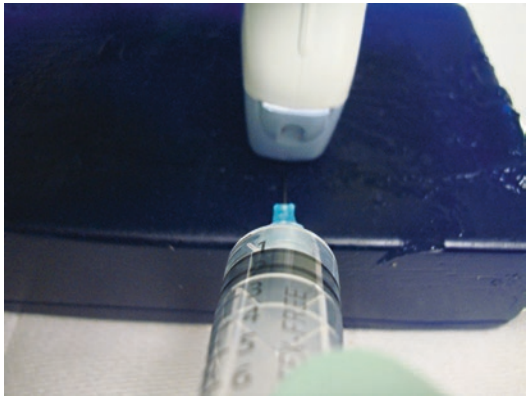

FIGURE 12.12 Parallel approach: Line up the needle with the azimuthal plane of the transducer. Commit to the line, and insert needle before looking up the monitor

hunt for the needle, rather than moving the needle. The parallel technique requires practice and experience to utilize successfully.

Perpendicular Approach

In the perpendicular (also known as "out of plane" or "short-axis") approach, the nodule is imaged and positioned in the midportion of the screen rather than off-center to either lateral side of the monitor. In this way, the point of needle introduction and the nodule beneath for aspiration are both centered in the midpoint of the transducer's side or long axis in order to transversely cross the azimuthal plane at 90° (Figs. 12.13 and 12.14). Advantages of the perpendicular technique are that the path to the target is shorter, so less tissue is traversed and the needle is moving parallel to the trachea and vessels, making it easier to avoid these structures. This again requires experience and skill since the needle itself will not be visualized during the performance of the biopsy. Nodules located in the lower neck may be best approached by the perpendicular technique [22]. The transducer is usually

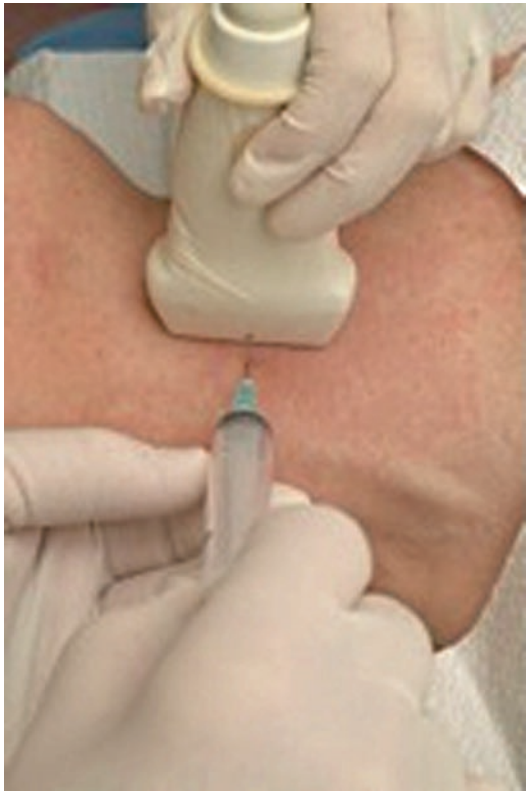

FIGURE 12.13 Assistant holding transducer at 90° to skin with needle entering at midpoint of transducer during perpendicular approach for UGFNA

oriented in the transverse fashion to visualize the trachea and vessels and is typically perpendicular to the skin but some prefer the transducer to be angled and the needle to be inserted at a 90° angle. The needle bevel is again introduced with the bevel facing upward toward the transducer to reflect the ultrasound waves and detect its bright image as it crosses the azimuthal plane during needle penetrance of the nodule (Fig. 12.15). Understanding and visualizing the various angles of needle descent are most important in order to match the

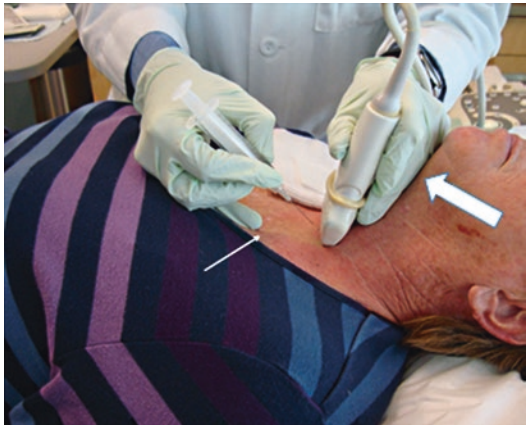

FIGURE 12.14 Perpendicular approach without assistant from inferior aspect of the transducer. Note the pulling skin tight (*small arrow*) to aid skin penetration and stabilizing the hand on the patient's neck (*large arrow*)

depth of the nodule in the neck when performing UGFNA in the perpendicular approach (Fig. 12.16). The angle of descent dictates whether the needle bevel will be visualized within the nodule (necessary to perform FNA) or above the nodule (descent angle too shallow) or below the nodule (descent angle too steep) as the bevel crosses the narrow beam of the azimuthal plane. One way to minimize the chance of passing over the nodule is to position the transducer at the caudal aspect (if approaching inferior to transducer or cranial if approaching superior to transducer) of the target to allow room to "drive" the needle toward the nodule, sliding the transducer to find the needle as necessary (Fig. 12.17). Repetitive practice and utilization of both the parallel approach and the perpendicular approach will result in optimizing the orientation and skills of the operator to enhance the performance of UGFNA.

Some prefer to use a micro-convex transducer for UGFNA of more inferiorly located targets or for all UGFNA. The nodule is placed in the middle of the screen, and the transducer tilted slightly and moved so the needle can be

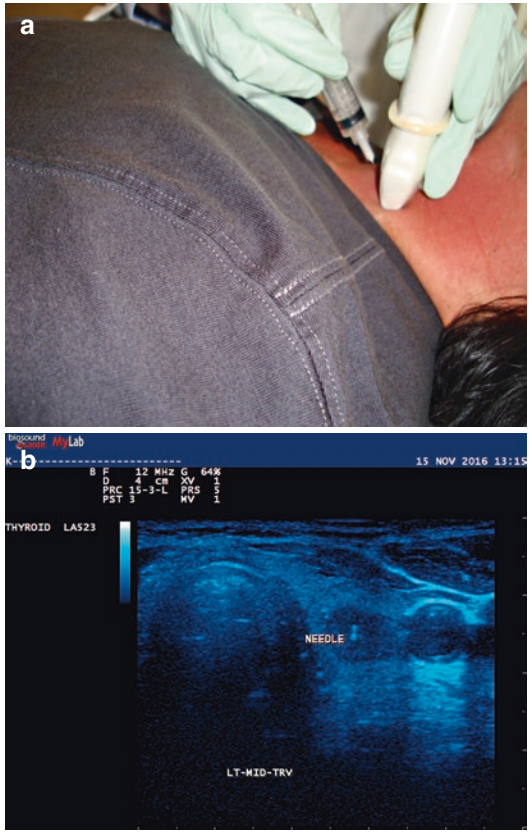

FIGURE 12.15 (**a**) Perpendicular approach without assistant. (**b**) Only the bevel tip of the needle is seen within the target nodule

introduced at 90° to the skin, and the entire needle is able to be seen coming from the side of the screen (Fig. 12.18).

Aspiration and Non-aspiration Techniques

The use of ultrasound at the time of planned FNA allows the operator to assess for solid, calcified/fibrotic, hypervascular, partially cystic, and multicompartmental cystic (complex) nodules. Based on this assessment and the initial pass of an

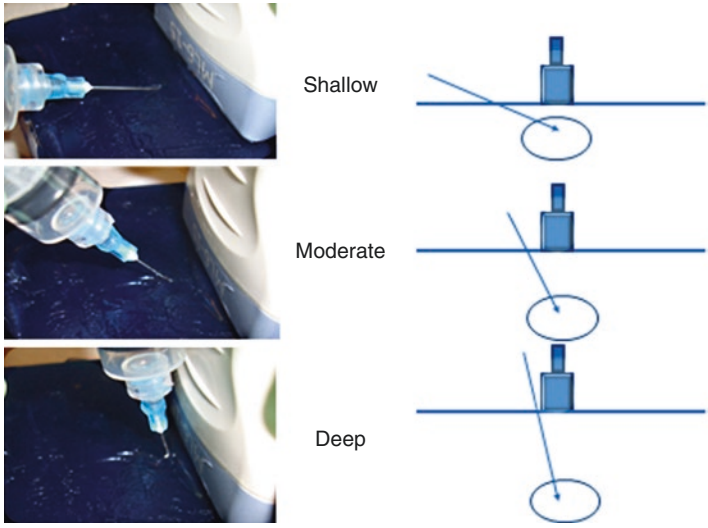

FIGURE 12.16 Perpendicular technique angle and insertion distance adjustments based on the depth of the target nodule

UGFNA, different approaches may be required to obtain adequate sampling and aspirated material for cytologic interpretation. There are two basic techniques for needle biopsy: suction (aspiration) or without suction (capillary action).

The closed suction technique is performed with a 27 or 25G needle attached to a 3–10 cc syringe (size of syringe is operator preference). The plunger is pulled back 1–2 cc, breaking the initial seal, making it easier to pull back on the plunger during the procedure. Then the needle is introduced into the nodule, under ultrasound guidance, and an additional 1–2 cc of negative pressure is applied to induce aspiration. The needle is moved back and forth along with slight twisting motion within the target area of the nodule at 3 cycles/s over 3–6 s; the aspiration pressure is released and the needle withdrawn. The goal is to withdraw the needle once a "flash" of material is seen in the needle hub. There are times when biopsy material is obtained without a flash, such as thick "pine tar" colloid or highly cellular tumors with little vascularity.

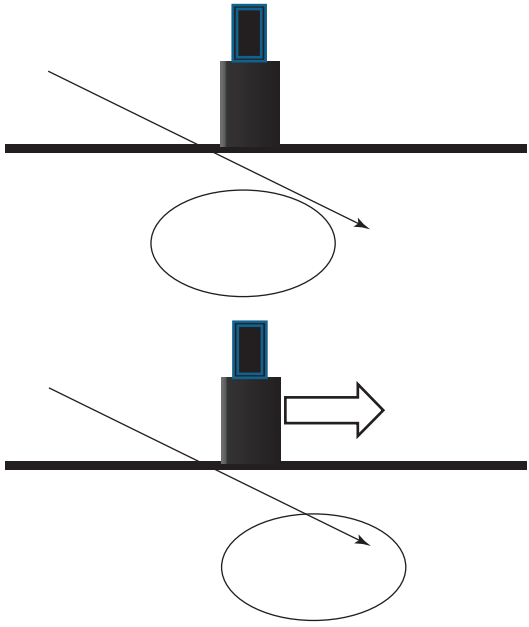

FIGURE 12.17 When using perpendicular approach, position the transducer toward the edge of the target closest to approaching needle to avoid passing over the target as seen in the top image. This way, the transducer can be moved (*large arrow*) to locate the needle tip within the target

The syringe is then detached from the needle, the plunger withdrawn (allowing 2 or 3 cc of air into the syringe), the needle reattached, and the plunger moved forward to extrude aspirated material onto a glass slide for smear and fixation preparation.

When draining a cyst, it is helpful to attach the needle to extension tubing, which is then attached to a large syringe, and suction is applied by an assistant (Fig. 12.7).

Often the nodule is composed of loosely formed microcystic and degenerating tissue and fluid, or the nodule is highly vascularized internally. In these situations a more dilute material rapidly appears in the syringe above the level of the needle hub. Using a non-suction, "needle-only" (Zajdela)

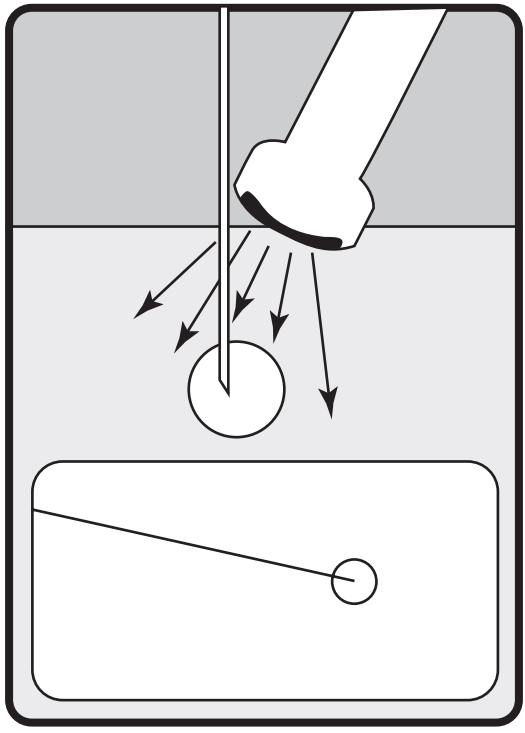

Figure 12.18 Micro-convex transducer UGFNA

technique usually improves acquisition of optimum cellular material for slide preparation for such nodules [23] (Fig. 12.19).

The "needle-only" or Zajdela technique utilizes a 27 or 25 gauge needle and the principle of capillary action uploading of cellular material into the needle without aspiration. The needle is grasped at the hub between the thumb and index finger and introduced into the nodule with quick up and down motions over 3–6 s. The index fingertip is then placed over the hub to close the system, and the needle is withdrawn, reattached to a syringe with the plunger retracted approximately 2–3 cc, and the material is extruded onto a slide for smear preparation and fixation. Usually two to four separate needle passes are made. One modification of this approach is to

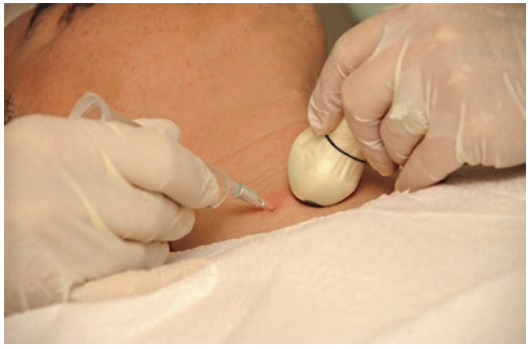

FIGURE 12.19 "Needle-only" or Zajdela technique where no aspiration or negative pressure is utilized. Note the plunger of the syringe has been removed from the body of the syringe during the procedure. Also demonstrated is a small footprint, curvilinear transducer

remove the plunger from the syringe, attach the needle to the syringe (for enhanced control of the needle), and perform an open-system aspirate. The thumb pad is placed over the end of the syringe at the time of needle withdrawal. The needle is detached and reattached to a syringe with a partially withdrawn plunger, and material is extruded onto a slide for smear and fixation. Another modification is to leave the plunger in the syringe and draw up 2–3 cc of air in the syringe prior to aspiration as seen in the setup in Fig. 12.6. Cellular material enters the needle via capillary action during the procedure, and the aspirate can then be extruded directly onto a slide. With this modification, the biopsy can be converted to a suction technique if no material is obtained without suction.

If the material obtained is frank blood or a watery mixture of interstitial, cystic, and degenerative or bloody fluid, a modification of the "needle-only" technique is often helpful. Again, two to four individual needle passes are performed, but an exceedingly rapid, cyclic penetration motion approximating 5–6 cycles/s for a few seconds is utilized rather than a 3 cycle/s motion. This allows for maximum needle bevel cutting and cellular acquisition with only minimal capillary action time to avoid fluid uploading into the needle.

The adequacy rate and accuracy is the same with suction and non-suction technique, and some feel that non-suction is simpler to perform and preferred over suction [24, 25]. Experience with both techniques allows the operator to modify the technique as the situation requires.

While the focus has been on thyroid nodule UGFNA, the same techniques are used for lymph node and parathyroid FNA. Suction is usually necessary for lymph nodes, and the needle can be rinsed in 1 cc of saline for thyroglobulin, PTH or calcitonin measurement from the FNA material.

Air drying, spray fixing, or immersion in alcohol of smears on glass slides is usually preferred for cytologic interpretation. Alternatively, a transport solution containing multiple FNA aspirates for liquid-based cytology (LBC) may be utilized as a primary approach. It is important to discuss these options with your pathologist who may have a preference. LBC can also be used as a secondary approach, especially if there is uncertainty of adequacy of material on slides for interpretation, and especially if the operator has a high-nondiagnostic/insufficient cellularity for interpretation rate. These latter issues can be overcome by utilizing smears and staining one or two slides immediately for assessment of cellular adequacy with a microscope in the laboratory. Rapid on-site evaluation (ROSE) is easy to perform in the office (Fig. 12.20), allowing for greater patient confidence that an adequate sample is obtained and initial assessment to determine if additional material for flow cytometry or molecular markers is needed [26, 27]. ROSE requires a moderate-complexity CLIA license. A written laboratory protocol for the performance of UGFNA and all laboratory associated procedures should be available for reference.

The essence and desired outcome of UGFNA is the acquisition of cellular material and the production of smears on glass slides for fixation and optimal cytologic interpretation. The capability to produce interpretable slides of aspirated material cannot be overemphasized. A high-nondiagnostic rate due to inadequate cellularity of smears or the need to

FIGURE 12.20 (**a**, **b**) In-office ROSE for immediate evaluation of adequacy and initial diagnostic assessment

solely depend on LBC is usually due to poor training in FNA technique, smearing techniques, or both. If the inadequacy rate is greater than 10%, it is recommended to either enroll in a slide-making cytology course or attend a training course to learn this and all skills associated with UGFNA. The use of ROSE will also help improve adequacy rates. Additionally, phantoms can be purchased and used for practice, however these are expensive. Alternatively, gelatin models are a cost-effective way to improve UGFNA technique [28].

Summary

There are numerous different methods of performing UGFNA, but there is no single *best method*. The techniques described are those widely utilized; they are not meant to be prescriptive but to provide a starting point for those who desire to start learning this procedure. You will discover many adaptations that can be customized to individual situations. It is important that the physician develop expertise in UGFNA in order to optimize patient care, safety, and outcomes.

References

1. Miller JM, Hamburger JI, Kini SR. The impact of needle biopsy on the preoperative diagnosis of thyroid nodules. Henry Ford Hosp Med J. 1980;28:145.
2. Takashima S, Fukuda H, Kobayashi T. Thyroid nodules: clinical effect of ultrasound-guided fine needle aspiration biopsy. J Clin Ultrasound. 1994;22:536–42.
3. Danese D, Sciacchitano S, Farsetti A, Andreoli M, Pontecorvi A. Diagnostic accuracy of conventional versus sonography-guided fine needle aspiration biopsy of thyroid nodules. Thyroid. 1998;8:15–21.
4. Carmeci C, Jeffery RB, McDougall IR, Noweis KW, Weigel RJ. Ultrasound-guided fine-needle aspiration biopsy of thyroid masses. Thyroid. 1998;8:283–9.
5. Yang GCH, Liebeskind D, Messina AV. Ultrasound-guided fine-needle aspiration of the thyroid assessed by ultrafast papanicolaou stain: data from 1,135 biopsies with a two to six year follow-up. Thyroid. 2001;11:581–9.
6. Haugen BR, Alexander EK, Bible KC, Doherty GM, Mandel SJ, Nikiforov YE, et al. 2015 American Thyroid Association management guidelines for adult patients with thyroid nodules and differentiated thyroid cancer: the American Thyroid Association guidelines task force on thyroid nodules and differentiated thyroid cancer. Thyroid. 2016;26(1):1–133.
7. Gharib H, Papini E, Garber JR, Duick DS, Harrell RM, Hegedus L, et al. American Association of Clinical Endocrinologists,

American College of Endocrinology, and Associazione Medici Endocrinologi medical guidelines for clinical practice for the diagnosis and Management of Thyroid Nodules – 2016 update. Endocr Pract. 2016;22(5):622–39.
8. Hagag P, Strauss S, Weiss M. Role of ultrasound-guided fine-needle aspiration biopsy in evaluation of nonpalpable nodules. Thyroid. 1998;8:989–95.
9. Leenhardt L, Hejblum G, Franc B, Fediaevsky LD, Delbot T, Le Guillozic D, et al. Indications and limits of ultrasound-guided cytology in the management of nonpalpable thyroid nodules. J Clin Endocrinol Metab. 1999;84:24–8.
10. Ito Y, Miyauchi A, Kobayashi K, Miya A. Prognosis and growth activity depend on patient age in clinical and subclinical papillary thyroid carcinoma. Endocr J. 2014;61(3):205–13.
11. Brito JP, Ito Y, Miyauchi A, Tuttle RM. A clinical framework to facilitate risk stratification when considering an active surveillance alternative to immediate biopsy and surgery in papillary microcarcinoma. Thyroid. 2016;26(1):144–9.
12. Lo WC, Cheng PW, Wang CT, Yeh ST, Liao LJ. Pain levels associated with ultrasound-guided fine-needle aspiration biopsy for neck masses. Head Neck. 2014;36(2):252–6.
13. Leboulleux S, Borget I, Labro S, Bidault S, Vielh P, Hartl D, Dauchy S, Chougnet CN, Girard E, Azoulay S, Mirghani H, Berdelou A, Lumbroso J, Deandreis D, Baudin E, Schlumberger M, Laurent S. Frequency and intensity of pain related to thyroid nodule fine-needle aspiration cytology. Thyroid. 2013;23(9):1113–8.
14. Polyzos SA, Anastasilakis AD. Clinical complications following thyroid fine-needle biopsy: as systematic review. Clin Endocrinol. 2009;71:157–65.
15. Khoo TK, Baker CH, Hallanger-Johnson J, Tom AM, Grant CS, Reading CC, et al. Comparison of ultrasound-guided fine-needle aspiration biopsy with core-needle biopsy in the evaluation of thyroid nodules. Endocr Pract. 2008;14(4):426–31.
16. Choi YJ, Baek JH, Suh CH, Shim WH, Jeong B, Kim JK, Song DE, Kim TY, Chung KW, Lee JH. Core-needle biopsy versus repeat fine-needle aspiration for thyroid nodules initially read as atypia/follicular lesion of undetermined significance. Head Neck. 2016;39(2):361–9. (epub).
17. Suh CH, Baek JH, Kim KW, Sung TY, Kim TY, Song DE, Choi YJ, Lee JH. The role of Core-needle biopsy for thyroid nodules with

initially nondiagnostic fine-needle aspiration results: a systematic review and meta-analysis. Endocr Pract. 2016;22(6):679–88.
18. Abu-Yousef MM, Larson JH, Kuehn DM, Wu AS, Laroia AT. Safety of ultrasound-guided fine needle aspiration biopsy of neck lesions in patients taking antithrombotic/anticoagulant medications. Ultrasound Q. 2011;27(3):157–9.
19. Lyle MA, Dean DS. Ultrasound-guided fine-needle aspiration biopsy of thyroid nodules in patients taking novel oral anticoagulants. Thyroid. 2015;25(4):373–6.
20. Denham SL, Ismail A, Bolus DN, Lockhart ME. Effect of anticoagulation medication on the thyroid fine-needle aspiration pathologic diagnostic sufficiency rate. J Ultrasound Med. 2016;35(1):43–8.
21. Tsao G, Orloff L. Clinician-performed thyroid ultrasound-guided fine-needle aspiration. Otolaryngol Clin N Am. 2014;47:509–18.
22. Crockett JC. "The thyroid nodule" fine-needle aspiration biopsy technique. J Ultrasound Med. 2011;30:685–94.
23. Zajdela A, de Maublanc MA, Schlienger P, Haye C. Cytologic diagnosis of orbital and periorbital palpable tumors using fine-needle sampling without aspiration. Diagn Cytopathol. 1986;2:17–20.
24. de Carvalho GA, Paz-Filho G, Cavalcanti TC, Graf H. Adequacy and diagnostic accuracy of aspiration vs. capillary fine needle thyroid biopsies. Endocr Pathol. 2009;20(4):204–8.
25. Tublin ME, Martin JA, Rollin LJ, Pealer K, Kurs-Lasky M, Ohori NP. Ultrasound-guided fine-needle aspiration versus fine-needle capillary sampling biopsy of thyroid nodules: does technique matter? J Ultrasound Med. 2007;26(12):1697–701.
26. Witt BL, Schmidt RL. Rapid onsite evaluation improves the adequacy of fine-needle aspiration for thyroid lesions: as systematic review and meta-analysis. Thyroid. 2013;23:428–35.
27. Lupo MA. Thyroid nodule evaluation: US-FNA and on-site cytology assessment. Endocr Pract. 2013;19(4):732–4.
28. Abraham D. A method using superconcentrated gelatin and a novel phantom suspension system for ultrasound-guided thyroid biopsy training. Thyroid. 2014;24(11):1662–3.

Chapter 13
Laser and Radiofrequency Ablation Procedures

Petros Tsamatropoulos and Roberto Valcavi

Introduction

The term interventional thyroidology refers to minimally invasive ultrasound-guided techniques to treat diseases of the endocrine neck, i.e., diseases of thyroid and parathyroid glands. Laser ablation (LA) and radiofrequency ablation (RFA) are two of these procedures used to destroy thyroid nodules and tumors using hyperthermia without surgical removal. Indications of LA and RFA technique for the treatment of endocrine neck diseases include symptomatic benign cold thyroid nodules, symptomatic thyroid cysts, autonomously functioning thyroid nodules, and recurrent thyroid cancer. Both thermal techniques have also been used for the treatment of parathyroid adenomas, but with several drawbacks and are no longer recommended.

The advantages of in situ tumor ablation are reduced costs, the possibility of performing procedures on outpatients, the possibility of treating patients who are poor candidates for surgery due to age or comorbidity, and the possibility of treat-

P. Tsamatropoulos, MD • R. Valcavi, MD, FACE (✉)
Endocrinology Unit, Centro Palmer, Reggio Emilia, Italy
e-mail: roberto.valcavi@gmail.com

D.S. Duick et al. (eds.), *Thyroid and Parathyroid Ultrasound and Ultrasound-Guided FNA*,
https://doi.org/10.1007/978-3-319-67238-0_13

ing patients who refuse surgery. LA and RFA are performed by endocrinologists, interventional radiologists, and surgeons.

Laser Ablation Principles

LASER is the acronym for light amplified stimulated emission of radiation. Light energy is applied via optical fibers directly inserted into the tissue [1–5]. Laser technology directs high-level energy to a well-delimited area of tissue in a predictable, precise, and controlled way. A number of laser sources and wavelengths are currently available, and different types of laser fibers, modified tips, and applicators can be used. For example, neodymium:yttrium aluminum garnet (Nd:YAG) or diode (solid state) lasers with a wavelength of 820–1064 nm are used for percutaneous LA because penetration of light is optimal in the near-infrared spectrum. High power destroys tissue by means of vaporization, charring around the fiber tip surrounded by a coagulation zone, as seen on ultrasound images (Fig. 13.1). Heat deposition is greatest near the thermal source, with rapid energy decay. Cell death may continue up to 72 h after the procedure due to coagulation of microvessels and ischemic injury [6]. Microscopically, the coagulation zone is surrounded by a rim of reversible damage that separates necrotic from viable tissue [7]. Figure 13.2 shows gross histology with charring and coagulation zone in a laser nodule resected 1 month after LA. Shrinkage of the nodule will occur because of slow reabsorption of the coagulation zone, eventually resulting in a fibrotic tissue area. We have described microscopic findings after percutaneous LA in benign thyroid nodules [8]. Figures 13.3 and 13.4 exemplify the histology of a laser-ablated area of a thyroid nodule resected 2 years after LA, which consisted of a well-defined zone, surrounded by a fibrous capsule filled in by amorphous material. No significant pathologic features were found in the thyroid tissue adjacent to the treated area.

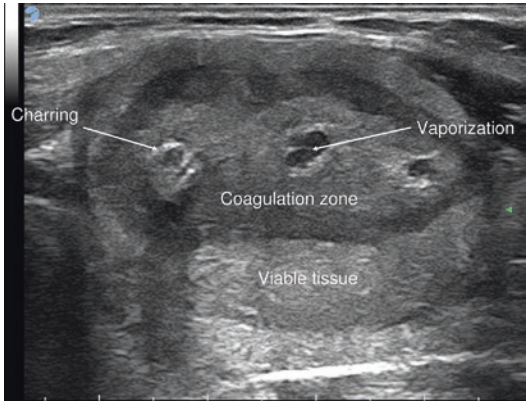

FIGURE 13.1 Ultrasound image of a three-fiber thyroid nodule laser ablation in a transverse US B-mode scan. Laser marks are seen as anechoic spots surrounded by hyperechoic rims. These are *cavitation*, due to tissue vaporization, and *charring*, respectively. The *coagulation zone* is hypoechoic parenchyma, clearly cleaved from *viable tissue*

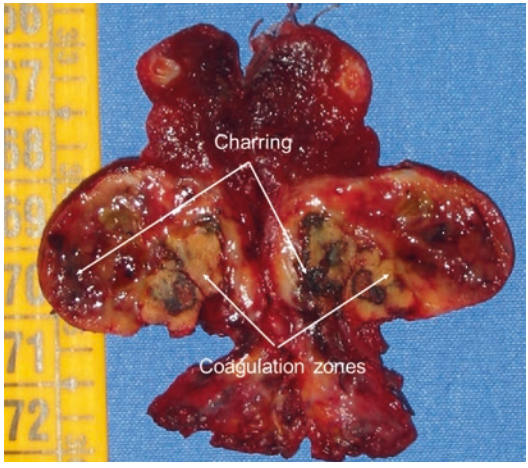

FIGURE 13.2 Macroscopic aspect of a benign nodule resected 1 month after LA treatment. *Arrows* show charring and coagulation zones

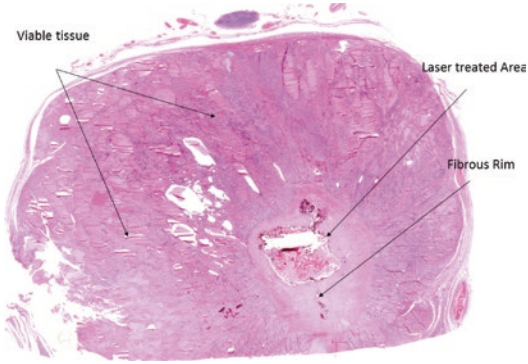

FIGURE 13.3 Microscopic changes (×5) occurring in a benign thyroid nodule resected after laser ablation. *Arrows mark* laser-treated area surrounded by a fibrous rim, within hyperplastic thyroid nodular viable tissue

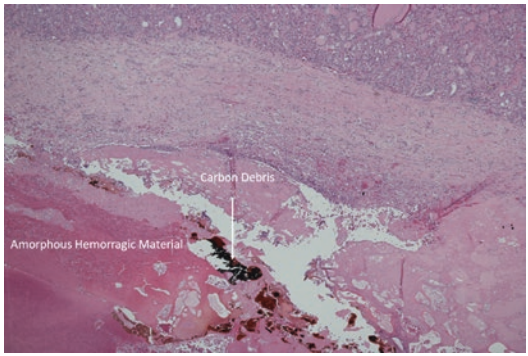

FIGURE 13.4 Nodule section at a further magnification (×20) shows amorphous hemorrhagic material with carbon debris (*arrows*) due to laser ablation

Charring is the main cause of decreased energy transmission, which in turn limits the coagulation zone. In addition, coagulation necrosis itself reduces optical penetration by about 20% in both normal and tumor tissue [4, 9]. Using a bare tip, almost spherical lesions with a maximum diameter of 12–16 mm can be produced. Lesion size can be increased

by simultaneous use of multiple fibers in an array around the tumor, rather than repositioning a single fiber.

Laser Ablation in the Thyroid Gland

Outpatient ultrasound-guided (UG) interventional procedures have been proposed to treat benign solid thyroid nodules without open surgery. This approach is possible, thanks to the combined use of ultrasonography (US) and fine-needle aspiration biopsy (FNA), which greatly reduces the need for diagnostic thyroidectomy [10–12]. The 2015 American Thyroid Association (ATA) management guidelines for patients with thyroid nodules and differentiated thyroid cancer suggest either no treatment or partial/total thyroid surgery for patients with benign solid thyroid nodular disease, depending on nodule size, growth, and symptoms [13], and the 2010 American Association of Clinical Endocrinologists—Associazione Medici Endocrinologi (Italian Association of Clinical Endocrinologists)—European Thyroid Association (AACE-AME-ETA) thyroid nodule guidelines have for the first time introduced UG interventional approaches as a possible choice for thyroid nodule clinical management [14]. In 2016 the AACE, American College of Endocrinology (ACE) and AME medical guidelines for clinical practice for the diagnosis and management of thyroid nodules confirmed the importance of UG minimally invasive procedures, namely, LA and radiofrequency ablation, for the treatment of benign, symptomatic, thyroid nodules [15]. The basic principle of locoregional treatment is to induce shrinkage of solid thyroid nodules using heat for tissue destruction. Thyroid LA was introduced by Pacella et al. in 2000 [16]. Since then several studies have been published on its effects on thyroid cold [17–29], cystic [30, 31], and hot nodules [32–38], including controlled trials [39–43], demonstrating that this technique is effective and safe. Indeed, we have been using LA in patients with benign thyroid cold nodules in Reggio Emilia, Italy, since 2002.

Technique

LA is an outpatient procedure carried out on fasting subjects. The flat tip technique is based on the insertion of a 300 μm plane-cut optic fiber through the sheath a 21G Chiba needle, exposing the bare fiber in direct contact with thyroid tissue for a length of 5 mm. In the thyroid gland, multiple fibers are inserted cranio-caudally one at a side of the other at 1.0 cm distance, in order to obtain an ellipsoid ablation that matches the ellipsoid shape of most thyroid nodules (Fig. 13.5). At variance with the square multiple fiber technique used for the liver, in the thyroid gland optimal geometrical configuration may be achieved inserting simultaneously the fibers (Fig. 13.6) in a triangle or in a line array depending on the nodule shape and size. With four fibers inserted simultaneously, combined with pullbacks, volume ablations up to 30 mL may be attained in a single session.

The goal of LA procedure is to achieve the maximum ablation volume in a single outpatient session. The patient is placed on an operating table in the supine position with hyperextended neck. The operator, seated behind patient's head, watches real-time US images. US equipment is used by

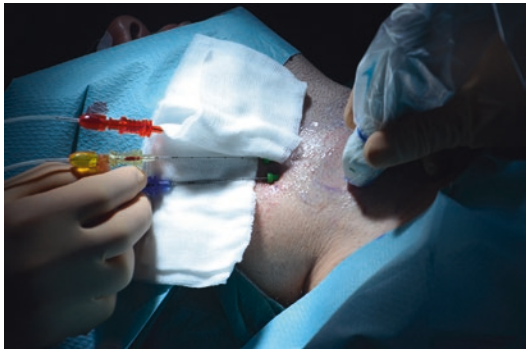

Figure 13.5 Three laser fibers inserted in Chiba 21-gauges needles along cranio-caudal major nodule axis; needles are separated by 1.0 cm

an assistant sitting to the right of the patient. A nurse helps in maneuvers. Procedure is carried out in the dark; a scialytic lamp is used only for needle placement. Real-time imaging is the key support and it is used throughout all procedure steps. In Reggio Emilia, in the years 2002–2008, we used an Nd:YAG laser with 1064 nm near-infrared wavelength emission, equipped with a four-source beam splitter (DEKA M.E.L.A., Florence, Italy). In 2009, we substituted this with equipment composed of an ultrasound device and a laser unit (EcholaserX4®, Elesta, Florence, Italy). The EcholaserX4® (Fig. 13.7) permits the operator to use up to four laser sources, each with its own energy emission setting and independent activation. This helps matching the ablation zone to nodule size and shape. Contrast enhancement ultrasound (CEUS) study can be performed before and after LA in order to estimate ablation volume. Contrast media (Sonovue®, sulfur exafluoride microbubbles) is rapidly injected intravenously. Conscious sedation is obtained with i.v. midazolam (2–5 mg) in fractionated boli. Emergency care drugs and equipment, including a defibrillator, are in the interventional suite. Although an anesthesiologist is not present during LA sessions, we recommend performing LA in a healthcare facility where an anesthesiologist is available on call. Local anesthesia with 2% ropivacaine HCl subcutaneous and pericapsular infiltration (2–5 mL) is performed under US

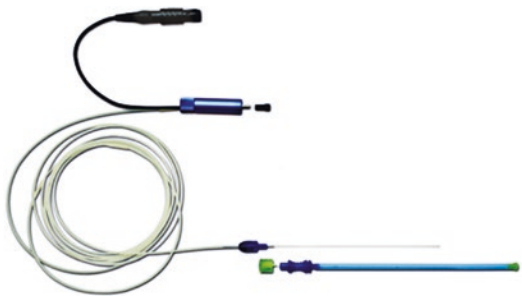

Figure 13.6 A laser fiber used for thyroid LA. (Photograph courtesy of ELESTA s.r.l. Calenzano, Italy)

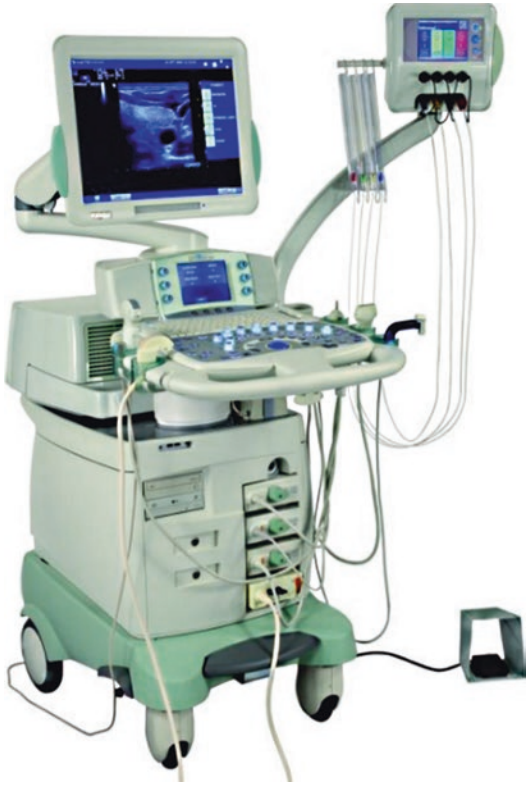

FIGURE 13.7 The Echolaser X4® (Elesta, Florence, Italy) equipment, composed of an ultrasound device and a laser unit. The small monitor is the touch screen laser display, permitting the operator to use up to four sources each with its own activation and energy emission setting. (Photograph courtesy of ELESTA s.r.l., Calenzano, Italy)

assistance with a thin (27 gauge) needle. Chiba 21-gauge needles (1–4) are placed manually along the longitudinal, cranio-caudal, major nodule axis at a distance of 10 mm, matching the anatomy of nodules as closely as possible. Fibers are inserted and laser is immediately turned on. An initial energy of 1200–1800 J/fiber with a mean output power of 3 W (range 2–4 W) is delivered starting 10 mm from the

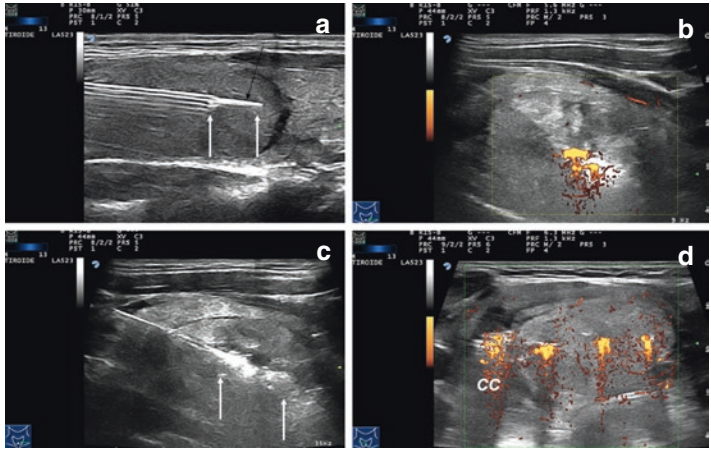

Figure 13.8 Multiplanar ultrasound imaging of a LA procedure with three fibers in a thyroid nodule. (**a**) Fiber exposed out of the tip of the needle (*arrows*). (**b**) Laser firing, color-Doppler imaging, longitudinal scan. (**c**) Laser firing, B-mode, longitudinal scan, first pullback. Arrows indicate the pullback area. (**d**) Laser firing, transverse scan, color-Doppler images during laser illumination showing the three needles at the same time. *CC* common carotid artery

bottom of the lesion. A highly echogenic area due to tissue heating and vaporization gradually increases over time until coalescence between fibers is observed. Multiplanar US images on axial and longitudinal scans are performed by the assistant/sonographer throughout laser illumination, allowing real-time visual control of each source. By upward needle/fiber pullbacks of 10 mm, additional doses of laser energy are administered at each step until a distance of 5 mm from the cranial portion of the nodule is reached (Fig. 13.8). While small thyroid nodules may be ablated using a single optic fiber, large nodules up to 40–50 mm in width, 30–35 mm in thickness, and 50–70 mm in length (i.e., up to 30–60 mL) may be treated by combining multiple fiber placement, needle/fiber pullback, and high energies. The number of fibers, number of pullbacks, and total energy delivered are tailored to nodule volume. The duration of laser illuminations ranges

from 6 to 30 min, depending on nodule size. Light irradiation is continuous; it is shortly suspended for fiber repositioning only in the event of pain, cough, or other side effects.

Laser Ablation Post-procedural Care

Immediately after the LA procedure, all patients receive prednisone 20 mg i.v. bolus. An ice pack with mild pressure is applied on the neck. Patients are then taken to the recovery room, where they receive ketoprofen 100 mg or paracetamol 1 g and are kept under observation for about 2 h. Before leaving hospital, all patients undergo US examination. The day after the LA procedure, patients are started on a tapering oral methylprednisolone therapy of 16 mg daily for 5 days, 8 mg daily for 4 days, and 4 mg daily for 3 days. Oral pump inhibitors are simultaneously administered (lansoprazole 30 mg) for the 12 days of oral prednisone therapy.

Side Effects

Few complications and side effects have been reported in the published data [23, 28, 43, 44]. In our own large clinical experience, no patient has ever required emergency care or emergency surgery. Intra-operatory pain is usually absent or minimal. Should it occur, laser should be turned off, and fibers repositioned in a more central area of the nodule. Post-operatory pain may occur in 8–40% of patients, requiring additional medication. Intranodular bleeding during needle placement is controlled by rapid fiber insertion and laser illumination and should not prevent regular ablation procedure from being completed. In our hands, infrequent (less than 2.5%) complications were thyroid pericapsular bleeding; vagal symptoms with bradycardia; cough; reversible voice change (complete recovery in 1–2 months after an additional corticosteroid course); tumor rupture with subfascial effusion, disappeared in 3–4 months, with no permanent

consequences; cutaneous burn; transient stridor; and hyper- or hypothyroidism.

A single case of tracheal laceration 50 days after LA has been reported in the literature. The patient underwent total thyroidectomy and tracheal repair [45].

Clinical Results in Benign Cold Thyroid Nodules

Nodule shrinkage in the available literature ranges from 36 to 82% of initial volume [17–43]. In our center, we reported safety and effects of Nd:YAG LA treatment in patients with benign nonfunctioning thyroid nodules in a 3-year follow-up [23]. In 2012 we presented data on a 5-year follow-up in 72 patients (51 females, 21 males, age 52.2 ± 12.3 years) treated with LA for nonfunctioning thyroid nodules [46]. Energy delivered was (mean ± SD) 8842 ± 6086 J with an output power of 3.1 ± 0.5 W. Five years after LA, mean ± SD nodule volume decreased from 28.1 ± 29.3 to 14.5 ± 17.6 mL, with a percent reduction of −49.6%. Volume reduction was related with good clinical response, i.e., cosmetic improvement and compressive symptoms reduction.

According to internal content, nodules were classified as follows: (a) compact (solid, iso-/hypoechoic, homogeneous, ≤10% of cystic content), (b) mixed (solid, inhomogeneous, with a 20–50% cystic content), and (c) spongiform (aggregation of multiple microcystic components in more than 50% of the nodule). Cystic nodules (fluid content ≥50%) were excluded from this series. In 25 spongiform nodules, volume decreased from 24.8 ± 25.9 to 7.7 ± 7.5 mL, with a reduction of −58.7%. In 14 mixed nodules, volume decreased from 41.1 ± 47.3 to 16.1 ± 17.4 mL, with a reduction of −48.3%. In 33 solid nodules, volume decreased from 26.4 ± 24.5 to 17.9 ± 22.0 mL, with a reduction of −26.8%. Hence, LA was more effective in patients with spongiform thyroid nodules as compared to mixed ($P \leq 0.01$) and compact ($P \leq 0.001$) nodules. Our data demonstrate that LA procedure was more effective and durable in patients with spongiform nodules.

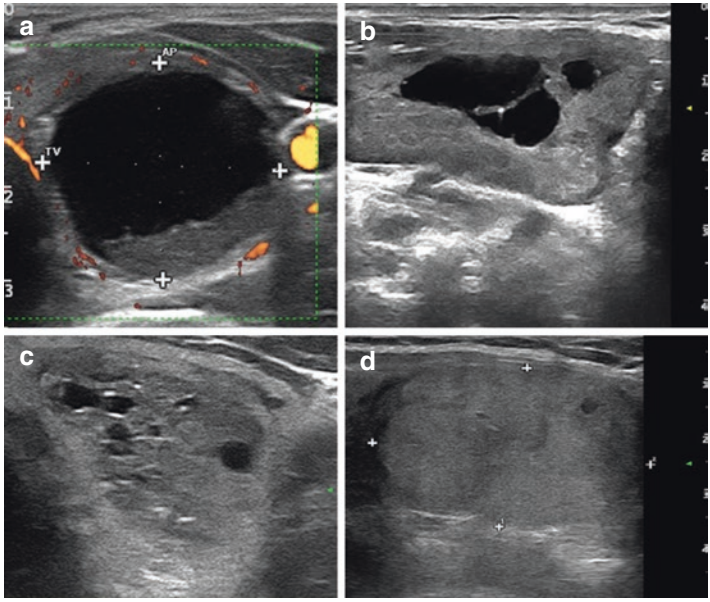

FIGURE 13.9 (**a**) Cystic thyroid nodule. (**b**) Mixed thyroid nodule. (**c**) Spongiform thyroid nodule. (**d**) Solid thyroid nodule

These results were confirmed by a study of Negro et al. published in 2016 [29]. The patients with spongiform nodules are therefore the best candidates for percutaneous LA procedure (Fig. 13.9).

Clinical Results in Autonomously Functioning Thyroid Nodules

In a few case series studies, LA was found effective in treating patients with autonomously functioning thyroid nodules (AFTNs) in terms of hyperthyroidism control [32, 33, 35]. Nonetheless, other studies demonstrated that LA achieved only partial results in normalizing thyroid hormone levels in patients with AFTNs, and more treatment sessions were required [16, 34, 36, 41]. A combined treatment with LA and 131-iodine has been proposed for large toxic nodular goiters

[37, 38]. In conclusion, the routine use of LA is not recommended for the routine treatment of AFTNs, but laser therapy may be considered when surgery or radioiodine are contraindicated or declined.

Clinical Results in Thyroid Cysts

Ethanol ablation (EA) is the first-line treatment for recurrent, benign, symptomatic, cystic (cystic portion >90%) or predominantly cystic (cystic portion less than 90% and greater than 50%) thyroid nodules [13–15, 47]. However, aspiration combined with LA is also effective in treating thyroid cysts [30, 31], albeit more expensive than EA. There are no studies comparing EA to LA for the treatment of thyroid cystic nodules. In our center we use EA for pure thyroid cysts and LA for multilocular thyroid cysts or predominantly cystic thyroid nodules since heat can destroy cystic septa and solid nodular tissue (Fig. 13.10).

Clinical Results in Recurrent Thyroid Cancer

Occasionally well-differentiated thyroid cancer (DTC) may recur, mainly in the thyroid bed or in lymph nodes [48]. In this case, surgical removal and radioiodine is recommended [13]. However, repeated neck dissection is difficult due to distortion of normal tissue planes by scar tissue formation, and such operations are associated with a higher rate of complications such as recurrent laryngeal nerve injury, hypoparathyroidism, and skin scar formation [49]. In 2013 two case series studies reported the efficacy of LA for the local control of neck recurrences from papillary thyroid cancer (PTC) [50, 51]. Ablated metastatic lymph nodes shrunk, and serum thyroglobulin (Tg) levels declined significantly. Recently, two other studies confirmed the potential role of LA for the treatment of cervical recurrences from PTC [52, 53]. It seems that LA may be used in high-risk surgical patients or in patients refusing additional surgery as an alternative to repeated surgical resection of metastatic disease of PTC.

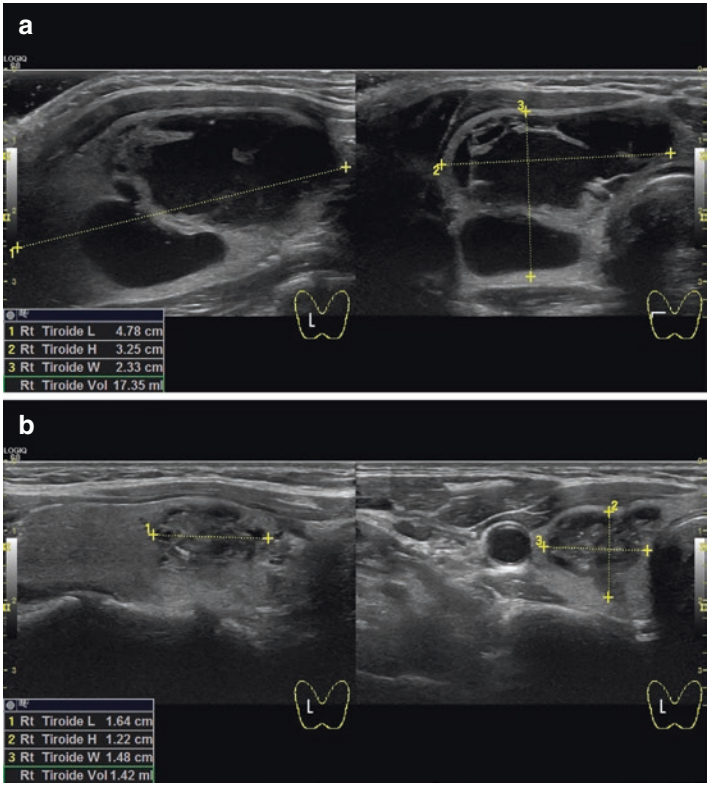

Figure 13.10 B-mode ultrasound images of a right complex multilocular thyroid cyst before (**a**) and 3 months after (**b**) aspiration and laser ablation in the same session. The thyroid nodule shrunk from 4.78 cm L × 2.33 cm H × 3.25 cm W (volume of 17.35 mL) to 1.64 c m L × 1.22 cm H × 1.48 cm W (volume of 1.42 mL) with a volume reduction of 91.8%

Laser Ablation in Primary Thyroid Papillary Microcarcinoma

Papillary thyroid microcarcinoma (PTMC) is usually associated with an excellent outcome. For patients with PTMC without extrathyroidal extension, and without clinical

evidence of any lymph node metastases, the initial surgical procedure can be either a total thyroidectomy or a thyroid lobectomy [13]. However, management of PTMC may become a dilemma because of patients' reluctance to have surgery or due to comorbidities. In 2013 we published a study with the aim to evaluate the clinical feasibility of LA on PTMC as a primary treatment and to prove histologically the absence of residual viable tumor after the LA procedure [54]. Three patients diagnosed by fine-needle aspiration cytology as positive for malignancy consistent with papillary thyroid carcinoma (category Thy 6 according to the Bethesda fine-needle aspiration cytology classification system) [55] were enrolled in the study after a full explanation of the protocol. These patients had positive fine-needle aspiration cytology for papillary thyroid cancer with US evidence of only one nodule 10 mm or less in greatest dimension and no other evidence of tumor in the thyroid gland or neck. All patients underwent percutaneous LA of the PTMC in the operating room under general anesthesia immediately before surgical removal of the thyroid gland.

After LA completion, the surgeon directly started a standard total thyroidectomy. Subsequent to surgery, the thyroid glands were submitted for histological evaluation. Tumor and surrounding parenchymal cellular vitality analysis were evaluated by immunohistochemistry on selected paraffin-embedded blocks using both thyroid transcription factor-1 (TTF-1) and antihuman mitochondria antibodies (clone 113-I). TTF-1 positivity was defined by nuclear labeling, while antihuman mitochondria antibody reactivity corresponded to a granular cytoplasmic staining.

The histological features were comparable in all three cases; that is, the neoplastic tissue around the cavitation showed typical changes of thermal damage, including cell shape distortion or cell shrinkage and nuclear chromatin condensation. On higher-power view, cases 2 and 3 were found to have incidental papillary microfoci far from the ablated zone. In case 2, a micrometastasis was observed in 1 perithyroidal lymph node out of 3 resected lymph nodes. There was no

continuity between intrathyroidal PTMC foci and the lymph node metastasis.

The signs of thermal damage included a 2–3 mm rim of normal tissue around the tumor that faded away at the border of the cavitation. In the residual thyroid tissue, the follicular architecture was maintained, and there was no extrafollicular colloid spillage or hemorrhage. No vascular invasion was seen. In all cases, there was complete loss of TTF-1 and antimitochondria antibody staining in the whole ablated area and in the rim of normal tissue surrounding the tumor. In contrast, the immunoreactivity for TTF-1 and antimitochondrial antibodies was easily detectable in nontargeted tissue. This demonstrates that the ablated neoplastic tissue was irreversibly damaged.

In conclusion, this study proves that percutaneous LA is technically feasible for complete PTMC destruction. Now, LA may be useful in selected patients with PTMC, either when the surgeon or a patient refuses surgery or when the patient is at high surgical risk. However, LA cannot be recommended as a routine primary choice of treatment for PTMC since recognition of micro-multifocality and lymph node micrometastasis is not possible at present.

Clinical Results in Functional Parathyroid Adenomas

In 2012 we published a study assessing the long-term efficacy of LA in the treatment of primary hyperparathyroidism (PHPT) due to functional parathyroid adenomas (PAs) in six patients [56]. Two months after laser ablation, serum parathyroid hormone (PTH) and calcium levels decreased in six and five patients, respectively. At the last follow-up examination, i.e., 1–7 years after LA, serum PTH and calcium levels were above the normal range in six and three patients, respectively. Three patients underwent surgery for persistent PHPT. LA therapy was safe and without permanent side effects, albeit one patient reported transient dysphonia. In conclusion, we

found that LA produces a transient reduction of serum PTH and calcium levels in patients with PAs, but it is not a lasting solution of hyperparathyroidism.

Radiofrequency Ablation in the Thyroid Gland

The goal of radiofrequency ablation (RFA) is to induce thermal injury to the tissue through electromagnetic energy deposition. Passage of alternating high-frequency current, between 200 and 1200 kHz through tissue, leads to a rise in temperature, without muscle contraction or pain [11]. The alternating electric field created in the tissue displaces molecules first in one direction, then in the opposite direction. Such agitation creates frictional heat. In the monopolar mode, which is the one most commonly used, the patient is part of a closed-loop circuit that includes a radiofrequency generator, an electrode needle, and a large dispersive electrode (ground pads) (Fig. 13.11). The discrepancy between the small surface area of the needle electrode and the large area of the ground pads causes the heat generated to be

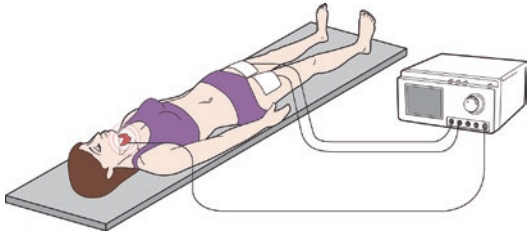

FIGURE 13.11 Thyroid RFA system. The patient is part of a closed-loop circuit that includes a radiofrequency generator, an electrode needle, and a large dispersive electrode (ground pads). The discrepancy between the small surface area of the needle electrode and the large area of the ground pads causes the heat generated to be concentrated around the needle electrode inserted into target area. (Illustration courtesy of STARmed Co., Ltd., Gyeonggi-do, Korea)

concentrated around the needle electrode inserted into target area. A typical treatment produces temperatures of 90 °C or more, resulting in coagulation necrosis within a few minutes, tissue desiccation, and consequent rise in impedance [57]. Small vessels are completely destroyed, and large vessels up to 3 mm in diameter are thrombosed. As for the laser, overheating with carbonization would limit heat transmission and tissue destruction. Instead, internally cooled tip needles maintain probe tip temperatures at around 90 °C without tissue charring. This improves the ability of the radiofrequency applicator to cause tissue ablation.

Devices

For monopolar thyroid RFA straight, internally cooled, short (7 or 10 cm), thin (18 or 19 gauge) electrode needles connected to a radiofrequency generator are currently used (Fig. 13.12). The active tips of the electrode needles may have a different length (0.5–2.0 cm) according to the desired ablation area [58, 59]. Experience with bipolar radiofrequency electrode needles for thyroid ablation is still limited [60–62]. In the past other types of electrode needles (e.g., multi-tined expandable electrodes) had been used for thyroid RFA, but their use is no longer recommended [63–65].

Technique

Thyroid RFA is performed as an outpatient procedure in an interventional suite. Patients should be fasting. The patient is placed on an operation bed in the supine position with hyperextended neck, and a venous catheter is inserted in a forearm vein. The operator is seated behind the patient's head and controls the US monitor throughout the procedure (Fig. 13.13). A multiparametric monitor is connected to the patient displaying a continuous single lead electrocardiogram, pulse oximetry, blood pressure, and respiratory rate.

Figure 13.12 The VIVA RF Generator® (STARmed, Korea) creates predictable and consistent ablation zones by using optimized ablation modes for various nodules. It also has a smart user interface to provide the exact information related to procedure details, and it records patient treatment data. The **star RF electrodes Fixed®** (STARmed, Korea) are used in percutaneous thyroid radiofrequency ablation procedures. The coolant circulation system of the electrode needle maintains the suitable impedance at the surface of the electrode. It also prevents tissue adjacent to the active tip from charring and helps to make a spherical ablation zone. (Photograph courtesy of STARmed Co., Ltd., Gyeonggi-do, Korea)

Conscious sedation is obtained with intravenous (i.v.) midazolam (2–5 mg) in fractionated boli in order to decrease the patient's anxiety, swallowing, cough, and movements. Local anesthesia with 2% HCl ropivacaine subcutaneous and pericapsular infiltration (2–5 mL) is performed under US assistance with thin (27 gauge) needles (Fig. 13.14).

In the RFA monopolar technique, the patient is part of a closed-loop circuit: ground pads (dispersive electrodes), applied to both thighs, are connected to a radiofrequency generator, and the generator is connected to an electrode needle. These electrode needles are straight, internally cooled, 7 cm, and 18 gauge and have active tips of usually 1.0 cm for most thyroid nodules. The ablation is performed according to the "moving shot" technique: the nodule is divided into multiple conceptual areas, and thereafter the nodule is ablated unit by unit by moving the electrode tip (Fig. 13.15) [66–68].

FIGURE 13.13 During thyroid RFA the operator is seated behind the patient's head and controls the US monitor throughout the procedure. An assistant (nurse, sonographer, or 2nd operator) is helpful during the thyroid ablation

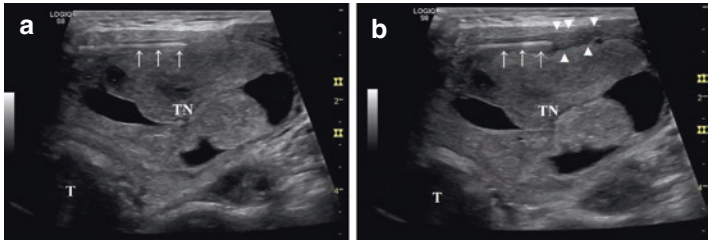

FIGURE 13.14 Local anesthesia with 2% ropivacaine HCl pericapsular infiltration (2–5 mL) before RFA. (**a**) A 27-gauge spinal needle (*arrows*) is inserted into the pericapsular space above the anterior surface of the thyroid nodule (TN). (**b**) The anesthetic liquid (*arrowheads*), which appears hypoechoic in US imaging, accumulates around the needle (*arrows*). B-mode, longitudinal, US image of a large, predominantly solid, right thyroid nodule. T: trachea

The ablation starts from the deepest portion of the nodule with a trans-isthmic approach (Fig. 13.16). The needle is inserted transisthmically at the higher level according to patient anatomy. This insertion allows the repositioning of the needle as much as 60–90 degrees with respect to the entry point in order to achieve ablation of more medially located tissue. This maneuver does not increase side effects, particularly vocal cord palsy, because while continuously tilt-

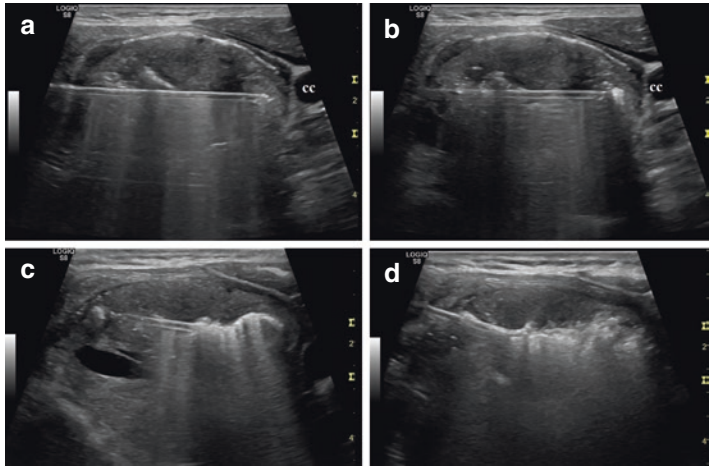

FIGURE 13.15 Longitudinal ultrasound images of the "moving shot" thyroid RFA technique. The needle is inserted transisthmically. The thyroid nodule is divided into multiple imaginary ablation units, and RFA is performed unit by unit. (**a**) Insertion of the electrode needle toward the common carotid (*cc*) artery. (**b–d**) The needle is moved within the thyroid mass by pulling it back and tilting it upward from deep to superficial layers of the nodule. The ablated area appears hyperechoic because of tissue vaporization

ing the probe, careful surveillance of the area medial to the needle is required to detect US signs of heating (gas microbubbles) when the needle is inserted close to the tracheoesophageal groove where the inferior laryngeal nerve runs (the so-called danger triangle). When a hyperechoic area appears and when impedance increases, the tip is moved backward to an untreated more superficial area. The maneuver is repeated with repositioning the needle, until all areas are ablated. Usually RF power starts with 30 W, and 5 W upward adjustments are made up to 60 W. Higher RFA power is used in Korea [69]. The successful ablation of a unit is confirmed by the appearance of a hyperechoic area—due to microbubbles—and the abrupt increase of impedance (the so-called break point) registered on the RF generator monitor.

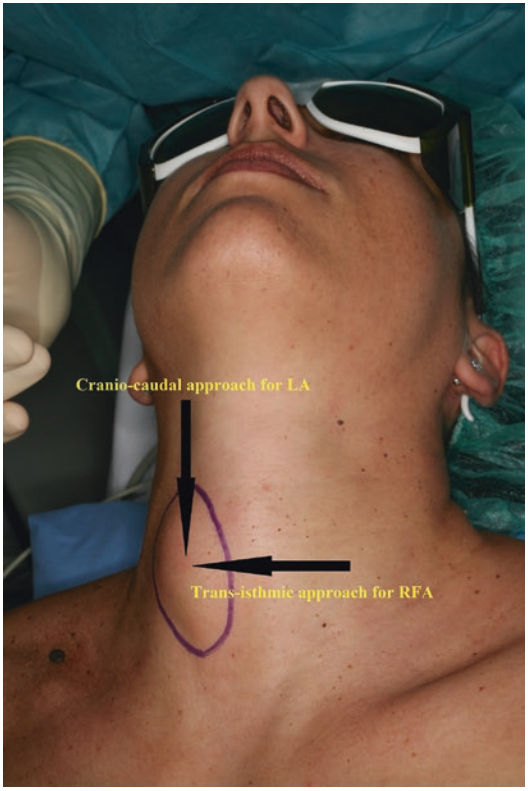

Figure 13.16 Approaches for thyroid LA and RFA. Cranio-caudal (longitudinal) approach, through long axis of the thyroid nodule, is used for LA. Trans-isthmic approach, via short axis of thyroid nodule (from medial to lateral aspect), is used for RFA

To treat mixed nodules, the cystic fluid is first aspirated and then the ablation is performed.

Radiofrequency Ablation Post-procedural Care

The procedural care after the RFA is the same as for the LA (see above).

Side Effects

Complications during thyroid RFA are uncommon, but they should be taken into account. A large multicenter Korean study reported an overall complication rate of 3.3% associated with the RFA treatment of benign thyroid nodules [70]. In order to prevent complications, it is important to have a thorough knowledge of sonographic anatomy of the neck [71].

Intraoperative pain is usually well controlled by means of local anesthesia with ropivacaine and conscious sedation with midazolam [68]. Notwithstanding, in case of intense pain, local or radiating to the jaw, teeth, chest, or back, the RF generator is turned off. Subsequently, the electrode needle is repositioned in a more central area of the nodule and the ablation can proceed. Intranodular bleeding during needle insertion may occur and is seen as a rapidly expanding hypo/anechoic signal within nodular tissue. It can be stopped by swift needle-electrode insertion and heat administration. Intranodular bleeding does not prevent ablation procedure. Thyroid pericapsular bleeding is seen as a hypoechoic layer surrounding the thyroid. Pericapsular hematomas can be controlled by compression of the neck for a few minutes. Neck bruising may follow a few days later, and it disappears in about 3–4 weeks. A rarely reported complication is vasovagal reaction which presents with bradycardia, hypotension, vomiting, and defecation. If this reaction is observed, the bed is tilted in Trendelenburg position, and maneuvers are temporarily interrupted until spontaneous recovery, which occurs in a few minutes. This possible event is due to vagus nerve stimulation as the nodule may displace the common carotid artery and the internal jugular vein. For this reason, knowledge of cervical vagus nerve localization is essential in thyroid RFA [72]. Cough during thermal ablation is due to trachea stimulation, and the tip of the needle should be pulled back.

Nodule rupture presents with sudden neck bulging and pain usually during the early follow-up period (2–4 weeks) [73]. The rupture might occur due to volume expansion because of intranodular bleeding. An initial conservative

treatment with compression is recommended. Another cause for tumor rupture may be liquefaction which occurs typically 2–4 weeks after RFA procedure. However, in case of symptoms deterioration, drainage or excision may be required. Infection or abscess formation is rare, since the skin is sterilized with povidone iodine solution. Skin burns have been reported at the electrode needle puncture site. Application of an ice bag during ablation or injection of fluid between the nodule and skin has been proposed in order to prevent skin burns. Voice change is a serious complication of thyroid RFA which is due to thermal injury of the recurrent laryngeal nerve. This phenomenon can be prevented by undertreating the area near the danger triangle (i.e., the tracheoesophageal groove which contains the recurrent laryngeal nerve). Finally, RFA may cause the new appearance of thyroid antibodies (anti-thyroglobulin, antithyroid peroxidase, or anti-thyrotropin receptor antibodies), but no subsequent clinical consequences (hypo- or hyperthyroidism) have been reported so far.

Clinical Results in Benign Cold Thyroid Nodules

The main indication for RFA in the endocrine neck is to reduce the volume of benign cold thyroid nodules in patients with local pressure symptoms or cosmetic complaints. Benignity of thyroid nodules with non-suspicious sonographic features is usually confirmed by at least two separate fine-needle aspiration (FNA) biopsies prior to RFA. Indeed, the risk of malignancy after two benign cytology results is extremely low [74–77]. The alternative of patients with both cytologically and sonographically benign thyroid nodules causing compressive and esthetic symptoms, who refuse surgery, is US follow-up.

The first study suggesting the use of RFA to treat symptomatic thyroid nodules was published in 2006 [78]. Since then, many studies have confirmed the efficacy and safety of treating benign thyroid nodules with RFA. Until now three systematic reviews with meta-analyses have confirmed that

RFA is effective in both reducing the volume of thyroid nodules and improving the related compressive symptoms and esthetic problems, without causing thyroid dysfunction or serious complications [79–81]. Moreover, we have demonstrated that RFA of symptomatic thyroid nodules improves patients' health-related quality of life [68]. Some authors have found that the efficacy of thyroid RFA is similar to that of thyroid surgery [82, 83].

The reduction in thyroid nodule volume after RFA ranges from 50 to 90% [84–90]. The heterogeneity of results among studies can be explained by a number of factors: (a) different types of electrodes used, (b) a single treatment versus repeated RFA sessions, (c) different initial volume of treated nodules, and (d) different composition (solid, cystic, or mixed) of the target nodules. Nodule volume reduction is gradual, and final results are achieved approximately 1 year after RFA or even more in case of large lesions. The aim of thyroid RFA is to perform the procedure only once. Additional ablation sessions can be performed in case of partial results or if thyroid nodule regrowth occurs [91–93]. In a 4-year follow-up study, thyroid nodule regrowth was recorded in only 5.6% of the patients (7/126) [93]. Notably, RFA does not affect eventual subsequent thyroid surgery [94]. In Figs. 13.17 and 13.18, we

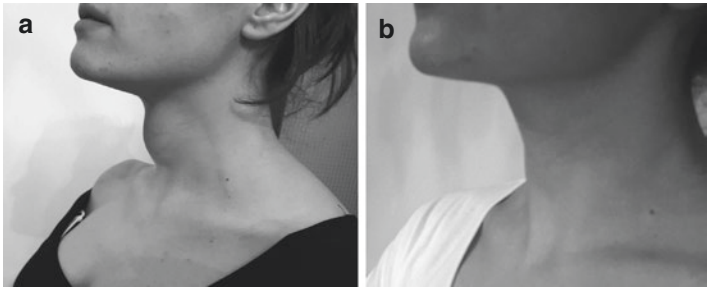

Figure 13.17 Photos of a 29-year-old Caucasian female patient's neck before (**a**) and 10 months after (**b**) radiofrequency ablation (RFA) of a large, benign, thyroid nodule. The thyroid ultrasound images of this patient are shown in Fig. 13.18

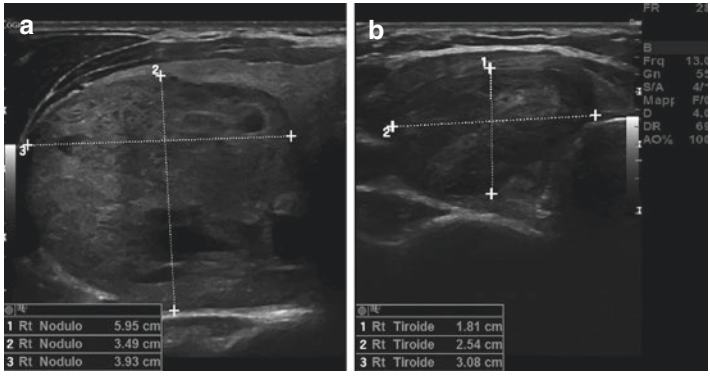

FIGURE 13.18 Ultrasound images in B-mode showing the thyroid nodule before (**a**) and 10 months after (**b**) radiofrequency ablation of the patient in Fig. 13.17. The predominantly solid, isoechoic, heterogeneous, thyroid nodule of the right lobe with regular margin 5.95 cm L × 3.49 cm H × 3.93 cm W (volume of 42.44 mL) and twice benign cytology shrunk to 3.08 cm L × 1.81 cm H × 2.54 cm W (volume of 7.36 mL) after one RFA session, resulting in a volume reduction percentage of 82.7%

show the results of a patient treated in our center with RFA for a large, benign, symptomatic, thyroid nodule.

RFA does not alter the thyroid function [68]. This is also true for extended thyroid tissue thermal ablation. Indeed, in patients with previous lobectomy, RFA does not affect blood thyroid hormone levels [95]. Similarly, the thyroid function of patients treated with RFA for bilateral benign nodules is also preserved [96]. We need to be aware that an ablated thyroid nodule becomes hypoechoic, inhomogeneous, and avascular on color Doppler ultrasonography [97]. Therefore, it is important not to confound a treated thyroid nodule with a thyroid cancer.

Clinical Results in Thyroid Cysts

As we discussed previously, EA is the first-line treatment for benign, symptomatic, benign, recurring cysts and complex nodules with a large fluid component [13, 15, 47].

Notwithstanding, RFA is also effective in treating cystic or predominantly cystic thyroid nodules, but is more expensive than EA and might require more sessions [98–100]. Despite the effectiveness of EA, some patients may have unsatisfactory results, mostly because of the solid component of the nodule which does not respond to alcohol. In this case, RFA has been used successfully to solve persistent clinical problems after an EA session [101, 102].

Clinical Results in Autonomously Functioning Thyroid Nodules

The first case report of the successful treatment of an autonomous functioning thyroid nodule (AFTN) was published in 2008 [103]. Subsequently, additional articles demonstrate that RFA is effective in patients with AFTNs since it reduces the nodule volume and controls hyperthyroidism [64, 65, 104]. RFA ablation of AFTNs requires a complete ablation, as untreated peripheral areas tend to regrow, causing relapse of hyperthyroidism. It has been shown that for the treatment of AFTNs, more than one RFA session may be necessary. However, at the present time, there are no studies comparing RFA to radioiodine for the treatment of AFTNs. Our opinion is that RFA should be used for AFTNs only when other treatment options are unavailable or refused.

Clinical Results in Recurrent Thyroid Cancer

In 2001, RFA was proposed as a treatment for regional recurrence from DTC [105]. Subsequently, other studies have also confirmed the efficacy of RFA for treating thyroid cancer recurrences to cause volume reduction or complete disappearance of tumor in some cases, decrease of serum thyroglobulin concentrations, and improvement of clinical symptoms if present [106–113].

The RFA technique used for the treatment of DTC recurrences is similar to that used for benign thyroid nodules, but

has additional precautions. First, the lesion has to be confirmed to be malignant by UG-FNA biopsy and FNA thyroglobulin measurement. Second, since these lesions are usually small, the use of electrode needles with a shorter active tip (i.e., 0.5 cm or 0.7 cm) is generally more appropriate. RFA starts with low power (5 W) and the power is gradually increased until a hyperechoic area forms. Thermal damage to nerves, especially recurrent laryngeal nerve and vagus nerve, during RFA treatment is of more concern than damage to blood vessels, as blood flow within the vessels dissipates the heat (the so-called heat sink effect). On the other hand, there is the possibility that the heat sink effect might reduce RFA efficacy if treating lesions close to a large vessel (common carotid artery or internal jugular vein) because of the cooling effect of blood flow. In order to avoid thermal injury of neck nerves during RFA, sterile water or 5% dextrose solution can be injected with a 23-gauge needle between the expected location of these vital structures and the tumor (hydrodissection technique). Thus, a protective barrier displaces the target from critical structures (not only nerves but also trachea and esophagus). Saline solution is not recommended for hydrodissection in RFA because it conducts electricity. During hydrodissection technique, if a continuous infusion of fluid is deemed necessary, the tip of the hydrodissection needle should be placed at least 1 cm away from the tip of the RF applicator. Another strategy that prevents thermal injury is the use of the electrode needle as a lever to increase the distance between tumor and critical structures. Using this technique, tumor is pulled away from vital structures by tilting the electrode needle during ablation under continuous US guidance.

Clinical Results in Functional Parathyroid Adenomas

There is very limited experience of treating parathyroid adenomas causing hyperparathyroidism [114–116] and secondary hyperparathyroidism [117] with RFA, and thus no recommendation can be made.

Comparison Between Radiofrequency Ablation and Laser Ablation for the Treatment of Benign Solid Thyroid Nodules and Final Remarks

There are no head-to-head comparisons between RFA and LA for the treatment of benign solid thyroid nodules. However, a recent systematic review including traditional pooling and Bayesian network meta-analysis found that RFA is superior to laser ablation in reducing benign solid thyroid nodule volume, despite the smaller number of treatment sessions without major side effects [61]. In our center we prefer treating large, benign, solid or predominantly solid, thyroid nodules with RFA. Instead, as discussed before, we use LA for multilocular thyroid cysts and predominantly cystic thyroid nodules. Finally, we treat pure thyroid cysts with EA. In conclusion, these three main interventional thyroidology techniques, i.e., RFA, LA, and EA, are valid alternatives to surgery in well-selected patients suffering from symptomatic, solid, mixed or cystic, thyroid nodules [118].

References

1. Bown SG. Phototherapy in tumors. World J Surg. 1983;7(6):700–9.
2. Nolsøe CP, Torp-Pedersen S, Burcharth F, Horn T, Pedersen S, Christensen NE, et al. Interstitial hyperthermia of colorectal liver metastases with a US-guided Nd-YAG laser with a diffuser tip: a pilot clinical study. Radiology. 1993;187(2):333–7.
3. Amin Z, Harries SA, Lees WR, Bown SG. Interstitial tumour photocoagulation. Endosc Surg Allied Technol. 1993;1(4):224–9.
4. Germer CT, Roggan A, Ritz JP, Isbert C, Albrecht D, Müller G, et al. Optical properties of native and coagulated human liver tissue and liver metastases in the near infrared range. Lasers Surg Med. 1998;23(4):194–203.
5. Heisterkamp J, van Hillegersberg R, Ijzermans JN. Interstitial laser coagulation for hepatic tumours. Br J Surg. 1999;86(3):293–304.
6. Nikfarjam M, Muralidharan V, Malcontenti-Wilson C, Christophi C. Progressive microvascular injury in liver and colorectal liver

metastases following laser induced focal hyperthermia therapy. Lasers Surg Med. 2005;37(1):64–73.
7. Ritz JP, Lehmann KS, Zurbuchen U, Knappe V, Schumann T, Buhr HJ, et al. Ex vivo and in vivo evaluation of laser-induced thermotherapy for nodular thyroid disease. Lasers Surg Med. 2009;41(7):479–86.
8. Piana S, Riganti F, Froio E, Andrioli M, Pacella CM, Valcavi R. Pathological findings of thyroid nodules after percutaneous laser ablation: a series of 22 cases with cyto-histological correlation. Endocr Pathol. 2012;23(2):94–100.
9. Ritz JP, Roggan A, Isbert C, Müller G, Buhr HJ, Germer CT. Optical properties of native and coagulated porcine liver tissue between 400 and 2400 nm. Lasers Surg Med. 2001;29(3):205–12.
10. Hegedus L. Therapy: a new nonsurgical therapy option for benign thyroid nodules? Nat Rev Endocrinol. 2009;5(9):476–8.
11. Baek JH, Lee JH, Valcavi R, Pacella CM, Rhim H, Na DG. Thermal ablation for benign thyroid nodules: radiofrequency and laser. Korean J Radiol. 2011;12(5):525–40.
12. Gharib H, Hegedüs L, Pacella CM, Baek JH, Papini E. Clinical review: nonsurgical, image-guided, minimally invasive therapy for thyroid nodules. J Clin Endocrinol Metab. 2013;98(10):3949–57.
13. Haugen BR, Alexander EK, Bible KC, Doherty GM, Mandel SJ, Nikiforov YE, et al. 2015 American Thyroid Association management guidelines for adult patients with thyroid nodules and differentiated thyroid cancer: the American Thyroid Association guidelines task force on thyroid nodules and differentiated thyroid cancer. Thyroid. 2016;26(1):1–133.
14. Gharib H, Papini E, Paschke R, Duick DS, Valcavi R, Hegedüs L, AACE/AME/ETA Task Force on Thyroid Nodules, et al. American Association of Clinical Endocrinologists, Associazione Medici Endocrinologi, and European Thyroid Association medical guidelines for clinical practice for the diagnosis and management of thyroid nodules. Endocr Pract. 2010;16(Suppl 1):1–43.
15. Gharib H, Papini E, Garber JR, Duick DS, Harrell RM, Hegedüs L. American Association of Clinical Endocrinologists, American College of Endocrinology, and Associazione Medici Endocrinologi medical guidelines for clinical practice for the diagnosis and management of thyroid nodules – 2016 update. Endocr Pract. 2016;22(5):622–39.

16. Pacella CM, Bizzarri G, Guglielmi R, Anelli V, Bianchini A, Crescenzi A, et al. Thyroid tissue: US-guided percutaneous interstitial laser ablation-a feasibility study. Radiology. 2000;217(3):673–7.
17. Døssing H, Bennedbaek FN, Karstrup S, Hegedüs L. Benign solitary solid cold thyroid nodules: US-guided interstitial laser photocoagulation—initial experience. Radiology. 2002;225(1):53–7.
18. Pacella CM, Bizzarri G, Spiezia S, Bianchini A, Guglielmi R, Crescenzi A, et al. Thyroid tissue: US-guided percutaneous laser thermal ablation. Radiology. 2004;232(1):272–80.
19. Papini E, Guglielmi R, Bizzarri G, Pacella CM. Ultrasound-guided laser thermal ablation for treatment of benign thyroid nodules. Endocr Pract. 2004;10(3):276–83.
20. Cakir B, Topaloglu O, Gul K, Agac T, Aydin C, Dirikoc A, et al. Effects of percutaneous laser ablation treatment in benign solitary thyroid nodules on nodule volume, thyroglobulin and anti-thyroglobulin levels, and cytopathology of nodule in 1 yr follow-up. J Endocrinol Investig. 2006;29(10):876–84.
21. Amabile G, Rotondi M, De Chiara G, Silvestri A, Di Filippo B, Bellastella A, et al. Low-energy interstitial laser photocoagulation for treatment of nonfunctioning thyroid nodules: therapeutic outcome in relation to pretreatment and treatment parameters. Thyroid. 2006;16(8):749–55.
22. Døssing H, Bennedbaek FN, Hegedüs L. Effect of ultrasound-guided interstitial laser photocoagulation on benign solitary solid cold thyroid nodules: one versus three treatments. Thyroid. 2006;16(8):763–8.
23. Valcavi R, Riganti F, Bertani A, Formisano D, Pacella CM. Percutaneous laser ablation of cold benign thyroid nodules. A three-year follow-up in 122 patients. Thyroid. 2010;20(11):1253–61.
24. Døssing H, Bennedbæk FN, Hegedüs L. Long-term outcome following interstitial laser photocoagulation of benign cold thyroid nodules. Eur J Endocrinol. 2011;165(1):123–8.
25. Amabile G, Rotondi M, Pirali B, Dionisio R, Agozzino L, Lanza M, et al. Interstitial laser photocoagulation for benign thyroid nodules: time to treat large nodules. Lasers Surg Med. 2011;43(8):797–803.
26. Gambelunghe G, Fede R, Bini V, Monacelli M, Avenia N, D'Ajello M, et al. Ultrasound-guided interstitial laser ablation for thyroid nodules is effective only at high total amounts

of energy: results from a three-year pilot study. Surg Innov. 2013;20(4):345–50.
27. Achille G, Zizzi S, Di Stasio E, Grammatica A, Grammatica L. Ultrasound-guided percutaneous laser ablation in treating symptomatic solid benign thyroid nodules: our experience in 45 patients. Head Neck. 2016;38(5):677–82.
28. Pacella CM, Mauri G, Achille G, Barbaro D, Bizzarri G, De Feo P, et al. Outcomes and risk factors for complications of laser ablation for thyroid nodules: a Multicenter study on 1531 patients. J Clin Endocrinol Metab. 2015;100(10):3903–10.
29. Negro R, Salem TM, Greco G. Laser ablation is more effective for spongiform than solid thyroid nodules. A 4-year retrospective follow-up study. Int J Hyperth. 2016;32(7):822–8.
30. Døssing H, Bennedbaek FN, Hegedüs L. Beneficial effect of combined aspiration and interstitial laser therapy in patients with benign cystic thyroid nodules: a pilot study. Br J Radiol. 2006;79(948):943–7.
31. Døssing H, Bennedbæk FN, Hegedüs L. Interstitial laser photocoagulation (ILP) of benign cystic thyroid nodules—a prospective randomized trial. J Clin Endocrinol Metab. 2013;98(7):E1213–7.
32. Døssing H, Bennedbaek FN, Hegedüs L. Ultrasound-guided interstitial laser photocoagulation of an autonomous thyroid nodule: the introduction of a novel alternative. Thyroid. 2003;13(9):885–8.
33. Spiezia S, Vitale G, Di Somma C, Pio Assanti A, Ciccarelli A, Lombardi G, et al. Ultrasound-guided laser thermal ablation in the treatment of autonomous hyperfunctioning thyroid nodules and compressive nontoxic nodular goiter. Thyroid. 2003;13(10):941–7.
34. Barbaro D, Orsini P, Lapi P, Pasquini C, Tuco A, Righini A, et al. Percutaneous laser ablation in the treatment of toxic and pretoxic nodular goiter. Endocr Pract. 2007;13(1):30–6.
35. Cakir B, Gul K, Ugras S, Ersoy R, Topaloglu O, Agac T, et al. Percutaneous laser ablation of an autonomous thyroid nodule: effects on nodule size and histopathology of the nodule 2 years after the procedure. Thyroid. 2008;18(7):803–5.
36. Rotondi M, Amabile G, Leporati P, Di Filippo B, Chiovato L. Repeated laser thermal ablation of a large functioning thyroid nodule restores euthyroidism and ameliorates constrictive symptoms. J Clin Endocrinol Metab. 2009;94(2):382–3.

37. Chianelli M, Bizzarri G, Todino V, Misischi I, Bianchini A, Graziano F, et al. Laser ablation and 131-iodine: a 24-month pilot study of combined treatment for large toxic nodular goiter. J Clin Endocrinol Metab. 2014;99(7):E1283–6.
38. Negro R, Greco G. Large multinodular toxic goiter: is surgery always necessary? Case Rep Endocrinol. 2016;2016:1320827.
39. Døssing H, Bennedbaek FN, Hegedüs L. Effect of ultrasound-guided interstitial laser photocoagulation on benign solitary solid cold thyroid nodules – a randomised study. Eur J Endocrinol. 2005;152(3):341–5.
40. Papini E, Guglielmi R, Bizzarri G, Graziano F, Bianchini A, Brufani C, et al. Treatment of benign cold thyroid nodules: a randomized clinical trial of percutaneous laser ablation versus levothyroxine therapy or follow-up. Thyroid. 2007;17(3):229–35.
41. Døssing H, Bennedbaek FN, Bonnema SJ, Grupe P, Hegedüs L. Randomized prospective study comparing a single radioiodine dose and a single laser therapy session in autonomously functioning thyroid nodules. Eur J Endocrinol. 2007;157(1):95–100.
42. Gambelunghe G, Fatone C, Ranchelli A, Fanelli C, Lucidi P, Cavaliere A, et al. A randomized controlled trial to evaluate the efficacy of ultrasound-guided laser photocoagulation for treatment of benign thyroid nodules. J Endocrinol Investig. 2006;29(9):RC23–6.
43. Papini E, Rago T, Gambelunghe G, Valcavi R, Bizzarri G, Vitti P, et al. Long-term efficacy of ultrasound-guided laser ablation for benign solid thyroid nodules. Results of a three-year multicenter prospective randomized trial. J Clin Endocrinol Metab. 2014;99(10):3653–9.
44. Cakir B, Gul K, Ersoy R, Topaloglu O, Korukluoglu B. Subcapsular hematoma complication during percutaneous laser ablation to a hypoactive benign solitary thyroid nodule. Thyroid. 2008;18(8):917–8.
45. Di Rienzo G, Surrente C, Lopez C, Quercia R. Tracheal laceration after laser ablation of nodular goitre. Interact Cardiovasc Thorac Surg. 2012;14(1):115–6.
46. Valcavi R, Stecconi Bortolani G, Riganti F, Pacella C. Thyroid spongiform nodules are the best candidates for percutaneous laser ablation. A 5 year follow-up study in 72 patients. Presented at 15th International & 14th European Congress of Endocrinology, 2012, Florence, Italy. Endocrine Abstracts 29 OC2.5.

47. Valcavi R, Frasoldati A. Ultrasound-guided percutaneous ethanol injection therapy in thyroid cystic nodules. Endocr Pract. 2004;10(3):269–75.
48. Durante C, Montesano T, Torlontano M, Attard M, Monzani F, Tumino S, et al. Papillary thyroid cancer: time course of recurrences during post surgery surveillance. Clin Endocrinol Metab. 2013;98(2):636–42.
49. Samaan NA, Schultz PN, Hickey RC, Goepfert H, Haynie TP, Johnston DA, et al. The results of various modalities of treatment of well differentiated thyroid carcinomas: a retrospective review of 1599 patients. J Clin Endocrinol Metab. 1992;75(3):714–20.
50. Papini E, Bizzarri G, Bianchini A, Valle D, Misischi I, Guglielmi R, et al. Percutaneous ultrasound-guided laser ablation is effective for treating selected nodal metastases in papillary thyroid cancer. J Clin Endocrinol Metab. 2013;98(1):E92–7.
51. Mauri G, Cova L, Tondolo T, Ierace T, Baroli A, Di Mauro E, et al. Percutaneous laser ablation of metastatic lymph nodes in the neck from papillary thyroid carcinoma: preliminary results. J Clin Endocrinol Metab. 2013;98(7):E1203–7.
52. Zhou W, Zhang L, Zhan W, Jiang S, Zhu Y, Xu S. Percutaneous laser ablation for treatment of locally recurrent papillary thyroid carcinoma <15 mm. Clin Radiol. 2016;71(12):1233–9. https://doi.org/10.1016/j.crad.2016.07.010.
53. Mauri G, Cova L, Ierace T, Baroli A, Di Mauro E, Pacella CM, et al. Treatment of metastatic lymph nodes in the neck from papillary thyroid carcinoma with percutaneous laser ablation. Cardiovasc Intervent Radiol. 2016;39(7):1023–30. https://doi.org/10.1007/s00270-016-1313-6.
54. Valcavi R, Piana S, Bortolan GS, Lai R, Barbieri V, Negro R. Ultrasound-guided percutaneous laser ablation of papillary thyroid microcarcinoma: a feasibility study on three cases with pathological and immunohistochemical evaluation. Thyroid. 2013;23(12):1578–82.
55. Baloch ZW, LiVolsi VA, Asa SL, Rosai J, Merino MJ, Randolph G, et al. Diagnostic terminology and morphologic criteria for cytologic diagnosis of thyroid lesions: a synopsis of the National Cancer Institute thyroid fine-needle aspiration state of the science conference. Diagn Cytopathol. 2008;36(6):425–37.
56. Andrioli M, Riganti F, Pacella CM, Valcavi R. Long-term effectiveness of ultrasound-guided laser ablation of hyperfunctioning

parathyroid adenomas: present and future perspectives. AJR Am J Roentgenol. 2012;199(5):1164–8.
57. Ha EJ, Baek JH, Lee JH. The efficacy and complications of radiofrequency ablation of thyroid nodules. Curr Opin Endocrinol Diabetes Obes. 2011;18(5):310–4.
58. Na DG, Lee JH, Jung SL, Kim JH, Sung JY, Shin JH, Korean Society of Thyroid Radiology (KSThR); Korean Society of Radiology, et al. Radiofrequency ablation of benign thyroid nodules and recurrent thyroid cancers: consensus statement and recommendations. Korean J Radiol. 2012;13(2):117–25.
59. Garberoglio R, Aliberti C, Appetecchia M, Attard M, Boccuzzi G, Boraso F, et al. Radiofrequency ablation for thyroid nodules: which indications? The first Italian opinion statement. J Ultrasound. 2015;18(4):423–30.
60. Korkusuz Y, Erbelding C, Kohlhase K, Luboldt W, Happel C, Grünwald F. Bipolar radiofrequency ablation of benign symptomatic thyroid nodules: initial experience. Rofo. 2016;188(7):671–5.
61. Li XL, Xu HX, Lu F, Yue WW, Sun LP, Bo XW, et al. Treatment efficacy and safety of ultrasound-guided percutaneous bipolar radiofrequency ablation for benign thyroid nodules. Br J Radiol. 2016;89(1059):2015085. https://doi.org/10.1259/bjr.20150858.
62. Kohlhase KD, Korkusuz Y, Gröner D, Erbelding C, Happel C, Luboldt W, et al. Bipolar radiofrequency ablation of benign thyroid nodules using a multiple overlapping shot technique in a 3-month follow-up. Int J Hyperth. 2016;32(5):511–6. https://doi.org/10.3109/02656736.2016.1149234.
63. Spiezia S, Garberoglio R, Di Somma C, Deandrea M, Basso E, Limone PP, et al. Efficacy and safety of radiofrequency thermal ablation in the treatment of thyroid nodules with pressure symptoms in elderly patients. J Am Geriatr Soc. 2007;55(9):1478–9.
64. Deandrea M, Limone P, Basso E, Mormile A, Ragazzoni F, Gamarra E, et al. US-guided percutaneous radiofrequency thermal ablation for the treatment of solid benign hyperfunctioning or compressive thyroid nodules. Ultrasound Med Biol. 2008;34(5):784–91.
65. Spiezia S, Garberoglio R, Milone F, Ramundo V, Caiazzo C, Assanti AP, et al. Thyroid nodules and related symptoms are stably controlled two years after radiofrequency thermal ablation. Thyroid. 2009;19(3):219–25.

66. Baek JH, Moon WJ, Kim YS, Lee JH, Lee D. Radiofrequency ablation for the treatment of autonomously functioning thyroid nodules. World J Surg. 2009;33(9):1971–7.
67. Shin JH, Baek JH, Ha EJ, Lee JH. Radiofrequency ablation of thyroid nodules: basic principles and clinical application. Int J Endocrinol. 2012;2012:919650.
68. Valcavi R, Tsamatropoulos P. Health-related quality of life after percutaneous radiofrequency ablation of cold, solid, benign thyroid nodules: a 2-year follow-up study in 40 patients. Endocr Pract. 2015;21(8):887–96.
69. Deandrea M, Sung JY, Limone P, Mormile A, Garino F, Ragazzoni F, et al. Efficacy and safety of radiofrequency ablation versus observation for nonfunctioning benign thyroid nodules: a randomized controlled international collaborative trial. Thyroid. 2015;25(8):890–6.
70. Baek JH, Lee JH, Sung JY, Bae JI, Kim KT, Sim J, et al. Korean Society of Thyroid Radiology. Complications encountered in the treatment of benign thyroid nodules with US-guided radiofrequency ablation: a multicenter study. Radiology. 2012;262(1):335–42.
71. Ha EJ, Baek JH, Lee JH. Ultrasonography-based thyroidal and perithyroidal anatomy and its clinical significance. Korean J Radiol. 2015;16(4):749–66.
72. Ha EJ, Baek JH, Lee JH, Kim JK, Shong YK. Clinical significance of vagus nerve variation in radiofrequency ablation of thyroid nodules. Eur Radiol. 2011;21(10):2151–7.
73. Shin JH, Jung SL, Baek JH, Kim JH. Rupture of benign thyroid tumors after radio-frequency ablation. AJNR Am J Neuroradiol. 2011;32(11):2165–9.
74. Chehade JM, Silverberg AB, Kim J, Case C, Mooradian AD. Role of repeated fine-needle aspiration of thyroid nodules with benign cytologic features. Endocr Pract. 2001;7(4):237–43.
75. Illouz F, Rodien P, Saint-André JP, Triau S, Laboureau-Soares S, Dubois S, et al. Usefulness of repeated fine-needle cytology in the follow-up of non-operated thyroid nodules. Eur J Endocrinol. 2007;156(3):303–8.
76. Kwak JY, Koo H, Youk JH, Kim MJ, Moon HJ, Son EJ, et al. Value of US correlation of a thyroid nodule with initially benign cytologic results. Radiology. 2010;254(1):292–300.
77. Piana S, Frasoldati A, Ferrari M, Valcavi R, Froio E, Barbieri V, et al. Is a five-category reporting scheme for thyroid fine needle aspiration cytology accurate? Experience of over 18,000

FNAs reported at the same institution during 1998–2007. Cytopathology. 2011;22(3):164–73.
78. Kim YS, Rhim H, Tae K, Park DW, Kim ST. Radiofrequency ablation of benign cold thyroid nodules: initial clinical experience. Thyroid. 2006;16(4):361–7.
79. Fuller CW, Nguyen SA, Lohia S, Gillespie MB. Radiofrequency ablation for treatment of benign thyroid nodules: systematic review. Laryngoscope. 2014;124(1):346–53.
80. Bandeira-Echtler E, Bergerhoff K, Richter B. Levothyroxine or minimally invasive therapies for benign thyroid nodules. Cochrane Database Syst Rev. 2014;6:CD004098.
81. Chen F, Tian G, Kong D, Zhong L, Jiang T. Radiofrequency ablation for treatment of benign thyroid nodules: a PRISMA-compliant systematic review and meta-analysis of outcomes. Medicine (Baltimore). 2016;95(34):e4659.
82. Bernardi S, Dobrinja C, Fabris B, Bazzocchi G, Sabato N, Ulcigrai V, et al. Radiofrequency ablation compared to surgery for the treatment of benign thyroid nodules. Int J Endocrinol. 2014;2014:934595.
83. Che Y, Jin S, Shi C, Wang L, Zhang X, Li Y, Baek JH. Treatment of benign thyroid nodules: comparison of surgery with radiofrequency ablation. AJNR Am J Neuroradiol. 2015;36(7):1321–5.
84. Baek JH, Kim YS, Lee D, Huh JY, Lee JH. Benign predominantly solid thyroid nodules: prospective study of efficacy of sonographically guided radiofrequency ablation versus control condition. AJR Am J Roentgenol. 2010;194(4):1137–42.
85. Faggiano A, Ramundo V, Assanti AP, Fonderico F, Macchia PE, Misso C, et al. Thyroid nodules treated with percutaneous radiofrequency thermal ablation: a comparative study. J Clin Endocrinol Metab. 2012;97(12):4439–45.
86. Wong KP, Lang BH. Use of radiofrequency ablation in benign thyroid nodules: a literature review and updates. Int J Endocrinol. 2013;2013:428363.
87. Turtulici G, Orlandi D, Corazza A, Sartoris R, Derchi LE, Silvestri E, et al. Percutaneous radiofrequency ablation of benign thyroid nodules assisted by a virtual needle tracking system. Ultrasound Med Biol. 2014;40(7):1447–52.
88. Cesareo R, Pasqualini V, Simeoni C, Sacchi M, Saralli E, Campagna G, et al. Prospective study of effectiveness of ultrasound-guided radiofrequency ablation versus control group in patients affected by benign thyroid nodules. J Clin Endocrinol Metab. 2015;100(2):460–6.

89. Ugurlu MU, Uprak K, Akpinar IN, Attaallah W, Yegen C, Gulluoglu BM. Radiofrequency ablation of benign symptomatic thyroid nodules: prospective safety and efficacy study. World J Surg. 2015;39(4):961–8.
90. De Bernardi IC, Floridi C, Muollo A, Giacchero R, Dionigi GL, Reginelli A, et al. Vascular and interventional radiology radiofrequency ablation of benign thyroid nodules and recurrent thyroid cancers: literature review. Radiol Med. 2014;119(7):512–20.
91. Jeong WK, Baek JH, Rhim H, Kim YS, Kwak MS, Jeong HJ, et al. Radiofrequency ablation of benign thyroid nodules: safety and imaging follow-up in 236 patients. Eur Radiol. 2008;18(6):1244–50.
92. Huh JY, Baek JH, Choi H, Kim JK, Lee JH. Symptomatic benign thyroid nodules: efficacy of additional radiofrequency ablation treatment session-prospective randomized study. Radiology. 2012;263(3):909–16.
93. Lim HK, Lee JH, Ha EJ, Sung JY, Kim JK, Baek JH. Radiofrequency ablation of benign non-functioning thyroid nodules: 4-year follow-up results for 111 patients. Eur Radiol. 2013;23(4):1044–9.
94. Dobrinja C, Bernardi S, Fabris B, Eramo R, Makovac P, Bazzocchi G, et al. Surgical and pathological changes after radiofrequency ablation of thyroid nodules. Int J Endocrinol. 2015;2015:576576.
95. Ha EJ, Baek JH, Lee JH, Sung JY, Lee D, Kim JK, et al. Radiofrequency ablation of benign thyroid nodules does not affect thyroid function in patients with previous lobectomy. Thyroid. 2013;23(3):289–93.
96. Ji Hong M, Baek JH, Choi YJ, Lee JH, Lim HK, Shong YK, et al. Radiofrequency ablation is a thyroid function-preserving treatment for patients with bilateral benign thyroid nodules. J Vasc Interv Radiol. 2015;26(1):55–61.
97. Andrioli M, Valcavi R. The peculiar ultrasonographic and elastographic features of thyroid nodules after treatment with laser or radiofrequency: similarities and differences. Endocrine. 2014;47(3):967–8.
98. Sung JY, Kim YS, Choi H, Lee JH, Baek JH. Optimum first-line treatment technique for benign cystic thyroid nodules: ethanol ablation or radiofrequency ablation? AJR Am J Roentgenol. 2011;196(2):W210–4.
99. Sung JY, Baek JH, Kim KS, Lee D, Yoo H, Kim JK, Park SH. Single-session treatment of benign cystic thyroid nodules

with ethanol versus radiofrequency ablation: a prospective randomized study. Radiology. 2013;269(1):293–300.
100. Baek JH, Ha EJ, Choi YJ, Sung JY, Kim JK, Shong YK. Radiofrequency versus ethanol ablation for treating predominantly cystic thyroid nodules: a randomized clinical trial. Korean J Radiol. 2015;16(6):1332–40.
101. Lee JH, Kim YS, Lee D, Choi H, Yoo H, Baek JH. Radiofrequency ablation (RFA) of benign thyroid nodules in patients with incompletely resolved clinical problems after ethanol ablation (EA). World J Surg. 2010;34(7):1488–93.
102. Jang SW, Baek JH, Kim JK, Sung JY, Choi H, Lim HK, et al. How to manage the patients with unsatisfactory results after ethanol ablation for thyroid nodules: role of radiofrequency ablation. Eur J Radiol. 2012;81(5):905–10.
103. Baek JH, Jeong HJ, Kim YS, Kwak MS, Lee D. Radiofrequency ablation for an autonomously functioning thyroid nodule. Thyroid. 2008;18(6):675–6.
104. Sung JY, Baek JH, Jung SL, Kim JH, Kim KS, Lee D, et al. Radiofrequency ablation for autonomously functioning thyroid nodules: a multicenter study. Thyroid. 2015;25(1):112–7.
105. Dupuy DE, Monchik JM, Decrea C, Pisharodi L. Radiofrequency ablation of regional recurrence from well-differentiated thyroid malignancy. Surgery. 2001;130(6):971–7.
106. Monchik JM, Donatini G, Iannuccilli J, Dupuy DE. Radiofrequency ablation and percutaneous ethanol injection treatment for recurrent local and distant well-differentiated thyroid carcinoma. Ann Surg. 2006; 244(2):296–304.
107. Baek JH, Kim YS, Sung JY, Choi H, Lee JH. Locoregional control of metastatic well-differentiated thyroid cancer by ultrasound-guided radiofrequency ablation. AJR Am J Roentgenol. 2011;197(2):W331–6.
108. Park KW, Shin JH, Han BK, Ko EY, Chung JH. Inoperable symptomatic recurrent thyroid cancers: preliminary result of radiofrequency ablation. Ann Surg Oncol. 2011;18(9):2564–8.
109. Shin JE, Baek JH, Lee JH. Radiofrequency and ethanol ablation for the treatment of recurrent thyroid cancers: current status and challenges. Curr Opin Oncol. 2013;25(1):14–9.
110. Lee SJ, Jung SL, Kim BS, Ahn KJ, Choi HS, Lim DJ, et al. Radiofrequency ablation to treat loco-regional recurrence of well-differentiated thyroid carcinoma. Korean J Radiol. 2014;15(6):817–26.

111. Wang L, Ge M, Xu D, Chen L, Qian C, Shi K, et al. Ultrasonography-guided percutaneous radiofrequency ablation for cervical lymph node metastasis from thyroid carcinoma. J Cancer Res Ther. 2014;10(Suppl):C144–9.
112. Lim HK, Baek JH, Lee JH, Kim WB, Kim TY, Shong YK, et al. Efficacy and safety of radiofrequency ablation for treating locoregional recurrence from papillary thyroid cancer. Eur Radiol. 2015;25(1):163–70.
113. Kim JH, Yoo WS, Park YJ, Park do J, Yun TJ, Choi SH, et al. Efficacy and safety of radiofrequency ablation for treatment of locally recurrent thyroid cancers smaller than 2 cm. Radiology. 2015;276(3):909–18.
114. Kim HS, Choi BH, Park JR, Hahm JR, Jung JH, Kim SK, et al. Delayed surgery for parathyroid adenoma misdiagnosed as a thyroid nodule and treated with radiofrequency ablation. Endocrinol Metab (Seoul). 2013;28(3):231–5.
115. Xu SY, Wang Y, Xie Q, Wu HY. Percutaneous sonography guided radiofrequency ablation in the management of parathyroid adenoma. Singap Med J. 2013;54(7):e137–40.
116. Kim BS, Eom TI, Kang KH, Park SJ. Radiofrequency ablation of parathyroid adenoma in primary hyperparathyroidism. J Med Ultrason (2001). 2014;41(2):239–43.
117. Carrafiello G, Laganà D, Mangini M, Dionigi G, Rovera F, Carcano G, et al. Treatment of secondary hyperparathyroidism with ultrasonographically guided percutaneous radiofrequency thermoablation. Surg Laparosc Endosc Percutan Tech. 2006;16(2):112–6.
118. Lupo MA. Radiofrequency ablation for benign thyroid nodules – a look towards the future of interventional thyroidology. Endocr Pract. 2015;21(8):972–4.

Chapter 14
Percutaneous Ethanol Injection (PEI) for Thyroid Cysts and Other Neck Lesions

Andrea Frasoldati, Petros Tsamatropoulos, and Daniel S. Duick

Introduction

Percutaneous ethanol injection (PEI) is an ultrasound (US)-guided technique deployed to achieve a chemical ablation (based on the sclerosing effects of alcohol) of benign and malignant thyroid lesions [1, 2]. Originally proposed for sclerotherapy of hepatocellular carcinoma, hepatic, and renal

A. Frasoldati, MD, PhD (✉)
Endocrinology Unit, Medical Specialities Department, Arcispedale S. Maria Nuova – IRCCS, Reggio Emilia, Italy
e-mail: andrea.frasoldati@asmn.re.it; andrea.frasoldati@gmail.com

P. Tsamatropoulos, MD
Endocrinology Unit, Centro Palmer, Reggio Emilia, Italy

D.S. Duick, MD, MACE
University of Arizona College of Medicine, Phoenix, AZ, USA

Endocrinology Associates, PA, Scottsdale, AZ, USA

D.S. Duick et al. (eds.), *Thyroid and Parathyroid Ultrasound and Ultrasound-Guided FNA*,
https://doi.org/10.1007/978-3-319-67238-0_14

cysts [3–5], PEI was soon applied to the treatment of parathyroid hyperplasia in patients with chronic renal failure [6, 7] and of autonomously functioning nodules as well as cystic lesions in the thyroid gland [8–14]. Once instilled into the tissues, ethanol exerts rapid toxic effects, with coagulative necrotic changes and fibrosis triggered by cell dehydration and protein denaturation. Tissue damage is amplified by ischemic changes secondary to small vessel thrombosis, as shown by histological evidence of hemorrhagic infarcts and fibrosis [15, 16]. From a terminological perspective, alcohol or ethanol ablations are frequently used synonyms for PEI [1, 2].

Today, PEI sclerotherapy is unanimously recognized as the first-line treatment of benign thyroid cysts which recur after initial drainage, whereas its utility in the management of solid thyroid nodules has progressively declined [17, 18]. Hence, PEI treatment of thyroid cysts will be the main focus of the present chapter. Ethanol ablation of other neck lesions (e.g., thyroglossal duct cysts, hyperplastic parathyroid, and metastatic lymph nodes) will also be concisely addressed.

PEI of Thyroid Cystic Nodules: Clinical Results

Cystic thyroid nodules may correspond to "pure" colloidal cysts or, far more frequently, to "mixed" nodules, which feature a significant fluid component, usually an inhomogeneous collection of colloid, blood, and cell debris (Fig. 14.1) [19]. Most thyroid cystic nodules are indolent and asymptomatic; nevertheless, the sudden occurrence of a thyroid hemorrhagic cyst is usually revealed by a visible neck lump and may be accompanied by tenderness, if not overt pain, and other pressure symptoms. Hoarseness and dysphagia may be observed in a minority of cases. Although these lesions may recede either spontaneously or after drainage of the fluid by fine needle aspiration (FNA), they frequently tend to recur [20–23]. We have gleaned from studies comparing ethanol sclerotherapy to FNA alone that the chance of a stable regression is at least

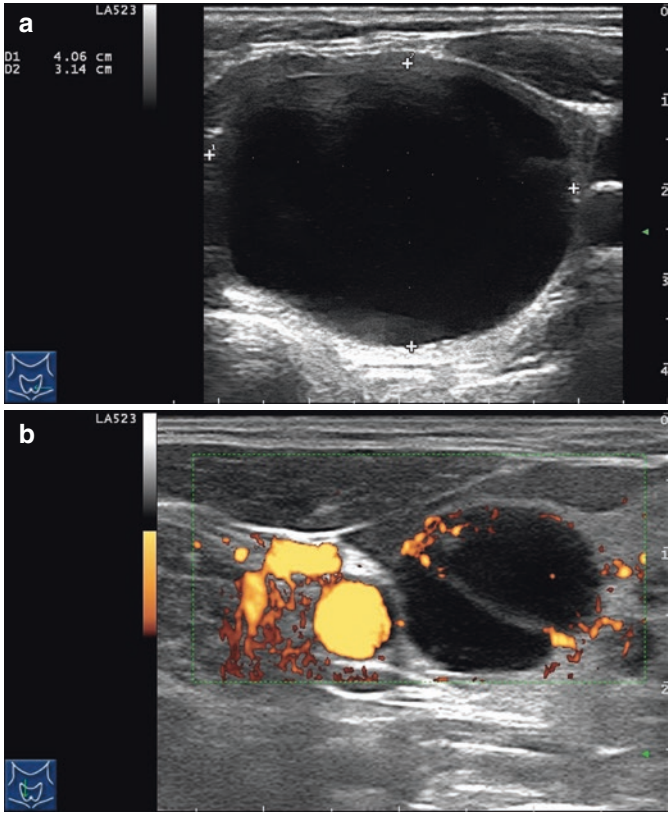

Figure 14.1 Types of cystic and mixed thyroid nodules: (**a**) a unilocular, "pure" thyroid cyst of the left lobe that appears anechoic (B-mode US, transverse view); (**b**) a multilocular (in this case bilocular), complex thyroid cyst of the right lobe with an internal septation (power Doppler US, transverse view); (**c**) a right thyroid cyst with solid and vascularized wall (color Doppler US, transverse view); (**d**) a left, hemorrhagic thyroid cyst (color Doppler US, transverse view on the left, sagittal view on the right); (**e**) a right, mixed thyroid nodule 50% solid, 50% cystic (B-mode US, transverse view on the left, sagittal view on the right); (**f**) a right, predominantly solid, mixed thyroid nodule (B-mode US, transverse view on the left, sagittal view on the right); (**g**) a left, predominantly cystic, mixed thyroid nodule (B-mode US, transverse view on the left, sagittal view on the right). All these types of thyroid nodules, except from the predominantly solid mixed type (**f**), are good candidates for PEI

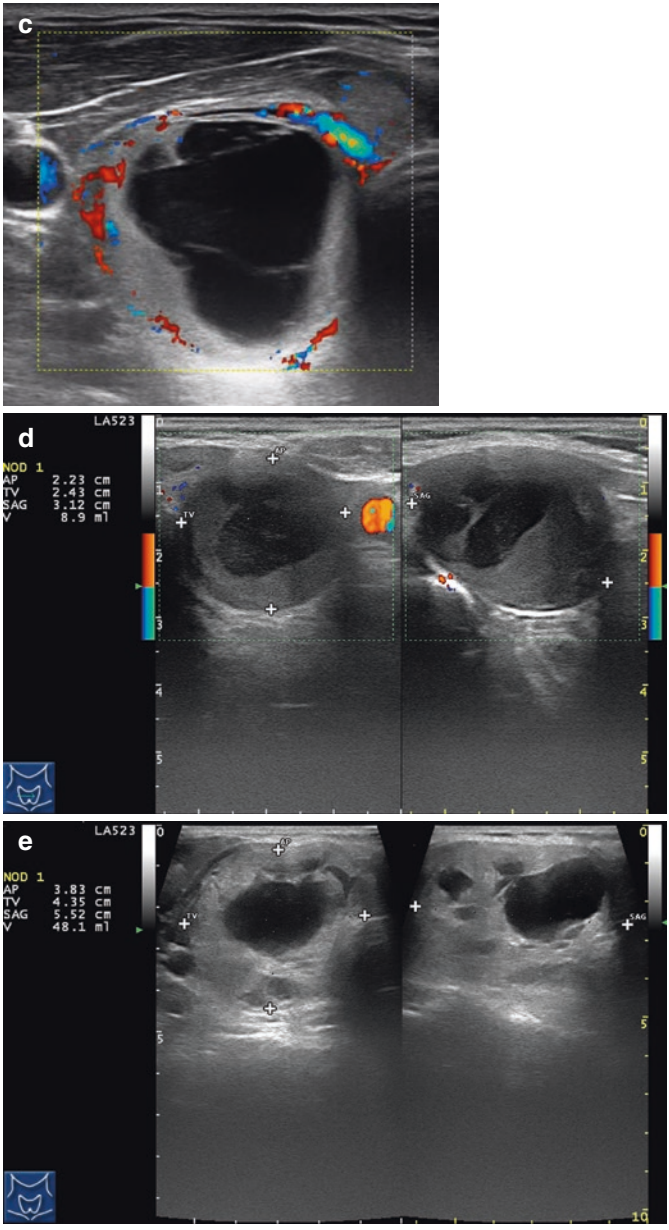

Figure 14.1 (continued)

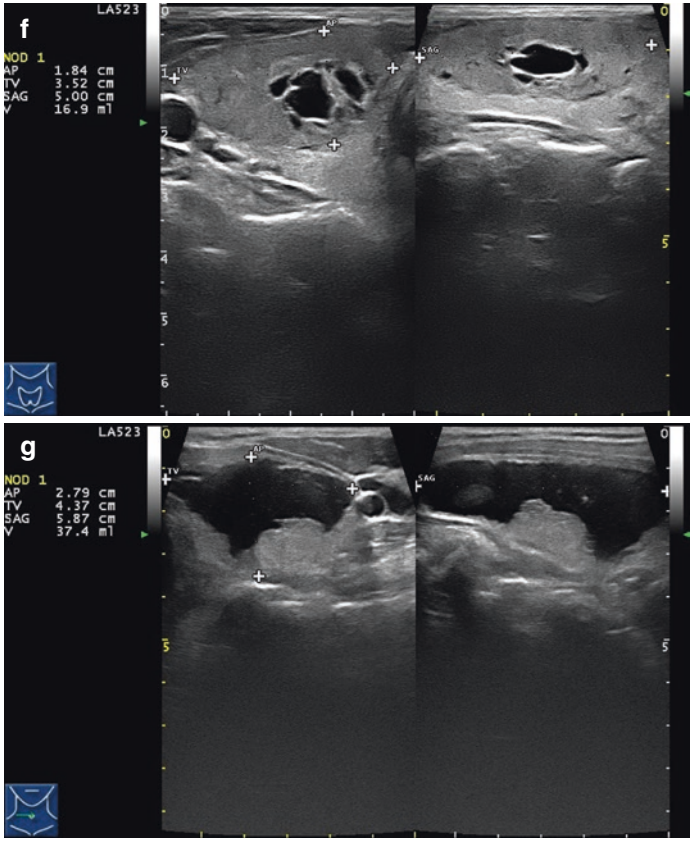

Figure 14.1 (continued)

doubled after PEI [24–26] (Fig. 14.2). The results of ethanol injection vs. isotonic saline flushing, both followed by fluid aspiration, were compared in a randomized prospective study: after a 6-month surveillance, PEI achieved a 82% cure rate, whereas saline infusion was successful in less than 50% of treated subjects [25]. Importantly, the beneficial effects of PEI are long-lasting, as the recurrence rate is minimal: 3.4% and 6.5% over 5 and 10 years, respectively [27, 28].

Clinical studies focused on PEI treatment of thyroid cystic nodules have consistently demonstrated that alcohol ablation achieves a significant volume reduction, ranging in most series

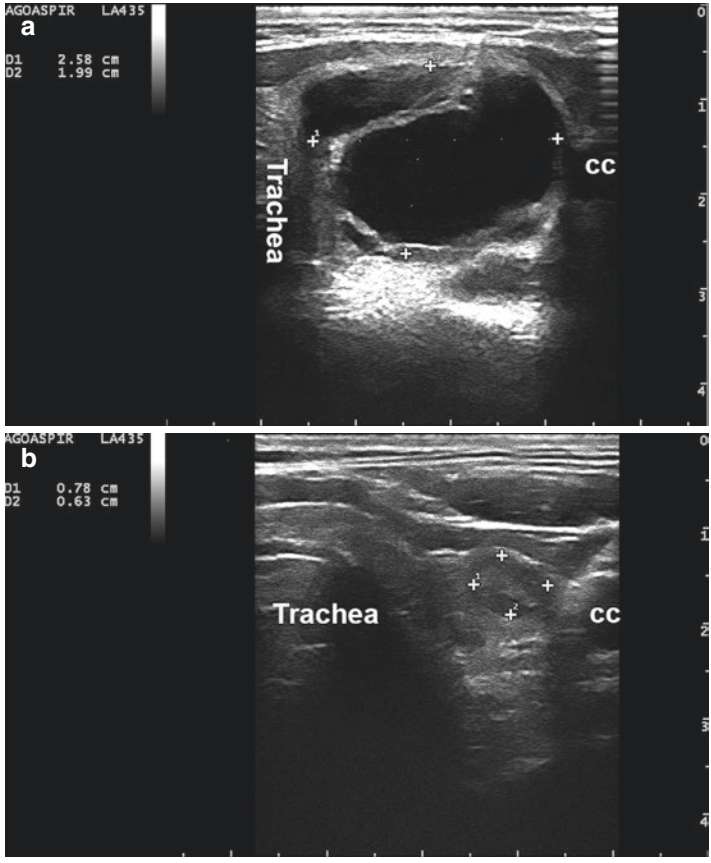

FIGURE 14.2 A complex thyroid cyst (calipers) before (**a**) and 6 months after (**b**) percutaneous ethanol injection. *cc*, common carotid artery

between 65% and 90%. Accordingly, the procedure is expected to attain a ≥50% reduction of thyroid cyst volume in the large majority (70–95%) of patients [14, 21, 22, 25–33]. The consistency of PEI results is supported by reports from numerous different centers and authors over the last two decades, notwithstanding minor variations of the technique [14, 21, 22, 25–33] (Table 14.1). The preference of alcohol versus other sclerosing agents, e.g., tetracycline, polydecanol, arginine

Table 14.1 PEI sclerotherapy in thyroid cystic nodules: clinical outcome

	Patients	Mean follow-up (months)	Mean volume at baseline (mL)	Number of PEI sessions	Mean volume reduction (%)	Success rate (%)[a]
Yasuda et al. [13]	61	6	n.r.	1–3	n.r.	72.1
Monzani et al. [21]	20	12	~12.0	1–2	n.r.	95
Verde et al. [14]	32	12	14.5 (1.5–65.8)	n.r.	71	75
Antonelli et al. [22]	26	12	16.8 ± 9.9	1–5 (mean 2.5)	n.r.	77
Zingrillo et al. [30]	43	37.0 ± 14.0	38.4 (4.8–166)	1–4 (mean 1.5)	91.9	93
Cho et al. [40]	22 (13/9)	3.5 (1–10)	13.0 (3.5–42.0)	1–6	64.0	68.1
Del Prete et al. [27]	98	120 ± 14	35.2 ± 20	1–4 (mean 1.8)	59.9	93.8
Kim et al. [29]	20	4.4 (1–6)	15.7 (12.0–48.6)	1–3 (mean 1.8)	64.0	65.0
Bennedbaek et al. [25]	33 (26/7)	6	8.0 (5.0–14.0)	1–3	100[b]	82.0
Valcavi et al. [26]	135	12	19.0 ± 19.0	1–3	85.6[b]	n.r.
Guglielmi et al. [28]	58	82	13.7 ± 14.0	2.2 ± 1.3	86.6	86.2
Lee et al. [31]	432	36.5 ± 12.9	15.6 ± 12.6	1–7 (mean 2.3)	66.1	79.4

(continued)

Table 14.1 (continued)

	Patients	Mean follow-up (months)	Mean volume at baseline (mL)	Number of PEI sessions	Mean volume reduction (%)	Success rate (%)[a]
Kanotra et al. [32]	40 (24/16)	13.8 ± 5	12.2 (5.8–18.5)	1–3 (mean 1.5)	70.0	85.0
Sung et al. [33]	36	17.0 ± 7.46	13.8 ± 11.9	1–2 (mean 1.2)	93.0	94.4
Kim et al. [42, 43]	217	6.0 ± 5.6	15.7 ± 18.1	1–3	85.2	90.3
In et al. 2015	62	14.1 (12–24)	7.2 mL (1.3–54.1)	1–2	n.r.	81.3
Reverter et al. [38]	30	2.1 ± 1.4	18.2 ± 15.5	1–3	85.9	100
Suh et al. [44]	107	17.1 ± 12.2	20.8 ± 31.1	1–2	61.6	61.7

[a]Success rate defined in most studies a ≥50% volume reduction
[b]Median volume reduction

hydrochloride, and sodium tetradecyl sulfate [34–37], resides in its safety and affordability: the cost of the material is negligible, and the procedure may be repeated several times, if needed. In addition to measuring the cyst volume before and after ethanol instillation, the outcomes of PEI may be evaluated on clinical ground. Amelioration of pressure symptoms and cosmetic complaints is the rule, being recorded in about 75–95% of patients treated with PEI [24]. The measurement of the volume of the lesion before and after treatment provides an objective parameter, while the clinical outcome usually relies on subjective evaluations. In a recent Spanish study, a comprehensive ten-item questionnaire investigating goiter symptoms was proposed to the patients: each item was defined by a 1–5 score, and a final sum was calculated [38]. In another recent study from Korea, subjective pressure symptoms were rated on a 10-cm visual analog scale by the patients, while a 1–4 grade cosmetic score was attributed by the physician [33].

Three major determinants are known to negatively impact the success of the procedure: (a) an exceedingly large volume (e.g., ≥40–50 mL) of the lesion; (b) a mixed instead of a "pure" anechoic cystic structure; and (c) a thick and dense, as opposed to a watery, content of the cyst. The first two potential limitations, both likely to preclude a thorough and homogeneous alcohol diffusion within the lesion, are easily foreseen, while the third one, which stands as the main obstacle to the drainage phase, cannot always be anticipated before performing the procedure. In order to avoid this latter issue, the viscosity of the cystic content is usually assessed during the diagnostic fine needle aspiration which precedes the PEI procedure. This information is used to select the optimal needle gauge for aspiration. As a general rule, US evidence of echoic particles which, under the gentle pressure of the probe, float across the anechoic space like snowflakes under a gust of wind ("snow-globe" effect) is a reliable index of a watery, quite fluid content of the lesion, likely to allow an easy and complete drainage. Alternatively, when the fluid content is highly viscous, there may be insufficient withdrawal

of material to ensure an adequate volume of the ethanol reinstillation within the lesion [39].

Very large cystic nodules may represent a challenging target because the PEI procedure usually turns out to be more difficult on practical ground: longer time is required for the drainage as well as the instillation phases to be carried out, and the compliance of the patient may be compromised by the prolonged duration of the procedure. Furthermore, an even and complete distribution of the ethanol on the inner surface of the cyst may not be optimally accomplished. Nevertheless, according to the available evidence, an inverse correlation between cyst volume and success rate of PEI procedure has not been conclusively demonstrated [25, 30–32, 40]. Far more convincing and concordant among different studies are the evidence collected on the role of the nodule structure as a major factor determining the final outcome of PEI treatment. While "pure" cystic nodules may achieve an impressive (>90%) volume decrease, similar results are usually not achieved in case of "mixed" nodules [39, 41–44]; and the latter are also more likely to require multiple PEI sessions. In order to achieve a successful treatment of this kind of lesion, a two-step approach has recently been proposed, based on an initial PEI session focused on the cystic component and a second PEI procedure performed 1 month later on the solid portion of the nodule [45].

Alcohol Ablation of Thyroid Cystic Lesions: The Technique

The patient is requested to lie in a supine position, with a pillow placed under the shoulders in order to ensure an adequate hyperextension of the neck. The neck area is prepped with an antibacterial/sterilizing solution; a sterile blanket is deployed over the patient's chest; sterile gloves are worn by the operators; and the use of sterile gel and probe covers are utilized during US-guided procedures. The patient's eyes may be sheltered from the risk of accidental contact with alcohol by a pair of protective glasses. Local anesthesia is optional

and can be beneficial when larger (e.g., 16–18 gauge) needles are required. The selection of the needle size is a crucial step in order to ensure a fast and complete drainage of the fluid; as a general rule, most cystic lesions can be emptied using 20- to 23-gauge needles, and larger needles are to be reserved to extremely viscous lesions. At our hospital, we routinely use a 22-gauge spinal needle initially and move to a larger caliber stylus needle when suggested by the circumstances (Fig. 14.3).

For didactical purposes, PEI is generally described as the succession of four phases: (a) insertion of the needle, (b) drainage of the cyst content, (c) injection of ethanol into the lesion, and (d) needle extraction. All the above listed phases should be performed under US guidance, with a constant attention to the positioning of the needle tip (Fig. 14.4a, b). Sometimes, before PEI, pericapsular anesthesia with lidocaine is performed (Fig. 14.4c).

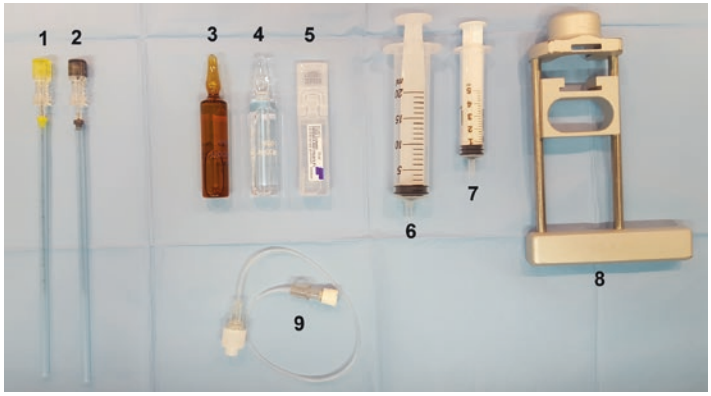

Figure 14.3 Equipment for the ethanol ablation of a thyroid cyst: (**1**) a 20-gauge spinal needle with stylet, (**2**) a 22-gauge spinal needle with stylet, (**3**) 2% lidocaine for local anesthesia (seldom necessary), (**4**) 95% sterile alcohol, (**5**) saline solution for washing the needle at the end of the procedure, (**6**) a 20 mL syringe for alcohol injection, (**7**) a 5 mL syringe for the administration of lidocaine in case of local anesthesia, (**8**) a pistol syringe holder for applying negative aspiration pressure, and (**9**) a flexible extension tube for connecting the hub of the needle to the tip of syringe

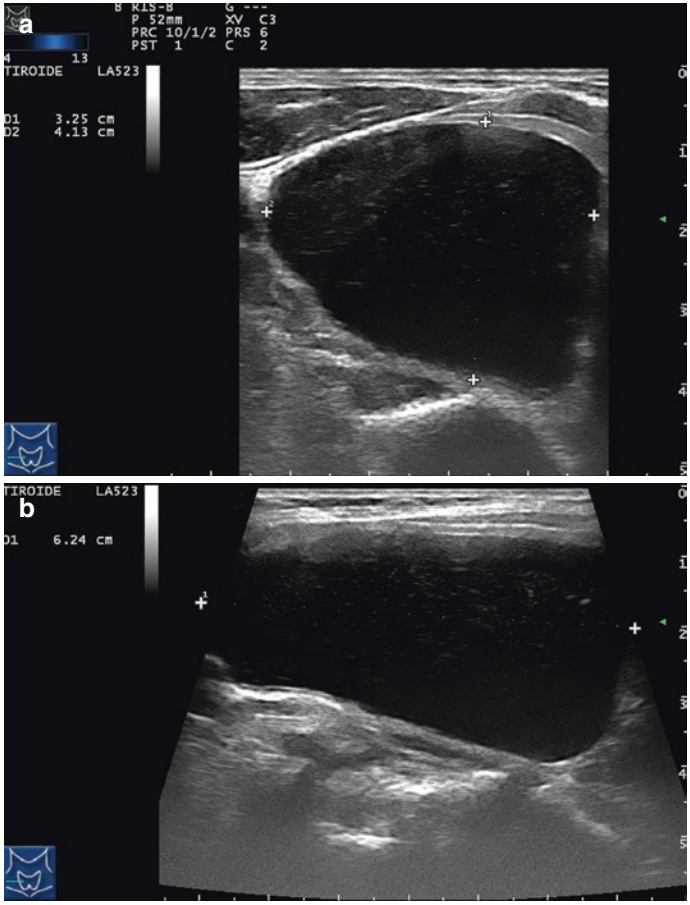

FIGURE 14.4 US-guided PEI of a thyroid cyst. (**a**) Basal US image of a right lobe thyroid cyst (B-mode, transverse view). (**b**) Basal US image of the right lobe thyroid cyst (B-mode, longitudinal view). (**c**) Pericapsular anesthesia with a 27-gauge needle (*arrow*). (**d**) Needle insertion into the cyst. (**e**) Aspiration of fluid content of the cyst (longitudinal view). (**f**) Aspiration continues and the cyst shrinks—tip of the needle (*arrow*)—(transverse view). (**g**) Thyroid cyst immediately before ethanol injection—tip of the needle (*arrow*)—(transverse view). (**h**) Ethanol instillation—ethanol is visible as hyperechoic material (*arrows*). (**i**) The thyroid cyst is filled with an amount of ethanol equal to 50% of the aspirated liquid volume. (**j**) The thyroid cyst at the end of the procedure

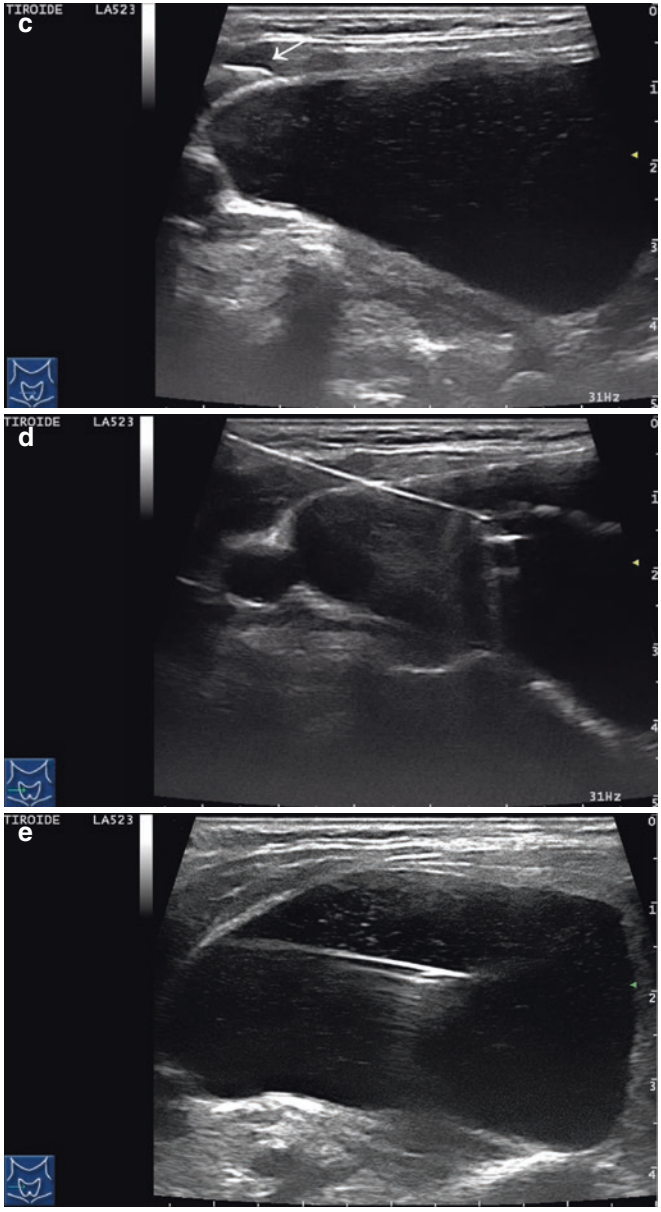

FIGURE 14.4 (continued)

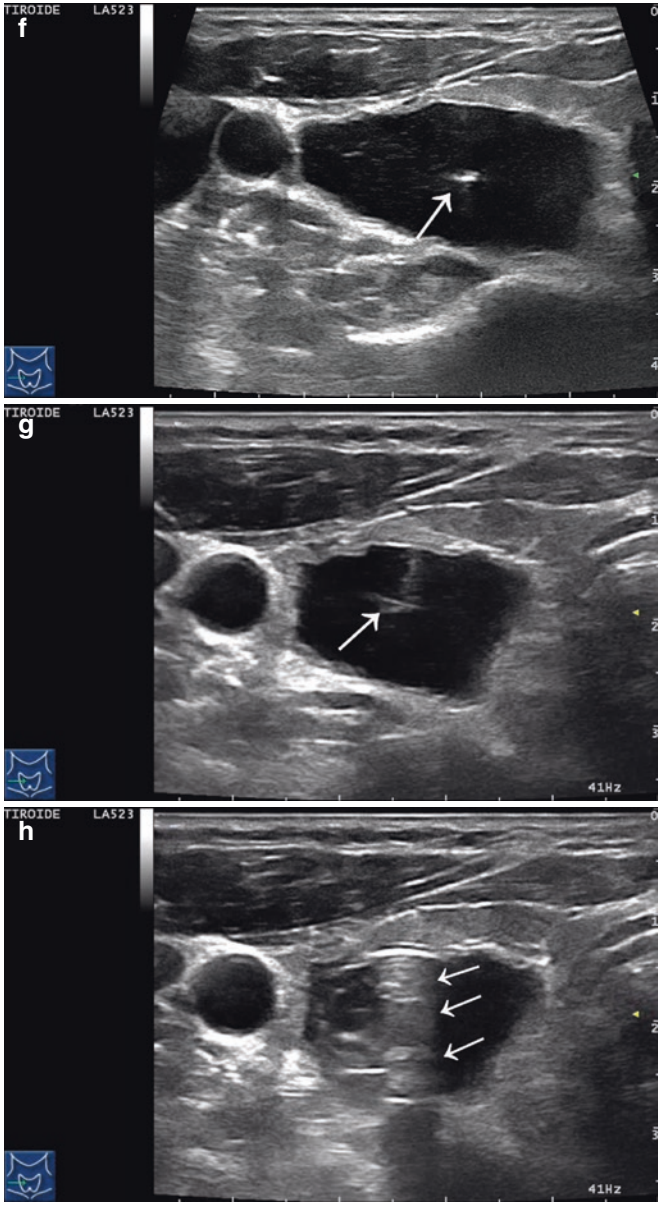

Figure 14.4 (continued)

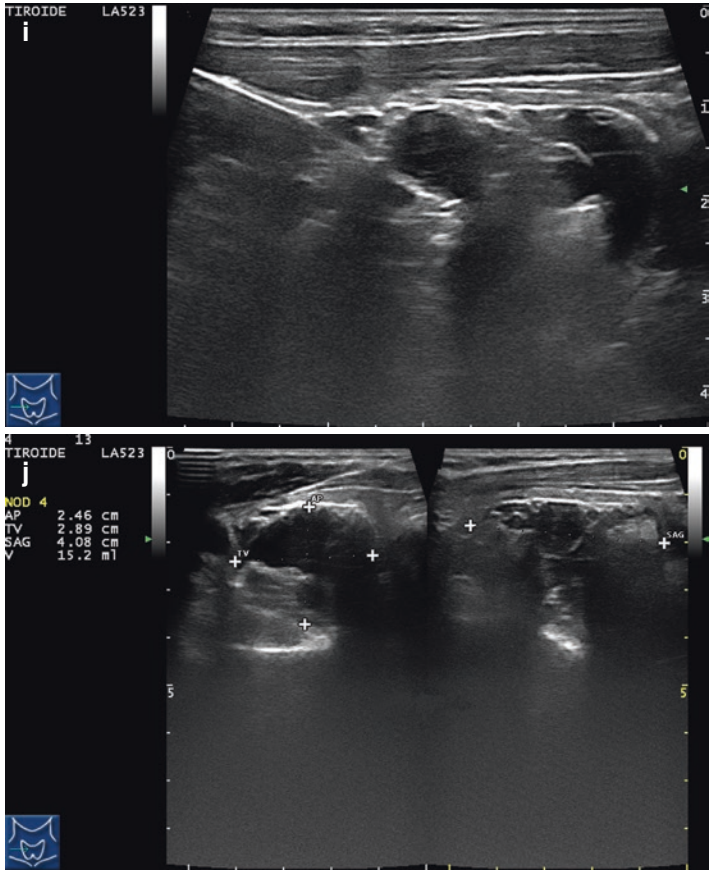

Figure 14.4 (continued)

Insertion of the Needle

In analogy with the different techniques for needle insertion suggested for FNA (see Chap. 12), this phase may be accomplished according to two basically different approaches: either the needle is inserted through a guiding device mounted on the US transducer, or it is directed "free-hand" into the lesion according to a perpendicular or a parallel approach. The needle should always be kept under visual

control by gentle adjustments of the transducer (Fig. 14.4d), which can be held by the first operator or by an assistant as well. According to the reported outcomes, neither procedure can be claimed as clearly superior to the other: the adoption of a guiding device usually makes the operator more confident, and fast, throughout the injection phase, whereas the free-hand technique permits continuous repositioning of the needle along different spatial axes. It should also be considered that, once the needle has been inserted, the guiding device can be removed thus warranting a full-range motion of the needle.

Drainage of the Fluid Content

As soon as the stylet (if used) is removed, the fluid rapidly reaches the needle hub ready to spill out. A 20 mL syringe connected through a catheter (20–25 cm length) allows a smooth and effortless drainage of the fluid content and preserves the needle from the risk of being misplaced under the strain forces induced by traction as well by the deformation of the cyst along the drainage phase (Fig. 14.4e–g). The use of two devices may quite effectively facilitate this phase: a pistol syringe holder and a catheter connecting the needle and the syringe. Both devices contribute to easing the drainage of the fluid content, as well as the subsequent alcohol injection; at the same time, the connecting tube prevents the transmission of abrupt traction and strain movements to the needle.

It should be kept in mind that voluminous cysts may need to be emptied with more than 1–2 syringes, and all the potentially necessary materials and devices should always be at full disposal of the operators. In case of large lesions as well as dense, viscous cyst content and longer duration of the procedure may lead to the occlusion of the needle. This inconvenience may be obviated by reaming the needle with a stylet. Although the attention of the less experienced operators tends to be maximally focused on the insertion of the needle, while the drainage phase is usually perceived as less troublesome, this is quite a delicate step, likely to influence the full

success of the procedure. Ideally, the fluid should be aspirated at a constant, slow speed, while keeping the needle tip under visual control: the progressive reduction of the cavity volume may frequently cause the needle tip to be plugged up by the cyst walls, which would require its gentle repositioning. In addition, an excessive energy applied to the suction may lead to capillary hemorrhage, causing a real-time refilling of the cyst. Operators facing the ascending phase of their learning curve should refrain from draining the fluid content to the last drop, as the visualization of the needle tip is easier if a small anechoic remnant of the cyst is left.

When the content of the cyst is made of viscous colloid not readily susceptible to drainage, a two-step approach is traditionally recommended: a small (e.g., 1–2 mL) volume of ethanol is injected with the aim of modifying the physicochemical properties of the material and the aspiration is postponed (1–4 weeks) [46, 47]. According to our experience, this strategy is almost invariably rewarding. Another, quite more cumbersome, approach is based on the use of a 16-gauge needle connected to a suction pump working at a 10–100 mmHg vacuum. In case the drainage is still ineffective, the 16-gauge needle may be substituted with an 8.5-French pigtail catheter. Once the fluid has been successfully drained, the ethanol is injected through the same device and after 10 min completely removed [48]. More recently, an open-window needle likely to drain quite dense material has been proposed for treating the most viscous cysts [49].

Ethanol Instillation

The injection of ethanol into the cyst should always be performed with extreme caution: the keystone which should guide this part of the PEI procedure is that the maneuver should be interrupted as soon as either resistance against further instillation is perceived by the operator in charge of injecting the alcohol, or the patient starts complaining of a sudden, burning pain. The access of the ethanol into the anechoic structure of the cyst is easily appreciated at US as a

hyperechoic dense material refilling the anechoic space of the cyst (Fig. 14.4h). The lack of resistance to the injection and the progressive volume gain of the cyst indicate that ethanol is being correctly instilled inside the lesion. Similar as in the drainage phase, the prolongation of the ethanol instillation may cause the obstruction of the needle thus requiring the action of reaming. The central issue of the instillation phase deals with the calculation of the right amount of ethanol to be injected. As regards to this issue, there are no absolute rules to follow nor exact formulas to apply: in general, the quantity of ethanol required roughly corresponds in most procedures to the 50% of the total drained fluid (Fig. 14.4i). Taking this principle as a standard guideline, the operators should be prepared to adapt to the various circumstances and factors which may limit, or alternatively broaden, the volume of the instilled ethanol. In other terms, the onset of a major resistance to further injection, not amenable to be counteracted by repositioning of the needle tip, may require to stop the maneuver, irrespectively of the fact that the ideal quantity of ethanol has not yet been instilled. On the contrary, if the PEI procedure goes smoothly, with the patient fully compliant and the needle tip under optimal visual control, the amount of alcohol may exceed the theoretical target. Although the maximum amount of ethanol usually required for sclerotherapy of most thyroid cysts is <10–15 mL, larger volumes (e.g., up to 30 mL) can be occasionally used. Once the instillation phase is ended, two different modalities are available: (a) leave all the injected ethanol inside the lesion in order to permit the sclerosing properties of the agent to be exerted throughout the following days and (b) drain all the injected alcohol after a short while (e.g., 3–10 min). Apparently, these two alternative approaches share similar results and an identical safety profile [50]. The theoretical advantage of the latter strategy, likely to make the procedure slightly more complicated and time-consuming, resides in the reduced exposition of tissues to ethanol leakage. In addition, when dealing with a large cyst refilled with a conspicuous amount of ethanol, the reabsorption of the agent may be less than

complete preventing a fully satisfactory reduction of the lesion size. Again, we would recommend avoiding dogmatic position in favor of or against each of the above-described techniques but rather try and verify both of them in the clinical practice in order to determine the most suitable and effective approach for each individual case.

Needle Extraction

Once the injection phase is ended, the needle should be rapidly extracted in order to minimize the contact of subcutaneous tissues with the tract of the needle dunked into the alcohol (Fig. 14.4j). This part of the procedure is usually the most painful for the patient but is fortunately transient, lasting usually less than 30 and sometimes up to 60 s: having the needle tip rinsed with a small amount of saline before being extracted may attenuate the subsequent transient, yet intense, pain. Systematic placement of an ice pack may reduce the risk of minor bleeding.

Side Effects

PEI of thyroid cystic nodules is a safe procedure: no major side effects are usually seen, and this evidence, consistently reported in all published series [24], is well asserted by the worldwide diffusion of this technique. Nevertheless, the relative safety of the procedure should not generate an excess of confidence in the operators: although the risk of recurrent laryngeal nerve (RLN) injury is exceedingly low, a maximum level of alertness should be always observed during the various phases of the treatment, and hazardous behaviors, such as the prolonged instillation of ethanol while there is a progression of resistance to the injection, should always be avoided. Normally, the integrity of the fibrous capsule of the cyst ensures that ethanol is fully contained within the lesion making its leakage into the perinodular tissues unlikely. Yet, even

if every detail concerning the position of the needle, as well as the pressure transmitted back to the syringe, is in order, the occurrence of an intense pain suddenly signaled by the patient should prompt the operator to immediately stop the procedure. Only few data are available regarding factors possibly correlated to a higher risk of laryngeal nerve palsy: according to two studies, the larger the ethanol dose used, the higher the probability of dysphonia [25]. As previously mentioned, needle extraction is followed by a mild to moderate pain which typically lasts a minute and sometimes longer. Pain usually is described as radiating to the mandible angle or to the ear, and more seldom to the shoulder, to the chest or to the dorsal region. In order to alleviate painfulness associated with needle extraction, we suggest rinsing the needle with saline before extraction. On empiric basis, this simple expedient seems to some extent effective in reducing, although not completely preventing, the onset of pain.

Solid "Hot" and "Cold" Benign Thyroid Nodules

PEI was first been proposed for the treatment of patients with autonomously functioning thyroid nodules (AFTNs) in the early 1990s [8–11, 51]. As reported by many published studies, mostly Italian groups, the initial results were quite encouraging. Successful outcomes both in terms of recovery of normal thyroid function and in terms of volume decrease (about 60–90%) of the lesion [8, 9, 11, 52–54] occurred in about nine out of ten of the treated subjects, with the best results achieved in patients with subclinical as compared to overt hyperthyroidism [54] smaller nodules (e.g., <20–40 mL volume) and in complex nodules, versus more reports of suboptimal outcomes when treating solid "hot" nodules [28, 55–57]. Unfortunately, PEI effects in AFTN proved to be only temporary with hyperthyroidism recurring in about 15–35% of the patients [58, 59]. This evidence is in line with the observation

that studies based on thyroid scintiscan showed a persisting enhanced uptake by the nodular tissue in a large fraction (35–50%) of the autonomously functioning nodules treated with PEI [60, 61].

In addition to the disappointing results recorded by studies based on prolonged surveillance periods, two other major limitations have also transpired leading to a general loss of enthusiasm toward the utility of PEI in AFTNs. Firstly, treatment was time-consuming with multiple sessions (often as many as 5–10 sessions) of treatment required in the vast majority of patients. Secondly, at deep variance with the results of PEI applied to cystic nodules, PEI treatment of AFTNs was not devoid of important side effects. Laryngeal nerve palsy was recorded in most series, ranging from 0.7 to about 4.0% [53, 56, 59]. Moreover, a number of occasional serious adverse events (e.g., ipsilateral facial dysesthesia, transient Horner's syndrome, septic complications, jugular vein thrombosis, and severe thyrotoxicosis) have also been reported [62, 63]. Multimodal therapeutic strategies based on the combination of PEI and radioiodine ^{131}I and/or other interventional techniques have been proposed in patients with large AFTNs in more recent years in order to limit the therapeutic dose of ^{131}I, with promising results [60].

PEI may achieve a significant volume decrease also in nonfunctioning solid thyroid nodules as shown by retrospective studies and a prospective randomized trial comparing ethanol injection and l-thyroxine (LT4) administration [31, 64, 65]. As for AFTNs, multiple PEI sessions are needed, and volume reduction is achieved at the expense of a not negligible rate of adverse events [6, 29, 66]. For this reasons, and in light of the expanding use of other interventional techniques (e.g., laser thermal ablation or radio frequency) likely to provide more consistent results, the role of PEI in the treatment of solid cold nodules is to be restricted to anecdotal situations, not susceptible to other, more effective treatment [17, 18, 24, 67, 68].

PEI in Cystic and Solid Lesions of the Parathyroid Glands

PEI has long been used for sclerotherapy of PT hyperplasia in patients with chronic renal failure and secondary (or tertiary) hyperparathyroidism (HPT), with the first published studies in the 1980s [6, 7]. Although the management of HPT in patients with end-stage renal disease can now benefit from medical treatment, many patients still become refractory to drug therapy, thus requiring surgery or alternative options. Postsurgical recurrence of HPT can also occur quite frequently in these patients [69, 70]. It has been shown that PEI is effective in controlling HPT in this clinical setting: after PEI, PTH levels markedly decrease in parallel with amelioration of hypercalcemia with no major complications, although cases of transient mild dysphonia or "hoarseness" have been reported [69–72]. Therefore, PEI treatment in patients with secondary or tertiary HPT has not yet become obsolete [73]. Preferential candidates for PEI are patients at high surgical risk with frankly elevated PTH levels (300–1500 pg/mL) and less than all four (e.g., 1–2) grossly enlarged, hyperplastic PT glands [73]. In primary hyperparathyroidism, PEI has been tried in cases of patients exhibiting contraindications to surgery, with a reported 30% cure rate, to be weighed against the rare occurrence of transient dysphonia [74, 75]. Therefore, in analogy with what has been said for PEI in AFTNs, today PEI does not stand as a first-line option for sporadic primary HPT. Interestingly, PEI has been recently revived in patient with multiple endocrine neoplasia type 1 and recurrent HPT [76].

Ethanol sclerotherapy of "solid" PT lesions is usually performed through multiple (e.g., 3–5) sessions, using 23–25-gauge needles, with small amounts of ethanol, corresponding to 50–85% of the PT volume, injected in each single procedure, under real-time US monitoring. Ethanol should be slowly injected with extreme caution, due to the high risk of its dispersion into surrounding tissues with potential chemical damage to the recurrent laryngeal nerve. The procedure is usually considered successful in

case the typically hypoechoic parathyroid texture changes to hyperechoic following ethanol injection.

Cystic lesions of PT origin usually correspond to "functionally silent" parathyroid cysts, which derive from embryological remnants [77, 78] (Fig. 14.5). However, the chance of a large hyperfunctioning PT adenoma presenting with a dominant cystic portion should always be ruled out. Typically, at

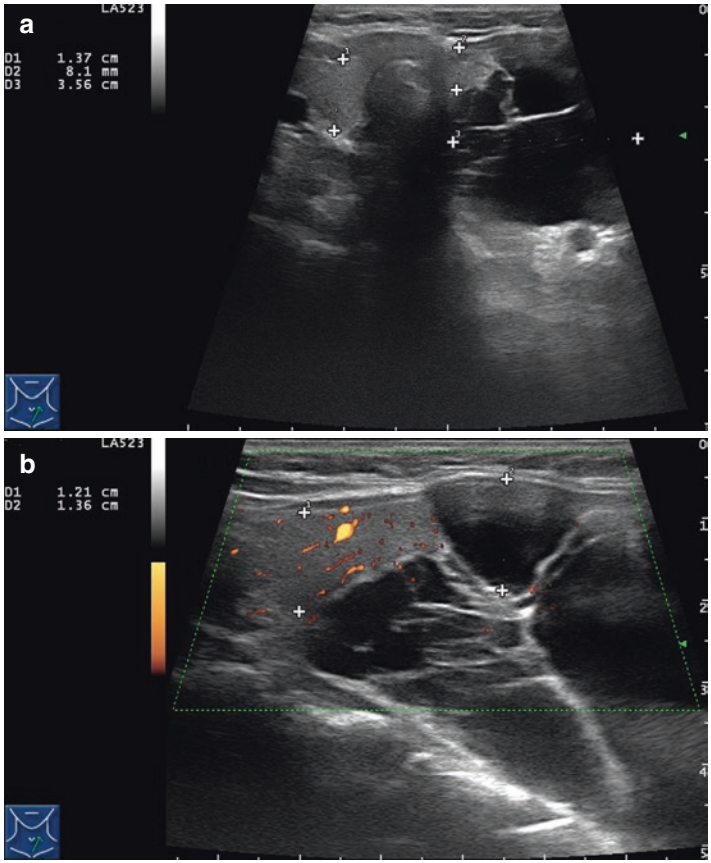

FIGURE 14.5 A large, left, inferior, complex, parathyroid cyst in B-mode US, transverse view (**a**) and in color Doppler US, longitudinal view (**b**)

closer US examination, PT adenomas show a solid, highly vascularized component, while PT cysts have a pure anechoic US appearance, due to a colorless and "clear water" fluid content, which has been [79–81]. Due to their deep position, below the thyroid lobes and partially included in the upper mediastinum, PT cysts are usually incidentally found during a neck US or a CT scan, being often initially misdiagnosed as voluminous thyroid cystic nodules [81, 82]. Although most patients are asymptomatic, pressure symptoms (e.g., dysphagia, cough, hiccups) may occur. The correct diagnosis is achieved by US-guided FNA completed with parathyroid hormone (PTH) assay in the needle washout [82, 83]. After drainage by FNA, PT cysts tend to recur; and in this case, PEI may offer an alternative option to surgery [69, 84–86]. The technique of PEI for parathyroid cysts is identical to the one described above for thyroid cysts, with careful attention and enhanced vigilance to avoid any alcohol leakage due to the adjacency to the laryngeal nerve.

PEI in Neck Metastasis from Thyroid Cancer

PEI of cervical lymphadenopathy was originally introduced in 1993 at Mayo Clinic, Rochester, MN, as a palliative therapy for patients with advanced thyroid cancer already submitted to multiple surgical procedures and/or radioiodine sessions [87, 88]. PEI of metastatic lymph nodes has recently been established as a curative treatment option in patients with neck recurrences, with a near 90% average success rate recorded across different institutions. There is a 16.5–66.0% rate of complete lesion regression and a very low (1.2%) risk of major complications [88–96] (Table 14.2). In light of these data, PEI can be considered a valuable therapeutic option for patients not amenable to second surgery and/or radioiodine therapy. Treatment is performed through administration of small (0.1–3 mL) amount of ethanol, delivered at a variable number of sessions. Since most of the treated lymph nodes feature a solid structure, maximum attention should be paid

Table 14.2 PEI sclerotherapy in thyroid cancer neck recurrences (NR): clinical outcome

	NR (pts)	Mean follow-up (months)	Location (central vs. lateral)	Mean basal volume	Mean volume decrease (%)	Complete regression (%)
Lewis et al. [88]	29 (14)	18 (2–77)	n.r.	492 mm^3	95.9	31.0
Monchik et al. [89]	11 (6)	18.7	1 vs. 10	n.r.	n.r.	n.r.
Lin et al. [90]	24 (16)	24 (13–43)	11 vs. 13	9.9 mm (mean Ø)	37.5–43.5	16.5
Kim et al. [91]	47 (27)	26 (10–38)	7 vs. 40	678.8 mm^3	93.6 ± 12.6	44.7
Heilo et al. [92]	109 (63)	32 (3–72)	49 vs. 60	340 mm^3	n.r.	66.0
Hay et al. [93]	37 (25)	65.0	16 vs. 21	223 mm^3	95.0%	46.0
Guenette et al. [94]	21 (14)	38.5	5 vs. 16	10 mm (mean Ø)	n.r.	69.0°

to prevent ethanol leakage into the surrounding tissues, especially when the target lesion is located in the central neck compartment. Doppler US examination is used to evaluate the short-term response to treatment with reduction of vascularization, while the measurement of serum thyroglobulin (Tg) levels over time provides a reliable index of the clinical outcome [88–96]. Notwithstanding the excellent results reported, PEI therapy should not be viewed as always curative: even in case of marked reduction of the treated lesion, it is not possible to be positive about the complete and definitive eradication of neoplastic cells. While pathologic specimens have been shown to be void of viable cancer cells after PEI [97], microscopic detection of residual cancer cells between fibrotic tissues has also been reported during post-treatment follow-up [90]. Additional studies are awaited to define a definitive role of PEI vs. other interventional techniques in patients with neck recurrences from thyroid cancer [98–100].

Conclusions

Currently, the main application of PEI in thyroid disease refers to sclerotherapy of pure thyroid cysts as well as mixed, predominantly cystic thyroid nodules. In these clinical settings, PEI has been unequivocally shown to achieve excellent results both in terms of volume reduction of the target lesion and in terms of consistency and stability of results. This, at the expense of minimal side effects. Instead, the use of PEI for treating thyroid solid hyperfunctioning nodules has been almost completely abandoned, being relegated to a minor role in the frame of multimodal strategies based on the combined use of radioiodine, PEI, and ablation interventional techniques (e.g., RF, LTA) for exceedingly large nodules in patients at high surgical risk or in patients who refuse surgery.

In addition, PEI has also long been used with good results for treating PT lesions in patients with chronic renal failure

and secondary (tertiary) parathyroid hyperplasia and in patients with primary hyperparathyroidism not candidate to parathyroid surgery. Nevertheless, the adoption of parathyroid ethanol ablation should always be carefully weighed in light of the increase risk of injury to the recurrent laryngeal nerve. In recent years, the use of PEI for neck node metastasis from differentiated thyroid carcinoma has gained increasing interest; although the published series are still limited, satisfactory results have been consistently reported.

References

1. Lubiensky A, Simon M, Helmberger TK. Percutaneous Alcohol Instillation In: Vogl TJ, Helmberger T, Mack MG, Reiser MF, editors. Percutaneous tumor ablation in medical radiology. Berlin Heidelberg: Springer-Verlag; 2008. p. 123–8.
2. Ahmed M, Solbiati L, Brace CL, Breen DJ, Callstrom MR, Charboneau JW, et al. International Working Group on Image-guided Tumor Ablation; Interventional Oncology Sans Frontières Expert Panel; Technology Assessment Committee of the Society of Interventional Radiology; Standard of Practice Committee of the Cardiovascular and Interventional Radiological Society of Europe. Image-guided tumor ablation: standardization of terminology and reporting criteria—a 10-year update. Radiology. 2014;273:241–60.
3. Bean WJ. Renal cysts: treatment with alcohol. Radiology. 1981;138:329–31.
4. Livraghi T, Giorgio A, Marin G, Salmi A, de Sio I, Bolondi L, et al. Hepatocellular carcinoma and cirrhosis in 746 patients: long term results of percutaneous ethanol injection. Radiology. 1985;197:101–8.
5. Bean WJ, Rodan BA. Hepatic cysts: treatment with alcohol. Am J Radiol. 1985;144:237–41.
6. Solbiati L, Giangrande A, De Pra L, Bellotti E, Cantù P, Ravetto C. Percutaneous ethanol injection of parathyroid tumors under US guidance: treatment for secondary hyperparathyroidism. Radiology. 1985;155:607–10.
7. Giangrande A, Castiglioni A, Solbiati L, Allaria P. Ultrasound-guided percutaneous fine-needle ethanol injection into

parathyroid glands in secondary hyperparathyroidism. Nephrol Dial Transplant. 1992;7(5):412–21.
8. Livraghi T, Paracchi A, Ferrari C, Bergonzi M, Garavaglia G, Raineri P, et al. Treatment of autonomous thyroid nodule with percutaneous ethanol injection: preliminary results. Radiology. 1990;175:827–9.
9. Martino E, Murtas ML, Loviselli A, Piga M, Petrini L, Miccoli P, et al. Percutaneous intranodular ethanol injection for treatment of autonomously functioning thyroid nodules. Surgery. 1992;112:1161–5.
10. Goletti O, Monzani F, Caraccio N, Del Guerra P, Lippolis PV, Pucciarelli M, et al. Percutaneous ethanol injection treatment of autonomously functioning single thyroid nodules: optimization of treatment and short term outcome. World J Surg. 1992;16:784–9; discussion 789-90.
11. Papini E, Panunzi C, Pacella CM, Bizzarri G, Fabbrini R, Petrucci L, et al. Percutaneous ultrasound-guided ethanol injection: a new treatment of toxic autonomously functioning thyroid nodules? J Clin Endocrinol Metab. 1993;76:411–6.
12. Rozman B, Bence-Zigman Z, Tomic-Brzac H, Skreb F, Pavlinovic Z, Simonovic I. Sclerosation of thyroid cysts by ethanol. Period Biol. 1989;91:1116–8.
13. Yasuda K, Ozaki O, Sugino K, Yamashita T, Toshima K, Ito K, et al. Treatment of cystic lesions of the thyroid by ethanol instillation. World J Surg. 1992;16:958–61.
14. Verde G, Papini E, Pacella CM, et al. Ultrasound guided percutaneous ethanol injection in the treatment of cystic thyroid nodules. Clin Endocrinol. 1994;41:719–24.
15. Crescenzi A, Papini E, Pacella CM, Rinaldi R, Panunzi C, Petrucci L, et al. Morphological changes in a hyperfunctioning thyroid adenoma after percutaneous ethanol injection: histological, enzymatic and sub-microscopical alterations. J Endocrinol Investig. 1996;19:371–6.
16. Monzani F, Caraccio N, Basolo F, Iacconi P, LiVolsi V, Miccoli P. Surgical and pathological changes after percutaneous ethanol injection therapy of thyroid nodules. Thyroid. 2000;10:1087–92.
17. Gharib H, Papini E, Garber JR, Duick DS, Harrell RM, Hegedüs L, Paschke R, Valcavi R, Vitti P. AACE/ACE/AME Task Force on Thyroid Nodules. American Association of Clinical Endocrinologists (AACE), American College of Endocrinology (ACE), and Associazione Medici Endocrinologi (AME) medical guidelines for clinical practice for the diagnosis

and management of thyroid nodules- 2016 update. Endocr Pract. 2016;22:622–39.
18. Haugen BR, Alexander EK, Bible KC, Doherty GM, Mandel SJ, Nikiforov YE, Pacini F, Randolph GW, Sawka AM, Schlumberger M, Schuff KG, Sherman SI, Sosa JA, Steward DL, Tuttle RM, Wartofsky L. 2015 American Thyroid Association management guidelines for adult patients with thyroid nodules and differentiated thyroid cancer: the American Thyroid Association (ATA) guidelines task force on thyroid nodules and differentiated thyroid cancer. Thyroid. 2016;26(1):1–133.
19. De Los Santos ET, Keyhani-Rofagha S, Cunningham JJ, et al. Cystic thyroid nodules:the dilemma of malignant lesions. Arch Intern Med. 1990;150:422–7.
20. Jensen F, Rasmussen SN. The treatment of thyroid cysts by ultrasonographically-guided fine needle aspiration. Acta Chir Scand. 1976;142:209–11.
21. Monzani F, Lippi F, Goletti O, et al. Percutaneous aspiration and ethanol sclerotherapy for thyroid cysts. J Clin Endocrinol Metab. 1994;78:800–2.
22. Antonelli A, Campatelli A, Di Vito A, et al. Comparison between ethanol sclerotherapy and emptying with injection of saline in treatment of thyroid cysts. Clin Investig. 1994;72(12):971–4.
23. Kim DW. Ultrasound-guided fine-needle aspiration of benign thyroid cysts or partially cystic thyroid nodules: a preliminary study for factors predicting successful collapse. Endocrine. 2014;45:67–72.
24. Bandeira-Echtler E, Bergerhoff K, Richter B. Levothyroxine or minimally invasive therapies for benign thyroid nodules. Cochrane Database Syst Rev. 2014;6:CD004098.
25. Bennedbaek FN, Hegedus L. Treatment of recurrent thyroid cysts with ethanol: a randomized double blind controlled trial. J Clin Endocrinol Metab. 2003;88:5773–7.
26. Valcavi R, Frasoldati A. Ultrasound-guided percutaneous ethanol injection therapy in thyroid cystic nodules. Endocr Pract. 2004;10:269–75.
27. Del Prete S, Caraglia M, Russo D, Vitale G, Giuberti G, Marra M, et al. Percutaneous ethanol injection efficacy in the treatment of large symptomatic thyroid cystic nodules: ten-year follow-up of a large series. Thyroid. 2002;12:815–21.
28. Guglielmi R, Pacella CM, Bianchini A, Bizzarri G, Rinaldi R, Graziano FM, et al. Percutaneous ethanol injection treatment in benign thyroid lesions: role and efficacy. Thyroid. 2004;14:125–31.

29. Kim JH, Lee HK, Lee JH, Ahn IM, Choi CG. Efficacy of sonographically guided percutaneous ethanol injection for treatment of thyroid cysts versus solid thyroid nodules. Am J Roentgenol. 2003;180:1623–726.
30. Zingrillo M, Torlontano M, Chiarella R, et al. Percutaneous ethanol injection may be a definitive treatment for symptomatic thyroid cystic nodules not treatable by surgery: five-year follow-up study. Thyroid. 1999;9:763–7.
31. Lee SJ, Ahn I-M. Effectiveness of percutaneous ethanol injection therapy in benign nodular and cystic thyroid disease: long-term follow-up experience. Endocr J. 2005;52:455–62.
32. Kanotra SP, Lateef M, Kirmani O. Non-surgical management of benign thyroid cysts: use of ultrasound-guided ethanol ablation. Postgrad Med J. 2008;84(998):639–43.
33. Sung JY, Kim YS, Choi H, et al. Optimum first-line treatment technique for benign cystic thyroid nodules: ethanol ablation or radiofrequency ablation. AJR Am J Roentgenol. 2011;196(2):W210–4.
34. Porenta M, Fettich JJ. Treatment of thyroid cysts by sclerosation. Radiobiol Radiother. 1985;26:249–54.
35. Hegedüs L, Hansen JM, Karstrup S, Torp-Pedersen S, Juul N. Tetracycline for sclerosis of thyroid cysts. A randomized study. Arch Intern Med. 1988;148(5):1116–8.
36. Kalra N, Ahuja CK, Dutta P, Rajwanshi A, Mittal BR, Bhansali A, et al. Comparison of sonographically guided percutaneous sodium tetradecyl sulfate injection with ethanol injection in the treatment of benign nonfunctioning thyroid nodules. J Vasc Interv Radiol. 2014;25:1218–24.
37. Zhao Y, Guan X, Liu Y, Liu S, Hussain A, Shi B. The efficacy of percutaneous AHI (arginine hydrochloride injection) for the treatment of recurrent thyroid cysts. Ann Endocrinol. 2015;76:281–5.
38. Reverter JL, Alonso N, Avila M, Lucas A, Mauricio D, Puig-Domingo M. Evaluation of efficacy, safety, pain perception and health-related quality of life of percutaneous ethanol injection as first-line treatment in symptomatic thyroid cysts. BMC Endocr Disord. 2015;15:73.
39. In HS, Kim DW, Choo HJ, Jung SJ, Kang T, Ryu JH. Ethanol ablation of benign thyroid cysts and predominantly cystic thyroid nodules: factors that predict outcome. Endocrine. 2014;46:107–13.

40. Cho YS, Lee HK, Ahn IM, Lim SM, Kim DH, Choi CG, et al. Sonographically guided ethanol sclerotherapy for benign thyroid cysts: results in 22 patients. AJR Am J Roentgenol. 2000;174:213–6.
41. Kim DW, Rho MH, Park HJ, Kwag HJ. Ultrasonography-guided ethanol ablation of predominantly solid thyroid nodules: a preliminary study for factors that predict the outcome. Br J Radiol. 2012;85:930–6.
42. Kim YJ, Baek JH, Ha EJ, Lim HK, Lee JH, Sung JY, et al. Cystic versus predominantly cystic thyroid nodules: efficacy of ethanol ablation and analysis of related factors. Eur Radiol. 2012;22:1573–8.
43. Baek JH, Ha EJ, Choi YJ, Sung JY, Kim JK, Shong YK. Radiofrequency versus ethanol ablation for treating predominantly cystic thyroid nodules: a randomized clinical trial. Korean J Radiol. 2015;16:1332–40.
44. Suh CH, Baek JH, Ha EJ, Choi YJ, Lee JH, Kim JK, et al. Ethanol ablation of predominantly cystic thyroid nodules: evaluation of recurrence rate and factors related to recurrence. Clin Radiol. 2015;70:42–7.
45. Kim DW. Usefulness of two-stage ethanol ablation in the treatment of benign predominantly cystic thyroid nodules. Endocr Pract. 2014;20:548–55.
46. Zingrillo M, Torlantano M, Ghiggi MR, D'Aloiso L, Nirchino V, Bisceglia M, et al. Percutaneous ethanol injection of large thyroid cystic nodules. Thyroid. 1996;6:403–8.
47. Zieleźnik W, Kawczyk-Krupka A, Peszel Barlik M, Cebula W, Sieroń A. Modified percutaneous ethanol injection in the treatment of viscous cystic thyroid nodules. Thyroid. 2005;15:683–7.
48. Sung JY, Baek JH, Kim YS, Jeong HJ, Kwak MS, Lee D, Moon W. One-step ethanol ablation viscous cystic thyroid nodules. AJR. 2008;191:1730–173.
49. Lv G, Chen S, Li B, Chen X, Li S. Efficacy assessment of newly developed open-window intervention needles for the treatment of cystic thyroid nodules that cannot be aspirated. Thyroid. 2014;24:1012–7.
50. Kim DW, Rho MH, Kim HJ, Kwon JS, Sung YS, Lee SW. Percutaneous ethanol injection for benign cystic thyroid nodules: is aspiration of ethanol-mixed fluid advantageous? AJNR Am J Neuroradiol. 2005;26:2122–7.
51. Monzani F, Goletti O, Caraccio N, Del Guerra P, Ferdeghini M, Pucci E, et al. Percutaneous ethanol injection treatment of

autonomous thyroid adenoma: hormonal and clinical evaluation. Clin Endocrinol. 1992;36:491–7.
52. Di Lelio A, Rivolta M, Casati M, Capra M. Treatment of autonomous thyroid nodules: value of percutaneous ethanol injection. Am J Roentgenol. 1995;164:207–13.
53. Ferrari C, Reschini E, Paracchi A. Treatment of the autonomous thyroid nodule: a review. Eur J Endocrinol. 1996;135:383–90.
54. Lippi F, Ferrari C, Manetti L, Rago T, Santini F, Monzani F, et al. Treatment of solitary autonomous thyroid nodules by percutaneous etanol injection. Results of an Italian multicenter study. J Clin Endocrinol Metab. 1996;81:3261–4.
55. Monzani F, Caraccio N, Goletti O. Five year follow-up of percutaneous ethanol injection for the treatment of hyperfunctioning thyroid nodules: a study of 117 patients. Clin Endocrinol. 1997;46:9–15.
56. Zingrillo M, Torlontano M, Ghiggi MR, Frusciante V, Varraso A, Liuzzi A, et al. Radioiodine and percutaneous ethanol injection in the treatment of large toxic thyroid nodule: a long-term study. Thyroid. 2000;10:985–9.
57. Del Prete S, Russo D, Caraglia M, Giuberti G, Marra M, Vitale G, et al. Percutaneous ethanol injection of autonomous thyroid nodules with a volume larger than 40 ml: three years of follow-up. Clin Radiol. 2001;56:895–901.
58. Tarantino L, Francica G, Sordelli I, Sperlongano P, Parmeggiani D, Ripa C, et al. Percutaneous ethanol injection of hyperfunctioning thyroid nodules: long-term follow-up in 125 patients. AJR Am J Roentgenol. 2008;190:800–8.
59. Yano Y, Sugino K, Akaishi J, Uruno T, Okuwa K, Shibuya H, et al. Treatment of autonomously functioning thyroid nodules at a single institution: radioiodine therapy, surgery, and ethanol injection therapy. Ann Nucl Med. 2011;25:749–54.
60. Zingrillo M, Modoni S, Conte M, Frusciante V, Trischitta V. Percutaneous ethanol injection plus radioiodine versus radioiodine alone in the treatment of large toxic thyroid nodules. J Nucl Med. 2003;44:207–10.
61. Pacini F. Role of percutaneous ethanol injection in management of nodular lesions of the thyroid gland. J Nucl Med. 2003;44:211–2.
62. Pishdad GR, Pishdad P, Pishdad R. Horner's syndrome as a complication of percutaneous ethanol treatment of thyroid nodule. Thyroid. 2011;21:327–8.

63. Regalbuto C, Le Moli R, Muscia V, Russo M, Vigneri R, Pezzino V. Severe graves' ophthalmopathy after percutaneous ethanol injection in a nontoxic thyroid nodule. Thyroid. 2012;22:210–3.
64. Zingrillo M, Collura D, Ghiggi MR, Nirchio V, Trischitta V. Treatment of large cold benign thyroid nodules not eligible for surgery with percutaneous ethanol injection. J Clin Endocrinol Metab. 1998;83:3905–7.
65. Bennedbaek FN, Nielsen LK, Hegedus L. Effect of percutaneous ethanol injection therapy versus suppressive doses of L-thyroxine on benign solitary solid cold thyroid nodules: a randomized trial. J Clin Endocrinol Metab. 1998;83:830–5.
66. Bennedbaek FN, Hegedüs L. Percutaneous ethanol injection therapy in benign solitary solid cold thyroid nodules: a randomized trial comparing one injection with three injections. Thyroid. 1999;9:225–33.
67. Papini E, Pacella CM, Hegedus L. Diagnosis of endocrine disease: thyroid ultrasound (US) and US-assisted procedures: from the shadows into an array of applications. Eur J Endocrinol. 2014;170:R133–46.
68. Papini E, Pacella CM, Misischi I, Guglielmi R, Bizzarri G, Døssing H, et al. The advent of ultrasound-guided ablation techniques in nodular thyroid disease: towards a patient-tailored approach. Best Pract Res Clin Endocrinol Metab. 2014;28:601–18.
69. Douthat WG, Cardozo G, Garay G, Orozco S, Chiurchiu C, de la Fuente J, et al. Use of percutaneous ethanol injection therapy for recurrent secondary hyperparathyroidism after subtotal parathyroidectomy. Int J Nephrol. 2011;2011:246734.
70. Chen HH, Lin CJ, Wu CJ, Lai CT, Lin J, Cheng SP, et al. Chemical ablation of recurrent and persistent secondary hyperparathyroidism after subtotal parathyroidectomy. Ann Surg. 2011;253:786–90.
71. Kitaoka M. Ultrasonographic diagnosis of parathyroid glands and percutaneous ethanol injection therapy. Nephrol Dial Transplant. 2003;18(Suppl 3):ii27–30.
72. Tanaka M, Itoh K, Matsushita K, Matsushita K, Fukagawa M. Efficacy of percutaneous ethanol injection therapy for secondary hyperparathyroidism in patients on hemodialysis as evaluated by parathyroid hormone levels according to K/DOQI guidelines. Ther Apher Dial. 2005;9:48–52.
73. Douthat WG, Chiurchiu CR, Massari PU. New options for the management of hyperparathyroidism after renal transplantation. World J Transplant. 2012;2(3):41–5.

74. Harman CR, Grant CS, Hay ID, et al. Indications, technique, and efficacy of alcohol injection of enlarged parathyroid glands in patients with primary hyperparathyroidism. Surgery. 1998;124:1011–9.
75. Cercueil JP, Jacob D, Verges B, Holtzmann P, Lerais JM, Krause D. Percutaneous ethanol injection into parathyroid adenomas: mid- and long-term results. Eur Radiol. 1998;8:1565–156.
76. Singh Ospina N, Thompson GB, Lee RA, Reading CC, Young WF Jr. Safety and efficacy of percutaneous parathyroid ethanol ablation in patients with recurrent primary hyperparathyroidism and multiple endocrine Neoplasia type 1. J Clin Endocrinol Metabol. 2015;100(1):E87–90.
77. Clark OH, Okerlund MD, Cavalieri RR, Greenspan FS. Diagnosis and treatment of thyroid parathyroid and thyroglossal duct cysts. J Clin Endocrinol Metab. 1979;48:983–8.
78. Ippolito G, Palazzo FF, Sebag F, Sierra M, De Micco C, Henry JF. A single institution 25-year review of true parathyroid cysts. Langenbecks Arch Surg. 2006;391:13–8.
79. Goomany A, Rafferty A, Smith I. An unusual neck mass: a case of a parathyroid cyst and review of the literature. Case Rep Surg. 2015;2015:243527.
80. Prinz RA, Peters JR, Kane JM, Wood J. Needle aspiration of nonfunctioning parathyroid cysts. Am Surg. 1990;56:420–2.
81. Akel M, Salti I, Azar ST. Successful treatment of parathyroid cyst using ethanol sclerotherapy. Am J Med Sci. 1999;317:50–2.
82. Baskin HJ. New applications of thyroid and parathyroid ultrasound. Minerva Endocrinol. 2004;29:195–206.
83. Frasoldati A, Valcavi R. Challenges in neck ultrasonography: lymphadenopathy and parathyroid glands. Endocr Pract. 2004;10:261–8.
84. Koiwa F, Hasegawa T, Tanaka R, Kakuta T. Indication and efficacy of PEIT in the management of secondary hyperparathyroidism. NDT Plus. 2008;1(Suppl 3):14–7.
85. Sung JY, Baek JH, Kim KS, Lee D, Ha EJ, Lee JH. Symptomatic nonfunctioning parathyroid cysts: role of simple aspiration and ethanol ablation. Eur J Radiol. 2013;82:316–20.
86. Kim JH. Ultrasound-guided sclerotherapy for benign nonthyroid cystic mass in the neck. Ultrasonography. 2014;33:83–90.
87. Hay ID, Charboneau JW. The coming of age of ultrasound-guided percutaneous ethanol ablation of selected neck nodal metastases in well-differentiated thyroid carcinoma. J Clin Endocrinol Metab. 2011;96:2717–20.

88. Lewis BD, Hay ID, Charboneau JW, McIver B, Reading CC, Goellner JR. Percutaneous ethanol injection for treatment of cervical lymph node metastases in patients with papillary thyroid carcinoma. Am J Roentgenol. 2002;178:699–704.
89. Monchik JM, Donatini G, Iannuccilli J, Dupuy DE. Radiofrequency ablation and percutaneous ethanol injection treatment for recurrent local and distant well-differentiated thyroid carcinoma. Ann Surg. 2006;244:296–304.
90. Lim CY, Yun JS, Lee J, Nam KH, Chung WY, Park CS. Percutaneous ethanol injection therapy for locally recurrent papillary thyroid carcinoma. Thyroid. 2007;17:347–35.
91. Kim BM, Kim MJ, Kim EK, et al. Controlling recurrent papillary thyroid carcinoma in the neck by ultrasonography-guided percutaneous ethanol injection. Eur Radiol. 2008;18:835–42.
92. Heilo A, Sigstad E, Fagerlid KH, Håskjold OI, Grøholt KK, Berner A, et al. Efficacy of ultrasound-guided percutaneous ethanol injection treatment in patients with a limited number of metastatic cervical lymph nodes from papillary thyroid carcinoma. J Clin Endocrinol Metab. 2011;96:2750–5.
93. Hay ID, Lee RA, Davidge-Pitts C, Reading CC, Charboneau JW. Long-term outcome of ultrasound-guided percutaneous ethanol ablation of selected "recurrent" neck nodal metastases in 25 patients with TNM stages III or IVA papillary thyroid carcinoma previously treated by surgery and 131I therapy. Surgery. 2013;154:1448–54; discussion 1454-5.
94. Guenette JP, Monchik JM, Dupuy DE. Image-guided ablation of postsurgical locoregional recurrence of biopsy-proven well-differentiated thyroid carcinoma. J Vasc Interv Radiol. 2013;24(5):672–9.
95. Vannucchi G, Covelli D, Perrino M, De Leo S, Fugazzola L. Ultrasound-guided percutaneous ethanol injection in papillary thyroid cancer metastatic lymph-nodes. Endocrine. 2014;47:648–51.
96. Fontenot TE, Deniwar A, Bhatia P, Al-Qurayshi Z, Randolph GW, Kandil E. Percutaneous ethanol injection vs reoperation for locally recurrent papillary thyroid cancer: a systematic review and pooled analysis. JAMA Otolaryngol Head Neck Surg. 2015;141:512–8.
97. Sohn YM, Hong SW, Kim EK, Kim MJ, Moon HJ, Kim SJ, et al. Complete eradication of metastatic lymph node after percutaneous ethanol injection therapy: pathologic correlation. Thyroid. 2009;19:317–9.

98. Pacella CM, Papini E. Image-guided percutaneous ablation therapies for local recurrences of thyroid tumors. J Endocrinol Investig. 2013;36:61–70.
99. Yue W, Chen L, Wang S, Yu S. Locoregional control of recurrent papillary thyroid carcinoma by ultrasound-guided percutaneous microwave ablation: a prospective study. Int J Hyperth. 2015;3:403–8.
100. Lim HK, Baek JH, Lee JH, Kim WB, Kim TY, Shong YK, et al. Efficacy and safety of radiofrequency ablation for treating locoregional recurrence from papillary thyroid cancer. Eur Radiol. 2015;25:163–70.

Chapter 15
Utilization of Molecular Markers in the Diagnosis and Management of Thyroid Nodules

Susan J. Hsiao and Yuri E. Nikiforov

Introduction

Advances in molecular testing have made it possible to routinely incorporate molecular markers in guiding management of patients with indeterminate cytology thyroid nodules. Ultrasound and cytopathologic examination of thyroid nodules are crucially important diagnostic methodologies, and utilization of these methodologies is able to definitively classify the majority (70–80%) of thyroid nodules as benign or malignant [1, 2]. The Bethesda reporting system, first proposed in 2007 by the National Cancer Institute, provides diagnostic categories with risk stratification and recommendations for

S.J. Hsiao, MD, PhD
Department of Pathology & Cell Biology, Columbia University Medical Center, New York, NY, USA

Y.E. Nikiforov, MD, PhD (✉)
Department of Pathology, Division of Molecular & Genomic Pathology, University of Pittsburgh Medical Center, Pittsburgh, PA, USA
e-mail: nikiforovye@upmc.edu

D.S. Duick et al. (eds.), *Thyroid and Parathyroid Ultrasound and Ultrasound-Guided FNA*,
https://doi.org/10.1007/978-3-319-67238-0_15

clinical management [3, 4]. However, 20–30% of thyroid nodules fall into one of the three indeterminate categories: atypia of undetermined significance/follicular lesion of undetermined significance (AUS/FLUS) (Bethesda III), follicular or oncocytic (Hürthle cell) neoplasm/suspicious for follicular or oncocytic (Hürthle cell) neoplasm (FN/SFN) (Bethesda IV), or suspicious for malignant cells (SMC) (Bethesda V) [4, 5].

The AUS/FLUS category carries a risk of malignancy of 5–15%; patients with AUS/FLUS nodules typically undergo a repeat fine needle aspiration (FNA) procedure. For the FN/SFN category, the risk of malignancy is 15–30%, and patients are typically recommended to undergo a diagnostic lobectomy. The SMC category carries the highest risk of malignancy at 60–70%. Patients with SMC category thyroid nodules are recommended to undergo either thyroidectomy or lobectomy [3].

On resection, the majority of indeterminate thyroid nodules are found to be benign [4–6]. Avoiding or reducing diagnostic surgeries for indeterminate nodules that turn out to be benign would be of great benefit to patients. For the 10–40% of patients with indeterminate thyroid nodules that turn out to be malignant, if the malignant nodule is greater than 1 cm in size, those patients who have undergone a diagnostic lobectomy then undergo a completion lobectomy. These patients could have benefitted from an upfront thyroidectomy rather than two separate procedures.

To increase the level of granularity in preoperative risk assessments and reduce the number of diagnostic surgeries, ancillary approaches such as molecular profiling of indeterminate nodules are increasingly being utilized. In a recent survey of practice patterns of members of the Endocrine Society, American Thyroid Association, and American Association of Clinical Endocrinologists, 38.8% of respondents obtain molecular profiles to guide management of patients with AUS/FLUS nodules, and 29.0% obtain molecular profiles for patients with FN/SFN nodules [7].

Several molecular tests are currently commercially available (Table 15.1). These tests utilize a variety of methodologies to characterize thyroid nodules by gene mutations/rearrangements, mRNA expression, or microRNA (miRNA) expression [8–12].

Table 15.1 Commercially available molecular tests for indeterminate thyroid nodules

	Mutation testing			**mRNA gene expression classifier**	**miRNA classifier**	
Test	ThyroSeq v2	ThyGenX	Thyroid Cancer Mutation Panel	Afirma	ThyraMIR (offered as reflex test if ThyGenX test is negative)	RosettaGX Reveal
Company	UPMC, via CBLPath	Interpace Diagnostics	Quest	Veracyte	Interpace Diagnostics	Rosetta Genomics
Methodology	Next-generation sequencing	Next-generation sequencing	Real-time PCR, pyrosequencing	mRNA expression array	qRT-PCR	qRT-PCR
Number of targets tested	Hotspot mutations in 14 genes and 42 types of gene fusions involving RET, PPARG, NTRK1, NTRK3, BRAF, THADA, and ALK genes	Hotspot mutations in five genes and RET/PTC1, RET/PTC3, PAX8/PPARG fusions	Hotspot mutations in four genes and RET/PTC1, RET/PTC3, PAX8/PPARG fusions	142 mRNAs	Ten miRNAs	24 miRNAs

(continued)

Table 15.1 (continued)

	Mutation testing			**mRNA gene expression classifier**	**miRNA classifier**	
Sample requirements	1–2 drops from first FNA pass into collection tube	One dedicated FNA pass into collection tube	Needle washing in alcohol-based fixative (eg., Cytolyt), two unstained tissue slides, or four unstained FNA slides	Two dedicated FNA passes into collection tube	One dedicated FNA pass into collection tube	One stained FNA smear slide

Gene Mutation/Rearrangement Testing

Gene mutation and rearrangement testing are based upon decades of characterization of the molecular alterations responsible for driving thyroid tumorigenesis. These studies have culminated in recent large-scale sequencing projects, such as The Cancer Genome Atlas (TCGA) sequencing study, and have resulted in a comprehensive profile of the landscape of alterations in thyroid tumors.

The TCGA study of papillary thyroid cancer examined single-nucleotide variants, small indels, copy number alterations, rearrangements, mRNA expression, miRNA expression, and DNA methylation of 496 papillary thyroid carcinomas [13]. Driver alterations were identified by this analysis for 96.5% of cases [13]. Thus, driver mutations that account for nearly all papillary thyroid cancers have now been described. The majority of alterations seen in papillary thyroid carcinoma involve the mitogen-activated protein kinase (MAPK) and phosphatidylinositol-3-kinase (PI3K) pathways. The knowledge gained through prior studies and large-scale sequencing projects have guided the design of gene mutation/rearrangement panels.

Seven-Gene Mutation/Rearrangement Panels

A seven-gene panel of the mutations and rearrangements most frequently seen in thyroid cancer (accounting for approximately 70% of thyroid cancers) is one approach for mutational testing. These panels typically include hotspot mutations in *BRAF*, *NRAS*, *HRAS*, and *KRAS,* and testing for the fusion genes *RET/PTC1*, *RET/PTC3*, and *PAX8/PPARG*.

BRAF is a serine threonine kinase that plays an integral role in the MAPK pathway and is important in cell division and differentiation. Mutations in *BRAF* are seen in approximately 40–45% of papillary thyroid carcinomas [14, 15]. The most commonly seen *BRAF* mutation is the activating V600E mutation. Other mutations such as K601E or small in-frame insertions or deletions have been reported [16–19]. Additionally, activation of BRAF signaling may occur

through fusion of *BRAF* with partners such as *AKAP9*, *SND1*, or *MKRN1* [13, 20].

NRAS, *HRAS*, and *KRAS* are oncogenes frequently mutated in several tumors. Activating mutations typically occur at codon 61 (most frequently) and also at codons 12 and 13. Mutations in *NRAS*, *HRAS*, or *KRAS* have been reported in 40–50% of follicular carcinomas and 20–40% of follicular adenomas [21–24]. *NRAS*, *HRAS*, or *KRAS* mutations have also been reported in noninvasive follicular thyroid neoplasm with papillary-like nuclear features (NIFTP) and invasive follicular variant of papillary thyroid carcinoma [25–27].

The fusions interrogated in seven-gene mutation/rearrangement panels are the RET/PTC1 (fusion of *RET* with *CCDC6*), RET/PTC3 (fusion of *RET* with *NCOA4*), and *PAX8/PPARG* fusions. RET/PTC1 and RET/PTC3 fusions are seen in papillary thyroid carcinomas. The incidence of which is approximately 10% of the cases (down from 20–30% incidence two decades ago [28–30]. *PAX8/PPARG* fusions are seen primarily in follicular carcinomas (30–40% of cases) [31–33]. This *PAX8/PPARG* fusion may also be seen, albeit at lower frequencies, in follicular adenomas and the follicular variant of papillary thyroid carcinomas [31–35].

All genes and rearrangements in the seven-gene mutation/rearrangement panel show high specificity and positive predictive value (PPV) for cancer (although the PPV for *NRAS*, *HRAS*, and *KRAS* is lower) [12, 36, 37]. A seven-gene mutation/rearrangement panel (or a similar eight- gene panel that also includes TRK rearrangements that occur in 5% of papillary thyroid cancers) was initially validated in three prospective studies at two institutions and was found to have a high specificity of 97–100% and high PPV of 86–100% [12, 36, 37]. In subsequent studies of similar seven-gene panels, including a single-institution retrospective study and two prospective multi-institutional studies of the Asuragen miRInform test (now currently commercially offered by Interpace Diagnostics as the ThyGenX test), similar high specificities of 86–92% and PPV of 71–80% were seen in FN/SFN thyroid nodules

[38–40]. Seven-gene mutation/rearrangement panels are commercially available from providers such as Quest Diagnostics or Interpace Diagnostics (ThyGenX). The ThyGenX test has been modified from the miRInform test to also include mutations in *PIK3CA*. *PIK3CA* alterations have been primarily described in poorly differentiated and anaplastic thyroid carcinomas [41–43].

ThyroSeq v2 Mutation/Rearrangement Panel

The ThyroSeq v2 panel is a large, next-generation sequencing (NGS)-based test. Use of NGS technology allows for the simultaneous interrogation of multiple genes in a cost-effective and high-throughput manner. This test includes the seven genes in other mutation/rearrangement panels (*BRAF*, *NRAS*, *HRAS*, *KRAS*, *RET/PTC1*, *RET/PTC3*, *PAX8/PPARG*), as well as additional genes that have been implicated in thyroid cancer: *AKT1*, *PTEN*, *TP53*, *TSHR*, *GNAS*, *CTNNB1*, *RET*, *PIK3CA*, *EIF1AX*, and *TERT* and rearrangements of *RET*, *BRAF*, *NTRK1*, *NTRK3*, *PPARG*, and *THADA* [44].

EIF1AX is a novel gene recently described to be recurrently mutated in the TCGA study of papillary thyroid carcinoma [13]. *EIF1AX* is a translational initiation factor and was seen in 2% of papillary thyroid carcinomas; however, in a subsequent study, mutations in *EIF1AX* were also identified in two follicular adenomas and one hyperplastic nodule, suggesting that the presence of *EIF1AX* mutations is not specific for carcinoma [45]. *EIF1AX* mutations have also been observed in 11% of poorly differentiated and 9% of anaplastic thyroid carcinomas [46, 47]. Interestingly, as opposed to papillary thyroid carcinoma where *EIF1AX* mutations were generally mutually exclusive with other driver mutations, in poorly differentiated and anaplastic thyroid carcinomas, a tendency toward co-occurrence of *EIF1AX* and *RAS* mutations was seen [13, 46, 47]. Further study is needed to fully elucidate the role of *EIF1AX* in thyroid cancer and to

investigate whether there may be a cooperative effect between *EIF1AX* and *RAS* in poorly differentiated and anaplastic thyroid carcinomas.

TERT promoter mutations are another important alteration present on the ThyroSeq v2 panel. *TERT* promoter mutations, located either 124 or 146 bp upstream of the start codon, have been described as recurrent alterations in follicular cell thyroid cancers; they have not been detected in medullary thyroid carcinomas or benign thyroid lesions [48–51]. These mutations, while present in well-differentiated papillary thyroid and follicular carcinomas, are present at increased frequency in aggressive tumors such as poorly differentiated carcinoma, anaplastic thyroid carcinoma, and widely invasive oncocytic carcinoma [48–51]. Furthermore, studies have found an association of *TERT* promoter mutation with increased risk for disease-specific mortality, distant metastases, and persistent disease [51].

The ThyroSeq v2 panel also includes *TP53*, *PIK3CA*, and *AKT1* genes. These genes are associated with aggressive behavior and tumor progression, and mutations in these genes are seen more frequently in poorly differentiated and anaplastic thyroid carcinomas [41–43, 52–56]. Genes that predict benign behavior, such as activating mutations of *TSHR* and *GNAS*, are also included in the panel [57–61]. Approximately 50–80% of hyperfunctioning nodules harbor *TSHR* mutations, and approximately 3–6% of hyperfunctioning nodules harbor *GNAS* mutations [57–61]. Mutations in either *TSHR* or *GNAS* have only rarely been reported in follicular carcinomas [62].

The ThyroSeq v2 panel can additionally detect mutations in *RET* which are seen in medullary thyroid carcinoma. Both mutations associated with sporadic medullary thyroid carcinoma or MEN2B syndrome such as the activating tyrosine kinase domain mutation M918T or extracellular domain cysteine mutations associated with MEN2A syndrome or familial medullary thyroid carcinoma are detectable by the panel.

Finally, the ThyroSeq v2 panel can detect an expanded set of fusion genes. Rearrangements involving *NTRK1* and

NTRK3 are seen in 5% of papillary thyroid carcinomas [62–66]. In pediatric cases of papillary thyroid carcinoma, the incidence of *NTKR1* or *NTRK3* rearrangements may be even higher [67]. Fusions involving *THADA* have been reported in approximately 1% of papillary thyroid carcinomas [13]. Fusions involving the *ALK* gene are potentially targetable and have been seen in approximately 1–2% of papillary thyroid carcinomas, 4–9% of poorly differentiated carcinomas, 4% of anaplastic thyroid carcinomas, and 1–2% of medullary thyroid carcinomas [47, 68, 69].

ThyroSeq v2 was initially validated in a single-institution, combined retrospective and prospective study of 143 FN/SFN cytology thyroid nodules [44]. Results from this study showed overall very good performance with a specificity of 93%, sensitivity of 90%, PPV of 83%, and NPV of 96% [44]. In a follow-up, single-institution, prospective study of 465 AUS/FLUS thyroid nodules, similar good performance of the assay was seen, with sensitivity of 90.9%, specificity of 92.1%, PPV of 76.9%, and NPV of 97.2% [70].

Expression Classifier Testing

mRNA Gene Expression Classifier

The Afirma gene expression classifier (GEC), offered by Veracyte, was developed by examining the gene expression profile patterns of thyroid nodules and using this data to train a molecular classifier [71]. The Afirma classifier uses the pattern of expression of 142 genes to classify nodules into one of two categories: benign or suspicious [8, 71]. Initial validation of the Afirma test was done using 265 indeterminate nodules in a multi-institutional study [71]. Both high sensitivity (90%) and NPV (94%) were seen; lower values were seen for specificity (52%) and PPV (37%) [71]. Subsequent studies at other institutions with higher disease prevalence reported lower NPVs [72–75]. In many of these studies, the rate of true negatives or false negatives was difficult to definitively ascertain

as many patients with benign results by Afirma testing did not undergo surgical resection. A recent meta-analysis of seven studies reported a pooled sensitivity of 95.7% and pooled specificity of 30.5% [76].

In addition to the Afirma GEC, Afirma offers two malignancy classifiers, Afirma MTC and Afirma BRAF. These malignancy classifiers are recommended to be performed on thyroid nodules that have a suspicious result by the Afirma GEC or are SMC on cytology. The Afirma MTC classifier examines the expression of genes differentially expressed in medullary thyroid carcinoma. In a recent small validation study of the MTC classifier, a sensitivity of 96.3% was reported [77]. The Afirma BRAF classifier analyzes the expression of genes differentially expressed in thyroid nodules with the *BRAF* V600E mutation.

miRNA Expression Classifier

MicroRNAs (miRNAs) are small, noncoding RNAs that are important in regulation of gene expression. Studies have demonstrated the differential expression of several miRNAs in thyroid carcinoma; some have additionally shown association with prognostic features such as advanced disease or extrathyroidal extension [78, 79].

A miRNA classifier assay is offered by Rosetta Genomics (Rosetta GX Reveal). This assay examines the expression of 24 miRNAs from a single stained diagnostic smear to classify nodules as "suspicious for malignancy by miRNA profiling," "positive for medullary marker," or "benign" [80]. In a multicenter, retrospective study that utilized a total of 109 Bethesda III and IV cytology samples, this test was reported to show a sensitivity of 85%, a specificity of 72%, and an NPV of 91% [9].

The ThyraMIR test (Interpace Diagnostics) also utilizes a panel of miRNAs to classify thyroid nodules as "positive" or "negative." The ThyraMIR test analyzes the expression of ten miRNAs and is currently offered as reflex testing on nodules

that are negative by the eight-gene ThyGenX mutation/rearrangement panel. The performance of this assay, as reported in the initial validation study based on the analysis of a total of 150 Bethesda III and IV cytology samples (which did not include any cases of Hurthle cell carcinomas), is sensitivity of 57%, specificity of 92%, NPV of 82%, and PPV of 77% [40].

Comparison of Test Performance

Sensitivity measures the proportion of actual positives which are true positives, and specificity measures the proportion of negatives which are true negatives. Sensitivity and specificity reflect the performance characteristics of a test. PPV and NPV, however, will vary depending on the prevalence of disease. For example, a patient population with higher incidence of thyroid cancer than the population where the test was validated will have a lower NPV. Another factor that may affect observed NPV and PPV may be institutional differences in the malignancy rates for each indeterminate cytology category. Published test performance characteristics are summarized in Table 15.2.

Strengths of gene mutation/rearrangement panels are their high specificity and PPV for malignancy. In general, these tests are being utilized to "rule in" malignancy. Strengths of gene expression classifiers are their high sensitivity and NPV. This test is being used to "rule out" malignancy. The ideal diagnostic test would have high sensitivity, specificity, NPV, and PPV and would be able to both rule in and rule out malignancy. Combination testing is one approach being pursued: for example, addition of the ThyraMIR test to the ThyGenX test gives a sensitivity of 89%, specificity of 85%, NPV of 94%, and PPV of 74%. Also, addition of the Afirma MTC or Afirma BRAF malignancy classifiers may add some specificity to the Afirma GEC, although no data regarding this has been published yet.

Of the currently commercially available tests, the ThyroSeq v2 test shows much promise as a stand-alone test that could

Table 15.2 Comparison of published thyroid molecular test performance characteristics

	Type of study	Cytology (Bethesda category)	Number of cases	Sensitivity	Specificity	NPV	PPV
ThyroSeq	Prospective	III	96	91%	92%	97%	77%
	Retrospective and prospective	IV	143	90%	93%	96%	83%
Afirma	Prospective	III	129	90%	53%	95%	38%
		IV	81	90%	49%	94%	37%
RosettaGX Reveal	Retrospective	III, IV	150	74%	74%	92%	43%
ThyGenX and ThyraMIR	Prospective	III	58	94%	80%	97%	68%
		IV	51	82%	91%	91%	82%

be used to both rule in and rule out malignancy, with a NPV of 96% and PPV of 83% in FN/SFN nodules and a NPV of 97.2% and PPV of 76.9% in AUS/FLUS nodules. Further understanding of thyroid pathogenesis and the potential role of cooperating genes or mutations may help in further refining the NPV and PPV of the panel. In particular, *RAS* alterations, which may be seen in carcinomas as well as benign/indolent neoplasms such as follicular adenomas or NIFTP, confer a lower risk of malignancy of 74 to 87% than other alterations such as the *BRAF* V600E mutation which has a >95% risk of malignancy [12, 36, 37]. Knowledge of the differences in risk based on the specific gene mutation present can guide patient management. Furthermore, use of large, NGS-based mutation panels would allow for the discovery of co-occurring mutations (e.g., in *TP53* or *EIF1AX*) that may prove to be associated with increased risk.

Utilizing the Results of Molecular Profiling in Clinical Management

Test performance characteristics have formed the basis of clinical algorithms to guide the use of molecular testing in guiding perioperative decision making [81]. For a positive result on seven-gene mutation/rearrangement panels, which have high specificity and high PPV, indeterminate cytology thyroid nodules may be managed with oncologic thyroidectomy. A negative result on a seven-gene mutation/rearrangement panel may be managed by observation or diagnostic thyroid lobectomy for AUS/FLUS nodules and by diagnostic thyroid lobectomy for FN/SFN or SMC nodules. Gene expression classifiers have high sensitivity and high NPV. For a benign result, observation or diagnostic thyroid lobectomy would be appropriate, and for a suspicious result on AUS/FLUS or FN/SFN nodules, at least a diagnostic lobectomy should be considered.

For the ThyroSeq v2 panel, which has good overall sensitivity, specificity, NPV, and PPV, the following clinical

algorithm can be considered (Fig. 15.1). When test is negative for all alterations, in nodules with Bethesda III and IV cytology (and pretest cancer probability is that expected for these Bethesda categories), the residual probability of cancer is expected to be 3–4%. According to the NCCN guidelines, these patients can be followed by observation, similar to the recommendations for benign cytology nodules. For nodules with a positive ThyroSeq result, the type of mutation and other test results allow one to predict the probability of cancer in the nodule and estimate how aggressive the cancer is, helping to define the most appropriate surgical approach. An isolated *RAS* or *RAS*-like mutation predicts a high probability (~80%) of either low-risk cancer or a precancerous tumor, NIFTP. Many of these patients can be treated with

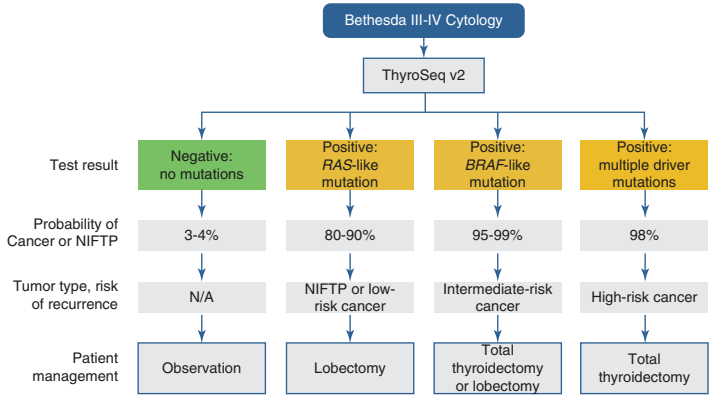

Figure 15.1 Algorithm for clinical management using the ThyroSeq v2 test, based on the risk conferred by specific mutations. Negative nodules have a risk of cancer of 3–4%, similar to that for benign cytology nodules, and can be managed with observation. Nodules positive for a *RAS*-like mutation have a risk of either low-risk cancer or NIFTP and can be managed with lobectomy. Nodules positive for a *BRAF*-like mutation are intermediate-risk cancers and can be managed with total thyroidectomy or lobectomy. Nodules positive for multiple driver mutations are high-risk cancers and can be managed with total thyroidectomy, with possible local lymph node dissection

therapeutic lobectomy, which is currently recommended for low-risk thyroid cancers. Isolated *BRAF* V600E or other *BRAF* V600E-like mutations confer a very high (>95%) probability of cancer of intermediate risk for disease recurrence. The risk may be further modified by clinical parameters; for example, small (<1 cm) tumors may still be of low risk. These patients can be treated with total thyroidectomy or lobectomy. Test positivity for multiple driver mutations is virtually diagnostic of cancer and predicts a significant risk of disease recurrence and tumor-related mortality. These patients would benefit from total thyroidectomy, with consideration for central compartment lymph node dissection.

Studies have suggested that use of molecular testing can help avoid unnecessary surgeries and can reduce the number of two-step surgeries (initial lobectomy followed by completion thyroidectomy). In a study of 471 patients with AUS/FLUS or FN/SFN cytology nodules, patients who did not have seven-gene mutation/rearrangement testing were 2.5 more times likely to require a two-step surgery [82]. Cost-effectiveness modeling studies of seven-gene mutation/rearrangement panels, gene expression classifier testing, and combined mutation and miRNA testing all show potential cost savings [83, 84].

Conclusions

Advances in technology and further elucidation of the molecular mechanisms underlying thyroid tumor pathogenesis have made possible the incorporation of molecular testing to ultrasound and cytopathologic examination in guiding the management of the patient with a thyroid nodule. Multiple tests are commercially available, and each utilizes different methodologies to profile the molecular alterations in indeterminate thyroid nodules. These tests have their own strengths and weakness; some have excellent utility in ruling in malignancy, and some have excellent utility in ruling out malignancy. Usage of these tests is increasingly being adopted in clinical practice and has potential to reduce costs by reducing

the number of unnecessary surgeries. Further advances in testing and test performance are likely to occur and may prove to have additional utility, for example, by predicting tumor aggressiveness or response to therapy.

References

1. Cooper DS, Doherty GM, Haugen BR, Kloos RT, Lee SL, Mandel SJ, et al. Revised American Thyroid Association management guidelines for patients with thyroid nodules and differentiated thyroid cancer. Thyroid. 2009;19(11):1167–214.
2. Gharib H, Papini E, Paschke R, Duick DS, Valcavi R, Hegedus L, et al. American Association of Clinical Endocrinologists, Associazione Medici Endocrinologi, and European Thyroid Association medical guidelines for clinical practice for the diagnosis and management of thyroid nodules: executive summary of recommendations. J Endocrinol Investig. 2010;33(Suppl 5):51–6.
3. Ali SZ, Cibas ES. The Bethesda system for reporting thyroid cytopathology. New York: Springer; 2010.
4. Baloch ZW, LiVolsi VA, Asa SL, Rosai J, Merino MJ, Randolph G, et al. Diagnostic terminology and morphologic criteria for cytologic diagnosis of thyroid lesions: a synopsis of the National Cancer Institute thyroid fine-needle aspiration state of the science conference. Diagn Cytopathol. 2008;36(6):425–37.
5. Baloch ZW, Fleisher S, LiVolsi VA, Gupta PK. Diagnosis of "follicular neoplasm": a gray zone in thyroid fine-needle aspiration cytology. Diagn Cytopathol. 2002;26(1):41–4.
6. Mazzaferri EL. Management of a solitary thyroid nodule. N Engl J Med. 1993;328(8):553–9.
7. Burch HB, Burman KD, Cooper DS, Hennessey JV, Vietor NO. A 2015 survey of clinical practice patterns in the management of thyroid nodules. J Clin Endocrinol Metab. 2016;101(7):2853–62.
8. Alexander EK, Kennedy GC, Baloch ZW, Cibas ES, Chudova D, Diggans J, et al. Preoperative diagnosis of benign thyroid nodules with indeterminate cytology. N Engl J Med. 2012;367(8):705–15.
9. Lithwick-Yanai G, Dromi N, Shtabsky A, Morgenstern S, Strenov Y, Feinmesser M, et al. Multicentre validation of a microRNA-based assay for diagnosing indeterminate thyroid nodules utilising fine needle aspirate smears. J Clin Pathol. 2017;70(6):500–7.

10. Bartolazzi A, Orlandi F, Saggiorato E, Volante M, Arecco F, Rossetto R, et al. Galectin-3-expression analysis in the surgical selection of follicular thyroid nodules with indeterminate fine-needle aspiration cytology: a prospective multicentre study. Lancet Oncol. 2008;9(6):543–9.
11. Keutgen XM, Filicori F, Crowley MJ, Wang Y, Scognamiglio T, Hoda R, et al. A panel of four miRNAs accurately differentiates malignant from benign indeterminate thyroid lesions on fine needle aspiration. Clin Cancer Res. 2012;18(7):2032–8.
12. Nikiforov YE, Ohori NP, Hodak SP, Carty SE, LeBeau SO, Ferris RL, et al. Impact of mutational testing on the diagnosis and management of patients with cytologically indeterminate thyroid nodules: a prospective analysis of 1056 FNA samples. J Clin Endocrinol Metab. 2011;96(11):3390–7.
13. Cancer Genome Atlas Research N. Integrated genomic characterization of papillary thyroid carcinoma. Cell. 2014;159(3):676–90.
14. Cohen Y, Xing M, Mambo E, Guo Z, Wu G, Trink B, et al. BRAF mutation in papillary thyroid carcinoma. J Natl Cancer Inst. 2003;95(8):625–7.
15. Kimura ET, Nikiforova MN, Zhu Z, Knauf JA, Nikiforov YE, Fagin JA. High prevalence of BRAF mutations in thyroid cancer: genetic evidence for constitutive activation of the RET/PTC-RAS-BRAF signaling pathway in papillary thyroid carcinoma. Cancer Res. 2003;63(7):1454–7.
16. Chiosea S, Nikiforova M, Zuo H, Ogilvie J, Gandhi M, Seethala RR, et al. A novel complex BRAF mutation detected in a solid variant of papillary thyroid carcinoma. Endocr Pathol. 2009;20(2):122–6.
17. Ciampi R, Nikiforov YE. Alterations of the BRAF gene in thyroid tumors. Endocr Pathol. 2005;16(3):163–72.
18. Hou P, Liu D, Xing M. Functional characterization of the T1799-1801del and A1799-1816ins BRAF mutations in papillary thyroid cancer. Cell Cycle. 2007;6(3):377–9.
19. Soares P, Trovisco V, Rocha AS, Lima J, Castro P, Preto A, et al. BRAF mutations and RET/PTC rearrangements are alternative events in the etiopathogenesis of PTC. Oncogene. 2003;22(29):4578–80.
20. Ciampi R, Knauf JA, Kerler R, Gandhi M, Zhu Z, Nikiforova MN, et al. Oncogenic AKAP9-BRAF fusion is a novel mechanism of MAPK pathway activation in thyroid cancer. J Clin Invest. 2005;115(1):94–101.

21. Lemoine NR, Mayall ES, Wyllie FS, Williams ED, Goyns M, Stringer B, et al. High frequency of ras oncogene activation in all stages of human thyroid tumorigenesis. Oncogene. 1989;4(2):159–64.
22. Motoi N, Sakamoto A, Yamochi T, Horiuchi H, Motoi T, Machinami R. Role of ras mutation in the progression of thyroid carcinoma of follicular epithelial origin. Pathol Res Pract. 2000;196(1):1–7.
23. Namba H, Rubin SA, Fagin JA. Point mutations of ras oncogenes are an early event in thyroid tumorigenesis. Mol Endocrinol. 1990;4(10):1474–9.
24. Suarez HG, du Villard JA, Severino M, Caillou B, Schlumberger M, Tubiana M, et al. Presence of mutations in all three ras genes in human thyroid tumors. Oncogene. 1990;5(4):565–70.
25. Nikiforov YE, Seethala RR, Tallini G, Baloch ZW, Basolo F, Thompson LD, et al. Nomenclature revision for encapsulated follicular variant of papillary thyroid carcinoma: a paradigm shift to reduce overtreatment of indolent tumors. JAMA Oncol. 2016;2(8):1098.
26. Adeniran AJ, Zhu Z, Gandhi M, Steward DL, Fidler JP, Giordano TJ, et al. Correlation between genetic alterations and microscopic features, clinical manifestations, and prognostic characteristics of thyroid papillary carcinomas. Am J Surg Pathol. 2006;30(2):216–22.
27. Zhu Z, Gandhi M, Nikiforova MN, Fischer AH, Nikiforov YE. Molecular profile and clinical-pathologic features of the follicular variant of papillary thyroid carcinoma. An unusually high prevalence of ras mutations. Am J Clin Pathol. 2003;120(1):71–7.
28. Jung CK, Little MP, Lubin JH, Brenner AV, Wells SA Jr, Sigurdson AJ, et al. The increase in thyroid cancer incidence during the last four decades is accompanied by a high frequency of BRAF mutations and a sharp increase in RAS mutations. J Clin Endocrinol Metab. 2013. https://doi.org/10.1210/jc.2013-2503.
29. Nikiforov YE. RET/PTC rearrangement—a link between Hashimoto's thyroiditis and thyroid cancer…or not. J Clin Endocrinol Metab. 2006;91(6):2040–2.
30. Zhu Z, Ciampi R, Nikiforova MN, Gandhi M, Nikiforov YE. Prevalence of RET/PTC rearrangements in thyroid papillary carcinomas: effects of the detection methods and genetic heterogeneity. J Clin Endocrinol Metab. 2006;91(9):3603–10.
31. Dwight T, Thoppe SR, Foukakis T, Lui WO, Wallin G, Hoog A, et al. Involvement of the PAX8/peroxisome proliferator-

activated receptor gamma rearrangement in follicular thyroid tumors. J Clin Endocrinol Metab. 2003;88(9):4440–5.
32. French CA, Alexander EK, Cibas ES, Nose V, Laguette J, Faquin W, et al. Genetic and biological subgroups of low-stage follicular thyroid cancer. Am J Pathol. 2003;162(4):1053–60.
33. Nikiforova MN, Lynch RA, Biddinger PW, Alexander EK, Dorn GW 2nd, Tallini G, et al. RAS point mutations and PAX8-PPAR gamma rearrangement in thyroid tumors: evidence for distinct molecular pathways in thyroid follicular carcinoma. J Clin Endocrinol Metab. 2003;88(5):2318–26.
34. Marques AR, Espadinha C, Catarino AL, Moniz S, Pereira T, Sobrinho LG, et al. Expression of PAX8-PPAR gamma 1 rearrangements in both follicular thyroid carcinomas and adenomas. J Clin Endocrinol Metab. 2002;87(8):3947–52.
35. Nikiforova MN, Biddinger PW, Caudill CM, Kroll TG, Nikiforov YE. PAX8-PPARgamma rearrangement in thyroid tumors: RT-PCR and immunohistochemical analyses. Am J Surg Pathol. 2002;26(8):1016–23.
36. Cantara S, Capezzone M, Marchisotta S, Capuano S, Busonero G, Toti P, et al. Impact of proto-oncogene mutation detection in cytological specimens from thyroid nodules improves the diagnostic accuracy of cytology. J Clin Endocrinol Metab. 2010;95(3):1365–9.
37. Nikiforov YE, Steward DL, Robinson-Smith TM, Haugen BR, Klopper JP, Zhu Z, et al. Molecular testing for mutations in improving the fine-needle aspiration diagnosis of thyroid nodules. J Clin Endocrinol Metab. 2009;94(6):2092–8.
38. Beaudenon-Huibregtse S, Alexander EK, Guttler RB, Hershman JM, Babu V, Blevins TC, et al. Centralized molecular testing for oncogenic gene mutations complements the local cytopathologic diagnosis of thyroid nodules. Thyroid. 2014;24(10):1479–87.
39. Eszlinger M, Piana S, Moll A, Bosenberg E, Bisagni A, Ciarrocchi A, et al. Molecular testing of thyroid fine-needle aspirations improves presurgical diagnosis and supports the histologic identification of minimally invasive follicular thyroid carcinomas. Thyroid. 2015;25(4):401–9.
40. Labourier E, Shifrin A, Busseniers AE, Lupo MA, Manganelli ML, Andruss B, et al. Molecular testing for miRNA, mRNA, and DNA on fine-needle aspiration improves the preoperative diagnosis of thyroid nodules with indeterminate cytology. J Clin Endocrinol Metab. 2015;100(7):2743–50.

41. Garcia-Rostan G, Costa AM, Pereira-Castro I, Salvatore G, Hernandez R, Hermsem MJ, et al. Mutation of the PIK3CA gene in anaplastic thyroid cancer. Cancer Res. 2005;65(22):10199–207.
42. Hou P, Liu D, Shan Y, Hu S, Studeman K, Condouris S, et al. Genetic alterations and their relationship in the phosphatidylinositol 3-kinase/Akt pathway in thyroid cancer. Clin Cancer Res. 2007;13(4):1161–70.
43. Ricarte-Filho JC, Ryder M, Chitale DA, Rivera M, Heguy A, Ladanyi M, et al. Mutational profile of advanced primary and metastatic radioactive iodine-refractory thyroid cancers reveals distinct pathogenetic roles for BRAF, PIK3CA, and AKT1. Cancer Res. 2009;69(11):4885–93.
44. Nikiforov YE, Carty SE, Chiosea SI, Coyne C, Duvvuri U, Ferris RL, et al. Highly accurate diagnosis of cancer in thyroid nodules with follicular neoplasm/suspicious for a follicular neoplasm cytology by ThyroSeq v2 next-generation sequencing assay. Cancer. 2014;120(23):3627–34.
45. Karunamurthy A, Panebianco F, Hsiao S, Vorhauer J, Nikiforova M, Chiosea SI, et al. Prevalence and phenotypic characteristics of EIF1AX mutations in thyroid nodules. Endocr Relat Cancer. 2016;23(4):295–301.
46. Kunstman JW, Juhlin CC, Goh G, Brown TC, Stenman A, Healy JM, et al. Characterization of the mutational landscape of anaplastic thyroid cancer via whole-exome sequencing. Hum Mol Genet. 2015;24(8):2318–29.
47. Landa I, Ibrahimpasic T, Boucai L, Sinha R, Knauf JA, Shah RH, et al. Genomic and transcriptomic hallmarks of poorly differentiated and anaplastic thyroid cancers. J Clin Invest. 2016;126(3):1052–66.
48. Landa I, Ganly I, Chan TA, Mitsutake N, Matsuse M, Ibrahimpasic T, et al. Frequent somatic TERT promoter mutations in thyroid cancer: higher prevalence in advanced forms of the disease. J Clin Endocrinol Metab. 2013;98(9):E1562–6.
49. Liu T, Wang N, Cao J, Sofiadis A, Dinets A, Zedenius J, et al. The age- and shorter telomere-dependent TERT promoter mutation in follicular thyroid cell-derived carcinomas. Oncogene. 2013;33(42):4978–84.
50. Liu X, Bishop J, Shan Y, Pai S, Liu D, Murugan AK, et al. Highly prevalent TERT promoter mutations in aggressive thyroid cancers. Endocr Relat Cancer. 2013;20(4):603–10.
51. Melo M, Rocha AG, Vinagre J, Batista R, Peixoto J, Tavares C, et al. TERT promoter mutations are a major indicator of poor

outcome in differentiated thyroid carcinomas. J Clin Endocrinol Metab. 2014. https://doi.org/10.1210/jc.2013-3734.
52. Fagin JA, Matsuo K, Karmakar A, Chen DL, Tang SH, Koeffler HP. High prevalence of mutations of the p53 gene in poorly differentiated human thyroid carcinomas. J Clin Invest. 1993;91(1):179–84.
53. Donghi R, Longoni A, Pilotti S, Michieli P, Della Porta G, Pierotti MA. Gene p53 mutations are restricted to poorly differentiated and undifferentiated carcinomas of the thyroid gland. J Clin Invest. 1993;91(4):1753–60.
54. Dobashi Y, Sugimura H, Sakamoto A, Mernyei M, Mori M, Oyama T, et al. Stepwise participation of p53 gene mutation during dedifferentiation of human thyroid carcinomas. Diagn Mol Pathol. 1994;3(1):9–14.
55. Ho YS, Tseng SC, Chin TY, Hsieh LL, Lin JD. p53 gene mutation in thyroid carcinoma. Cancer Lett. 1996;103(1):57–63.
56. Takeuchi Y, Daa T, Kashima K, Yokoyama S, Nakayama I, Noguchi S. Mutations of p53 in thyroid carcinoma with an insular component. Thyroid. 1999;9(4):377–81.
57. Fuhrer D, Holzapfel HP, Wonerow P, Scherbaum WA, Paschke R. Somatic mutations in the thyrotropin receptor gene and not in the Gs alpha protein gene in 31 toxic thyroid nodules. J Clin Endocrinol Metab. 1997;82(11):3885–91.
58. Trulzsch B, Krohn K, Wonerow P, Chey S, Holzapfel HP, Ackermann F, et al. Detection of thyroid-stimulating hormone receptor and Gsalpha mutations: in 75 toxic thyroid nodules by denaturing gradient gel electrophoresis. J Mol Med. 2001;78(12):684–91.
59. Parma J, Duprez L, Van Sande J, Hermans J, Rocmans P, Van Vliet G, et al. Diversity and prevalence of somatic mutations in the thyrotropin receptor and Gs alpha genes as a cause of toxic thyroid adenomas. J Clin Endocrinol Metab. 1997;82(8):2695–701.
60. Garcia-Jimenez C, Santisteban P. TSH signalling and cancer. Arq Bras Endocrinol Metabol. 2007;51(5):654–71.
61. Nishihara E, Amino N, Maekawa K, Yoshida H, Ito M, Kubota S, et al. Prevalence of TSH receptor and Gsalpha mutations in 45 autonomously functioning thyroid nodules in Japan. Endocr J. 2009;56(6):791–8.
62. Leeman-Neill RJ, Kelly LM, Liu P, Brenner AV, Little MP, Bogdanova TI, et al. ETV6-NTRK3 is a common chromosomal rearrangement in radiation-associated thyroid cancer. Cancer. 2013;120(6):799–807.

63. Greco A, Pierotti MA, Bongarzone I, Pagliardini S, Lanzi C, Della PG. TRK-T1 is a novel oncogene formed by the fusion of TPR and TRK genes in human papillary thyroid carcinomas. Oncogene. 1992;7(2):237–42.
64. Greco A, Mariani C, Miranda C, Lupas A, Pagliardini S, Pomati M, et al. The DNA rearrangement that generates the TRK-T3 oncogene involves a novel gene on chromosome 3 whose product has a potential coiled-coil domain. Mol Cell Biol. 1995;15(11):6118–27.
65. Martin-Zanca D, Hughes SH, Barbacid M. A human oncogene formed by the fusion of truncated tropomyosin and protein tyrosine kinase sequences. Nature. 1986;319(6056):743–8.
66. Radice P, Sozzi G, Miozzo M, De Benedetti V, Cariani T, Bongarzone I, et al. The human tropomyosin gene involved in the generation of the TRK oncogene maps to chromosome 1q31. Oncogene. 1991;6(11):2145–8.
67. Prasad ML, Vyas M, Horne MJ, Virk RK, Morotti R, Liu Z, et al. NTRK fusion oncogenes in pediatric papillary thyroid carcinoma in northeast United States. Cancer. 2016;122(7):1097–107.
68. Kelly LM, Barila G, Liu P, Evdokimova VN, Trivedi S, Panebianco F, et al. Identification of the transforming STRN-ALK fusion as a potential therapeutic target in the aggressive forms of thyroid cancer. Proc Natl Acad Sci U S A. 2014;111(11):4233–8.
69. Ji JH, Oh YL, Hong M, Yun JW, Lee HW, Kim D, et al. Identification of driving ALK fusion genes and genomic landscape of medullary thyroid cancer. PLoS Genet. 2015;11(8):e1005467.
70. Nikiforov YE, Carty SE, Chiosea SI, Coyne C, Duvvuri U, Ferris RL, et al. Impact of the multi-gene thyroSeq next-generation sequencing assay on cancer diagnosis in thyroid nodules with atypia of undetermined significance/follicular lesion of undetermined significance cytology. Thyroid. 2015;25(11):1217–23.
71. Chudova D, Wilde JI, Wang ET, Wang H, Rabbee N, Egidio CM, et al. Molecular classification of thyroid nodules using high-dimensionality genomic data. J Clin Endocrinol Metab. 2010;95(12):5296–304.
72. Alexander EK, Schorr M, Klopper J, Kim C, Sipos J, Nabhan F, et al. Multicenter clinical experience with the Afirma gene expression classifier. J Clin Endocrinol Metab. 2014;99(1):119–25.
73. Harrell RM, Bimston DN. Surgical utility of Afirma: effects of high cancer prevalence and oncocytic cell types in patients with indeterminate thyroid cytology. Endocr Pract. 2014;20(4):364–9.

74. Marti JL, Avadhani V, Donatelli LA, Niyogi S, Wang B, Wong RJ, et al. Wide inter-institutional variation in performance of a molecular classifier for indeterminate thyroid nodules. Ann Surg Oncol. 2015;22(12):3996–4001.
75. McIver B, Castro MR, Morris JC, Bernet V, Smallridge R, Henry M, et al. An independent study of a gene expression classifier (Afirma) in the evaluation of cytologically indeterminate thyroid nodules. J Clin Endocrinol Metab. 2014;99(11):4069–77.
76. Santhanam P, Khthir R, Gress T, Elkadry A, Olajide O, Yaqub A, et al. Gene expression classifier for the diagnosis of indeterminate thyroid nodules: a meta-analysis. Med Oncol. 2016;33(2):14.
77. Pankratz DG, Hu Z, Kim SY, Monroe RJ, Wong MG, Traweek ST, et al. Analytical performance of a gene expression classifier for medullary thyroid carcinoma. Thyroid. 2016;26(11):1573–80.
78. Chou CK, Chen RF, Chou FF, Chang HW, Chen YJ, Lee YF, et al. miR-146b is highly expressed in adult papillary thyroid carcinomas with high risk features including extrathyroidal invasion and the BRAF(V600E) mutation. Thyroid. 2010;20(5):489–94.
79. Chou CK, Yang KD, Chou FF, Huang CC, Lan YW, Lee YF, et al. Prognostic implications of miR-146b expression and its functional role in papillary thyroid carcinoma. J Clin Endocrinol Metab. 2013;98(2):E196–205.
80. Benjamin H, Schnitzer-Perlman T, Shtabsky A, VandenBussche CJ, Ali SZ, Kolar Z, et al. Analytical validity of a microRNA-based assay for diagnosing indeterminate thyroid FNA smears from routinely prepared cytology slides. Cancer Cytopathol. 2016;124(10):711–21.
81. Ferris RL, Baloch Z, Bernet V, Chen A, Fahey TJ 3rd, Ganly I, et al. American Thyroid Association statement on surgical application of molecular profiling for thyroid nodules: current impact on perioperative decision making. Thyroid. 2015;25(7):760–8.
82. Yip L, Wharry LI, Armstrong MJ, Silbermann A, McCoy KL, Stang MT, et al. A clinical algorithm for fine-needle aspiration molecular testing effectively guides the appropriate extent of initial thyroidectomy. Ann Surg. 2014;260(1):163–8.
83. Labourier E. Utility and cost-effectiveness of molecular testing in thyroid nodules with indeterminate cytology. Clin Endocrinol. 2016;85(4):624–31.
84. Yip L, Farris C, Kabaker AS, Hodak SP, Nikiforova MN, McCoy KL, et al. Cost impact of molecular testing for indeterminate thyroid nodule fine-needle aspiration biopsies. J Clin Endocrinol Metab. 2012;97(6):1905–12.

Chapter 16
Ultrasound Elastography of Thyroid Nodules

Ghobad Azizi and Carl D. Malchoff

Abbreviations

ARFI	Acoustic radiation force impulse
ES	Elastography score
FNAB	Fine needle aspiration biopsy
kPa	Kilopascals
m/s	Meters per second
NPV	Negative predictive value
PPV	Positive predictive value
PTC	Papillary thyroid cancer
ROI	Region of interest
SWE	Shear wave elastography
SWV	Shear wave velocity
US	Ultrasound
VTIQ	Virtual tissue imaging quantification
VTQ	Virtual touch quantification

G. Azizi, MD (✉)
Endocrinology, Wilmington Endocrinology, Wilmington, NC, USA
e-mail: azizi@wilmingtonendo.com

C.D. Malchoff, MD, PhD
Internal Medicine and Neag Comprehensive Cancer Center, UConn Health, Farmington, CT, USA

D.S. Duick et al. (eds.), *Thyroid and Parathyroid Ultrasound and Ultrasound-Guided FNA*,
https://doi.org/10.1007/978-3-319-67238-0_16

Introduction

Elastography is a promising new technology for noninvasively distinguishing benign thyroid nodules from thyroid cancer through tissue stiffness measurement [1]. Elastography was developed in 1991 by Ophir and colleagues at the University of Texas Medical School, Houston [2]. B-mode ultrasound (US) imaging provides excellent visualization of thyroid nodules. However, it has a low sensitivity for predicting thyroid cancer and provides only limited information about the mechanical properties of benign and malignant thyroid nodules [3].

Several large studies in recent years have demonstrated that both strain and shear wave elastography can stratify the malignant potential of thyroid nodules independently from other US features [4–9]. In this chapter, we will first discuss strain elastography and then shear wave elastography (SWE). Tissue inflammation and neoplastic processes can change tissue composition and stiffness [10]. Elastography investigates differences in the mechanical properties of structures by applying an external force and monitoring the deformation response. Low relative displacement is linked to decreased elasticity and a higher probability of malignancy [11, 12].

Why do most thyroid cancers have a higher tissue stiffness or lower elasticity than regular thyroid tissue? There are at least three reasons to explain the increased stiffness of thyroid cancer at the microscopic level: (1) increased cellularity or increased tumor epithelial cells; (2) increased tumor nonepithelial cells (fibroblasts, endothelial cells, squamous metaplasia, spindle cell metaplasia, and inflammatory cells); and (3) increased matrix substances (collagen, calcifications, amyloid, and mucin). These features increase tissue stiffness that is detected by elastography. In vitro studies with various tumors show tenfold greater stiffness of malignant neoplasms compared with normal tissues [13].

The effectiveness of elastography in detecting papillary thyroid cancer (PTC) is in large part due the presence of

microcalcifications in malignant nodules. This phenomenon is often attributed to psammoma bodies in PTC and is also frequently seen in medullary thyroid carcinoma [13]. Psammoma bodies are assemblies of calcium, seen microscopically. The origin of the word is Greek, meaning sand [14]. They are postulated to arise from infarction and subsequent calcification of the tips of papillae.

Microcalcifications are defined as small bright punctate densities measuring <2 mm, without acoustic shadowing, demonstrated on US [15]. Some microcalcifications may not be visualized on B-mode US due to small size, especially in small and newly formed thyroid cancers. However, they contribute to increased tissue stiffness. It is important to note that psammoma bodies are not pathognomonic of PTC. They can infrequently be seen in benign hyperplastic thyroid nodules as well [16].

The findings of Cooper et al. [16] confirm our clinical experience that high tissue stiffness seen with strain elastography or SWE is not always specific for thyroid cancer.

Strain Elastography

Strain elastography requires minimal manual compression of the tissue being visualized, which then displaces the underlying tissue. The more elastic the tissue, the more displacement is produced. The displacement or distortion of the tissue is then measured and visualized as an elastogram [17].

Imaging of Strain Elastography: Color Maps

Elastography superimposes information regarding elasticity, in color, on B-mode images. Each color represents a certain level of elasticity [18]. The elastography image is displayed next to the B-mode image. Most US machines have multiple different modes for color maps. In the most common elastography map, the color red represents hard tissue and the color

purple represents soft tissue. Figure 16.1 shows examples of strain elastography images for a solid isoechoic thyroid nodule, using three different color maps. Fine needle aspiration biopsy (FNAB) of this nodule was positive for PTC. In the first color map, purple represents soft and red represents hard tissue. For the second map, white/black represents soft/hard tissue. The third map shows red/blue as soft/hard tissue.

Several factors can affect the quality of the images including motion of the patient during the exam, respiratory motion, the location of thyroid nodules, and the practitioner's experience. The presence of fluid or calcifications in a thyroid nodule can also create conflicting results. During the examination, the US monitor may show continuously changing images, similar to a video.

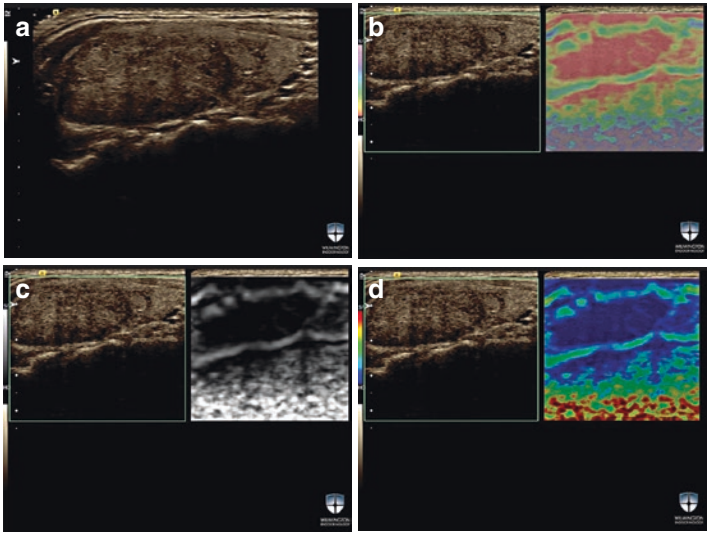

Figure 16.1 (**a**–**d**) Three different strain elastography images of a solid isoechoic right thyroid nodule measuring 37 × 17 × 18 mm; FNAB was positive for PTC. The result for all three maps showed similar result and suggestive of a hard thyroid nodule

How to Grade Strain Elastography Images

One of the challenges of strain elastography is how to grade an image. There are different approaches to grading strain elastography images. Different authors have divided these images into four or five different groups [4, 19–21]. In this chapter, we present our four-group scoring system to grade strain elastography images. We have been using this grading system routinely since January 2010 and are able to explain the discrepancies in interpretation. In the past few years, we worked with several different US machines, and our elastography classification system was useful regardless of which US manufacturer was used for strain elastography exam. Figures 16.2, 16.3, 16.4, and 16.5 illustrate different strain elastography scores (ES) using color map 1.

In the more frequently used color map, the color red represents hard or stiff tissue and the color purple represents soft or elastic tissue. The color green indicates the median stiffness. In our experience, most benign thyroid nodules are either purple or green. B-mode image and elastography image are displayed next to each other. For our study, an elastography score of ES0 was assigned to a thyroid nodule with more elasticity than surrounding thyroid tissue, for example, when a nodule is purple and the surrounding thyroid tissue is green. These nodules are uncommon (5% of total thyroid nodules) and have very low risk for malignancy (<3%). ES1 represents the largest group (about 60–65%) of thyroid nodules. In this group, both the thyroid nodule and the surrounding thyroid tissue have green appearance. This category of thyroid nodules also has a low risk for malignancy (<3%).

ES2 represents the yellow-orange thyroid nodules with intermediate risk for malignancy. This group of nodules has slightly higher tissue stiffness than their surrounding thyroid tissue, and the risk for malignancy is approximately 7.7%. ES3 was assigned to thyroid nodules with little or no elasticity (hard) and included all thyroid nodules that had over 30% red color on elastogram. This group is considered as high risk

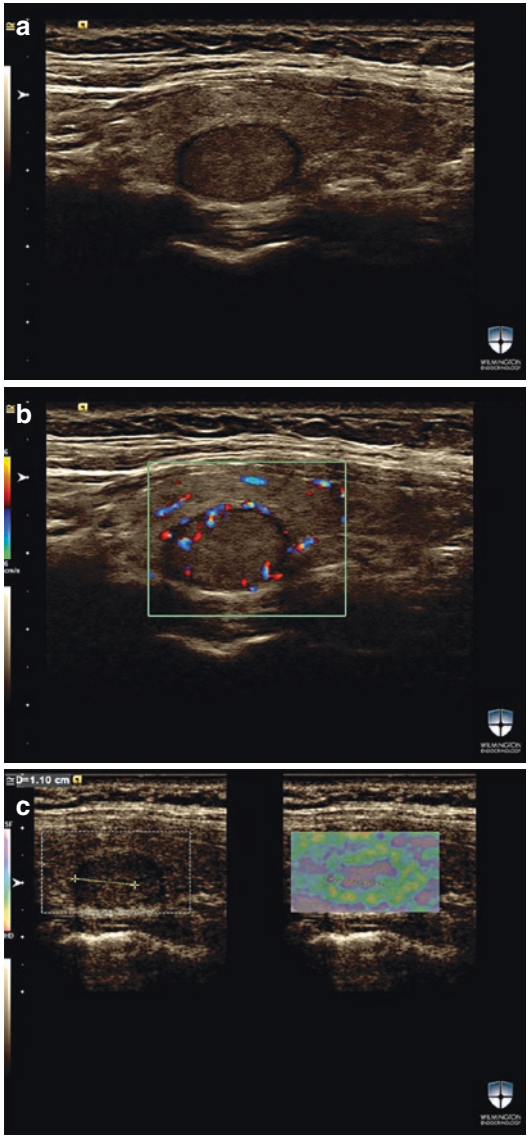

FIGURE 16.2 (**a**–**c**) A solid thyroid nodule with strain elastography score ES0. The stiffness of this solid nodule is less than the surrounding thyroid tissue. FNAB of this nodule was benign

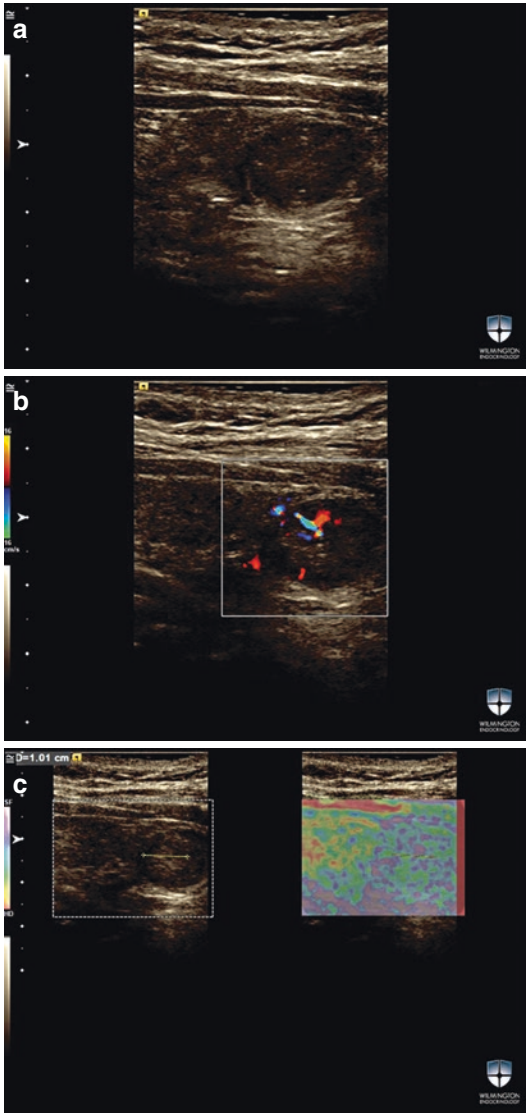

Figure 16.3 (**a**–**c**) A strain elastography image of a solid isoechoic thyroid nodule with ES1. FNAB for this nodule was benign

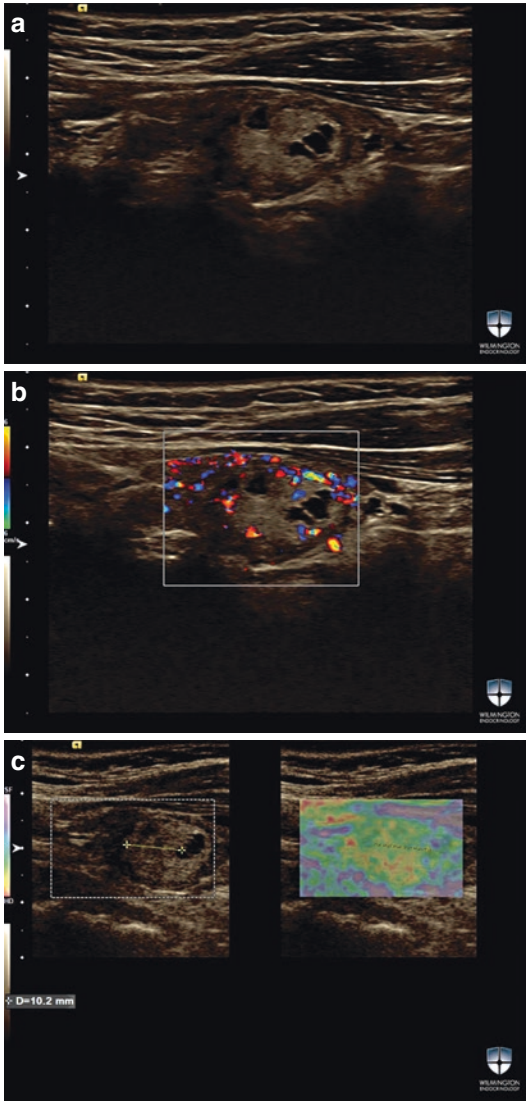

Figure 16.4 (**a**–**c**) An example of a thyroid nodule with ES2. This nodule is isoechoic and complex but mainly solid. FNAB for this nodule was benign

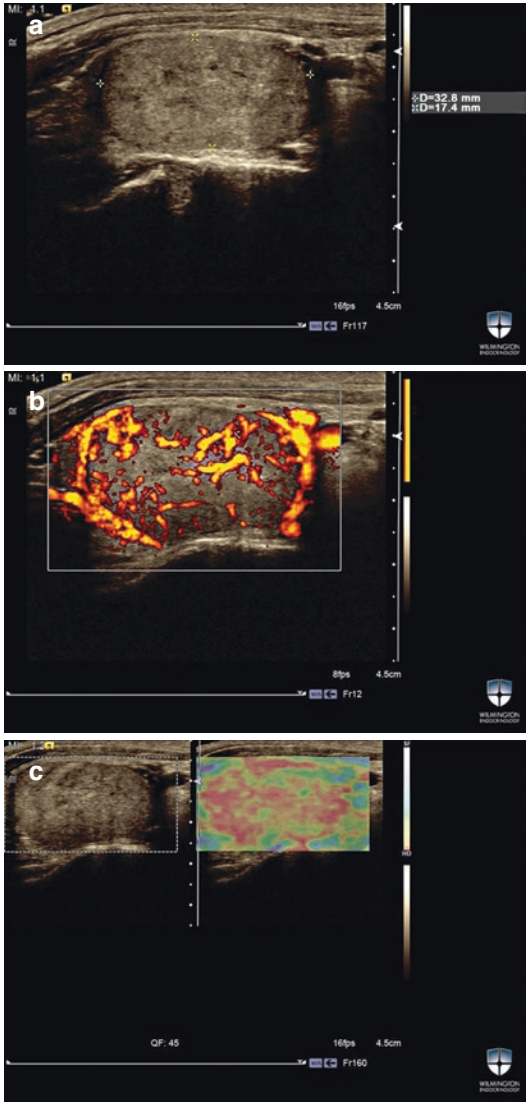

FIGURE 16.5 (**a**–**c**) An example of ES3; FNAB of this solid vascular thyroid nodule was suspicious for follicular neoplasm. The surgical pathology was suggestive of follicular cancer

for malignancy, and the prevalence for thyroid cancer was 36%. However, if a thyroid nodule only had a small amount of red color on elastogram (between 1 and 30% of the thyroid nodule), the nodule was considered as ES2 or intermediate risk for malignancy.

Artifacts on Elastography Images

The presence of thyroid fibrosis and severe heterogeneity (as seen in autoimmune thyroiditis) can cause increased tissue stiffness and subsequent higher elastography scores. The image of both the thyroid nodule and the surrounding thyroid tissue can present as red color affecting a large part of the thyroid gland beyond the nodule under investigation. Figure 16.6 shows an example of a strain elastography image of a thyroid nodule with diffuse artifact surrounding the lesion. In this case, the complete gland was red or hard in color map 1. FNAB showed a benign cytopathology.

Elastography Exam Technique

The elastography exam should follow the B-mode exam of the thyroid gland and nodule(s). The entire thyroid lobe should be included in region of interest (ROI) box. The US probe should be placed longitudinally. First, the thyroid nodule should be identified with B-mode US. The patient should not swallow or breathe for 5 s during exam. The elastography exam should be repeated at least twice, to confirm that the studies are similar. If the results of the studies are inconsistent or conflicting, this may indicate artifact due to poor exam technique, Hashimoto thyroiditis in the thyroid parenchyma, and/or possible heterogeneity within the thyroid nodule. A 2D image only provides information about one layer of a thyroid gland and nodule. The location of a thyroid nodule can affect the elastography exam as well. For example, close proximity to carotid, trachea, or isthmus may interfere with elastography and may result in false positive interpretation.

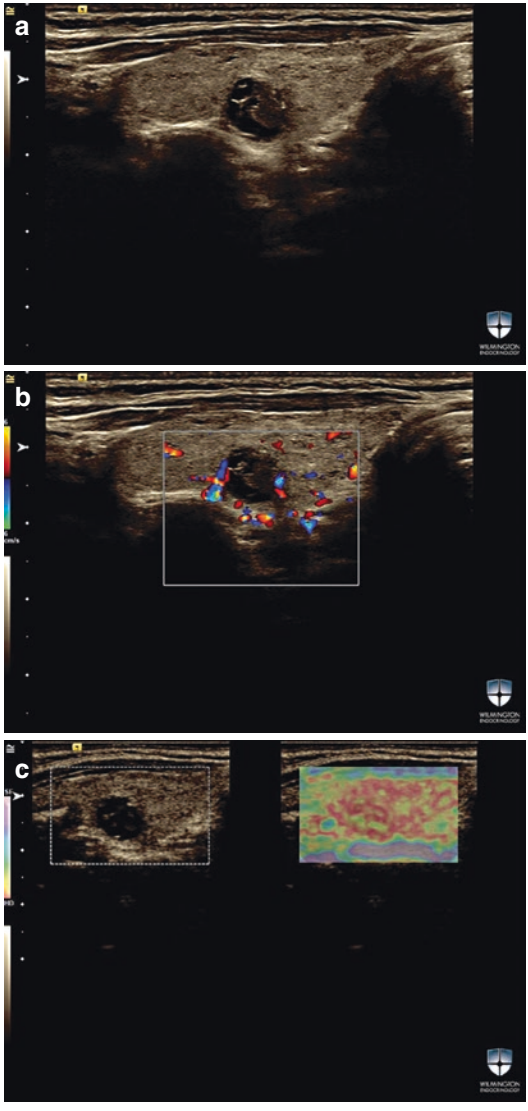

FIGURE 16.6 (**a**–**c**) A complex thyroid nodule. This patient has a history of hypothyroidism for many years. Strain elastography image shows diffuse red color throughout the right thyroid lobe, indicating artifact

Shear Wave Elastography

In shear wave elastography a separate ultrasound pulse is delivered at an angle to the imaging US waves [22–24]. One such technique is referred to as acoustic radiation force impulse (ARFI). The propagation velocity of this pulse is calculated and reported in meters per second (m/s) or converted to a measurement of stiffness reported as kilopascals (kPa) that is proportional to the square of the velocity (kPa = $3pc^2$; where c is the shear wave speed in m/s and p is the tissue density constant) [24]. Unlike strain elastography, shear wave elastography does not require manual compression techniques and it is less operator-dependent [25]. A number of different studies have applied this technology to risk stratification of thyroid nodules [6–9, 25–29].

One early shear wave technology, referred to as virtual touch quantification (VTQ), could produce quantitative tissue velocity data but did not provide a qualitative map that could demonstrate the heterogeneity within the thyroid nodule. VTQ measures an average elasticity within a region of interest (ROI) measuring 6 × 5 mm. Figure 16.7 shows a solid hypoechoic thyroid nodule with shear elastography measurement using VTQ software. Two recent studies showed that VTQ was useful in differentiating between benign and malignant thyroid nodules [7, 9]. In the larger of these studies, Xu et al. prospectively examined 441 thyroid nodules in 375 patients with VTQ and determined that the best cutoff to differentiate benign from malignant thyroid nodules was a SWV of 2.87 m/s [7]. The disadvantage of this technology is that heterogeneity in stiffness within a thyroid nodule cannot be easily evaluated.

Advances in shear wave technology now provide qualitative images that reflect the heterogeneity of stiffness within the thyroid nodule and allow for measurement of tissue stiffness in specific areas of the nodule. The tissue stiffness is expressed qualitatively throughout the entire nodule and surrounding tissue. Continuous images are recorded as video clips. The size of the elastography box should encompass

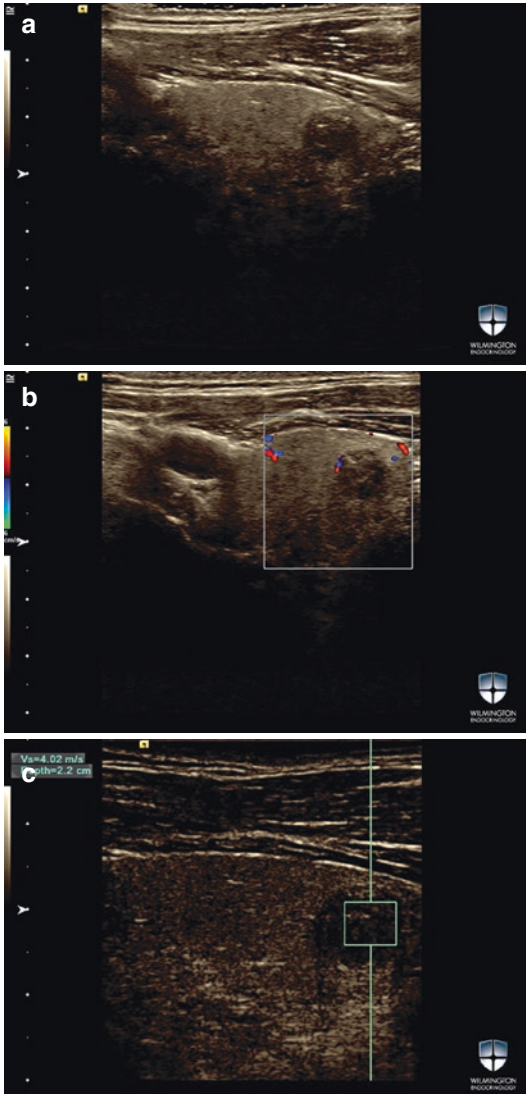

FIGURE 16.7 (**a–c**) A solid hypoechoic thyroid nodule in the left thyroid lobe. B-mode image SWV measurement was performed with VTQ software. SWV for this nodule was 4.02 m/s. FNAB was suspicious for malignancy. Surgical pathology showed 10 mm follicular variant of PTC

both the thyroid nodule under investigation and the surrounding tissue. After the shear wave image is taken, the ROI box can be modified to measure the stiffness of the entire thyroid nodule or the stiffest area within the thyroid nodule. The software can calculate maximum, median, minimum velocity within the ROI box, defined as area of interest by examiner, who determines which elastography images to select.

Figures 16.8 and 16.9 show two different examples of SWE images with one such device. In two relatively small studies, this technique has been used to estimate the risk of thyroid cancer in thyroid nodules [6, 25]. Both studies evaluated the performance of SWE in patients that had been preselected for surgery, so large prospective studies are necessary. While the second study reported the measurement of the stiffest part of the thyroid nodule, the first study did not specify how the region of interest was determined.

Another technique employing shear wave technology referred to as virtual touch imaging quantification (VTIQ) was approved for use in the United States in 2013 [24] and has been studied more extensively for the evaluation of thyroid nodules. This method creates qualitative and quantitative shear wave images in one display. Figure 16.10 shows examples for qualitative and quantitative SWE images using VTIQ software. In our prospective study using VTIQ, we evaluated 707 thyroid nodules in 676 patients with FNAB [8]. Conventional US exam was performed prior to SWV measurement. The transducer was held in the longitudinal axis, and the patient was instructed to refrain from swallowing and breathing for 3–5 s. A qualitative shear wave image was created next to B-mode image, and the SWV was measured quantitatively with a ROI box of 1.5 × 1.5 mm. The qualitative stiffness map guided the practitioner to measure the area with highest SWV. The exam was performed three times. The best cutoff to distinguish between benign and malignant thyroid nodules was 3.54 m/s [8].

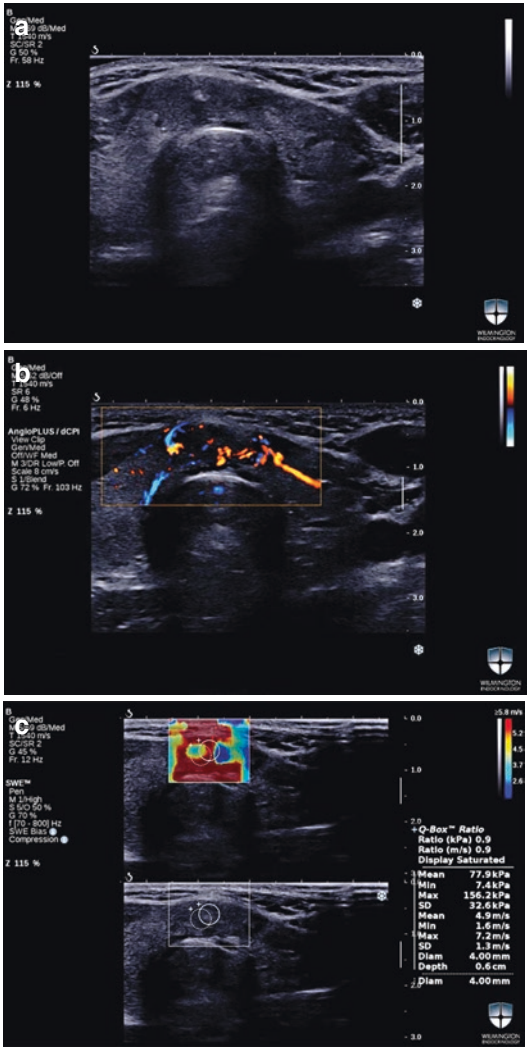

FIGURE 16.8 (**a**–**c**) SWE image of a solid thyroid nodule in the isthmus. Max and mean SWV were 156.2 kPa and 77.9 kPa, respectively. The instant conversions for these values in m/s were 7.2 m/s and 4.9 m/s for max and mean SWV. FNAB was diagnostic for PTC. The surgical pathology report confirmed the diagnosis

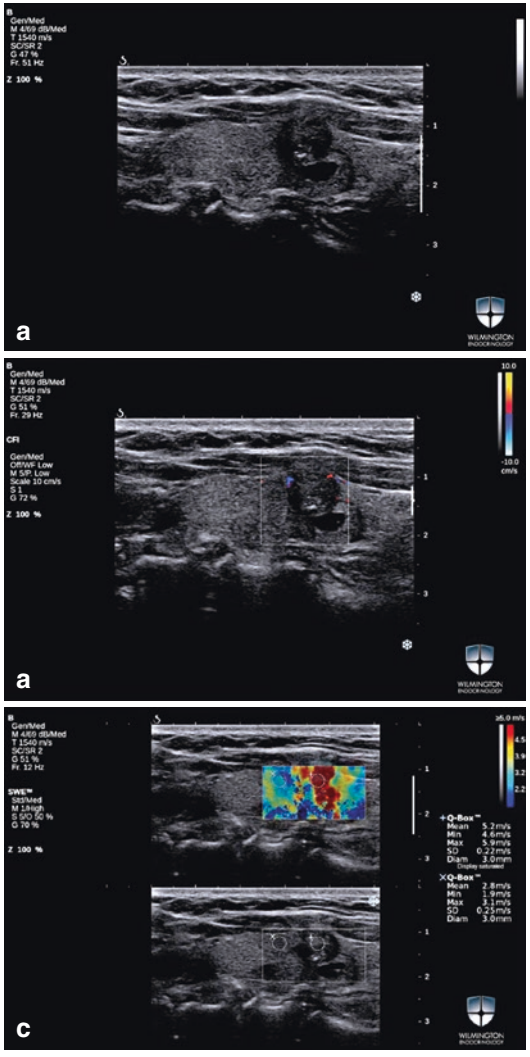

FIGURE 16.9 (**a**–**c**) B-mode and SWE images of a thyroid nodule measuring 10 mm. Max SWV and mean SWV for this lesion were 5.9 m/s and 5.2 m/s, respectively. FNAB was read as suspicious for malignancy. The surgical pathology showed a 10 mm PTC

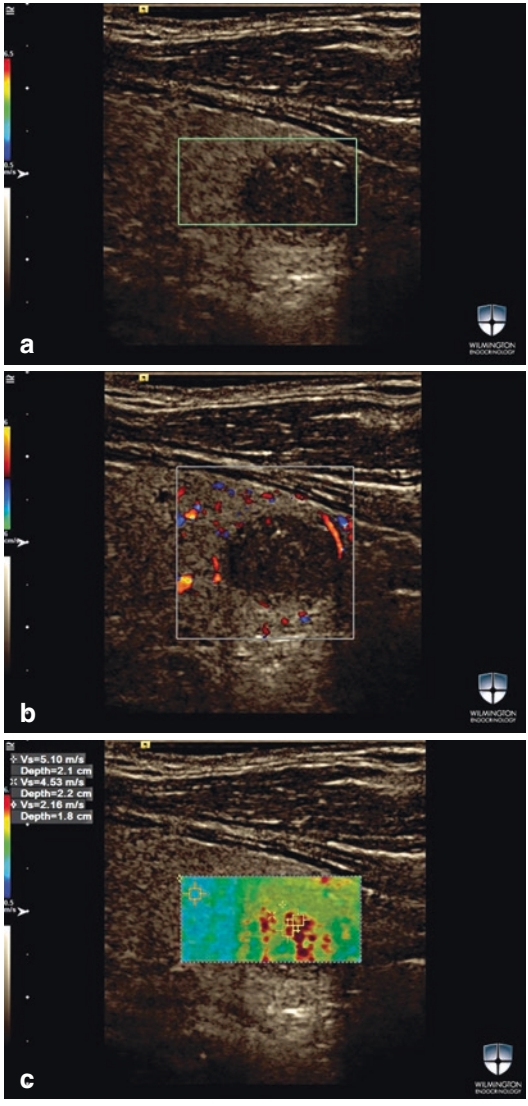

FIGURE 16.10 (**a**–**c**) A solid thyroid nodule with foci of microcalcifications. The max SWV for this nodule using VTIQ was 5.1 m/s and 4.53 m/s. Tissue velocity was 2.53 m/s. FNAB for this nodule was suspicious for malignancy. The surgical pathology showed a 10 mm PTC

Discussion

Studies of Strain Elastography and Shear Wave Elastography

Several recent studies have demonstrated that both strain elastography and SWE predict thyroid cancer risk independently of other ultrasound characteristics. Strain elastography technology can only produce qualitative images and is not capable of quantifying stiffness. This technology is more subjective and is more operator-dependent than SWE. The image can be difficult to reproduce in certain thyroid nodules with mixed tissue stiffness. There is no consensus regarding color map classification and how much pressure to apply when creating strain elastography images.

The largest prospective study of strain elastography, by Azizi et al., was reported on a population with 9% prevalence of thyroid cancer [4]. There were 86 malignant thyroid nodules. Strain elastography was a significant predictor of thyroid cancer ($p = 0.0001$). By multivariate regression analysis, the independent predictors of thyroid cancer were elastography score, microcalcifications, hypoechogenicity, and isthmus location. The positive predictive value (PPV) of ES was 36.1%, which was similar to the PPV of microcalcifications (35.9%), but greater than hypoechogenicity (13.6%) and isthmus location (16.9%). The negative predictive value (NPV) of ES was 97.2%, which was better than any other predictors of benignity. In this study the sensitivity and specificity for thyroid nodules with an elastography score of 3 (the group with the highest stiffness) for the diagnosis of malignancy were 77.0% and 85.2%, respectively. The NPV of 97.2% for strain elastography was greater than all conventional US criteria [4].

A recent large multicenter prospective study of strain elastography, by Friedrich-Rust et al., examined 657 thyroid nodules in 602 patients. The sensitivity, specificity, NPV, and PPV for strain elastography were 56%, 81%, 92%, and 32%, respectively. In this study FNAB was performed on only 214

thyroid nodules in 198 patients. Four hundred and eighty three patients had thyroid surgery [5].

Our large prospective shear wave study, using VTIQ, examined 707 thyroid nodules in 676 patients with FNAB [8]. Both conventional B-mode US and SWE were performed. The prevalence of thyroid cancer was 11.6%. The best SWV cutoff to distinguish between benign and malignant thyroid nodules was 3.54 m/s. SWE was an independent predictor for thyroid cancer. The sensitivity and specificity were 79.3% and 71.5%, respectively. PPV was 26.7% and NPV was 96.3%. Other independent predictors for thyroid cancer in this study included microcalcifications and irregular margins. SWE had higher sensitivity, specificity, PPV, and NPV when compared with B-mode. In a second analysis of these results, thyroid nodules were divided into five predetermined groups based on SWV values. For the group with highest SWV (>4.5 m/s), PPV was 39%, and 32 of 82 thyroid nodules in this group were malignant. We concluded that SWE can enhance B-mode findings and might improve thyroid nodule selection and increase thyroid cancer detection rate [8].

Shear Wave Elastography and Thyroid Cancer Pathology

Some studies suggest that among thyroid cancers, papillary thyroid cancer has a greater SWV than follicular thyroid cancer [4, 6]. However, these findings should be considered preliminary since the initial studies are not adequately powered to be certain of this distinction.

Interobserver Variability

Interobserver variability can be considerable when using elastography to evaluate thyroid nodules. The quality of US machine and practitioner's experience in elastography and thyroid US are important factors affecting the quality and result of the exam [26].

Elastography and Hashimoto Thyroiditis

Elastography calculates nodule stiffness relative to the surrounding thyroid tissue. Autoimmune thyroid disease is a potential interfering factor that can cause changes in the tissue stiffness. In this environment, elastography can incorrectly estimate the malignancy risk of thyroid nodules [27]. Having information about autoimmune thyroid disease of a patient prior to elastography exam and FNAB is helpful in our experience. Hypoechogenicity and heterogeneity on B-mode imaging should alert the examiner to the possibility of autoimmune thyroid dysfunction and resultant interference with accuracy of elastography measurements. Checking thyroid antibodies, including thyroid peroxidase and thyroglobulin antibodies, may be useful.

In our study, the presence of mild to moderate heterogeneity did not affect elastography measurement, but severe heterogeneity and fibrosis in the gland can increase ES and give false positive results. Many of the patients in this group have a prior history of hypothyroidism. The elastography image usually shows diffuse and uniform red color either affecting a large part or entire thyroid lobe, beyond the thyroid nodule under investigation. Figure 16.6 shows an example of a patient with Hashimoto thyroiditis and a complex thyroid nodule.

Elastography Exam of Complex Nodules

The diagnostic assessment of complex thyroid nodules with elastography can be limited due to presence of fluid in the lesion. Several publications have suggested that a cystic portion may create artifact, and therefore, the solid portion of the thyroid nodule should be evaluated [4, 21, 28].

Complex thyroid nodules should be evaluated based on the percentage of the nodule that is solid or cystic. While complex nodules with >50% solid portion are more likely to be malignant, the presence of artifact is more prevalent in nodules with larger cystic component (>50% cystic). In our view, the prevalence of thyroid malignancy in complex nodules with <50% solid portion is very low (1%). We recommend

dividing complex nodules into four groups: group 1, <25% solid tissue; group 2, 25–50% solid tissue; group 3, 51–75% solid tissue; and group 4, >75% solid tissue. We found only one cancer in the first two groups. The remaining 22 thyroid cancers were in group 3 and group 4. In our study, complex thyroid nodules had a similar prevalence of cancer when compared with the solid group [4].

Shear waves do not exist in fluids [22]. When the content of a lesion is fluid only, pressure is the same in all directions. In certain complex thyroid nodules, SWV might be measurable when the fluid contains viscous material and debris. We recommend avoiding the cystic component in large complex lesions with >50% fluid.

When examining complex thyroid nodules with SWE, the size of the elastography box should be modified accordingly. During the initial exam the entire nodule should be studied with SWE. Then the elastography box should be focused on the solid component of the nodule. The exam should be repeated at least twice. If the complex thyroid nodule is >20 mm, the nodule should be divided in two or three parts and each part should be evaluated individually. In our experience, elastography can provide valuable information for needle placement during FNAB for larger complex or solid thyroid nodules to detect partially malignant lesions. Larger thyroid nodules (>20 mm) may have several different levels of stiffness within the nodule under investigation. We recommend FNAB of the areas with greater stiffness first. We have observed several large thyroid nodules that were partially malignant.

Elastography Exam of Nodules Less Than 10 mm

In a subgroup analysis of thyroid nodules evaluated by strain elastography, we found that strain elastography was less accurate in nodules <10 mm [4]. Other sonographic features such as microcalcifications and hypoechogenicity may be more powerful in predicting thyroid malignancy in these nodules. Shear wave elastography may be more accurate than strain elastography when evaluating thyroid nodules <10 mm [8]. Further studies with a larger data sample are needed to examine this issue.

Comparison of Elastography Technologies (Strain and Shear Wave Elastography)

There are few publications comparing shear wave and strain elastography. These studies are small with the largest examining less than 200 thyroid nodules. In the most recent publication, Liu et al. reported that SWE and strain elastography had similar performance characteristics [28]. This publication examined only 64 thyroid nodules in 49 patients. Nineteen (29.6%) nodules were malignant. Figure 16.11 shows strain elastography and SWE exam of a thyroid nodule with two different US machines, one performing strain elastography and the second SWE; the results were similar. However, published studies are too small to assess the true value of combining these two technologies [28, 29].

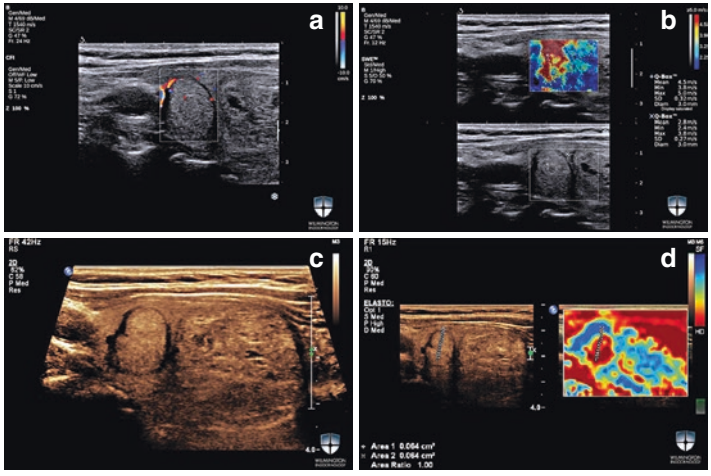

FIGURE 16.11 (**a**–**d**) Left thyroid lobe with a large dominant thyroid nodule and a smaller nodule in the upper pole using strain elastography and SWE with two different US machines. The image for strain elastography is ES3 for the smaller nodule and ES1 for dominant nodule. For the smaller nodule, the maximum and mean SWV were 5.0 m/s and 4.5 m/s, respectively. FNAB for larger nodule was benign and for smaller nodule was suspicious for follicular neoplasm. Surgical pathology showed 15 mm follicular variant of PTC

Elastography of Cervical Lymph Nodes

SWE seems to be helpful in evaluating cervical lymph nodes. Several recent publications with SWE reported good result in differentiating between benign and malignant cervical lymph nodes [30–32]. Cheng et al. evaluated 100 lymph nodes with SWE. Fifty seven lymph nodes were malignant and 43 benign. In this study, the mean SWV was significantly higher in metastatic cervical nodes (4.46 ± 1.46 m/s) than in benign nodes (2.71 ± 0.85 m/s) ($p < 0.001$). ROC curve analysis revealed that the best SWV cutoff for differentiating between benign and metastatic lymph nodes was 3.34 m/s (area under the ROC curve: 0.855, 95% confidence interval [CI]: 0.770–0.917) [33]. A second larger prospective study evaluated 270 cervical lymph nodes. Surgical pathology confirmed 54 malignant nodes [32]. In this publication, based on the ROC curve, the best single cutoff maximum SWV for predicting malignant lymph nodes was 2.93 m/s with sensitivity of 92.6%. The specificity, PPV, and NPV were 75.5%, 48.5%, and 97.6%, respectively [32]. Larger prospective multicenter studies are needed to validate these results.

Limitations of Strain and Shear Wave Elastography Exam

While SWE appears to be less operator-dependent, both technologies have similar limitations. These limitations include:

1. Complex thyroid nodules with high fluid content, with >50% cystic component.
2. Isthmus location of thyroid nodules, due to proximity to trachea, can produce high strain elastography score or SWV values.
3. Deep location of thyroid nodules with >4 cm distance to the surface can limit the exam. Examples for this group include patients with large neck and/or when thyroid nodules are located in the lower pole of the thyroid gland.

4. Calcified thyroid nodules can pose a challenge for both technologies. Many benign but calcified thyroid nodules can have a high SWV or high strain elastography score.
5. Thyroid fibrosis and severe Hashimoto thyroiditis can also cause elevated ES in thyroid nodules and surrounding tissue, despite benign FNAB.

In our experience, both strain elastography and SWE have a learning curve of many months, similar to performing neck US. Elastography is not helpful in evaluating all thyroid nodules. Some malignant thyroid nodules can be soft and some benign thyroid nodules are hard, and this may lead to misdiagnosis. This technology should be considered as a new tool added to our diagnostic capacity to help predict the probability of thyroid cancer.

Conclusion

We conclude that both strain elastography and shear wave elastography stratify the malignancy risk for thyroid nodules as a single variable and in conjunction with other B-mode US features. It can be added to US examinations of thyroid nodules. This technology may improve our ability to detect thyroid cancer and lead to fewer unnecessary thyroid biopsies and surgeries. However, more prospective studies are required to determine the precise value of these new technologies in specific thyroid nodule subgroups.

Disclosure The authors have no conflicts of interest to disclose.

References

1. Garra BS. Elastography: current status, future prospects, and making it work for you. Ultrasound Q. 2011;27(3):177–86. https://doi.org/10.1097/RUQ.0b013e31822a2138.
2. Ophir J, Céspedes I, Ponnekanti H, Yazdi Y, Li X. Elastography: a quantitative method for imaging the elasticity of biological tissues. Ultrason Imaging. 1991;13(2):111–34.

3. Gharib H, Papini E, Paschke R, Duick DS, Valcavi R, Hegedüs L, Vitti P, AACE/AME/ETA Task Force on thyroid nodules. American Association of Clinical Endocrinologists, Associazione Medici Endocrinologi, and European Thyroid Association Medical guidelines for clinical practice for the diagnosis and management of thyroid nodules: executive summary of recommendations. Endocr Pract. 2010;16(3):468–75.
4. Azizi G, Keller J, Lewis M, Puett D, Rivenbark K, Malchoff C. Performance of elastography for the evaluation of thyroid nodules: a prospective study. Thyroid. 2013;23(6):734–40. https://doi.org/10.1089/thy.2012.0227.
5. Friedrich-Rust M, Vorlaender C, Dietrich CF, Kratzer W, Blank W, Schuler A, Broja N, Cui XW, Herrmann E, Bojunga J. Evaluation of strain elastography for differentiation of thyroid nodules: results of a prospective degum multicenter study. Ultraschall Med. 2016;37(3):262–70. https://doi.org/10.1055/s-0042-104647.
6. Veyrieres JB, Albarel F, Lombard JV, Berbis J, Sebag F, Oliver C, Petit P. A threshold value in shear wave elastography to rule out malignant thyroid nodules: a reality? Eur J Radiol. 2012;81:3965–72.
7. Xu JM, Xu XH, Xu HX, Zhang YF, Zhang J, Guo LH, Liu LN, Liu C, Zheng SG. Conventional US, US elasticity imaging, and acoustic radiation force impulse imaging for prediction of malignancy in thyroid nodules. Radiology. 2014;272(2):577–86. https://doi.org/10.1148/radiol.14132438.
8. Azizi G, Keller JM, Mayo ML, Piper K, Puett D, Earp KM, Malchoff CD. Thyroid nodules and shear wave elastography: a new tool in thyroid cancer detection. Ultrasound Med Biol. 2015;41(11):2855–65. https://doi.org/10.1016/j.ultrasmedbio.2015.06.021.
9. Zhang FJ, Han RL. The value of acoustic radiation force impulse (ARFI) in the differential diagnosis of thyroid nodules. Eur J Radiol. 2013;82(11):e686–90. https://doi.org/10.1016/j.ejrad.2013.06.027.
10. Goertz RS, Amann K, Heide R, Bernatik T, Neurath MF, Strobel D. An abdominal and thyroid status with acoustic radiation force impulse elastometry–a feasibility study: acoustic radiation force impulse elastometry of human organs. Eur J Radiol. 2011;80(3):e226–30. https://doi.org/10.1016/j.ejrad.2010.09.025.
11. Ianculescu V, Ciolovan LM, Dunant A, Vielh P, Mazouni C, Delaloge S, Dromain C, Blidaru A, Balleyguier C. Added value of virtual touch IQ shear wave elastography in the ultrasound

assessment of breast lesions. Eur J Radiol. 2014;83(5):773–7. https://doi.org/10.1016/j.ejrad.2014.01.021.
12. Krouskop TA, Wheeler TM, Kallel F, Garra BS, Hall T. Elastic moduli of breast and prostate tissues under compression. Ultrason Imaging. 1998;20(4):260–74.
13. Asteria C, Giovanardi A, Pizzocaro A, Cozzaglio L, Morabito A, Somalvico F, Zoppo A. US-elastography in the differential diagnosis of benign and malignant thyroid nodules. Thyroid. 2008;18(5):523–31. https://doi.org/10.1089/thy.2007.0323.
14. Johannessen JV, Sobrinho-Simões M. The origin and significance of thyroid psammoma bodies. Lab Investig. 1980;43(3):287–96.
15. Komolafe F. Radiological patterns and significance of thyroid calcification. Clin Radiol. 1981;32(5):571–5.
16. Cooper DS, Tiamson E, Ladenson PW. Psammoma bodies in fine needle aspiration biopsies of benign thyroid nodules. Thyroidology. 1988;1:55–9.
17. Lazebnik RS. Whitepaper: tissue strain analytics virtual touch tissue imaging and quantification. Ultrasound, Mountain View: Siemens Medical Solutions, USA, Inc.; 2008.
18. Xing P, Wu L, Zhang C, Li S, Liu C, Wu C. Differentiation of benign from malignant thyroid lesions: calculation of the strain ratio on thyroid sonoelastography. J Ultrasound Med. 2011;30(5):663–9.
19. Itoh A, Ueno E, Tohno E, Kamma H, Takahashi H, Shiina T, Yamakawa M, Matsumura T. Breast disease: clinical application of US elastography for diagnosis. Radiology. 2006;239(2):341–50.
20. Rago T, Di Coscio G, Basolo F, Scutari M, Elisei R, Berti P, Miccoli P, Romani R, Faviana P, Pinchera A, Vitti P. Combined clinical, thyroid ultrasound and cytological features help to predict thyroid malignancy in follicular and Hupsilonrthle cell thyroid lesions: results from a series of 505 consecutive patients. Clin Endocrinol. 2007;66(1):13–20.
21. Rago T, Scutari M, Santini F, Loiacono V, Piaggi P, Di Coscio G, Basolo F, Berti P, Pinchera A, Vitti P. Real-time elastosonography: useful tool for refining the presurgical diagnosis in thyroid nodules with indeterminate or nondiagnostic cytology. J Clin Endocrinol Metab. 2010;95(12):5274–80. https://doi.org/10.1210/jc.2010-0901.
22. Benson J, Fan L. Tissue strain analytics, a complete ultrasound solution for elastography. https://www.cee.siemens.com/web/ua/ru/medecine/detection_diagnosis/ultrasaund/Tissue-Strain-

Analytics/Documents/whitepaper_tissue_strain_pdf. Accessed 1 Dec 2012.
23. Bell J. Siemens announces FDA clearance of virtual touch elastography imaging. Siemens Healthcare USA. Siemens, 24 June 2013. Web. 27 Oct 2014. http://usa.healthcare.siemens.com/press/pressreleases/healthcare-news-2013-06-24-1/.
24. Bercoff J. SuperSonic imagine white paper: shear wave elastography. http://www.supersonicimagine.com/content/view/full/. Accessed 30 Oct 2012.
25. Sebag F, Vaillant-Lombard J, Berbis J, Griset V, Henry JF, Petit P, Oliver C. Shear wave elastography: a new ultrasound imaging mode for the differential diagnosis of benign and malignant thyroid nodules. J Clin Endocrinol Metab. 2010;95:5281–8.
26. Park SH, Kim SJ, Kim EK, Kim MJ, Son EJ, Kwak JY. Interobserver agreement in assessing the sonographic and elastographic features of malignant thyroid nodules. Am J Roentgenol. 2009;193:W416–23.
27. Sporea I, Vlad M, Bota S, Sirli RL, Popescu A, Danila M, Sendroiu M, Zosin I. Thyroid stiffness assessment by acoustic radiation force impulse elastography (ARFI). Ultraschall Med. 2011;32(3):281–5. https://doi.org/10.1055/s-0029-1246048.
28. Liu BX, Xie XY, Liang JY, Zheng YL, Huang GL, Zhou LY, Wang Z, Xu M, Lu MD. Shear wave elastography versus real-time elastography on evaluation thyroid nodules: a preliminary study. Eur J Radiol. 2014;83(7):1135–43. https://doi.org/10.1016/j.ejrad.2014.02.024.
29. Bojunga J, Dauth N, Berner C, Meyer G, Holzer K, Voelkl L, Herrmann E, Schroeter H, Zeuzem S, Friedrich-Rust M. Acoustic radiation force impulse imaging for differentiation of thyroid nodules. PLoS One. 2012;7(8):e42735. https://doi.org/10.1371/journal.pone.0042735.
30. Desmots F, Fakhry N, Mancini J, Reyre A, Vidal V, Jacquier A, Santini L, Moulin G, Varoquaux A. Shear wave elastography in head and neck lymph node assessment: image quality and diagnostic impact compared with B-mode and Doppler ultrasonography. Ultrasound Med Biol. 2016;42(2):387–98. https://doi.org/10.1016/j.ultrasmedbio.2015.10.019.
31. Choi YJ, Lee JH, Lim HK, Kim SY, Han MW, Cho KJ, Baek JH. Quantitative shear wave elastography in the evaluation of metastatic cervical lymph nodes. Ultrasound Med Biol. 2013;39(6):935–40. https://doi.org/10.1016/j.ultrasmedbio.2012.12.009.

32. Azizi G, Keller JM, Mayo ML, Piper K, Puett D, Earp KM, Malchoff CD. Shear wave elastography and cervical lymph nodes: predicting malignancy. Ultrasound Med Biol. 2016;42(6): 1273–81. https://doi.org/10.1016/j.ultrasmedbio.2016.01.012.
33. Cheng KL, Choi YJ, Shim WH, Lee JH, Baek JH. Virtual touch tissue imaging quantification shear wave elastography: prospective assessment of cervical lymph nodes. Ultrasound Med Biol. 2016;42(2):378–86. https://doi.org/10.1016/j.ultrasmedbio.2015.10.003.

Chapter 17
Authoring Quality Ultrasound Reports

J. Woody Sistrunk

Introduction

It has now been almost two decades since endocrinologists began routinely performing thyroid ultrasound studies. The first American Association of Clinical Endocrinologists (AACE) Thyroid Ultrasound Course was held in 1998. Point of service ultrasound, performed by the treating physician, has clearly benefitted patients with thyroid and parathyroid disorders. Treating physician-performed ultrasound evaluation, ultrasound-guided FNA (USGFNA), and ultrasound thyroid cancer surveillance have changed thyroid and parathyroid disease management forever.

With this relatively new science, inherent responsibilities of the physician sonologist (physician performing ultrasound) exist. Quality measures such as AACE Endocrine Certification in Neck Ultrasound (ECNU) certification and American Institute of Ultrasound Medicine (AIUM) practice accreditation are in place [1, 2].

Clear documentation of the information gathered from an ultrasound study is essential to quality patient care. The

J. Woody Sistrunk, MD, FACE, ECNU
Jackson Thyroid & Endocrine Clinic, PLLC, Jackson, MS, USA
e-mail: woodysistrunk@gmail.com

D.S. Duick et al. (eds.), *Thyroid and Parathyroid Ultrasound and Ultrasound-Guided FNA*,
https://doi.org/10.1007/978-3-319-67238-0_17

report should be complete, yet succinct. It should fully describe the ultrasonographic findings and provide useful interpretation and recommendation.

The aim of this chapter is to review the basic requirements of documenting a thyroid/parathyroid ultrasound adhering to both the requirements of the Endocrine Certification in Neck Ultrasound (ECNU) and the Practice Parameter for the Performance of a Thyroid and Parathyroid Ultrasound Examination set forth by the American Institute of Ultrasound in Medicine (AIUM) in conjunction with the American College of Radiology (ACR). Examples will provide the basis of what comprises a quality ultrasound report. For additional thyroid ultrasound reporting examples, please see https://www.aace.com/files/ecnu-sample-submission.pdf.

Suboptimal Reports Can Be Clinically Misleading

Unfortunately, thyroid ultrasound reports with unanswered clinical questions may lead to unnecessary or inappropriate surgery. Below are actual real-world ultrasound reports as examples of what to avoid. Hopefully, these will highlight the necessity of combining the patient history, physical exam, real-time ultrasound, and lab findings in order to author a report of optimal quality.

These are actual examples taken from real-world thyroid ultrasound reports:

"Impression: There are multiple nonspecific hypodensities and small cystic nodules in the thyroid gland. Their appearance is nonspecific."

How much more nonspecific can one be?

"Impression: Enlarged multinodular thyroid consistent with a goiter. The nodules cannot be further characterized by ultrasound. If further evaluation is clinically indicated, nuclear medicine thyroid scan would be recommended."

Only to be answered with the superb, insightful nuclear medicine scan:

"Impression: What appears to be a cold nodule in the inferior aspect of the right lobe of the thyroid gland? Correlation with ultrasound recommended."

Isn't this where the question began?

"Impression: Multinodular thyroid gland likely related to a multinodular goiter."

Consider the audience/recipient of the report: *the referring clinician*, to whom an effective thyroid ultrasound report will provide an answer to the question prompting referral; *the thyroid/parathyroid surgeon*, whose appropriate operative decision will depend upon an effective report; and *the medical record*, in which consistency will benefit longitudinal follow-up of the patient.

An ultrasound report should be readily available as a separate, narrative document. It should not be composed of check boxes, buried in an electronic medical record clinic note, nor should it contain medication lists or any other extraneous information that is not applicable to the ultrasound study at hand. A separate and identifiable document is necessary in providing documentation for reimbursement and for good patient care; however, many integrate the ultrasound report into a concise clinical note which is meaningful and does not result in reimbursement problems.

For additional information required for a comprehensive ultrasound report, see AIUM Documentation of an Ultrasound Examination [3].

Practice Identification Data

Identification of the imaging facility/physician's office should be at the top of the report with facility location and sufficient contact information. The clinician performance of the study should be clearly indicated.

Patient Identification Data

At a minimum, patient name, date of birth, ID number (social security or patient/clinic number). Note: Reports submitted for ECNU certification must have all identifying patient demographics removed to comply with HIPPA regulations [1].

Date of Procedure

It is imperative that a date of service be *clearly identified.*

Indication

Aside from being necessary for third party payment, a quality thyroid ultrasound examination is performed to answer a clinical question. Consider the clinical question to be answered by ultrasound. Be succinct in giving the indication, for example, *multinodular goiter*, *diffuse thyroid enlargement*, *hyperthyroidism*, *right thyroid nodule found on CT scan*, *or history of papillary thyroid cancer in sister*.

Occasionally, a more complicated indication may be clinically necessary such as "1.9 cm BRAF mutation positive right lobe tall cell papillary cancer, s/p total thyroidectomy and subsequent I^{131} therapy. T1b, N1b, M0 (Stage I) now with an elevated thyroglobulin tumor marker."

Remember to keep the indication brief, relevant, and to the point.

Explanation of Procedure

This should be a simple overview of how the procedure was performed.

For routine thyroid/parathyroid ultrasound—"Using physician-performed, real-time ultrasound limited to the thyroid gland and anterior neck, longitudinal and transverse images were obtained of both lobes and isthmus."

For thyroid cancer surveillance—"Using physician-performed, real-time ultrasound limited to the thyroid bed and neck, including nodes (Levels I, II, III, IV, V, VI), longitudinal and transverse images were obtained."

The AIUM Practice Parameter for the Performance of a Thyroid and Parathyroid Examination states "Recorded images of the thyroid should include transverse images of the superior, mid and inferior portions of the right and left lobes; longitudinal images of the media, mid, and lateral portions of both lobes; and at least a transverse image of the isthmus." [2] These 13 images are also now required as a part of the Validation of Competency (VCP) portion of the ECNU certification process [1]. When a sonographer is taking images for a physician to review later, as routinely performed in a radiology department, clearly more images are needed to demonstrate/document complete study.

Physician sonologists performing real-time ultrasound may require fewer images. An effective approach should be that if a comprehensive report can be generated from the archived images with no other clinical data 1 year from now, then a sufficient number of images have been obtained. Enough images should be obtained to answer the clinical question at hand for performing the ultrasound study.

Thyroid Size

The size of a normal thyroid gland correlates with the amount of iodine in the diet. The United States is replete with dietary iodine, and each normal thyroid lobe has anterior-posterior and transverse dimensions of 2 cm or less with a longitudinal dimension of 4.5–5.5 cm, and overall the thyroid weighs approximately 15–20 g. In Europe, where dietary iodine intake is lower, the normal gland may be up to 40 g.

The AIUM Thyroid/Parathyroid Practice Guideline states: "The size of each thyroid lobe should be recorded in 3 dimensions, anteroposterior, transverse, and longitudinal. The thickness of the isthmus on the transverse view should be recorded" [2].

It is best to avoid words such as length, depth, width, etc. since these do not refer to a definite plane of measurement. A limited vocabulary will yield consistency in reporting.

Calculating or reporting the volume of the thyroid gland has no routine role in clinical thyroidology and is considered optional. Measurements can be given in centimeters or millimeters but is important to remain consistent throughout the report.

Note: The preferred ECNU standard for reporting all measurements is *longitudinal x anterior-posterior x transverse unless otherwise stated* [1]. The order in which dimensions are reported should be stated on the report.

Thyroid Description

An overall description of the thyroid parenchyma and an assessment of the vascularity of the gland should be provided.

This allows an overview of the gland prior to focusing on pathology-specific nodule or cyst. Otherwise, considerations such as diffuse autoimmune thyroid disease or thyroid lymphoma may be lost in the effort to identify a small nodule. This is a frequent omission made by radiologists.

Begin the statement with "Overall" to make certain that the reader understands this is a summation statement of the gland parenchyma. Examples would include:

"Overall, the thyroid is symmetrically enlarged with a heterogeneous echotexture."

For autoimmune thyroid disease including Hashimoto's thyroiditis and Graves' disease:

"Overall, the thyroid gland is symmetrically enlarged, diffusely heterogeneous, and hypervascular." Additional descriptors could include "significantly hypoechoic" and "diffusely heterogeneous." Describe what is seen. "Overall, the thyroid gland is enlarged and asymmetric with a prominent right lobe. The gland has homogeneous echotexture."

Comment on the presence (or absence) of tracheal deviation and substernal extension.

With Hashimoto's thyroiditis, additional information can be added including a short description of fibrosis and/or the pseudo-nodular appearance of the gland.

Description of posterior enhancement of the thyroid parenchyma is another identifiable, relevant feature in infiltrative/lymphocytic autoimmune thyroid disease.

As rarely the parenchyma of the right and left lobes is significantly discordant, it is recommended that the entire gland be described as a whole instead of describing each lobe separately.

Description of Pathology

What was seen and where was it seen?

Location is critical; the more descriptive the report, the more reproducible the exam will be. Surgeons will appreciate consistent, effective locations of pathology.

No absolute convention of reporting order exists. It is recommended to be consistent in reporting, for example, findings in the right upper pole to the right inferior pole are described first, the isthmus, and then the left upper pole to the left lower pole. Nothing is more disturbing and confusing than an ultrasound report that describes anatomic findings in a random pattern. Describing the location of a nodule within the right/left thyroid lobes, upper/ mid/lower lobe, anterior/posterior position, and lateral/medial position provides a consistent, reproduceable pattern that can be eaily followed by the reader.

Nodules

The AIUM Practice Parameter for Thyroid and Parathyroid Ultrasound Examination recommends:

"Thyroid abnormalities should be imaged in a way that allows for reporting and documentation of the following…."

> "The location, size, number, and character of significant abnormalities, including measurements of nodules and focal abnormalities in 3 dimensions."
> "The sonographic features of any thyroid abnormality with respect to echogenicity, composition (degree of cystic change), margins (smooth or irregular), presence and type of calcification (if present), and other relevant sonographic patterns" [2].

These recommendations mirror the requirements of the Validation of Competency (VCP) portion of ECNU [1].

In describing a nodule start with the basics:

- Is the nodule *solid*, *cystic*, *or complex*?
- Is the nodule *hypoechoic*, *hyperechoic*, or *isoechoic*?
- Is the nodule *homogeneous* or *heterogeneous*?
- Are there *calcifications*? If so, what type?
- Are the borders *regular*, *discrete*, or *infiltrative*?
- What is the *Doppler flow pattern/grade*?
- What is the *shape* of the nodule?

By considering these basic questions, an ongoing process begins that will help identify suspicious or benign nodules while performing the study.

As recommended by AIUM [2] and required by ECNU [1], measure each nodule in three dimensions. A volume calculation can be considered as a more accurate indicator for long-term nodule size surveillance. Nodules that are *taller than wide* (anterior-posterior > transverse) should be noted and described as such. This characteristic is considered a "High Suspicion" sonographic pattern by the 2015 ATA Guidelines [4].

Remember, both benign and malignant nodules are still nodules. They are not lesions, masses, growths, hypodensities, polyps, goiters, areas, nodularities, geographic hypoechogenicities, or nodulations. *They are nodules!* Keep the language consistent.

> This actual example "Impression – A 3.4 mm complex mass is seen in the right lobe" seems to be designed to create anxiety if read by the patient and could easily become an invitation for unnecessary surgery.

Avoid redundant synonyms like inhomogeneous, nonhomogeneous, etc. If a nodule is seen that has the typical appearance, describing it as a *spongiform colloid nodule* is helpful. As referenced in the 2015 American Thyroid Association guidelines, "A spongiform appearance is defined as the aggregation of multiple microcystic components in more than 50% of the volume of the nodule" [4]. The description of a spongiform colloid nodule is a highly specific appearance suggesting benign disease. It can be of critical importance in reassurance of the clinician and the patient of its benign nature. Other nodule characteristics must also be considered:

Calcifications can be broadly classified into *eggshell calcifications*, *dense calcifications* (with posterior acoustic shadowing), or *microcalcifications* (without shadowing). Some overlap exists between the use of the term punctuate calcifications and microcalcifications. "Interrupted peripheral calcifications" as mentioned in the 2015 ATA Guidelines infer a high risk of malignancy [4]. Proper description is imperative. Note: As per the ECNU requirements, calcifications or lack thereof should be described with every nodule [1].

The margins of a nodule may be described as *smooth (with or without a halo)*, *irregular*, *infiltrative*, *or irregular/infiltrative.* This is recommended in the AIUM Practice Parameter and required with the ECNU VCP.

Vascularity of nodules is documented utilizing Grades 1 through 4 as described by Fukunari [5]. This has become the standard for description of Doppler flow in nodules. Consider these simple descriptions:

- *Grade 1 (Absent) Doppler flow is seen.*
- *Grade 2 (Peripheral) Doppler flow is seen.*
- *Grade 3 (Penetrating) Doppler flow is seen.*
- *Grade 4 (Chaotic) Doppler flow is seen.*

Please note: Doppler grades are reported as Arabic numbers, not Roman numerals. Doppler grades do not apply to parathyroids or lymph nodes. Doppler is a proper name and is always capitalized.

Comet tail artifact in a colloid nodule should always be mentioned. Although often mistaken on static images by radiologists for microcalcifications, this reverberation artifact is a benign finding.

Cysts

Cysts can be subdivided into *simple cysts* (only cystic content) and *complex cysts* (more cystic than solid material). A *complex nodule* is used to describe a nodule that is more solid than cystic. If a nodule is complex, specify what percentage is solid versus cystic.

Invariably, some nodules will have a small amount of cystic degeneration. "Minimal cystic degeneration is seen" is a sufficient descriptor in this circumstance.

Lymph Nodes

It is recommended that with every neck ultrasound, imaging is performed of cervical lymph nodes. This can be a cursory look, not necessarily comprehensive thyroid cancer lymph node mapping. If no nodes with a short-/long-axis ratio > 0.5 (i.e., not rounded), with calcifications, cystic change, or abnormal Doppler pattern, are seen, a summation statement in the impression can be "No significant cervical adenopathy is seen." Any lymph node with an anterior-posterior dimension >0.5 cm and a short-/long-axis ratio (S:L ratio) >0.5 should be reported along with comment regarding presence or absence of a hilar line, cystic necrosis (often revealed by posterior acoustic enhancement), and calcifications. Doppler descriptions for nodes such as "No intra-nodal Doppler flow is seen," "Doppler flow is seen at the central hilum," or "Peripheral Doppler flow is seen" are all very adequate succinct descriptions that can be utilized. Again, Doppler grades used in describing nodules do not apply with lymph nodes. In the setting of an evaluation of a thyroid nodule with ultrasound, documenting absence of suspicious lymph nodes serves as an indication that the nodes were indeed investigated. If a single

node is seen of doubtful or uncertain clinical significance, document that node in the body of the report. Any node may become clinically relevant, particularly after the confirmation of malignancy of a nodule with an FNA biopsy.

Preoperative evaluation of patients with suspicious nodules and postoperative surveillance of documented thyroid cancer patients require a more comprehensive lymph node exam. A consistent protocol is of critical importance. It is imperative that the physician sonographer/sonologist have a working understanding of lymph node compartments (Fig. 17.1). Although no absolute convention exists, mapping/reporting nodes is easier to interpret when a consistent

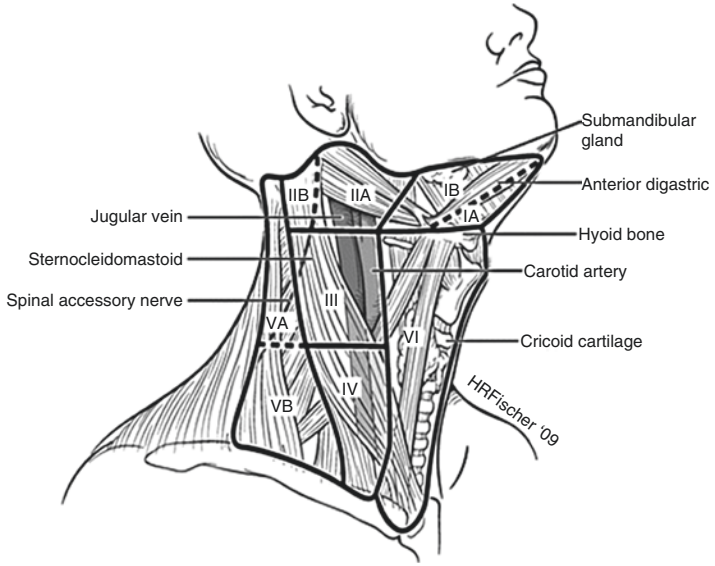

Figure 17.1 Lymph node map. From 2015 American Thyroid Association Management Guidelines for Adult Patients with Thyroid Nodules and Differentiated Thyroid Cancer: The American Thyroid Association Guidelines Task Force on Thyroid Nodules and Differentiated Thyroid Cancer. Haugen, Alexander, et al., Thyroid. Jan 2016, 26(1): p. 30. Reprinted with permission from American Thyroid Association

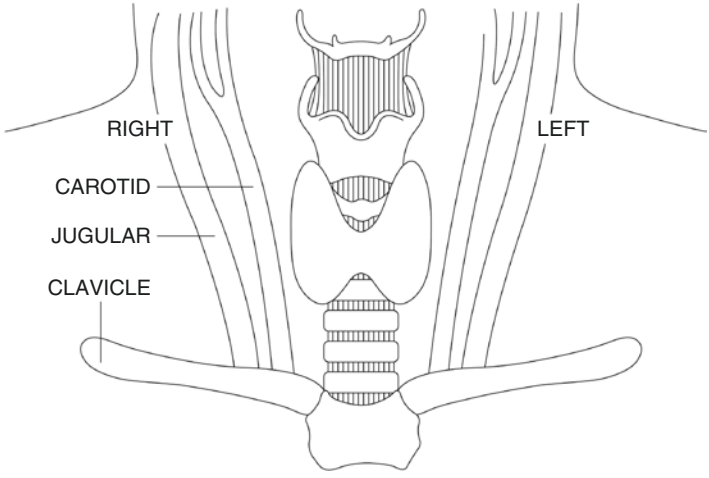

Figure 17.2 AACE ECNU cartoon

pattern is followed. The criteria mentioned above are used to identify suspicious nodes that may be malignant. The official ECNU cartoon (Fig. 17.2) can be used to diagram the size and location of suspicious lymph nodes for communication with the surgeon and/or serial ultrasound follow-up.

Parathyroid Glands

Because normal parathyroid glands are not typically seen with ultrasound, those that are seen enlarged likely represent pathology such as an adenoma, hyperplasia, cyst, or carcinoma. Parathyroid glands should be measured in three dimensions, lateralized right or left, and location noted (i.e., posterior to thyroid, intrathyroidal, in thyro-thymic ligament, etc.). State the echogenicity (almost always hypoechoic) and describe the vascularity, especially the presence or absence of a polar artery or vascular pedicle. *Additionally, see* Chap. 9 *regarding the ultrasound characteristics of parathyroid glands.*

Impression/Plan

One should not consider the impression as a restatement of the entire body of your report; it is a *diagnostic impression*. Keep it brief. Although a number of styles could be considered, consistency counts here. Numbered bullet points make a report easily readable and understood. Remember this is often the only portion of the report that will be read by others. Make it count!

Impression Bullet #1: Summation Statement

Some examples include:

- "Prominent thyroid gland with a heterogeneous echotexture."
- "Multinodular goiter with nodules seen in both lobes."
- "Symmetrically enlarged, diffusely heterogeneous, densely hypoechoic, fibrotic, goiter, compatible with the clinical history of Hashimoto's thyroiditis with hypothyroidism."
- "Symmetrically enlarged, diffusely heterogeneous, hypervascular goiter (suggestive of/consistent with the clinical diagnosis of) Graves' disease/hyperthyroidism"
- "The thyroid gland is surgically absent compatible with the clinical history of thyroidectomy (± and subsequent I^{131} therapy) for papillary cancer."

Impression Bullet #2: Pathology Description

- "Dominant right mid-lobe nodule, 1.8 cm."
- "No discrete nodules are seen." A powerful, succinct description.
- "Posterior to the right mid- to lower lobe is a significantly (or profoundly) hypoechoic nodule measuring 1.3 cm. By its anatomic location and appearance, this is likely a parathyroid gland consistent with the findings of the parathyroid sestamibi scan of XX/XX/XXXX from X hospital."

- For nodules that have been biopsied previously:
  - "Right mid-lobe densely hypoechoic nodule, 2.5 cm. This nodule was previously biopsied with benign result on XX/XX/XXXX."

Impression Bullet #3: Lymph Node Comment

- Describe any pathologic nodes seen.
- "No significant cervical adenopathy is seen."
- Or for thyroid cancer: "Nodes are seen in both sides of the neck, none of which have an overtly suspicious appearance."

Impression Bullet #4: Comparison to Prior Studies

Although relatively straightforward, this should be succinct and compared to prior study with an exact date.

- "When compared to the prior study of XX/XX/XXXX, no significant change is seen."

Recommendations/Plan

As required in the ECNU certification, recommendations should be included in the report [1]. The AIUM Practice Parameter – Documentation of and Ultrasound Examination recommends the addition of recommendations for follow-up imaging or other testing [3].

For example:

- "A follow-up ultrasound in 1 year is recommended."
- "Correlation with pending thyroperoxidase antibody is planned/recommended."
- "Correlation with antibodies for Graves' disease and an I123 thyroid uptake(± and scan) is planned."
- "FNA biopsy of the dominant nodule (with molecular markers collected and held pending results of cytology) is planned/recommended."

The impression and specific recommendations may be combined:

- "A suspicious dominant 2.5 cm right mid to lower lobe thyroid nodule with microcalcifications is seen. An ultrasound-guided FNA biopsy (±with molecular markers collected and held pending results of cytology) is recommended." This type of statement will benefit the referring physician and explains to the third party payer why the biopsy is necessary.

Cartoon

Although not a requirement of either ECNU certification or AIUM accreditation, a drawing demonstrating pathology may be of helpful significance to the referring physician, the surgeon, and the patient. Sketching the findings in the presence of the patient immediately following the study solidifies in the mind of the patient and the physician sonographer an overview of the pathology and its clinical relevance. Figure 17.2 is the official ECNU cartoon. This can be duplicated for use as needed in clinical practice.

Documentation of FNA Biopsy

The AIUM and ECNU are both very explicit in their recommendations of what should be documented in with an USGFNA. The AIUM Practice Parameter for Documentation of an Ultrasound Examination in the subheading "Reporting of Ultrasound-Guided Procedures" also recommends:

- "Date and time of the ultrasound guidance of the procedure."
- "Needle/device type and gauge."
- "Number of passes performed."
- "Specimen type and amount of removed if any as well as its disposition."

- "Complications" [3].
- Note the time of FNA biopsy can be easily obtained from the ultrasound image demonstrating the needle in the target lesion, as required by ECNU [1].

Evolution of Ultrasound Reporting

What will the future hold for thyroid ultrasound reporting? The 2015 American Thyroid Association Guidelines describe specific sonographic patterns including "High Suspicion," "Intermediate Suspicion," "Low Suspicion," "Very Low Suspicion," and "Benign" [4]. These classifications may be very useful in an ultrasound report. Based on the BI-RADS (Breast Imaging Reporting and Data System) for breast imaging, several Thyroid Imaging, Reporting and Data Systems (TIRADS) have been proposed (see Chap. 7) [6]. For now, endocrinologists/thyroidologists must stand for quality by exemplifying the most effective use of thyroid ultrasound and generating a meaningful report. As the science advances to the use of USGFNA-based molecular markers, elastography, and ultrasound-guided ethanol ablative procedures, ultrasound reports will need to be expanded and improved to keep up with the state of the science, at the same time maintaining high quality and consistency.

Summary

An excellent ultrasound examination may have little value if the documented report is deficient. Extracting all the useful information from the study and presenting it in a cohesive, concise manner is a skill that one develops with practice over time.

This chapter has outlined an approach to writing an informative, constructive, and practical ultrasound report. Consistency, quality, and reproducibility are the hallmarks of a good thyroid ultrasound report.

Acknowledgment Dr. Sistrunk wishes to acknowledge the vast contributions that H. Jack Baskin, Sr., MD, made to the original version of this chapter in the third edition of this book. Much of his original content has been propagated with continued updates based on ECNU and AIUM requirements. Without the guidance of Dr. Jack Baskin, there would have been no AACE Ultrasound Course and no Endocrine Certification in Neck Ultrasound.

References

1. Endocrine Certification in Neck Ultrasound (ECNU) Handbook. https://www.aace.com/files/CandidateHandbook.pdf. Accessed 02 Oct 2016.
2. American Institute of Ultrasound in Medicine (AIUM) Practice Guidelines for Performance of a Thyroid and Parathyroid Ultrasound Examination. http://www.aium.org/resources/guidelines/thyroid.pdf. Accessed 20 Sept 2016.
3. American Institute of Ultrasound in Medicine (AIUM) Practice Parameter for Documentation of an Ultrasound Examination. http://www.aium.org/resources/guidelines/documentation.pdf. Accessed 20 Sept 2016.
4. Haugen BR, et al. 2015 American Thyroid Association management guidelines for adult patients with thyroid nodules and differentiated thyroid cancer. Thyroid. 2016;26(1):1–133.
5. Fukunari N, et al. Clinical evaluation of color Doppler imaging for the differential diagnosis of thyroid follicular lesions. World J Surg. 2004;28(12):1261–5.
6. Grant EG, et al. Thyroid ultrasound reporting lexicon: white paper of the ACR thyroid imaging, reporting and data system (TIRADS) committee. J Am Coll Radiol. 2015;12:1272–9.

Index

D.S. Duick et al. (eds.), *Thyroid and Parathyroid Ultrasound and Ultrasound-Guided FNA*,
https://doi.org/10.1007/978-3-319-67238-0